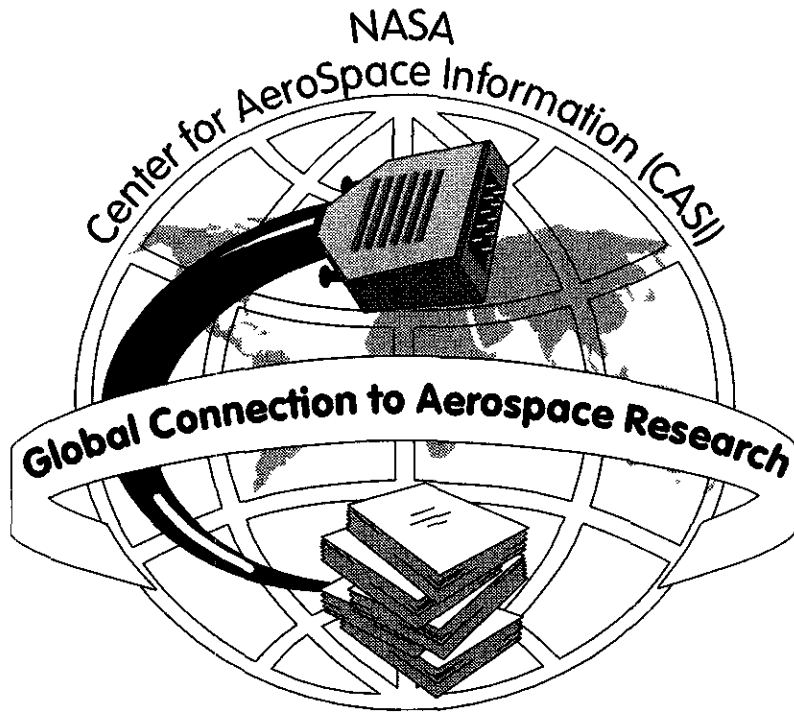


STI CENTER -GS 53-45/100
NASA JOHNSON SPACE CENTER
2101 NASA ROAD ONE
HOUSTON, TX 77058-3696

19690094145



A Service of:
National Aeronautics and
Space Administration



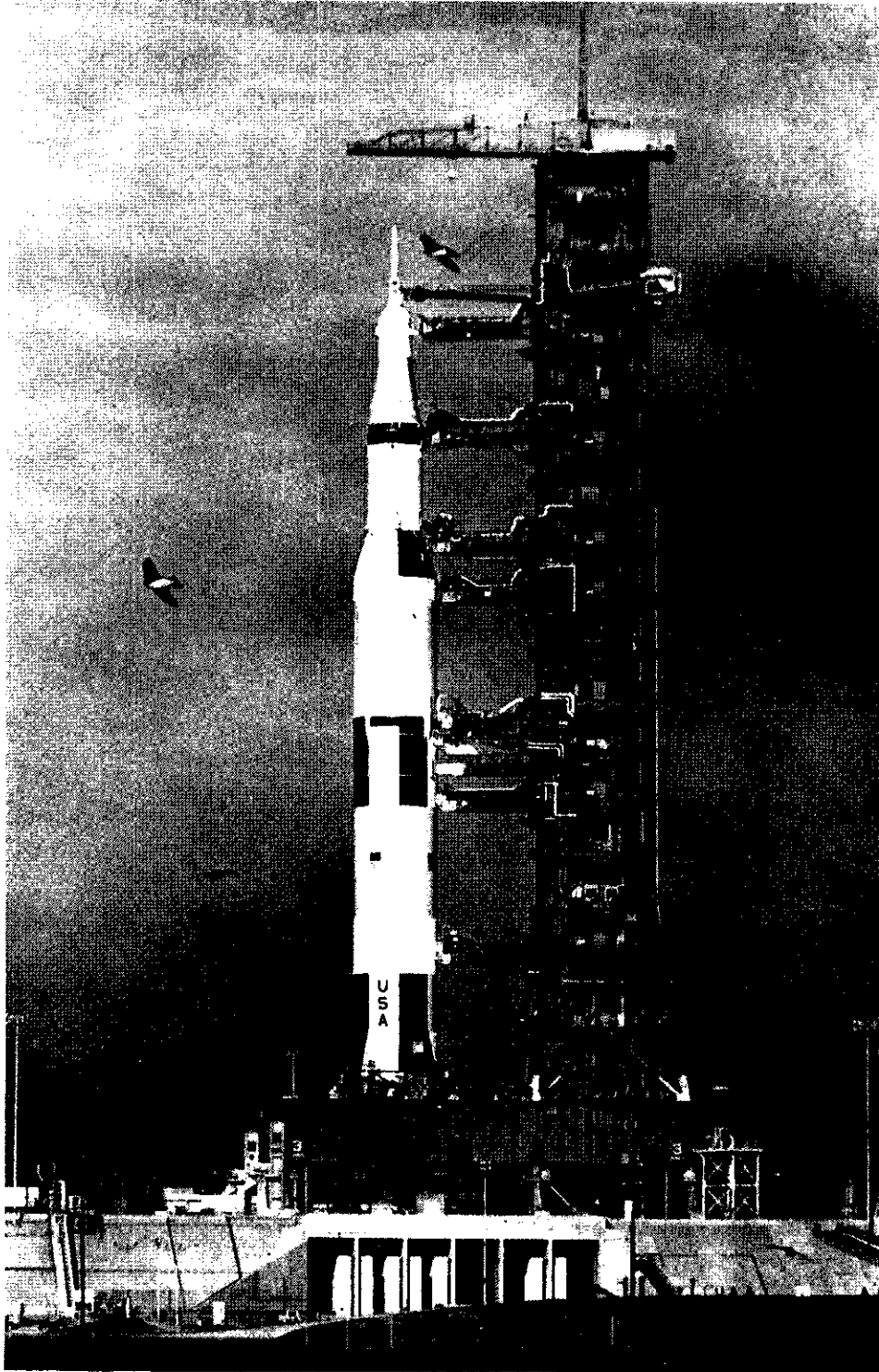
SCIENTIFIC &
TECHNICAL INFORMATION

GEORGE C. MARSHALL SPACE FLIGHT CENTER

MPR-SAT-FE-69-7

SATURN V LAUNCH VEHICLE
FLIGHT EVALUATION REPORT - AS-505
APOLLO 10 MISSION

PREPARED BY
SATURN FLIGHT EVALUATION WORKING GROUP



AS-505 LAUNCH VEHICLE

MPR-SAT-FE-69-7

SATURN V LAUNCH VEHICLE FLIGHT EVALUATION REPORT - AS-505

APOLLO 10 MISSION

BY

Saturn Flight Evaluation Working Group
George C. Marshall Space Flight Center

ABSTRACT

Saturn V AS-505 (Apollo 10 Mission) was launched at 12:49:00 Eastern Daylight Time on May 18, 1969, from Kennedy Space Center, Complex 39, Pad B. The vehicle lifted off on schedule on a launch azimuth of 90 degrees east of north and rolled to a flight azimuth of 72.028 degrees east of north.

The launch vehicle successfully placed the manned spacecraft in the planned translunar injection coast mode. The S-IVB/IU was placed in a solar orbit with a period of 344.9 days by a combination of continuous LH₂ vent, the contingency experiment of propellant lead, a LOX dump and APS ullage burn.

The Major Flight Objectives and the Detailed Test Objectives of this mission were completely accomplished. No failures, anomalies, or deviations occurred that seriously affected the flight or mission.

Any questions or comments pertaining to the information contained in this report are invited and should be directed to:

Director, George C. Marshall Space Flight Center
Huntsville, Alabama 35812
Attention: Chairman, Saturn Flight Evaluation Working
Group, S&E-CSE-LF (Phone 453-2575)

TABLE OF CONTENTS

Section		Page
	TABLE OF CONTENTS	iii
	LIST OF ILLUSTRATIONS	xii
	LIST OF TABLES	xix
	ACKNOWLEDGEMENT	xxiii
	ABBREVIATIONS	xxiv
	MISSION PLAN	xxvii
	FLIGHT TEST SUMMARY	xxix
1	INTRODUCTION	
	1.1 Purpose	1-1
	1.2 Scope	1-1
2	EVENT TIMES	
	2.1 Summary of Events	2-1
	2.2 Variable Time and Commanded Switch Selector Events	2-3
3	LAUNCH OPERATIONS	
	3.1 Summary	3-1
	3.2 Prelaunch Milestones	3-1
	3.3 Countdown Events	3-1
	3.4 Propellant Loading	3-1
	3.4.1 RP-1 Loading	3-1
	3.4.2 LOX Loading	3-3
	3.4.3 LH ₂ Loading	3-3
	3.4.4 Auxiliary Propulsion System Propellant Loading	3-3
	3.5 S-II Insulation, Purge and Leak Detection	3-3
	3.5.1 Forward Bulkhead Insulation	3-3
	3.5.2 Forward Bulkhead Uninsulated Area	3-4
	3.5.3 LH ₂ Tank Sidewall	3-4

TABLE OF CONTENTS (CONTINUED)

Section		Page
	3.5.4 Bolting/J-Ring	3-4
	3.5.5 Feedline Elbow	3-4
	3.5.6 Common Bulkhead	3-4
	3.6 Ground Support Equipment	3-5
	3.6.1 Ground/Vehicle Interface	3-5
	3.6.2 MSFC Furnished Ground Support Equipment	3-5
	3.6.3 GSE Camera Coverage	3-6
4	TRAJECTORY	
	4.1 Summary	4-1
	4.2 Tracking Data Utilization	4-1
	4.2.1 Tracking During the Ascent Phase of Flight	4-1
	4.2.2 Tracking During Orbital Flight	4-2
	4.2.3 Tracking During the Injection Phase of Flight	4-2
	4.3 Trajectory Evaluation	4-2
	4.3.1 Ascent Trajectory	4-2
	4.3.2 Parking Orbit Trajectory	4-3
	4.3.3 Injection Trajectory	4-5
	4.3.4 Post TLI Trajectory	4-6
	4.3.5 S-IVB/IU Post Separation Trajectory	4-10
5	S-IC PROPULSION	
	5.1 Summary	5-1
	5.2 S-IC Ignition Transient Performance	5-1
	5.3 S-IC Mainstage Performance	5-4
	5.4 S-IC Engine Shutdown Transient Performance	5-6
	5.5 S-IC Stage Propellant Management	5-6
	5.6 S-IC Pressurization Systems	5-6
	5.6.1 S-IC Fuel Pressurization System	5-6
	5.6.2 S-IC LOX Pressurization System	5-7
	5.7 S-IC Pneumatic Control Pressure System	5-8
	5.8 S-IC Purge Systems	5-9
	5.9 POGO Suppression System	5-9

TABLE OF CONTENTS (CONTINUED)

Section		Page
6	S-II PROPULSION	
6.1	Summary	6-1
6.2	S-II Chillydown and Buildup Transient Performance	6-2
6.3	S-II Mainstage Performance	6-5
6.4	S-II Shutdown Transient Performance	6-7
6.5	S-II Stage Propellant Management	6-9
6.6	S-II Pressurization Systems	6-10
6.6.1	S-II Fuel Pressurization System	6-10
6.6.2	S-II LOX Pressurization System	6-11
6.7	S-II Pneumatic Control Pressure System	6-11
6.8	S-II Helium Injection System	6-12
7	S-IVB PROPULSION	
7.1	Summary	7-1
7.2	S-IVB Chillydown and Buildup Transient Performance for First Burn	7-2
7.3	S-IVB Mainstage Performance for First Burn	7-2
7.4	S-IVB Shutdown Transient Performance for First Burn	7-5
7.5	S-IVB Parking Orbit Coast Phase Conditioning	7-6
7.6	S-IVB Chillydown and Restart for Second Burn	7-6
7.7	S-IVB Mainstage Performance for Second Burn	7-12
7.8	S-IVB Shutdown Transient Performance for Second Burn	7-14
7.9	S-IVB Stage Propellant Management	7-14
7.10	S-IVB Pressurization System	7-14
7.10.1	S-IVB Fuel Pressurization System	7-14
7.10.2	S-IVB LOX Pressurization System	7-18

TABLE OF CONTENTS (CONTINUED)

Section		Page
7.11	S-IVB Pneumatic Control Pressure System	7-22
7.12	S-IVB Auxiliary Propulsion System	7-26
7.13	S-IVB Propellant Lead Experiment and Orbital Safing Operation	7-27
7.13.1	LOX and LH ₂ Lead Chillydown Experiment	7-28
7.13.2	LOX Tank Ambient Repressurization	7-31
7.13.3	LH ₂ Tank Ambient Repressurization	7-32
7.13.4	Fuel Tank Safing	7-32
7.13.5	LOX Tank Dump and Safing	7-33
7.13.6	Cold Helium Dump	7-33
7.13.7	Ambient Helium Dump	7-34
7.13.8	Stage Pneumatic Control Sphere Safing	7-35
7.13.9	Engine Start Sphere Safing	7-35
7.13.10	Engine Control Sphere Safing	7-35
8	HYDRAULIC SYSTEMS	
8.1	Summary	8-1
8.2	S-IC Hydraulic System	8-1
8.3	S-II Hydraulic System	8-1
8.4	S-IVB Hydraulic System (First Burn)	8-1
8.5	S-IVB Hydraulic System (Parking Orbit Coast Phase)	8-2
8.6	S-IVB Hydraulic System (Second Burn)	8-3
8.7	S-IVB Hydraulic System (Translunar Injection Coast and Propellant Dump)	8-3
9	STRUCTURES	
9.1	Summary	9-1
9.2	Total Vehicle Structures Evaluation	9-1
9.2.1	Longitudinal Loads	9-1
9.2.2	Bending Moments	9-3
9.2.3	Vehicle Dynamic Characteristics	9-5
9.3	Vibration Evaluation	9-11
9.3.1	S-IC Stage and Engine Evaluation	9-11
9.3.2	S-II Stage and Engine Evaluation	9-12
9.3.3	S-IVB Stage and Engine Evaluation	9-23

TABLE OF CONTENTS (CONTINUED)

Section		Page
10	GUIDANCE AND NAVIGATION	
	10.1 Summary	10-1
	10.1.1 Flight Program	10-1
	10.1.2 Instrument Unit Components	10-1
	10.2 Guidance Comparisons	10-1
	10.3 Navigation and Guidance Scheme Evaluation	10-7
	10.4 Guidance System Component Evaluation	10-8
	10.4.1 LVDC Performance	10-8
	10.4.2 LVDA Performance	10-8
	10.4.3 Ladder Outputs	10-8
	10.4.4 Telemetry Outputs	10-11
	10.4.5 Discrete Outputs	10-11
	10.4.6 Switch Selector Functions	10-11
	10.4.7 ST-124M-3 Inertial Platform Performance	10-11
11	CONTROL SYSTEM	
	11.1 Summary	11-1
	11.2 Control System Description	11-1
	11.3 S-IC Control System Evaluation	11-2
	11.3.1 Liftoff Clearances	11-2
	11.3.2 S-IC Flight Dynamics	11-2
	11.4 S-II Control System Evaluation	11-7
	11.5 S-IVB Control System Evaluation	11-14
	11.5.1 Control System Evaluation During First Burn	11-14
	11.5.2 Control System Evaluation During Parking Orbit	11-14
	11.5.3 Control System Evaluation During Second Burn	11-17
	11.5.4 Control System Evaluation After S-IVB Second Burn	11-18
12	SEPARATION	
	12.1 Summary	12-1
	12.2 S-IC/S-II Separation Evaluation	12-1
	12.2.1 S-IC Retro Motor Performance	12-1
	12.2.2 S-II Ullage Motor Performance	12-1
	12.2.3 S-IC/S-II Stage Separation	12-1

TABLE OF CONTENTS (CONTINUED)

Section		Page
	12.3 S-II Second Plane Separation Evaluation	12-1
	12.4 S-II/S-IVB Separation Evaluation	12-2
	12.4.1 S-II Retro Motor Performance	12-2
	12.4.2 S-IVB Ullage Motor Performance	12-2
	12.4.3 S-II/S-IVB Separation Dynamics	12-2
	12.5 S-IVB/IU/LM/CSM Separation Evaluation	12-2
	12.6 Lunar Module Docking and Ejection Evaluation	12-2
13	ELECTRICAL NETWORKS	
	13.1 Summary	13-1
	13.2 S-IC Stage Electrical System	13-1
	13.3 S-II Stage Electrical System	13-2
	13.4 S-IVB Stage Electrical System	13-3
	13.5 Instrument Unit Electrical System	13-6
14	RANGE SAFETY AND COMMAND SYSTEMS	
	14.1 Summary	14-1
	14.2 Secure Range Safety Command Systems	14-1
	14.3 Command and Communications System	14-1
15	EMERGENCY DETECTION SYSTEM	
	15.1 Summary	15-1
	15.2 System Evaluation	15-1
	15.2.1 General Performance	15-1
	15.2.2 Propulsion System Sensors	15-1
	15.2.3 Flight Dynamics and Control Sensors	15-1
	15.2.4 EDS Event Times	15-2
16	VEHICLE PRESSURE AND ACOUSTIC ENVIRONMENT	
	16.1 Summary	16-1
	16.2 Surface Pressures and Compartment Venting	16-1
	16.2.1 S-IC Stage	16-1
	16.2.2 S-II Stage	16-5

TABLE OF CONTENTS (CONTINUED)

Section		Page
	16.3 Base Pressures	16-5
	16.3.1 S-IC Base Pressures	16-5
	16.3.2 S-II Base Pressures	16-7
	16.4 Acoustic Environment	16-8
	16.4.1 External Acoustics	16-8
	16.4.2 Internal Acoustics	16-17
17	VEHICLE THERMAL ENVIRONMENT	
	17.1 Summary	17-1
	17.2 S-IC Base Heating and Stage Separation Environment	17-1
	17.2.1 S-IC Base Heating	17-1
	17.2.2 S-IC/S-II Separation Environment	17-3
	17.3 S-II Base Region Environment	17-3
	17.4 Vehicle Aeroheating Thermal Environment	17-10
	17.4.1 S-IC Stage Aeroheating Environment	17-10
	17.4.2 S-II Stage Aeroheating Environment	17-12
	17.4.3 S-IVB Stage Aeroheating Environment	17-17
18	ENVIRONMENTAL CONTROL SYSTEM	
	18.1 Summary	18-1
	18.2 S-IC Environmental Control	18-1
	18.3 S-II Environmental Control	18-5
	18.4 IU Environmental Control	18-5
	18.4.1 Thermal Conditioning System	18-6
	18.4.2 Gas Bearing Supply System	18-8
19	DATA SYSTEMS	
	19.1 Summary	19-1
	19.2 Vehicle Measurements Evaluation	19-1
	19.3 Airborne Telemetry Systems	19-5
	19.4 Airborne Tape Recorders	19-5
	19.5 RF Systems Evaluation	19-7
	19.5.1 Telemetry System RF Propagation Evaluation	19-7
	19.5.2 Tracking Systems RF Propagation Evaluation	19-8

TABLE OF CONTENTS (CONTINUED)

Section		Page
	19.5.3 Command Systems RF Evaluation	19-9
	19.6 Optical Instrumentation	19-13
20	MASS CHARACTERISTICS	
	20.1 Summary	20-1
	20.2 Mass Evaluation	20-1
21	MISSION OBJECTIVES ACCOMPLISHMENT	21-1
22	FAILURES, ANOMALIES AND DEVIATIONS	
	22.1 Summary	22-1
	22.2 System Failures and Anomalies	22-1
	22.3 System Deviation	22-1
23	SPACECRAFT SUMMARY	23-1
Appendix		
A	ATMOSPHERE	
	A.1 - Summary	A-1
	A.2 General Atmospheric Conditions at Launch Time	A-1
	A.3 Surface Observations at Launch Time	A-1
	A.4 Upper Air Measurements	A-2
	A.4.1 Wind Speed	A-2
	A.4.2 Wind Direction	A-3
	A.4.3 Pitch Wind Component	A-3
	A.4.4 Yaw Wind Component	A-7
	A.4.5 Component Wind Shears	A-7
	A.4.6 Extreme Wind Data in the High Dynamic Pressure Region	A-7
	A.5 Thermodynamic Data	A-7
	A.5.1 Temperature	A-7
	A.5.2 Atmospheric Pressure	A-7
	A.5.3 Atmospheric Density	A-13
	A.5.4 Optical Index of Refraction	A-13
	A.6 Comparison of Selected Atmospheric Data for Saturn V Launches	A-13

TABLE OF CONTENTS (CONTINUED)

Appendix		Page
B	AS-505 SIGNIFICANT CONFIGURATION CHANGES	
B.1	Introduction	B-1

LIST OF ILLUSTRATIONS

Figure		Page
2-1	Telemetry Time Delay	2-2
4-1	Ascent Trajectory Position Comparison	4-3
4-2	Ascent Trajectory Space-Fixed Velocity and Flight Path Angle Comparisons	4-4
4-3	Ascent Trajectory Acceleration Comparison	4-5
4-4	Dynamic Pressure and Mach Number Comparisons	4-6
4-5	Ground Track	4-12
4-6	Injection Phase Space-Fixed Velocity and Flight Path Angle Comparisons	4-13
4-7	Injection Phase Acceleration Comparison	4-13
4-8	Velocity Increments Due to Slingshot Activity	4-15
4-9	S-IVB/IU Velocity Relative to Earth Distance	4-17
5-1	S-IC Start Box Requirements	5-2
5-2	S-IC Engine Buildup Transients	5-3
5-3	S-IC Stage Propulsion Performance	5-5
5-4	S-IC Fuel Ullage Pressure	5-8
5-5	S-IC LOX Tank Ullage Pressure	5-9
5-6	S-IC Center Engine LOX Suction Line Pressure	5-10
5-7	S-IC Prevalve Liquid Level, Typical Outboard Engine	5-11
6-1	S-II Engine Start Tank Performance	6-2
6-2	S-II Engine Pump Inlet Start Requirements	6-4
6-3	S-II Propulsion Performance	6-6
6-4	S-II Inflight LOX Level History	6-8
6-5	S-II Fuel Tank Ullage Pressure	6-12
6-6	S-II Fuel Pump Inlet Conditions	6-13
6-7	S-II LOX Tank Ullage Pressure	6-14

LIST OF ILLUSTRATIONS (CONTINUED)

Figure		Page
6-8	S-II LOX Pump Inlet Conditions	6-15
7-1	S-IVB Start Box and Run Requirements - First Burn	7-3
7-2	S-IVB Steady State Performance - First Burn	7-4
7-3	S-IVB CVS Performance - Coast Phase	7-7
7-4	S-IVB Ullage Pressure During Repressurization Using O ₂ /H ₂ Burner	7-9
7-5	S-IVB O ₂ /H ₂ Burner Thrust and Pressurant Flowrate	7-10
7-6	S-IVB Start Box and Run Requirements - Second Burn	7-11
7-7	S-IVB Steady State Performance - Second Burn	7-13
7-8	S-IVB LH ₂ Ullage Pressure - First Burn and Parking Orbit	7-16
7-9	S-IVB LH ₂ Ullage Pressure - Second Burn and Translunar Coast	7-17
7-10	S-IVB Fuel Pump Inlet Conditions - First Burn	7-19
7-11	S-IVB Fuel Pump Inlet Conditions - Second Burn	7-20
7-12	S-IVB LOX Tank Ullage Pressure - First Burn and Parking Orbit	7-21
7-13	S-IVB LOX Tank Ullage Pressure - Second Burn, Translunar Coast	7-22
7-14	S-IVB LOX Pump Inlet Conditions - First Burn	7-23
7-15	S-IVB LOX Pump Inlet Conditions - Second Burn	7-24
7-16	S-IVB Cold Helium Supply History	7-25
7-17	S-IVB APS Helium Bottle Mass	7-26
7-18	S-IVB APS Helium Bottle Temperature	7-28
7-19	S-IVB APS Propellants Remaining Versus Range Time, Module No. 1 and Module No. 2	7-29
7-20	S-IVB Propellant Lead Experiment and Orbital Safing Sequence	7-32
7-21	LOX Pump Inlet Chillover Effectiveness	7-34
7-22	LOX Pump Discharge Chillover Effectiveness	7-35
7-23	S-IVB Fuel Lead Chillover Effectiveness	7-36
7-24	S-IVB LOX Dump	7-37

LIST OF ILLUSTRATIONS (CONTINUED)

Figure		Page
8-1	S-IC Engine, Valve Closing Pressure	8-2
8-2	S-IVB Hydraulic System Pressure - Second Burn	8-4
8-3	S-IVB Hydraulic System Actuator Position - Second Burn	8-5
8-4	S-IVB Auxiliary Hydraulic Pump Performance - Second Burn	8-6
8-5	S-IVB Auxiliary Hydraulic Pump Performance - Coast Phase and Third Thermal Cycle	8-7
8-6	S-IVB Hydraulic System Actuator Positions - Coast Phase and Third Thermal Cycle	8-8
8-7	S-IVB Auxiliary Hydraulic Pump Performance - Coast Phase and Passivation	8-9
8-8	S-IVB Hydraulic System Actuator Positions - Coast Phase and Passivation	8-10
9-1	Release Rod Force - Displacement Curves	9-2
9-2	Longitudinal Loads at Maximum Bending Moment, Center Engine Cutoff, and Outboard Engine Cutoff	9-3
9-3	Longitudinal Structural Dynamic Response Due to Outboard Engine Cutoff	9-4
9-4	Maximum Bending Moment Near Max Q	9-5
9-5	First Longitudinal Modal Frequencies During S-IC Powered Flight	9-6
9-6	Peak Amplitudes of Vehicle First Longitudinal Mode for AS-504 and AS-505	9-7
9-7	Comparison of AS-504 and AS-505 S-II Stage Low Frequency Oscillations	9-9
9-8	S-IVB Second Burn 45 Hertz Oscillations	9-10
9-9	AS-505 Lateral Analysis/Measured Modal Frequency Correlation	9-12
9-10	S-IC Stage Structure Vibration Envelopes	9-14
9-11	S-IC Stage Engine Vibration Envelopes	9-15
9-12	S-IC Stage Components Vibration Envelopes	9-16
9-13	S-IC Vibration Measurement Locations	9-17
9-14	S-II Stage Structure Vibration Envelopes	9-19

LIST OF ILLUSTRATIONS (CONTINUED)

Figure		Page
9-15	S-II Stage Engine Vibration Envelopes	9-20
9-16	S-II Stage Component Vibration Envelopes	9-21
9-17	S-IVB Stage Vibration Envelopes	9-24
9-18	S-IVB Stage Engine Vibration Envelopes	9-25
10-1	Tracking and ST-124M-3 Platform Velocity Comparison (Trajectory Minus Guidance)	10-2
10-2	Attitude Commands During Active Guidance Period	10-9
10-3	Orbital Attitude Commands	10-10
11-1	Pitch Plane Dynamics During S-IC Burn	11-4
11-2	Yaw Plane Dynamics During S-IC Burn	11-5
11-3	Roll Plane Dynamics During S-IC Burn	11-6
11-4	Normal Acceleration During S-IC Burn	11-8
11-5	Pitch and Yaw Plane Wind Velocity and Free-Stream Angle-of-Attack During S-IC Burn	11-9
11-6	Pitch Plane Dynamics During S-II Burn	11-11
11-7	Yaw Plane Dynamics During S-II Burn	11-12
11-8	Roll Plane Dynamics During S-II Burn	11-13
11-9	Pitch Attitude Control During S-IVB First Burn	11-15
11-10	Yaw Attitude Control During S-IVB First Burn	11-15
11-11	Roll Attitude Control During S-IVB First Burn	11-16
11-12	Pitch Attitude Control During Parking Orbit	11-17
11-13	Pitch Attitude Control During S-IVB Second Burn	11-19
11-14	Yaw Attitude Control During S-IVB Second Burn	11-20
11-15	Roll Attitude Control During S-IVB Second Burn	11-20
11-16	Pitch Attitude Control After S-IVB Second Burn	11-21
13-1	S-IVB Stage Forward Battery No. 1 Voltage and Current	13-4
13-2	S-IVB Stage Forward Battery No. 2 Voltage and Current	13-4
13-3	S-IVB Stage Aft Battery No. 1 Voltage and Current	13-5
13-4	S-IVB Stage Aft Battery No. 2 Voltage and Current	13-5

LIST OF ILLUSTRATIONS (CONTINUED)

Figure		Page
13-5	Battery 6D10 Voltage, Current and Temperature	13-7
13-6	Battery 6D30 Voltage, Current and Temperature	13-8
13-7	Battery 6D40 Voltage, Current and Temperature	13-9
16-1	S-IC Engine Fairing Compartment Pressure Differential	16-2
16-2	S-IC Compartment Pressure Differentials	16-3
16-3	S-IC Compartment Pressure Loading	16-4
16-4	S-II Forward Skirt Pressure Loading	16-6
16-5	S-IC Base Pressure Differential	16-7
16-6	S-IC Base Heat Shield Pressure Loading	16-8
16-7	Thrust Cone and Base Heat Shield Forward Face Pressures	16-9
16-8	S-II Heat Shield Aft Face Pressures	16-10
16-9	Vehicle External Overall Sound Pressure Level at Liftoff	16-11
16-10	Vehicle External Sound Pressure Spectral Densities at Liftoff	16-12
16-11	Vehicle External Overall Fluctuating Pressure Level	16-14
16-12	Vehicle External Fluctuating Pressure Spectral Densities at Maximum Inflight Aerodynamic Noise	16-16
16-13	S-IC Heat Shield Panels Internal Acoustic Environment	16-17
16-14	S-IC Intertank Internal Acoustic Environment	16-18
16-15	S-II Internal Acoustics History	16-19
16-16	S-IVB Acoustics Levels During S-IC Burn	16-20
17-1	S-IC Base Heat Shield Thermal Environment	17-2
17-2	F-1 Engine Thermal Environment	17-2
17-3	S-IC Heat Shield Forward Surface Temperature	17-4
17-4	S-IC Heat Shield Bondline Temperature	17-4
17-5	S-IC Base Heat Shield Measurement Locations	17-5
17-6	S-IC Temperature Under Insulation, Inboard Side Engine No. 1	17-6

LIST OF ILLUSTRATIONS (CONTINUED)

Figure		Page
17-7	S-IC Forward Skirt Compartment Ambient Air Temperature During S-IC/S-II Stage Separation	17-6
17-8	S-II Heat Shield Base Region Heating Rates	17-7
17-9	S-II Thrust Cone Heating Rate	17-8
17-10	S-II Base Gas Temperature	17-8
17-11	S-II Heat Shield Aft Face Temperatures	17-9
17-12	S-IC Intertank Aerodynamic Heating	17-11
17-13	S-IC Forward Skirt Aerodynamic Heating	17-11
17-14	Forward Location of Separated Flow	17-12
17-15	S-IC LOX Tank Skin Temperature	17-13
17-16	S-IC Fuel Tank Skin Temperature	17-13
17-17	S-IC Intertank Skin Temperatures	17-14
17-18	S-IC Forward Skirt Skin Temperature	17-14
17-19	S-II Aft Interstage Aeroheating Environment	17-15
17-20	S-II Aft Interstage Aeroheating Environment, Ullage Motor Fairing	17-16
17-21	S-II Aft Interstage Aeroheating Environment, LH ₂ Feedline Aft Fairing	17-17
17-22	S-II Body Aeroheating Environment, LH ₂ Feedline Forward Fairing	17-18
17-23	S-II Body Aeroheating Environment, Forward Skirt	17-18
17-24	S-II Body Aeroheating Environment, Systems Tunnel Forward Fairing	17-19
18-1	S-IC Forward Compartment Canister Temperature	18-2
18-2	S-IC Forward Compartment Ambient Temperature	18-3
18-3	S-IC Aft Compartment Temperature Range	18-4
18-4	RTG Purge Ducting Modification	18-6
18-5	IU Sublimator Performance During Ascent	18-7
18-6	Thermal Conditioning System GN ₂ Sphere Pressure (D25-601)	18-9
18-7	Flight Control Computer Temperatures (C69-602)	18-9
18-8	Selected Component Temperatures	18-10

LIST OF ILLUSTRATIONS (CONTINUED)

Figure		Page
18-9	Gas Bearing GN ₂ Sphere Pressure	18-11
18-10	Inertial Platform GN ₂ Pressures	18-11
19-1	VHF Telemetry Coverage Summary	19-8
19-2	C-Band Radar Coverage Summary	19-10
19-3	CCS Signal Strength Fluctuations at Guaymas	19-11
19-4	CCS Signal Strength Fluctuations at Goldstone	19-12
19-5	CCS System Block Diagram	19-14
19-6	Electrical Schematic of CCS Coaxial Switch	19-14
19-7	CCS Coverage Summary	19-15
A-1	Scalar Wind Speed at Launch Time of AS-505	A-4
A-2	Wind Direction at Launch Time of AS-505	A-5
A-3	Pitch Wind Speed Component (w_x) at Launch Time of AS-505	A-6
A-4	Yaw Wind Speed Component at Launch Time of AS-505	A-8
A-5	Pitch (S_x) and Yaw (S_z) Component Wind Shears at Launch Time of AS-505	A-9
A-6	Relative Deviation of Temperature and Density From the PRA-63 Reference Atmosphere, AS-505	A-11
A-7	Relative Deviation of Pressure and Absolute Deviation of the Index of Refraction From the PRA-63 Reference Atmosphere, AS-505	A-12

LIST OF TABLES

Table		Page
2-1	Time Base Summary	2-3
2-2	Significant Event Times Summary	2-4
2-3	Variable Time and Commanded Switch Selector Events	2-10
3-1	AS-505 Prelaunch Milestones	3-2
4-1	Comparison of Significant Trajectory Events	4-7
4-2	Comparison of Cutoff Events	4-8
4-3	Comparison of Separation Events	4-9
4-4	Stage Impact Location	4-10
4-5	Parking Orbit Insertion Conditions	4-11
4-6	Translunar Injection Conditions	4-14
4-7	Comparison of Slingshot Maneuver	4-14
4-8	Lunar Close Approach Parameters	4-16
4-9	Heliocentric Orbit Parameters	4-16
5-1	S-IC Engine Performance Deviations	5-4
5-2	S-IC Stage Propellant Mass History	5-7
6-1	S-II Engine Performance Deviations (ESC +61 Seconds)	6-7
6-2	S-II Propellant Mass History	6-10
7-1	S-IVB Steady State Performance - First Burn (ESC +140-Second Time Slice at Standard Altitude Conditions)	7-5
7-2	S-IVB Steady State Performance - Second Burn (ESC +180-Second Time Slice at Standard Altitude Conditions)	7-15
7-3	S-IVB Stage Propellant Mass History	7-15
7-4	S-IVB APS Propellant Conditions	7-27
7-5	S-IVB APS Propellant Consumption	7-30

LIST OF TABLES (CONTINUED)

Table		Page
7-6	S-IVB Helium Bottle Conditions	7-31
9-1	S-IVB Stage Low Frequency Vibration Summary	9-11
9-2	S-IC Stage Vibration Summary	9-13
9-3	S-II Stage Maximum Overall Vibration Levels	9-18
9-4	S-IVB Vibration Summary	9-26
10-1	Inertial Platform Velocity Comparisons	10-3
10-2	Guidance Comparisons	10-5
10-3	Guidance Component Comparisons	10-7
10-4	Start and Stop Times for IGM Guidance Commands	10-8
10-5	Translunar Injection Parameters	10-11
11-1	AS-505 Misalignment and Liftoff Conditions Summary	11-3
11-2	Maximum Control Parameters During S-IC Boost Flight	11-7
11-3	Maximum Control Parameters During S-II Boost Flight	11-10
11-4	Maximum Control Parameters During S-IVB First Burn	11-16
11-5	Maximum Control Parameters During S-IVB Second Burn	11-18
13-1	S-IC Stage Battery Power Consumption	13-1
13-2	S-II Stage Battery Power Consumption	13-2
13-3	S-IVB Stage Battery Power Consumption	13-3
13-4	IU Battery Power Consumption	13-6
14-1	Command and Communications System Commands History, AS-505	14-2
15-1	Maximum Angular Rates	15-1
15-2	EDS Related Event Times	15-2
15-3	EDS Associated Discrettes	15-3
16-1	Sound Pressure Level Comparison of AS-505 With Previous Saturn V Flight Data	16-19
18-1	TCS Coolant Flowrates and Pressures	18-7
19-1	AS-505 Flight Measurement Summary	19-2

LIST OF TABLES (CONTINUED)

Table		Page
19-2	AS-505 Flight Measurements Waived Prior to Launch	19-2
19-3	AS-505 Measurement Malfunctions	19-3
19-4	AS-505 Questionable Flight Measurements	19-5
19-5	AS-505 Launch Vehicle Telemetry Links	19-6
19-6	Tape Recorder Summary	19-6
20-1	Total Vehicle Mass - S-IC Burn Phase - Kilograms	20-3
20-2	Total Vehicle Mass - S-IC Burn Phase - Pounds Mass	20-4
20-3	Total Vehicle Mass - S-II Burn Phase - Kilograms	20-5
20-4	Total Vehicle Mass - S-II Burn Phase - Pounds Mass	20-6
20-5	Total Vehicle Mass - S-IVB First Burn Phase - Kilograms	20-7
20-6	Total Vehicle Mass - S-IVB First Burn Phase - Pounds Mass	20-8
20-7	Total Vehicle Mass - S-IVB Second Burn Phase - Kilograms	20-9
20-8	Total Vehicle Mass - S-IVB Second Burn Phase - Pounds Mass	20-10
20-9	Flight Sequence Mass Summary	20-11
20-10	Mass Characteristics Comparison	20-13
21-1	Mission Objectives Accomplishment Summary	21-1
22-1	Hardware Criticality Categories for Flight Hardware	22-1
22-2	Summary of Failures and Anomalies	22-2
22-3	Summary of Deviations	22-2
A-1	Surface Observations at AS-505 Launch Time	A-1
A-2	Solar Radiation at AS-505 Launch Time, Launch Pad 39B	A-2
A-3	Systems Used to Measure Upper Air Wind Data for AS-505	A-3
A-4	Maximum Wind Speed in High Dynamic Pressure Region for Apollo/Saturn 501 through Apollo/Saturn 505 Vehicles	A-10

LIST OF TABLES (CONTINUED)

Table		Page
A-5	Extreme Wind Shear Values in the High Dynamic Pressure Region for Apollo/Saturn 501 through Apollo/Saturn 505 Vehicles	A-10
A-6	Selected Atmospheric Observations for Apollo/Saturn 501 through Apollo/Saturn 505 Vehicle Launches at Kennedy Space Center, Florida	A-13
B-1	S-IC Significant Configuration Changes	B-2
B-2	S-II Significant Configuration Changes	B-2
B-3	S-IVB Significant Configuration Changes	B-3
B-4	IU Significant Configuration Changes	B-4

ACKNOWLEDGEMENT

This report is published by the Saturn Flight Evaluation Working Group--composed of representatives of Marshall Space Flight Center, John F. Kennedy Space Center, and MSFC's prime contractors--and in cooperation with the Manned Spacecraft Center. Significant contributions to the evaluation have been made by:

George C. Marshall Space Flight Center

Science and Engineering

Central Systems Engineering
Aero-Astroynamics Laboratory
Astrionics Laboratory
Computation Laboratory
Astronautics Laboratory

Program Management

John F. Kennedy Space Center

Manned Spacecraft Center

The Boeing Company

McDonnell Douglas Astronautics Company

International Business Machines Corporation

North American Rockwell/Space Division

North American Rockwell/Rocketdyne Division

ABBREVIATIONS

ACN	Ascension	DTO	Detailed Test Objective
AEDC	Arnold Engineering Development Center	EBW	Exploding Bridge Wire
AGC	Automatic Gain Control	ECO	Engine Cutoff
ANT	Antigua	ECP	Engineering Change Proposal
AOS	Acquisition of Signal	ECS	Environmental Control System
APS	Auxiliary Propulsion System	EDS	Emergency Detection System
ASI	Augmented Spark Igniter	EDT	Eastern Daylight Time
AUX	Auxiliary	EMR	Engine Mixture Ratio
BDA	Bermuda	ESC	Engine Start Command
CCS	Command and Communications System	EVA	Extra-Vehicular Activity
CDDT	Countdown Demonstration Test	FCC	Flight Control Computer
CECO	Center Engine Cutoff	FM/FM	Frequency Modulation/ Frequency Modulation
CG	Center of Gravity	GBI	Grand Bahama Island
CKAFS	Cape Kennedy Air Force Site	GBM	Grand Bahama Island
CM	Command Module	GFCV	GOX Flow Control Valve
CNV	Canaveral	GDS	Goldstone
CRO	Carnarvon	GG	Gas Generator
CRP	Computer Reset Pulse	GMT	Greenwich Mean Time
CSM	Command and Service Module	GOX	Gaseous Oxygen
CVS	Continuous Vent System	GRR	Guidance Reference Release
CYI	Grand Canary Island	GSE	Ground Support Equipment
DEE	Digital Events Evaluator	GTI	Grand Turk Island
		GWM	Guam

GYM	Guaymas	MER	Mercury (ship)
HAW	Hawaii	MFCV	Modulating Flow Control Valve
HDA	Holddown Arm	MFO	Major Flight Objective
HEP	Hardware Evaluation Program	MFV	Main Fuel Valve
HFCV	Helium Flow Control Valve	MILA	Merritt Island Launch Area
HSK	Honeysuckle (Canberra)	MLV	Main LOX Valve
IGM	Iterative Guidance Mode	MOV	Main Oxidizer Valve
IMU	Inertial Measurement Unit	MR	Mixture Ratio
IP&C	Instrumentation Program and Components	MSC	Manned Spacecraft Center
IU	Instrument Unit	MSFC	Marshall Space Flight Center
KSC	Kennedy Space Center	MSFN	Manned Space Flight Network
LES	Launch Escape System	MSS	Mobile Service Structure
LET	Launch Escape Tower	MTF	Mississippi Test Facility
LIEF	Launch Information Exchange Facility	NPSP	Net Positive Suction Pressure
LM	Lunar Module	NPV	Non Propulsive Vent
LOI	Lunar Orbit Insertion	NASA	National Aeronautics and Space Administration
LOS	Loss of Signal	OAFPL	Overall Fluctuating Pressure Level
LUT	Launch Umbilical Tower	OASPL	Overall Sound Pressure Level
LV	Launch Vehicle	OAT	Overall Test
LVDA	Launch Vehicle Data Adapter	OCP	Orbital Correction Program
LVDC	Launch Vehicle Digital Computer	ODOP	Offset Frequency Doppler
MAD	Madrid	OECO	Outboard Engine Cutoff
MCC-H	Mission Control Center - Houston	OMNI	Omni Directional

PAM/ FM/FM	Pulse Amplitude Modulation/ Frequency Modulation/ Frequency Modulation	SPL	Sound Pressure Level
PAFB	Patrick Air Force Base	SRSCS	Secure Range Safety Command System
PCM	Pulse Code Modulation	SS/FM	Single Sideband/Frequency Modulation
PCM/ FM	Pulse Code Modulation/ Frequency Modulation	STDV	Start Tank Discharge Valve
PMR	Programed Mixture Ratio	SV	Space Vehicle
PRA	Patrick Reference Atmosphere	T ₁	Time Base 1
PSD	Power Spectral Density	T ₁ I	Time to go in 1st Stage IGM
PTCS	Propellant Tanking Control System	T ₂ I	Time to go in 2nd Stage IGM
PU	Propellant Utilization	TAN	Tananarive
RED	Redstone (ship)	TCS	Thermal Conditioning System
RF	Radio Frequency	TD&E	Transposition, Docking and Ejection
RMS	Root Mean Square	TEL 4	Cape Telemetry 4
RP-1	Designation for S-IC Stage Fuel (kerosene)	TEX	Corpus Christi (Texas)
RPM	Revolutions Per Minute	TLI	Translunar Injection
RTG	Radio Isotope Thermo- Electrical Generator	TM	Telemeter, Telemetry
SA	Service Arm	TMR	Triple Modular Redundant
SC	Spacecraft	TSM	Tail Service Mast
SEC	Seconds	TVC	Thrust Vector Control
SLA	Spacecraft LM Adapter	UHF	Ultra High Frequency
SM	Service Module	USB	Unified S-Band
SMC	Steering Misalignment Correction	UT	Universal Time
		VAN	Vanguard (ship)
		VHF	Very High Frequency
		WHS	White Sands

MISSION PLAN

The AS-505 (Apollo 10 mission) is the fifth flight of the Apollo-Saturn V flight test program. It is a Lunar Development Flight; the primary objectives are: (1) demonstrate crew/space vehicle/mission support facilities performance during a manned lunar mission with the Command and Service Module (CSM) and Lunar Module (LM); (2) evaluate LM performance in the cislunar and lunar environment. The crew is composed of Lt. Col. Thomas Stafford, Cdmr. John Young and Cdmr. Eugene Cernan.

The space vehicle is composed of the AS-505 Launch Vehicle (LV) consisting of the S-IC-5, S-II-5, S-IVB-5 and Instrument Unit (IU) stages and spacecraft consisting of the Spacecraft LM Adapter (SLA), LM-4 and CSM-106.

The vehicle is launched from Complex 39B at Kennedy Space Center. The launch azimuth is 90 degrees with a roll to a variable flight azimuth of 72 to 108 degrees east of true north.

The vehicle mass at launch (Ground Ignition) is about 2,945,069 kilograms (6,492,766 lbm). The S-IC and S-II stage powered flight times are approximately 160 and 392 seconds, respectively. The S-IVB first burn time is approximately 145 seconds. The S-IVB/IU/LM/CSM is inserted into a 185 kilometer (100 n mi) altitude (referenced to the earth's equatorial radius) circular parking orbit. The vehicle mass at parking orbit insertion is about 133,760 kilograms (294,891 lbm).

About 10 seconds after insertion into earth orbit, the vehicle assumes a horizontal attitude. During this coast in earth orbit, the LV and CSM system is checked out for Translunar Injection (TLI). During the second or third revolution the second burn (344 seconds) of the S-IVB injects the S-IVB/IU/LM/CSM into a free-return, translunar trajectory. Fifteen minutes after S-IVB cutoff, the LV maneuvers to an inertial attitude hold for CSM separation, docking and LM extraction. After the maneuver, the CSM separates from the LV and the SLA panels jettison. The CSM then transposes and docks to the LM. After docking, the CSM/LM is ejected, by springs, from the S-IVB/IU.

After the CSM/LM has been ejected, the S-IVB stage achieves a slingshot trajectory behind the moon and a solar orbit by activating propulsion venting, the contingency experiment of propellant lead, LOX dump through the J-2 engine, and firing the Auxiliary Propulsion System (APS) ullage engines.

During the 3-day translunar coast of the CSM/LM, the astronauts perform star/earth landmark sighting, Inertial Measurement Unit (IMU) alignments and general lunar navigation procedures. At approximately 76.5 hours, a Lunar Orbit Insertion (LOI) burn puts the CSM/LM into a 111 by 315 kilometer (60 by 170 n mi) elliptical orbit by an approximate 380-second Service Propulsion System (SPS) burn. After two revolutions, the CSM circularizes the orbit at 111 kilometers (60 n mi) by a 15-second SPS burn. The LM is then entered by two astronauts and checkout accomplished. At approximately 98.8 hours, CSM undocking occurs. At 101 hours, a Descent Propulsion System (DPS) phasing burn places the LM in a 394 by 18 kilometer (213 by 9.9 n mi) orbit. The LM simulates the descent attitude profile during approach to the phasing burn. At approximately 103 hours, an APS burn initiates LM active rendezvous; LM docking occurs at approximately 107 hours followed by LM deactivation and crew transfer to the CSM. The LM is jettisoned at approximately 109 hours and the CSM injected into the transearth trajectory. The coast period lasts approximately 89 hours. The Service Module (SM) separates from the Command Module (CM) 15 minutes prior to reentry. Splashdown in the Pacific Ocean occurs approximately 191 hours after liftoff.

FLIGHT TEST SUMMARY

The third manned Saturn V Apollo space vehicle, AS-505 (Apollo 10 Mission), was launched at Kennedy Space Center (KSC), Florida on May 18, 1969 at 12:49:00 Eastern Daylight Time (EDT) from Launch Complex 39, Pad B. This fifth launch of the Saturn V Apollo was the second Saturn V/Apollo Spacecraft in full lunar mission configuration. The three major flight objectives and the six Detailed Test Objectives (DTO's) were completely accomplished.

The launch countdown was completed without any unscheduled countdown holds. Ground system performance was satisfactory. The problems encountered during countdown were overcome such that vehicle launch readiness was not compromised.

The vehicle was launched on an azimuth of 90 degrees east of north and after 13.05 seconds of vertical flight, the vehicle began to roll into a flight azimuth of 72.028 degrees east of north. Actual trajectory parameters of the AS-505 were close to nominal. Space-fixed velocity at S-IC Outboard Engine Cutoff (OECO) was 10.81 m/s (35.47 ft/s) greater than nominal. At S-II OECO the space-fixed velocity was 13.22 m/s (43.37 ft/s) lower than nominal. At S-IVB first cutoff the space-fixed velocity was 0.07 m/s (0.23 ft/s) greater than nominal. The altitude at S-IVB first burn cutoff was 0.03 kilometers (0.01 n mi) lower than nominal, and the surface range was 0.92 kilometers (0.50 n mi) greater than nominal. The space-fixed velocity at parking orbit insertion was 0.07 m/s (0.23 ft/s) less than nominal. At translunar injection the total space-fixed velocity was 2.39 m/s (7.84 ft/s) less than nominal. The value of C_3 was 868 m²/s² (9345 ft²/s²) lower than nominal.

All S-IC propulsion systems performed satisfactorily. At the 35 to 38-second time slice, average engine thrust reduced to standard conditions was 0.20 percent lower than predicted. Average reduced specific impulse was 0.03 percent lower than predicted, and reduced propellant consumption rate was 0.158 percent lower than predicted. Center Engine Cutoff (CECO) was initiated by the Instrument Unit (IU) at 135.16 seconds as planned. OECO, initiated by LOX low level sensors, occurred at 161.63 seconds which was 1.43 seconds later than predicted in the Flight Trajectory.

The S-II propulsion system performed satisfactorily throughout the flight. As sensed by the engines, Engine Start Command (ESC) occurred at 163.05 seconds. OECO occurred at 552.64 seconds with a burn time of 389.59 seconds or 1.70 seconds longer than predicted. Due to center engine low

frequency performance oscillations on the two previous flights, the center engine was shut down early on AS-505 successfully avoiding these oscillations. CECO occurred at 460.61 seconds. Total stage thrust, as determined by computer analysis of telemetered propulsion measurements at 61 seconds after S-II ESC, was 0.35 percent below predicted. Total engine propellant flowrate (excluding pressurization flow) was 0.43 percent below predicted and average specific impulse was 0.09 percent above predicted at this time slice. Average Engine Mixture Ratio (EMR) was 0.18 percent below predicted.

The J-2 engine performed satisfactorily throughout the operational stage of S-IVB stage first and second burns. Shutdowns for both burns were also normal. The engine performance during first burn, as determined from standard altitude reconstruction analysis, was 0.13 percent less than predicted for thrust and 0.26 percent greater than predicted for specific impulse. The first burn duration was 146.95 seconds from Start Tank Discharge Valve (STDV) open. This duration was 1.54 seconds longer than predicted. Engine Cutoff (ECO) was initiated by a velocity cutoff command from the Launch Vehicle Digital Computer (LVDC). The Continuous Vent System (CVS) adequately regulated LH₂ tank ullage pressure at 13.4 N/cm² (19.5 psia) during earth parking orbit. The Oxygen/Hydrogen (O₂/H₂) burner satisfactorily repressurized the LH₂ tank for restart. Repressurization of the LOX tank was not required. Engine restart conditions were within specified limits. Restart at full open Propellant Utilization (PU) valve position was successful and there were no indications of any problem. Second burn duration of 343.06 seconds from STDV open was 0.65 seconds shorter than predicted. Engine performance during second burn, as determined from the standard altitude reconstruction analysis, was 0.25 percent less than predicted for thrust and 0.30 percent greater than predicted for specific impulse. ECO was initiated by a LVDC velocity cutoff command. Subsequent to second burn, the propellant lead experiment was successfully accomplished and the stage propellant tanks and pneumatic systems were satisfactorily safed. The velocity change resulting from the experiment, the CVS operation, the LOX dump, and Auxiliary Propulsion System (APS) firings caused the stage to enter a solar orbit as planned. A helium leak in the APS Module No. 1 was noted at 23,400 seconds (06:30:00). The leak persisted until loss of data at 39,240 seconds (10:54:00); however, system performance was within the operational limits.

The stage hydraulic systems performed satisfactorily on the S-IC, S-II, and first burn and coast phase of the S-IVB stage. During this period all parameters were within specification limits and there were no deviations or anomalies. Subsequent to this time, during second burn and translunar coast, there was a minor problem with the engine driven hydraulic pump and an apparently unrelated problem with the auxiliary hydraulic pump. However, there was no indication of mission or program impact due to this anomaly.

The structural loads and dynamic environments experienced by the AS-505 launch vehicle were well within the vehicle structural capability. There was no evidence of coupled structure/propulsion system instability (POGO) during S-IC, S-II, or S-IVB powered flights. The early S-II stage center engine shutdown successfully eliminated the low frequency (16 to 19 hertz) oscillations that were experienced on AS-503 and AS-504. During S-IVB first and second burns, very mild low frequency (12 to 19 hertz) oscillations were experienced with the maximum amplitude of ± 0.30 g recorded by the gimbal block longitudinal accelerometer. During the last 70 seconds of second burn, the Apollo 10 astronauts reported (in real time) that higher frequency oscillations were superimposed on the low frequency oscillations. These vibrations are, however, well within the structural design capability.

The guidance and navigation system functioned satisfactorily. Translunar trajectory injection parameters were within tolerance, and S-IVB stage safing was satisfactorily accomplished, resulting in a heliocentric orbit for the S-IVB/IU as planned. The LVDC, the Launch Vehicle Data Adapter (LVDA), and the ST-124M-3 inertial platform functioned satisfactorily.

The AS-505 Flight Control Computer (FCC), Thrust Vector Control (TVC), and APS satisfied all requirements for vehicle attitude control during the flight. S-IC/S-II first and second plane separations were accomplished with no significant attitude deviations. At S-II planned CECO, the guidance parameters were modified by the loss in thrust. S-II/S-IVB separation occurred as expected and without producing any significant attitude deviations. Satisfactory control of the vehicle was maintained during first and second S-IVB burns and during parking orbit. During the Command and Service Module (CSM) separation from the S-IVB/IU and during the Transposition, Docking and Ejection (TD&E) maneuver, the control system maintained the vehicle in a fixed inertial attitude to provide a stable docking platform. After Translunar Injection (TLI), attitude control was maintained for the propellant dumps and chilldown experiment. For AS-505 the APS propellants were not depleted by the last ullage burn, and control was maintained until the batteries were exhausted.

The AS-505 launch vehicle electrical systems performed satisfactorily throughout all phases of flight. Data indicated that the redundant Secure Range Safety Command Systems (SRSCS) on the S-IC, S-II, and S-IVB stages were ready to perform their functions properly on command if flight conditions during the launch phase had required vehicle destruct. The system properly safed the S-IVB SRSCS on command from Bermuda (BDA). The performance of the Command and Communications System (CCS) in the IU was satisfactory, except during the time period from 23,601 seconds (06:33:21) when CCS downlink signal strength dropped sharply until 25,097 seconds (06:58:17), when the antenna was switched to the omni mode. The drop in signal strength is suspected to be a malfunction in the directional antenna system.

The Emergency Detection System (EDS) performance was nominal; no abort limits were reached. The AS-505 EDS configuration was essentially the same as AS-504.

The vehicle internal, external, and base region pressure environments were generally in good agreement with the predictions and compared well with previous flight data. The pressure environment was well below design levels. The measured acoustic levels were generally in good agreement with the liftoff and inflight predictions, and with data from previous flights.

The AS-505 vehicle thermal environment was similar to that experienced on earlier flights with the exception of the S-IC stage which showed minor changes due to differences of higher ambient temperatures at liftoff.

The Environmental Control Systems (ECS) performed satisfactorily during the AS-505 countdown. Available data shows the IU ECS performed satisfactorily. The IU environmental conditioning purge duct exhibited a pressure loss and flow increase during prelaunch operations but IU performance was unaffected.

All elements of the data system performed satisfactorily except for a problem with the CCS downlink during translunar coast. Measurement performance was excellent, as evidenced by 99.2 percent reliability. This is the highest reliability attained on any Saturn V flight. Telemetry performance was nominal, with the exception of a minor calibration deviation. The onboard tape recorder performance was satisfactory. Very High Frequency (VHF) telemetry Radio Frequency (RF) propagation was generally good; though the usual problems due to flame effects and staging were experienced. VHF data were received to 15,780 seconds (04:23:00). Command systems RF performance for both the SRSCS and CCS was nominal except for the CCS downlink problem noted. Goldstone (GDS) and Guaymas (GYM) reported receiving CCS signal to 40,191 seconds (11:09:51). Good tracking data were received from the C-Band radar with BDA indicating final Loss of Signal (LOS) at 35,346 seconds (09:49:06). The 73 ground engineering cameras provided good data during the launch.

SECTION 1

INTRODUCTION

1.1 PURPOSE

This report provides the National Aeronautics and Space Administration (NASA) Headquarters, and other interested agencies, with the launch vehicle evaluation results of the AS-505 flight test. The basic objective of flight evaluation is to acquire, reduce, analyze, evaluate and report on flight test data to the extent required to assure future mission success and vehicle reliability. To accomplish this objective, actual flight failures, anomalies and deviations must be identified, their causes accurately determined, and complete information made available so that corrective action can be accomplished within the established flight schedule.

1.2 SCOPE

This report presents the results of the early engineering flight evaluation of the AS-505 launch vehicle. The contents are centered on the performance evaluation of the major launch vehicle systems, with special emphasis on failures, anomalies, and deviations. Summaries of launch operations and spacecraft performance are included for completeness.

The official George C. Marshall Space Flight Center (MSFC) position at this time is represented by this report. It will not be followed by a similar report unless continued analysis or new information should prove the conclusions presented herein to be significantly incorrect. Final stage evaluation reports will, however, be published by the stage contractors. Reports covering major subjects and special subjects will be published as required.

SECTION 2

EVENT TIMES

2.1 SUMMARY OF EVENTS

Range zero time, the basic time reference for this report, is 12:49:00 Eastern Daylight Time (EDT) (16:49:00 Universal Time [UT]). This time is based on the nearest second prior to S-IC tail plug disconnect which occurred at 12:49:00.6 EDT. Range time is calculated as the elapsed time from range zero time and, unless otherwise noted, is the time used throughout this report. The actual and predicted range times are adjusted to ground telemetry received times. Figure 2-1 shows the time delay of ground telemetry received time versus Launch Vehicle Digital Computer (LVDC) time and indicates the magnitude and sign of corrections applied to correlate range time and vehicle time in Tables 2-1, 2-2 and 2-3.

Guidance Reference Release (GRR) occurred at -16.97 seconds and start of Time Base 1 (T_1) occurred at 0.58 seconds. GRR was established by the Digital Events Evaluator (DEE-6) and T_1 was initiated at detection of liftoff signal provided by de-energizing the liftoff relay in the Instrument Unit (IU) at IU umbilical disconnect.

Range time for each time base used in the flight sequence program and the signal for initiating each time base are presented in Table 2-1.

Start of T_2 was within nominal expectations for this event. Start of T_3 , T_4 and T_5 was initiated approximately 1.5, -1.4 and 0.3 seconds later than predicted, respectively, due to variations in the stage burn times. These variations are discussed in Sections 5, 6, and 7 of this document. Start of T_6 , which was initiated by the LVDC upon solving the restart equation, was 2.4 seconds later than predicted. Start of T_7 was 2.0 seconds later than predicted. T_8 , which was initiated by the receipt of a ground command, was started 186.8 seconds later than the predicted time.

A summary of significant events for AS-505 is given in Table 2-2. Since not all events listed in Table 2-2 are IU commanded switch selector functions, deviations are not to be construed as failures to meet specified switch selector tolerances. The events in Table 2-2 associated with guidance, navigation, and control have been identified as being accurate to within a major computation cycle.

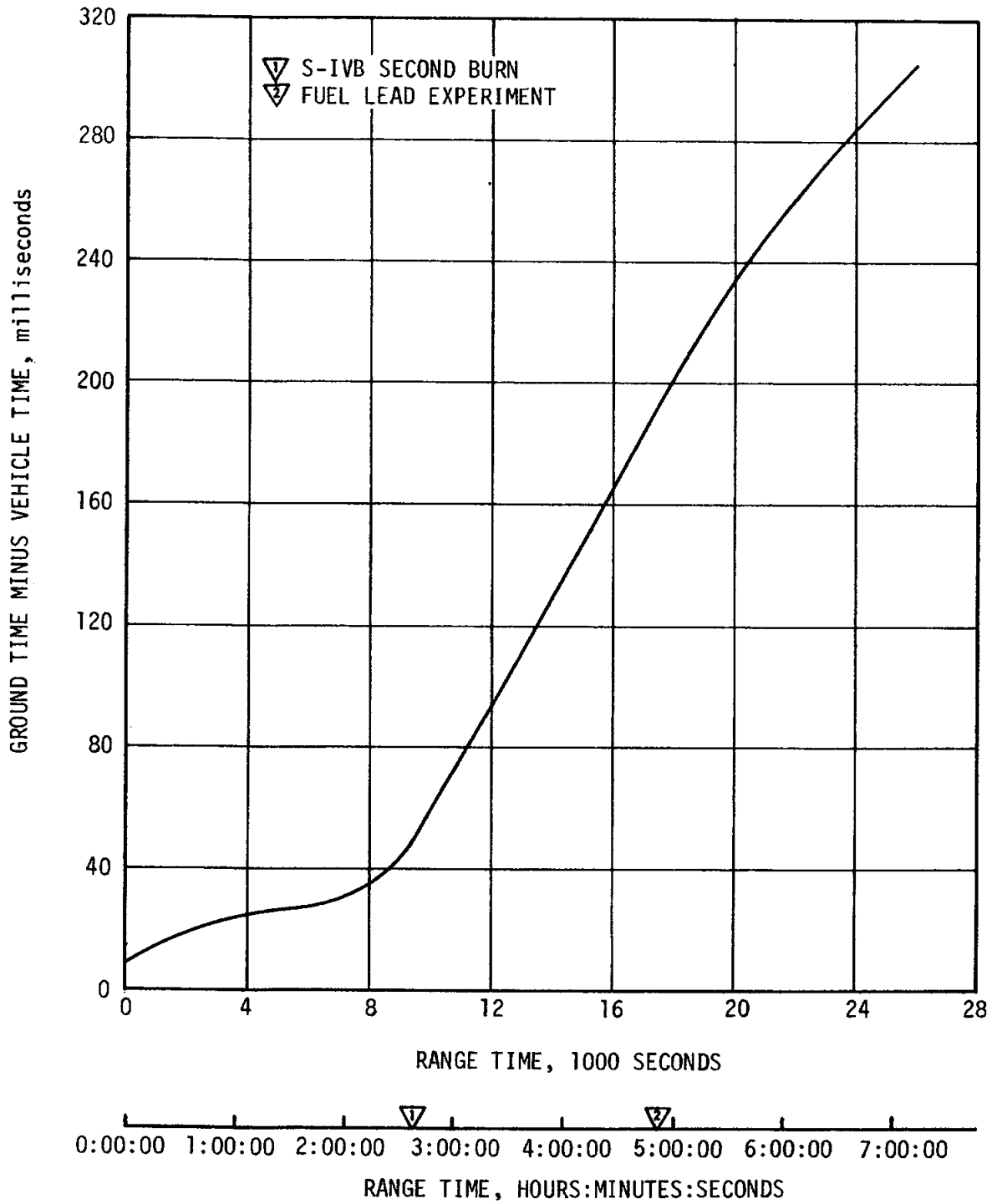


Figure 2-1. Telemetry Time Delay

Table 2-1. Time Base Summary

TIME BASE	RANGE TIME SEC (HR:MIN:SEC)	SIGNAL START
T ₀	-16.97	Guidance Reference Release
T ₁	0.58	IU Umbilical Disconnect Sensed by LVDC
T ₂	135.29	S-IC CECO Sensed by LVDC
T ₃	161.66	S-IC OECO Sensed by LVDC
T ₄	552.65	S-II ECO Sensed by LVDC
T ₅	703.98	S-IVB ECO (Velocity) Sensed by LVDC
T ₆	8629.26 (2:23:49.26)	Restart Equation Solution
T ₇	9550.83 (2:39:10.83)	S-IVB ECO Commanded by LVDC
T ₈	16,935.83 (4:42:15.83)	Enabled by Ground Command

The predicted times for establishing actual minus predicted times in Table 2-2 have been taken from 40M33625, "Interface Control Document Definition of Saturn SA-505 Flight Sequence Program" and from the "Saturn V AS-505 Post-Launch Predicted Operational Trajectory," dated May 23, 1969.

2.2 VARIABLE TIME AND COMMANDED SWITCH SELECTOR EVENTS

Table 2-3 lists known switch selector events which were issued during flight but which were not programed for specific times. The water coolant valve open and close switch selector commands were issued based upon the condition of two thermal switches in the Environmental Control System (ECS). The outputs of these switches were sampled once every 300 seconds, beginning at 180 seconds, and a switch selector command was issued to open and close the water valve to maintain proper temperature control.

Table 2-2. Significant Event Times Summary

EVENT DESCRIPTION	RANGE TIME		TIME FROM BASE	
	ACTUAL SEC	ACT-PRED SEC	ACTUAL SEC	ACT-PRED SEC
1 GUIDANCE REFERENCE RELEASE (GRR)	-17.0	0.0	-17.6	0.0
2 S-IC ENGINE START SEQUENCE COMMAND (GROUND)	-8.9	0.0	-9.5	0.1
3 S-IC ENGINE NO.1 START	-6.1	0.0	-6.7	0.0
4 S-IC ENGINE NO.2 START	-6.0	0.0	-6.6	0.0
5 S-IC ENGINE NO.3 START	-6.3	0.1	-6.9	0.1
6 S-IC ENGINE NO.4 START	-6.0	0.0	-6.6	0.0
7 S-IC ENGINE NO.5 START	-6.4	0.0	-7.0	0.0
8 ALL S-IC ENGINES THRUST OK	-1.6	-0.1	-2.2	-0.1
9 RANGE ZERO	0.0		-0.6	
10 ALL HOLDDOWN ARMS RELEASED (FIRST MOTION)	0.2	0.0	-0.3	0.1
11 IU UMBILICAL DISCONNECT, START OF TIME BASE 1 (T1)	0.6	0.0	0.0	0.0
12 BEGIN TOWER CLEARANCE YAW MANEUVER	1.6	0.0	1.0	0.0
13 END YAW MANEUVER	10.0	0.4	9.4	0.4
14 BEGIN PITCH AND ROLL MANEUVER	13.1	0.6	12.5	0.6
15 S-IC OUTBOARD ENGINE CANT	20.6	0.0	20.0	0.0
16 END ROLL MANEUVER	32.3	1.8	31.7	1.8
17 MACH 1	66.8	0.9	66.2	1.0
18 MAXIMUM DYNAMIC PRESSURE (MAX Q)	82.6	1.5	82.0	1.5
19 S-IC CENTER ENGINE CUTOFF (CECO)	135.2	-0.1	134.6	0.0
20 START OF TIME BASE 2 (T2)	135.3	0.1	0.0	0.0
21 END PITCH MANEUVER (TILT ARREST)	158.7	2.0	23.4	1.9
22 S-IC OUTBOARD ENGINE CUTOFF (DECO)	161.6	1.4	26.3	1.4
23 START OF TIME BASE 3 (T3)	161.7	1.5	0.0	0.0
24 START S-II LH2 TANK HIGH PRESSURE VENT MODE	161.7	1.4	0.1	0.0

Table 2-2. Significant Event Times Summary (Continued)

EVENT DESCRIPTION	RANGE TIME		TIME FROM BASE	
	ACTUAL SEC	ACT-PRED SEC	ACTUAL SEC	ACT-PRED SEC
25 S-II LH2 RECIRCULATION PUMPS OFF	161.8	1.4	0.2	0.0
26 S-II ULLAGE MOTOR IGNITION	162.1	1.4	0.5	0.0
27 S-IC/S-II SEPARATION COMMAND TO FIRE SEPARATION DEVICES AND RETRO MOTORS	162.3	1.4	0.7	0.0
28 S-IC RETRO MOTOR EFFECTIVE BURN TIME INITIATION (THRUST BUILDUP REACHES 75%) (AVERAGE OF 8)	162.4	1.4	0.8	0.0
29 S-II ENGINE START COMMAND (ESC)	163.1	1.5	1.4	0.0
30 S-II ENGINE IGNITION (STDV OPEN, AVERAGE OF FIVE)	164.1	1.5	2.4	0.0
31 S-II ULLAGE MOTOR BURN TIME TERMINATION (THRUST REACHES 75%)	166.0	1.2	4.4	-0.2
32 S-II MAINSTAGE	166.3	1.7	4.6	0.2
33 S-II CHILLDOWN VALVES CLOSE	168.0	1.4	6.4	0.0
34 ACTIVATE S-II PU SYSTEM	168.5	1.4	6.9	0.0
35 S-II SECOND PLANE SEPARATION COMMAND (JETTISON S-II AFT INTERSTAGE)	192.3	1.4	30.7	0.0
36 LAUNCH ESCAPE TOWER (LET) JETTISON	197.8	1.4	36.1	-0.9
37 ITERATIVE GUIDANCE MODE (IGM) PHASE 1 INITIATED	202.9	1.4	41.2	-0.1
38 S-II LOX STEP PRESSURIZATION	261.6	1.4	100.0	0.0
39 S-II CENTER ENGINE CUTOFF (CECO)	460.6	1.4	299.0	0.0
40 S-II LH2 STEP PRESSURIZATION	461.6	1.4	300.0	0.0
41 GUIDANCE SENSED TIME TO BEGIN EMR SHIFT (IGM PHASE 2 INITIATED & START OF ARTIFICIAL TAU MODE)	484.8	1.5	323.1	0.1
42 S-II LOW ENGINE MIXTURE RATIO (EMR) SHIFT (ACTUAL)	488.5	0.0	326.8	-1.5
43 END OF ARTIFICIAL TAU MODE	490.2	6.7	328.6	5.3

Table 2-2. Significant Event Times Summary (Continued)

EVENT DESCRIPTION	RANGE TIME		TIME FROM BASE	
	ACTUAL SEC	ACT-PRED SEC	ACTUAL SEC	ACT-PRED SEC
44 S-II OUTBOARD ENGINE CUTOFF (OECU)	552.6	-1.5	391.0	-2.9
45 S-II ENGINE CUTOFF INTERRUPT, START OF TIME BASE 4 (T4) (START OF IGM PHASE 3)	552.7	-1.4	0.0	0.0
46 S-IVB ULLAGE MOTOR IGNITION	553.4	-1.5	0.8	0.0
47 S-II/S-IVB SEPARATION COMMAND TO FIRE SEPARATION DEVICES AND RETRO MOTORS	553.5	-1.5	0.9	0.0
48 S-IVB ENGINE START COMMAND (FIRST ESC)	553.6	-1.5	1.0	0.0
49 FUEL CHILLDOWN PUMP OFF	554.8	-1.5	2.2	0.0
50 S-IVB IGNITION (STDV OPEN)	556.9	-1.2	4.2	0.2
51 S-IVB MAINSTAGE	559.3	-1.3	6.7	0.2
52 START OF ARTIFICIAL TAU MODE	560.1	-1.9	7.5	-0.4
53 S-IVB ULLAGE CASE JETTISON	565.4	-1.5	12.8	0.0
54 END OF ARTIFICIAL TAU MODE	568.9	-3.6	16.2	-2.2
55 BEGIN CHI BAR STEERING	669.4	0.6	116.7	2.1
56 END IGM PHASE 3	695.7	-0.6	143.1	1.0
57 BEGIN CHI FREEZE	697.3	1.0	144.6	2.5
58 S-IVB VELOCITY CUTOFF COMMAND (FIRST GUIDANCE CUTOFF) (FIRST ECO)	703.8	0.3	151.1	1.8
59 S-IVB ENGINE CUTOFF INTERRUPT, START OF TIME BASE 5 (T5)	704.0	0.3	0.0	0.0
60 S-IVB APS ULLAGE ENGINE NO. 1 IGNITION COMMAND	704.3	0.3	0.3	0.0
61 S-IVB APS ULLAGE ENGINE NO. 2 IGNITION COMMAND	704.4	0.3	0.4	0.0
62 LOX TANK PRESSURIZATION OFF	705.3	0.2	1.4	0.0
63 PARKING ORBIT INSERTION	713.8	0.3	9.8	0.0
64 BEGIN ORBITAL GUIDANCE, BEGIN MANEUVER TO LOCAL HORIZONTAL ATTITUDE	724.1	0.2	20.1	-0.1
65 S-IVB LH2 CONTINUOUS VENT SYSTEM (CVS) ON	763.0	0.3	59.0	0.0

Table 2-2. Significant Event Times Summary (Continued)

EVENT DESCRIPTION	RANGE TIME		TIME FROM BASE	
	ACTUAL SEC	ACT-PRED SEC	ACTUAL SEC	ACT-PRED SEC
66 S-IVB APS ULLAGE ENGINE NO. 1 CUTOFF COMMAND	791.0	0.3	87.0	0.0
67 S-IVB APS ULLAGE ENGINE NO. 2 CUTOFF COMMAND	791.0	0.2	87.1	0.0
68 FIRST ORBITAL NAVIGATION CALCULATIONS	805.2	-6.7	101.2	-6.8
69 BEGIN S-IVB RESTART PREPARA- TIONS, START OF TIME BASE 6 (T6)	8629.3	2.4	0.0	0.0
70 S-IVB O2/H2 BURNER LH2 ON	8670.5	2.3	41.3	0.0
71 S-IVB O2/H2 BURNER EXCITERS ON	8670.8	2.3	41.6	0.0
72 S-IVB O2/H2 BURNER LOX ON (HELIUM HEATER ON)	8671.2	2.3	42.0	0.0
73 S-IVB LH2 VENT OFF (CVS OFF)	8671.4	2.3	42.2	0.0
74 S-IVB LH2 REPRESSURIZATION CONTROL ON	8677.3	2.3	48.1	0.0
75 S-IVB LOX REPRESSURIZATION CONTROL ON	8677.5	2.3	48.3	0.0
76 S-IVB AUX HYDRAULIC PUMP FLIGHT MODE ON	8848.2	2.3	219.0	0.0
77 S-IVB LOX CHILLDOWN ON	8878.2	2.3	249.0	0.0
78 S-IVB LH2 CHILLDOWN ON	8883.2	2.3	254.0	0.0
79 S-IVB PREVALVES CLOSED	8888.2	2.3	259.0	0.0
80 S-IVB PU MIXTURE RATIO 4.5 ON	9079.3	2.3	450.1	0.0
81 S-IVB APS ULLAGE ENGINE NO. 1 IGNITION COMMAND	9125.5	2.3	496.3	0.0
82 S-IVB APS ULLAGE ENGINE NO. 2 IGNITION COMMAND	9125.6	2.3	496.4	0.0
83 S-IVB O2/H2 BURNER LH2 OFF (HELIUM HEATER OFF)	9126.0	2.3	496.8	0.0
84 S-IVB O2/H2 BURNER LOX OFF	9130.5	2.3	501.3	0.0
85 S-IVB LH2 CHILLDOWN OFF	9198.6	2.3	569.4	0.0
86 S-IVB LOX CHILLDOWN OFF	9198.8	2.3	569.6	0.0
87 S-IVB ENGINE RESTART COMMAND (FUEL LEAD INITIATION) (SECOND ESC)	9199.2	2.3	570.0	0.0

Table 2-2. Significant Event Times Summary (Continued)

EVENT DESCRIPTION	RANGE TIME		TIME FROM BASE	
	ACTUAL SEC	ACT-PRED SEC	ACTUAL SEC	ACT-PRED SEC
88 S-IVB APS ULLAGE ENGINE NO. 1 CUTOFF COMMAND	9202.2	2.3	573.0	0.0
89 S-IVB APS ULLAGE ENGINE NO. 2 CUTOFF COMMAND	9202.3	2.3	573.1	0.0
90 S-IVB SECOND IGNITION (STDV OPEN)	9207.5	2.6	578.3	0.3
91 S-IVB MAINSTAGE	9210.0	2.6	580.8	2.3
92 IGM PHASE 4 INITIATED	9218.2	6.8	589.0	4.5
93 ENGINE MIXTURE RATIO (EMR) SHIFT	9334.3	1.0	705.1	-1.3
94 S-IVB LH2 STEP PRESSURIZATION (SECOND BURN RELAY OFF)	9479.2	2.3	850.0	0.0
95 BEGIN CHI BAR STEERING	9521.1	1.7	891.9	-0.6
96 BEGIN CHI FREEZE	9549.3	2.4	920.1	0.1
97 S-IVB SECOND GUIDANCE CUTOFF COMMAND (SECOND ECO)	9550.6	2.0	-0.3	-0.1
98 S-IVB ENGINE CUTOFF INTERRUPT, START OF TIME BASE 7	9550.8	2.0	0.0	0.0
99 LH2 VENT ON COMMAND	9551.3	2.0	0.5	0.0
100 TRANSLUNAR INJECTION	9560.6	2.0	9.7	-0.1
101 BEGIN ORBITAL GUIDANCE	9569.6	0.1	18.9	-1.8
102 FIRST ORBITAL NAVIGATION CALCULATIONS	9572.5	2.0	21.7	0.0
103 CSM SEPARATION	10962.4	-42.5	1411.5	-44.6
104 CSM DOCK	11856.0	416.0	2305.1	414.0
105 SC/LV FINAL SEPARATION	14185.7	-719.3	4634.8	-721.3
106 INITIATE MANEUVER TO SLINGSHOT ATTITUDE	16935.8	186.8	0.0	0.0
107 START OF TIME BASE 8 (T8)	16935.8	186.8	0.0	0.0
108 S-IVB ULLAGE ENGINE NO. 1 ON	17136.4	187.4	200.6	0.6
109 S-IVB ULLAGE ENGINE NO. 2 ON	17137.8	188.8	202.0	2.0
110 BEGIN LOX REPRESSURIZATION	17153.1	189.1	217.3	2.3
111 BEGIN LOX LEAD	17301.3	187.3	365.5	0.5

Table 2-2. Significant Event Times Summary (Continued)

EVENT DESCRIPTION	RANGE TIME		TIME FROM BASE	
	ACTUAL SEC	ACT-PRED SEC	ACTUAL SEC	ACT-PRED SEC
112 END LOX LEAD	17310.3	188.3	374.5	1.5
113 END LOX REPRESSURIZATION	17355.5	268.5	419.6	81.6
114 BEGIN LH2 REPRESSURIZATION	17356.9	205.9	421.0	19.0
115 END LH2 REPRESSURIZATION	17386.2	175.2	450.4	-11.6
116 BEGIN FUEL LEAD	17409.9	187.9	474.1	1.1
117 S-IVB ULLAGE ENGINE NO. 1 OFF	17415.6	190.6	479.7	3.7
118 S-IVB ULLAGE ENGINE NO. 2 OFF	17417.0	192.0	481.1	5.1
119 END FUEL LEAD	17458.8	183.8	523.0	-3.0
120 H2 CONTINUOUS VENT ON	17496.1	204.1	560.2	17.2
121 BEGIN LOX DUMP	17655.8	186.8	720.0	0.0
122 END LOX DUMP	17956.0	186.8	1020.2	0.0
123 H2 NONPROPULSIVE VENT ON (NPV)	18969.8	186.8	2034.0	0.0
124 S-IVB ULLAGE ENGINE NO. 1 ON	19735.8	186.8	2800.0	0.0
125 S-IVB ULLAGE ENGINE NO. 2 ON	19736.0	187.0	2800.2	0.2
126 S-IVB ULLAGE ENGINE NO. 1 OFF	19743.3	39.3	2807.4	-147.6
127 S-IVB ULLAGE ENGINE NO. 2 OFF	19744.9	40.9	2809.0	-146.0

Table 2-3. Variable Time and Commanded Switch Selector Events

FUNCTION	STAGE	RANGE TIME (SEC)	TIME FROM BASE (SEC)	REMARKS
Water Coolant Valve Open	IU	180.8	T ₃ +19.2	LVDC Function
Water Coolant Valve Closed	IU	782.5	T ₅ +78.5	LVDC Function
Start Calibration Sequence		2293.3	T ₅ +1589.4	TAN Rev 1
Start Calibration Sequence		3205.3	T ₅ +2501.3	CRO Rev 1
Start Calibration Sequence		5373.4	T ₅ +4669.4	GYM Rev 1
Start Calibration Sequence		6677.4	T ₅ +5973.4	CYI Rev 1
Start Calibration Sequence		7821.4	T ₅ +7117.3	TAN Rev 2
Water Coolant Valve Closed	IU	8000.0	T ₅ +7296.0	LVDC Function
Start Calibration Sequence		9029.2	T ₆ +400.0	CRO Rev 2
Ambient Repress Mode Selector Off and Cryo On	S-IVB	9566.2	T ₇ +15.4	CCS Command
Water Coolant Valve Closed	IU	15,213.7	T ₇ +5662.9	LVDC Function
LH ₂ Tank Continuous Vent Valve Close On	S-IVB	16,953.4	T ₈ +17.5	CCS Command
LH ₂ Tank Continuous Vent Valve Close Off	S-IVB	16,956.2	T ₈ +20.3	CCS Command
LH ₂ Tank Repress Control Valve Open Off	S-IVB	17,096.6	T ₈ +160.8	CCS Command
LH ₂ Tank Repress Control Valve Open Off	S-IVB	17,098.5	T ₈ +162.7	CCS Command
Ambient Repress Mode Selector On and Cryo Off	S-IVB	17,100.0	T ₈ +164.1	CCS Command
S-IVB Ullage Engine No. 1 On	S-IVB	17,136.5	T ₈ +200.6	CCS Command
S-IVB Ullage Engine No. 2 On	S-IVB	17,137.8	T ₈ +202.0	CCS Command
LOX Tank Repress Control Valve Open On	S-IVB	17,153.1	T ₈ +217.3	CCS Command
Auxiliary Hydraulic Pump Flight Mode On	S-IVB	17,186.4	T ₈ +250.6	CCS Command
Passivation Enable	S-IVB	17,299.8	T ₈ +364.0	CCS Command
Engine Helium Control Valve Open On	S-IVB	17,300.6	T ₈ +364.8	CCS Command
Engine Mainstage Control Valve Open On	S-IVB	17,301.3	T ₈ +365.5	CCS Command
Engine Mainstage Control Valve Open Off	S-IVB	17,310.3	T ₈ +374.5	CCS Command
Prevalves Close On	S-IVB	17,311.4	T ₈ +375.5	CCS Command
Engine Helium Control Valve Open Off	S-IVB	17,312.2	T ₈ +376.3	CCS Command
Engine Helium Control Valve Open On	S-IVB	17,324.7	T ₈ +352.9	CCS Command
Engine Helium Control Valve Open Off	S-IVB	17,336.3	T ₈ +400.4	CCS Command
Passivation Disable	S-IVB	17,337.0	T ₈ +401.2	CCS Command
LOX Tank Repress Control Valve Open Off	S-IVB	17,355.5	T ₈ +419.6	CCS Command
LH ₂ Tank Repress Control Valve Open On	S-IVB	17,356.9	T ₈ +421.0	CCS Command
Prevalves Close Off	S-IVB	17,358.3	T ₈ +422.5	CCS Command
Ambient Repress Mode Selector Off and Cryo On	S-IVB	17,386.3	T ₈ +450.4	CCS Command

Table 2-3. Variable Time and Commanded Switch Selector Events (Continued)

FUNCTION	STAGE	RANGE TIME (SEC)	TIME FROM BASE (SEC)	REMARKS
Passivation Enable	S-IVB	17,408.5	T ₈ +472.6	CCS Command
Engine Ignition Phase Control Valve Open On	S-IVB	17,409.9	T ₈ +474.1	CCS Command
Engine Helium Control Valve Open On	S-IVB	17,411.3	T ₈ +475.5	CCS Command
S-IVB Ullage Engine No. 1 Off	S-IVB	17,415.6	T ₈ +479.7	CCS Command
S-IVB Ullage Engine No. 2 Off	S-IVB	17,417.0	T ₈ +481.1	CCS Command
Engine Ignition Phase Control Valve Open Off	S-IVB	17,458.9	T ₈ +523.0	CCS Command
Engine Helium Control Valve Open Off	S-IVB	17,460.3	T ₈ +524.4	CCS Command
LH ₂ Tank Continuous Vent Orifice Shutoff Valve Open On	S-IVB	17,496.1	T ₈ +560.2	CCS Command
LH ₂ Tank Continuous Vent Relief Override Shutoff Valve Open On	S-IVB	17,497.5	T ₈ +561.6	CCS Command
LH ₂ Tank Continuous Vent Orifice Shutoff Valve Open On	S-IVB	17,500.3	T ₈ +564.5	CCS Command
LH ₂ Tank Continuous Vent Relief Override Shutoff Valve Open Off	S-IVB	17,501.8	T ₈ +565.9	CCS Command
Water Coolant Valve Open	IU	17,919.4	T ₈ +983.5	LVDC Function
Water Coolant Valve Closed	IU	18,219.5	T ₈ +1283.6	LVDC Function
S-IVB Ullage Engine No. 1 Off	S-IVB	19,743.3	T ₈ +2807.4	CCS Command
S-IVB Ullage Engine No. 2 Off	S-IVB	19,744.9	T ₈ +2809.0	CCS Command
Auxiliary Hydraulic Pump Flight Mode On	S-IVB	19,792.3	T ₈ +2856.4	CCS Command
Auxiliary Hydraulic Pump Flight Mode Off	S-IVB	19,928.1	T ₈ +2992.3	CCS Command
Water Coolant Valve Closed	IU	23,329.3	T ₈ +6393.4	LVDC Function
PCM Coax Switch High Gain Antenna	IU	24,053.8	T ₈ +7118.0	CCS Command
CCS Coax Switch Fail Safe and High Gain Antenna	IU	24,053.9	T ₈ +7118.1	CCS Command
PCM Coax Switch High Gain Antenna	IU	24,054.0	T ₈ +7118.2	CCS Command
CCS Coax Switch Fail Safe and High Gain Antenna	IU	24,054.1	T ₈ +7118.2	CCS Command
Water Coolant Valve Open	IU	25,133.1	T ₈ +8197.2	LVDC Function
Water Coolant Valve Closed	IU	25,433.8	T ₈ +8497.9	LVDC Function

Table 2-3 also contains the times of initiation of the special sequence of switch selector events which were programed to be initiated by telemetry station acquisition and included the following calibration sequence:

<u>FUNCTION</u>	<u>STAGE</u>	<u>TIME (SEC)</u>
In-Flight Calibration Mode On	S-IVB	Acquisition +60.0
Telemetry Calibrator In-Flight Calibrator On	IU	Acquisition +60.2
TM Calibrate On	S-IVB	Acquisition +60.4
Telemetry Calibrator In-Flight Calibrate On	IU	Acquisition +65.2
TM Calibrate Off	S-IVB	Acquisition +65.4
In-Flight Calibration Mode Off	S-IVB	Acquisition +66.0

In addition, known ground commands sent to the LVDC are included in this table.

SECTION 3

LAUNCH OPERATIONS

3.1 SUMMARY

The ground systems supporting the AS-505/Apollo 10 countdown and launch performed exceptionally well. There were no significant failures or anomalies. Several systems experienced component failures and malfunctions, but these problems did not cause any holds or significant delays in the scheduled sequences of launch operations. Launch occurred at 12:49:00 Eastern Daylight Time (EDT), May 18, 1969.

The Apollo 10 vehicle was the first to be launched from Pad 39B of the Saturn complex. Damage to the pad, Launch Umbilical Tower (LUT) and support equipment from the blast and flame impingement was minor. A hydraulic oil fire occurred in Service Arm (SA) No. 1 control console.

3.2 PRELAUNCH MILESTONES

A chronological summary of events and preparations leading to the launch of the AS-505 is contained in Table 3-1.

3.3 COUNTDOWN EVENTS

The AS-505/Apollo 10 terminal countdown was picked up at 21:00:00 EDT, May 16, 1969. The countdown proceeded as planned with no unscheduled holds. The scheduled 1-hour hold at -3 hours 30 minutes in the count was utilized to overcome a slight delay in propellant loading. Launch occurred at 12:49:00 EDT, May 18, 1969.

3.4 PROPELLANT LOADING

3.4.1 RP-1 Loading

The RP-1 system successfully supported the launch countdown. During the automatic replenish operations at approximately -12 hours, the fast fill valve "open" indication dropped out causing system shutdown. Replenish operations were reinitiated in the manual mode and were completed satisfactorily. The problem was subsequently traced to improperly adjusted fast fill valve limit switches. Although attempts at readjustment were unsuccessful, there was no significant impact on remaining RP-1 operations. The fast fill valve is not used during the countdown after

Table 3-1. AS-505 Prelaunch Milestones

DATE	ACTIVITY OR EVENT
October 16, 1968	LM-4 Arrival
November 23, 1968	CSM-106 Arrival
November 27, 1968	S-IC Stage Arrival
December 3, 1968	S-II Stage Arrival
December 10, 1968	S-IVB Stage Arrival
December 15, 1968	IU Arrival
December 30, 1968	Launch Vehicle (LV) Erection Completed
January 17, 1969	Final Manned Altitude Run
February 3, 1969	LV Propellant Dispersion/Malfunction Overall Test (OAT)
February 6, 1969	Spacecraft (SC) Erection
February 27, 1969	Space Vehicle (SV) Electrical Mate
March 5, 1969	SV OAT (plugs in)
March 11, 1969	SV Transfer to Pad 39B
March 28, 1969	Emergency Egress Test Completed
April 19, 1969	SV Flight Readiness Test (FRT) Completed
April 25, 1969	SV Hypergol Load Completed
May 2, 1969	S-IC RP-1 Loaded
May 5, 1969	CDDT (Wet) Completed
May 6, 1969	CDDT (Dry) Completed
May 18, 1969	SV Launched on Schedule

replenish is completed. If unscheduled replenish had been required, it could have been accomplished, as before, in the manual mode.

During the automatic RP-1 level adjust at about -50 minutes, an anomaly occurred which caused the level adjust valve to close slightly late. As a result the RP-1 flight mass percentage (which can normally be adjusted to 100 ± 0.02 percent) was adjusted to 99.81 percent, but was still within Launch Mission Rules requirements of 100 ± 0.2 percent. The same problem occurred during Countdown Demonstration Test (CDDT), however post CDDT troubleshooting revealed no problems with the Propellant Tanking Control System (PTCS). Further postlaunch investigation has isolated the problem to a defective printed circuit card in the PTCS.

3.4.2 LOX Loading

The LOX system supported the launch countdown satisfactorily. During fill line chilldown in preparation of LOX loading at about -8 hours, the primary LOX replenish pump failed to start. The problem was traced to a blown fuse in the pump motor starter circuit. Troubleshooting and fuse replacement delayed LOX loading about 50 minutes. Completion of LOX loading was achieved at approximately -4 hours 22 minutes. The built-in 1-hour hold at -3 hours 30 minutes precluded a launch delay. Launch damage to the LOX system was minor.

3.4.3 LH₂ Loading

The LH₂ system successfully supported the launch countdown with no major incidents. The fill sequence began with initiation of S-II loading at about -4 hours and was completed during the scheduled 1-hour hold at -3 hours 30 minutes. Launch damage to the LH₂ system was minor.

3.4.4 Auxiliary Propulsion System Propellant Loading

Propellant loading of the S-IVB Auxiliary Propulsion System (APS) was accomplished satisfactorily. Total propellant mass in both modules at liftoff was 186.9 kilograms (412 lbm) of Nitrogen Tetroxide (N₂O₄) and 116.1 kilograms (256 lbm) of Monomethyl Hydrazine (MMH).

3.5 S-II INSULATION, PURGE AND LEAK DETECTION

The performance of the S-II-505 stage insulation was highly satisfactory. Joint closeouts of the external sidewall insulation were of the nylon wet-layup configuration as first utilized on the S-II-504 stage. Performance of this insulation displayed outstanding improvement over that used on S-II-503 and prior stages. All purge circuit pressures remained within the desired limits during countdown and contaminant gas concentrations were well below redline values. Television inspection of the LH₂ tank sidewall insulation during the countdown showed only two minor leaks in the vicinity of the systems tunnel. The total heat leakage through the insulation to the liquid hydrogen was well below specification allowable.

3.5.1 Forward Bulkhead Insulation

The inlet pressure of the forward bulkhead insulation circuit remained steady at 1.34 N/cm² (1.95 psig) from LH₂ load initiation until the time of launch. The outlet pressure was at or near zero throughout the countdown. Hydrogen and oxygen contamination levels were between 1500 and 2000 parts per million. Nitrogen indications exceeded 1 percent at the time of LH₂ loading but diminished after stable temperatures were reached.

3.5.2 Forward Bulkhead Uninsulated Area

The circuit inlet pressure for the forward bulkhead uninsulated area remained steady at 1.14 N/cm² (1.65 psig) through propellant loading and until the time of launch. The outlet pressure was at or near zero throughout the countdown. Nitrogen contamination exceeded one percent at the beginning of LOX load and diminished to an insignificant level after LH₂ loading.

3.5.3 LH₂ Tank Sidewall

The sidewall inlet pressure remained steady between 1.04 and 1.20 N/cm² (1.51 and 1.74 psig). The outlet pressure decayed from 1.09 to 0.72 N/cm² (1.58 to 1.05 psig) during LOX tanking, and further decayed to 0.41 N/cm² (0.6 psig) during LH₂ loading. At the time of launch the outlet pressure had recovered to 0.49 N/cm² (0.71 psig). Hydrogen and nitrogen contamination exceeded one percent about 2 hours before launch, but as the time of launch approached, all sidewall contamination readings became insignificant.

Insulation outer surface temperatures on the sidewall were warmer than on any preceding stage. Minimum temperature recorded during the countdown was 269°K (25°F). On S-II-504, the lowest temperature experienced was 219°K (-65°F). The absence of frost was noteworthy since all targets and other markings were clearly visible.

3.5.4 Bolting/J-Ring

The bolting ring inlet pressure diminished steadily from 1.19 to 0.98 N/cm² (1.73 to 1.42 psig) at launch. The outlet pressure decayed from 0.9 N/cm² (1.3 psig) to slightly below zero at the time of LH₂ loading, then remained at or below zero until launch. Hazardous gas concentration readings were questionable due to problems experienced with the ground analyzer system.

3.5.5 Feedline Elbow

The feedline elbow circuit inlet pressure remained steady between 2.28 and 2.48 N/cm² (3.3 and 3.6 psig). Outlet pressure varied from 0.71 to 1.2 N/cm² (1.04 to 1.74 psig) during tanking but otherwise remained steady until launch. There were no significant contamination readings.

3.5.6 Common Bulkhead

Purge pressures remained approximately steady during the period the bulkhead was purged. Evacuation began at -3 hours 24 minutes and pressures decreased below 2.07 N/cm² (3 psia) within 50 minutes. This is well within acceptable limits. There were no significant hazardous gas readings in this purge circuit.

3.6 GROUND SUPPORT EQUIPMENT (GSE)

3.6.1 Ground/Vehicle Interface

Detailed discussion of the GSE will be contained in the Kennedy Space Center Apollo/Saturn V (AS-505) Ground Systems Evaluation Report. Ground systems performance was highly satisfactory. The Holddown Arms (HDA), Tail Service Masts (TSM), SA and all other ground equipment functioned well in support of AS-505 launch. The HDA was released pneumatically at 0.25 second. TSM retraction was normal and all protective hoods closed properly.

SA systems performed within design limits during the launch sequence and SA total retract times to safe angle were within specifications. Based on the Digital Events Evaluator (DEE-6) data, SA No. 1 umbilical carrier withdrawal time was 0.43 second greater than specification maximum of 5 seconds. The slow withdrawal did not affect overall SA No. 1 retract time enough to cause terminal countdown sequence cutoff. Total SA No. 1 retract time to safe angle was 10 seconds, which is within the specification limit of 10.5 seconds, and was 3.8 seconds before SA No. 2 retract command. (Failure to achieve SA No. 1 safe angle prior to time for SA No. 2 retract would cause cutoff.) Overall damage to the SA at launch was considered minor. The SA No. 1 control console interior components and cables were destroyed by hydraulic oil fire. As on previous launches, latches were bent and control console doors were blown open on most arm levels of the LUT.

The Environmental Control System (ECS) GN₂ flowrate to the Instrument Unit (IU) exceeded Launch Vehicle (LV) specifications and criteria at -9 hours 50 minutes for approximately 5 minutes as a result of a reduction in back pressure from the IU. Adjustments were made to restore the purge flowrate to the previous levels and maintain the required IU compartment temperature. Inspection of the system from the ECS to the vehicle interface revealed no anomalies. The probable cause of the deviation was a separation of the IU purge duct.

3.6.2 MSFC Furnished Ground Support Equipment

3.6.2.1 S-IC Stage GSE. Performance of the GSE supporting the S-IC stage during countdown was satisfactory. There were no significant system failures or anomalies. Blast damage to the mechanical support equipment was minor. There was no reportable damage to the electrical support equipment. The following are minor discrepancies which were corrected during the countdown:

- a. During functional testing the high pressure helium bottle fill regulator failed (helium system overpressurization switch actuated at -23 hours 47 minutes) and required replacement.
- b. The 400 hertz frequency changer (LUT 3) failed at -18 hours 10 minutes. Three defective inverter capacitors were replaced and the frequency changer performed satisfactorily for the remainder of the countdown.

3.6.2.2 S-II Stage GSE. The S-II stage GSE performed satisfactorily during countdown and launch. Blast damage to the mechanical and electrical equipment was very minor. During the postlaunch inspection a LOX umbilical debris valve was found to be open, although the proper closed signal was received at launch. There were no significant system failures or anomalies, and all minor discrepancies were promptly corrected during the countdown. One of the minor discrepancies was leakage of a pressure regulator in the pneumatic supply console at -22 hours 30 minutes. This regulator was replaced. Another regulator in this console required adjustment at -8 hours 25 minutes.

3.6.2.3 S-IVB Stage GSE. All S-IVB GSE systems operated satisfactorily during the countdown. The only problem reported was a faulty connection in the pneumatic console distributor cable. No major damage was found during the postlaunch inspection.

3.6.2.4 IU Stage GSE. The IU GSE performance during countdown was satisfactory. No anomalies were encountered with the mechanical equipment. Several malfunctions and anomalies occurred in the electrical GSE during launch preparations and countdown which were promptly corrected to maintain launch readiness. The systems involved were the Ground Computer, Integration Networks, Digital Data Acquisition System, Stabilizer, Count Clock and DEE-6.

Support of the DEE-6 was lost after liftoff. Due to high discrete activity encountered at liftoff, it is normal for the DEE-6 to run behind in the processing of backlogged discrete events. As a result, the last indication of data output occurred at -1.63 seconds. Post-launch inspection indicated a possibility of a memory parity halt as the reason for DEE-6 failure. Through software manipulation, the liftoff data were obtained from the backlogged information and transmitted to the master printer.

3.6.3 GSE Camera Coverage

On review of the film coverage of the GSE at launch the following anomalies were noted:

- a. S-II Stage Forward SA (SA No. 5) electrical umbilical access panel was observed not secured and flapping after liftoff.
- b. The retracting cable on the Service Module SA (SA No. 8) did not retract the umbilical carrier to the boom after disconnection and was observed hanging 1.2 to 1.5 meters (4 to 5 ft) after full retraction of the arm.
- c. A GSE cabinet on the east side 18.3 meter (60 ft) level of the LUT was observed on fire, and the cabinet doors open after S-IC flame impingement. Flame impingement obscured time of door opening. Last appearance of cabinet intact was at 8 seconds and the doors were observed open at 17 seconds.

SECTION 4

TRAJECTORY

4.1 SUMMARY

The trajectory parameters from launch to translunar injection were close to nominal. The vehicle was launched on an azimuth 90 degrees east of north. A roll maneuver was initiated at 13.05 seconds range time that placed the vehicle on a flight azimuth of 72.028 degrees east of north.

The space-fixed velocity at S-IC Outboard Engine Cutoff (OECO) was 10.81 m/s (35.47 ft/s) greater than nominal. The space-fixed velocity at S-II OECO was 13.22 m/s (43.37 ft/s) less than nominal. The space-fixed velocity at S-IVB first guidance cutoff was 0.07 m/s (0.23 ft/s) greater than nominal. The altitude at S-IVB first guidance cutoff was 0.03 kilometer (0.01 n mi) lower than nominal and the surface range was 0.92 kilometer (0.50 n mi) greater than nominal.

The space-fixed velocity at parking orbit insertion was 0.07 m/s (0.23 ft/s) less than nominal and the flight path angle was 0.0059 degree less than nominal. The eccentricity was 0.000037 greater than nominal. The apogee and perigee were 0.13 kilometer (0.07 n mi) and 0.62 kilometer (0.33 n mi) lower than nominal, respectively.

The parameters at translunar injection were also very close to nominal. The eccentricity was 0.00002 less than nominal, the inclination was 0.007 degree greater than nominal, the node was 0.022 degree lower than nominal and C_3 was 868 m²/s² (9345 ft²/s²) less than nominal. The total space-fixed velocity was 2.39 m/s (7.84 ft/s) less than nominal and the altitude was 2.87 kilometers (1.55 n mi) higher than nominal.

The actual impact locations for the spent S-IC and S-II stages were determined by a theoretical free-flight simulation. The surface range for the S-IC impact point was 4.19 kilometers (2.26 n mi) less than nominal. The surface range for the S-II impact point was 34.57 kilometers (18.67 n mi) less than nominal.

4.2 TRACKING DATA UTILIZATION

4.2.1 Tracking During the Ascent Phase of Flight

Tracking data were obtained during the period from the time of first motion through parking orbit insertion.

The best estimate trajectory was established by using telemetered guidance velocities as generating parameters to fit data from five different C-Band tracking stations. Approximately 15 percent of the various tracking data was eliminated due to inconsistencies. A comparison of the reconstructed ascent trajectory with the remaining tracking data showed excellent agreement. The launch phase portion of the trajectory (liftoff to approximately 20 seconds) was established by constraining integrated telemetered guidance accelerometer data to the early phase of the best estimate trajectory.

4.2.2 Tracking During Orbital Flight

Orbital tracking was conducted by the NASA Manned Space Flight Network (MSFN). C-Band radar stations furnished data for use in determining the orbital trajectory. There were also considerable S-Band tracking data available which were not used in determining the orbital trajectory due to the abundance of C-Band radar data.

The orbital trajectory was obtained by integrating corrected insertion conditions forward. The insertion conditions, as determined by the Orbital Correction Program (OCP), were obtained by a differential correction procedure which adjusted the estimated insertion conditions to fit the C-Band radar tracking data in accordance with the weights assigned to the data. After all available C-Band radar tracking data were analyzed, the stations and passes providing the better quality data were used in the determination of the insertion conditions.

4.2.3 Tracking During the Injection Phase of Flight

C-Band radar data were obtained from the ship Mercury during the major portion of the injection phase of flight. These tracking data were found to be invalid and were not used in the trajectory determination. Thus the injection trajectory was obtained by integrating the restart vector forward utilizing telemetered guidance velocities.

4.3 TRAJECTORY EVALUATION

4.3.1 Ascent Trajectory

Actual and nominal altitude, surface range, and cross range for the ascent phase are presented in Figure 4-1. Actual and nominal space-fixed velocity and flight path angle during ascent are shown in Figure 4-2. Comparisons of total inertial accelerations are shown in Figure 4-3. The maximum acceleration during S-IC burn was 3.9 g. The accuracy of the trajectory at S-IVB first cutoff is estimated to be ± 0.7 m/s (± 2.3 ft/s) in velocity components and ± 250 meters (± 820 ft) in position components.

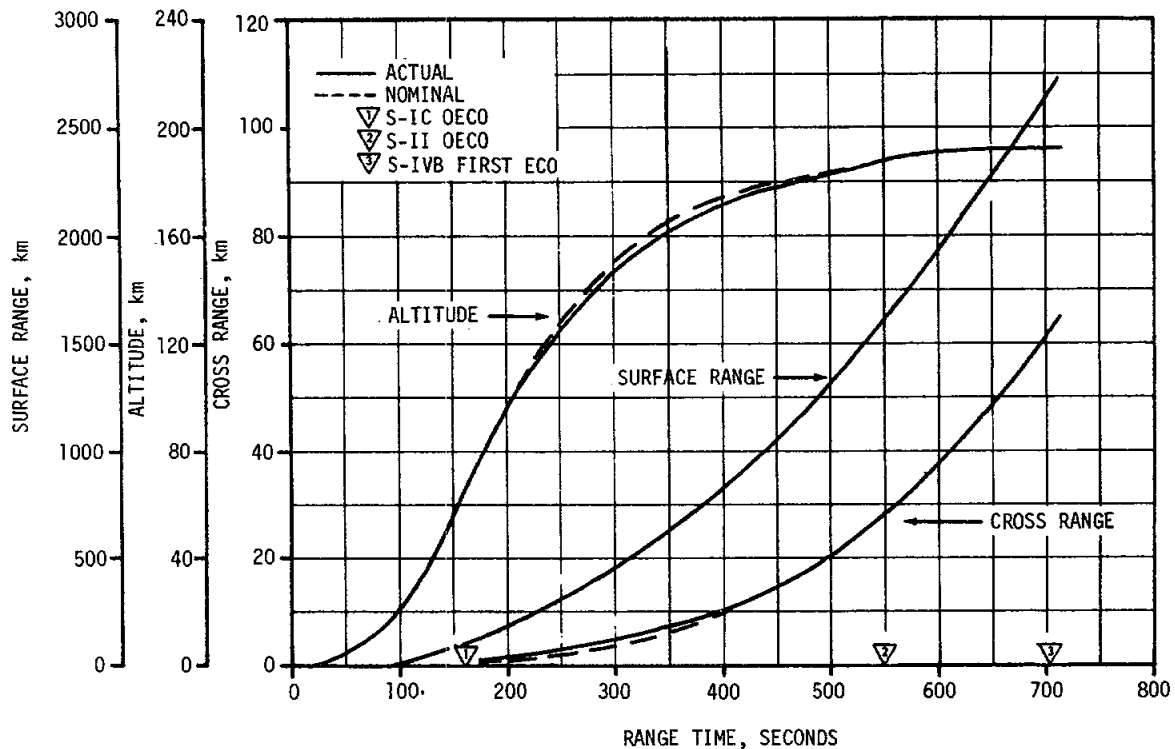


Figure 4-1. Ascent Trajectory Position Comparison

Mach number and dynamic pressure are shown in Figure 4-4. These parameters were calculated using meteorological data measured to an altitude of 89.75 kilometers (46.46 n mi). Above this altitude the measured data were merged into the U. S. Standard Reference Atmosphere.

Actual and nominal values of parameters at significant trajectory event times, cutoff events, and separation events are shown in Tables 4-1, 4-2, and 4-3, respectively.

The free-flight trajectories of the spent S-IC and S-II stages were simulated using initial conditions from the final postflight trajectory. The simulation was based upon the separation impulses for both stages and nominal tumbling drag coefficients. No tracking data were available for verification. Table 4-1 presents a comparison of nominal and free-flight parameters at apex for the S-IC and S-II stages. Table 4-4 presents a comparison of free-flight parameters to nominal at impact for the S-IC and S-II stages.

4.3.2 Parking Orbit Trajectory

A family of values for the insertion parameters was obtained depending upon the combination of data used and the weights applied to the data. The solutions that were considered reasonable had a spread of about

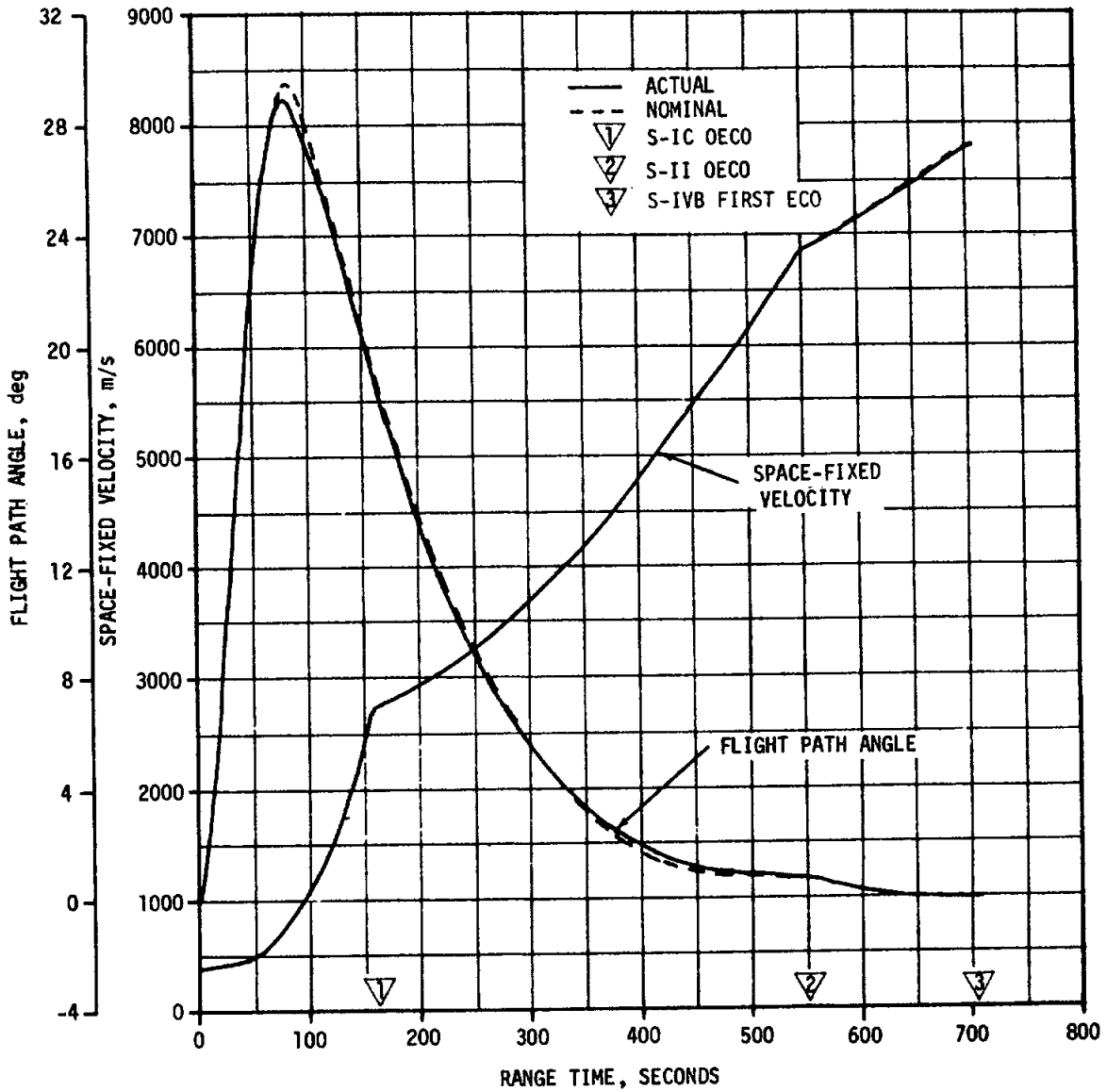


Figure 4-2. Ascent Trajectory Space-Fixed Velocity and Flight Path Angle Comparisons

± 250 meters (± 820 ft) in position components and ± 0.7 m/s (± 2.3 ft/s) in velocity components. The actual and nominal parking orbit insertion parameters are presented in Table 4-5. The ground track from insertion to S-IVB/CSM separation is given in Figure 4-5.

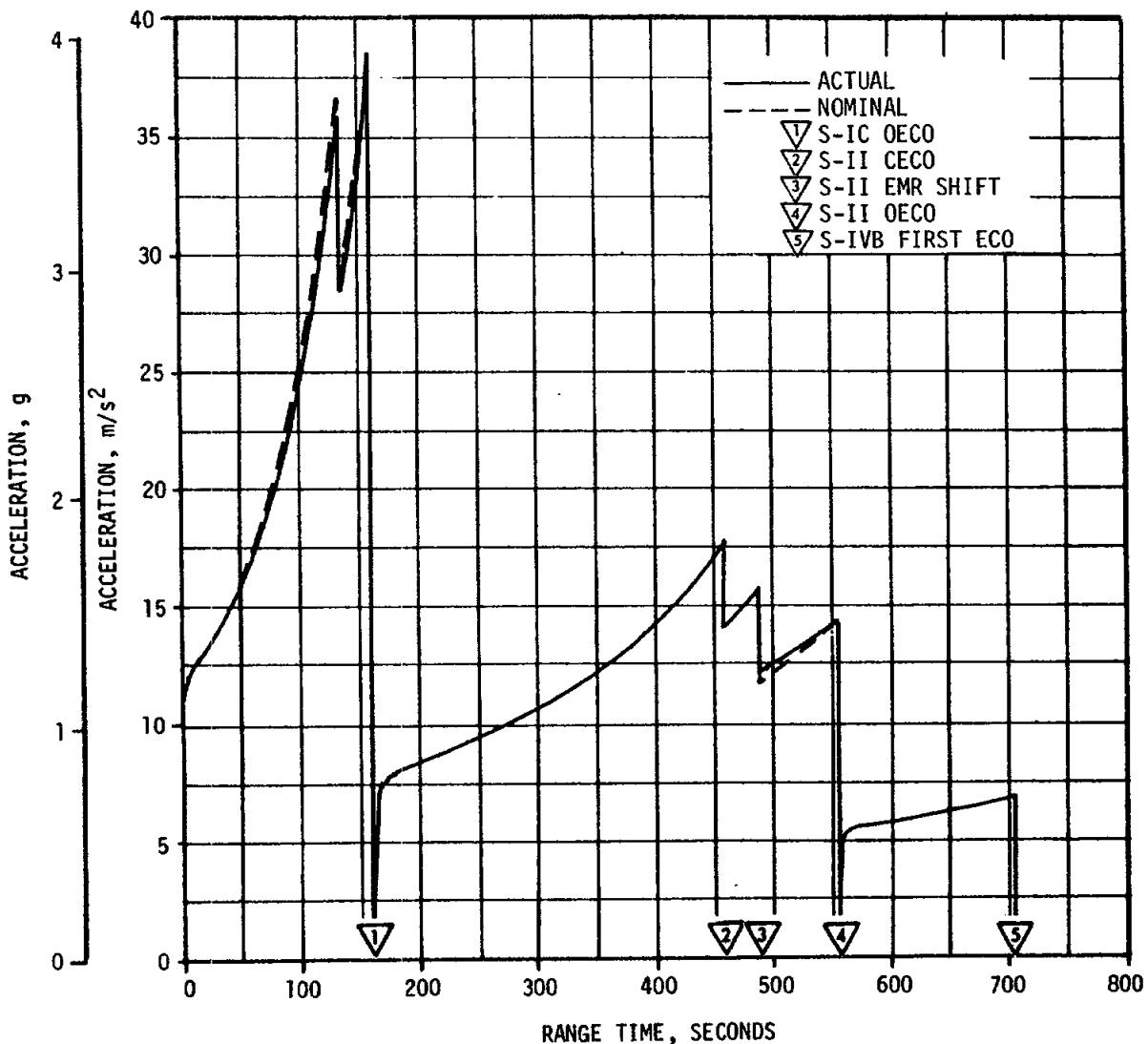


Figure 4-3. Ascent Trajectory Acceleration Comparison

4.3.3 Injection Trajectory

Comparisons between the actual and nominal total space-fixed velocity and flight path angle are shown in Figure 4-6. The actual and nominal total inertial acceleration comparisons are presented in Figure 4-7. Throughout the S-IVB second burn phase of flight, the space-fixed velocity and the flight path angle were very close to nominal with deviations more noticeable towards the end of the time period.

The trajectory and targeting parameters at S-IVB second guidance cutoff and translunar injection are presented in Tables 4-2 and 4-6, respectively.

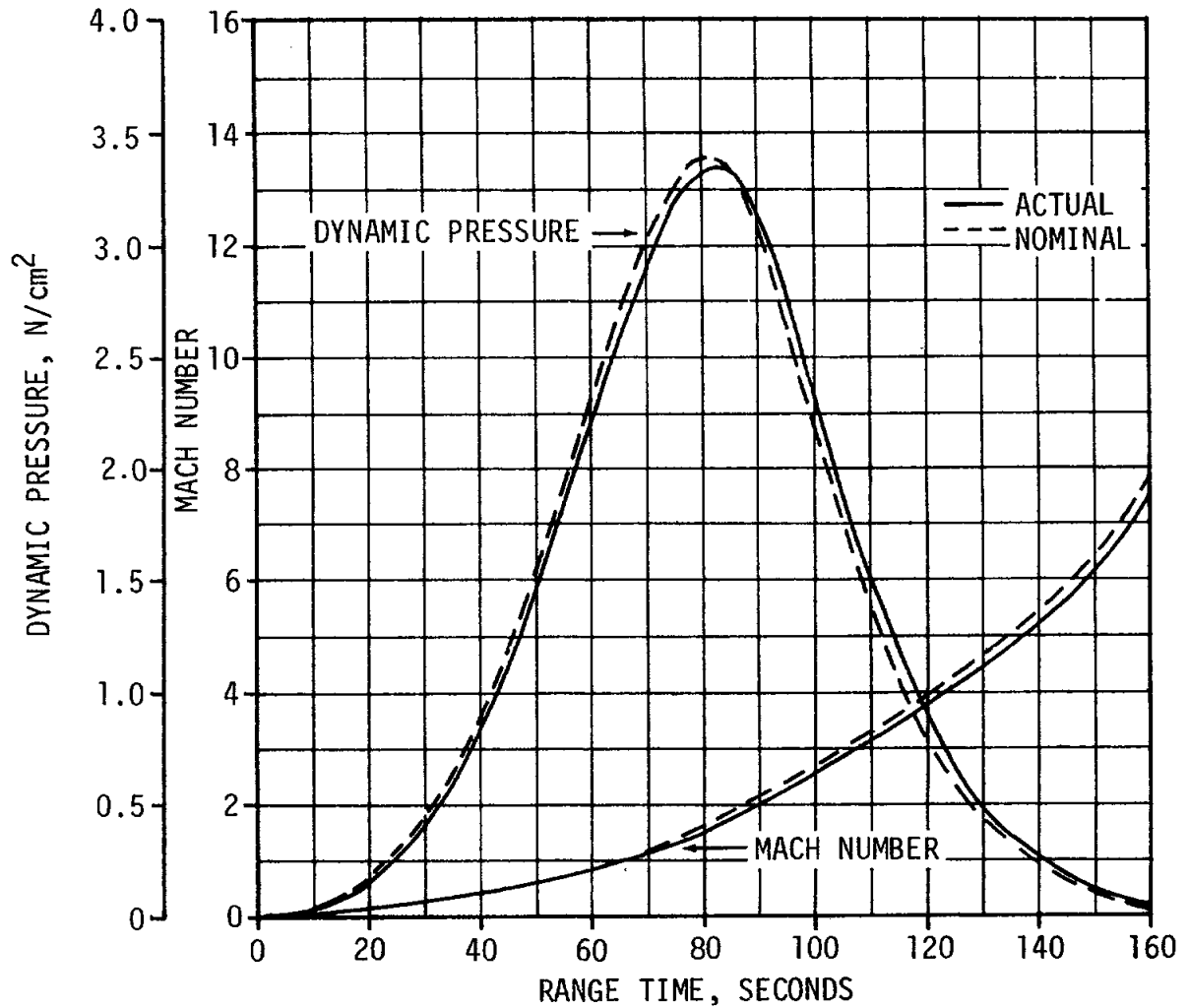


Figure 4-4. Dynamic Pressure and Mach Number Comparisons

4.3.4 Post TLI Trajectory

The post Translunar Injection (TLI) trajectory spans the time interval from TLI to S-IVB/CSM separation. The post TLI trajectory was obtained by integrating the translunar injection conditions, derived from the injection trajectory solution, to S-IVB/CSM separation. A comparison of S-IVB/CSM separation conditions is presented in Table 4-3. The post TLI tracking data were received and were used to verify the post TLI trajectory.

Table 4-1. Comparison of Significant Trajectory Events

EVENT	PARAMETER	ACTUAL	NOMINAL	ACT-NOM		
First Motion	Range Time, sec	0.25	0.25	0.0		
	Total Inertial Acceleration, m/s^2 (ft/s^2)	10.40 (34.12)	10.92 (35.83)	-0.52 (-1.71)		
Mach 1	Range Time, sec	66.8	65.9	0.9		
	Altitude, km (n mi)	7.86 (4.24)	7.74 (4.18)	0.12 (0.06)		
Maximum Dynamic Pressure	Range Time, sec	82.6	81.1	1.5		
	Dynamic Pressure, N/cm^2 (lbf/ft^2)	3.324 (694.2)	3.384 (706.8)	-0.060 (-12.6)		
	Altitude, km (n mi)	13.22 (7.14)	12.91 (6.97)	0.31 (0.17)		
Maximum Total Inertial Acceleration:	S-IC	Range Time, sec	161.71	160.16	1.55	
		Acceleration, m/s^2 (ft/s^2)	38.47 (126.21)	38.01 (124.70)	0.46 (1.51)	
	S-II	Range Time, sec	460.69	459.28	1.41	
		Acceleration, m/s^2 (ft/s^2)	17.82 (58.46)	17.75 (58.23)	0.07 (0.23)	
	S-IVB 1st Burn	Range Time, sec	703.84	703.56	0.28	
		Acceleration, m/s^2 (ft/s^2)	6.89 (22.60)	6.85 (22.47)	0.04 (0.13)	
	S-IVB 2nd Burn	Range Time, sec	9,550.66	9,548.67	1.99	
		Acceleration, m/s^2 (ft/s^2)	14.60 (47.90)	14.63 (48.00)	-0.03 (-0.10)	
	Maximum Earth-Fixed Velocity:	S-IC	Range Time, sec	161.96	160.91	1.05
			Velocity, m/s (ft/s)	2,388.34 (7,835.76)	2,380.96 (7,811.55)	7.38 (24.21)
S-II		Range Time, sec	553.50	555.04	-1.54	
		Velocity, m/s (ft/s)	6,497.67 (21,317.81)	6,511.84 (21,364.30)	-14.17 (-46.49)	
S-IVB 1st Burn		Range Time, sec	713.76	713.48	0.28	
		Velocity, m/s (ft/s)	7,389.65 (24,244.26)	7,389.70 (24,244.42)	-0.05 (-0.16)	
S-IVB 2nd Burn		Range Time, sec	9,551.30	9,549.25	2.05	
		Velocity, m/s (ft/s)	10,439.91 (34,251.67)	10,442.07 (34,258.76)	-2.16 (-7.09)	
Apex:		S-IC Stage	Range Time, sec	266.87	267.88	-1.01
			Altitude, km (n mi)	112.25 (60.61)	115.24 (62.22)	-2.99 (-1.61)
		Surface Range, km (n mi)	320.21 (172.90)	321.45 (173.57)	-1.24 (-0.67)	
	S-II Stage	Range Time, sec	597.21	596.33	0.88	
		Altitude, km (n mi)	189.48 (102.31)	190.25 (102.73)	-0.77 (-0.42)	
		Surface Range, km (n mi)	1,916.93 (1,035.06)	1,912.52 (1,032.68)	4.41 (2.38)	

Table 4-2. Comparison of Cutoff Events

PARAMETER	ACTUAL	NOMINAL	ACT-NOM	ACTUAL	NOMINAL	ACT-NOM
	S-1C CECO (ENGINE SOLENOID)			S-1C OECD (ENGINE SOLENOID)		
Range Time, sec	135.16	135.26	-0.10	161.63	160.20	1.43
Altitude, km (n mi)	43.39 (23.43)	44.56 (24.06)	-1.17 (-0.63)	65.28 (35.25)	65.79 (35.52)	-0.51 (-0.27)
Surface Range, km (n mi)	46.32 (25.01)	46.88 (25.31)	-0.56 (-0.30)	93.38 (50.42)	91.33 (49.31)	2.05 (1.11)
Space-Fixed Velocity, m/s (ft/s)	1,973.03 (6,473.20)	2,001.52 (6,566.67)	-28.49 (-93.47)	2,751.91 (9,028.58)	2,741.10 (8,993.11)	10.81 (35.47)
Flight Path Angle, deg	22.807	23.153	-0.346	18.946	19.545	-0.599
Heading Angle, deg	76.461	76.217	0.244	75.538	75.360	0.178
Cross Range, km (n mi)	0.23 (0.12)	0.17 (0.09)	0.06 (0.03)	0.60 (0.32)	0.33 (0.18)	0.27 (0.14)
Cross Range Velocity, m/s (ft/s)	10.49 (34.42)	4.21 (13.81)	6.28 (20.61)	17.89 (58.69)	9.08 (29.79)	8.81 (28.90)
	S-1I CECO (ENGINE SOLENOID)			S-1I OECD (ENGINE SOLENOID)		
Range Time, sec	460.61	459.21	1.40	552.64	554.13	-1.49
Altitude, km (n mi)	179.00 (96.65)	180.43 (97.42)	-1.43 (-0.77)	187.43 (101.20)	188.32 (101.68)	-0.89 (-0.48)
Surface Range, km (n mi)	1,109.50 (599.08)	1,102.86 (595.50)	6.64 (3.58)	1,636.56 (883.67)	1,646.50 (889.04)	-9.94 (-5.37)
Space-Fixed Velocity, m/s (ft/s)	5,678.47 (18,630.15)	5,667.07 (18,592.75)	-11.40 (-37.40)	6,898.24 (22,632.02)	6,911.46 (22,675.39)	-13.22 (-43.37)
Flight Path Angle, deg	1.029	0.864	0.165	0.741	0.735	0.006
Heading Angle, deg	79.585	79.612	-0.027	82.458	82.544	-0.086
Cross Range, km (n mi)	15.89 (8.58)	15.02 (8.11)	0.87 (0.47)	28.68 (15.49)	28.76 (15.53)	-0.08 (-0.04)
Cross Range Velocity, m/s (ft/s)	109.59 (359.55)	114.99 (377.26)	-5.40 (-17.71)	172.16 (564.83)	176.64 (579.53)	-4.48 (-14.70)
	S-1VB 1ST GUIDANCE CUTOFF SIGNAL			S-1VB 2ND GUIDANCE CUTOFF SIGNAL		
Range Time, sec	703.76	703.48	0.28	9,550.58	9,548.64	1.94
Altitude, km (n mi)	191.47 (103.39)	191.50 (103.40)	-0.03 (-0.01)	319.81 (172.68)	317.02 (171.18)	2.79 (1.50)
Surface Range, km (n mi)	2,650.21 (1,431.00)	2,649.29 (1,430.50)	0.92 (0.50)			
Space-Fixed Velocity, m/s (ft/s)	7,791.42 (25,562.40)	7,791.35 (25,562.17)	0.07 (0.23)	10,846.56 (35,585.83)	10,849.12 (35,594.23)	-2.56 (-8.40)
Flight Path Angle, deg	-0.0064	-0.0002	-0.0062	6.927	6.867	0.060
Heading Angle, deg	88.497	88.483	0.014	61.258	61.301	-0.043
Cross Range, km (n mi)	62.10 (33.53)	62.12 (33.54)	-0.02 (-0.01)			
Cross Range Velocity, m/s (ft/s)	275.31 (903.25)	274.12 (899.34)	1.19 (3.91)			
Eccentricity				0.97688	0.97698	-0.00010
C_3^* , m^2/s^2 (ft^2/s^2)				-1,396,436 (-15,031,112)	-1,390,603 (-14,968,326)	-5833 (-62,786)
Inclination, deg				31.701	31.693	0.008
Descending Node, deg				123.511	123.536	-0.025

* C_3 is twice the specific energy of orbit

$$C_3 = v^2 - \frac{2\mu}{R}$$

where v = Inertial Velocity
 μ = Gravitational Constant
 R = Radius vector from center of earth

Table 4-3. Comparison of Separation Events

PARAMETER	ACTUAL	NOMINAL	ACT-NOM
	S-IC/S-II SEPARATION		
Range Time, sec	162.31	160.91	1.40
Altitude, km (n mi)	65.89 (35.58)	66.43 (35.87)	-0.54 (-0.29)
Surface Range, km (n mi)	94.88 (51.23)	92.85 (50.13)	2.03 (1.10)
Space-Fixed Velocity, m/s (ft/s)	2,759.29 (9,052.79)	2,750.70 (9,024.61)	8.59 (28.18)
Flight Path Angle, deg	18.848	19.444	-0.596
Heading Angle, deg	75.538	75.355	0.183
Cross Range, km (n mi)	0.61 (0.33)	0.33 (0.18)	0.28 (0.15)
Cross Range Velocity, m/s (ft/s)	18.05 (59.22)	9.20 (30.18)	8.85 (29.04)
Geodetic Latitude, deg N	28.883	28.879	0.004
Longitude, deg E	-79.694	-79.714	0.020
S-II/S-IVB SEPARATION			
Range Time, sec	553.50	555.04	-1.54
Altitude, km (n mi)	187.51 (101.25)	188.40 (101.73)	-0.89 (-0.48)
Surface Range, km (n mi)	1,642.05 (886.64)	1,652.19 (892.11)	-10.14 (-5.47)
Space-Fixed Velocity m/s (ft/s)	6,900.65 (22,639.93)	6,914.90 (22,686.68)	-14.25 (-46.75)
Flight Path Angle, deg	0.730	0.725	0.005
Heading Angle, deg	82.490	82.577	-0.087
Cross Range, km (n mi)	28.83 (15.57)	28.92 (15.62)	-0.09 (-0.05)
Cross Range Velocity, m/s (ft/s)	172.65 (566.44)	177.13 (581.14)	-4.48 (-14.70)
Geodetic Latitude, deg N	31.925	31.939	-0.014
Longitude, deg E	-63.965	-63.858	-0.107
S-IVB/CSM SEPARATION			
Range Time, sec	10,962.4	11,004.9	-42.5
Altitude, km (n mi)	6,486.86 (3,502.63)	6,722.07 (3,629.63)	-235.21 (-127.00)
Space-Fixed Velocity, m/s (ft/s)	7,787.25 (25,548.72)	7,715.38 (25,312.93)	71.87 (235.79)
Flight Path Angle, deg	43.93	44.45	-0.52
Heading Angle, deg	67.47	67.88	-0.41
Geodetic Latitude, deg N	22.967	23.359	-0.392
Longitude, deg E	-139.826	-138.933	-0.893

Table 4-4. Stage Impact Location

PARAMETER	ACTUAL	NOMINAL	ACT-NOM
S-IC STAGE IMPACT			
Range Time, sec	539.12	542.07	-2.95
Surface Range, km (n mi)	645.98 (348.80)	650.17 (351.06)	-4.19 (-2.26)
Cross Range, km (n mi)	9.96 (5.38)	7.69 (4.15)	2.27 (1.23)
Geodetic Latitude, deg N	30.188	30.217	-0.029
Longitude, deg E	-74.207	-74.172	-0.035
S-II STAGE IMPACT			
Range Time, sec	1,217.89	1,222.49	-4.60
Surface Range, km (n mi)	4,424.97 (2,389.29)	4,459.54 (2,407.96)	-34.57 (-18.67)
Cross Range, km (n mi)	144.35 (77.94)	147.44 (79.61)	-3.09 (-1.67)
Geodetic Latitude, deg N	31.522	31.457	0.065
Longitude, deg E	-34.512	-34.158	-0.354

4.3.5 S-IVB/IU Post Separation Trajectory

The S-IVB/IU was placed on a lunar slingshot trajectory close to nominal. This was accomplished by orienting the stage in a retrograde attitude (pitch = 194 degrees with respect to local horizontal, yaw = 0 degree, roll = 189 degrees) and applying a velocity increase along the positive X body axis. The velocity increase was derived from a combination of LOX dump, LH₂ vent, Auxiliary Propulsion System (APS) burn and J-2 engine propellant lead experiment. The engine propellant lead experiment consisted of a 273-second APS burn, a 9-second LOX lead and a 53-second LH₂ lead. The final APS burn was shortened in real time from 155 seconds to approximately 8 seconds based on updated LOX residuals which were not considered at the time preflight slingshot targeting was performed. A time history of the longitudinal velocity increase subsequent to Time

Table 4-5. Parking Orbit Insertion Conditions

PARAMETER	ACTUAL	NOMINAL	ACT-NOM
Range Time, sec	713.76	713.48	0.28
Altitude, km (n mi)	191.37 (103.33)	191.51 (103.41)	-0.14 (-0.08)
Space-Fixed Velocity, m/s (ft/s)	7,793.09 (25,567.88)	7,793.16 (25,568.11)	-0.07 (-0.23)
Flight Path Angle, deg	-0.0049	0.0010	-0.0059
Heading Angle, deg	88.933	88.918	0.015
Inclination, deg	32.546	32.545	0.001
Descending Node, deg	123.132	123.148	-0.016
Eccentricity	0.000086	0.000049	0.000037
Apogee*, km (n mi)	185.79 (100.32)	185.92 (100.39)	-0.13 (-0.07)
Perigee*, km (n mi)	184.66 (99.71)	185.28 (100.04)	-0.62 (-0.33)
Period, min	88.20	88.20	0.00
Geodetic Latitude, deg N	32.700	32.699	0.001
Longitude, deg E	-52.526	-52.537	0.011

*Based on a spherical earth of radius 6378.165 km (3443.934 n mi).

Base 8 (T_8) is presented in Figure 4-8 and Table 4-7 lists the velocity gained during the various portions of slingshot maneuver.

The S-IVB/IU closest approach of 3112 kilometers (1680 n mi) above the lunar surface occurred at 78.851 hours into the mission. The actual and nominal conditions at closest approach are presented in Table 4-8. The velocity of the S-IVB/IU relative to earth is presented in Figure 4-9. This illustrates how the influence of the moon's gravity imparted energy to the S-IVB/IU.

Some of the heliocentric orbit parameters of the S-IVB/IU are presented in Table 4-9. The same parameters for the earth's orbit are also listed for comparison.

- ① FIRST REVOLUTION
- ② SECOND REVOLUTION

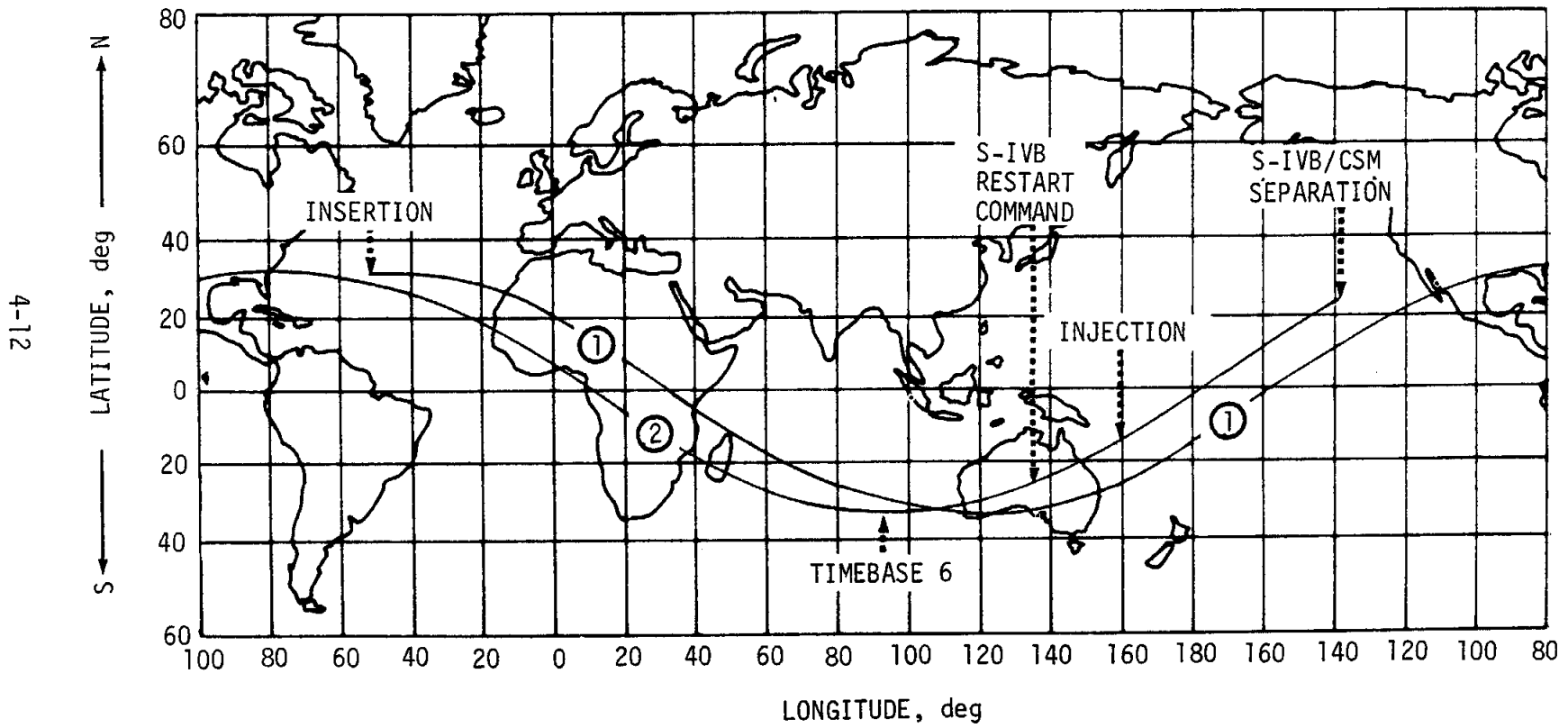


Figure 4-5. Ground Track

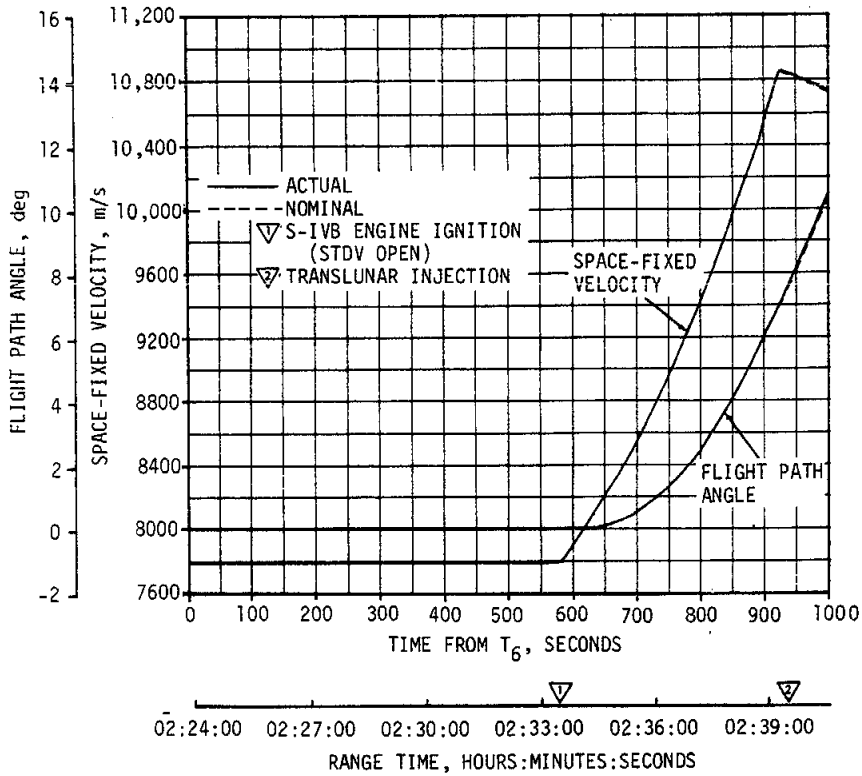


Figure 4-6. Injection Phase Space-Fixed Velocity and Flight Path Angle Comparisons

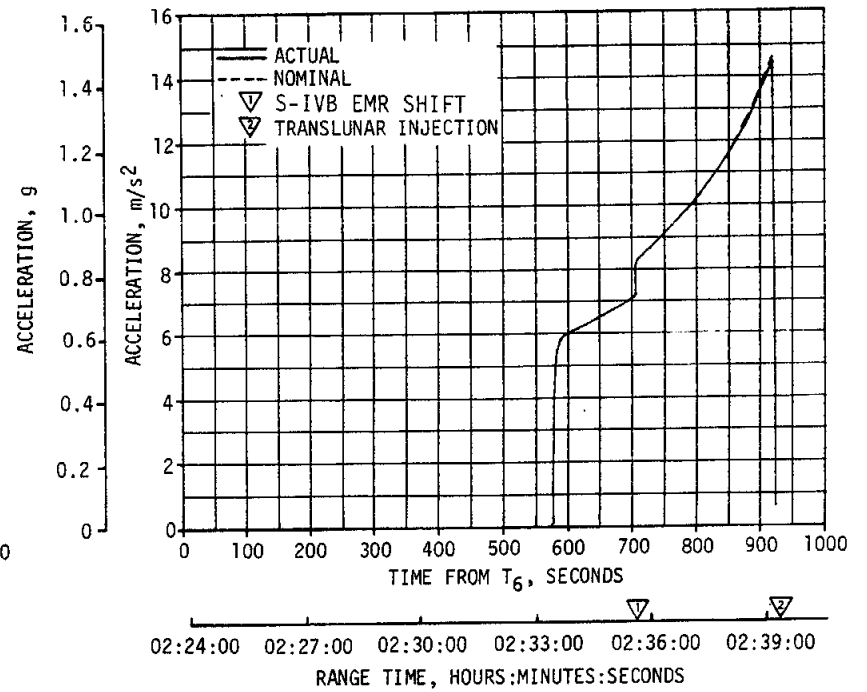


Figure 4-7. Injection Phase Acceleration Comparison

Table 4-6. Translunar Injection Conditions

PARAMETER	ACTUAL	NOMINAL	ACT-NOM
Range Time, sec	9,560.58	9,558.64	1.94
Altitude, km (n mi)	333.21 (179.92)	330.34 (178.37)	2.87 (1.55)
Space-Fixed Velocity, m/s (ft/s)	10,839.59 (35,562.96)	10,841.98 (35,570.80)	-2.39 (-7.84)
Flight Path Angle, deg	7.379	7.322	0.057
Heading Angle, deg	61.065	61.103	-0.038
Inclination, deg	31.698	31.691	0.007
Descending Node, deg	123.515	123.537	-0.022
Eccentricity	0.97834	0.97836	-0.00002
C_3 , m^2/s^2 (ft^2/s^2)	-1,308,471 (-14,084,267)	-1,307,603 (-14,074,922)	-868 (-9,345)

Table 4-7. Comparison of Slingshot Maneuver

PARAMETER	UNITS	ACTUAL ΔV	NOMINAL ΔV	TOLERANCES	
				-3 SIGMA	+3 SIGMA
Propellant Lead Experiment	m/s (ft/s)	13.4 (44.0)	13.8 (45.3)	-2 (-6.6)	+2 (+6.6)
LOX Dump	m/s (ft/s)	23.0 (75.5)	22.3 (73.2)	-10 (-32.8)	+10 (+32.8)
APS	m/s (ft/s)	\sim 0.3 (8 sec) (\sim 0.98)	6.2 (155 sec) (20.3)	\sim 0	\sim 0
Miscellaneous (CVS Performance and Hardware)	m/s (ft/s)	7.5 (24.6)	2.0 (6.6)	-11.0 (-36.1)	+11.0 (+36.1)
Total ΔV	m/s (ft/s)	44.2 (145.0)	44.3 (145.3)	-15.0 (-49.2)	+15.0 (+49.2)

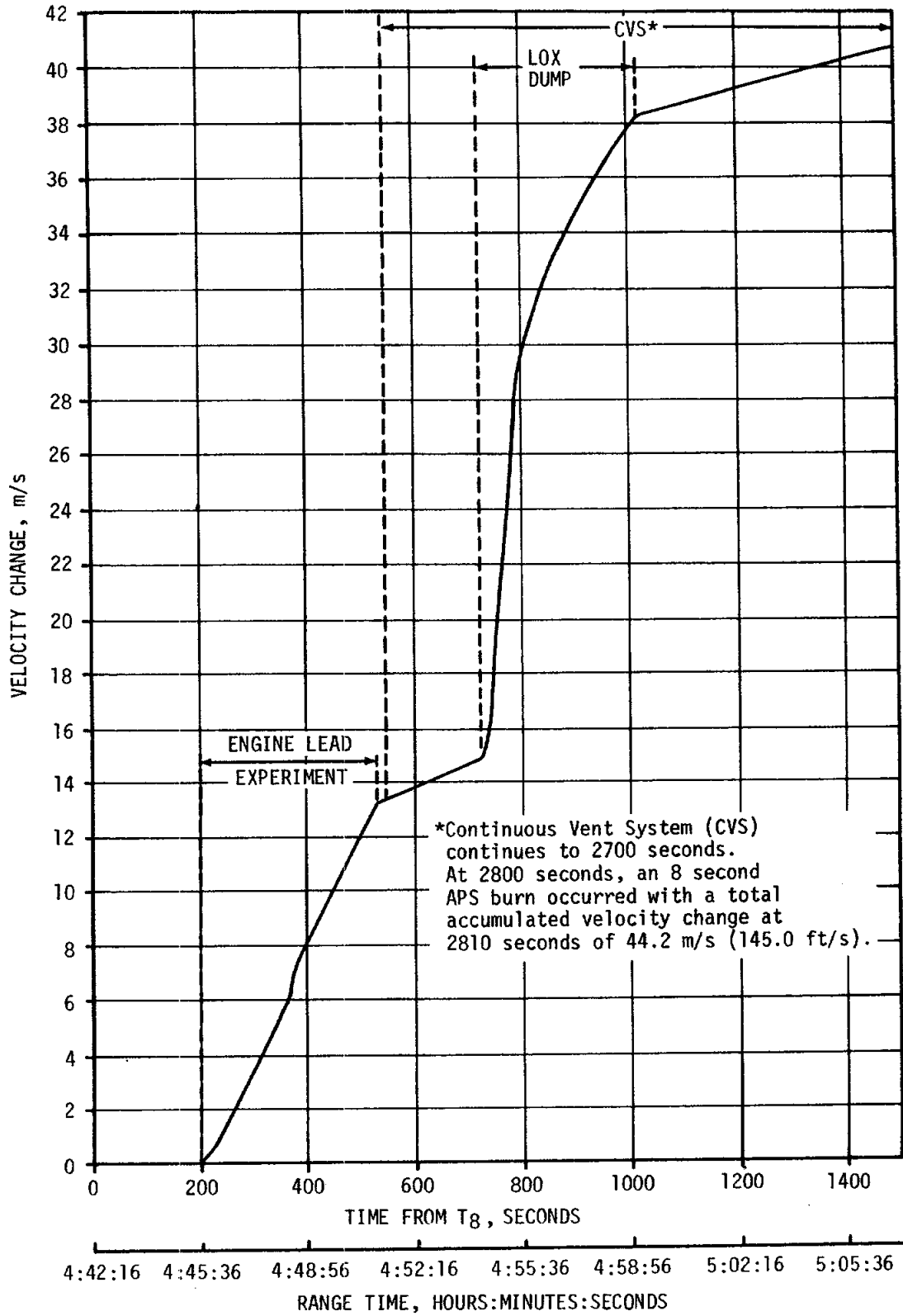


Figure 4-8. Velocity Increments Due to Slingshot Activity

Table 4-8. Lunar Close Approach Parameters

PARAMETER	UNITS	ACTUAL	NOMINAL
Lunar Radius of Closest Approach	km (n mi)	4850 (2619)	4748 (2564)
Altitude Above Lunar Surface	km (n mi)	3112 (1680)	3010 (1625)
Time from Launch	hr	78.9	78.5
Velocity Increase Relative to Earth, Due to Lunar Influence	km/s (n mi/s)	0.850 (0.459)	0.861 (0.465)

Table 4-9. Heliocentric Orbit Parameters

PARAMETER	UNITS	S-IVB/IU	EARTH
Semi-major Axis	km (n mi)	1.4398×10^8 (0.7774×10^8)	1.4900×10^8 (0.8045×10^8)
Aphelion	km (n mi)	1.5216×10^8 (0.8216×10^8)	1.5115×10^8 (0.8161×10^8)
Perihelion	km (n mi)	1.3581×10^8 (0.7333×10^8)	1.4684×10^8 (0.7929×10^8)
Inclination	deg	23.46	23.44
Period	days	344.88	365.25

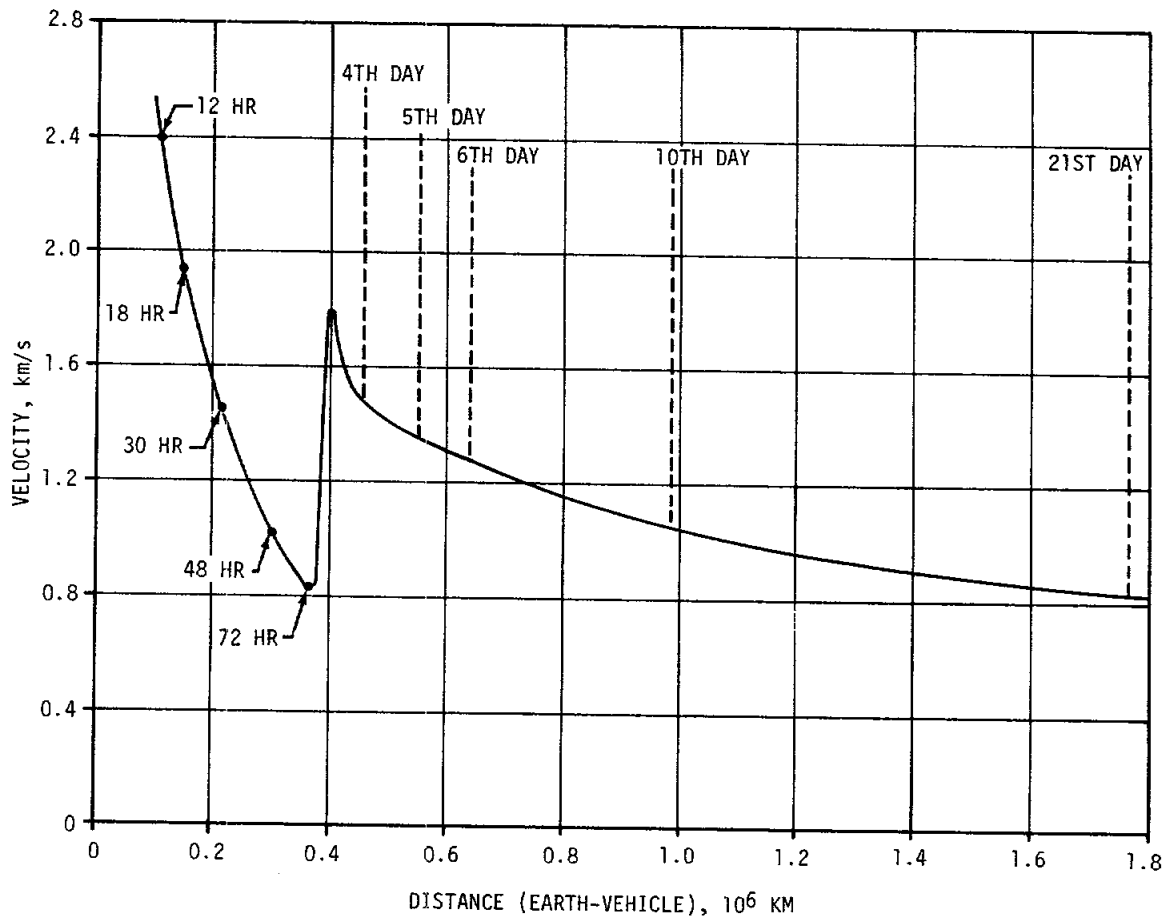


Figure 4-9. S-IVB/IU Velocity Relative to Earth Distance

SECTION 5

S-IC PROPULSION

5.1 SUMMARY

Unless otherwise stated, all predicted propulsion performance parameters used in this section are based on the latest prelaunch S-IC propulsion performance prediction, which was not incorporated in the Launch Vehicle Operational Flight Trajectory, dated April 17, 1969. The principal change in the latest S-IC propulsion prediction was in the predicted thrust levels of the five F-1 engines. This amounted to decreasing the thrusts used in the earlier predictions by approximately 40,000 Newtons (9000 lbf) per engine.

All S-IC propulsion systems performed satisfactorily. At the 35 to 38-second time slice, average engine thrust reduced to standard conditions was 0.20 percent lower than predicted. Average reduced specific impulse was 0.03 percent lower than predicted, and reduced propellant consumption rate was 0.158 percent lower than predicted. Although the average thrust deviation from predicted was small, engine No. 1 did run at a level of 6,611,000 Newtons (1,486,000 lbf) at the 35 to 38-second time slice, which was significantly lower than the predicted level of 6,708,000 Newtons (1,508,000 lbf).

Center Engine Cutoff (CECO) was initiated by the Instrument Unit (IU) at 135.16 seconds as planned. Outboard Engine Cutoff (OECO), initiated by LOX low level sensors, occurred at 161.63 seconds which was 1.43 seconds later than predicted in the Flight Trajectory. However, based on the latest S-IC propulsion prediction, OECO occurred only 0.63 second later than predicted. This is a small difference compared to the predicted 3 sigma limits of ± 7.05 seconds. The LOX residual at OECO was 18,412 kilograms (40,592 lbm) compared to the predicted 17,579 kilograms (38,756 lbm). The fuel residual at OECO was 12,944 kilograms (28,537 lbm) compared to the predicted 16,029 kilograms (35,338 lbm).

5.2 S-IC IGNITION TRANSIENT PERFORMANCE

The fuel pump inlet preignition pressure and temperature were 32.1 N/cm^2 (46.5 psia) and 278°K (40.7°F), respectively. These fuel pump inlet conditions were within the F-1 Engine Model Specification limits (start box requirements) as shown in Figure 5-1.

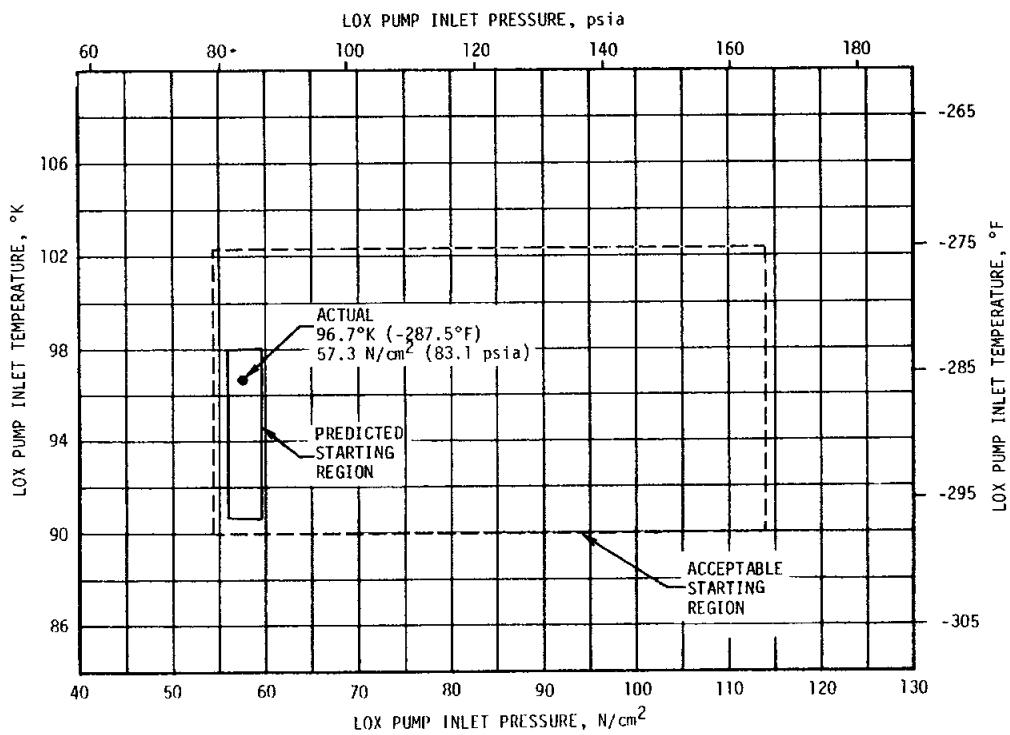
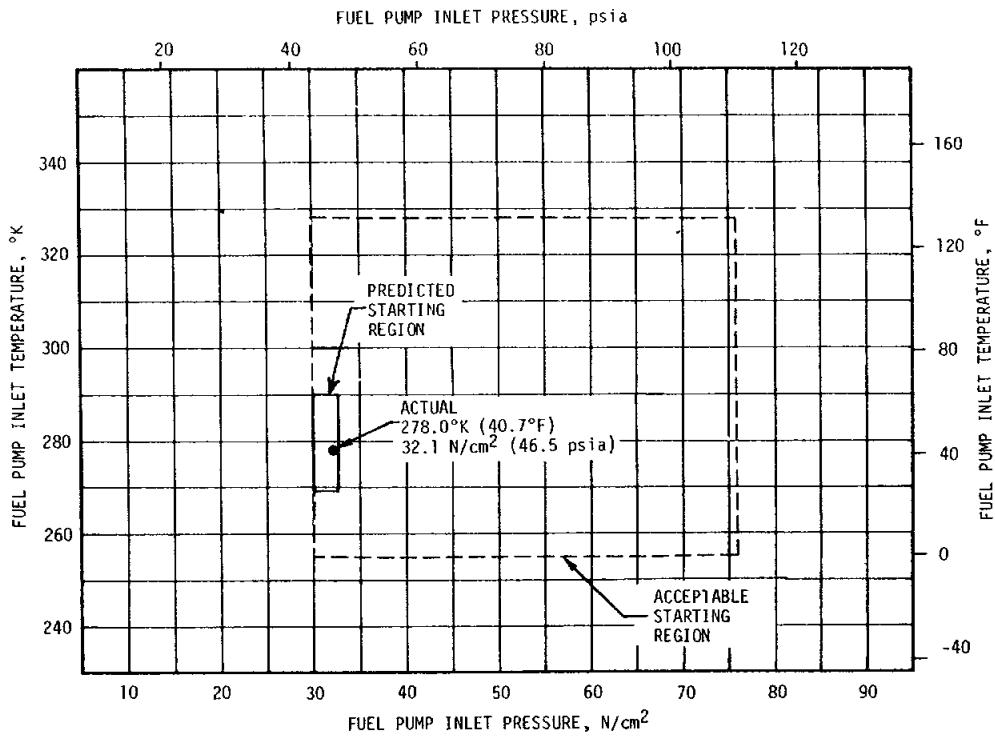


Figure 5-1. S-IC Start Box Requirements

The LOX pump inlet preignition pressure and temperature were 57.3 N/cm² (83.1 psia) and 96.7°K (-287.5°F), respectively. The LOX pump inlet conditions were also within the F-1 Engine Model Specification limits as shown in Figure 5-1.

Engine start-up sequence was nominal. A 1-2-2 start was planned and attained. Engine position starting order was 5, 3-1, 2-4. Two engines are considered to start together if their combustion chamber pressures reach 68.9 N/cm² (100 psig) in a 100-millisecond time period. Figure 5-2 shows the thrust buildup of each engine indicative of the successful 1-2-2 start.

All engines showed an 80-hertz thrust oscillation of approximately 445,000 Newtons (100,000 lbf) peak-to-peak amplitude during buildup (not shown in Figure 5-2). The oscillations began at the 1,550,000 Newton (350,000 lbf) level and had a duration of about 0.25 second. These oscillations are normal for F-1 engine thrust buildup and have been seen in static firings and previous flights. Data frequently fails to show these oscillations due to data filtering methods, but their presence is to be expected.

The best estimate of propellants consumed between ignition and hold-down arms release was 42,043 kilograms (92,689 lbf). The predicted consumption was 38,707 kilograms (85,333 lbf). The best estimate for liftoff propellant loads was 1,465,078 kilograms (3,229,944 lbf) for LOX and 636,593 kilograms (1,403,448 lbf) for fuel.

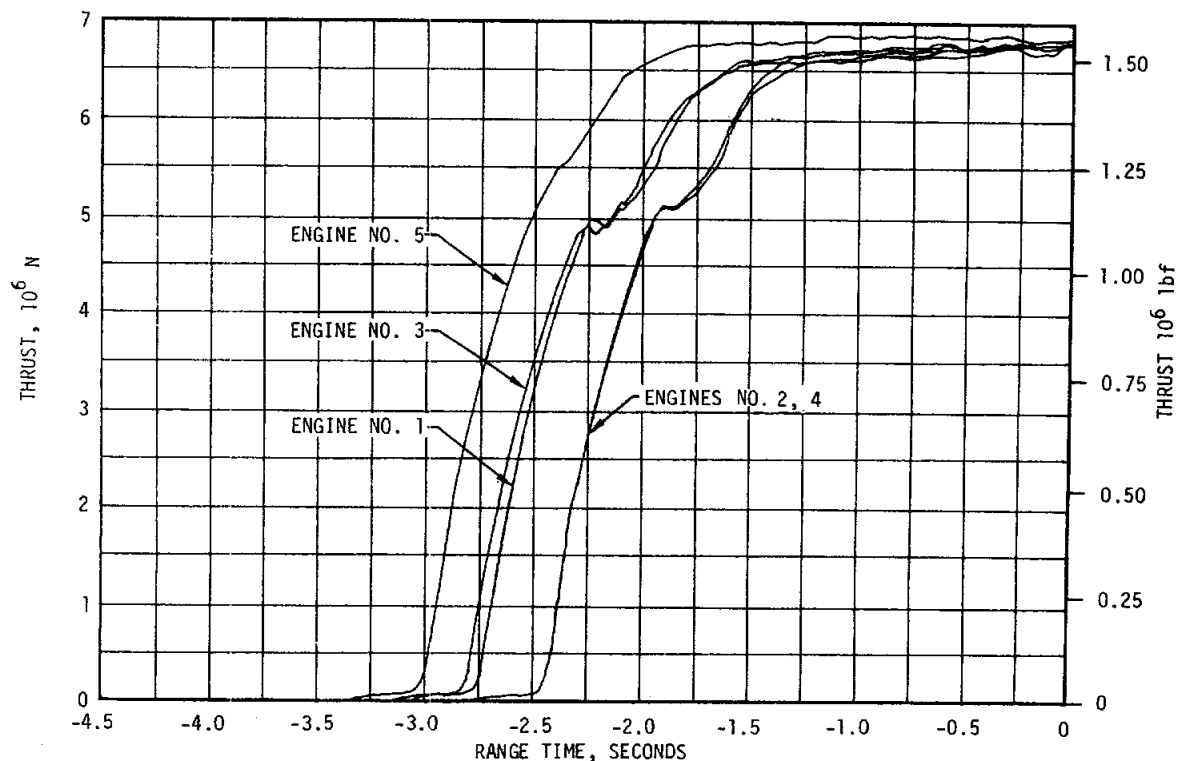


Figure 5-2. S-IC Engines Buildup Transients

5.3 S-IC MAINSTAGE PERFORMANCE

S-IC stage propulsion performance as determined by reconstruction was satisfactory. Site performance parameters and the nominal predictions are shown in Figure 5-3.

Individual engine parameters reduced to standard sea level conditions at the 35 to 38-second time slice are shown in Table 5-1. Individual engine deviations from predicted thrust ranged from 1.46 percent lower (engine No. 1) to 0.464 percent higher (engine No. 5). Individual engine deviations from predicted specific impulse ranged from 0.189 percent lower (engine No. 1) to 0.076 percent higher (engines No. 3 and 5). Reconstruction of engine No. 1 performance throughout the flight indicates that the engine reached its minimum thrust at approximately the 35 to 38-second time slice. The engine exhibited thrust climbout after the 35 to 38-second time slice, obtaining a maximum value of approximately 6,761,000 Newtons (1,520,000 lbf) at OECO which was close to the predicted value at that time. The performance of engine No. 1 caused no problems for the AS-505 flight.

Table 5-1. S-IC Engine Performance Deviations

PARAMETER	ENGINE	PREDICTED	RECONSTRUCTION ANALYSIS	DEVIATION PERCENT	AVERAGE DEVIATION PERCENT
Thrust 10 ³ N (10 ³ lbf)	1	6708 (1508)	6611 (1486)	-1.46	-0.20
	2	6748 (1517)	6739 (1515)	-0.132	
	3	6739 (1515)	6770 (1522)	0.462	
	4	6640 (1504)	6668 (1499)	-0.332	
	5	6703 (1507)	6735 (1514)	0.464	
Specific Impulse N-s/kg (lbf-s/lbm)	1	2588 (263.9)	2583 (263.4)	-0.189	-0.03
	2	2603 (265.4)	2602 (265.3)	-0.038	
	3	2596 (264.7)	2598 (264.9)	0.076	
	4	2586 (263.7)	2584 (263.5)	-0.076	
	5	2589 (264.0)	2591 (264.2)	0.076	
Total Flowrate kg/s (lbm/s)	1	2591 (5712)	2559 (5643)	-1.21	-0.158
	2	2593 (5717)	2591 (5712)	-0.087	
	3	2596 (5724)	2607 (5746)	0.384	
	4	2588 (5706)	2581 (5690)	-0.280	
	5	2590 (5709)	2600 (5732)	0.403	
Mixture Ratio LOX/Fuel	1	2.273	2.267	-0.264	-0.132
	2	2.267	2.264	-0.132	
	3	2.266	2.264	-0.088	
	4	2.273	2.269	-0.176	
	5	2.279	2.279	0	

NOTE: Analysis was reduced to standard sea level and pump inlet conditions at 35 to 38 seconds.

5-5

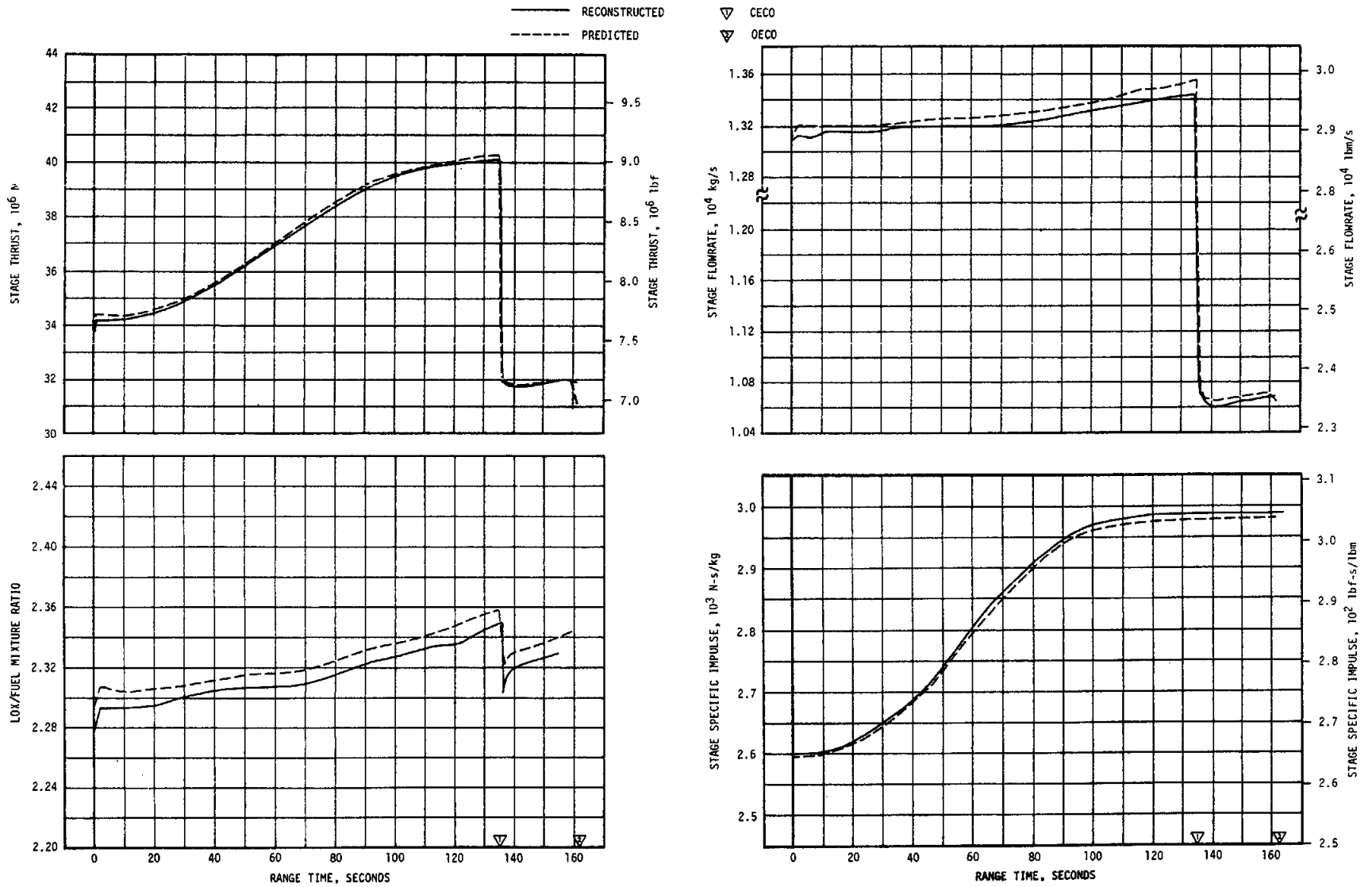


Figure 5-3. S-IC Stage Propulsion Performance

5.4 S-IC ENGINE SHUTDOWN TRANSIENT PERFORMANCE

CECO was initiated by a signal from the IU at 135.16 seconds as planned. OECO was initiated by LOX low level sensors and occurred 1.43 seconds later than the predicted time of 160.20 seconds that was used in the Final Flight Trajectory. This time is well within the 3 sigma range for OECO of ± 7.05 seconds. However, based on the latest prelaunch S-IC propulsion prediction, OECO occurred only 0.63 second later than predicted.

Thrust decay of the F-1 engines was nominal. The total impulse from OECO to separation was 10,530,035 N-s (2,367,247 lbf-s) which was well within the 3 sigma limits.

5.5 S-IC STAGE PROPELLANT MANAGEMENT

The S-IC does not have an active Propellant Utilization (PU) system. Minimum residuals are obtained by attempting to load the mixture ratio expected to be consumed by the engines plus the predicted unusable residuals. Also, a small additional amount of usable fuel (fuel bias) was loaded to minimize maximum residuals. An analysis of the usable residuals experienced during a flight is a good measure of the performance of the passive PU system. S-IC propellant residuals were within expected limits. Usable LOX residuals in the tank and suction ducts were approximately 748 kilograms (1650 lbm) more than predicted, as compared to 2540 kilograms (5600 lbm) more than predicted on AS-504. Approximately 1012 kilograms (2230 lbm) of usable fuel residuals were in the fuel tank at OECO. This was 3189 kilograms (7030 lbm) less than the fuel bias of 4200 kilograms (9260 lbm). A summary of the propellants remaining at major event times is presented in Table 5-2.

5.6 S-IC PRESSURIZATION SYSTEMS

5.6.1 S-IC Fuel Pressurization System

The fuel tank pressurization system performed satisfactorily keeping ullage pressure within acceptable limits during flight. Helium Flow Control Valves (HFCV's) No. 1 through No. 4 opened as planned and HFCV No. 5 was not required.

The low flow prepressurization system was commanded on at -97 seconds. High flow pressurization, accomplished by the onboard pressurization system, performed as expected. HFCV No. 1 was commanded on at -2.65 seconds and was supplemented by the high flow prepressurization system until umbilical disconnect.

Fuel tank ullage pressure was within the predicted limits throughout flight as shown in Figure 5-4. HFCV's No. 2, 3, and 4 were commanded open within acceptable limits during flight by the switch selector. Helium bottle pressure was 2110 N/cm² (3060 psia) at -2.75 seconds and decayed to 331 N/cm² (480 psia) at OECO. Total helium flowrate and heat exchanger performance were as expected.

Table 5-2. S-IC Stage Propellant Mass History

EVENT	PREDICTED		LEVEL SENSOR DATA		RECONSTRUCTED		
	LOX	FUEL	LOX	FUEL	LOX	FUEL	
Ignition Command	kg (1bm)	1,498,856 (3,304,412)	647,122 (1,426,660)	NA* NA*	645,577 (1,423,254)	1,498,137 (3,302,827)	645,577 (1,423,254)
Holddown Arm Release	kg (1bm)	1,468,474 (3,237,432)	638,797 (1,408,307)	1,464,974 (3,229,714)	637,054 (1,404,463)	1,465,078 (3,229,944)	636,594 (1,403,448)
CECO	kg (1bm)	211,087 (465,367)	98,730 (217,663)	216,081 (476,378)	98,444 (217,033)	216,491 (477,281)	97,976 (216,000)
OECO	kg (1bm)	17,579 (38,756)	16,029 (35,338)	18,347 (40,448)	12,874 (28,383)	18,412 (40,592)	12,944 (28,537)
Separation	kg (1bm)	15,326 (33,787)	14,946 (32,950)	-- --	-- --	16,037 (35,356)	11,815 (26,047)
Zero Thrust	kg (1bm)	15,018 (33,110)	14,650 (32,299)	-- --	-- --	15,760 (34,745)	11,497 (25,346)

NOTE: Predicted and reconstructed values do not include pressurization gas so they will compare with level sensor data.

* Not available because the LOX was above the level sensors at this time.

Fuel pump inlet pressure was maintained above the required Net Positive Suction Pressure (NPSP) during flight.

5.6.2 S-IC LOX Pressurization System

The LOX pressurization system performed satisfactorily and met all performance requirements. The ground prepressurization system maintained ullage pressure within acceptable limits until launch commit. The on-board pressurization system subsequently maintained ullage pressure within the GOX Flow Control Valve (GFCV) band during the flight. The heat exchangers performed as expected.

The prepressurization system was initiated at -71.99 seconds. Ullage pressure increased until it entered the prepressurization switch band zone which terminated the flow at -57.69 seconds. The low flow system was cycled on two additional times at -39.60 and -12.84 seconds. The high flow system was commanded on at -4.69 seconds and maintained ullage pressure within acceptable limits until launch commit.

The LOX tank ullage pressure, shown in Figure 5-5, was maintained within the required limits throughout flight by the GFCV. The maximum GOX flow-rate (at CECO) was 24.9 kg/s (55.0 lbm/s).

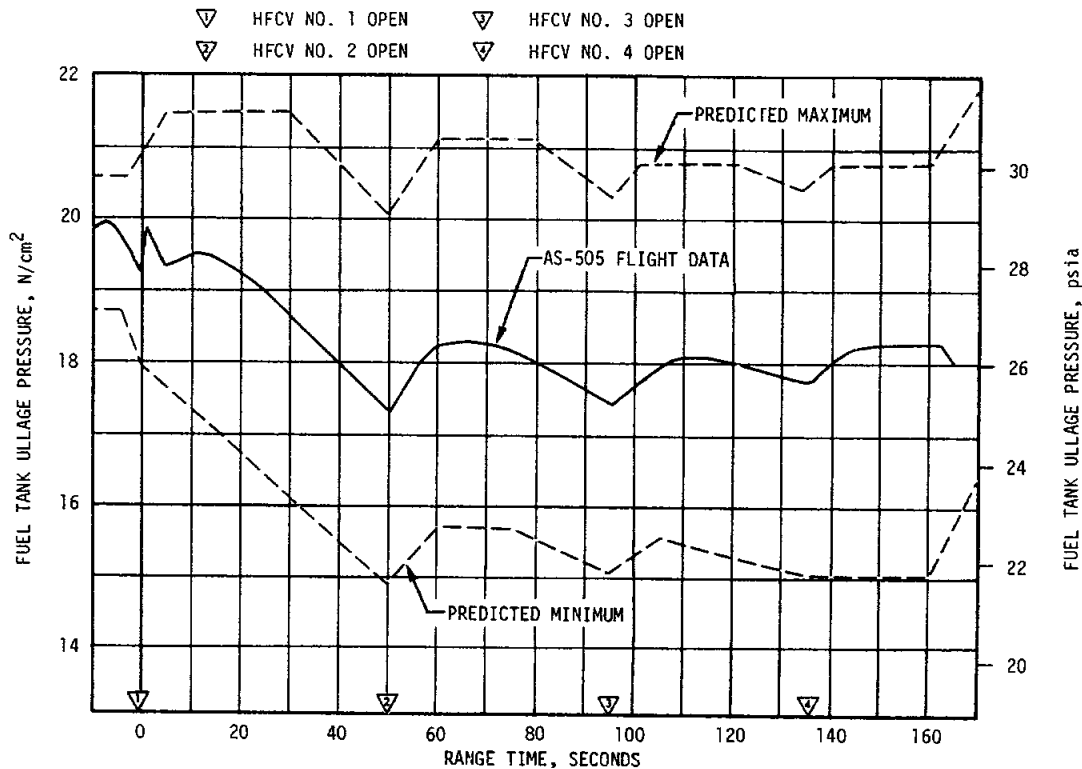


Figure 5-4. S-IC Fuel Ullage Pressure

The LOX pump inlet pressure met the NPSP requirements throughout flight. Engine No. 5 LOX suction duct pressure decayed after CECO as shown in Figure 5-6. The pressure decay rate was $1.38 N/cm^2/s$ ($2.0 psi/s$) and was similar to the decay on AS-503 ($1.65 N/cm^2/s$ [$2.4 psi/s$]) and AS-504 ($1.38 N/cm^2/s$ [$2.0 psi/s$]). The cause of this decay is unknown.

5.7 S-IC PNEUMATIC CONTROL PRESSURE SYSTEM

The control pressure system functioned satisfactorily throughout the S-IC flight.

Sphere pressure was $2130 N/cm^2$ ($3090 psia$) at liftoff and remained steady until CECO when it decreased to $2055 N/cm^2$ ($2980 psia$). The decrease was due to center engine prevalve actuation. There was a further decrease to $1782 N/cm^2$ ($2585 psia$) after OECO. Pressure downstream of the regulator initially read $530 N/cm^2$ ($768 psia$) and decreased to $520 N/cm^2$ ($755 psia$) at 160 seconds. Regulator performance was within limits. There were slight dips in outlet pressure at CECO and OECO due to prevalve actuation. These dips are to be expected.

The engine prevalves were closed after engine cutoff as required. Engine No. 5 prevalves closed at approximately 137 seconds. The prevalves for the other four engines closed at approximately 163.7 seconds.

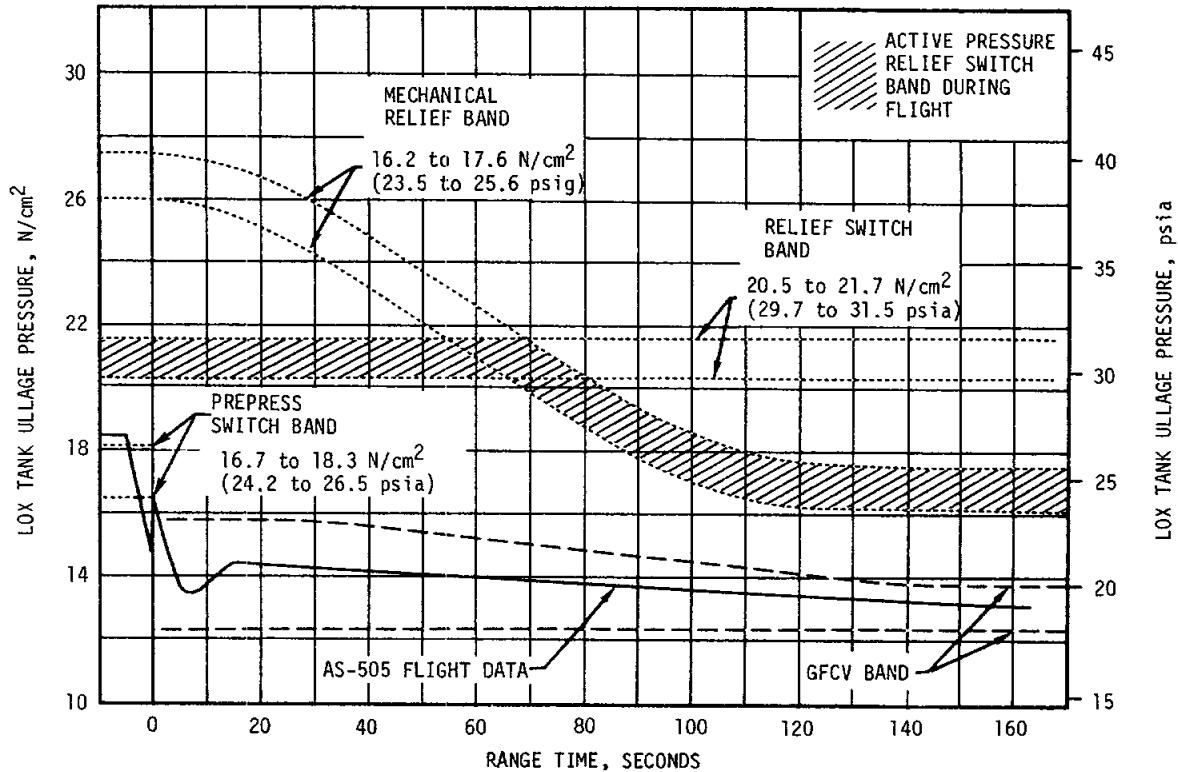


Figure 5-5. S-IC LOX Tank Ullage Pressure

5.8 S-IC PURGE SYSTEMS

Performance of the S-IC purge systems was satisfactory during the 162-second flight.

The turbopump LOX seal storage sphere pressure was within the limits of 1903 to 2275 N/cm² (2760 to 3300 psig) until ignition, and 2275 to 689 N/cm² (3300 to 1000 psig) from liftoff to cutoff. Regulator outlet pressure remained within the 59 ± 7 N/cm² (85 ± 10 psig) limits. Turbopump LOX seal pressure at the engine interface was within the required limits of 69 N/cm² (100 psig) maximum to 21 N/cm² (30 psig) minimum. The radiation calorimeter purge operated satisfactorily throughout flight.

5.9 POGO SUPPRESSION SYSTEM

The POGO suppression system performed satisfactorily prior to and during S-IC flight. The system was initially turned on approximately 26 minutes prior to launch to be sure the prevalues would fill with helium. Redline measurements indicated that the four outboard lines filled as scheduled.

The pressure measurement downstream of the solenoid valves indicated that flow was properly established in the system. Eleven minutes prior to launch, the system was turned on again and flow was established. The temperature measurements did not change since the system still contained helium

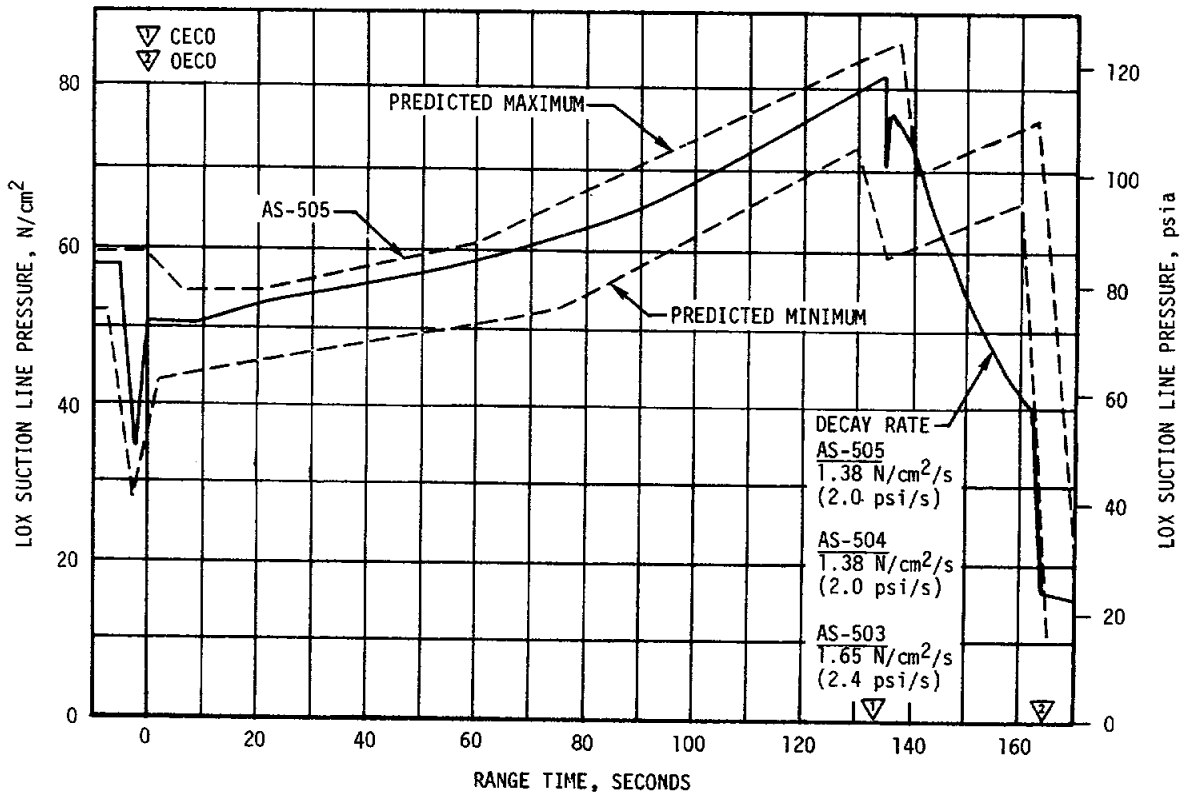


Figure 5-6. S-IC Center Engine LOX Suction Line Pressure

from the earlier initiation. The four resistance thermometers performed as expected during flight. In the outboard lines, the three upper measurements went cold momentarily at liftoff, indicating that the LOX level shifted on the probes. The probes remained warm throughout flight, indicating helium in the prevalues. Figure 5-7 shows a plot of liquid level in the prevalue. At cutoff, the increased pressure forced LOX into the prevalues. The fourth resistance thermometer, at the lip of the valve cavity, was cold throughout flight as expected.

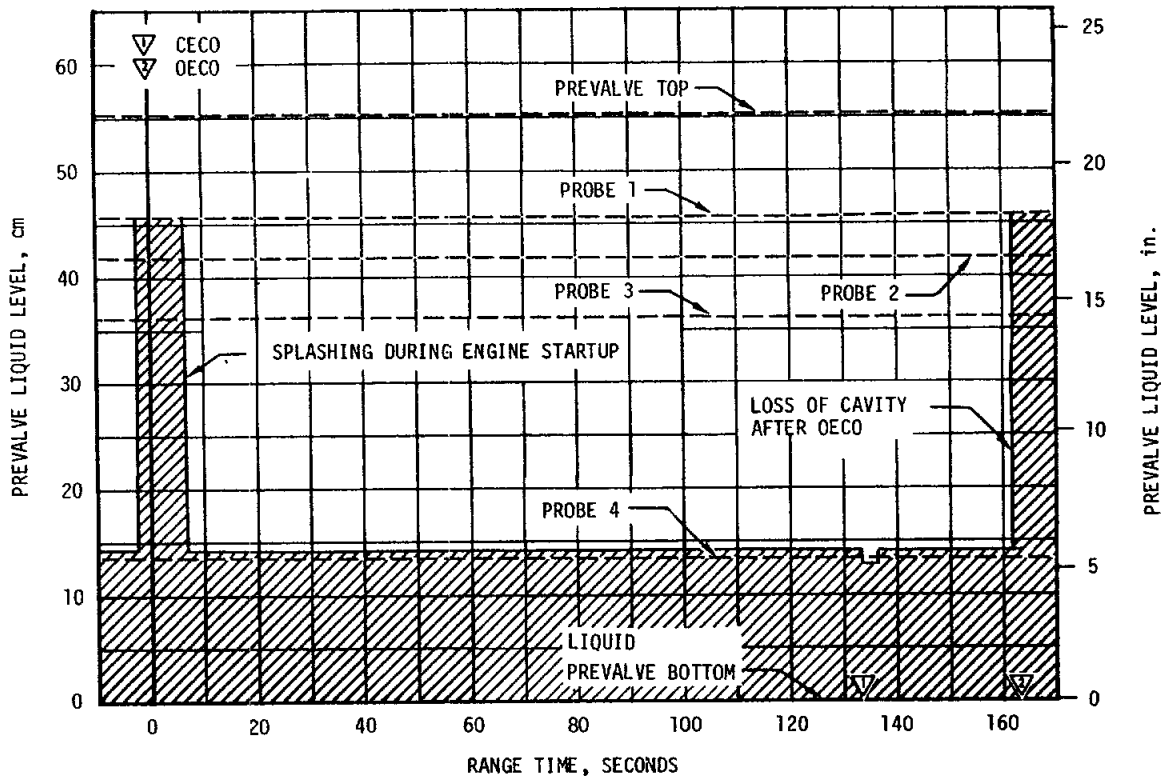


Figure 5-7. S-IC Prevalve Liquid Level, Typical Outboard Engine

SECTION 6

S-II PROPULSION

6.1 SUMMARY

The S-II propulsion system performed satisfactorily throughout the flight. As sensed by the engines, Engine Start Command (ESC) occurred at 163.05 seconds and Outboard Engine Cutoff (OECO) at 552.64 seconds with a burn time of 389.59 seconds or 1.70 seconds longer than predicted. The predicted propulsion performance parameters used in this section are based on a revised prelaunch S-II propulsion performance prediction, which was not incorporated in the AS-505 Launch Vehicle Operational Flight Trajectory (dated April 17, 1969). Due to center engine low frequency performance oscillations on the two previous flights, the center engine was shut down early on AS-505 successfully avoiding these oscillations. Center Engine Cutoff (CECO) occurred at 460.61 seconds. Total stage thrust, as determined by computer analysis of telemetered propulsion measurements at 61 seconds after S-II ESC was 0.35 percent below predicted. Total engine propellant flowrate (excluding pressurization flow) was 0.43 percent below predicted and average specific impulse was 0.09 percent above predicted at this time slice. Average Engine Mixture Ratio (EMR) was 0.18 percent below predicted.

The propellant management system met all performance requirements. The system differed from AS-504 by using open-loop control of the engine Propellant Utilization (PU) valves. Open-loop control was utilized on AS-503 and is planned for all subsequent flights. The PU valve movement resulted in an actual EMR shift at 488.48 seconds. OECO, initiated by the LOX low level cutoff sensors, was achieved following a planned 1.5-second time delay. A small engine performance decay was noted just prior to cutoff but was less severe than that observed on AS-504 due to only four engines burning at cutoff. Residual propellant remaining in the tanks at OECO signal were 2789 kilograms (6150 lbm) compared to a prediction of 2622 kilograms (5782 lbm).

The performance of the LOX and LH₂ tank pressurization systems was satisfactory. Ullage pressure in both tanks was more than adequate to meet engine inlet Net Positive Suction Pressure (NPSP) requirements throughout mainstage. As commanded by the Instrument Unit (IU), step pressurization occurred at 261.62 seconds for the LOX tank and 461.61 seconds for the LH₂ tank. The recirculation, engine servicing, pneumatic control and helium injection systems all performed satisfactorily.

6.2 S-II CHILLDOWN AND BUILDUP TRANSIENT PERFORMANCE

The prelaunch servicing operations satisfactorily accomplished the engine conditioning requirements. Thrust chamber temperatures were within predicted limits at launch and engine start. The thrust chamber temperatures ranged between 113 and 133°K (-256 and -221°F) at -187 seconds, 92 and 113°K (-294 and -256°F) at prelaunch commit and 124 and 145°K (-236 and -198°F) at engine start. Thrust chamber warmup rates during S-IC boost agreed closely with those experienced on previous flights.

Both temperature and pressure conditions of the J-2 engine start tanks were within the required prelaunch and engine start boxes as shown in Figure 6-1. Start tank temperatures at prelaunch and engine start averaged 13°K (23°F) warmer than on AS-504 as a result of the start tank servicing facility vent line modification. (The vent line flow area was increased by adding a 3.81 centimeter (1.5 in.) diameter line parallel to the existing vent line.) Results of this vent line change were highly satisfactory in that the increased flow area permitted a higher flowrate, and thus less cooling of the start tank prechill gas passing through the Ground Support Equipment (GSE) LH₂ heat exchanger. During S-IC boost, start tank pressure increase rates due to heatup averaged 3.4 N/cm²/min (5 psi/min) less than AS-504 results.

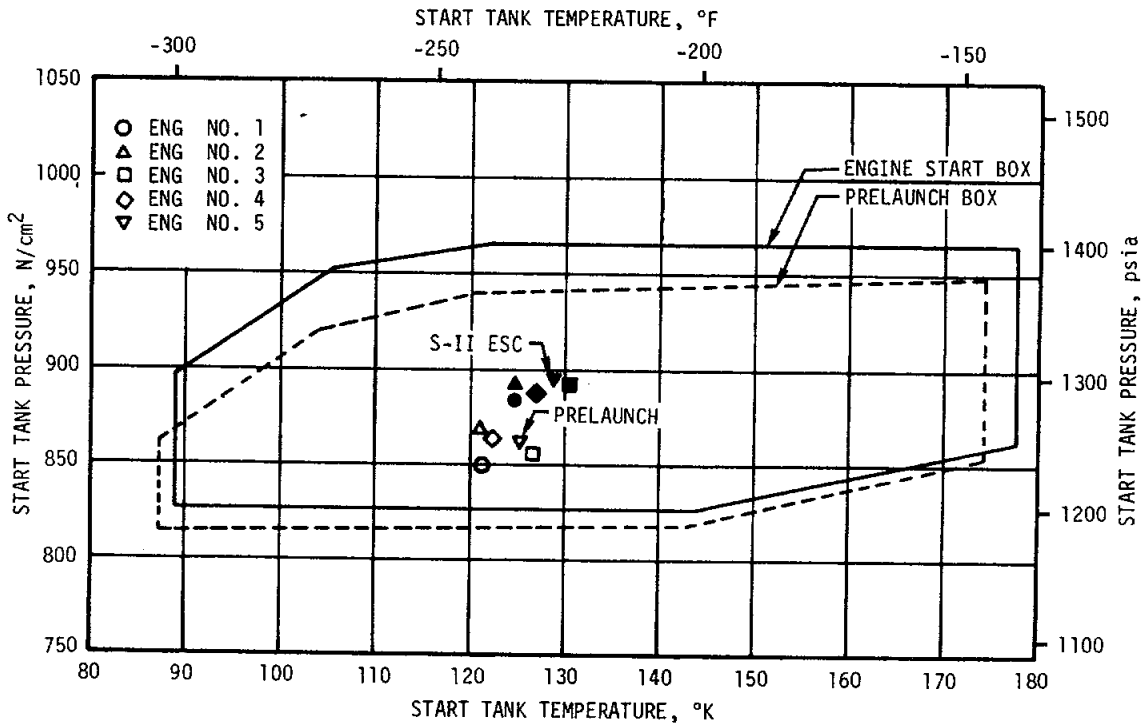


Figure 6-1. S-II Engine Start Tank Performance

All engine helium tank pressures were within the required prelaunch and engine start limits of 1931 to 2379 N/cm² (2800 to 3450 psia).

During flight, engine No. 5 regulator outlet pressure shifted from 281 to 276 N/cm² (408 to 400 psia) after approximately 63 seconds of S-II engine operation. Regulator operating range is 276 ±17.2 N/cm² (400 ±25 psia). The engine helium tank pressure also showed a change in decay rate at the same time the regulator shift occurred. Prior to the pressure regulator shift, the engine No. 5 helium tank pressure decay rate was 3.8 N/cm²/s (5.5 psi/s) compared to the other engines decay rate of about 1.9 N/cm²/s (2.8 psi/s). Subsequent to the shift the helium tank pressure decay rate was 0.57 N/cm²/s (0.83 psi/s) which is comparable to the decay rate of the other engines during the same time period. Even if the initial decay rate had been sustained throughout S-II burn, the supply pressure would have been sufficient to meet system demand.

A similar engine helium regulator shift occurred on engine No. 3 during AS-504 flight. The regulator outlet pressure shifted from 279 to 276 N/cm² (405 to 400 psia) after approximately 43 seconds of engine operation. Engine No. 3 helium tank pressure also showed a change in decay rate at the same time the regulator shift occurred. Prior to the shift the decay rate was 4.2 N/cm²/s (6.1 psi/s) compared to about 1.9 N/cm²/s (2.8 psi/s) for the other engines. Subsequent to the shift, the helium tank pressure decay rate was 0.76 N/cm²/s (1.1 psi/s).

Regulator outlet pressure shifts also occurred on AS-501 and AS-502 flights, but the helium tank pressure decay rate did not change at the same time. The regulator shifts were not experienced on AS-503. The probable cause of these minor regulator shifts and changes in engine helium tank pressure decay rates is internal regulator leakage.

The LOX and LH₂ recirculation systems used to chill the feed ducts, turbo-pumps, and other engine components performed satisfactorily during pre-launch and S-IC boost. Engine pump inlet temperatures and pressures at engine start were well within the requirements as shown in Figure 6-2. The LOX pump discharge temperatures at ESC were 6.2 to 7.3°K (11.2 to 13.2°F) subcooled, which is well below the 1.7°K (3°F) subcooling requirement.

Prepressurization of the propellant tanks was satisfactorily accomplished. Ullage pressures at S-II ESC were 26.9 N/cm² (39 psia) for LOX and 19.3 N/cm² (28 psia) for LH₂.

S-II ESC was received at 163.05 seconds and the Start Tank Discharge Valve (STDV) solenoid activation signal occurred 1.0 second later. The engine thrust buildup was satisfactory and was within the required thrust buildup envelope. The stage thrust reached mainstage level at 166.30 seconds. Engine thrust levels were between 854,059 and 898,541 Newtons (192,000 and 202,000 lbf) prior to "High EMR Select" command at 168.50 seconds.

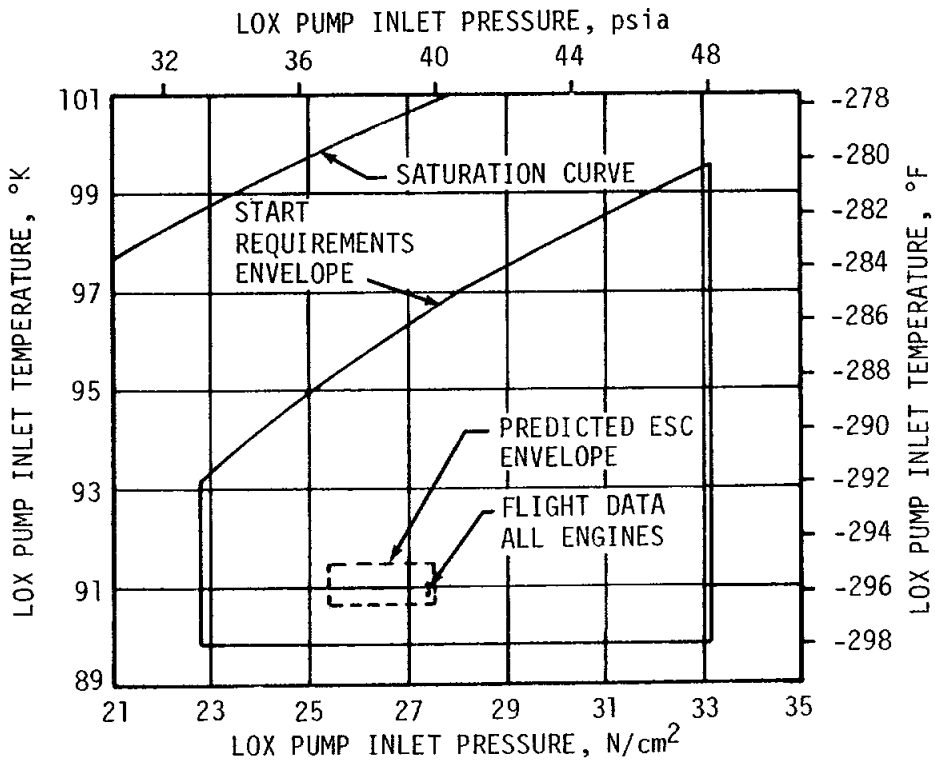
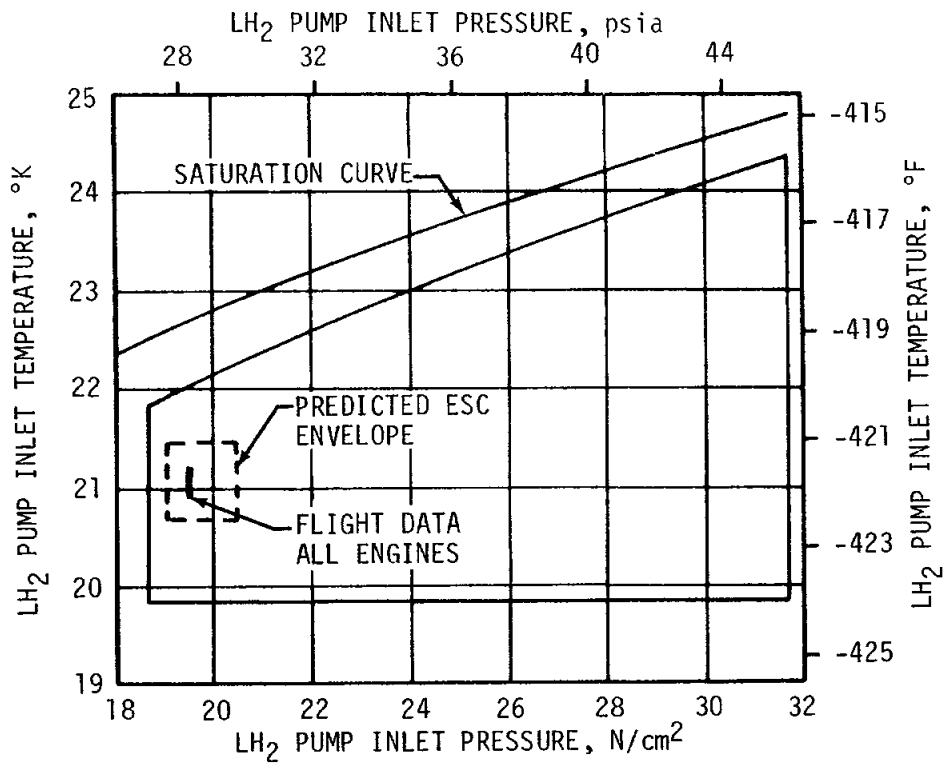


Figure 6-2. S-II Engine Pump Inlet Start Requirements

6.3 S-II MAINSTAGE PERFORMANCE

Stage performance during both the high and low EMR portions of the flight was very close to predicted as shown in Figure 6-3. At the ESC +61-second time slice, total vehicle thrust was 5,157,611 Newtons (1,159,477 lbf) which is only 18,064 Newtons (4061 lbf) or 0.35 percent below the pre-flight prediction. Average engine specific impulse was 4165.2 N-s/kg (424.7 lbf-s/lbm) or 0.09 percent above the predicted level. Propellant flowrate to the engines (excluding pressurization flow) was 1238.3 kg/s (2729.9 lbm/s) which was 0.43 percent below prediction, and the average EMR was 5.56 or 0.18 percent below preflight prediction.

At ESC +297.56 seconds, the center engine was shut down in order to prevent buildup of the low frequency oscillations that were observed on AS-503 and AS-504. This action reduced total vehicle thrust by 1,044,060 Newtons (234,714 lbf) to a level of 4,103,720 Newtons (922,553 lbf). Of this total, 1,024,274 Newtons (230,266 lbf) were directly due to CECO and the remaining 19,786 Newtons (4448 lbf) resulted from the effect of fuel step pressurization and loss of acceleration head.

The PU system was operated in the open-loop control mode for the AS-505 flight. At approximately 325 seconds after ESC, engine thrust chamber pressures reacted to the PU control valve step from the high to low EMR position. The action further reduced total vehicle thrust to 3,090,002 Newtons (694,660 lbf) at ESC +350 seconds. A change in stage thrust of 1,013,576 Newtons (227,861 lbf) is indicated between high (5.47) and low (4.27) EMR operation. Unlike previous flights, the deviation of actual from predicted performance did not increase at the lower mixture ratio levels. Vehicle thrust and propellant flowrate deviations at ESC +388 seconds were -11,161 Newtons (-2509 lbf) and 1.8 kg/s (3.9 lbm/s), respectively.

Individual J-2 engine data, excluding the effects of pressurization flowrate, are presented in Table 6-1 for the ESC +61-second time slice. With the exception of engine No. 5, very good correlation between prediction and flight was indicated by the small deviations. Flight data reconstruction procedures were directed toward matching the engine and stage acceptance specific impulse values while maintaining the engine flow and pump speed data as a baseline.

Examination of engine No. 5 data indicated that the low performance level resulted from a large increase in Gas Generator (GG) LOX bootstrap line hydraulic resistance. This lower engine power level was maintained throughout the flight. During vehicle acceptance testing, this engine exhibited two short intervals of reduced performance of 20,017 and 14,679 Newtons (4500 and 3300 lbf) thrust. Following the static test operations, a complete inspection was performed of the GG injector, control valve and bootstrap line. No contamination, restrictions, or out-of-tolerance conditions were detected.

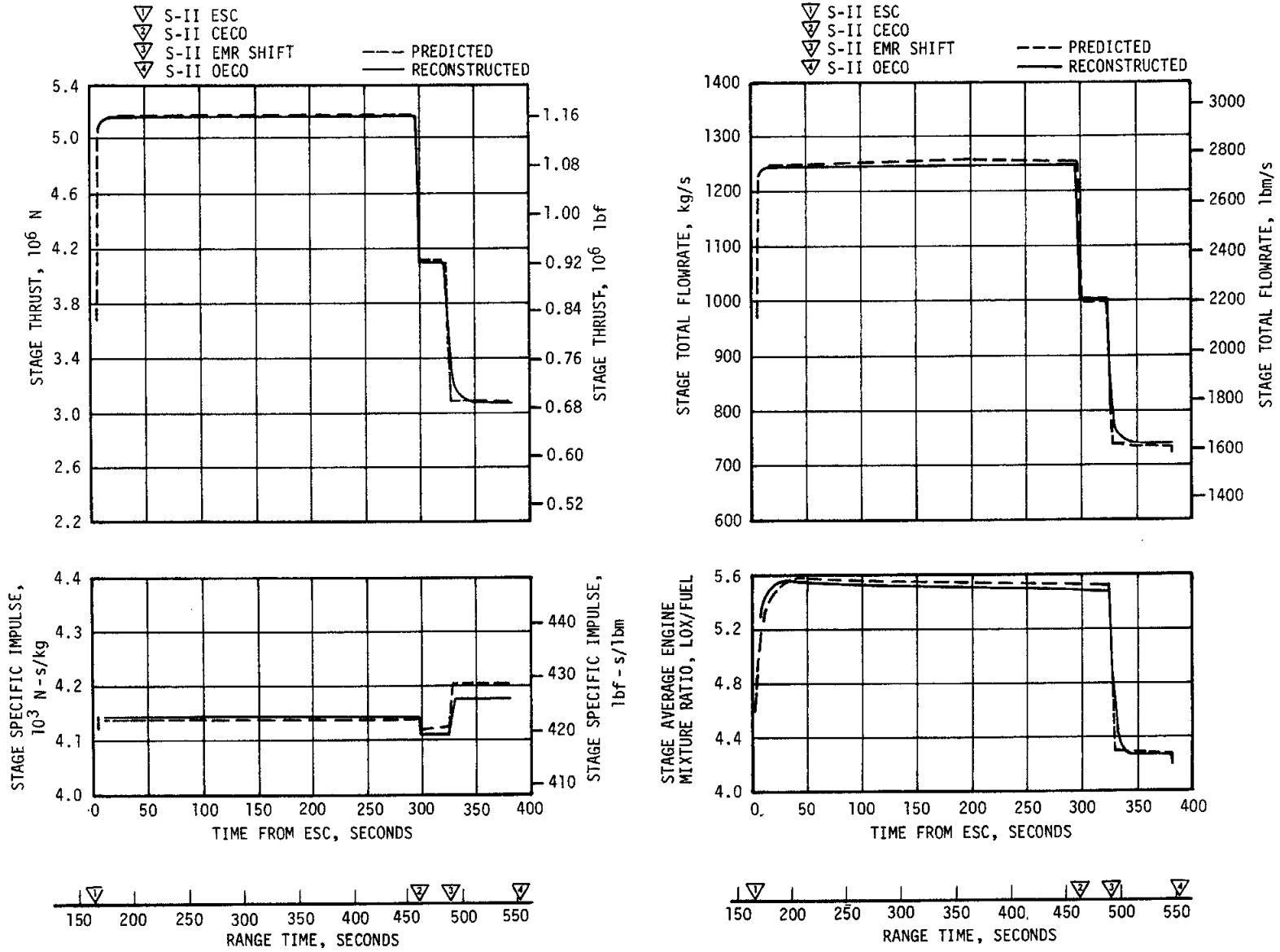


Figure 6-3. S-II Propulsion Performance

Table 6-1. S-II Engine Performance Deviations (ESC +61 Seconds)

PARAMETER	ENGINE	PREDICTED		RECONSTRUCTION ANALYSIS		PERCENT DEVIATION FROM PREDICTED	AVERAGE PERCENT DEVIATION FROM PREDICTED
Thrust, Newtons (lbf)	1	1,036,316	(232,973)	1,036,098	(232,924)	-0.02	-0.35
	2	1,032,704	(232,161)	1,027,855	(231,071)	-0.47	
	3	1,028,002	(231,104)	1,031,276	(231,840)	0.32	
	4	1,036,004	(232,903)	1,038,553	(233,476)	0.25	
	5	1,042,650	(234,397)	1,023,829	(230,166)	-1.81	
Specific Impulse, N-s/kg (lbf-s/lbm)	1	4161.9	(424.4)	4169.8	(425.2)	0.19	0.09
	2	4157.0	(423.9)	4162.9	(424.5)	0.14	
	3	4154.1	(423.6)	4152.1	(423.4)	-0.05	
	4	4161.9	(424.4)	4168.8	(425.1)	0.16	
	5	4172.7	(425.5)	4172.7	(425.5)	0	
Flowrate, kg/s (lbm/s)	1	249.0	(548.9)	248.5	(547.8)	-0.20	-0.43
	2	248.4	(547.7)	246.9	(544.3)	-0.62	
	3	247.5	(545.6)	248.4	(547.6)	0.37	
	4	248.9	(548.7)	249.2	(549.3)	0.11	
	5	249.9	(550.9)	245.3	(540.9)	-1.82	
Mixture Ratio, LOX/Fuel	1		5.58		5.53	-0.90	-0.18
	2		5.58		5.58	0	
	3		5.63		5.63	0	
	4		5.55		5.55	0	
	5		5.51		5.51	0	

Actual flight data are presented in Table 6-1 and have not been adjusted to standard J-2 engine conditions. Considering data that have been adjusted to standard conditions through use of a computer program, very little difference from the results shown in Table 6-1 is observed. In comparison to the vehicle acceptance test, the adjusted data showed engines No. 2 and 5 to be 1.0 and 1.86 percent low in thrust, respectively.

The low frequency oscillations which occurred on AS-503 and AS-504 did not occur on this flight. The oscillation problem appeared to be associated with inflight LOX liquid levels. The LOX level history for all S-II stage flights is shown in Figure 6-4. Early cutoff of the center engine on AS-505 precluded any oscillation buildup. Subsequent to CECO no adverse structural response characteristics were evident (for a detailed discussion refer to Section 9, paragraph 9.2.3). The flight results verify that early cutoff of the center engine successfully avoided the low frequency oscillation problem.

6.4 S-II SHUTDOWN TRANSIENT PERFORMANCE

Engine shutdown sequence was initiated by the stage LOX low level sensors. The OECO signal was delayed 1.5 seconds after the low level sensor dry indications by timers in the LOX depletion cutoff system. This resulted in engine performance decay prior to receipt of the cutoff signal, similar to that experienced during AS-504 flight. Due to early CECO however, the precutoff decay was greatly reduced. Only engine No. 1 exhibited a significant thrust chamber pressure decay prior to cutoff, decreasing approximately 79.3 N/cm² (115 psi) in the final 1.5 seconds. The decay of thrust

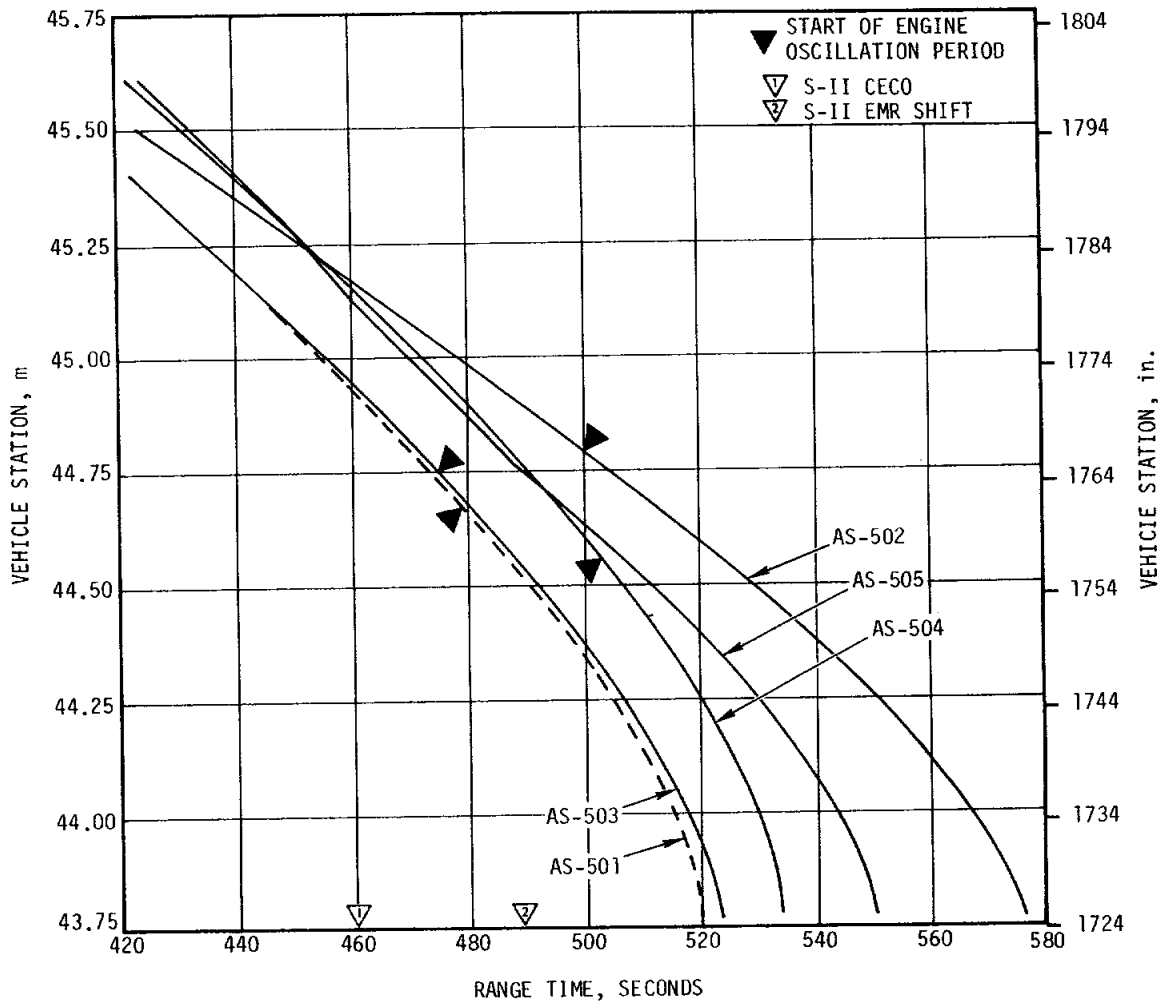


Figure 6-4. S-II Inflight LOX Level History

chamber pressures of the other outboard engines was approximately 13.8 N/cm² (20 psi). The order of outboard engine thrust chamber pressure decay was identical for the AS-504 and AS-505 flights (engines No. 1, 2, 3 and 4). One second before cutoff, with all outboard engines operating at low mixture ratio, total stage thrust was approximately 3,062,102 Newtons (688,388 lbf) with an average specific impulse of 4221.8 N-s/kg (430.5 lbf-s/lbm).

At OECO (552.64 seconds) the total vehicle thrust was down to 2,856,061 Newtons (642,068 lbf). Vehicle thrust dropped to 5 percent of this level within 0.66 second. The stage cutoff impulse through the 5 percent thrust level was estimated to be 563,145 N-s (126,600 lbf-s). Guidance data indicates the total impulse from OECO to S-II/S-IVB separation at 553.50 seconds to be 578,714 N-s (130,100 lbf-s) compared to a predicted value of 647,750 N-s (145,620 lbf-s) for this time period. No unusual features were apparent in the center engine thrust decay data following CECO. The 5 percent thrust level was reached approximately 0.3 second after cutoff.

Based on the latest propulsion performance prediction, burn time was 1.70 seconds longer than expected. A comparison of flight data with the Launch Vehicle Operational Flight Trajectory (dated April 17, 1969), which was based on a previous propulsion prediction, indicates a different burn time deviation.

6.5 S-II STAGE PROPELLANT MANAGEMENT

The propellant management system performed satisfactorily during the propellant loading operation and during flight. The S-II stage employed an open-loop system utilizing fixed, open-loop commands from the IU rather than feedback signals from the tank mass sensing probes. (Open-loop operation was also used on AS-503 and is planned for use on all subsequent vehicles).

The facility Propellant Tanking Control System (PTCS) and the propellant management system successfully accomplished S-II loading and replenishment. During the prelaunch countdown, all propellant management subsystems operated properly with no problems noted. Propellant fill and drain valve closure times were satisfactory (8.97 seconds for the LOX valve and 18.64 seconds for the LH₂ valve).

During CDDT, splashing of the LH₂ overfill shutoff (liquid level) sensor occurred. After the LH₂ tank was filled and the replenish mode was established during countdown, the GSE "revert" interlock for this sensor was deactivated.

Open-loop PU system operation commenced when "High EMR Select" was commanded at ESC +5.45 seconds as planned. The PU valves then moved to the high EMR position, providing a nominal EMR of 5.50 for the first phase of Programed Mixture Ratio (PMR). No propellant management system anomalies resulted from CECO. At ESC +323.49 seconds, the low EMR command was initiated, driving the PU valves against the low EMR stop. This provided an average EMR of 4.31 to 1 (predicted 4.32 to 1) for the remaining low mixture ratio portion of the flight.

The open-loop PU control system responded as expected during flight and no instabilities were noted. The open-loop PU error at OECO was

approximately -31.7 kilograms (-70 lbm) LH₂ versus a 3 sigma tolerance of ±1134 kilograms (±2500 lbm).

Based on point level sensor data, propellant residuals (mass in tanks and sumps) at OECO were 816 kilograms (1800 lbm) LOX, and 1973 kilograms (4350 lbm) LH₂, versus the predicted 656 kilograms (1447 lbm) LOX, and 1966 kilograms (4335 lbm) LH₂. An updated analysis using AS-504 LOX depletion data indicated a higher LOX residual would result on AS-505. Corrections for CECO and EMR differences resulted in a revised LOX predicted residual of 780 kilograms (1721 lbm). Table 6-2 presents a comparison of propellant masses as measured by the PU probes, engine flowmeters and point level sensors. The best estimate propellant mass is based on integration of flowmeter data utilizing the propellant residuals determined from point level sensor data at OECO. Best estimates of propellant mass loaded are 372,717 kilograms (821,700 lbm) LOX, and 71,808 kilograms (158,310 lbm) LH₂. These mass values are 0.14 percent less than predicted for LOX and 0.20 percent more than predicted for LH₂.

Table 6-2. S-II Propellant Mass History

EVENT RANGE TIME	UNITS	PREDICTED		PU SYSTEM ANALYSIS		FLOWMETER ANALYSIS (BEST ESTIMATE)		POINT SENSOR ANALYSIS	
		LOX	LH ₂	LOX	LH ₂	LOX	LH ₂	LOX	LH ₂
Ground Ignition	kg (lbm)	373,249 (822,874)	71,668 (158,000)	373,218 (822,805)	71,599 (157,848)	372,717 (821,700)	71,808 (158,310)	372,866 (822,028)	72,197 (159,168)
S-II ESC (163.05 sec)	kg (lbm)	373,249 (822,874)	71,668 (158,000)	373,004 (822,332)	71,548 (157,737)	372,717 (821,700)	71,808 (158,310)	372,866 (822,028)	72,197 (159,168)
High EMR Select (168.50 sec)	kg (lbm)	370,463 (816,731)	70,918 (156,348)	369,852 (815,384)	71,078 (156,700)	370,166 (816,076)	71,147 (156,852)	369,367 (814,314)	72,082 (158,914)
PU Valve Step (486.54 sec)	kg (lbm)	38,290 (84,415)	10,741 (23,679)	49,936 (110,089)	11,007 (24,267)	41,093 (90,594)	11,897 (26,229)	42,512 (93,723)	11,495 (25,343)
S-II OECO (552.64 sec)	kg (lbm)	656 (1447)	1966 (4335)	1433 (3160)	1694 (3735)	816 (1800)	1973 (4350)	816 (1800)	1973 (4350)
S-II Residual After Thrust Decay	kg (lbm)	542 (1194)	1916 (4224)	1305 (2878)	1651 (3639)	689 (1518)	1930 (4254)	689 (1518)	1930 (4254)

NOTE: This table does not include propellant trapped external to the tanks and LOX sump.

6.6 S-II PRESSURIZATION SYSTEMS

6.6.1 S-II Fuel Pressurization System

LH₂ tank ullage pressure, actual and predicted, is presented in Figure 6-5 for autosequence, S-IC boost and S-II boost. The LH₂ tank vent valves were closed at -96 seconds and the ullage was pressurized to 24.6 N/cm² (35.7 psia) in approximately 25 seconds. One makeup cycle was required at -38 seconds as a result of thermal pressure decay. Venting occurred during S-IC boost as anticipated. Two venting cycles were indicated on vent valve No. 1 between 63 and 88 seconds. There was no indication that vent valve No. 2 opened. Differential pressure across the vent valve was

kept below the low-mode upper limit of 20.3 N/cm^2 (29.5 psid). Ullage pressure at S-II engine start was 19.3 N/cm^2 (28 psia) meeting the minimum engine start requirement of 18.6 N/cm^2 (27 psia). The LH₂ tank valves were switched to the high vent mode immediately prior to S-II engine start.

LH₂ tank ullage pressure was maintained within the regulator range of 19.7 to 20.7 N/cm^2 (28.5 to 30 psia) during burn until the LH₂ tank pressure regulator was stepped open at 461.61 seconds. Ullage pressure increased to 22.1 N/cm^2 (32 psia). The LH₂ vent valves started venting at 483 seconds and continued venting throughout the remainder of the S-II flight. Ullage pressure remained within the high-mode vent range of 21 to 22.7 N/cm^2 (30.5 to 33 psia).

Figure 6-6 shows LH₂ total inlet pressure, temperature and NPSP. The parameters were close to predicted values. The NPSP supplied exceeded that required throughout the S-II burn phase of the flight.

6.6.2 S-II LOX Pressurization System

LOX tank ullage pressure, actual and predicted, is presented in Figure 6-7 for autosequence, S-IC boost and S-II burn. After a two-minute cold helium chilldown flow through the LOX tank, the vent valves were closed at -185.4 seconds and the LOX tank was prepressurized to the pressure switch setting of 26.6 N/cm^2 (38.6 psia) in approximately 50 seconds. No pressure makeup cycles were required. However, a slight pressure decay occurred, which was followed by the slight pressure increase caused by LH₂ tank prepressurization. Ullage pressure was 26.9 N/cm^2 (39 psia) at engine start.

The LOX regulator remained at its minimum position until 245 seconds because the ullage pressure was above the acceptable regulator range of 24.8 to 26.5 N/cm^2 (36 to 38.5 psia). A slight decrease in ullage pressure prior to LOX regulator step pressurization indicated normal performance of the LOX regulator. LOX step pressurization (261.62 seconds) caused the usual characteristic surge in ullage pressure followed by a slower increase until EMR shift. LOX tank ullage pressure reached a maximum of 28.2 N/cm^2 (40.9 psia) before the characteristic decay which follows EMR shift. Ullage pressure was 25 N/cm^2 (36.3 psia) at OECO.

LOX pump total inlet pressure, temperature and NPSP are presented in Figure 6-8. The NPSP supplied exceeded the requirement throughout the S-II boost phase. The total magnitude of LOX liquid stratification was slightly greater than predicted. The 1.5-second time delay in the LOX low level cutoff circuit used for AS-504 and AS-505 makes it very difficult to predict an accurate cutoff temperature.

6.7 S-II PNEUMATIC CONTROL PRESSURE SYSTEM

Performance of the stage pneumatic control system was satisfactory. Main receiver pressure and regulator outlet pressure were within predicted limits throughout system operation. Regulator outlet pressure was within

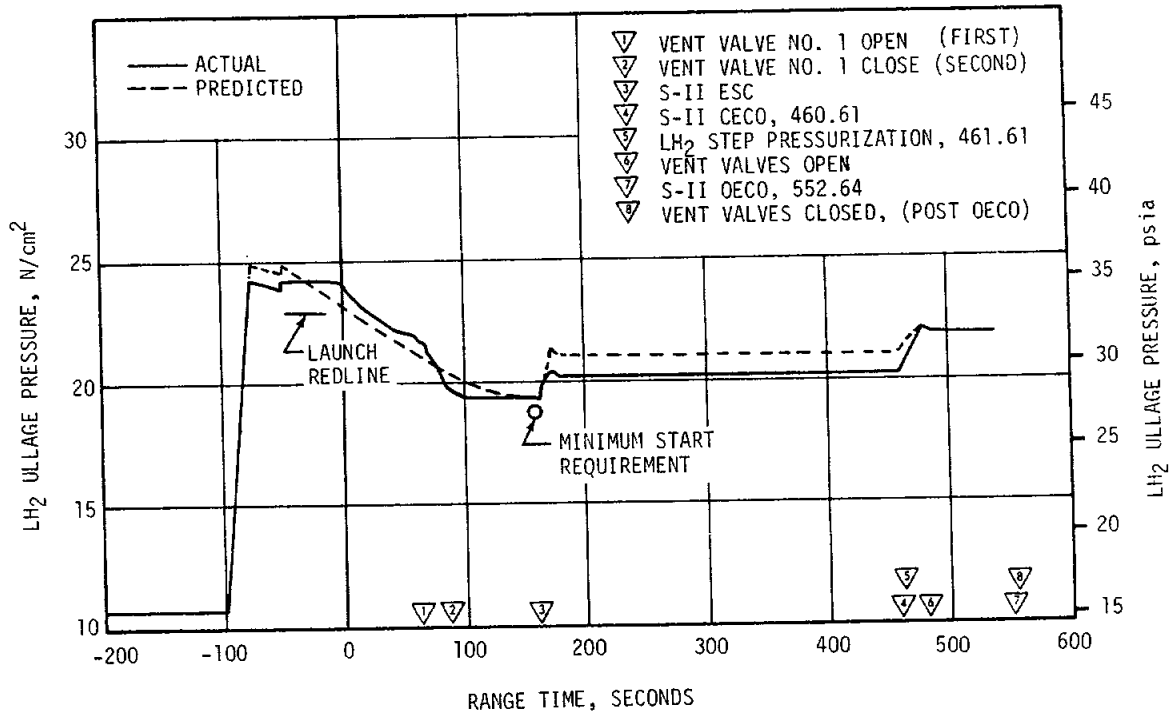


Figure 6-5. S-II Fuel Tank Ullage Pressure

the operating band of 476 to 527 N/cm² (690 to 765 psia) except during valve actuations which follow S-II ESC, CECO and OECO events. The makeup period for the regulator outlet pressure to return to its operating band after valve closures did not exceed 17 seconds. This is within the normal recovery time.

Pressure decay in the main receiver from facility supply vent at -30 seconds to the initial valve actuation at 168 seconds was negligible. Pressure decreased from 2065 to 2062 N/cm² (2995 to 2990 psia) during this period. Main receiver pressure was 1817 N/cm² (2635 psia) following the final valve actuation at OECO.

6.8 S-II HELIUM INJECTION SYSTEM

The performance of the helium injection system was satisfactory. Requirements were met and parameters were in good agreement with predictions. The supply bottle was pressurized to 2068 N/cm² (3000 psia) prior to lift-off and by ESC was 448 N/cm² (650 psia). Helium injection system average total flowrate during supply bottle blowdown (-30 to 161.75 seconds) was 2.01 SCMM (70.7 SCFM).

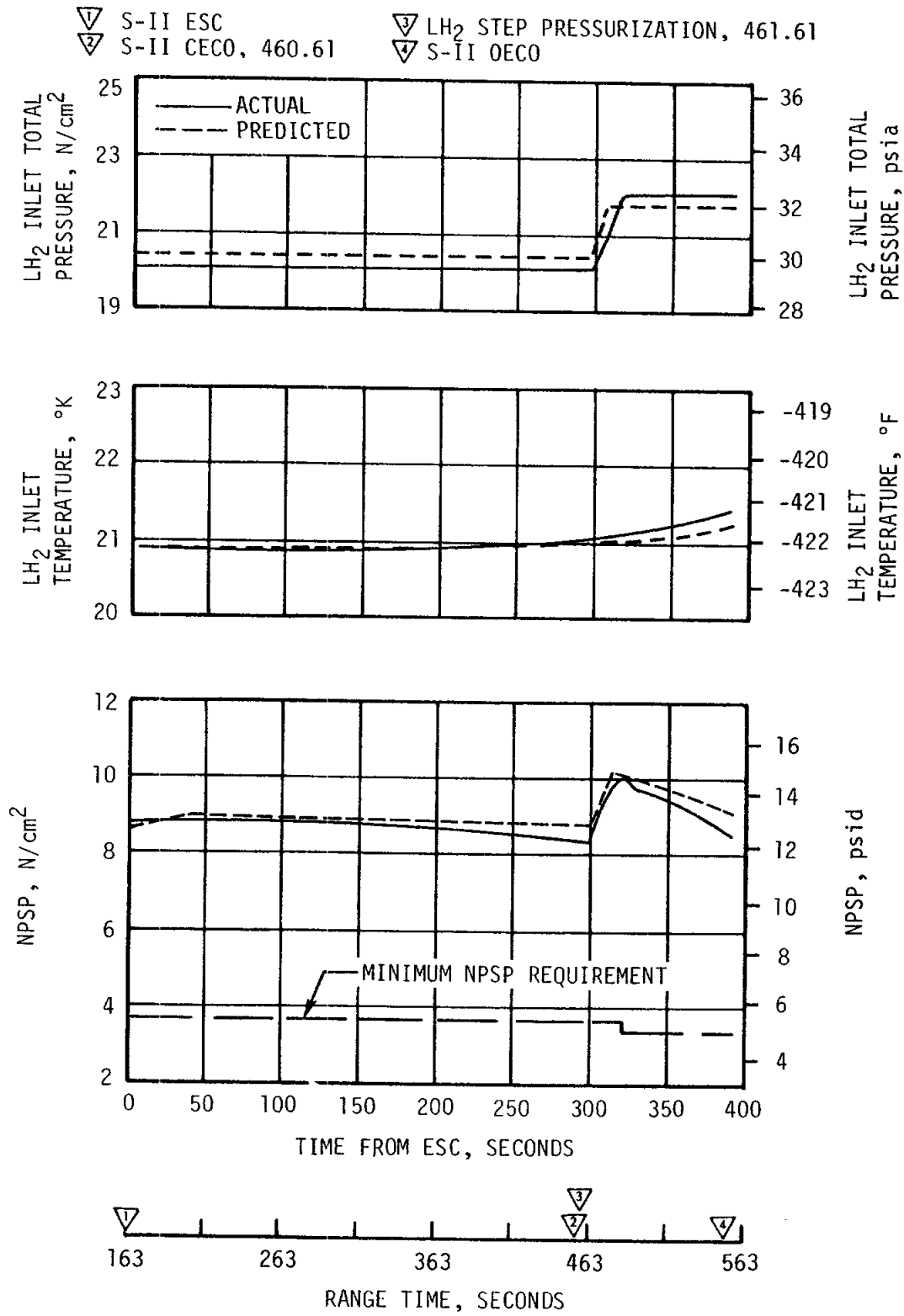


Figure 6-6. S-II Fuel Pump Inlet Conditions

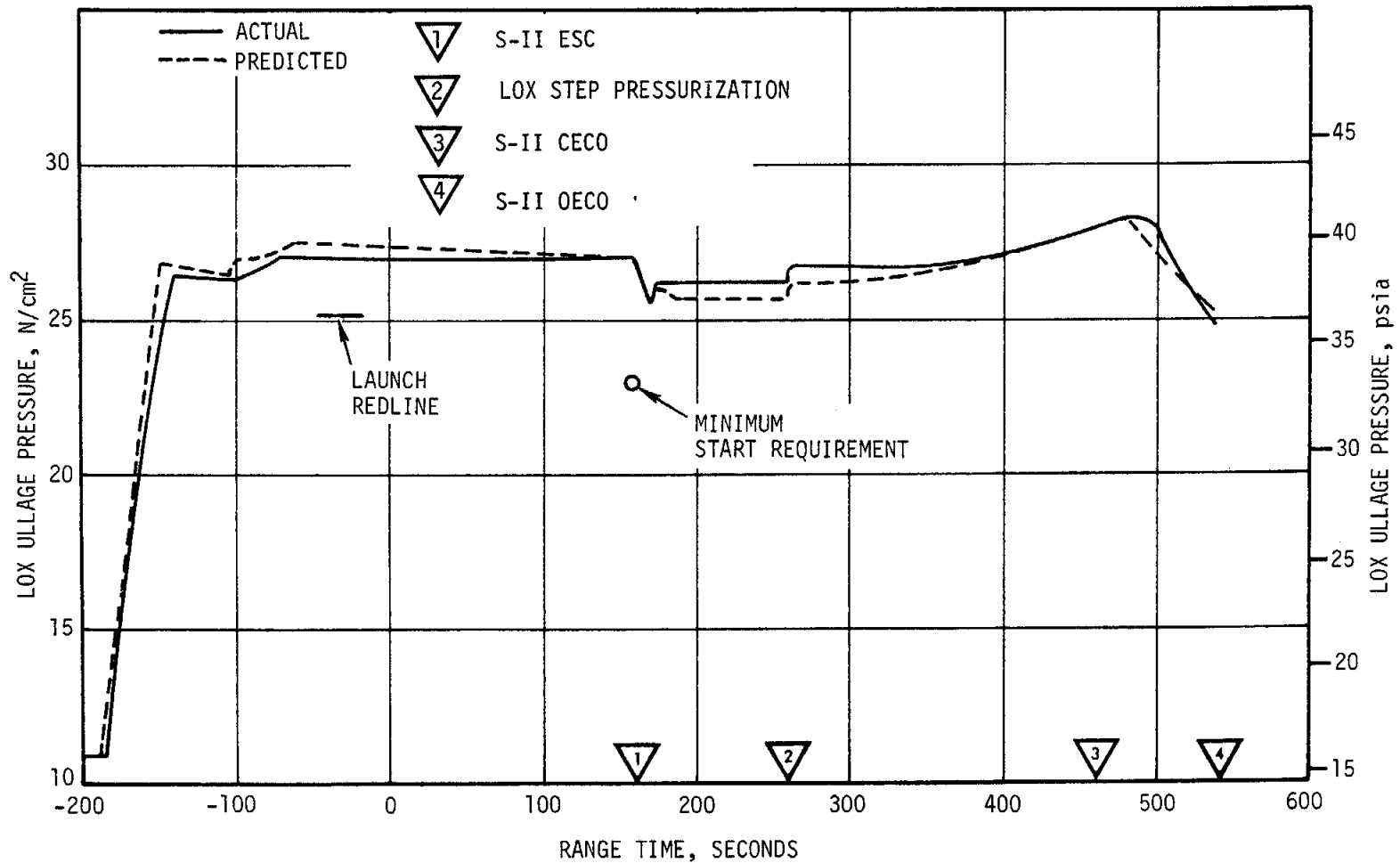


Figure 6-7. S-II LOX Tank Ullage Pressure

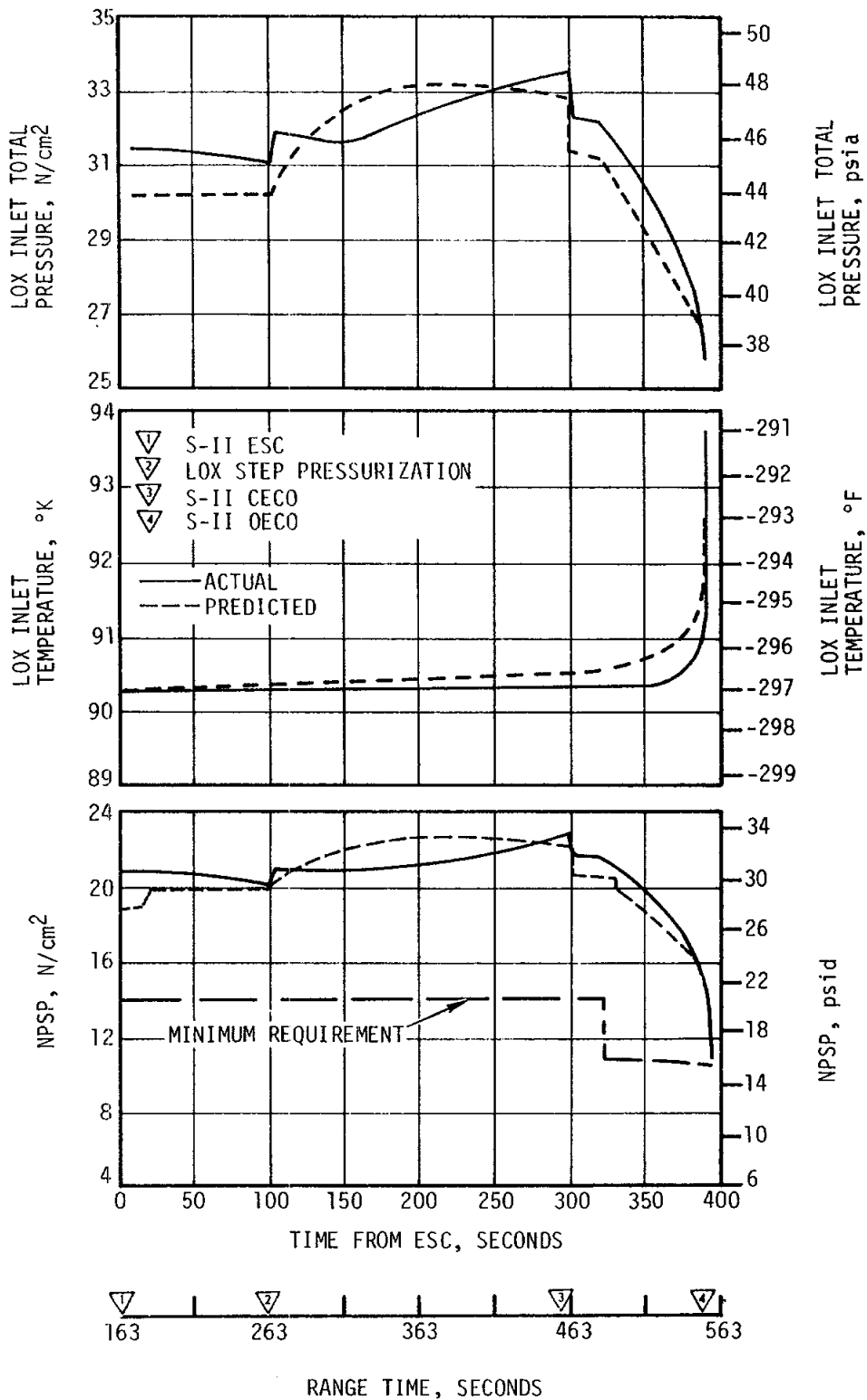


Figure 6-8. S-II LOX Pump Inlet Conditions

SECTION 7
S-IVB PROPULSION

7.1 SUMMARY

The J-2 engine operated satisfactorily throughout the operational phase of first and second burns. Shutdowns for both burns were also normal.

The engine performance during first burn, as determined from standard altitude reconstruction analysis, was 0.13 percent less than predicted for thrust and 0.26 percent greater than predicted for specific impulse. The first burn duration was 146.95 seconds from Start Tank Discharge Valve (STDV) open. This duration was 1.54 seconds longer than predicted. Engine Cutoff (ECO) was initiated by a velocity cutoff command from the Launch Vehicle Digital Computer (LVDC).

The Continuous Vent System (CVS) adequately regulated LH₂ tank ullage pressure at 13.4 N/cm² (19.5 psia) during earth parking orbit. The Oxygen/Hydrogen (O₂/H₂) burner satisfactorily repressurized the LH₂ tank for restart. Repressurization of the LOX tank was not required.

Engine restart conditions were within specified limits. Restart at full open Propellant Utilization (PU) valve position was successful and there were no indications of overtemperatures in the Gas Generator (GG).

Second burn duration was 343.06 seconds from STDV open which was 0.65 second shorter than predicted. Engine performance during second burn, as determined from the standard altitude reconstruction analysis, was 0.25 percent less than predicted for thrust and 0.30 percent greater than predicted for specific impulse. ECO was initiated by a LVDC velocity cutoff command.

Subsequent to second burn, the propellant lead experiment was successfully accomplished and the stage propellant tanks and pneumatic systems were satisfactorily safed. The velocity change resulting from the experiment, CVS, the LOX dump, and Auxiliary Propulsion System (APS) firings caused the stage to enter a solar orbit as planned.

A helium leak in the APS module No. 1 was noted at 23,400 seconds (06:30:00). The leak persisted until loss of data at 39,240 seconds (10:54:00); however, system performance was within operational limits.

7.2 S-IVB CHILLDOWN AND BUILDUP TRANSIENT PERFORMANCE FOR FIRST BURN

The propellant recirculation systems performed satisfactorily and met start and run box requirements for fuel and LOX as shown in Figure 7-1. The thrust chamber temperature at launch was well below the maximum allowable redline limit of 172°K (-150°F). At S-IVB first burn Engine Start Command (ESC), the temperature was 159.4°K (-173°F), which is within the requirement of 166 ±27.5°K (-160.9 ±49.5°F).

The chilldown and loading of the engine Gaseous Hydrogen (GH₂) start sphere and pneumatic control sphere prior to liftoff were satisfactory. At first ESC the start tank conditions were within the required S-IVB region of 896.3 ±68.9 N/cm² (1300 ±100 psia) and 133.2 ±44.4°K (-220 ±80°F) for initial start. The discharge was completed and the refill initiated at first burn ESC +4.40 seconds. The refill was satisfactory and in good agreement with the acceptance test.

The engine control bottle pressure and temperature at liftoff were 2082 N/cm² (3020 psia) and 178°K (-140°F), respectively.

LOX and LH₂ systems chilldowns, which were continuous from before liftoff until just prior to S-IVB first burn ESC, were satisfactory. At ESC the LOX pump inlet temperature was 91.3°K (-295.5°F) and the LH₂ pump inlet temperature was 21.4°K (-421.5°F).

The first burn start transient was satisfactory. The thrust buildup was within the limits set by the engine manufacturer. Faster thrust buildup to the 90 percent level as compared to the acceptance test results was observed on this flight. This buildup was similar to the thrust buildups observed on previous flights. The PU valve was in proper null position prior to first start. The total impulse from STDV to STDV +2.5 seconds was 832,943 N-s (187,253 lbf-s) for first start. This was greater than the value of 644,992 N-s (146,000 lbf-s) obtained during the same interval for the acceptance test.

Although the fuel injection temperature measurement behaved in an erratic manner, the first burn fuel lead appeared to follow predictions. Related measurements and subsequent performance indicated that satisfactory conditions were provided.

7.3 S-IVB MAINSTAGE PERFORMANCE FOR FIRST BURN

S-IVB stage propulsion system performance is evaluated using propulsion reconstruction analysis. This analysis utilizes telemetered engine and stage data to compute longitudinal thrust, specific impulse, and stage mass flowrate. The propulsion reconstruction analysis showed that the stage performance during mainstage operation was satisfactory. A comparison of predicted and actual performance of thrust, total flowrate, specific impulse, and mixture ratio versus time is shown in Figure 7-2. Table 7-1 shows the specific impulse, flowrates and mixture ratio

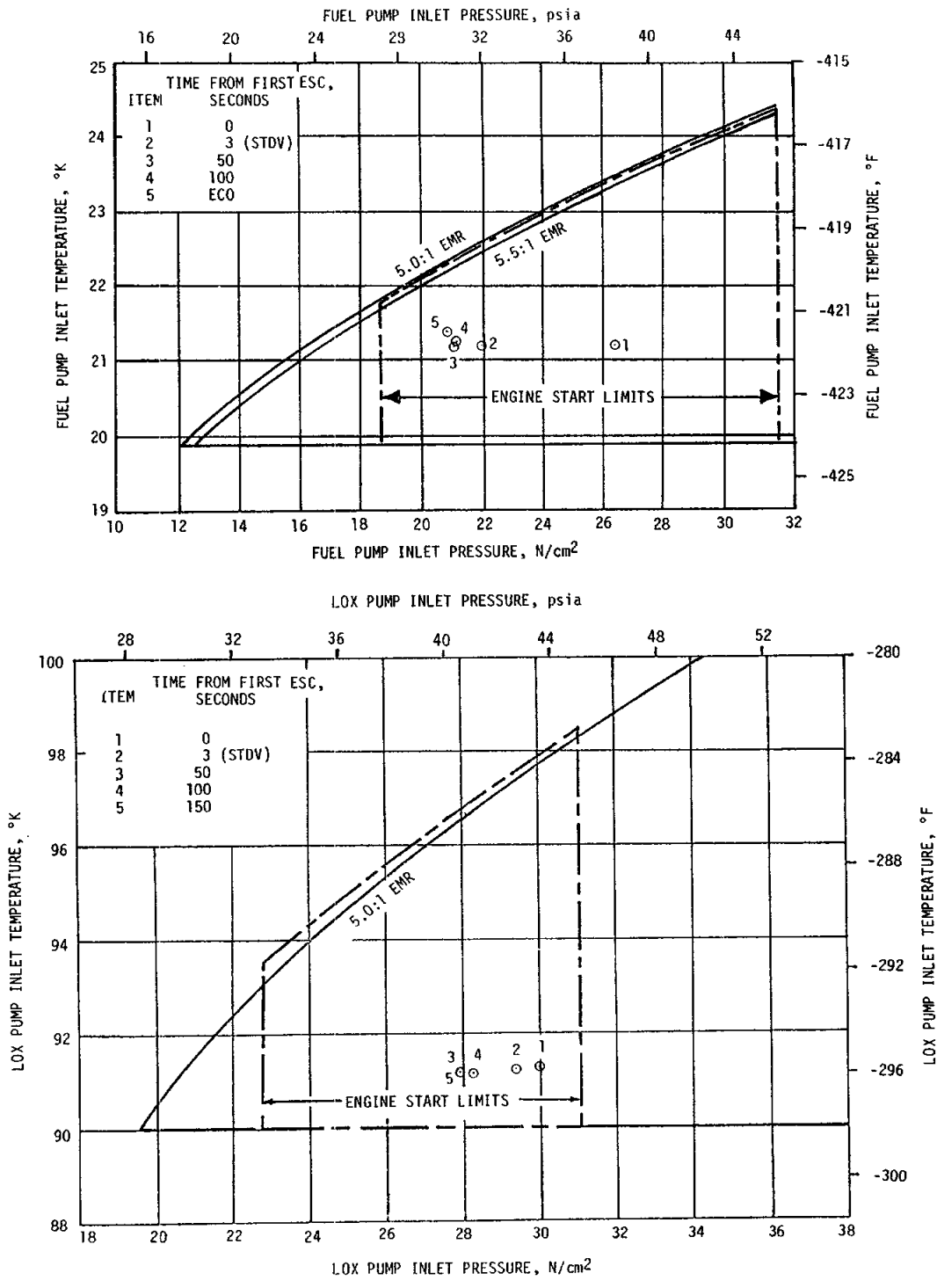


Figure 7-1. S-IVB Start Box and Run Requirements - First Burn

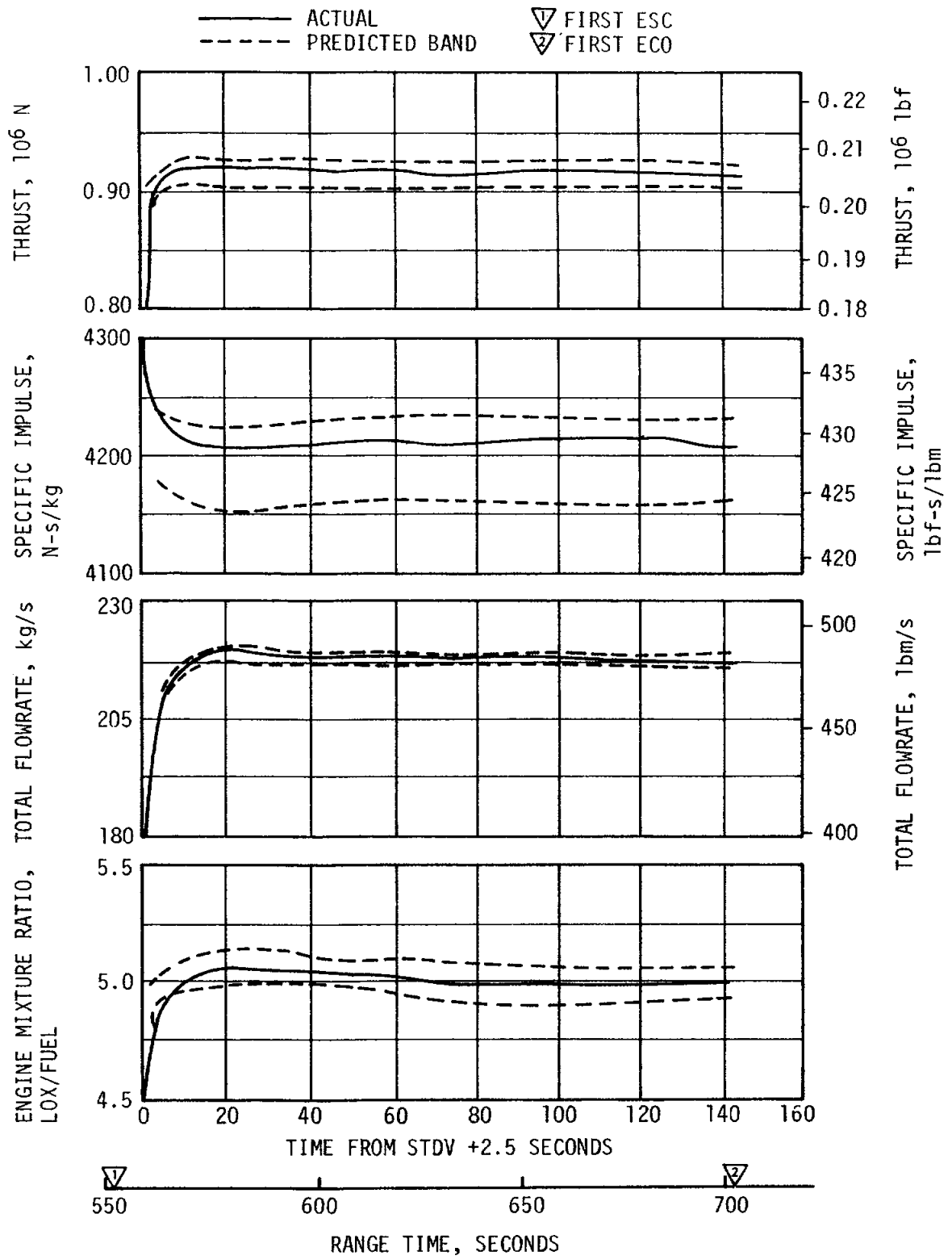


Figure 7-2. S-IVB Steady State Performance - First Burn

Table 7-1. S-IVB Steady State Performance - First Burn (ESC +140-Second Time Slice at Standard Altitude Conditions)

PARAMETER	PREDICTED	RECONSTRUCTION	FLIGHT DEVIATION	PERCENT DEVIATION FROM PREDICTED
Thrust N (lbf)	9,129,304 (205,235)	9,117,294 (204,965)	-12,010 (-270)	-0.13
Specific Impulse N-s/kg (lbf-s/lbm)	4201 (428.4)	4212 (429.5)	11 (1.1)	0.26
LOX Flowrate kg/s (lbm/s)	180.91 (398.83)	180.18 (397.24)	-0.73 (-1.59)	-0.40
Fuel Flowrate kg/s (lbm/s)	36.38 (80.21)	36.30 (80.02)	-0.08 (-0.19)	-0.24
Engine Mixture Ratio LOX/Fuel	4.972	4.964	-0.008	-0.16

deviations from the predicted at the ESC +140-second time slice when the engine performance characteristics stabilized. This time slice performance is the standardized altitude performance which is comparable to engine tests. The 140-second time slice performance for first burn thrust was 0.13 percent lower than predicted. Specific impulse performance for first burn was 0.26 percent higher than predicted.

First burn duration was 146.95 seconds from STDV open, which was 1.54 seconds longer than predicted burn time.

Instrumentation installed to monitor Augmented Spark Igniter (ASI) system performance responded as expected. Both LOX and LH₂ supply line temperatures chilled to expected levels during both burns and did not indicate any abnormal conditions.

The helium control system for the J-2 engine performed satisfactorily during first burn mainstage operation. Since the engine bottle was connected with the stage ambient repressurization bottles there was little pressure decay. Helium usage was estimated from flowrates during engine operation. Approximately 0.154 kilogram (0.34 lbm) was consumed during first burn.

7.4 S-IVB SHUTDOWN TRANSIENT PERFORMANCE FOR FIRST BURN

The ECO transient was satisfactory and agreed closely with the acceptance test and predictions. The total cutoff impulse to zero percent of rated thrust was 203,373 N-s (45,720 lbf-s). Cutoff occurred with the PU valve in the null position.

When cutoff impulse was adjusted for anticipated Main Oxidizer Valve (MOV) temperature and compared with the log book values at null PU valve position and 255°K (0°F) MOV actuator temperature, the flight value was near the log book value.

7.5 S-IVB PARKING ORBIT COAST PHASE CONDITIONING

The LH₂ CVS performed satisfactorily, maintaining the fuel tank ullage pressure at an average level of 13.4 N/cm² (19.5 psia).

The continuous vent regulator was activated at 762.95 seconds. Regulation continued with the expected operation of the main poppet periodically opening, cycling, and reseating. Continuous venting was terminated at 8671.42 seconds. The CVS performance is shown in Figure 7-3.

Calculations based on estimated temperatures indicated that the mass vented during parking orbit was 1014 kilograms (2236 lbm) and that the boiloff mass was 1092 kilograms (2407 lbm).

7.6 S-IVB CHILLDOWN AND RESTART FOR SECOND BURN

Propellant tank repressurization was satisfactorily accomplished by the O₂/H₂ burner. Helium heater "ON" command was initiated at 8671.2 seconds. LOX tank ullage pressure at helium heater "ON" command was approximately 27.1 N/cm² (39.3 psia); therefore, repressurization of the LOX tank was not required. The LH₂ repressurization control valves were opened at helium heater "ON" +6.1 seconds. The fuel tank was repressurized from 13.2 to 20.9 N/cm² (19.2 to 30.3 psia) in 182 seconds which yielded a ramp rate of 2.48 N/cm²/min (3.59 psi/min) as shown in Figure 7-4. There were 12.7 kilograms (28.0 lbm) of cold helium used from the cold helium spheres during repressurization. The burner continued to operate for a total of 460 seconds and provided nominal propellant settling forces.

The performance of the O₂/H₂ burner was satisfactory as shown in Figure 7-5.

The S-IVB stage provided adequate conditioning of propellants for engine restart. The engine start sphere was recharged properly and maintained sufficient pressure during coast. The engine control sphere gas usage was as predicted during the first burn; the ambient helium spheres recharged the control sphere to a nominal level adequate for a proper restart.

The propellant recirculation systems performed satisfactorily and met start and run box requirements for fuel and LOX as shown in Figure 7-6. The LH₂ pump inlet temperature at second burn ESC was 23.9°K (-416.6°F). At S-IVB second burn ESC the LOX pump inlet temperature was 91.1°K (-295.7°F). Second burn fuel lead generally followed the predicted pattern and resulted in satisfactory conditions as indicated by the thrust chamber temperatures and the associated fuel injector temperatures. The start tank performed satisfactorily during the second burn blowdown and recharge sequence.

▽ FIRST ECO

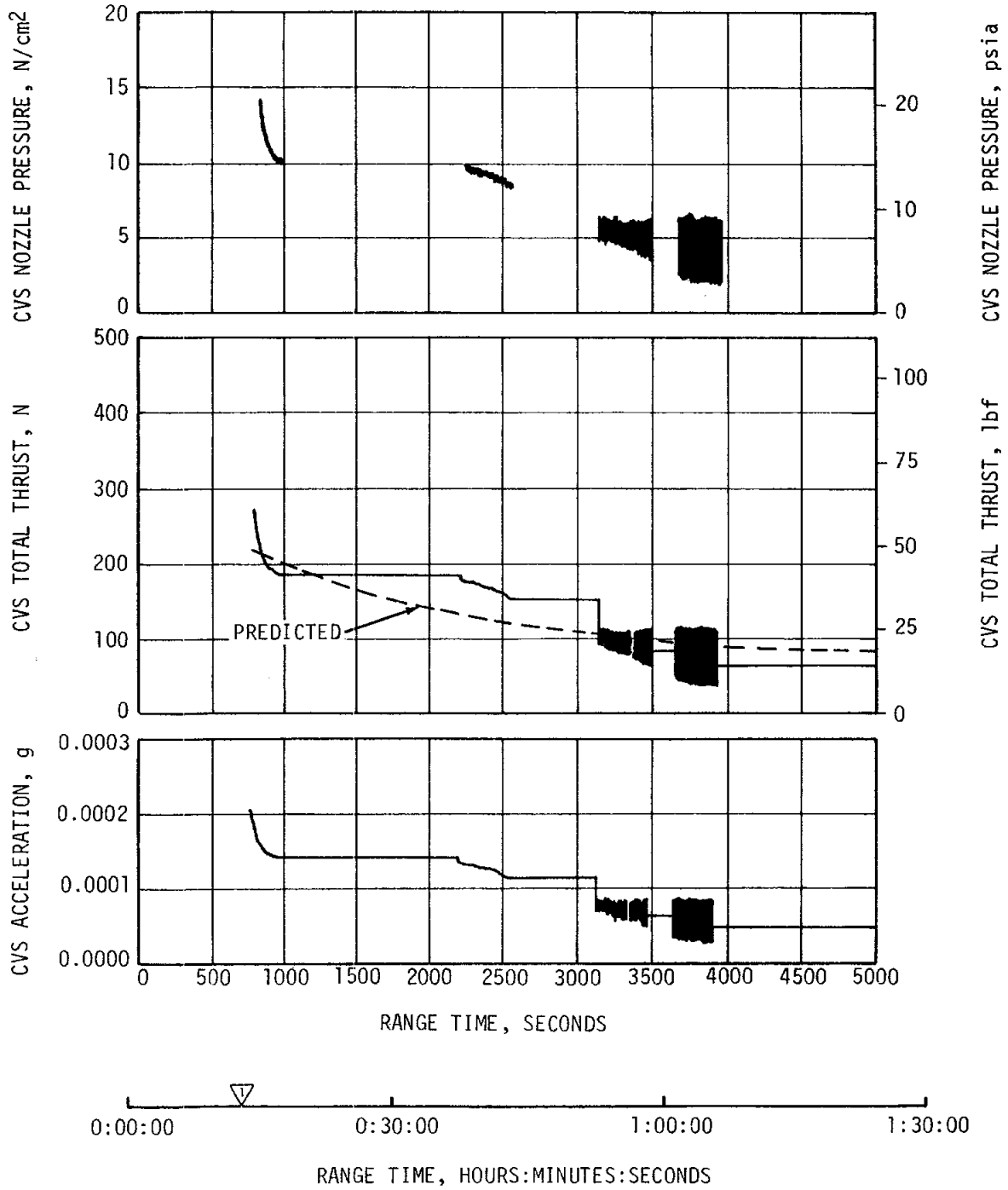


Figure 7-3. S-IVB CVS Performance - Coast Phase (Sheet 1 of 2)

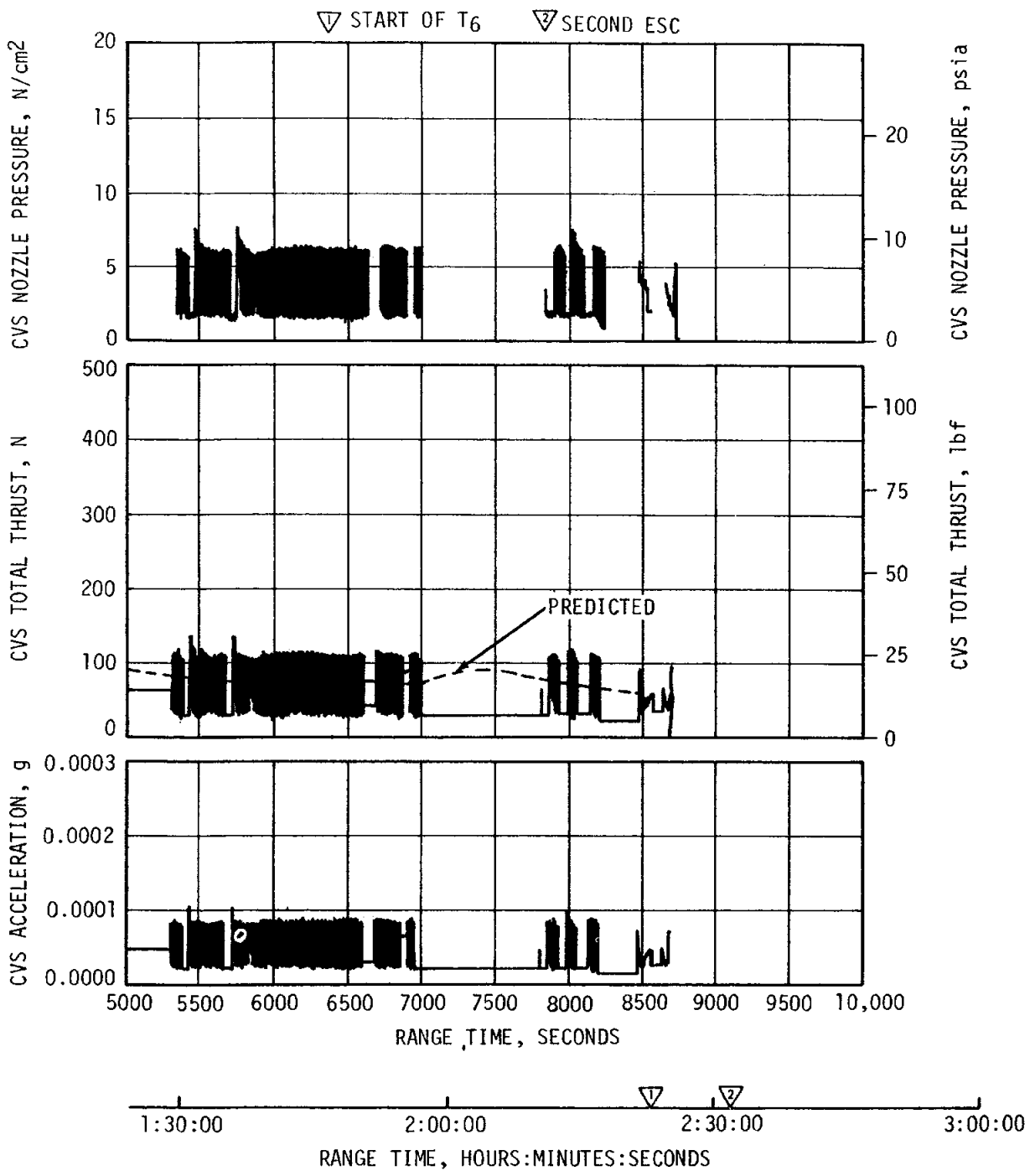


Figure 7-3. S-IVB CVS Performance - Coast Phase (Sheet 2 of 2)

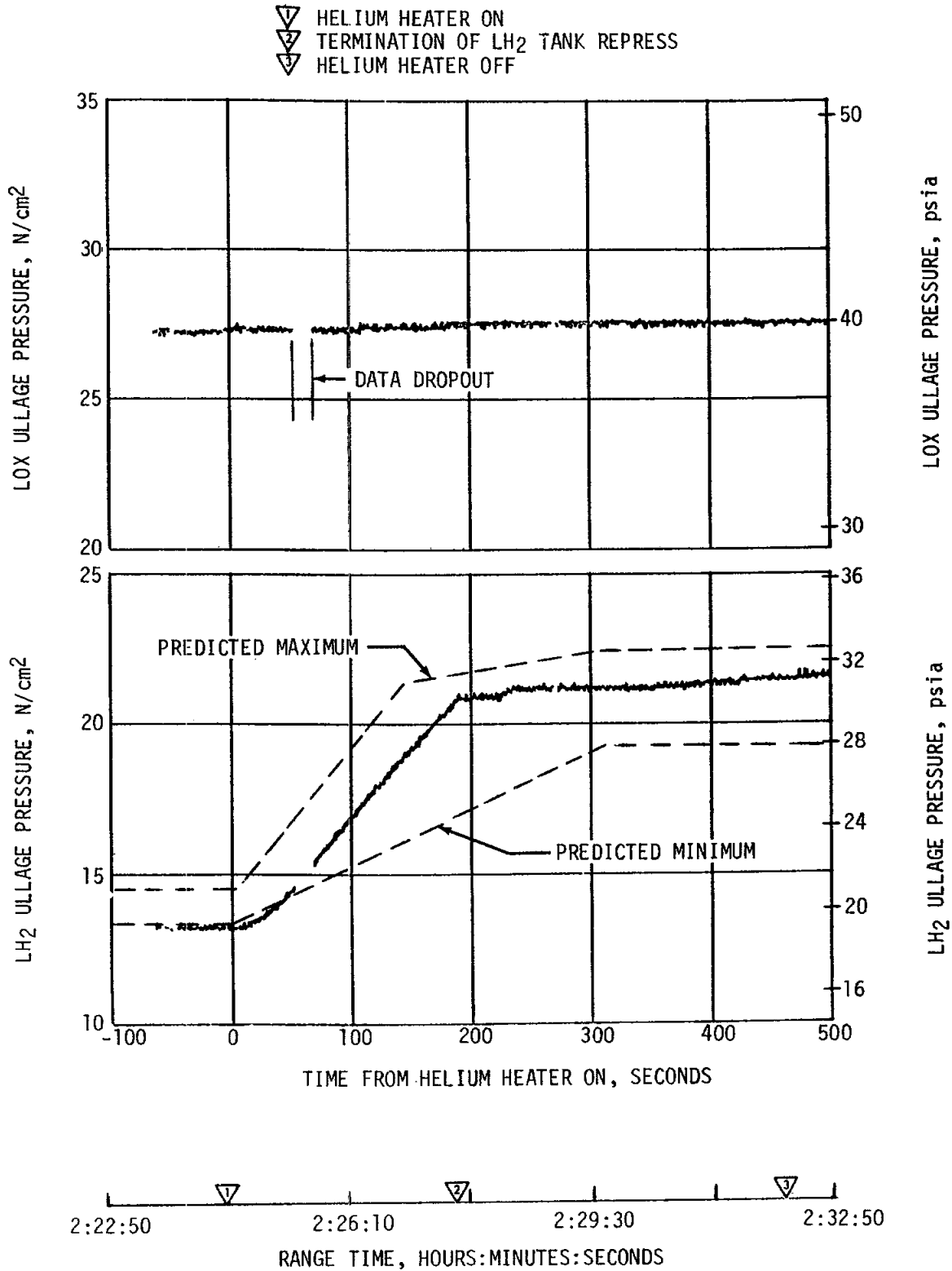


Figure 7-4. S-IVB Ullage Pressure During Repressurization Using O₂/H₂ Burner

- ▽ HELIUM HEATER ON
- ▽ TERMINATION OF LH₂ TANK REPRESS
- ▽ HELIUM HEATER OFF

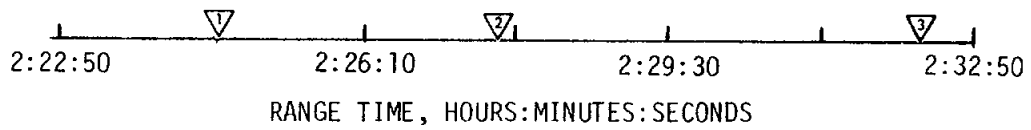
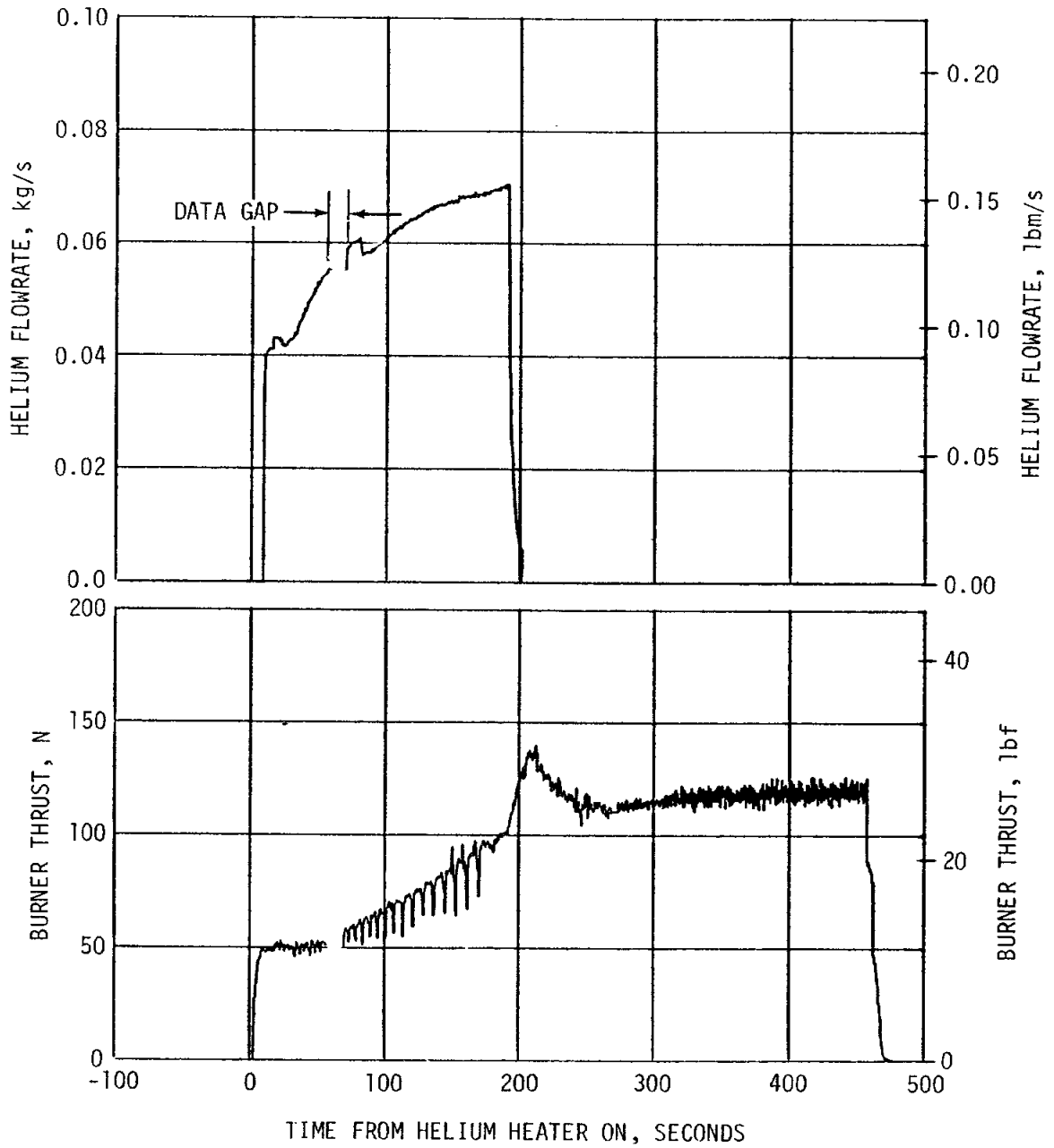


Figure 7-5. S-IVB O₂/H₂ Burner Thrust and Pressurant Flowrate

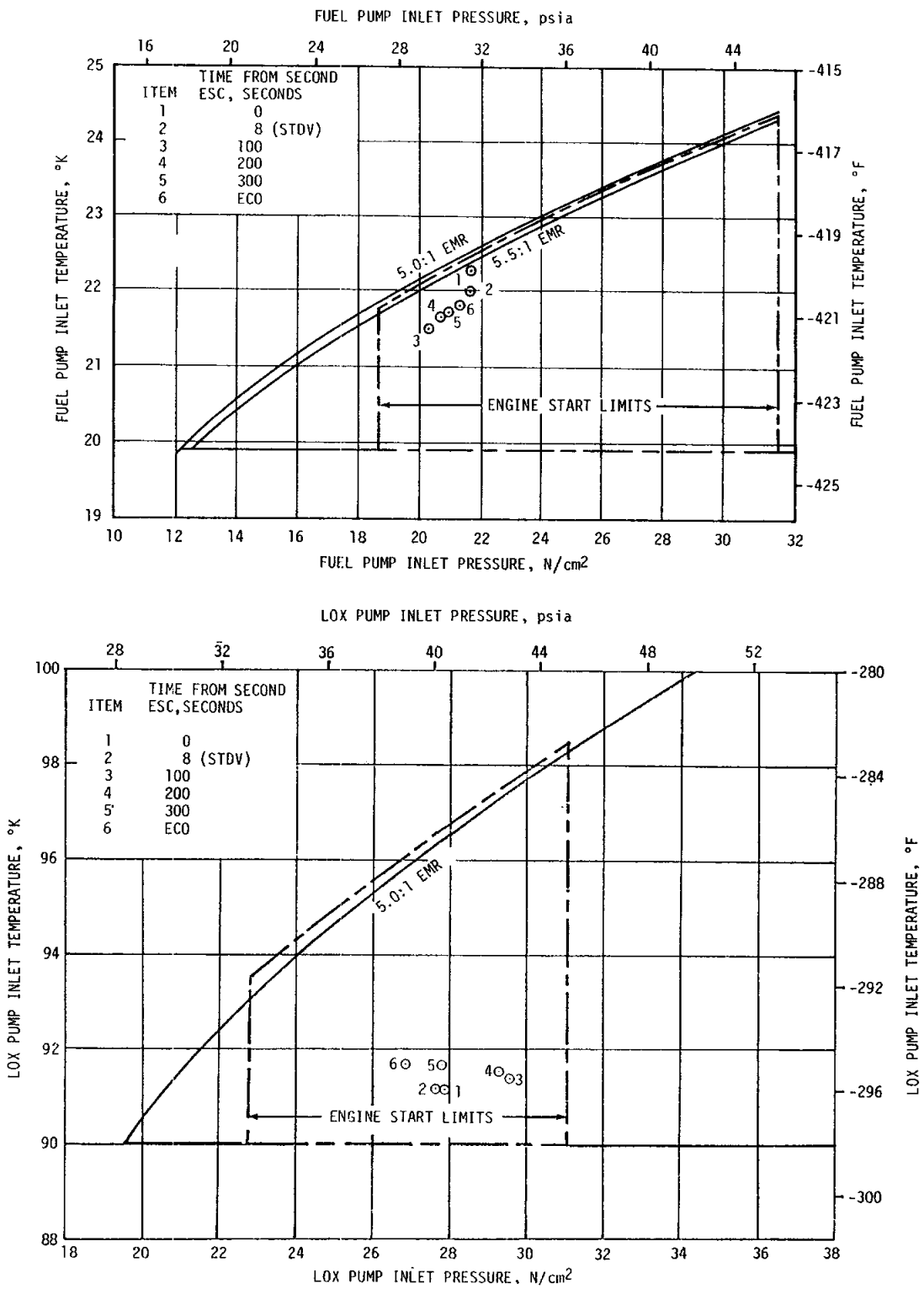


Figure 7-6. S-IVB Start Box and Run Requirements - Second Burn

The second burn start transient was satisfactory. The thrust buildup was within the limits set by the engine manufacturer. Faster thrust buildup to the 90 percent level, as compared to the acceptance test result, was observed on this flight. This buildup was similar to the thrust buildup on previous flights. The PU valve was in the proper full open (4.5 Engine Mixture Ratio [EMR]) position prior to the second start.

The total impulse from STDV to STDV +2.5 seconds was 797,335 N-s (179,248 lbf-s). This was greater than the value of 644,992 N-s (145,000 lbf-s) obtained during the same interval for the acceptance test.

Second burn fuel lead appeared to follow the predicted pattern. Even though the fuel injector temperature behaved in an erratic manner, the fuel lead apparently resulted in satisfactory conditions as indicated by other measurements and subsequent performance.

7.7 S-IVB MAINSTAGE PERFORMANCE FOR SECOND BURN

The propulsion reconstruction analysis showed that the stage performance during mainstage operation was satisfactory. A comparison of predicted and actual performance of thrust, total flowrate, specific impulse, and mixture ratio versus time is shown in Figure 7-7. Table 7-2 shows the specific impulse, flowrates and mixture ratio deviations from the predicted at the 180-second time slice. This time slice performance is the standardized altitude performance which is comparable to the first burn slice at 140 seconds.

The 180-second time slice performance for second burn thrust was 0.25 percent lower than predicted. Specific impulse performance for second burn was 0.30 percent higher than predicted.

Second burn duration was 343.06 seconds from STDV open, which was 0.65 second shorter than the predicted duration.

The helium control system performed satisfactorily during second burn mainstage. There was little pressure decay during the burn due to the connection to the stage repressurization system. Helium usage was estimated from flowrates during engine operation. Approximately 0.358 kilogram (0.79 lbm) was consumed during second burn.

Due to reports of excessive vibration during the flight, a special investigation has been undertaken concerning engine thrust variation in the 18 to 19 hertz frequency range. Since the POGO effect is a possible source of these vibrations, and it is known from previous experience that the LOX pump is responsive to POGO driving forces, investigation has been concentrated on the LOX pump. Frequency Modulation (FM) data suitable for evaluation in the expected frequency range, was evaluated for LOX pump discharge pressure measurements for the AS-503 and AS-505 flights. Other data from acceptance tests and other measurements were also evaluated. The data evaluated so far have not developed a positive indication of POGO or a positive correlation between thrust variations and other flights or propellant conditions.

81-2,

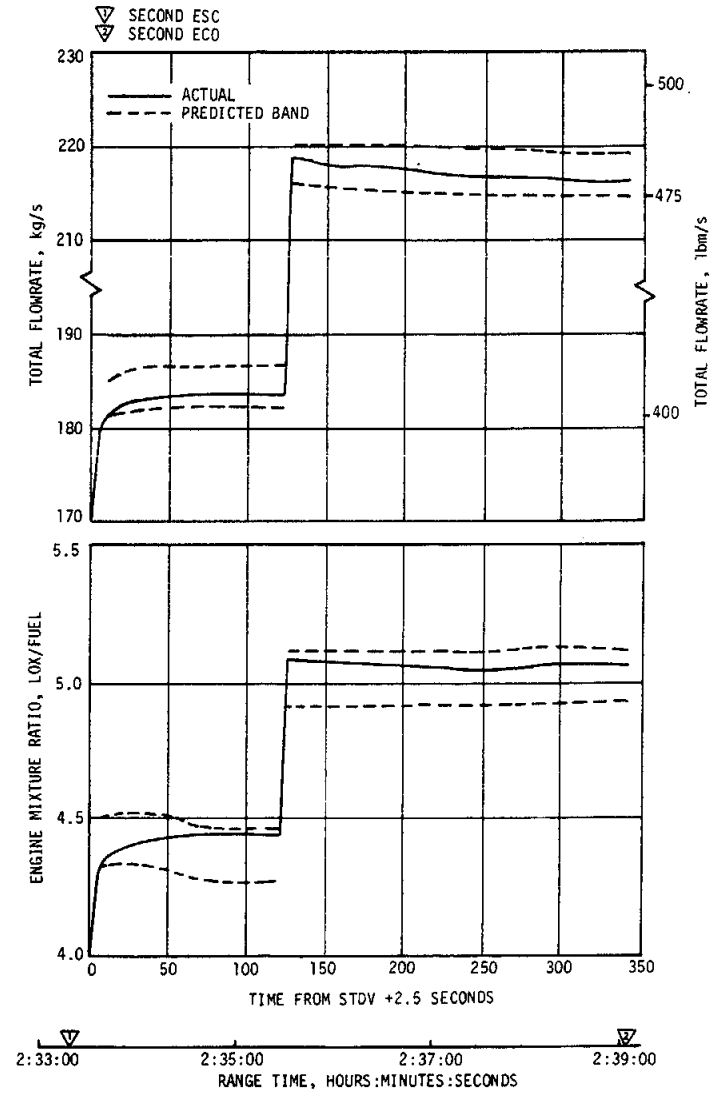
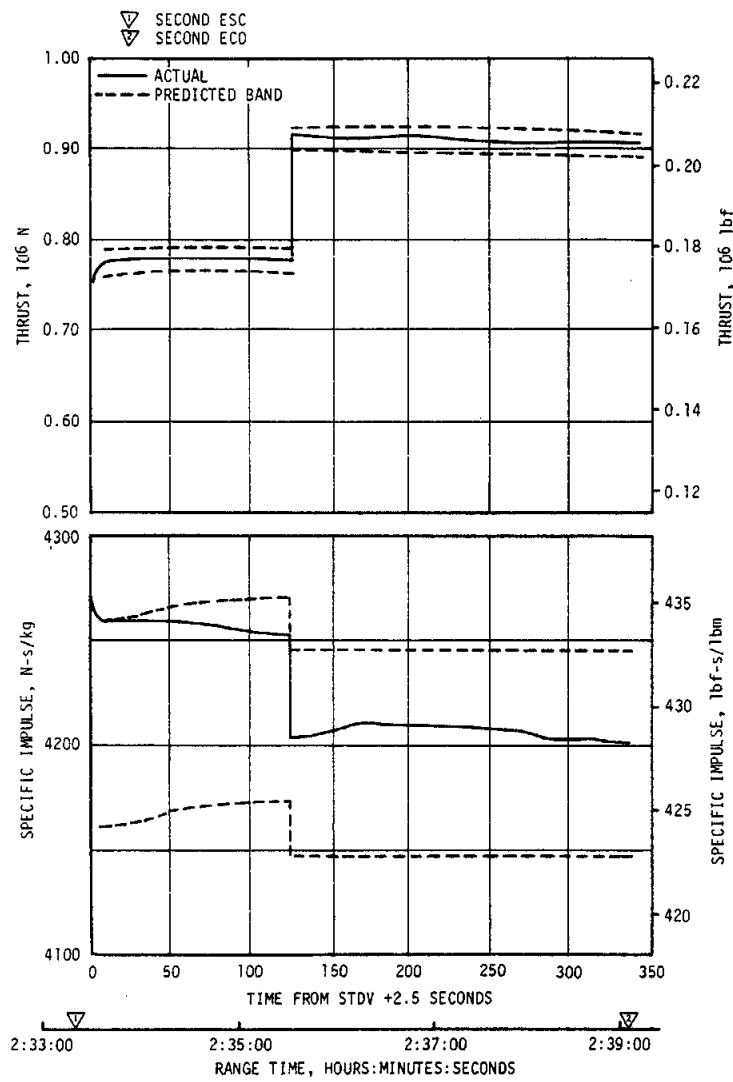


Figure 7-7. S-IVB Steady State Performance - Second Burn

Appropriate data from past flights and acceptance tests are being reviewed in a detailed manner in this continuing investigation.

7.8 S-IVB SHUTDOWN TRANSIENT PERFORMANCE FOR SECOND BURN

The shutdown transient was satisfactory and agreed closely with the acceptance test and predictions. The total cutoff impulse to zero percent of rated thrust was 210,650 N-s (47,356 lbf-s). ECO was initiated by a LVDC velocity cutoff command. Cutoff occurred with the PU valve in the null position.

7.9 S-IVB STAGE PROPELLANT MANAGEMENT

On AS-505 the PU system was operated in the open-loop mode, which means the LOX flowrate is not controlled to insure simultaneous depletion of propellants. The PU system successfully accomplished the requirements associated with propellant loading.

A comparison of propellant mass values at critical flight events, as determined by various analyses, is presented in Table 7-3. The best estimate full load propellant masses were 0.49 percent greater for LOX and 0.26 percent less for LH₂ than the predicted values. This deviation was well within the required loading accuracy.

The third stage statistical weighted average masses at ignition were 165,573 and 132,600 kilograms (365,025 and 292,332 lbm) for first and second burn, respectively. The cutoff masses were 133,830 and 62,450 kilograms (295,044 and 137,679 lbm) for first and second burn, respectively. Extrapolation of propellant level sensor data to depletion, using the propellant flowrates to depletion, indicated that a LOX depletion would have occurred approximately 10.64 seconds after second burn velocity cutoff.

The PU valve was positioned at null for start and remained there, as programmed, during first burn. The PU valve was commanded to the 4.5 EMR position at 9079.3 seconds and remained there for 255.02 seconds. At 9334.3 seconds the valve was commanded to the null position (approximately 5.0 EMR) and remained there throughout the remainder of the flight.

7.10 S-IVB PRESSURIZATION SYSTEM

7.10.1 S-IVB Fuel Pressurization System

The LH₂ pressurization system operationally met all engine performance requirements. The LH₂ pressurization system indicated acceptable performance during prepressurization, boost, first burn, coast phase, and second burn. The LH₂ tank pressurization command was received at -96.41 seconds. The pressurized signal was received 13.1 seconds later.

Table 7-2. S-IVB Steady State Performance - Second Burn (ESC +180-Second Time Slice at Standard Altitude Conditions)

PARAMETER	PREDICTED	SECOND BURN RECONSTRUCTION	FLIGHT DEVIATION	PERCENT DEVIATION FROM PREDICTED
Thrust N (lbf)	9,129,304 (205,235)	9,106,040 (204,712)	-23,264 (-523)	-0.25
Specific Impulse N-s/kg (lbf-s/lbm)	4201 (428.4)	4214 (429.7)	13 (1.3)	0.30
LOX Flowrate kg/s (lbm/s)	180.91 (398.83)	180.23 (397.34)	-0.68 (-1.49)	-0.35
Fuel Flowrate kg/s (lbm/s)	36.38 (80.21)	35.86 (79.05)	-0.53 (-1.16)	-1.4
Engine Mixture Ratio (LOX/Fuel)	4.972	5.026	0.054	1.09

Table 7-3. S-IVB Stage Propellant Mass History

EVENT	UNITS	PREDICTED		PU INDICATED (CORRECTED)		PU VOLUMETRIC		FLOW INTEGRAL		BEST ESTIMATE	
		LOX	LH2	LOX	LH2	LOX	LH2	LOX	LH2	LOX	LH2
S-IC Liftoff	kg (lbm)	86,705 (191,152)	19,731 (43,500)	86,848 (191,466)	19,680 (43,386)	87,478 (192,856)	19,752 (43,545)	86,796 (191,351)	19,605 (43,222)	87,130 (192,089)	19,681 (43,388)
First Ignition (ESC)	kg (lbm)	86,705 (191,152)	19,731 (43,500)	86,844 (191,458)	19,671 (43,367)	87,443 (192,778)	19,750 (43,542)	86,796 (191,351)	19,605 (43,222)	87,130 (192,089)	19,680 (43,388)
First Cutoff (ECO)	kg (lbm)	60,487 (133,350)	14,455 (31,868)	60,465 (133,302)	14,245 (31,405)	60,828 (134,102)	14,313 (31,555)	60,402 (133,164)	14,265 (31,450)	60,728 (133,883)	14,317 (31,564)
Second Ignition (ESC)	kg (lbm)	60,360 (133,072)	13,177 (29,051)	60,274 (132,882)	13,142 (28,973)	60,681 (133,779)	13,210 (29,123)	60,256 (132,841)	13,162 (29,018)	60,541 (133,471)	13,206 (29,116)
Second Cutoff (ECO)	kg (lbm)	2248 (4957)	918 (2025)	2448 (5396)	992 (2186)	2420 (5336)	977 (2153)	2410 (5314)	995 (2194)	2424 (5344)	999 (2204)

Following the termination of prepressurization, the ullage pressure reached relief conditions, approximately 21.8 N/cm² (31.6 psia), and remained just below this level at 21.7 N/cm² (31.5 psia) until liftoff, as shown in Figure 7-8. A small ullage pressure collapse occurred during the first 20 seconds of boost and was followed by a return to the relief level at 45 seconds due to self pressurization.

During first burn, the average pressurization flowrate was approximately 0.33 kg/s (0.72 lbm/s) providing a total flow of 47.7 kilograms (105 lbm). Ullage pressure was at the relief level throughout the burn, as predicted.

During the O₂/H₂ burner repressurization period, the LH₂ tank was pressurized from 13.3 to 20.8 N/cm² (19.3 to 30.2 psia). The LH₂ ullage pressure was 21.7 N/cm² (31.5 psia) at second burn ESC as shown in Figure 7-9. Approximately 12.7 kilograms (28.0 lbm) of helium were used in the repressurization operation. The average second burn pressurization flowrate was 0.30 and 0.32 kg/s (0.67 and 0.71 lbm/s) for 4.5 and 5.0 EMR, respectively. At step pressurization the flowrate increased to 0.52 kg/s (1.14 lbm/s). This provided a total flow of 122 kilograms (268 lbm) during second burn. Significant venting during second burn occurred at second ESC +280 seconds when step pressurization was initiated. This behavior was as predicted.

The ambient repressurization system was used to repressurize the tank from 11.6 to 14.3 N/cm² (16.8 to 20.8 psia) for the LH₂ lead experiment. The repressurization was satisfactory.

- ▽ PREPRESSURIZATION INITIATED
- ▽ FIRST ESC, 553.60
- ▽ FIRST ECO, 703.76
- ▽ REPRESSURIZATION INITIATED

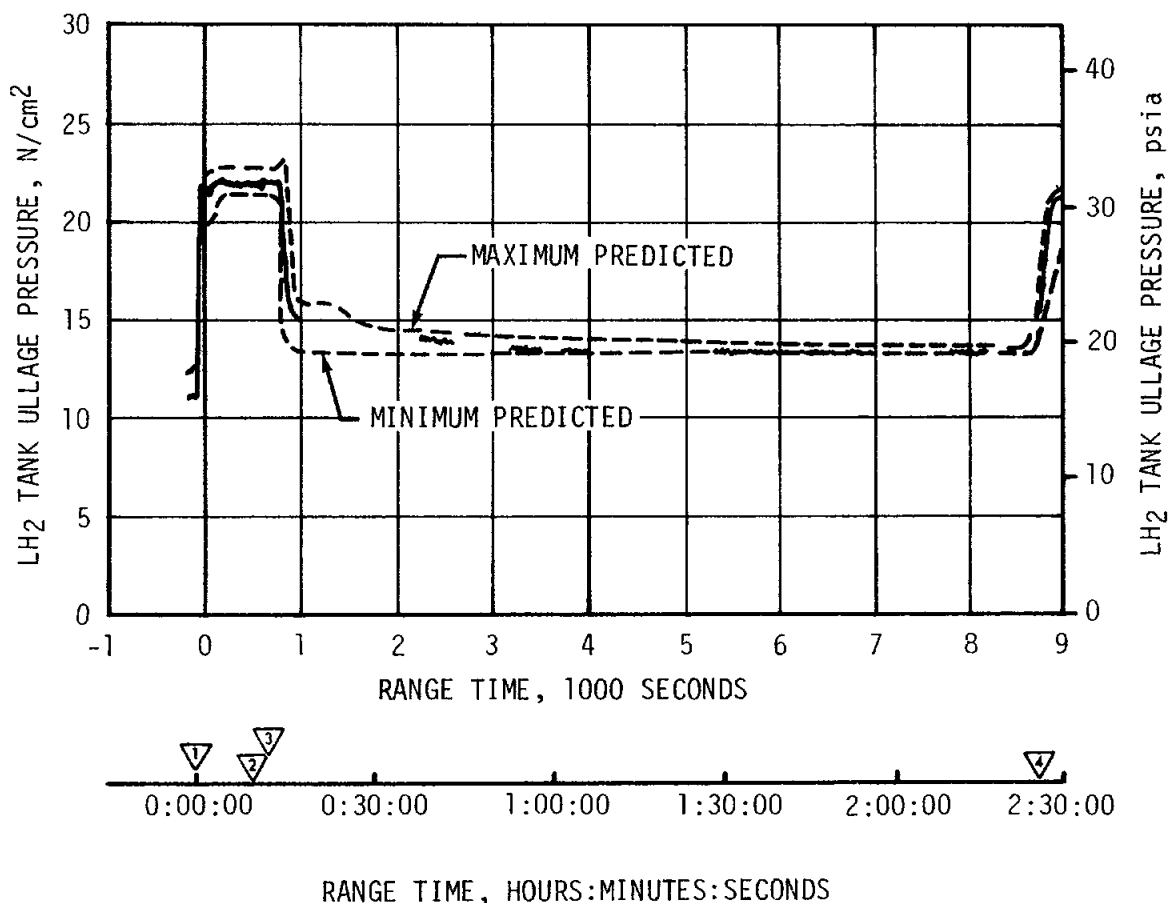


Figure 7-8. S-IVB LH₂ Ullage Pressure - First Burn and Parking Orbit

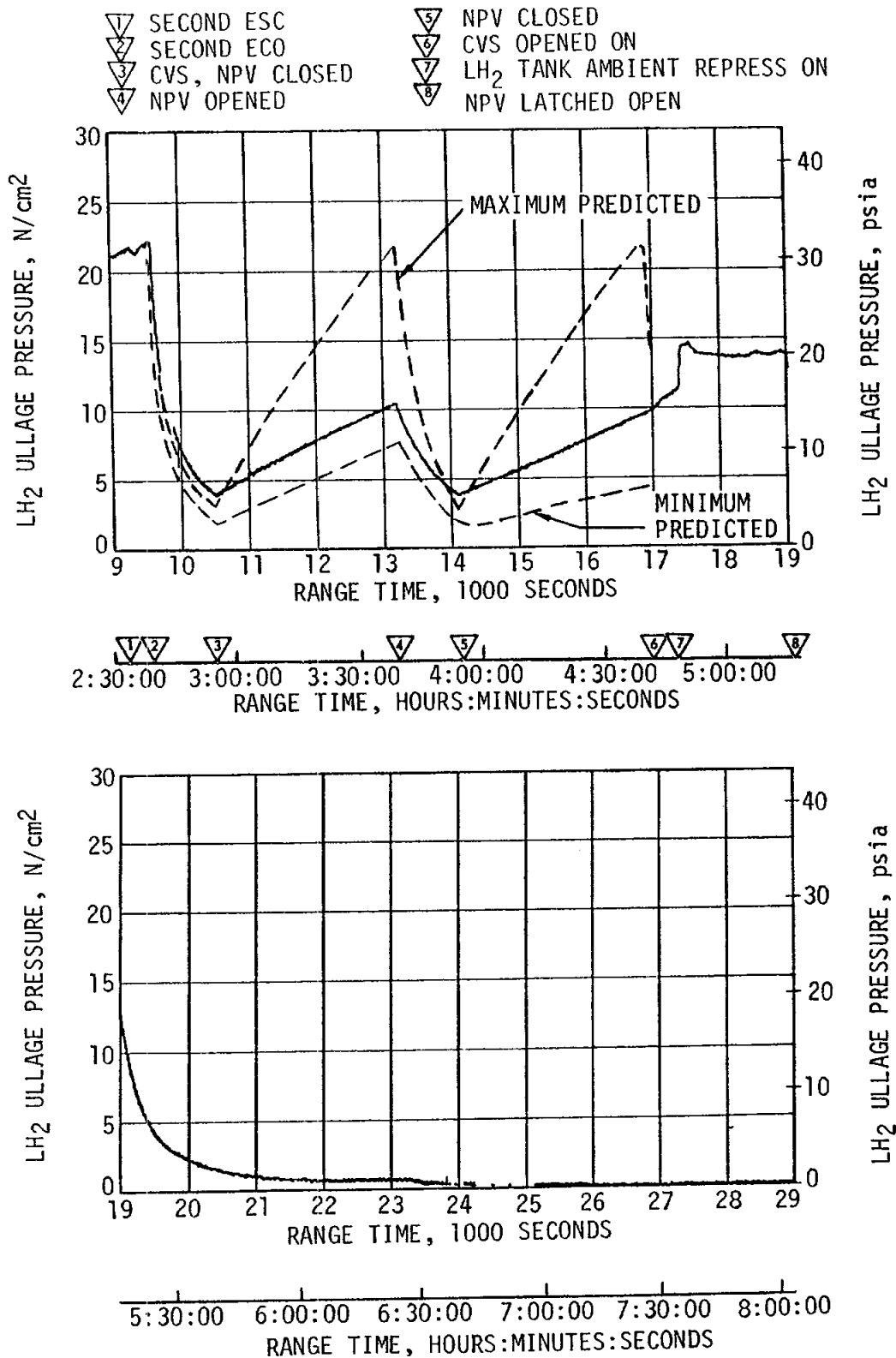


Figure 7-9. S-IVB LH₂ Ullage Pressure - Second Burn and Translunar Coast

The LH₂ pump inlet Net Positive Suction Pressure (NPSP) was calculated from the pump interface temperature and total pressure. These values indicated that the NPSP at first burn ESC was 10.5 N/cm² (15.2 psid). At the minimum point, the NPSP was 4.2 N/cm² (6.1 psid) above the required pressure. Throughout the burn, the NPSP satisfactorily agreed with the predicted value. The NPSP at second burn ESC was 5.2 N/cm² (7.6 psid) which was 1.8 N/cm² (2.6 psid) above the required pressure. Figures 7-10 and 7-11 summarize the fuel pump inlet conditions for first and second burns, respectively.

7.10.2 S-IVB LOX Pressurization System

LOX tank prepressurization was initiated at -167 seconds and increased the LOX tank ullage pressure from ambient to 28.3 N/cm² (41.1 psia) within 18 seconds as shown in Figure 7-12. Three makeup cycles were required to maintain the LOX tank ullage pressure before the ullage temperature stabilized. At -97 seconds the LOX tank ullage pressure increased from 27.4 to 28.5 N/cm² (39.8 to 41.4 psia) due to fuel tank prepressurization, LOX tank vent purge and LOX pressure sense line purge. The ullage pressure increased steadily to 29.5 N/cm² (42.9 psia) just before liftoff.

During S-IC boost there was a relatively moderate ullage pressure decay caused by an acceleration effect and temperature decrease.

No makeup cycles occurred until an inhibit was removed, approximately 50 seconds before ESC. At that time, one makeup cycle occurred. The LOX tank ullage pressure was 27.5 N/cm² (40.0 psia) at first ESC.

During first burn, three over-control cycles were initiated, as compared to the predicted one cycle. The LOX tank pressurization flowrate variation was 0.118 to 0.158 kg/s (0.26 to 0.35 lbm/s) during under-control system operation. This variation is normal because the bypass orifice inlet temperature changes as it follows the cold helium sphere temperature. Heat exchanger performance during first burn was satisfactory.

Repressurization of the LOX tank prior to second burn was not required. The tank ullage pressure was 27.5 N/cm² (39.9 psia) at second ESC, satisfying the requirements as shown in Figure 7-13.

Pressurization system performance during second burn was satisfactory, and had the same characteristics noted during first burn. As predicted, there were no over-control cycles. Flowrate varied between 0.25 and 0.31 kg/s (0.36 to 0.45 lbm/s). Heat exchanger performance was satisfactory.

The LOX NPSP calculated at the interface was 19.1 N/cm² (27.8 psid) at first burn ESC. The NPSP decreased after start and reached a minimum value of 17.3 N/cm² (25.1 psid) at 93 seconds after ESC. This was 6.8 N/cm² (9.9 psid) above the required NPSP at that time.

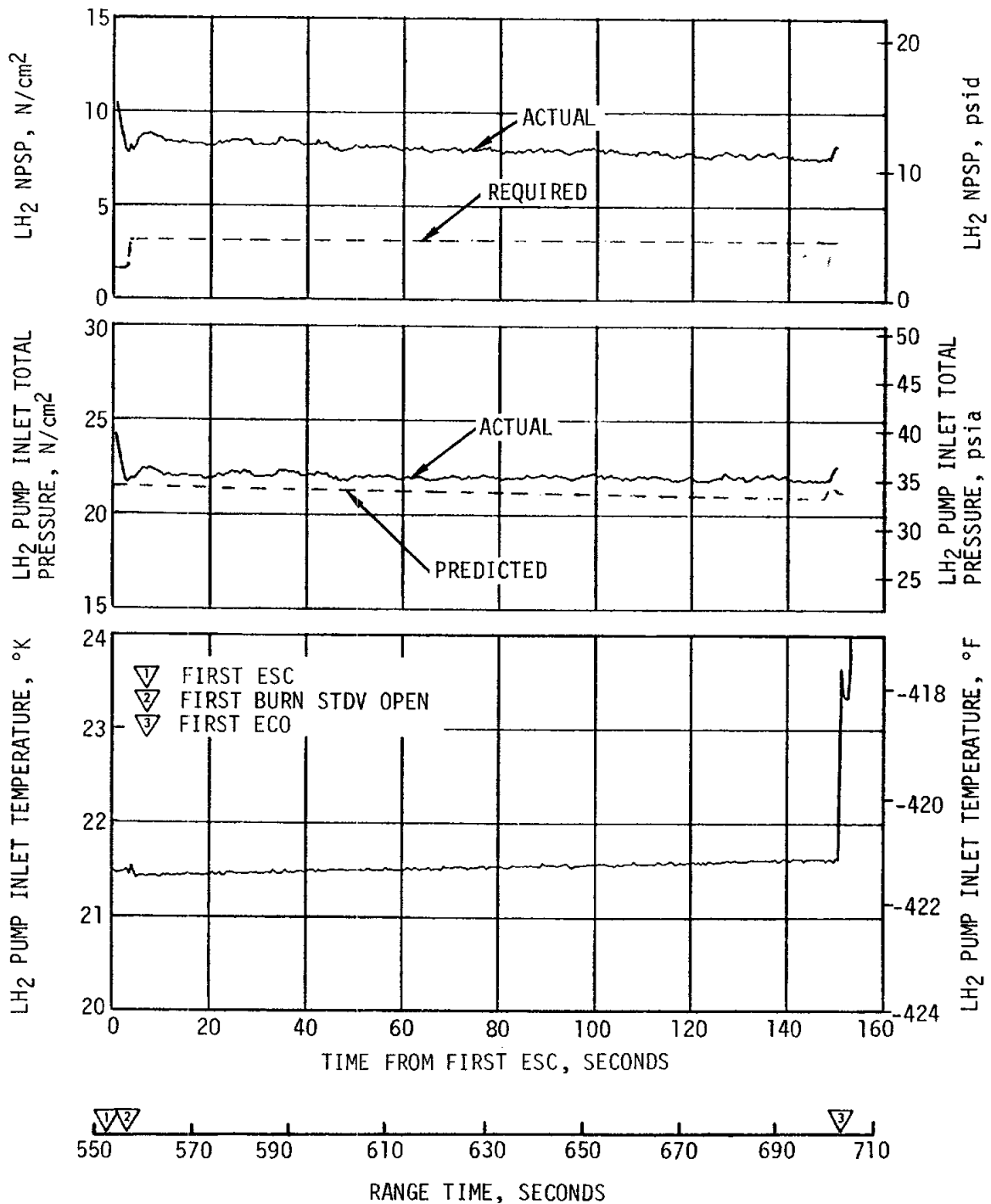


Figure 7-10. S-IVB Fuel Pump Inlet Conditions - First Burn

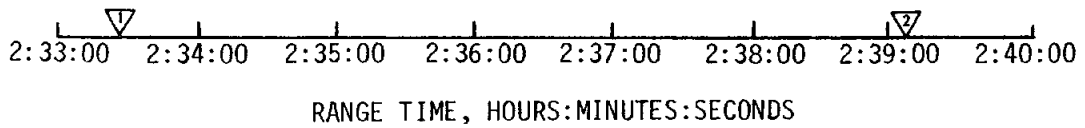
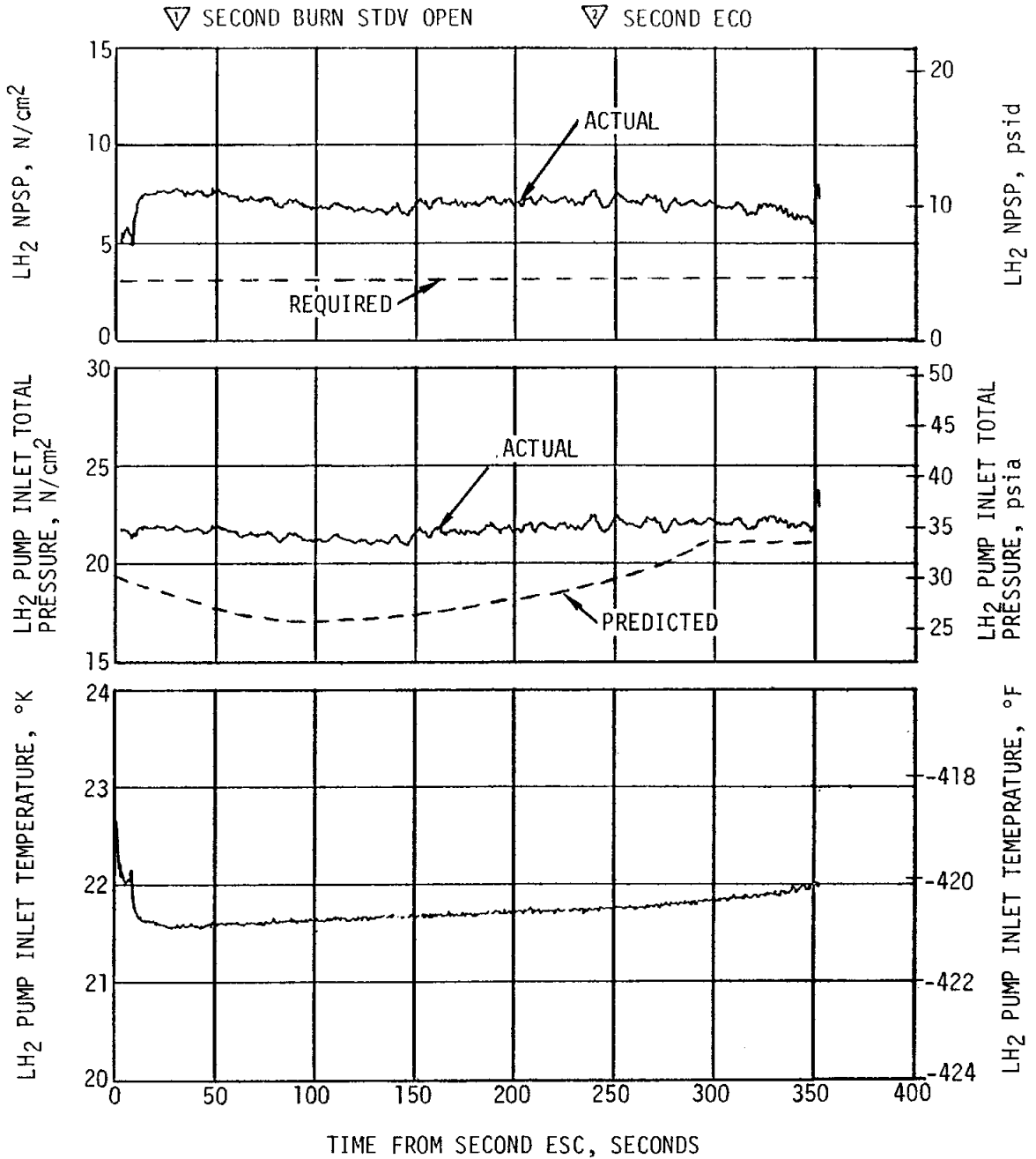


Figure 7-11. S-IVB Fuel Pump Inlet Conditions - Second Burn

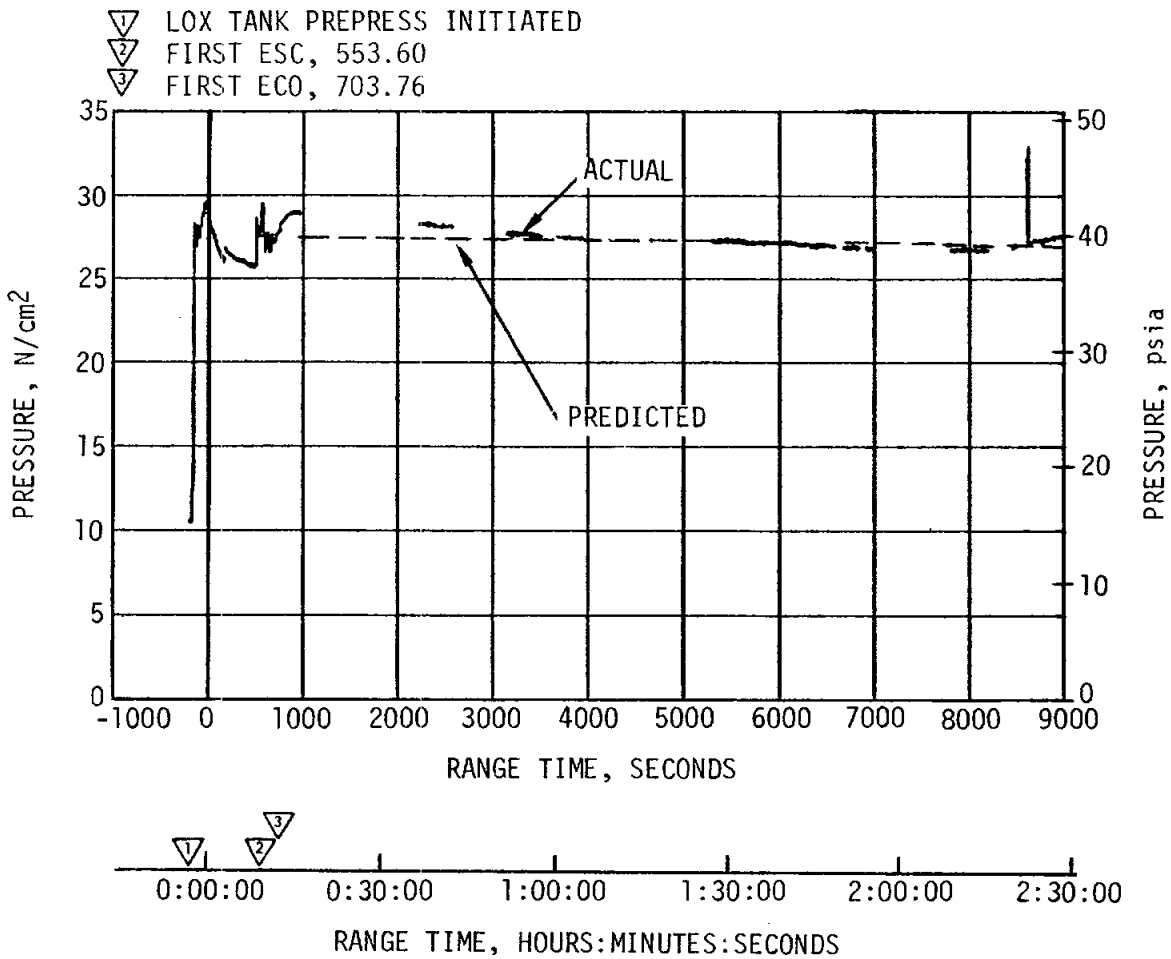


Figure 7-12. S-IVB LOX Tank Ullage Pressure - First Burn and Parking Orbit

The LOX pump static interface pressure during first burn followed the cyclic trends of the LOX tank ullage pressure. The NPSP calculated at the engine interface was 16.0 N/cm^2 (23.3 psid) at second burn ESC. At all times during second burn, NPSP was above the required level. Figures 7-14 and 7-15 summarize the LOX pump conditions for the first and the second burn, respectively.

The cold helium supply was adequate to meet all flight requirements. At first burn ESC the cold helium spheres contained 200 kilograms (442 lbm) of helium. At the end of the first burn, the helium mass had decreased to 176 kilograms (388 lbm). At second burn ESC the spheres contained 163.3 kilograms (360 lbm) of helium. At the end of second burn the helium mass had decreased to 99 kilograms (218 lbm). Figure 7-16 shows helium supply pressure history.

- ▽ SECOND ESC
- ▽ SECOND ECO
- ▽ INITIATE MANEUVER TO SEPARATION ATTITUDE
- ▽ CSM SEPARATION
- ▽ LOX TANK AMBIENT REPRESS
- ▽ START LOX TANK DUMP

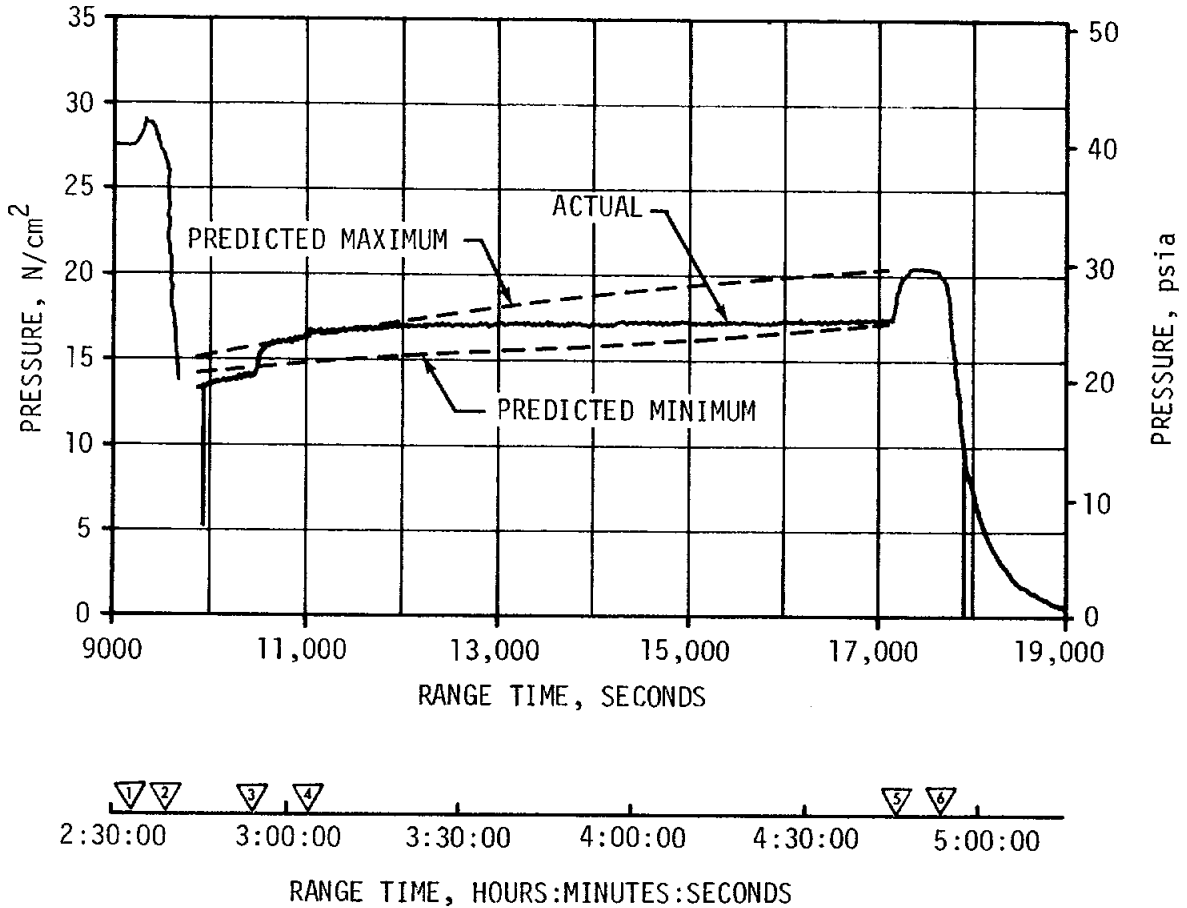


Figure 7-13. S-IVB LOX Tank Ullage Pressure - Second Burn, Translunar Coast

7.11 S-IVB PNEUMATIC CONTROL PRESSURE SYSTEM

The pneumatic control and purge system performed satisfactorily during all phases of the mission. For the first time on a S-IVB flight vehicle the stage pneumatics bottle was manifolded together with the LOX tank ambient repressurization spheres so that helium could flow from the LOX tank repressurization spheres to the stage pneumatic bottle and thus replenish it. System performance was as predicted during boost and first burn operations.

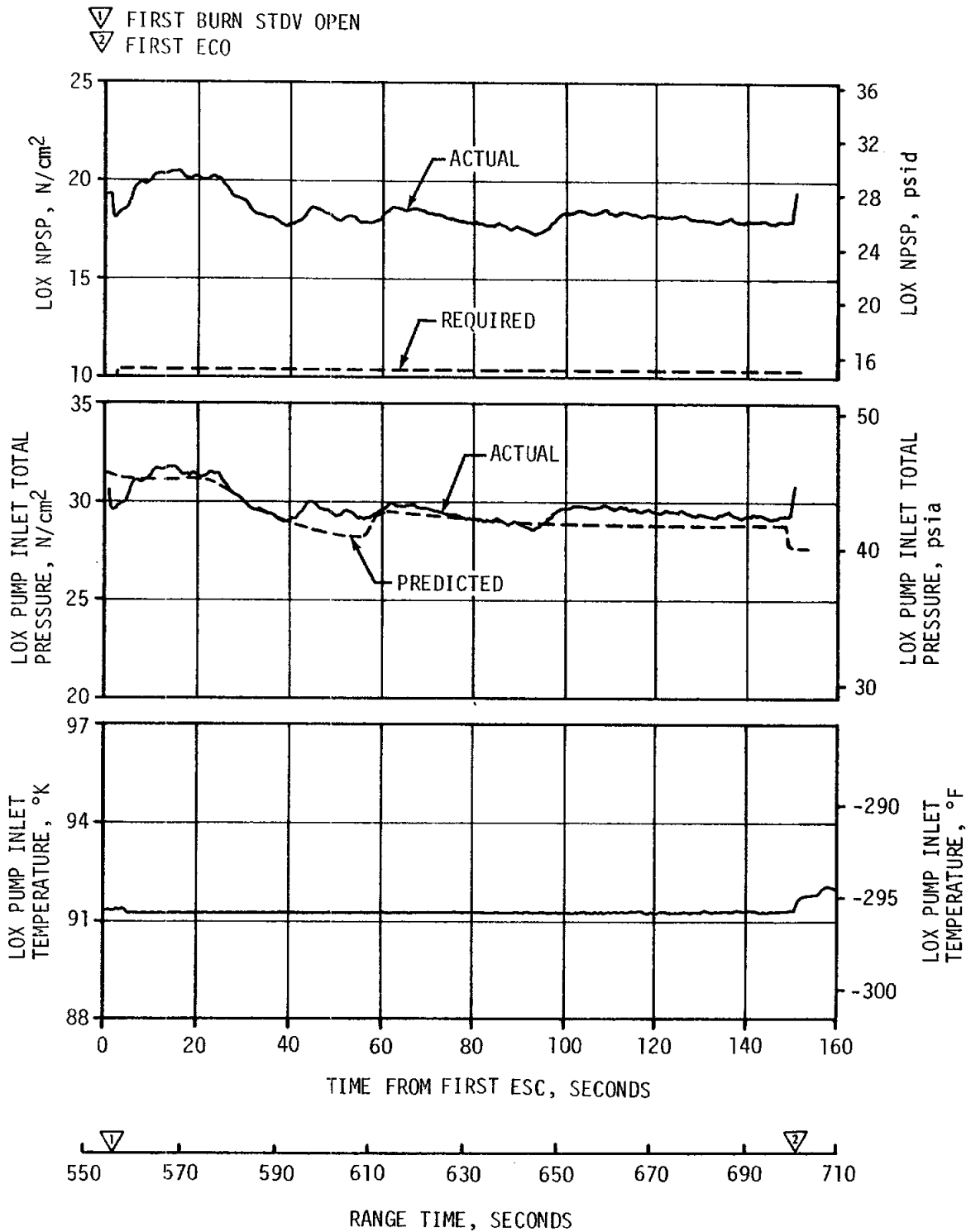


Figure 7-14. S-IVB LOX Pump Inlet Conditions - First Burn

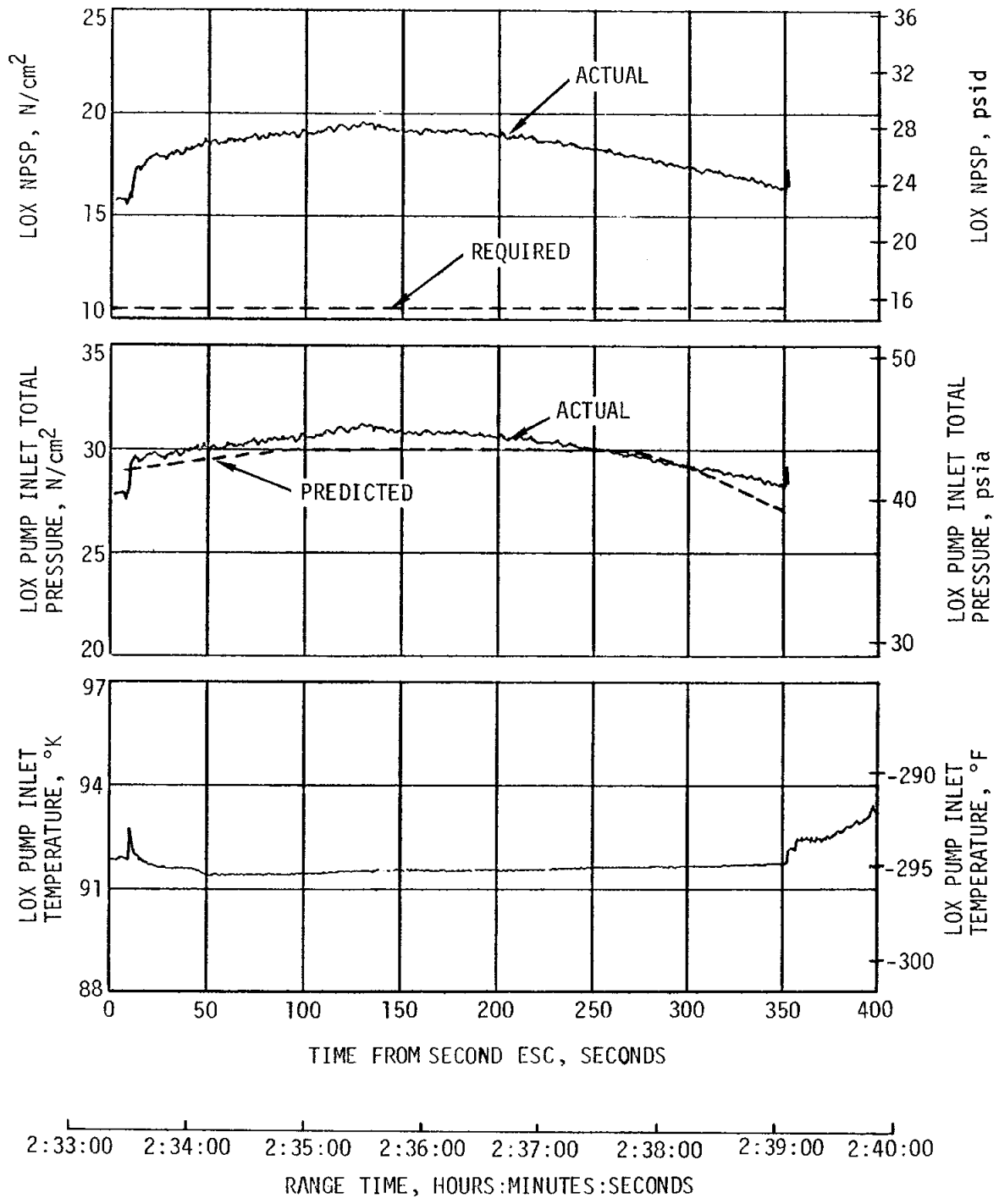


Figure 7-15. S-IVB LOX Pump Inlet Conditions - Second Burn

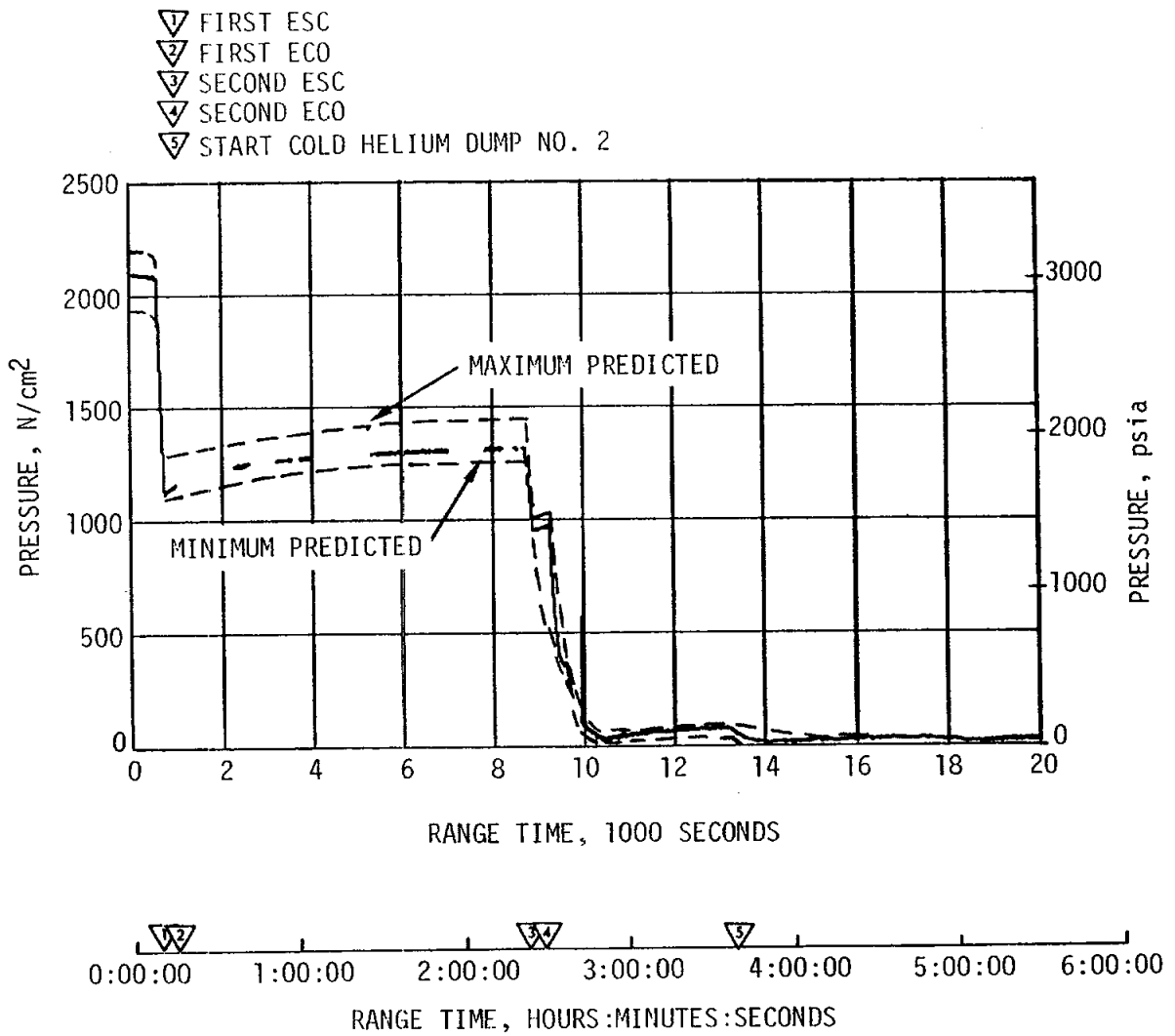


Figure 7-16. S-IVB Cold Helium Supply History

7.12 S-IVB AUXILIARY PROPULSION SYSTEM

The operations of the APS pressurization system was satisfactory with the exception of a helium leak in Module No. 1. The leak started approximately 6.5 hours after liftoff and extended through loss of data at 39,240 seconds (10:54:00). The leak rate at loss of data was approximately 3278 SCCM (200 SCIM). Figure 7-17 presents Modules No. 1 and 2 helium bottle mass at the time of the leak. The attitude control requirements for Modules No. 1 and 2 after 21,600 seconds (6:00:00) were approximately equal.

The range of regulator outlet pressure, ullage pressure, propellant manifold pressure, and propellant temperature is presented in Table 7-4.

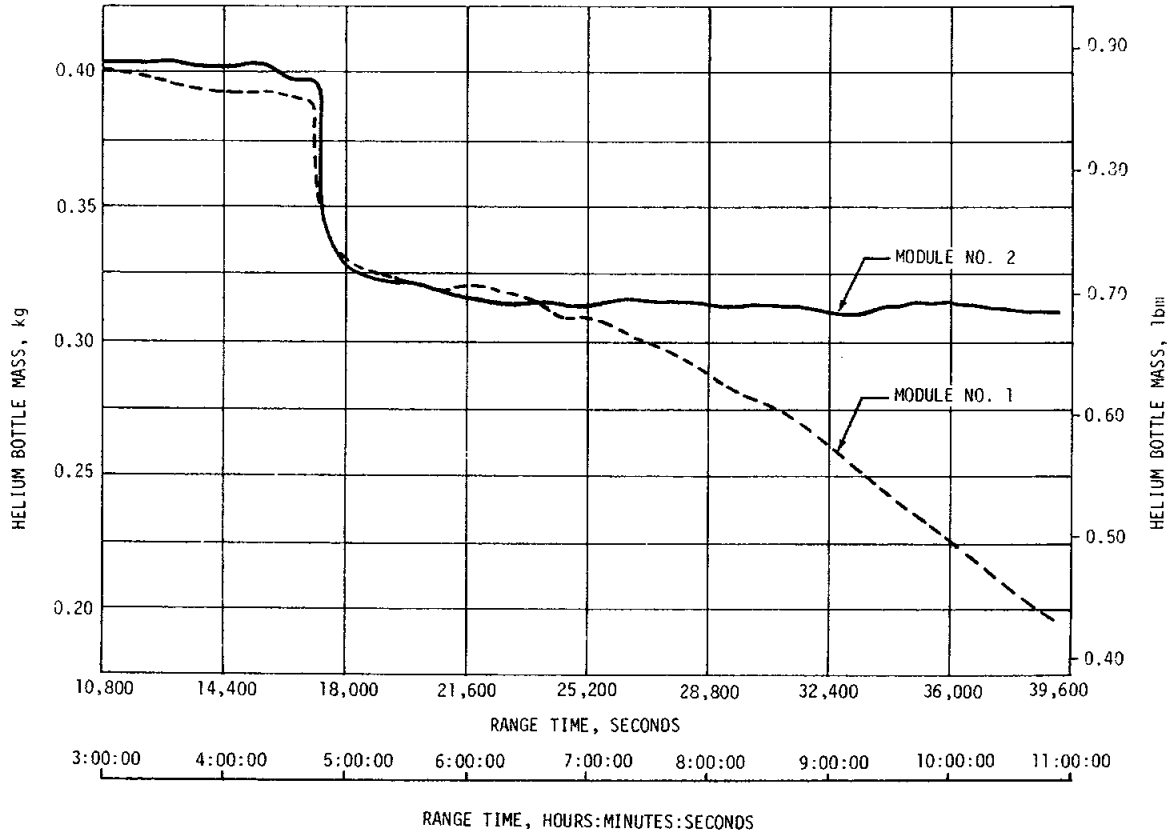


Figure 7-17. S-IVB APS Helium Bottle Mass

These pressure values were satisfactory and within instrumentation accuracy of the required values of 133 to 140 N/cm² (193 to 203 psia) for regulator outlet and 130 to 138 N/cm² (188 to 200 psia) for ullage and manifold pressure. However, temperature extremes of the regulator during the latter portion of the mission caused the Module No. 1 values to increase approximately 3.4 N/cm² (5 psia) and Module No. 2 values to decrease 2.1 N/cm² (3 psia). The regulator temperatures were in the same approximate range as the helium bottle temperatures presented in Figure 7-18. Since this regulator was not temperature compensated, these pressure trends were expected with the temperature extremes seen.

All engines performed satisfactorily. A time history of APS propellants for Modules No. 1 and 2 is presented in Figure 7-19. Table 7-5 presents the APS oxidizer and fuel consumption at significant events during the flight. Table 7-6 summarizes the APS status at loss of data.

7.13 S-IVB PROPELLANT LEAD EXPERIMENT AND ORBITAL SAFING OPERATION

A propellant lead experiment was performed after spacecraft and Lunar Module (LM) separation. LOX and LH₂ flow through the engine simulated the contingency restart preparation sequence. This contingency sequence, which could be used in case of recirculation chilldown system failure, provided data for evaluating the adequacy of the method. Before and after this experiment, the stage high pressure systems were safed. The thrust developed during the experiment and subsequent LOX dump was utilized to ensure that the spent S-IVB stage would be placed in solar orbit.

The manner and sequence in which the experiment and safing were performed are presented in Figure 7-20.

Table 7-4. S-IVB APS Propellant Conditions

PARAMETER	MODULE NO. 1		MODULE NO. 2	
	FUEL	OXIDIZER	FUEL	OXIDIZER
Ullage Pressure N/cm ² (psia)	131 to 137 (190 to 198)	128 to 137 (186 to 198)	128 to 132 (185 to 192)	124 to 126 (180 to 183)
Propellant Manifold Pressure N/cm ² (psia)	128 to 134 (186 to 194)	135 to 138 (196 to 200)	124 to 131 (180 to 190)	125 to 131 (182 to 190)
Propellant Temps (In Propellant Control Module) °K (°F)	290 to 304 (62 to 87)	290 to 307 (62 to 93)	305 to 316 (90 to 110)	304 to 315 (87 to 107)
Regulator Outlet Pressure N/cm ² (psia)	130 to 139 (188 to 202)	130 to 139 (188 to 202)	128 to 134 (186 to 194)	128 to 134 (186 to 194)

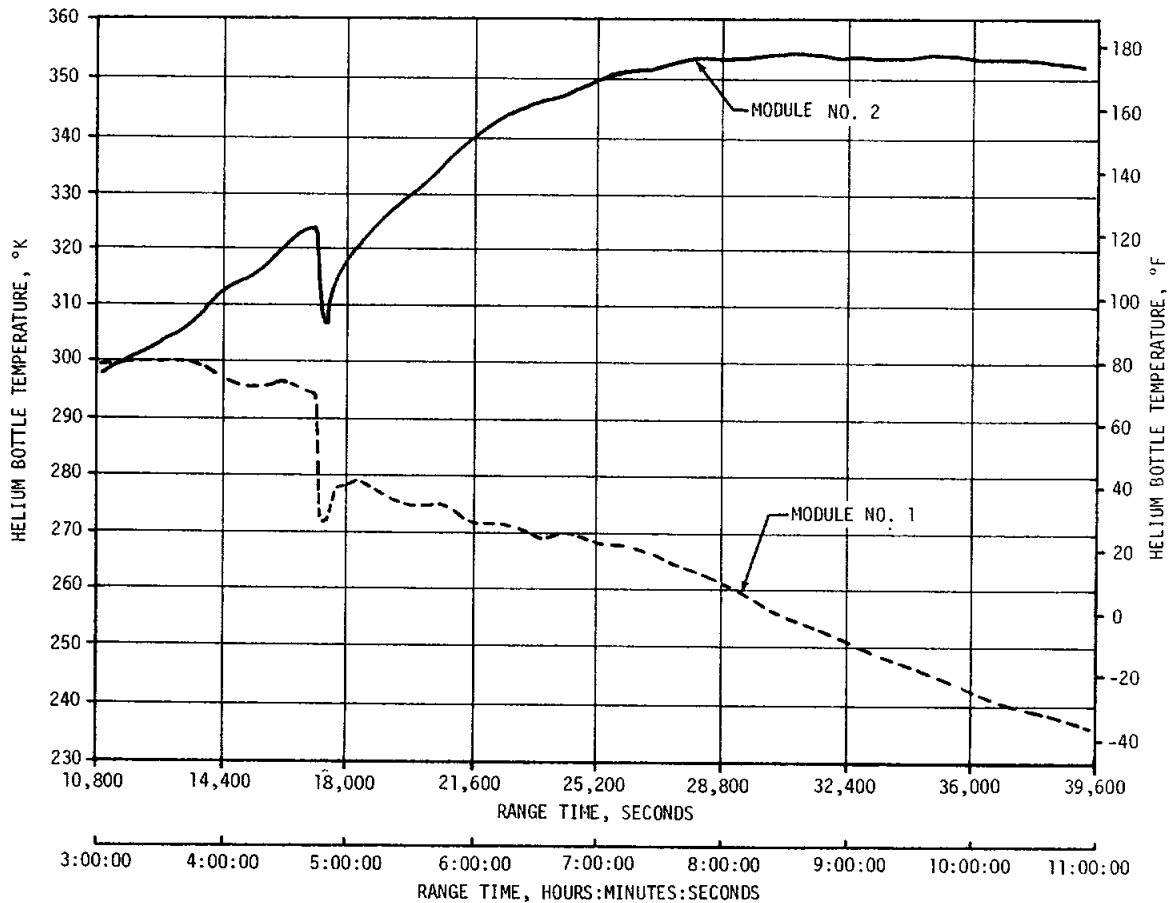


Figure 7-18. S-IVB APS Helium Bottle Temperature

7.13.1 LOX and LH₂ Lead Chillover Experiment

The LOX and LH₂ chillover experiment was successfully conducted as planned. Preliminary evaluations indicate that propellant tank repressurizations were within the limits predicted for the experiment and that the data received, with appropriate analysis and interpretation, will provide chillover criteria for contingency restart procedures. The main LOX valve was opened at 17,301 seconds and closed at 17,310 seconds, resulting in a LOX lead time of 9 seconds. The main fuel valve was opened at 17,410 seconds and closed at 17,459 seconds, resulting in a fuel lead time of 49 seconds.

The data received from this experiment have been evaluated from a "first-look" standpoint and are presented in Figures 7-21 through 7-23.

LOX pump inlet conditions are presented in Figure 7-21. The data indicated that the LOX pump inlet temperature went off-scale low 4 seconds after the MOV opened and came back on-scale 49 seconds after the MOV opened; this was 40 seconds after the MOV had closed. As shown in the figure, LOX pump inlet temperature was satisfactory for engine start at the end of an 8-second fuel lead.

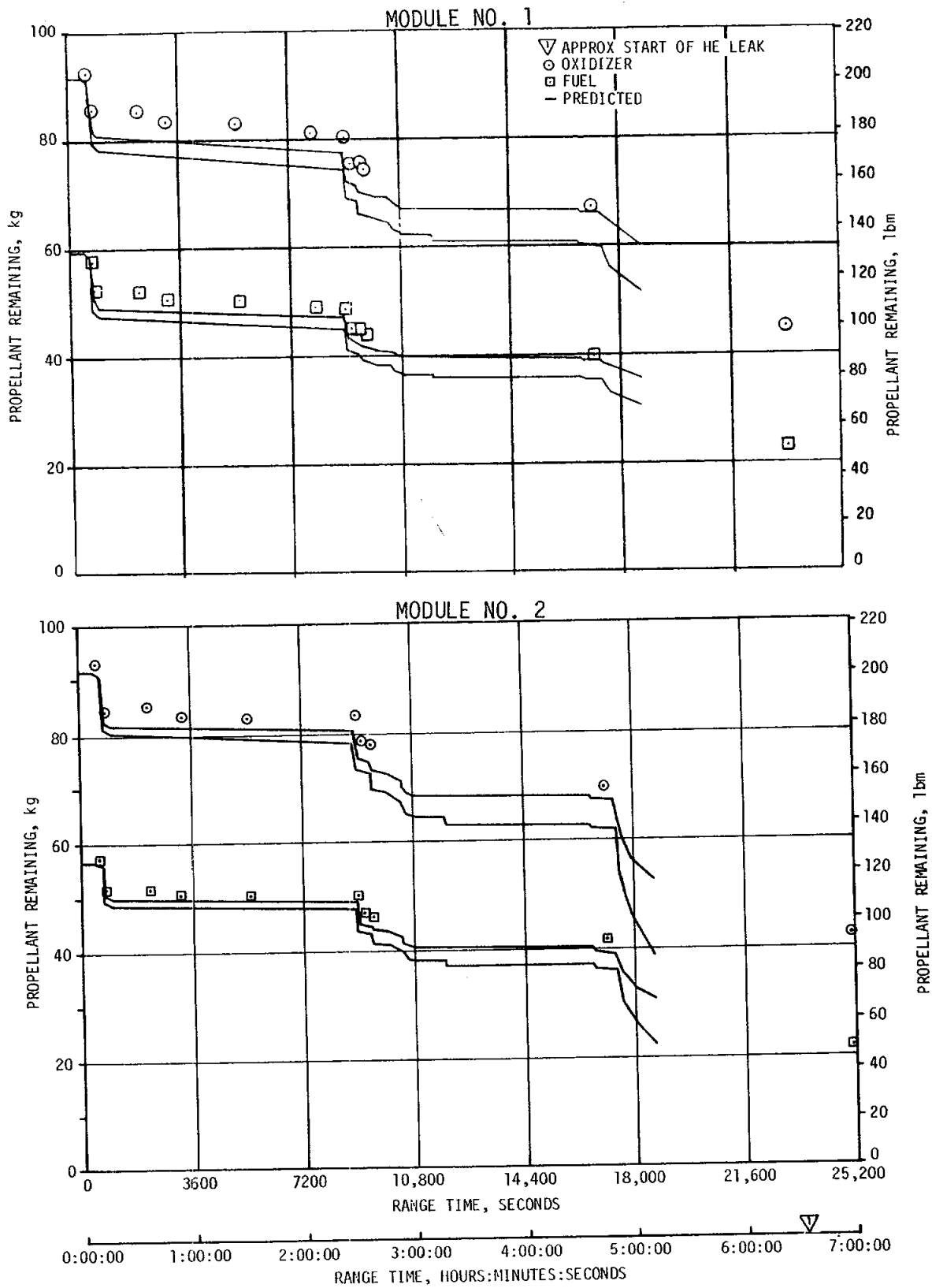


Figure 7-19. S-IVB APS Propellants Remaining Versus Range Time, Module No. 1 and Module No. 2

Table 7-5. S-IVB APS Propellant Consumption

TIME PERIOD	MODULE AT POSITION I				MODULE AT POSITION II			
	OXIDIZER KG	(LBM)	FUEL KG	(LBM)	OXIDIZER KG	(LBM)	FUEL KG	(LBM)
Liftoff	93.3	(205.8)	58.1	(128.0)	93.5	(206.2)	58.1	(128.0)
First Burn (Roll Control)	0.3	(0.7)	0.2	(0.4)	0.3	(0.7)	0.2	(0.4)
ECO to End of First APS Ullaging	5.8	(12.9)	4.6	(10.2)	5.8	(12.9)	4.6	(10.2)
End of First Ullage Burn to Start of T ₆	4.8	(10.6)	3.1	(6.9)	3.5	(7.7)	2.1	(4.6)
Restart Preparations	6.5	(14.3)	4.9	(10.8)	5.4	(11.8)	4.2	(9.2)
Second Burn (Roll Control)	0.3	(0.7)	0.2	(0.4)	0.3	(0.7)	0.2	(0.4)
ECO to Loss of Data	28.5*	(62.9)	20.5*	(45.2)	34.7	(76.6)	25.2	(55.4)
Total Usage	46.3	(102)	33.6	(74)	50.0	(110.3)	36.5	(80.2)

NOTE: The APS propellant consumption presented in this table was determined from helium bottle conditions (pressure, volume, temperature [PVT] method).

* The PVT method used in determining propellant consumption could not be used for Module No. 1 after 6.5 hours because of the Module No. 1 helium leak which started at approximately 6.5 hours.

LOX pump outlet conditions are presented in Figure 7-22. The data indicate that outlet conditions were satisfactory for start at the 8-second fuel lead time. There were indications that all-liquid flow was not present at the pump discharge. It is also noted that point 3 in the figure is near the saturation line and could actually be mixed phase rather than subcooled as indicated. However, it is believed that additional LOX tank pressure, subcooling the propellant as indicated by point 4, would have resulted in a satisfactory start condition. Saturated propellant conditions at the pump discharge are considered adequate for restart by the engine manufacturer.

Table 7-6. S-IVB Helium Bottle Conditions

PARAMETER	MODULE NO. 1		MODULE NO. 2	
	INITIAL CONDITIONS	CONDITIONS AT LOSS OF DATA 39,000 SEC	INITIAL CONDITIONS	CONDITIONS AT LOSS OF DATA 39,000 SEC
Pressure N/cm ² (psia)	2137 (3100)	663 (961)	2137 (3100)	1604 (2327)
Temperature °K (°F)	305 (90)	237 (-36)	304 (87)	351 (172)
Mass kg (lbm)	0.4654 (1.026)	0.197 (0.435)	0.467 (1.030)	0.314 (0.692)
Usage kg (lbm)		0.268 (0.591)		0.153 (0.338)

The conditions at the fuel pump inlet are presented in Figure 7-23. Fuel measurements obtained indicate that all-liquid flow was present at the pump inlet 3 seconds after fuel lead start. It is also indicated that pump inlet conditions remained substantially constant during the remainder of the 49-second fuel lead period. As shown in the figure, satisfactory start conditions are projected for a normal restart LOX tank pressure condition and an 8-second fuel lead.

Thrust chamber conditioning is depicted by the fuel injection temperature versus time curve in Figure 7-23. The measurements indicate that the injection temperature chilldown characteristic demonstrated was within the predicted range. However, it is not concluded at this time that a satisfactory condition would have existed if the fuel tank had been repressurized to a normal restart pressure level. This issue is clouded by erratic behavior of the fuel injection temperature measurement. The most appropriate adjustments have been made and are reflected in Figure 7-23; however, the response of this measurement is still under investigation.

7.13.2 LOX Tank Ambient Repressurization

Ambient helium repressurization of the LOX tank in preparation for the propellant lead experiment and LOX dump, was satisfactorily accomplished. Repressurization was initiated at approximately 17,153 seconds and was terminated 202 seconds later. Helium supply pressure dropped from 1960 to 90 N/cm² (2840 to 130 psia) and approximately 6.4 kilograms (14.2 lbm) of helium were added to the tank ullage. The ullage pressure only increased from 17.5 to 20.4 N/cm² (25.4 to 29.7 psia) because of the large ullage volume.

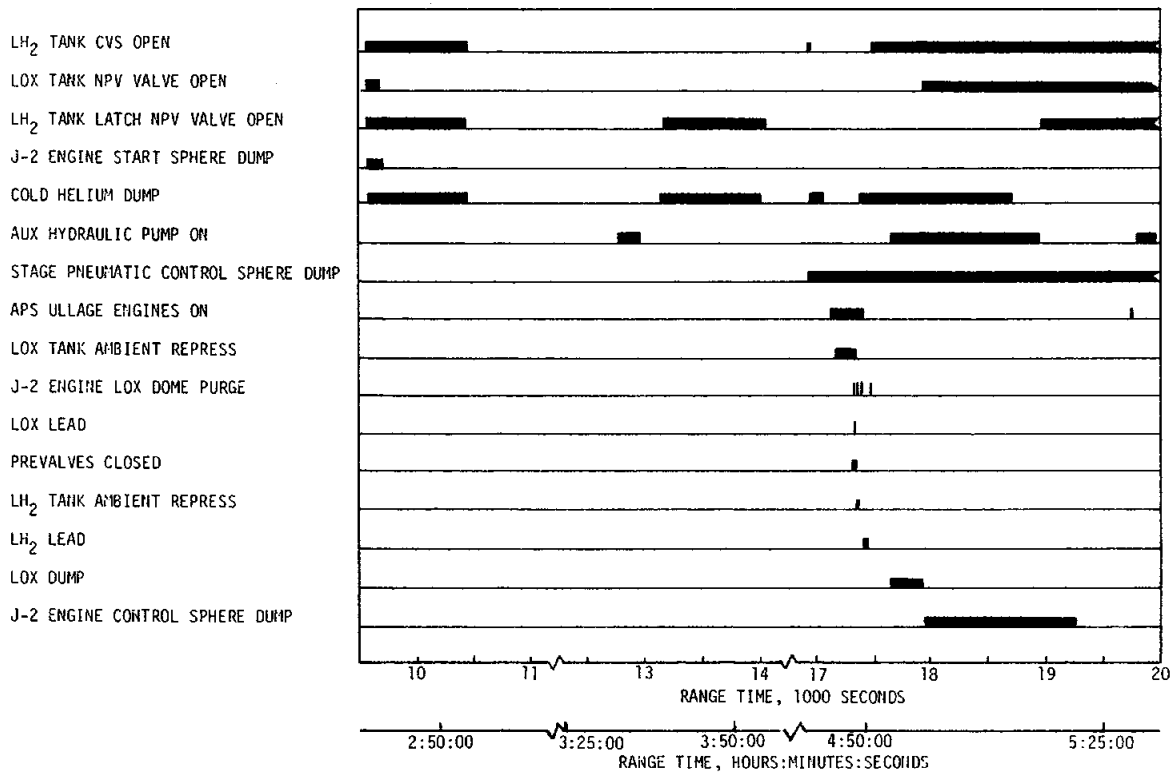


Figure 7-20. S-IVB Propellant Lead Experiment and Orbital Safing Sequence

7.13.3 LH₂ Tank Ambient Repressurization

Ambient helium repressurization of the LH₂ tank was satisfactorily accomplished in preparation for the propellant lead experiment. Repressurization was initiated at approximately 17,357 seconds and was terminated 29 seconds later. Helium supply pressure dropped from 1937 to 503 N/cm² (2810 to 730 psia) and approximately 11.2 kilograms (24.8 lbm) of helium were added to the tank ullage. The ullage pressure increased from 11.4 to 14.3 N/cm² (16.6 to 20.8 psia).

7.13.4 Fuel Tank Safing

The LH₂ tank was satisfactorily safed by accomplishing a programmed vent following the dual propellant lead experiment utilizing both the Non Propulsive Vent (NPV) and CVS as indicated in Figure 7-20. The LH₂ tank ullage pressure during safing is shown in Figure 7-9. At the start of safing, the LH₂ tank ullage pressure was 13.8 N/cm² (20.0 psia) and after venting for 2 hours it had decayed to approximately 0.07 N/cm² (0.1 psia).

7.13.5 LOX Tank Dump and Safing

Immediately following second burn cutoff, a programmed 150-second vent reduced LOX tank ullage pressure from 26.7 to 13.1 N/cm² (38.8 to 19.0 psia) as shown in Figure 7-13. Data levels were as expected with 44.9 kilograms (99 lbm) of helium and 72.5 kilograms (160 lbm) of GOX being vented overboard. As indicated in Figure 7-13, the ullage pressure then rose gradually due to self-pressurization, to 17.4 N/cm² (25.3 psia) at the initiation of ambient repressurization. Repressurization raised the ullage pressure to 20.5 N/cm² (29.7 psia).

The LOX tank dump was initiated at 17,665.79 seconds and was satisfactorily accomplished. A steady-state liquid flow of 0.0260 m³/s (411 gpm) was reached within 7 seconds.

Approximately 55 seconds after dump initiation, the measured LOX flowrate showed a sudden increase indicating that gas ingestion had begun. Shortly thereafter, the LOX ullage pressure began decreasing at a greater rate. Calculations indicate the LOX residual, approximately 2203 kilograms (4870 lbm), was dumped within 194 seconds. The tank pressure had decayed to 13.3 N/cm² (19.3 psia) at this time. Ullage gases continued to be dumped until the programmed termination.

LOX dump ended at 17,956 seconds as scheduled by closure of the MOV. A steady-state LOX dump thrust of 4340 Newtons (975 lbf) was obtained. The total impulse before MOV closure was 409,782 N-s (92,123 lbf-s), resulting in a calculated velocity increase of 25.4 m/s (83.2 ft/s). Figure 7-24 shows the LOX flowrate during dump and the mass of liquid and gas in the oxidizer tank. Figure 7-24 shows LOX ullage pressure and the LOX dump thrust produced. The predicted curves provided for the LOX flowrate and dump thrust correspond to the quantity of LOX dumped and the actual ullage pressure.

Three seconds following termination of LOX dump, the LOX NPV valve was opened and remained open for the duration of the mission. LOX tank ullage pressure decayed from 8.5 N/cm² (12.3 psia) at 17,956 seconds to zero pressure at approximately 25,000 seconds.

7.13.6 Cold Helium Dump

Cold helium was dumped through the O₂/H₂ burner heating coils and into the LH₂ tank, and overboard through the tank vents.

The cold helium spheres were safed by three cold helium dumps. Dump No. 1 was initiated at 9572 seconds and was programmed to continue for approximately 878 seconds as shown in Figure 7-16. During this period, the pressure decayed normally from 358.5 to 34.5 N/cm² (520 to 50 psia). Approximately 60.4 kilograms (113 lbm) of helium was dumped overboard. Dump No. 2 was initiated at 13,151 seconds and was programmed to continue for approximately 899 seconds as shown in Figure 7-16. During this period, the pressure decayed normally from 68.9 to 6.9 N/cm² (100 to 10 psia).

- ① START OF LOX LEAD +4 SECONDS
- ② START OF LOX LEAD +49 SECONDS
- ③ START OF FUEL LEAD
- ④ END OF 49 SECONDS FUEL LEAD
- ⑤ PROJECTED FOR FUEL LEAD START +8 SECONDS WITH NORMAL LOX TANK RESTART CONDITIONS

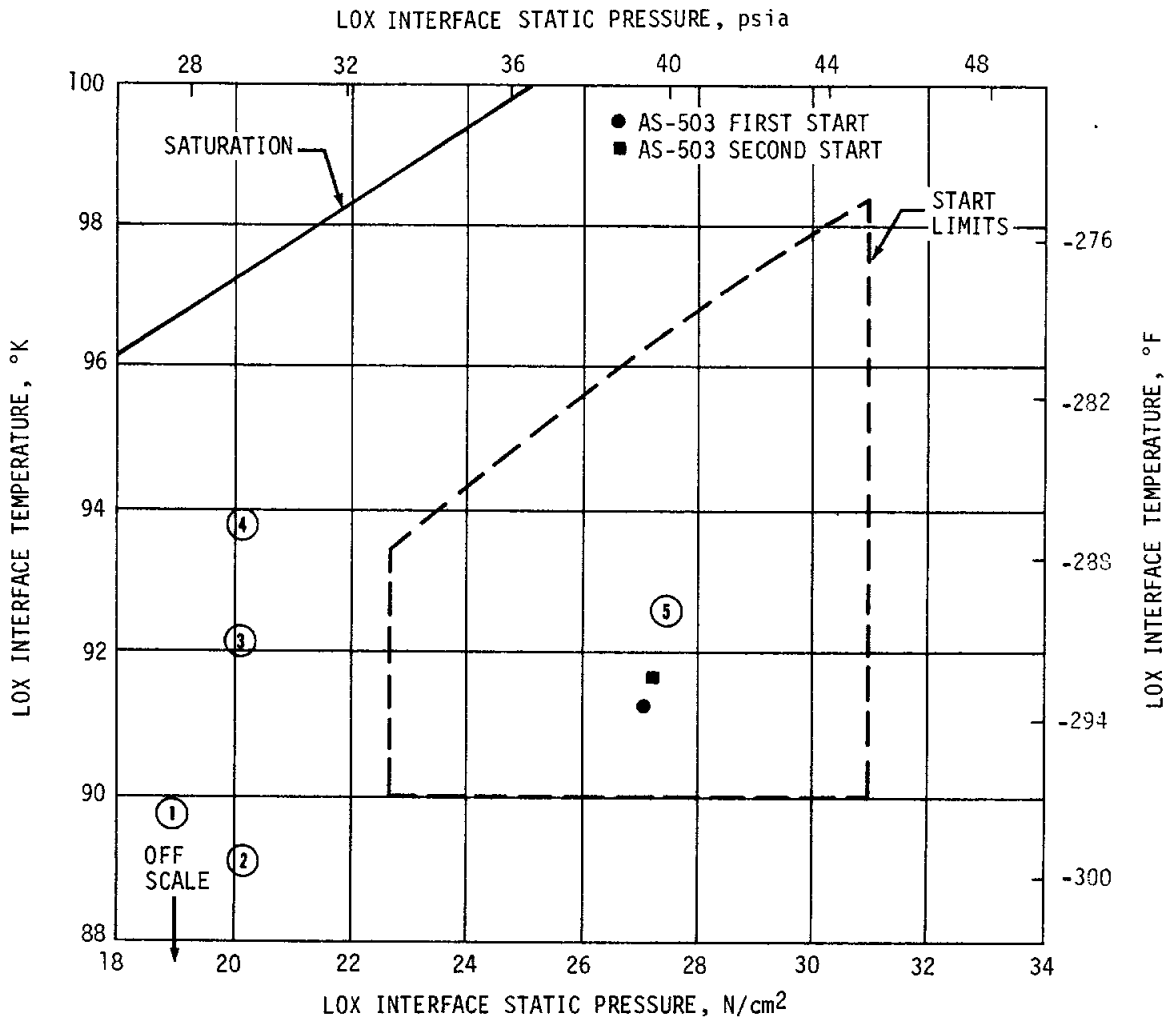


Figure 7-21. LOX Pump Inlet Chilldown Effectiveness

Approximately 12.7 kilograms (28 lbm) of helium was dumped overboard. An insignificant amount of helium was dumped overboard during the third cold helium dump which was initiated at 16,937 seconds and lasted 1511 seconds.

7.13.7 Ambient Helium Dump

The ambient helium remaining in the LOX and fuel repress spheres was dumped through the engine control helium regulator via the engine control sphere. The fuel repress spheres pressure decay began at 17,965 seconds and lasted for 2301 seconds. The pressure decayed from 620.1 to 75.8 N/cm² (900 to 110 psia). The LOX repress spheres pressure decay began at 18,300 seconds and lasted 966 seconds. The pressure decayed from 203.2 to 75.8 N/cm² (295 to 110 psia). The LOX and fuel repress spheres were secured by terminating the engine control bottle dump.

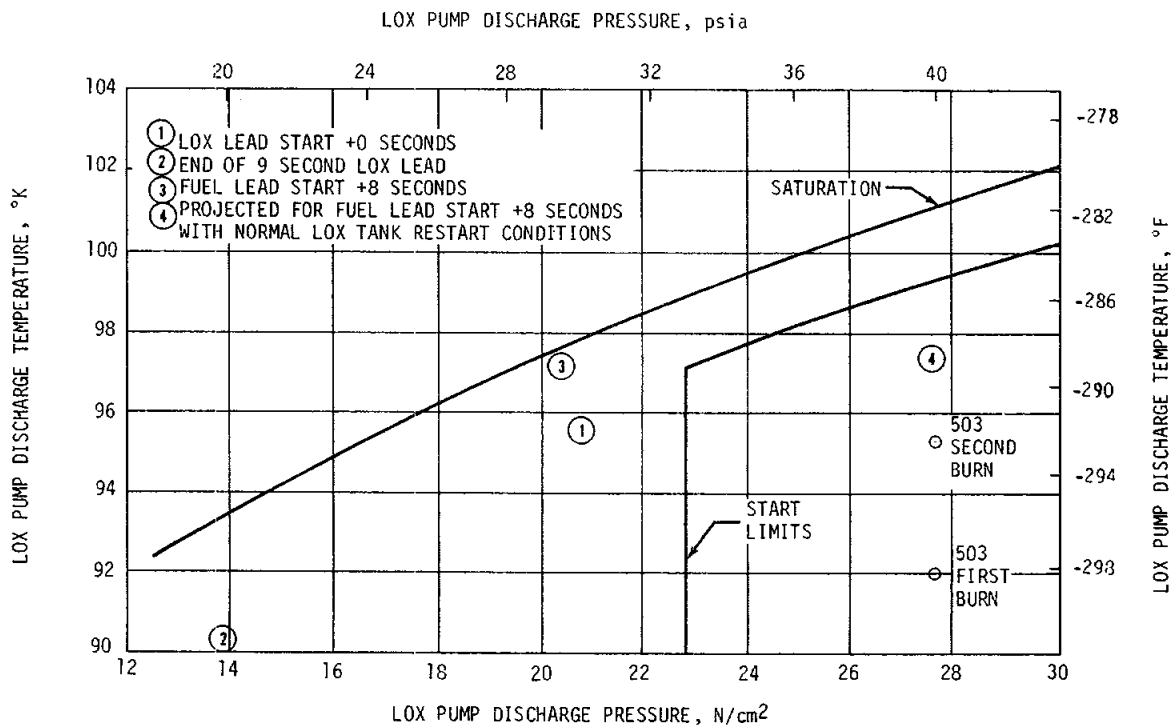


Figure 7-22. LOX Pump Discharge Chillover Effectiveness

7.13.8 Stage Pneumatic Control Sphere Safing

The stage pneumatic control sphere was safed by initiating the J-2 engine pump purge and flowing helium through the pump seal cavities to atmosphere. The stage pneumatic control sphere dump was initiated at 16,936 seconds and had a programmed duration of 3600 seconds. The pressure decayed normally from 2034 to 868 N/cm² (2950 to 1260 psia). The safing period satisfactorily reduced the potential energy in the sphere.

7.13.9 Engine Start Sphere Safing

The engine start sphere was safed during a 150-second period at approximately 9553 seconds. Safing was accomplished by opening the sphere vent valve. Pressure was decreased from 785.5 to 13.8 N/cm² (1140 to 20 psia) with 1.5 kilograms (3.3 lbm) of hydrogen being vented.

7.13.10 Engine Control Sphere Safing

The engine control sphere was safed beginning at 17,965 seconds and ending at 19,266 seconds. The helium control solenoid was energized to vent helium through the engine purge system. The pressure decayed from 620.1 to 75.8 N/cm² (900 to 110 psia). The ambient helium remaining in the LOX and fuel repress spheres was also dumped via the engine control sphere.

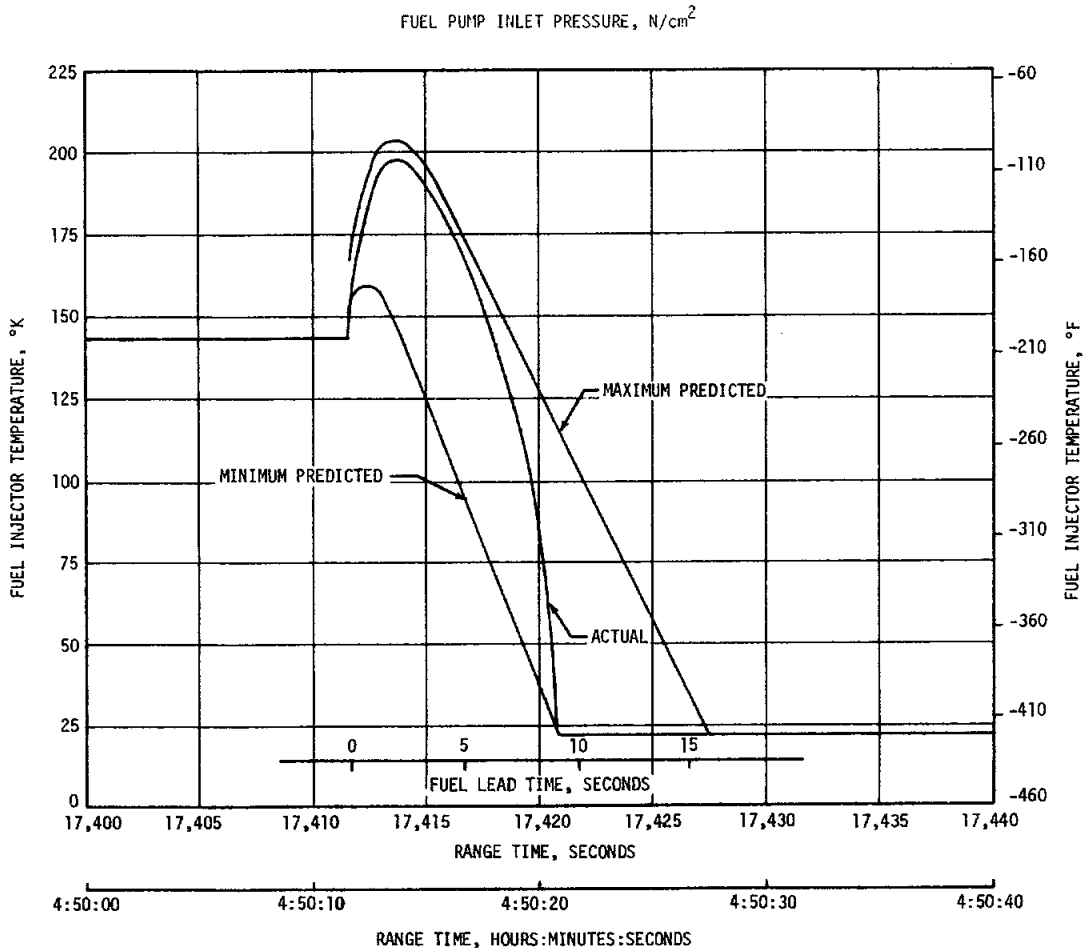
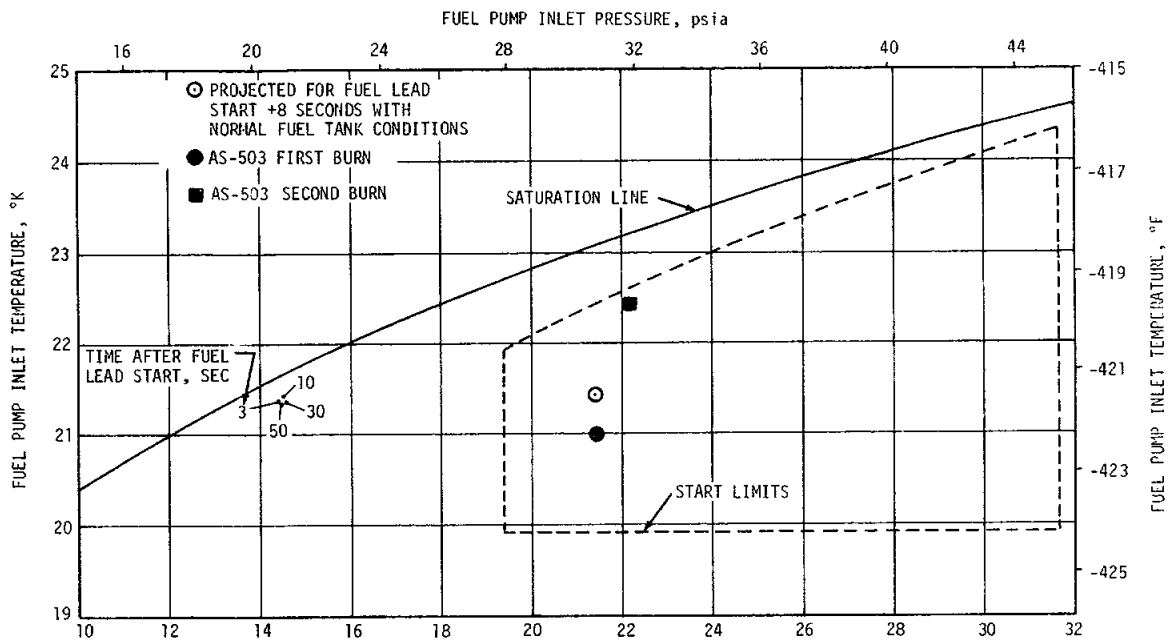


Figure 7-23. S-IVB Fuel Lead Chillover Effectiveness

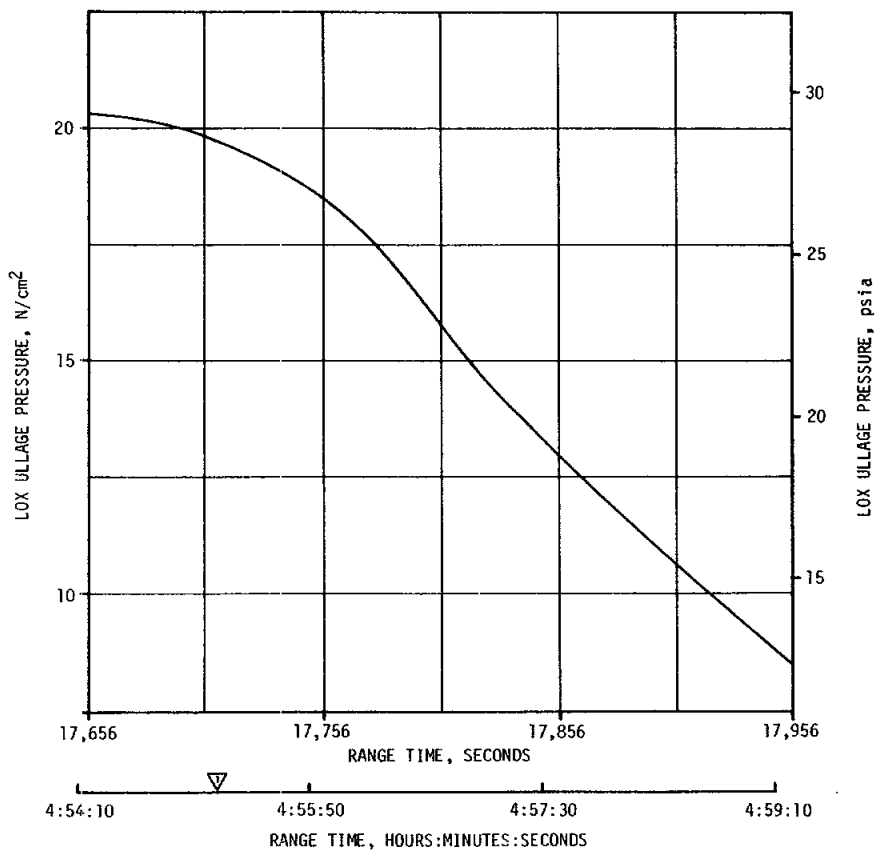
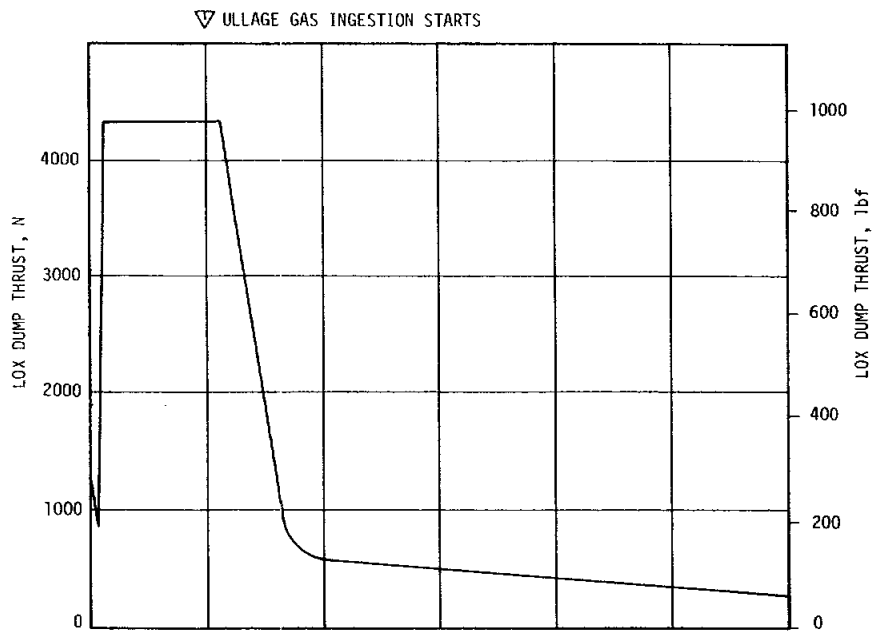


Figure 7-24. S-IVB LOX Dump (Sheet 1 of 2)

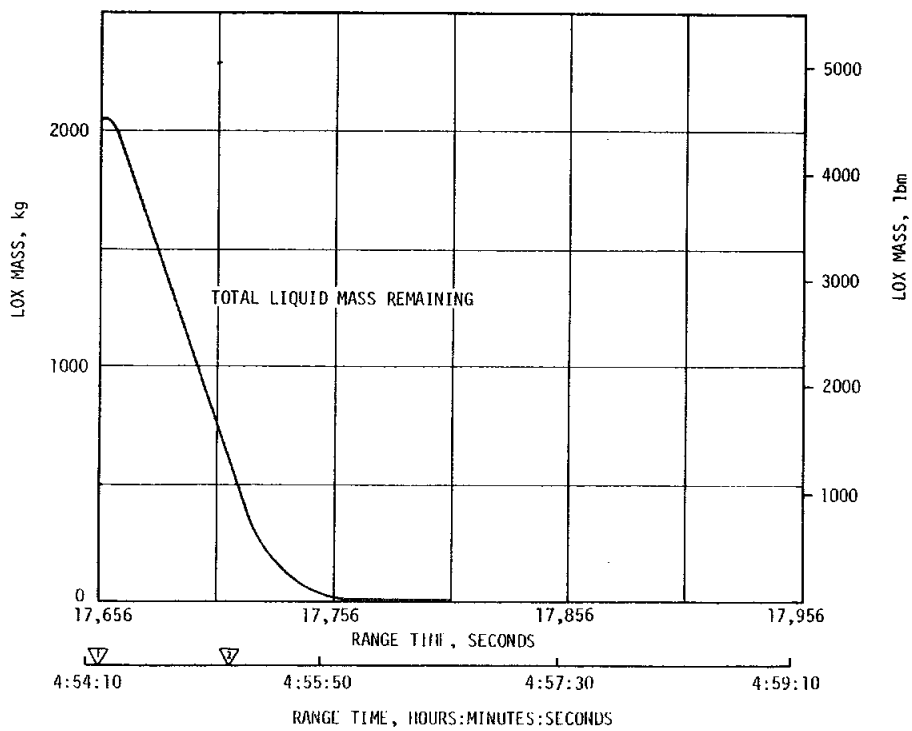
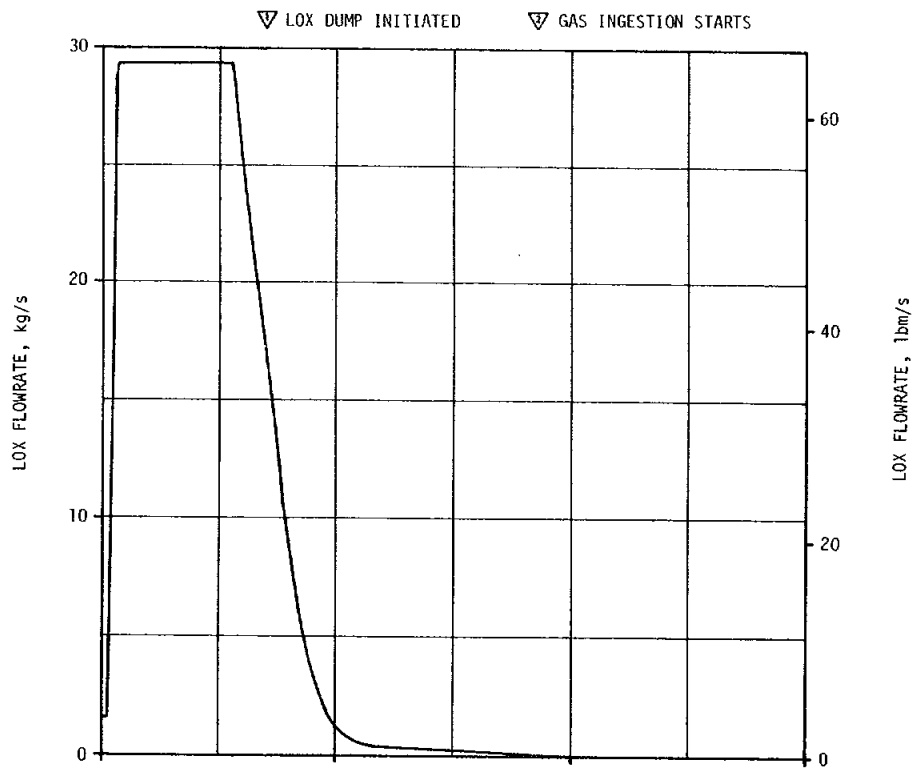


Figure 7-24. S-IVB LOX Dump (Sheet 2 of 2)

SECTION 8

HYDRAULIC SYSTEMS

8.1 SUMMARY

The stage hydraulic systems performed satisfactorily on the S-IC, S-II, and first burn and coast phase of the S-IVB stage. During this period all parameters were within specification limits and there were no deviations or anomalies. Subsequent to this time, during second burn and translunar coast, there was a minor problem with the engine driven hydraulic pump and an apparently unrelated problem with the auxiliary hydraulic pump. Shortly after second burn start command the engine driven pump output pressure slightly exceeded the compensator setting, but system performance continued to be nominal during the burn. Sometime during the second burn the auxiliary hydraulic pump performance was degraded as evidenced by system response after Engine Cutoff (ECO) and during coast phase activities. However, there was no indication of mission or program impact due to this anomaly.

8.2 S-IC HYDRAULIC SYSTEM

Analysis indicates that all servoactuators performed as commanded during the flight, with a maximum deflection equivalent to 2.15 degrees engine gimbal angle at approximately 82 seconds. All of the hydraulic supply pressures and temperatures were within operating limits with the exception of engine No. 1 closing pressure. This measurement started to increase unexpectedly at 80 seconds as shown in Figure 8-1, and reached a maximum of approximately 172 N/cm² (250 psia) near the end of S-IC flight. This apparent increase was due to instrument error.

8.3 S-II HYDRAULIC SYSTEM

The S-II hydraulic system performance was normal throughout the flight. System supply and return pressures, reservoir volumes, and system fluid temperatures were within predicted ranges. Reservoir fluid temperatures were close to the predicted rate of increase. All servoactuators responded to commands with good precision, and forces acting on the actuators were well below the predicted maximum.

8.4 S-IVB HYDRAULIC SYSTEM (FIRST BURN)

The S-IVB hydraulic system performance was nominal throughout S-IC/S-II boost and S-IVB first burn.

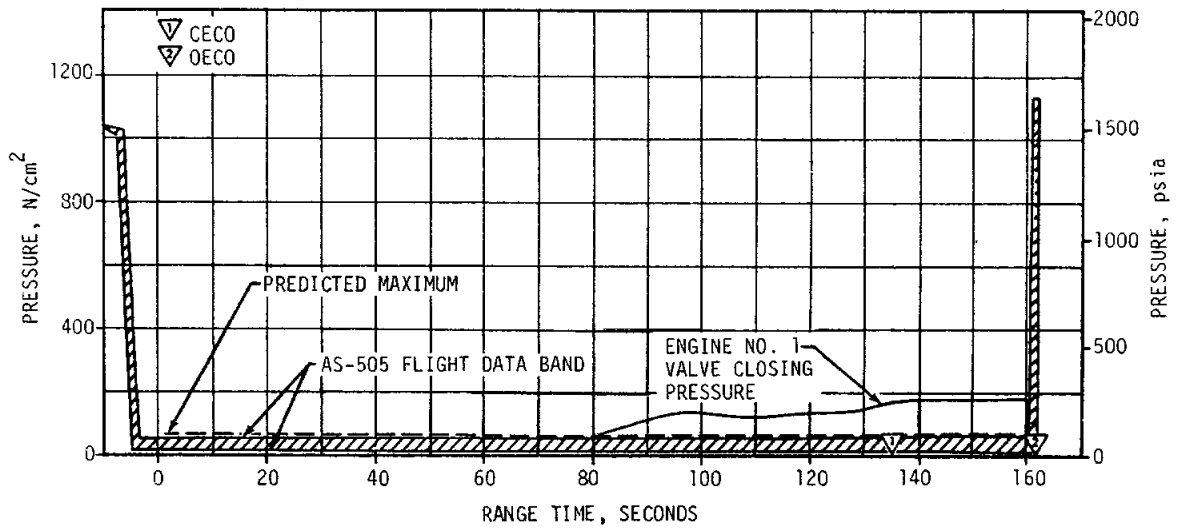


Figure 8-1. S-IC Engine, Valve Closing Pressure

The supply pressure was nearly constant at 2500 N/cm^2 (3630 psia), which is within the allowable 2413 to 2517 N/cm^2 (3500 to 3650 psia).

The system internal fluid leakage was shared by the main engine driven and auxiliary pumps during engine burn as characterized by a slight rise in system pressure after ignition and the auxiliary pump motor current drain of 32 amperes. The auxiliary pump, therefore, was supplying approximately $25.2 \text{ cm}^3/\text{s}$ (0.4 gpm) of the total leakage flowrate. The engine supplied 3.85 horsepower to the main pump during the burn.

Engine deflections were nominal throughout first burn. The actuator positions were offset from null during powered flight due to the displacement of the Center of Gravity (CG) off the vehicle center line, engine installation tolerances, thrust misalignment, and uncompensated gimbal clearances and thrust structure compression effects.

8.5 S-IVB HYDRAULIC SYSTEM (PARKING ORBIT COAST PHASE)

During the orbital coast phase, two hydraulic system thermal cycles of 48 seconds duration were programmed at 3304 and 6104 seconds. The purpose of these cycles is to distribute heat throughout the system by circulating hydraulic fluid periodically.

After ECO the pump inlet oil temperature increased from 323°K (119°F) to a maximum of 346°K (164°F) prior to the first thermal cycle, which was well within the upper limit of 408°K (275°F).

8.6 S-IVB HYDRAULIC SYSTEM (SECOND BURN)

The auxiliary pump was turned on during second burn prestart preparations at approximately 8848 seconds. System operation was normal throughout this period. Shortly after engine start, system pressure increased from 2502 to 2695 N/cm² (3635 to 3770 psia). This pressure step exceeded the pump compensator upper limit of 2508 N/cm² (3650 psia) as shown in Figure 8-2. However, pump inlet and reservoir oil temperatures increased at the nominal rates of 5.2 and 2.0°K/min (9.4 and 3.6°F/min), respectively. Engine deflections were nominal throughout the burn as shown in Figure 8-3. Therefore, this 3 percent excess in system pressure is not considered to be a problem.

System leakage during second burn was furnished by the engine driven pump. The engine supplied 4.85 horsepower to drive the pump during this period.

8.7 S-IVB HYDRAULIC SYSTEM (TRANSLUNAR INJECTION COAST AND PROPELLANT DUMP)

Degraded performance of the auxiliary hydraulic pump was observed during the period beginning with second burn ECO. Data indicated that the anomaly originated during second burn. System pressure decreased immediately after ECO as shown in Figure 8-2, whereas normal operation pressure would be maintained until the auxiliary pump "OFF" command was given 3.8 seconds later. Failure of the auxiliary pump motor amperage to rise during this period after ECO further substantiates degraded pump performance as shown in Figure 8-4.

A third thermal cycle, at 12,749 seconds, turned the auxiliary pump on for 48 seconds. No increase in system pressure, accumulator GN₂ pressure or reservoir oil pressure was observed. Aft battery No. 2 measurement indicated 17 amperes throughout the cycle as compared to a predicted value of 38 to 42 amperes as shown in Figure 8-5. The actuator position measurements shown in Figure 8-6 indicated that the actuators centered. It required 31 and 17 seconds, respectively, to center the pitch and yaw actuators. The engine driven pump inlet temperature dropped to a minimum value of 352°K (173°F). This actuator motion and oil temperature decrease confirms some auxiliary pump output pressure.

When the auxiliary hydraulic pump was activated for the propellant lead experiment and passivation, system performance was very similar to that of the third thermal cycle. However, a slight increase in reservoir oil pressure of 50 to 55 N/cm² (72 to 80 psia), as shown in Figure 8-7, was observed. Although the system was not performing properly, enough system pressure was maintained to center the actuators for passivation as shown in Figure 8-8.

Subsequent laboratory testing was accomplished by simulating failures that could have caused this anomaly. Of the simulated failures, the pressure

compensator spring guide failure test produced data closest to that observed during the flight. The pressure compensator spring guide has been replaced on AS-506 and AS-507 vehicles. There is no indication of any mission or program impact due to this anomaly.

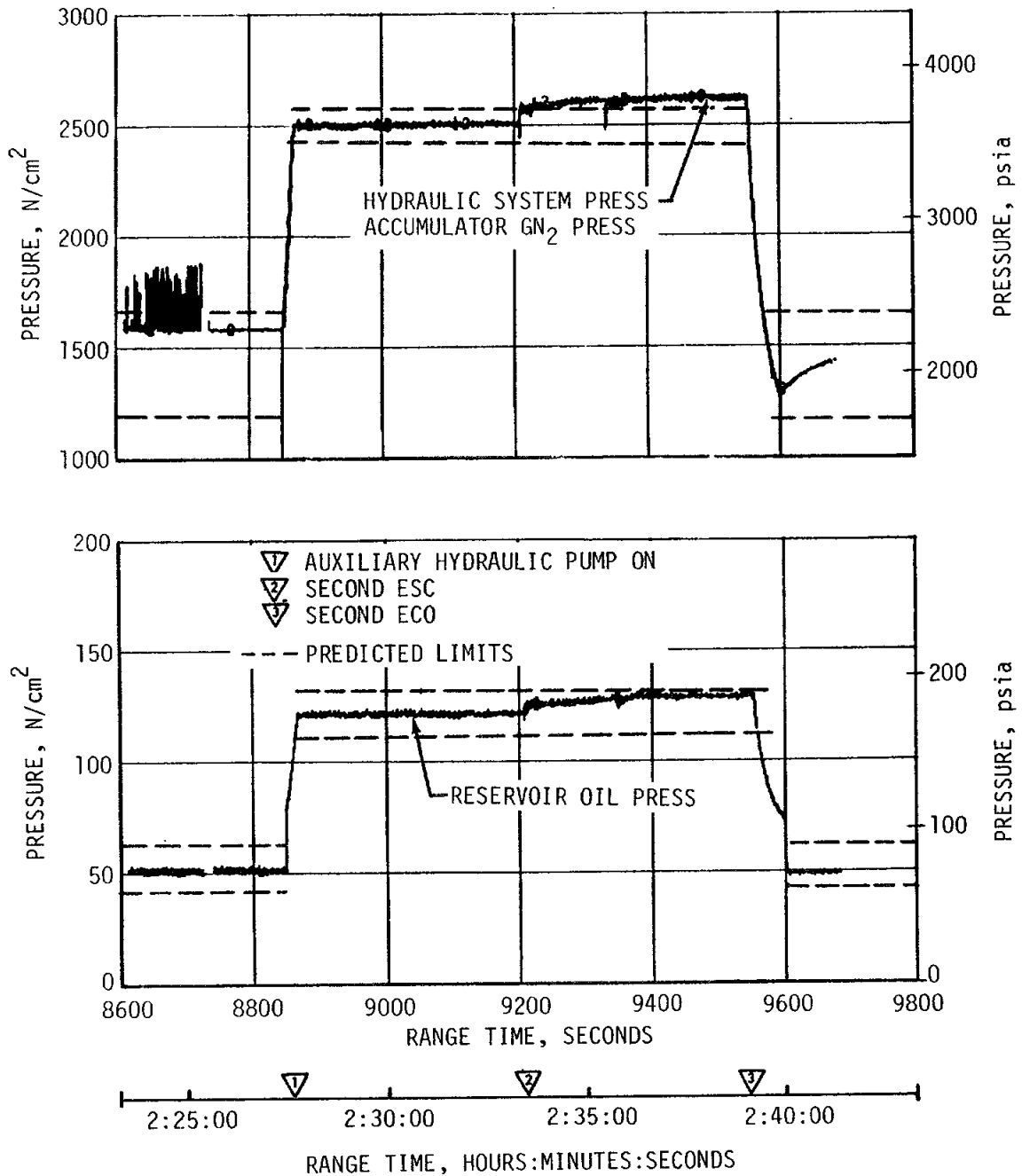


Figure 8-2. S-IVB Hydraulic System Pressure - Second Burn

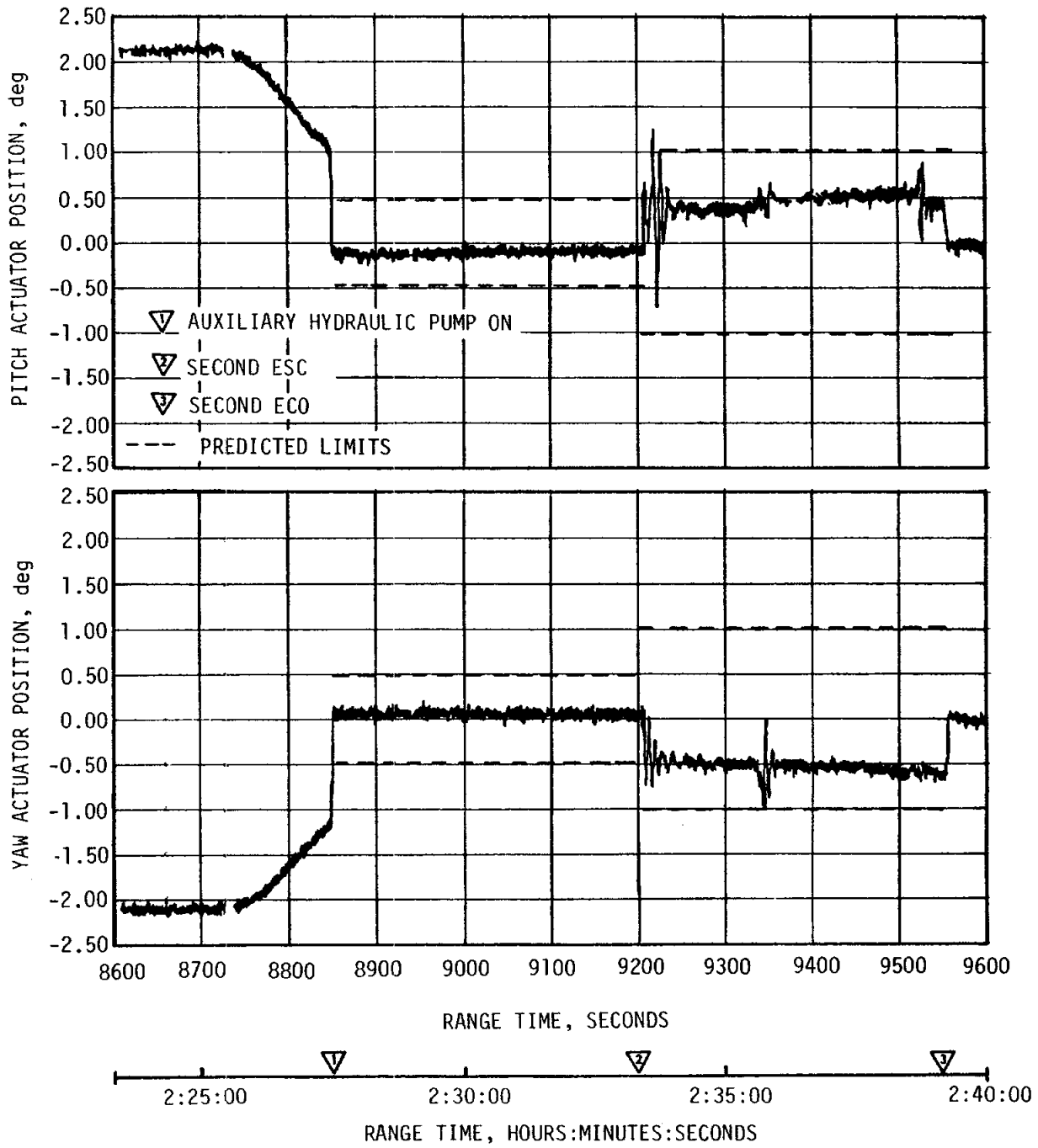


Figure 8-3. S-IVB Hydraulic System Actuator Positions - Second Burn

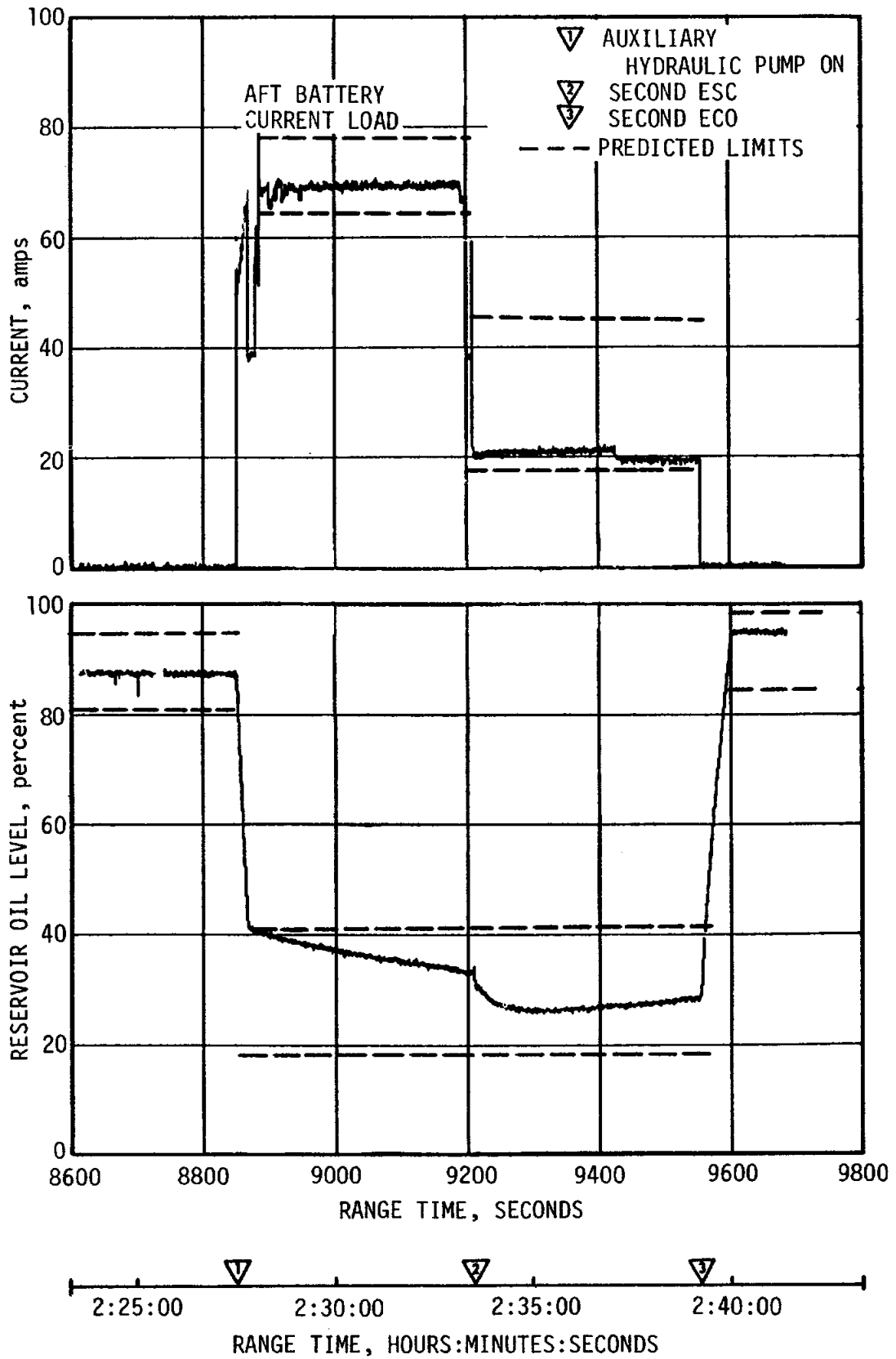


Figure 8-4. S-IVB Auxiliary Hydraulic Pump Performance - Second Burn

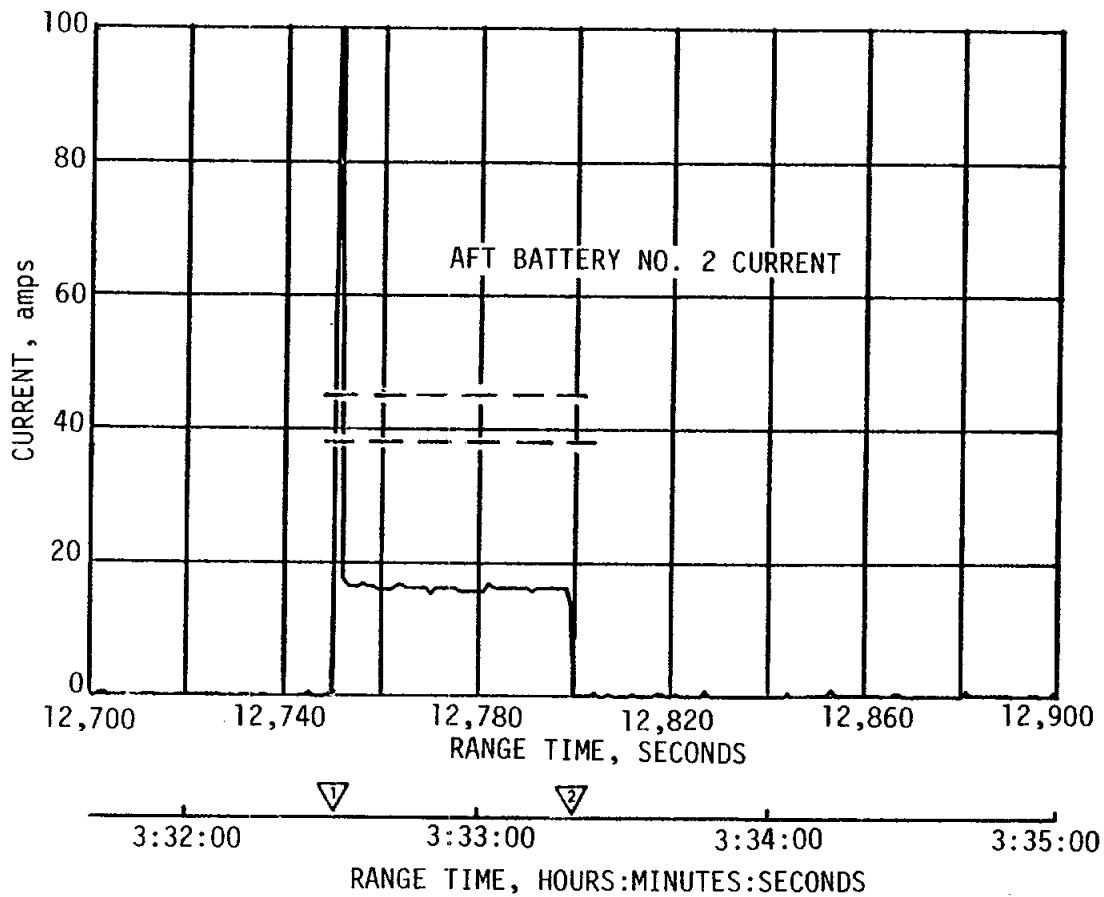
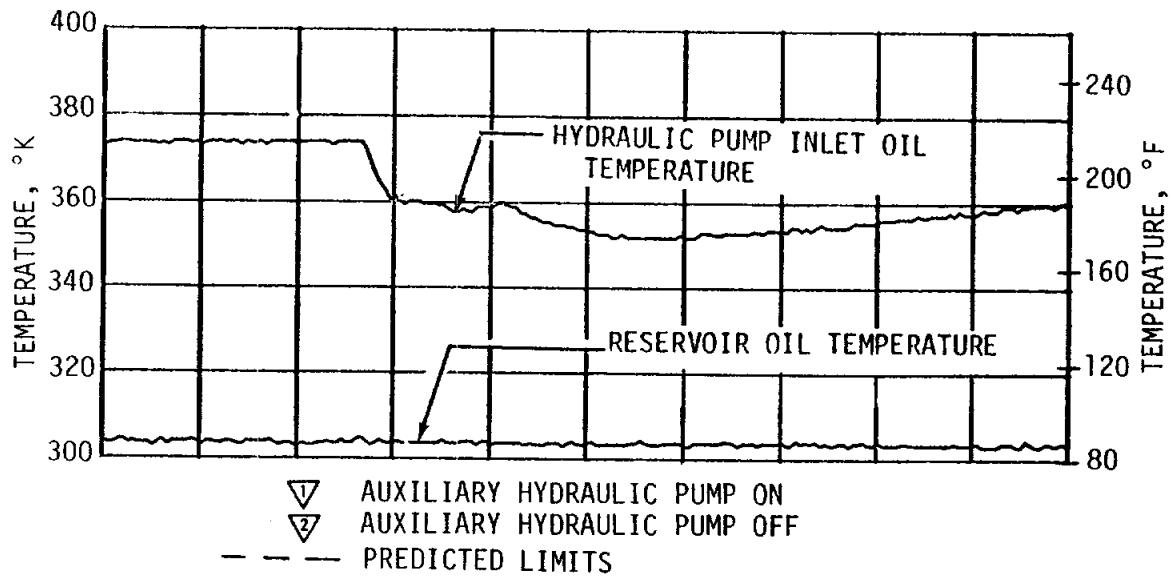


Figure 8-5. S-IVB Auxiliary Hydraulic Pump Performance - Coast Phase and Third Thermal Cycle

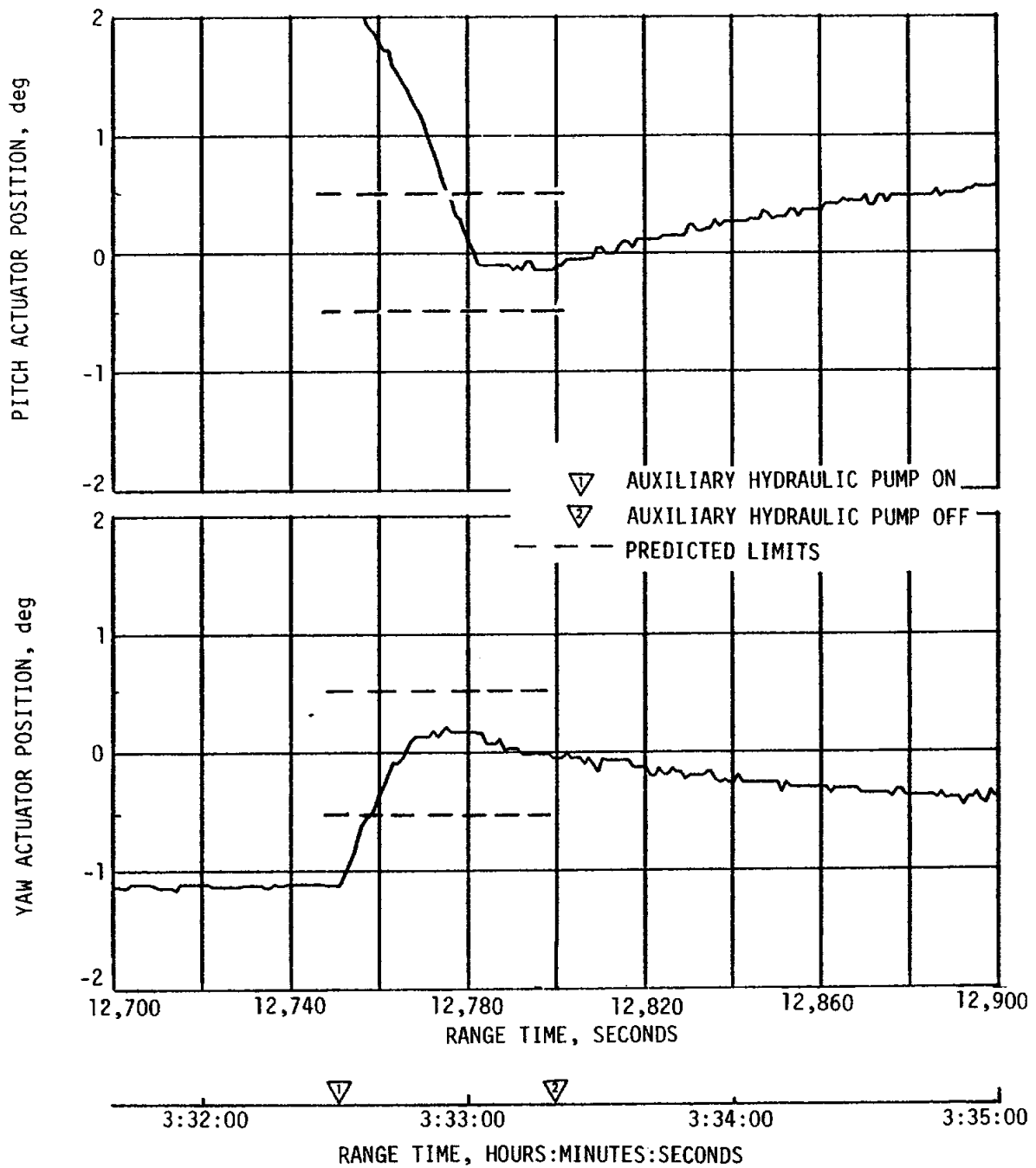


Figure 8-6. S-IVB Hydraulic System Actuator Positions - Coast Phase and Third Thermal Cycle

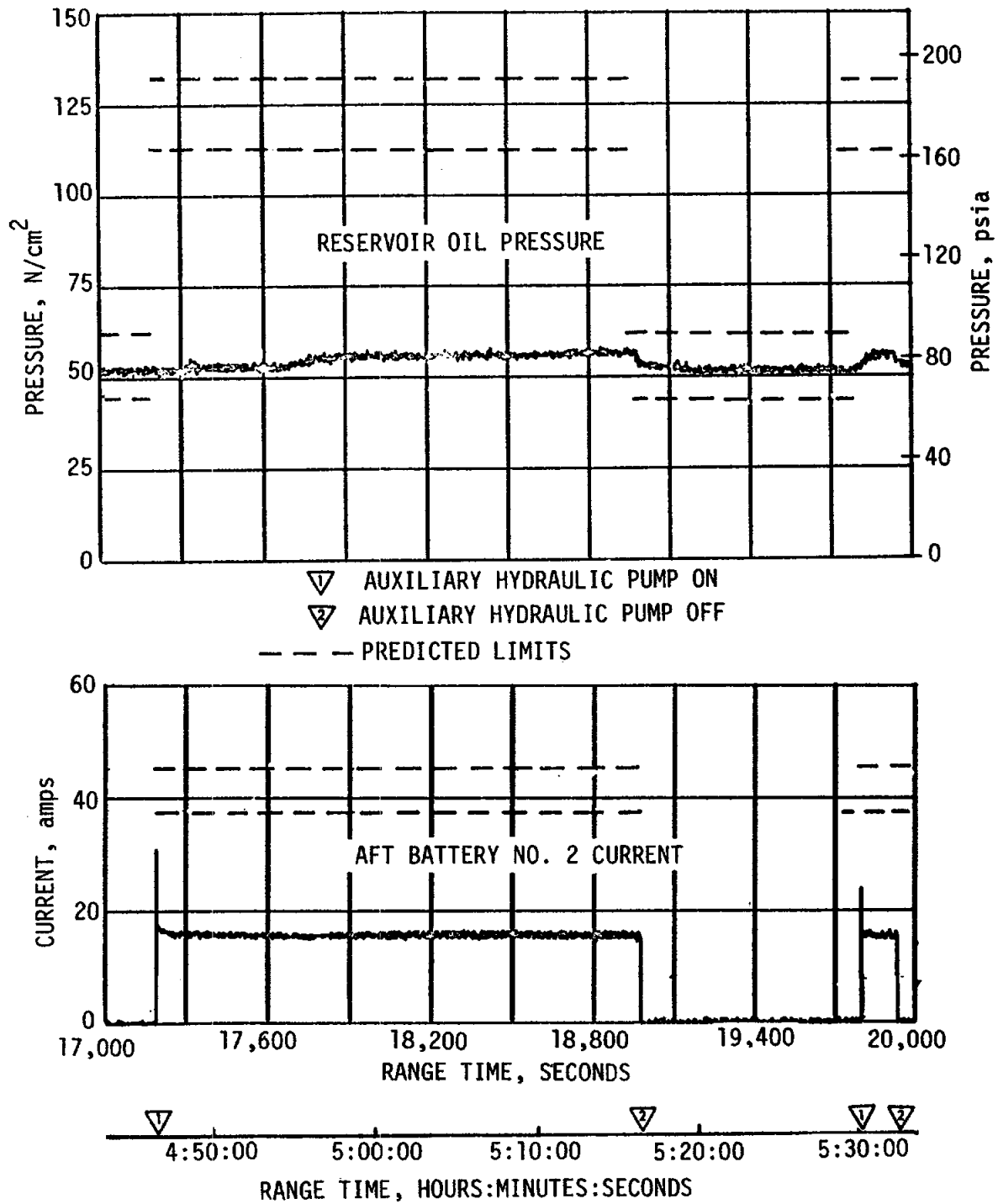


Figure 8-7. S-IVB Auxiliary Hydraulic Pump Performance - Coast Phase and Passivation

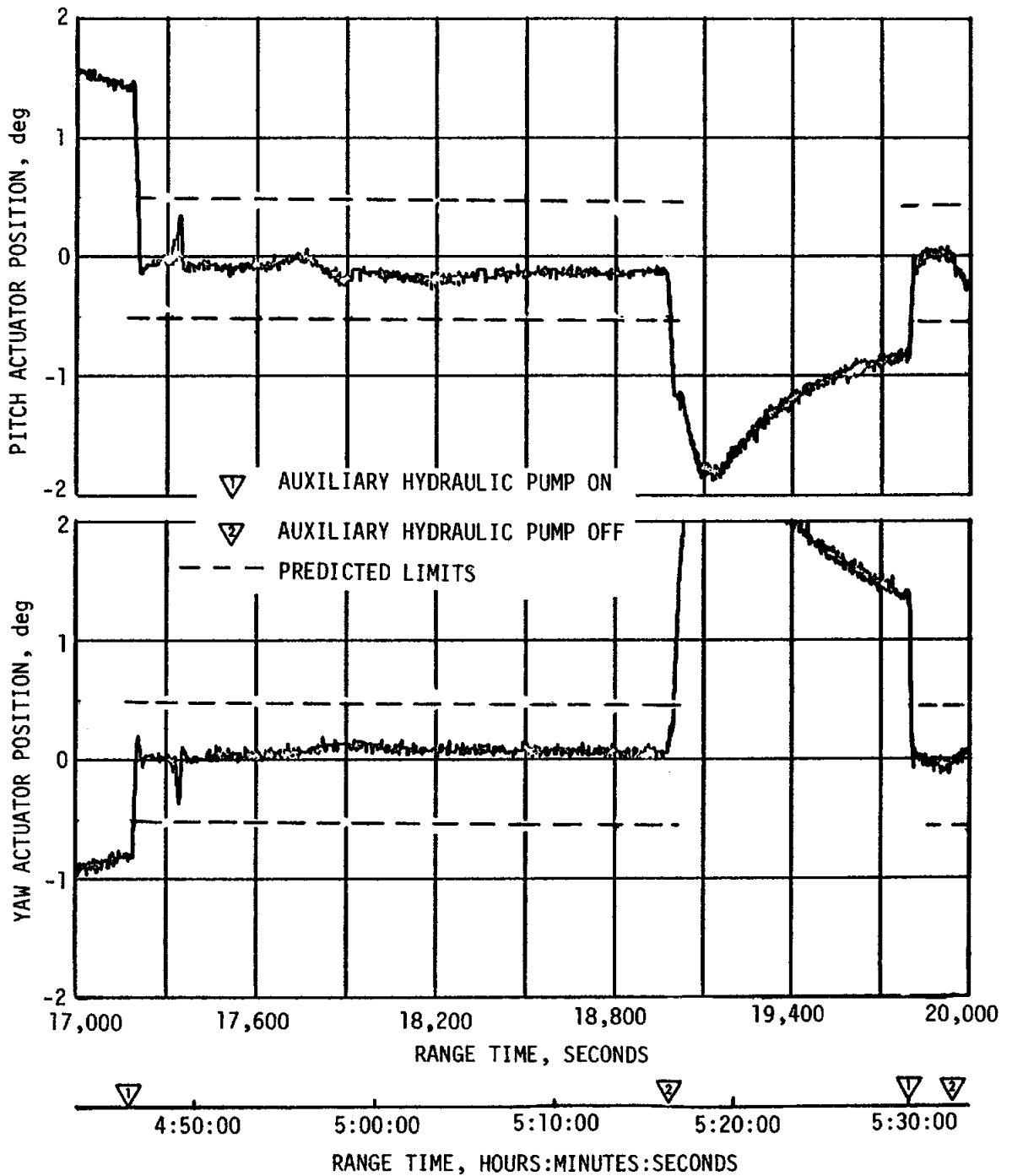


Figure 8-8. S-IVB Hydraulic System Actuator Positions - Coast Phase and Passivation

SECTION 9

STRUCTURES

9.1 SUMMARY

The structural loads and dynamic environments experienced by the AS-505 launch vehicle were well within the vehicle structural capability. The vehicle loads resulting from rigid-body and dynamic longitudinal load and bending moment were well below limit design values.

The maximum bending moment condition, 9.9×10^6 N-m (88×10^6 lbf-in.), was experienced at 84.6 seconds. The maximum longitudinal loads on the S-IC thrust structure, fuel tank, and intertank were experienced at 135.2 seconds, Center Engine Cutoff (CECO). On all the vehicle structure above the intertank, the maximum longitudinal loads were experienced at 161.6 seconds, Outboard Engine Cutoff (OECO), at the maximum longitudinal acceleration of 3.9 g.

Vehicle dynamic characteristics generally followed the preflight predictions. There was no evidence of coupled structure/propulsion system instability (POGO) during S-IC, S-II, or S-IVB powered flights. The early S-II stage center engine shutdown successfully eliminated the low-frequency (16 to 19 hertz) oscillations that were experienced on AS-503 and AS-504.

During S-IVB first and second burns, mild low-frequency (12 to 19 hertz) oscillations were experienced with the maximum amplitude of ± 0.30 g recorded by the gimbal block longitudinal accelerometer. During the last 70 seconds of second burn, the Apollo 10 astronauts reported (in real time) that higher frequency oscillations were superimposed on the low-frequency oscillations. These vibrations are, however, well within the structural design capability.

The AS-505 vehicle structure, component, and engine vibration measurements were, in general, within the envelopes established by previous flight data.

9.2 TOTAL VEHICLE STRUCTURES EVALUATION

9.2.1 Longitudinal Loads

The AS-505 vehicle liftoff occurred nominally at a steady-state acceleration of approximately 1.2 g. Transients due to thrust buildup and release

resulted in peak longitudinal dynamic accelerations, measured on the outboard and center engine thrust pads, of ± 0.5 g and ± 1.05 g, respectively. These responses were less than 20 percent of the 3-sigma 95-percent confidence design level.

The AS-505 slow-release rod force displacement characteristics are compared to the previous flight data in Figure 9-1. The higher release rod forces on AS-504 and AS-505 are believed due to less greasing of the rods.

The longitudinal loads that existed at the time of maximum aerodynamic loading (84.6 seconds) are shown in Figure 9-2. There were no discernible longitudinal dynamics at this time. The steady-state longitudinal acceleration of 2.19 g and the corresponding axial loads experienced were as expected.

The maximum longitudinal loads on the S-IC thrust structure, fuel tank, and intertank occurred at 135.2 seconds (CECO) at a longitudinal acceleration of 3.67 g. (See Figure 9-2). The maximum longitudinal loads on all vehicle structure above the S-IC intertank occurred at 161.6 seconds (OECO) at an acceleration of 3.9 g. The thrust cutoff transients experienced on the AS-505 vehicle are shown in Figure 9-3 and are essentially identical with those of the AS-504 vehicle.

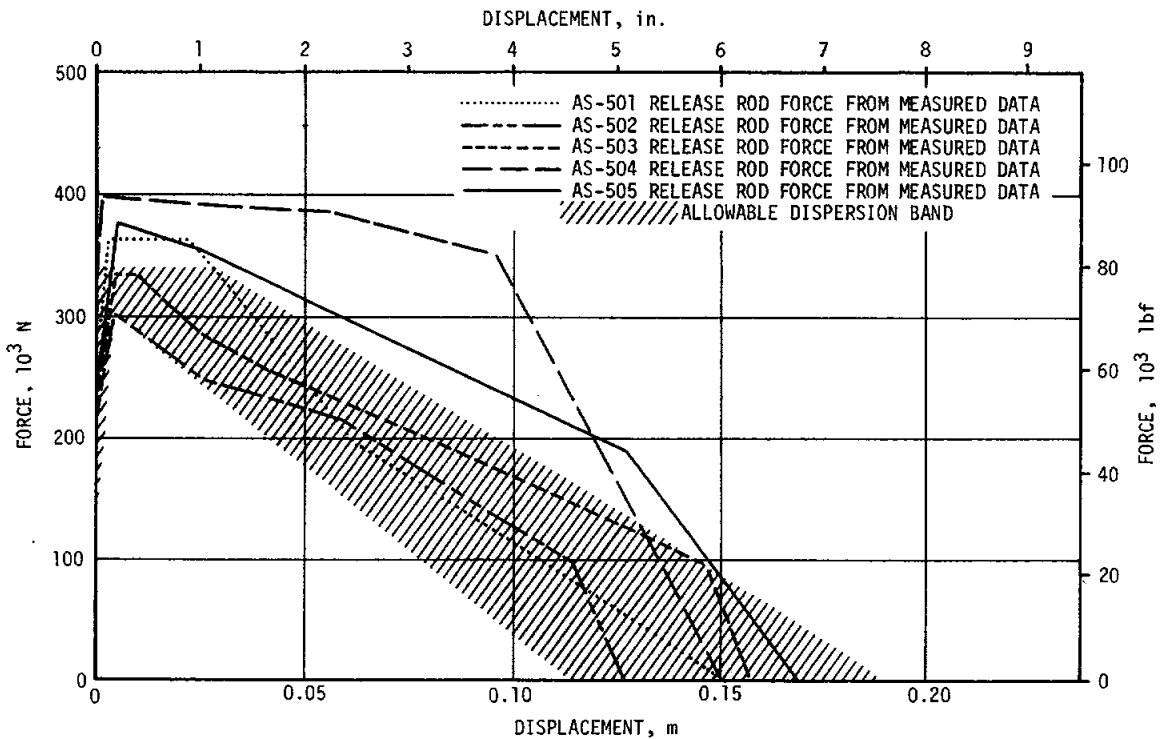


Figure 9-1. Release Rod Force - Displacement Curves

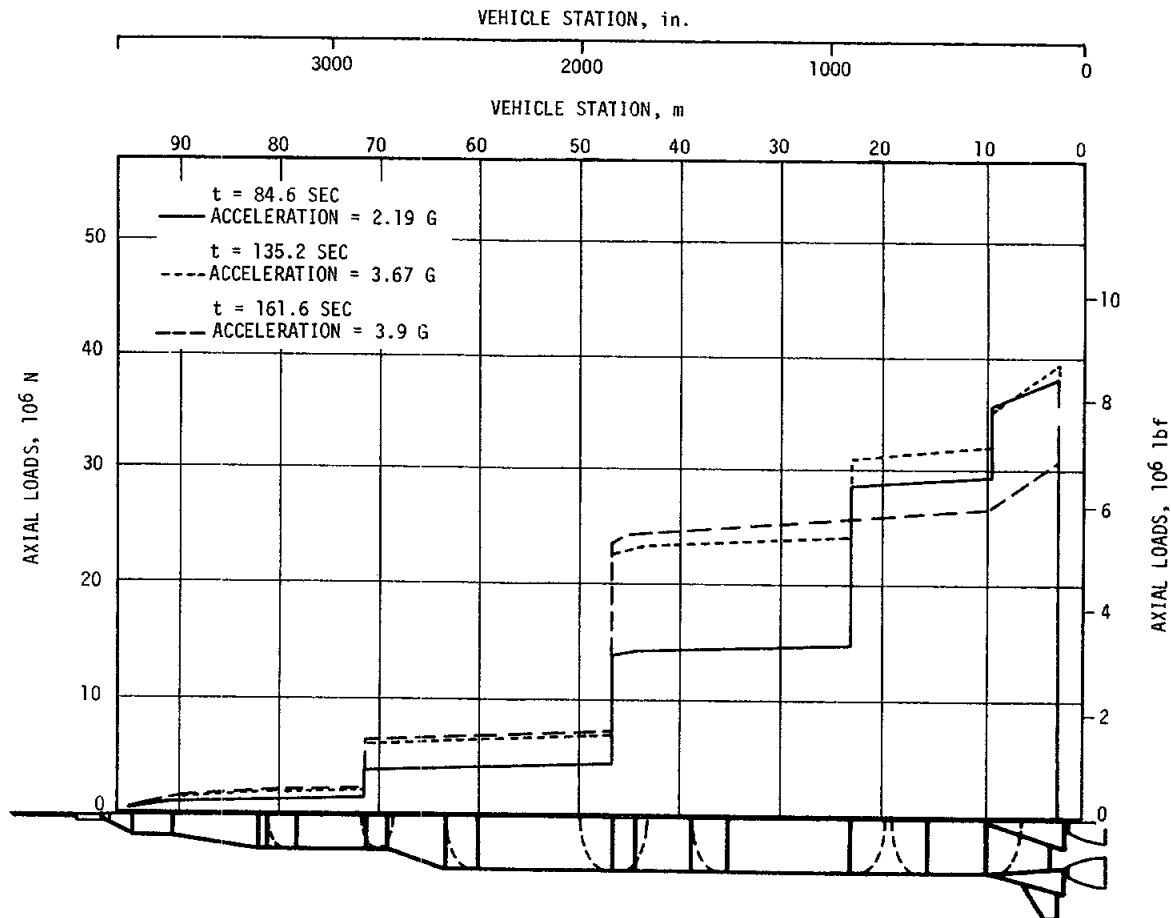


Figure 9-2. Longitudinal Loads at Maximum Bending Moment, Center Engine Cutoff, and Outboard Engine Cutoff

9.2.2 Bending Moments

The lateral loads experienced during thrust buildup and release were much lower than design because of the favorable winds experienced during launch. The wind speed at launch was low, 8.2 m/s (16 knots), at the 18.3-meter (60-ft) level. The comparable launch vehicle and spacecraft peak redline wind is 18.9 m/s (36.8 knots) and 14.4 m/s (28 knots), respectively.

The inflight winds that existed during the maximum aerodynamic loading phase of the flight were measured at 42 m/s (81.6 knots) at 14 kilometers (45,932 ft) altitude. These winds were approximately one-half the velocity of those encountered during the AS-504 flight. However, the trajectory for AS-505 was not wind biased (for the first time for Saturn V flights) and, as a result, the maximum bending moments experienced by AS-505 were about the same as for AS-504, about 40 percent of design value. As shown in Figure 9-4, the maximum bending moment of 9.9×10^6 N-m (88×10^6 lbf-in.) was experienced on the S-IC LOX tank at 84.6 seconds. Load

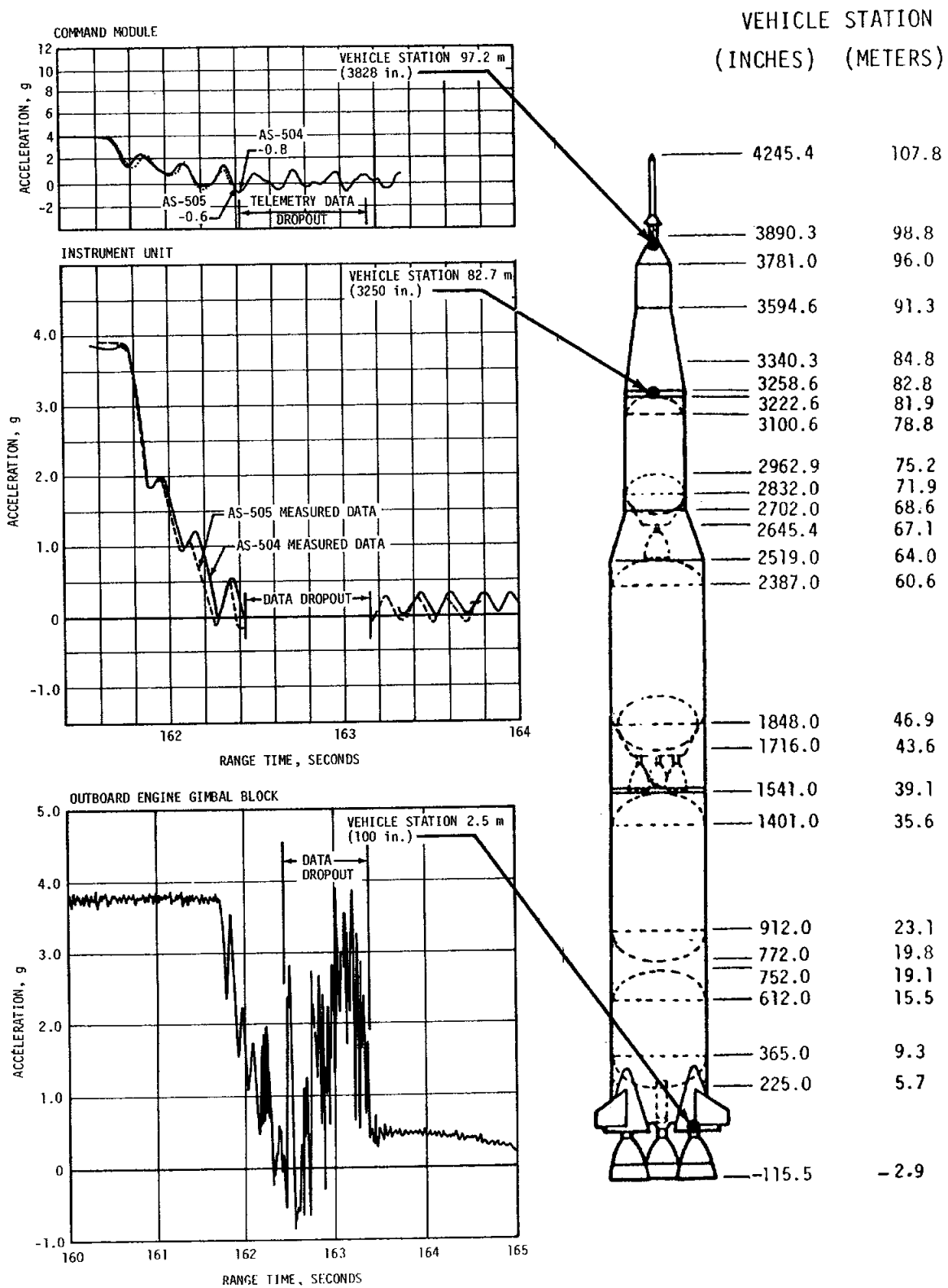


Figure 9-3. Longitudinal Structural Dynamic Response Due to Outboard Engine Cutoff

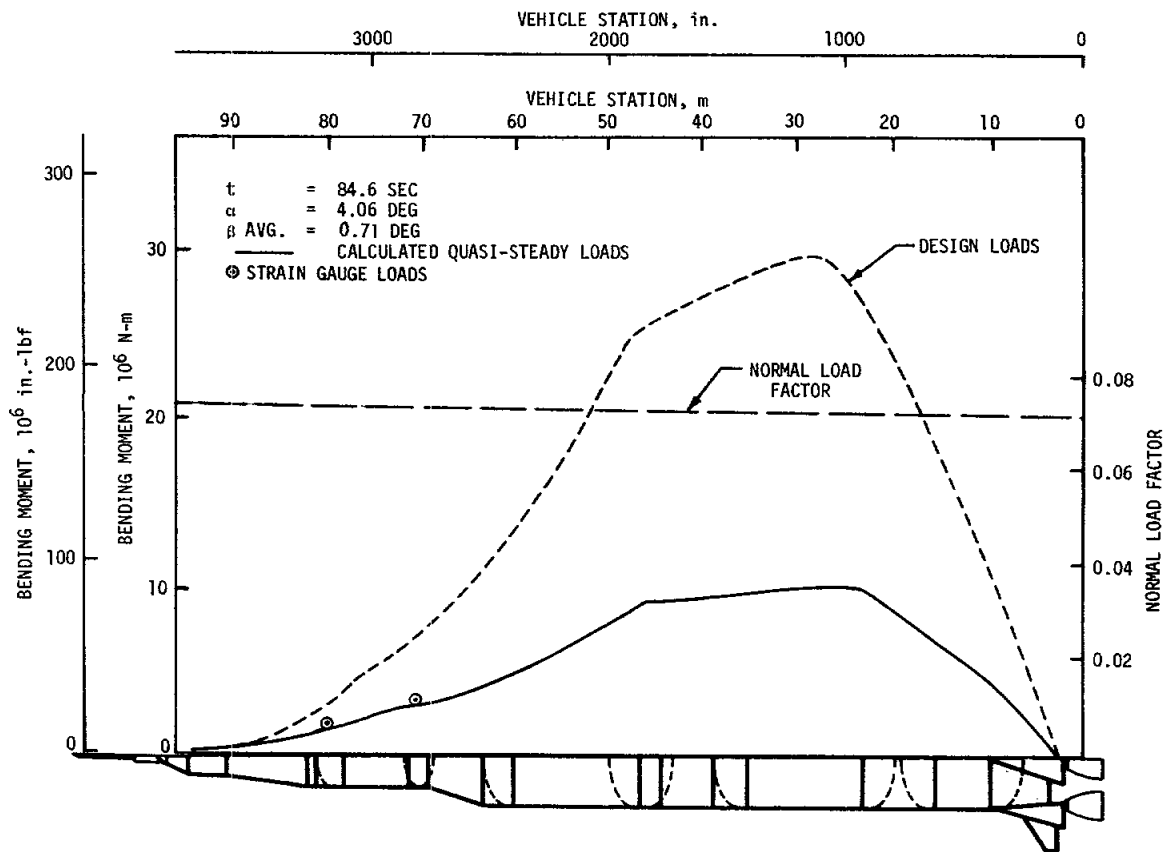


Figure 9-4. Maximum Bending Moment Near Max Q

computations are based upon measured inflight parameters such as thrust, gimballed angle, angle-of-attack, dynamic pressure, and accelerations. The bending moment values indicated by circles were derived from measured strain gage data.

9.2.3 Vehicle Dynamic Characteristics

9.2.3.1 Longitudinal Dynamic Characteristics. The predicted first longitudinal mode frequencies were present throughout the AS-505 S-IC boost phase. (See Figure 9-5.) The measured frequencies agree well with the analytical predictions. The frequencies are determined by spectral analysis using 5-second time slices.

The S-IC CECS transients were comparable in amplitude and frequency to those observed on AS-504. The amplitudes were slightly lower initially on AS-505, but decayed as slowly as on AS-504, indicating that vehicle damping in this mode was again low. The data of Figure 9-6 show peak amplitude of first mode oscillations versus body station for 135 through

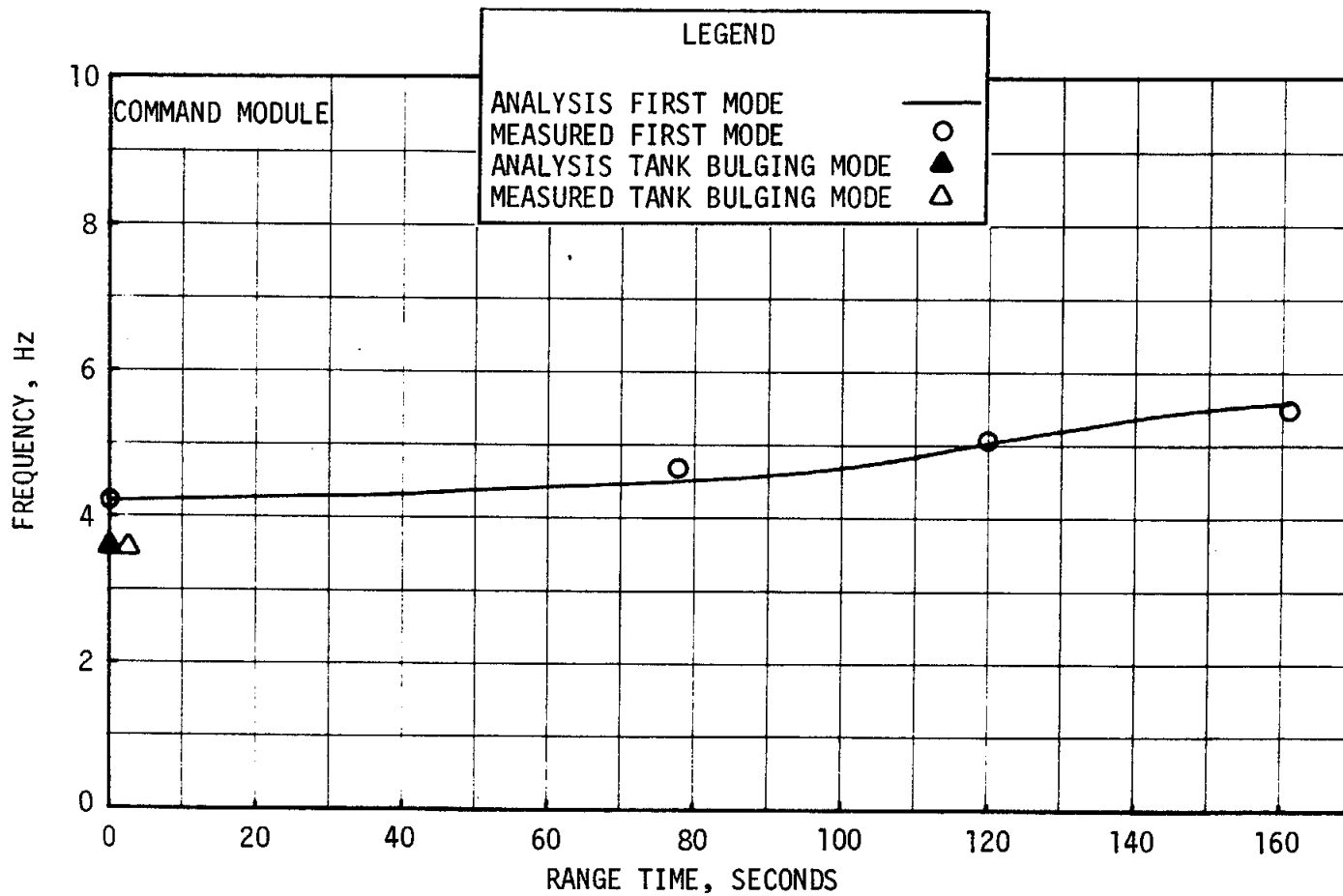


Figure 9-5. First Longitudinal Modal Frequencies During S-IC Powered Flight

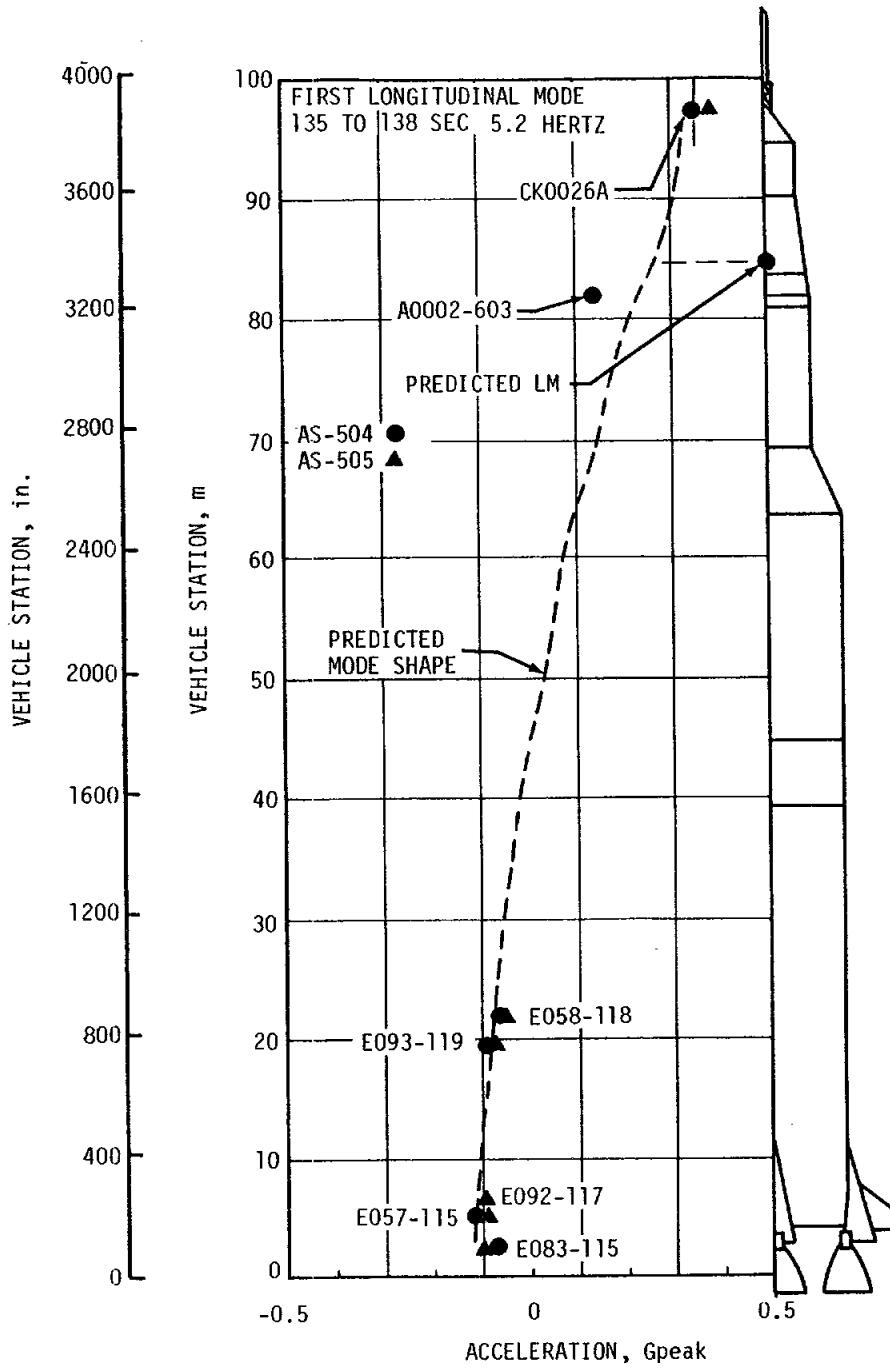


Figure 9-6 Peak Amplitudes of Vehicle First Longitudinal Mode for AS-504 and AS-505

138 seconds time slice. The amplitudes of measurements on both AS-504 and AS-505 flights are shown as well as a fit of the predicted first vehicle longitudinal mode through the data points.

The S-IC OEEO transients that were experienced by the AS-505 vehicle were nominal and were nearly identical to those experienced on AS-504. The S-IC/S-II separation dynamics were as expected. A maximum -0.6 Gpeak acceleration was measured in the command module as compared to a -0.8 Gpeak acceleration on AS-504 (See Figure 9-3).

The early S-II stage center engine shutdown successfully eliminated the low-frequency (16 to 19 hertz) oscillations that were experienced on the AS-503 and AS-504 flights. As shown in Figure 9-7, the AS-505 center engine crossbeam response levels after S-II CEEO were generally below the readable threshold level of ± 0.3 g as compared to the ± 12 g amplitudes on AS-504. The maximum amplitude measured on AS-505 was ± 2.0 g at S-II CEEO, and the maximum sustained response was about ± 1.0 g at approximately 294 seconds.

The most significant structural responses during the AS-505 flight occurred during S-IVB first and second burns. Low-frequency (12 to 19 hertz) oscillations were experienced during both burns. During first burn, a 19-hertz sinusoidal oscillation began on the J-2 engine gimbal block (A012) at about 592 seconds. The oscillation reached a maximum of ± 0.30 g at 620 seconds, and decayed to negligible vibration by 639 seconds. Both the oxidizer pump discharge pressure (D009) and the main LH₂ injector pressure (D004) showed increases in 19-hertz oscillations during this time period. Maximum pressure variations at 19 hertz were ± 3.03 N/cm² (± 4.4 psia) for D009 and ± 0.9 N/cm² (± 1.3 psia) for D004.

During S-IVB second burn, the Apollo 10 astronauts reported (in real time at 9486 seconds) experiencing high-frequency vibrations. Recapping later (at 10,415 seconds), they reported lateral and longitudinal low-frequency oscillations throughout first and second burns, and compared the flight to a rough-running Titan; they reconfirmed a definite shift to a high frequency superimposed upon the low frequency during second burn. The high frequency was estimated to be approximately 20 hertz. Another comment made at this time was ". . . we were sweating it all the way, but it shut down right on time." The comments from crew debriefing meetings since mission completion have not reflected the same severity as in real time and in inflight recaps; however, they confirmed that the S-IVB second burn high-frequency oscillations were audible and could be felt in the structure of the command module.

The flight measurements show a correlation with the astronauts reports. Several measurements detected the sudden shift to high-frequency (45-hertz) oscillations at 9481.8 seconds. These oscillations continued until S-IVB engine cutoff (second EEO). The amplitudes for many measurements, although low, also show a definite increase at this time. The maximum

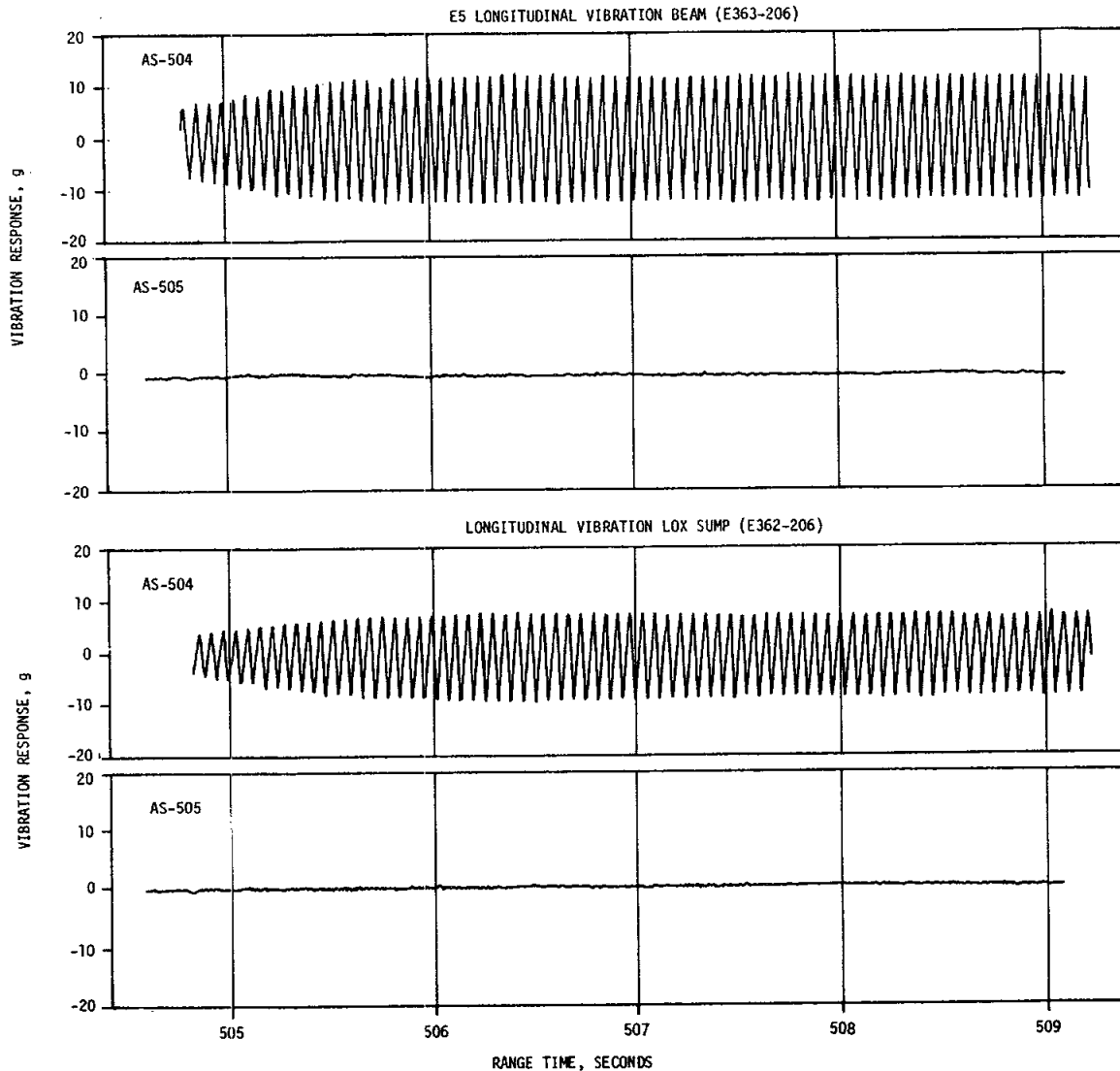


Figure 9-7. Comparison of AS-504 and AS-505 S-II Stage Low Frequency Oscillations

vibration levels at 45 hertz were measured by the S-IVB forward skirt pitch and yaw accelerometers as shown in Figure 9-8. The pitch measurement E099 indicated a maximum of ± 0.58 g.

The LH₂ step pressurization event occurred at 9479.2 seconds, which was 2.6 seconds before the vibration level increase. Following the step pressurization, the Non Propulsive Vent (NPV) nozzle pressures increased as expected. At 9481.3 seconds, the NPV pressures began oscillations at about ± 1.4 N/cm² (± 2 psia). It could not be determined if the pressure was oscillating at 45 hertz because of the low sample rate in the pressure measurements (D183 and D184); however, it does appear that the

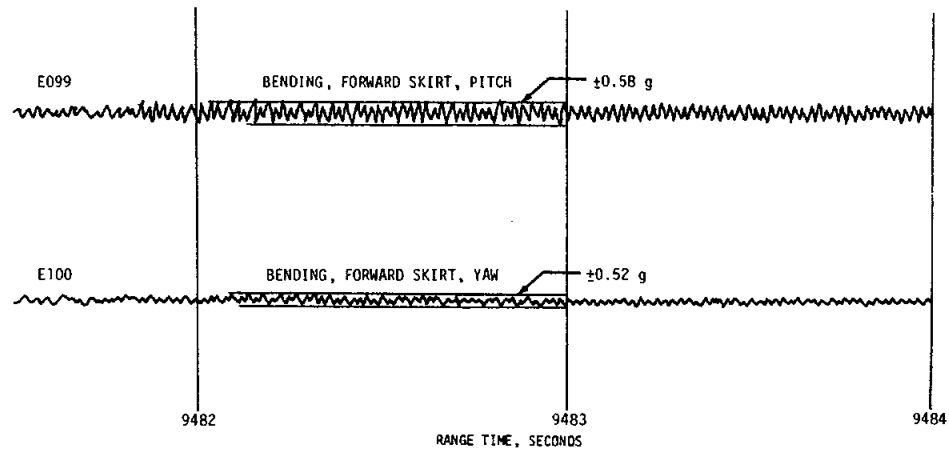


Figure 9-8. S-IVB Second Burn 45 Hertz Oscillations

oscillating pressures in the NPV system caused the forward skirt to vibrate at 45 hertz. One NPV nozzle is located approximately 1.02 meters (40 in.) from the accelerometer (E099-411) that recorded the maximum vibration level.

The cyclic interaction of the LH₂ vent and latching vent (NPV) valves is suspected to be the cause of these oscillations. On AS-505, the NPV valves had a small differential cracking pressure of 0.07 N/cm² (0.1 psi) as compared to 0.21 N/cm² (0.3 psi) on AS-503. A special test program is in progress to further understand the cause of the 45-hertz oscillations.

Also during S-IVB second burn, intermittent oscillations that began at about 9435 seconds were detected. Both the frequency and amplitude of these oscillations increased slightly during powered flight; the maximum was ±0.06 g at a frequency of 15 hertz on the gimbal block (A012) and occurred just before cutoff. Similar oscillations occurred during the AS-503 flight. The maximum level on the AS-503 gimbal block was ±0.04 g and occurred about 20 seconds prior to cutoff. Since the oscillations were intermittent rather than steadily increasing, there was no indication of a POGO instability. However, five POGO-type measurements (ECP 3218) have been requested for AS-506 for stability model analysis and for postflight evaluation of the low-frequency oscillations.

The maximum low-frequency vibration measured during the AS-505 flight and the maximum vibration measured during the 19-, 45-, and 15-hertz oscillations are shown in Table 9-1. These low-frequency vibrations are very low in amplitude; the maximum was only 40 percent of the stage dynamic design criteria. These vibrations did not affect structural integrity or stage performance.

Table 9-1. S-IVB Stage Low-Frequency Vibration Summary

MEAS. NO.	AREA MONITORED	MAXIMUM LEVEL GPEAK	RANGE TIME (SEC)	19 HERTZ LEVEL GPEAK	RANGE TIME (SEC)	45 HERTZ LEVEL GPEAK	RANGE TIME (SEC)	15 HERTZ LEVEL GPEAK	RANGE TIME (SEC)
E091	Fwd Field Splice - Thrust	1.20	2	0.08	620	0.10	9483	0.01	9550
E099	Fwd Bending Mode - Pitch	0.58	9483	0.04	610	0.58	9483	0.01	9550
E100	Fwd Bending Mode - Yaw	0.52	9483	0.07	600	0.52	9483	0.01	9550
E092	Aft Separation Plane - Thrust	0.58	87	0.16	620	0.08	9483	0.04	9550
A010	Gimbal Block - Pitch	0.06	6	0.01	620	----	----	----	----
A011	Gimbal Block - Yaw	0.14	6	0.01	620	0.01	9483	0.03	9550
A012	Gimbal Block - Thrust	0.30	620	0.30	620	0.08	9483	0.06	9550
E251	J-2 Chamber Dome - Thrust	0.82	9220	0.25	620	0.05	9520	0.07	9550
A013	J-2 Engine Skirt - Pitch	0.21	568	0.17	620	0.10	9483	0.13	9550
A014	J-2 Engine Skirt - Yaw	0.25	568	0.21	620	0.13	9483	0.17	9550

9.2.3.2 Lateral Dynamic Characteristics. Oscillations in the first four modes were detectable throughout S-IC powered flight. Spectral analyses were performed to determine modal frequencies using 5-second time slices. The frequencies of these oscillations agreed well with the analytical predictions. (See Figure 9-9.)

9.3 VIBRATION EVALUATION

9.3.1 S-IC Stage and Engine Evaluation

Structure, engine, and component vibration measurements taken on the S-IC stage are summarized in Table 9-2 and in Figures 9-10 through 9-12. A total of 44 single sideband vibration measurements were recorded, of which 42 yielded valid data throughout flight. Measurement locations are shown in Figure 9-13.

9.3.1.1 S-IC Stage Structure. Stage structure vibration data exhibited composite RMS levels and spectra shapes within the data envelopes of previous flights. The AS-505 maximum inflight intertank and forward skirt structure RMS levels lag those measured on previous flights because the Max Q region occurred later in flight.

9.3.1.2 F-1 Engines. The F-1 engine combustion chamber and turbopump measurements compare closely with previous flight data in both overall levels and spectra shapes. Measurement E038-101 shows a high Grms level when compared to previous valid data; consequently, it is questionable and is not included in the engine turbopump plot.

9.3.1.3 S-IC Components. All S-IC component vibration measurements were valid, and the levels measured agreed with those measured on previous flights.

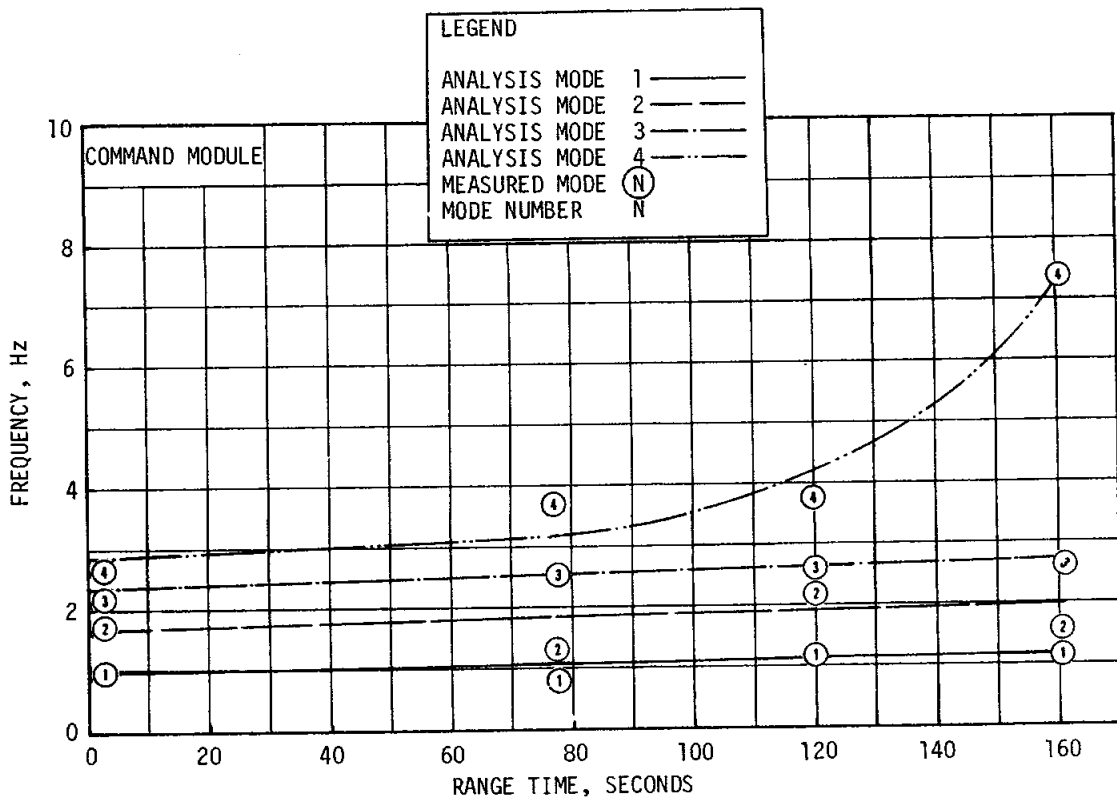


Figure 9-9. AS-505 Lateral Analysis/Measured Modal Frequency Correlation

9.3.2 S-II Stage and Engine Evaluation

Comparisons of Grms values for AS-505 and previous flight data are shown on Table 9-3 and in Figures 9-14 through 9-16. The AS-505 peak level at liftoff for the interstage frames radial measurement and all AS-505 values shown for the aft skirt stringers radial vibration measurement were determined from contractor digitized data. All other values shown were determined from NASA Grms history data. The variations between the five flights are considered normal.

9.3.2.1 S-II Stage Structure. In general, the S-II stage structure vibration levels were within the envelopes established by previous flights. The forward skirt stringers tangential vibration and aft skirt stringers radial peak value vibration levels were slightly above the envelopes established by previous flights. The interstage frames tangential vibration data were invalid and are not included in Figure 9-14.

9.3.2.2 S-II Stage J-2 Engines. The S-II engine combustion domes longitudinal and LH₂ pumps radial vibration envelopes (Figure 9-15) show a

Table 9-2. S-IC Stage Vibration Summary

MEASUREMENT	MAXIMUM GRMS AT RANGE TIME		OVERALL GRMS LIMIT	REMARKS
	PREVIOUS FLIGHT DATA	AS-505		
STRUCTURE				
Thrust Structure				
E023-115	14.7 at 0	10.8 at 0	22	AS-505 data are invalid.
E024-115	11.2 at 0	14.1 at -2.0	25	
E053-115	6.9 at 149.5	5.5 at 156.0	17	
E054-115	3.7 at 150		17	
E079-115	3.3 at 148	3.1 at 158.0	17	
E080-115	4.2 at 148	3.7 at 158.0	17	
Intertank Structure				
E020-118	7.7 at 2	5.6 at -2.0	27	
E021-118	9.1 at 4	9.4 at 0	27	
Forward Skirt Structure				
E046-120	3.6 at 94	5.0 at 85	30	Located near command destruct vibration isolated panel.
E047-120	6.1 at 3.9	5.2 at 5.7	30	
ENGINE				
Combustion Chamber				
E036-101	8.8 at 20.5	7.58 at 156	49	Data questionable, due to an amplifier calibration error.
E036-102	9.7 at 0	8.01 at 110.2	49	
E036-103	8.3 at 53	8.38 at 10.2	49	
E036-104	8.4 at 106.8	7.22 at 120.3	49	
E036-105	8.2 at 130.5	8.03 at 50.3	49	
Turbopump				
E037-101	41.5 at 20.0	23.8 at 157.0	41	
E038-101	39.0 at 1.0		41	
E039-101	26.5 at 125.0	16.8 at 132.4	41	
E040-101	17.3 at 123.8	15.4 at 154.0	41	
E041-101	20.9 at 158.0	17.6 at 157.0	41	
E041-102	17.5 at 144.5	18.8 at 154.0	41	
E042-102	9.6 at 86	8.6 at 157.0	41	
E042-103	10.9 at 148.1	9.1 at 154.0	41	
E042-104	11.2 at 79.0	9.4 at 144.5	41	
E042-105	10.7 at 26.6	9.0 at 126.2	41	
COMPONENTS				
Engine Actuators				
E030-101	9.4 at 111	4.4 at 125.5	30	
E030-102	5.0 at 123	4.6 at 0	30	
E031-101	6.7 at 118	6.0 at 156.0	30	
E031-102	7.8 at 107	6.7 at 134.3	30	
E032-101	15.1 at 111	7.4 at 150.0	30	
E032-102	14.0 at 89	13.0 at 155.0	30	
E033-101	8.8 at 100	8.5 at 71.4	30	
E033-102	7.0 at 127	6.3 at 159	30	
E034-101	5.3 at 124	4.1 at 150	30	
E034-102	5.5 at 135	10.2 at 0	30	
E035-101	15.0 at 68	14.7 at 71.3	30	
E035-102	10.5 at 127	8.4 at 134.3	30	
Heat Shield Panels				
E105-106	76.6 at -1	73.2 at 0	33	
E106-106	70.8 at 0	70.9 at 0	33	
E107-106	74.4 at 0	70.2 at 0	33	
Propellant Delivery System				
E025-118	2.7 at 132	1.7 at -2.0	9	
E026-118	3.1 at 118	2.8 at 0	9	
E027-115	10.4 at -0.5	8.3 at -2.0	22	
E028-115	11.3 at 118	10.8 at 0	22	

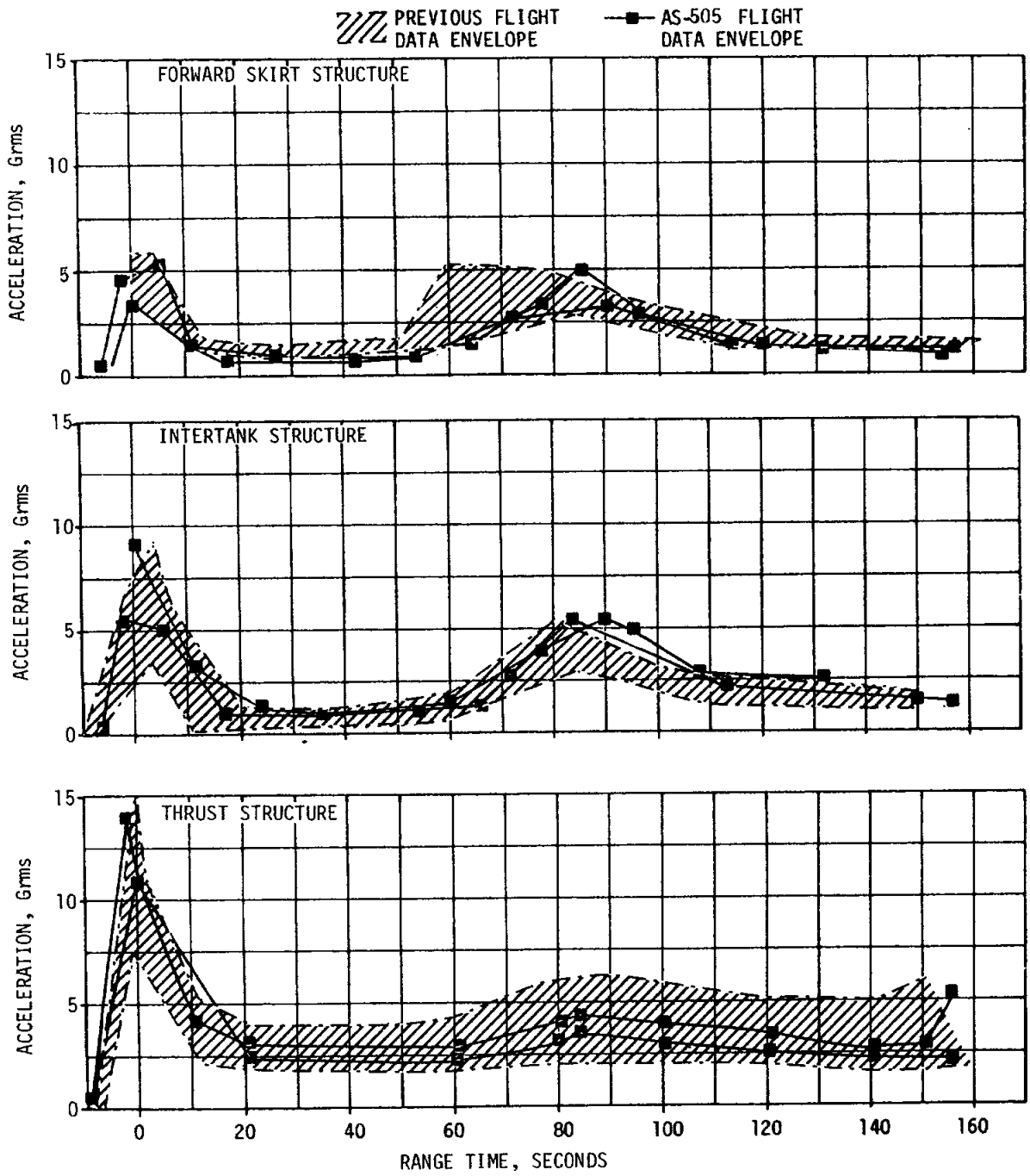


Figure 9-10 S-IC Stage Structure Vibration Envelopes

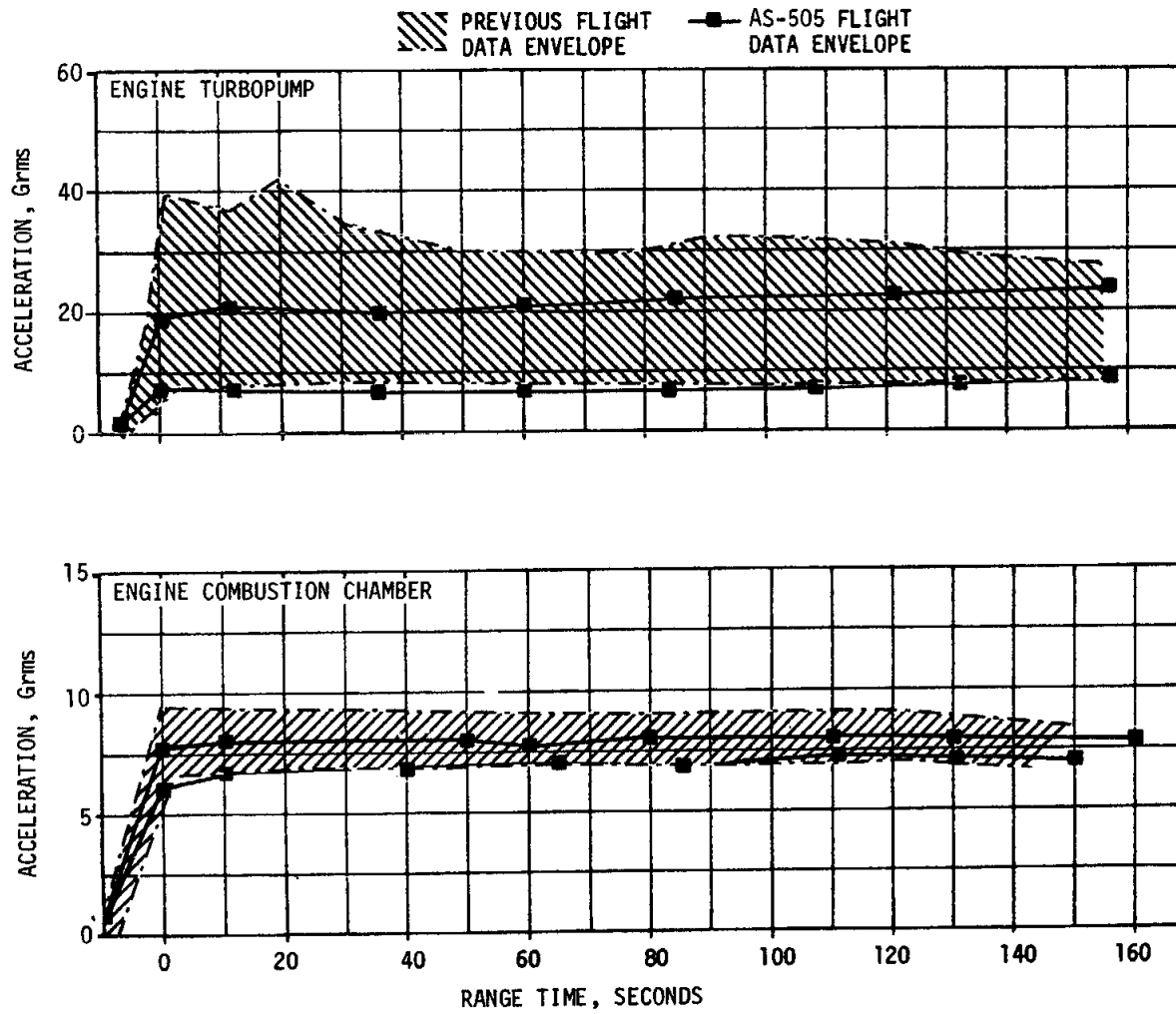


Figure 9-11 S-IC Stage Engine Vibration Envelopes

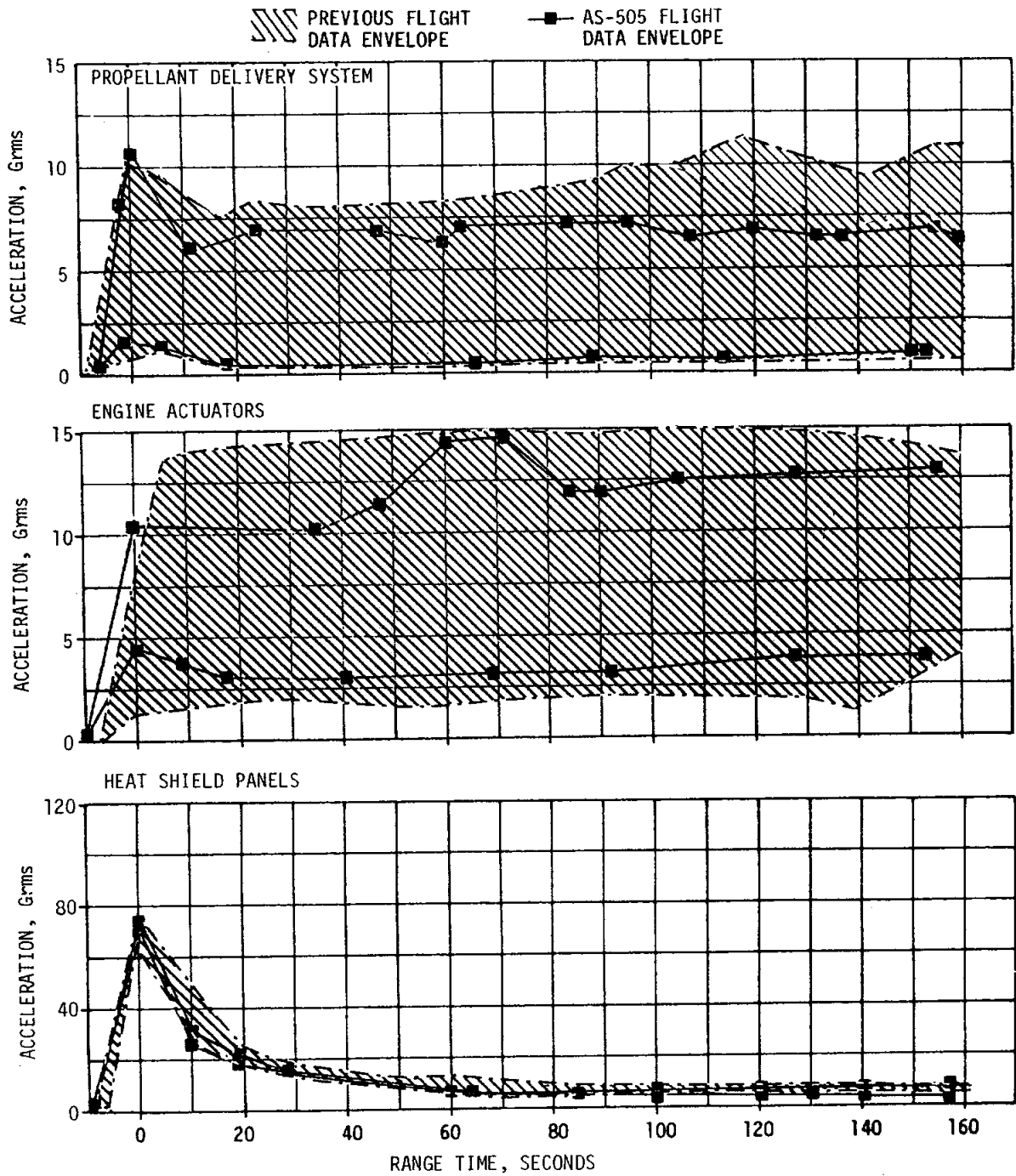


Figure 9-12 S-IC Stage Components Vibration Envelopes

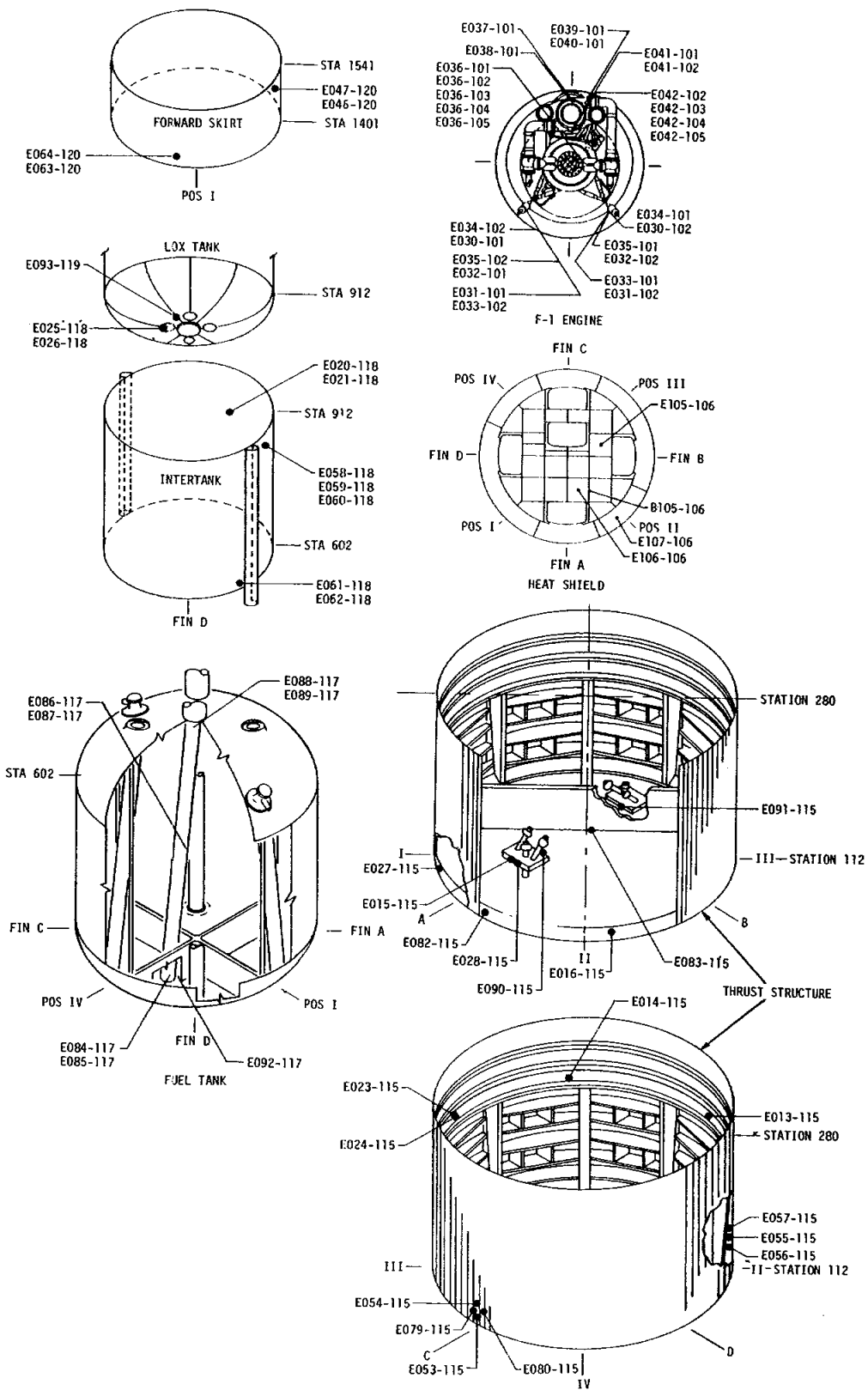


Figure 9-13. S-IC Vibration Measurement Locations

Table 9-3. S-II Stage Maximum Overall Vibration Levels

ZONE	STATIC FIRING		FLIGHT				
	VEHICLE	MAXIMUM GRMS RANGE	MAXIMUM GRMS RANGE				
			VEHICLE	LIFTOFF	TRANSONIC	MAX Q	MAINSTAGE
Forward Skirt Containers	S-II-1,2,3,4	0.7 to 3.1	AS-501,2,3,4	0.7 to 9.1	0.7 to 5.2	1.1 to 5.3	0.0 to 0.9
	S-II-5	0.9 to 2.1	AS-505	2.0 to 9.3	1.2 to 4.9	2.0 to 5.5	0.3 to 0.7
Forward Skirt Stringers	S-II-1,2,3,4	1.6 to 5.0	AS-501,2,3,4	1.2 to 13.1	1.0 to 11.3	1.7 to 9.2	0.3 to 1.3
	S-II-5	0.5 to 3.4	AS-505	2.1 to 9.0	2.2 to 9.3	2.4 to 9.0	0.4 to 1.2
Aft Skirt	S-II-1,2,3,4	9.8 to 19.6	AS-501,2,3,4	5.3 to 17.3	3.6 to 8.3	5.4 to 12.1	0.4 to 2.7
	S-II-5	10.6 to 20.7	AS-505	15.9	10.0	13.0	3.6
Interstage	S-II-1,2,3,4	Interstage Not Installed	AS-501,2,3,4	3.1 to 18.3	2.0 to 6.5	1.8 to 7.3	0.6 to 3.6
	S-II-5		AS-505	11.9 to 15.0	3.8 to 4.7	3.8 to 6.5	0.3 to 0.8
Thrust Cone Containers	S-II-1,2,3,4	2.2 to 15.8	AS-501,2,3,4	0.3 to 7.5	0.2 to 2.6	0.3 to 2.8	0.3 to 3.8
	S-II-5	5.0 to 8.5	AS-505	0.6 to 3.2	0.2 to 1.0	0.3 to 1.2	0.5 to 3.1
Thrust Cone Longerons	S-II-1,2,3,4	4.1 to 12.3	AS-501,2,3,4	0.2 to 5.1*	0.1 to 2.0	0.3 to 2.7*	0.5 to 7.2*
	S-II-5	5.2	AS-505	0.3 to 1.0	0.3 to 0.4	0.3 to 0.8	0.4 to 2.1
Engine Beam	S-II-1,2,3,4	5.4 to 15.3	AS-501,2,3,4	0.5 to 1.5	0.3 to 1.9	0.2 to 1.5	2.0 to 13.9
	S-II-5	2.8 to 9.8	AS-505	1.4	0.4	0.4	6.0
Engine Combustion Domes	S-II-1,2,3,4	Invalid Data	AS-503,4	0.0 to 3.8	0.0 to 4.6	0.0 to 3.8	2.8 to 10.6
	S-II-5	4.3 to 5.4	AS-505	1.9 to 2.2	1.4 to 2.0	1.7 to 2.4	8.0 to 10.8
LOX Pump	S-II-1,2,3,4	Invalid Data	AS-503,4	0.0 to 1.9	0.0 to 1.4	0.0 to 1.7	2.8 to 9.2
	S-II-5	4.7 to 6.0	AS-505	1.2 to 2.5	1.0 to 2.8	1.2 to 2.5	1.8 to 8.1
LH2 Pumps	S-II-1,2,3,4	Invalid Data	AS-503,4	3.0 to 7.3	0.0 to 6.2	1.5 to 6.2	8.8 to 19.9
	S-II-5	6.3 to 8.3	AS-505	1.4 to 3.1	1.7 to 2.0	1.9 to 2.3	9.1 to 14.9
LOX Sump Prevalves	S-II-1,2,3,4	Instrumentation Not Installed	AS-503	0.7 to 0.8	0.5	0.5	0.5 to 0.7
	S-II-5		AS-505	0.9	0.4	0.4	0.7
LH2 Prevalves	S-II-1,2,3,4	Instrumentation Not Installed	AS-503,4	0.8 to 1.3	0.2 to 0.8	0.3 to 1.1	0.9 to 1.8
	S-II-5		AS-505	1.5 to 1.7	0.7 to 0.8	0.7 to 1.0	0.9 to 1.4

*NOTE: These values are thrust cone longerons, normal data for which no graph is presented here. Refer to Saturn V Launch Vehicle Flight Evaluation Report AS-504, Apollo 9 Mission.

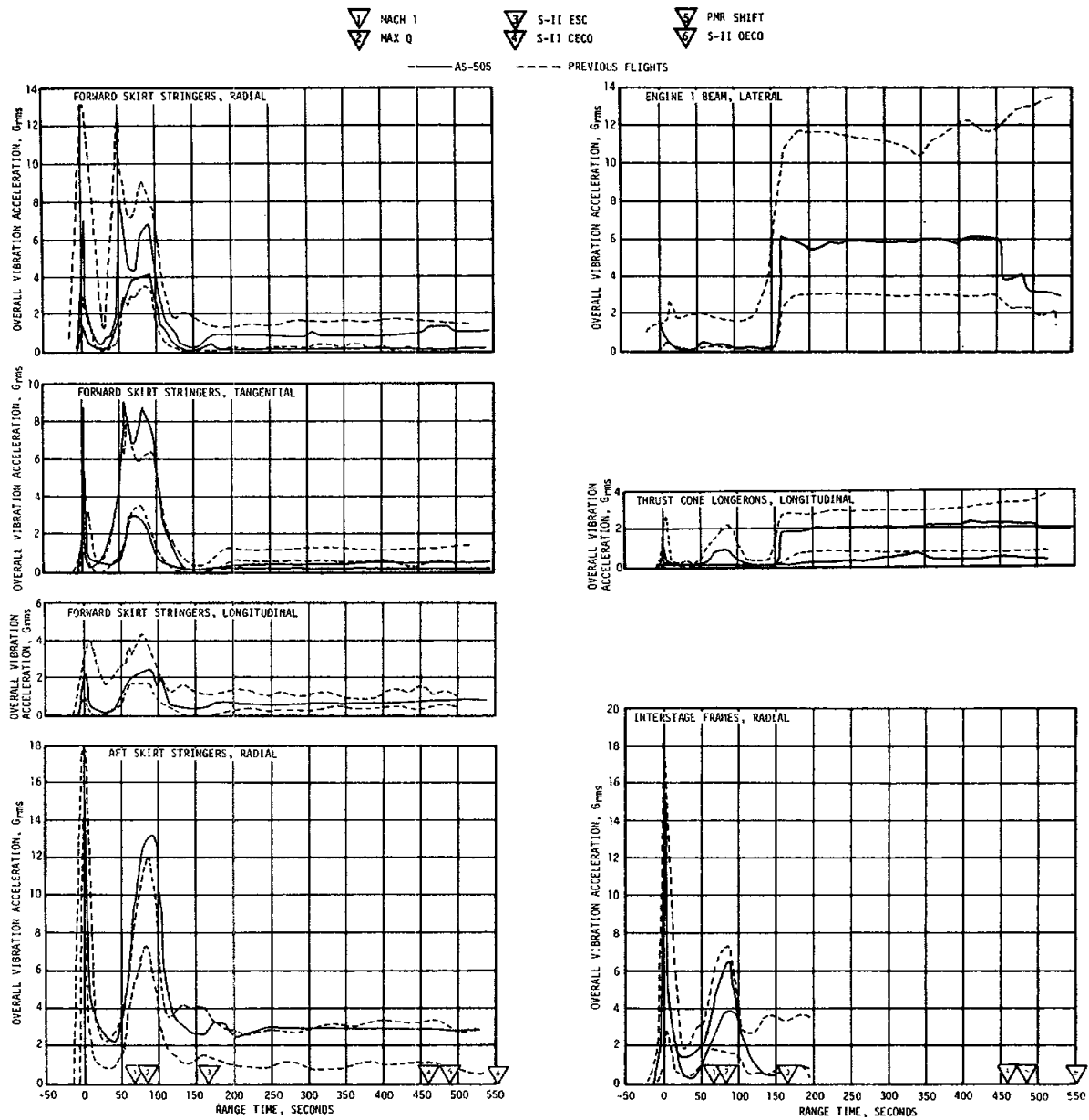


Figure 9-14. S-II Stage Structure Vibration Envelopes

1	MACH 1	3	S-II ESC	5	PMR SHIFT
2	MAX Q	4	S-II CEEO	6	S-II OEEO

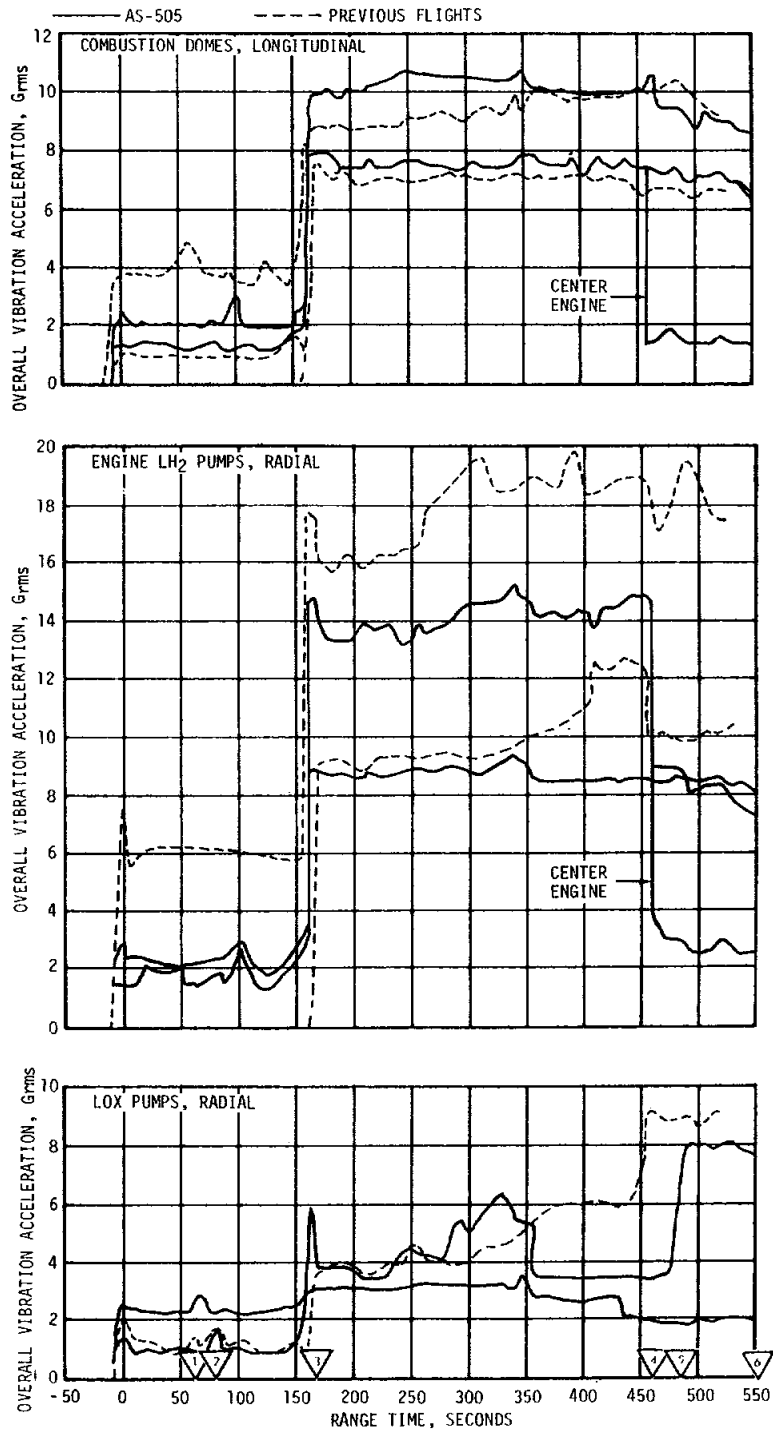


Figure 9-15. S-II Stage Engine Vibration Envelopes

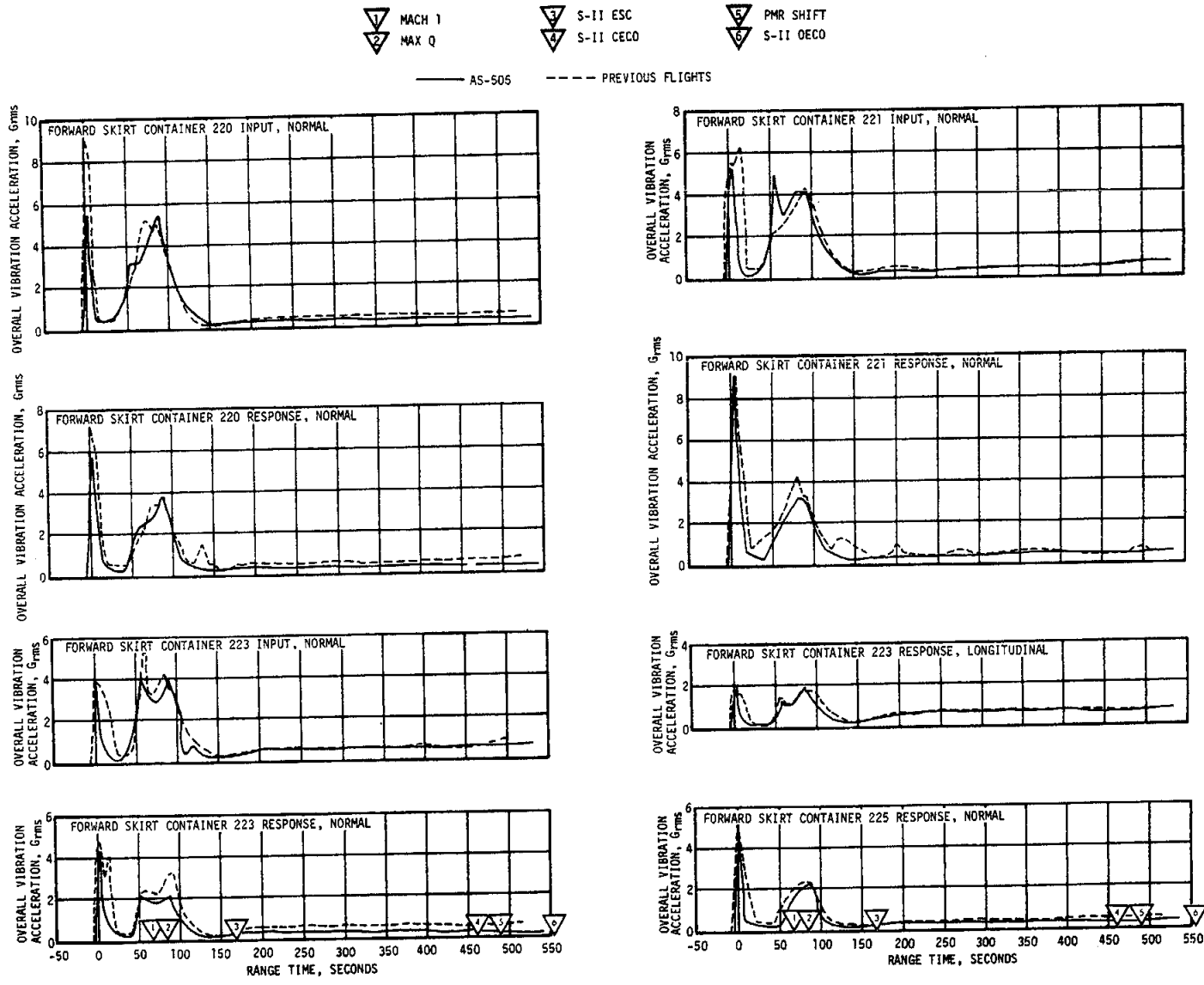


Figure 9-16. S-II Stage Component Vibration Envelopes (Sheet 1 of 2)

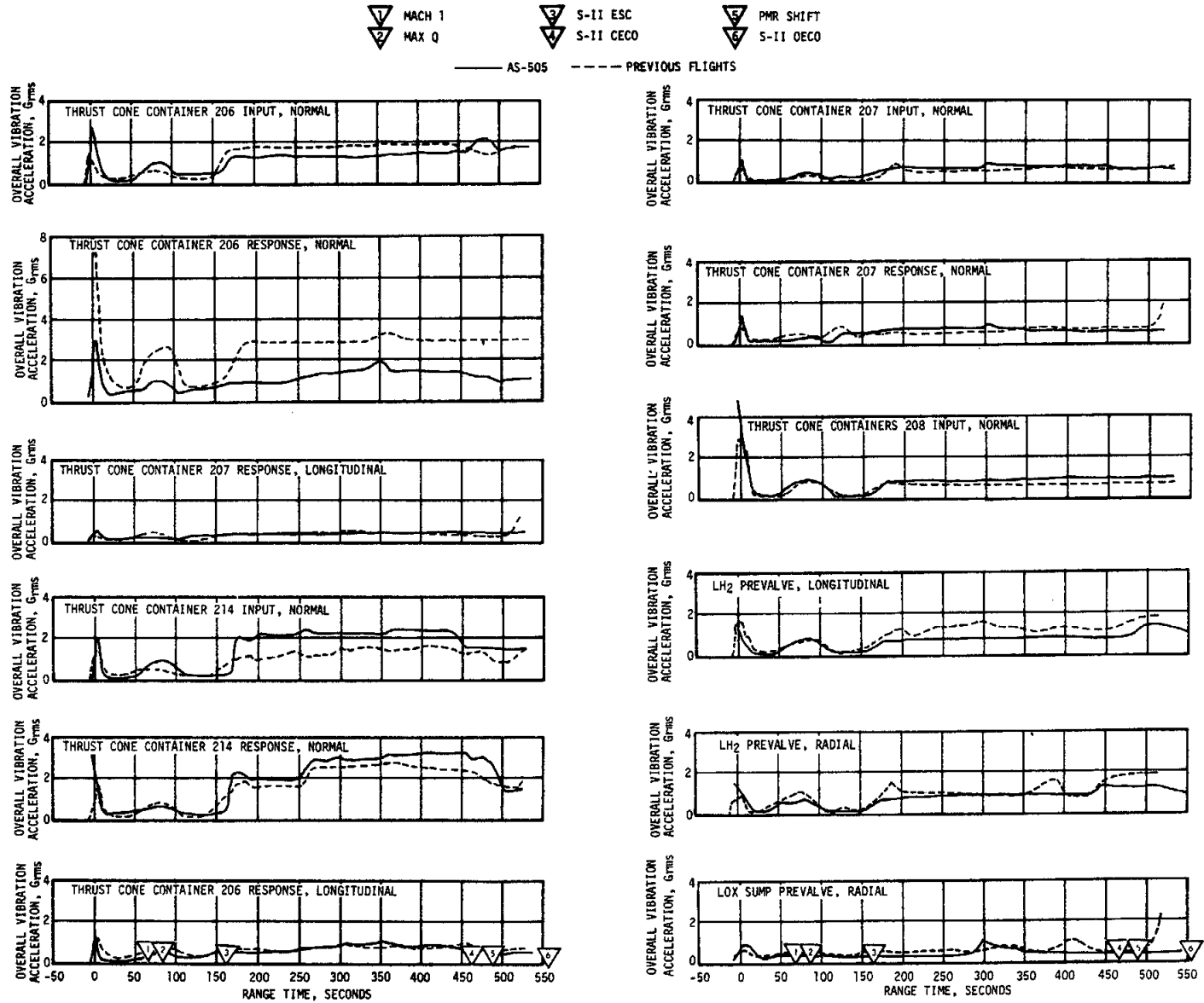


Figure 9-16. S-II Stage Component Vibration Envelopes
(Sheet 2 of 2)

drop in vibration level at CECO. A similar drop in level for the engine No. 5 LOX pump is not included in the figure because the reduced level remained within the envelope of the other four engines.

9.3.2.3 S-II Stage Components. In general, all S-II stage component vibration levels, as shown in Figure 9-16, agreed closely with the previous flight data.

9.3.3 S-IVB Stage and Engine Evaluation

Two vibration measurements were made on the structure, 15 at components mounted on the stage, and 13 at engine components. The maximum composite levels are indicated in Figures 9-17 and 9-18 and in Table 9-4.

9.3.3.1 S-IVB Stage Structure and Components. The envelope of vibration levels for the stage structure and components is shown in Figure 9-17. The data of the figure show the range of vibration levels at the input to components mounted on the forward and aft sections of the stage. The AS-505 levels were lower than the maximum measured during the AS-503 flight.

9.3.3.2 S-IVB Stage J-2 Engine. Data measured during the AS-505 flight on the two turbopumps and the combustion chamber dome are shown in Figure 9-18. The AS-503 levels presented for comparison include data from the turbopumps only. The differences between the measured vibration environment are within the normal scatter of the engines.

AS-505 S-IVB first and second burn data from components on the J-2 engine are shown in Figure 9-18. In addition, the nominal range of levels from similar measurements monitored on the AS-503 flight are shown. The AS-505 levels are within the range of the AS-503 data.

9.3.3.3 S-IVB Stage ASI Lines Dynamics. Dynamic strain measurements were made on the LOX and LH₂ ASI lines. The LOX ASI line strains ranged from 9 to 34 $\mu\text{in/in. RMS}$ (AS-503 flight line strains ranged from 10 to 20 $\mu\text{in/in. RMS}$). The LH₂ ASI line strains ranged from 17 to 60 $\mu\text{in/in. RMS}$ (AS-503 flight line strains ranged from 20 to 50 $\mu\text{in/in. RMS}$).

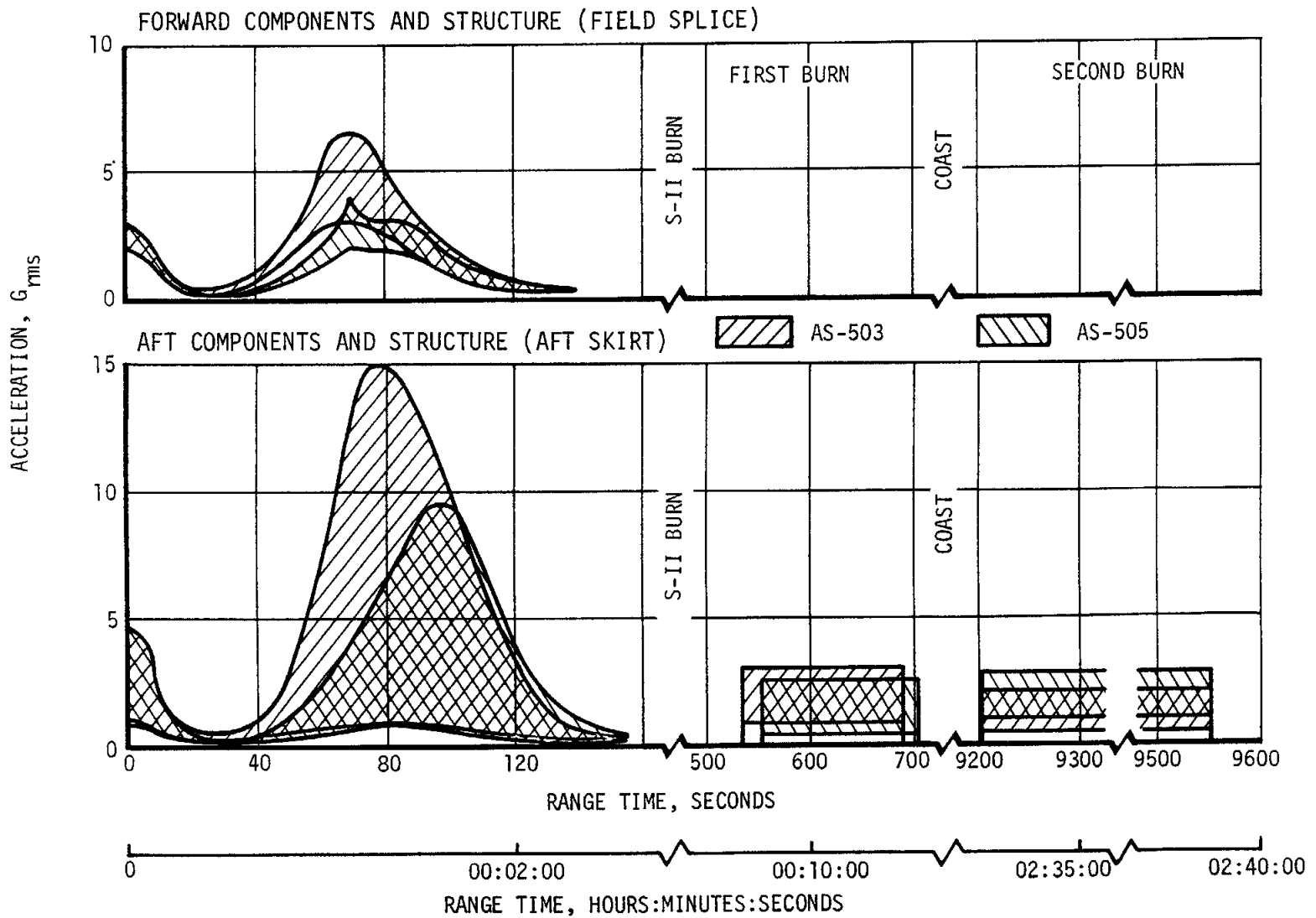


Figure 9-17. S-IVB Stage Vibration Envelopes

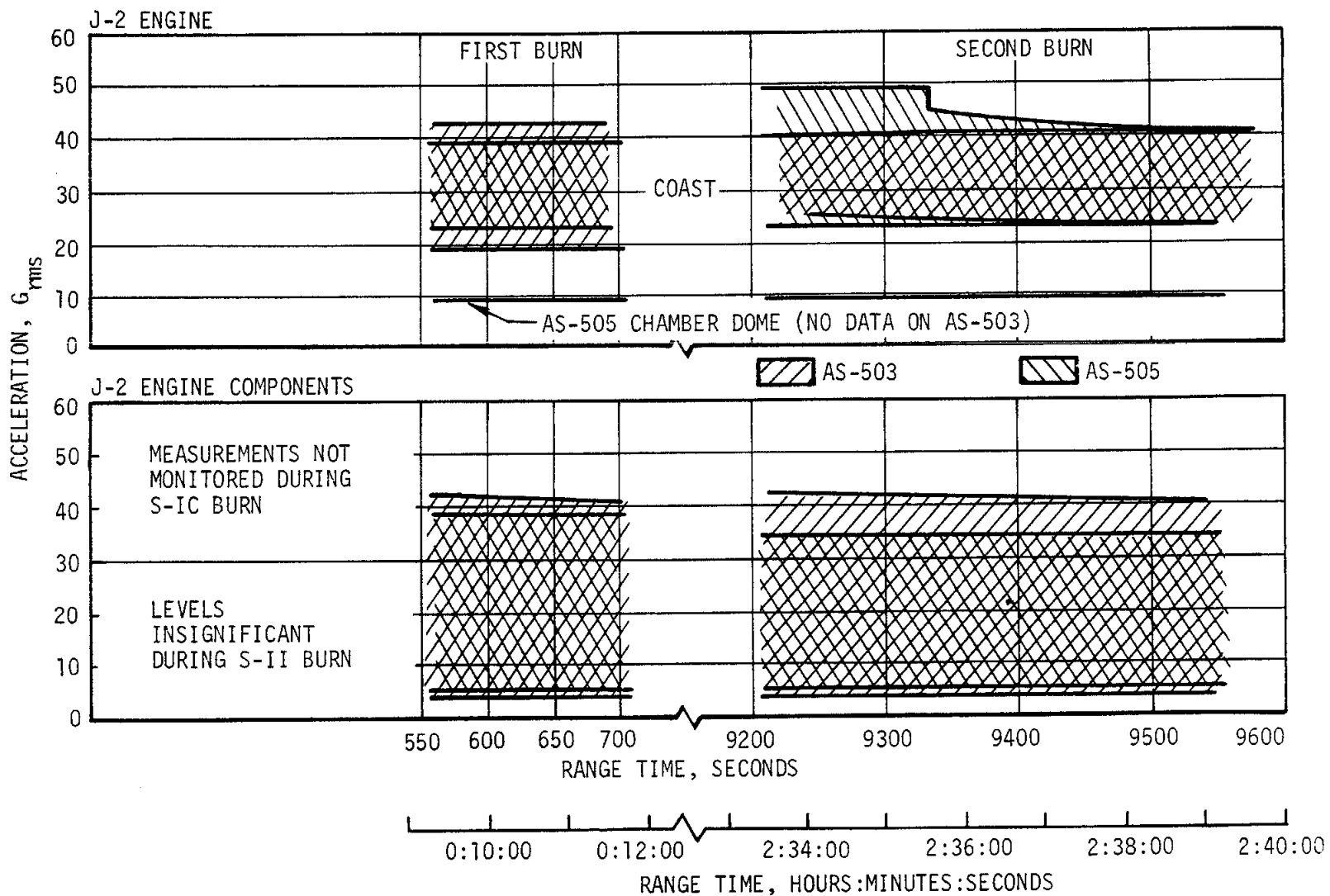


Figure 9-18. S-IVB Stage Engine Vibration Envelopes

Table 9-4. S-IVB Vibration Summary

	AREA MONITORED	MAX LEVEL GRMS	RANGE TIME (SEC)	REMARKS
Structure	Field Splice at Position I (Low Frequency), Thrust	0.8	1.5	Frequency Limited to 220 Hz
	Station 69.9 m (2748 in.) at Position II on Aft Skirt, Thrust	0.4	87	Frequency Limited to 220 Hz
Engine	Combustion Chamber Dome (Low Frequency), Thrust	0.6	9220	Frequency Limited to 220 Hz
	Combustion Chamber Dome Longitudinal	9.4	560	
	LH ₂ Turbopump, Lateral	25	9260	
	LOX Turbopump, Lateral	50	9210	
Stage Components (Forward) Stage Components (Aft)	Input to LH ₂ Vent Disconnect, Fwd Skirt, Thrust	2.5	85	
	Input to LH ₂ Vent Disconnect, Fwd Skirt, Radial	3.5	84	
	Input to Continuous Vent Module, Fwd Skirt, Radial	3.6	0.5	
	Helium Bottle, Thrust Structure, Pitch	3.4	700	
	Input to LH ₂ Feedline at LH ₂ Tank, Thrust	2.0	9216	
	Input to LH ₂ Feedline at LH ₂ Tank, Radial	2.9	67	
	Input to LH ₂ Prevalve in LH ₂ Feedline, Thrust	2.6	9219	
	Input to LH ₂ Prevalve in LH ₂ Feedline, Radial	2.1	560	
	Ambient Panel, Input to Chilledown Inverter, Thrust	1.4	0.5	
	Ambient Panel, Input to Chilledown Inverter, Radial	4.0	0.5	
	APS, Input to Propellant Control Module, Radial	4.6	83	
	APS, Input to Propellant Control Module, Tangential	5.7	83	
	APS, Input to Helium Regulator, Tangential	9.6	96	
	Input to Retrorocket Fwd Support, Aft	3.2	0.5	
	Input to LOX Chilledown Pump, Aft LOX Dome, Normal to Dome	3.9	0.5	

Table 9-4. S-IVB Vibration Summary (Continued)

AREA MONITORED		MAX LEVEL GRMS	RANGE TIME (SEC)	REMARKS
Component J-2 Engine	Main Fuel Valve, Tangential	6.5	702	Measurement Failed Second Burn
	Main Fuel Valve, Radial	6.5	702	
	Main Fuel Valve, Longitudinal	11.5	702	
	LOX Turbine Bypass Valve, Tangential	8.4	506	
	LOX Turbine Bypass Valve, Radial	8.6	560	
	LOX Turbine Bypass Valve, Longitudinal	18.2	702	
	ASI LOX Valve, Radial	14.7	702	
	ASI LOX Valve, Longitudinal	21.6	702	
	Fuel ASI Block, Radial	36.7	560	

SECTION 10

GUIDANCE AND NAVIGATION

10.1 SUMMARY

10.1.1 Flight Program

The guidance and navigation system performed satisfactorily during all periods for which data are available. The boost navigation and guidance schemes were properly executed, and translunar trajectory injection parameters were within tolerances. All orbital operations were nominal and S-IVB stage safing was satisfactorily accomplished, resulting in a heliocentric orbit for the S-IVB/IU as planned.

10.1.2 Instrument Unit Components

The Launch Vehicle Digital Computer (LVDC), the Launch Vehicle Data Adapter (LVDA), and the ST-124M-3 inertial platform functioned satisfactorily. No anomalies or deviations have been discovered.

10.2 GUIDANCE COMPARISONS

The postflight guidance hardware error analysis was based on comparisons of the ST-124M-3 platform measured velocities with the observed postflight trajectory established from external tracking data. No precision tracking data were available and the boost-to-parking orbit trajectory was established by a composite fit of C-band radar data. Figure 10-1 presents the comparisons of the platform measured velocities with corresponding values from the final observed postflight trajectory. A positive difference indicates trajectory data greater than the platform measurement. Although the overall differences are relatively small, they do not reflect a characteristic trend for platform hardware errors. The differences probably reflect more trajectory error than guidance error. The velocity differences at S-IVB first Engine Cutoff (ECO) were -0.8 m/s (-2.5 ft/s), 1.0 m/s (3.3 ft/s), and -0.6 m/s (-2.0 ft/s) for altitude, crossrange, and downrange velocity, respectively.

Due to limited tracking coverage of the second burn mode, that portion of the observed postflight trajectory was constructed by initializing the state vector and integrating the platform-measured velocities. Any velocity differences for the second burn were due to data transformation and interpolations.

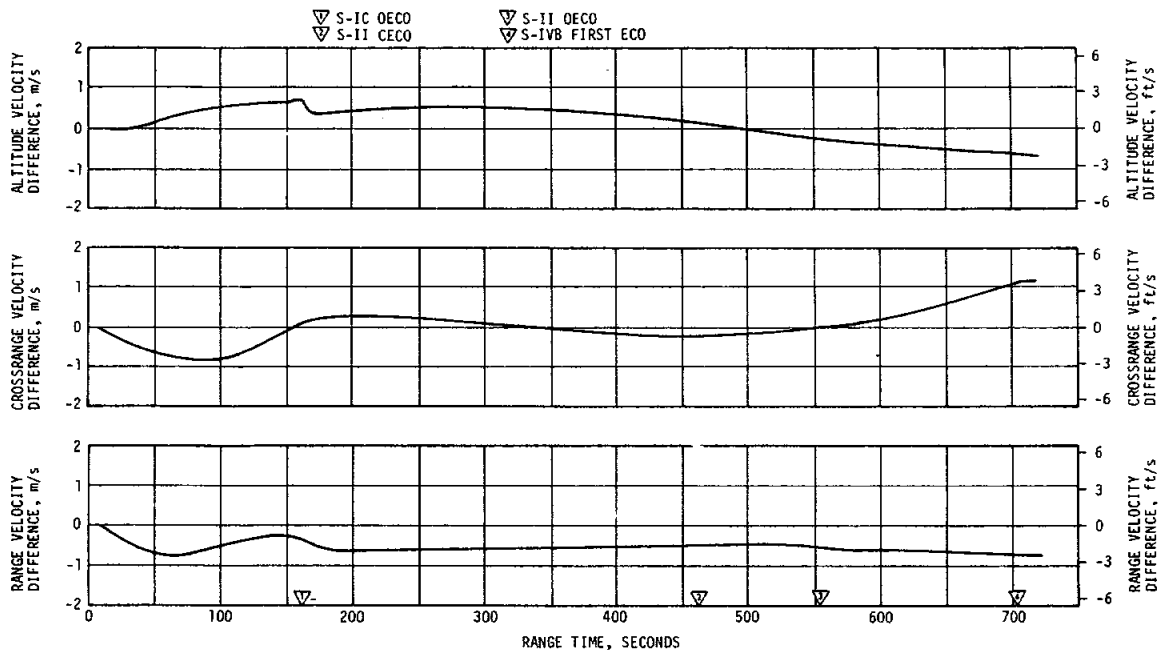


Figure 10-1. Tracking and ST-124M-3 Platform Velocity Comparison
(Trajectory Minus Guidance)

Velocities measured by the ST-124M-3 platform system at significant flight event times are shown in Table 10-1, along with corresponding values computed from the final AS-505 observed postflight trajectory and the preflight operational trajectory. Since the same thrust profile was used in the preflight and postflight operational trajectories, the inertial platform outputs should be equivalent. The differences between the telemetered velocities and the observed postflight trajectory values reflect some combination of small guidance hardware errors, tracking errors, and errors in interpolating data for event times. The differences between the telemetered and operational trajectory values reflected off-nominal flight conditions and vehicle performance.

Comparisons of navigation (PACSS 13 coordinate system) positions, velocities, and flight path angle at significant flight event times are presented in Table 10-2. The guidance (LVDC) and observed postflight trajectory values are in relatively good agreement throughout the flight. The component differences at parking orbit insertion and at Translunar Injection (TLI) are given in Table 10-3.

Table 10-1. Inertial Platform Velocity Comparisons

EVENTS	DATA SOURCE	VELOCITY M/S (FT/S)**		
		ALTITUDE (\dot{X}_m)	CROSSRANGE (\dot{Y}_m)	DOWN RANGE (\dot{Z}_m)
S-IC OECO	Guidance	2571.64 (8437.14)	7.90 (25.92)	2246.55 (7370.57)
	Postflight Trajectory	2572.05 (8438.48)	7.98 (26.18)	2245.74 (7367.91)
	Preflight Trajectory	2583.50 (8476.05)	-0.54 (-1.77)	2226.35 (7304.29)
S-II OECO	Guidance	3470.47 (11,386.06)	-3.60 (-11.81)	6751.83 (22,151.67)
	Postflight Trajectory	3470.27 (11,385.40)	-3.73 (-12.24)	6751.08 (22,149.21)
	Preflight Trajectory	3462.06 (11,358.46)	-0.72 (-2.36)	6763.89 (22,191.24)
First S-IVB ECO	Guidance	3210.19 (10,532.12)	2.05 (6.73)	7611.70 (24,972.77)
	Postflight Trajectory	3209.43 (10,529.63)	3.06 (10.04)	7611.08 (24,970.73)
	Preflight Trajectory	3206.03 (10,518.47)	1.54 (5.05)	7610.76 (24,969.68)
Parking Orbit Insertion	Guidance	3209.50 (10,529.86)	2.05 (6.73)	7613.35 (24,978.18)
	Postflight Trajectory	3208.78 (10,527.49)	3.10 (10.17)	7612.55 (24,975.56)
	Preflight Trajectory	3205.37 (10,516.30)	1.55 (5.08)	7612.46 (24,975.26)
Second S-IVB ECO *	Guidance	3079.06 (10,101.90)	204.90 (672.24)	-696.22 (-2284.19)
	Postflight Trajectory	3078.96 (10,101.57)	204.28 (670.21)	-695.95 (-2283.30)
	Preflight Trajectory	3094.33 (10,152.00)	14.53 (47.67)	-628.81 (-2063.02)
<p>* Second burn velocity data represent accumulated velocities from Time Base 6</p> <p>** PACSS 12 Coordinate System</p> <p>NOTE: Preflight trajectory data were adjusted for trajectory error in platform values at liftoff.</p>				

Table 10-1. Inertial Platform Velocity Comparisons (Continued)

EVENTS	DATA SOURCE	VELOCITY M/S (FT/S)**		
		ALTITUDE (\dot{x}_m)	CROSSRANGE (\dot{y}_m)	DOWN RANGE (\dot{z}_m)
Translunar Injection *	Guidance	3083.00 (10,114.83)	205.25 (673.39)	-696.60 (-2285.43)
	Postflight Trajectory	3083.01 (10,114.86)	205.35 (673.72)	-696.53 (-2285.20)
	Preflight Trajectory	3098.17 (10,164.60)	14.51 (47.60)	-629.10 (-2063.98)
<p>* Second burn velocity data represent accumulated velocities from Time Base 6</p> <p>** PACSS 12 Coordinate System</p> <p>NOTE: Preflight trajectory data were adjusted for trajectory error in platform values at liftoff.</p>				

Table 10-2. Guidance Comparisons

EVENT	DATA SOURCE	POSITIONS METERS (FT)				VELOCITIES M/S (FT/S)				FLIGHT PATH ANGLE (DEG)
		X _S	Y _S	Z _S	R	\dot{X}_S	\dot{Y}_S	\dot{Z}_S	V _S	γ
S-IC OECO	Guidance	6,436,333 (21,116,578)	39,704 (130,261)	158,973 (521,564)	6,438,417 (21,123,416)	827.45 (2714.72)	128.50 (421.59)	2621.08 (8699.35)	2751.72 (9027.96)	18.930
	Observed Postflight Trajectory	6,436,404 (21,116,812)	39,621 (129,990)	158,904 (521,337)	6,438,488 (21,123,647)	828.25 (2717.36)	128.58 (421.85)	2621.16 (8599.61)	2751.91 (9028.58)	18.9457
	Postflight Operational Trajectory	6,436,982 (21,118,708)	39,195 (128,593)	156,355 (512,977)	6,439,000 (21,125,328)	853.38 (2799.80)	120.16 (394.23)	2602.10 (8537.07)	2741.10 (8993.11)	19.5450
S-II OECO	Guidance	6,283,497 (20,615,150)	81,690 (268,010)	1,880,904 (6,170,946)	6,559,482 (21,520,610)	-1893.09 (-6210.92)	86.98 (285.38)	6633.39 (21,763.08)	6898.82 (22,633.92)	0.74600
	Observed Postflight Trajectory	6,283,760 (20,616,009)	81,586 (267,669)	1,880,627 (6,170,037)	6,559,653 (21,521,172)	-1893.09 (-6210.93)	86.90 (285.10)	6632.82 (21,761.22)	6898.24 (22,632.02)	0.74107
	Postflight Operational Trajectory	6,281,468 (20,608,492)	81,521 (267,458)	1,891,355 (6,205,231)	6,560,542 (21,524,088)	-1908.57 (-6261.71)	90.21 (295.97)	6642.10 (21,791.67)	6911.46 (22,675.40)	0.7346
First S-IVB ECO	Guidance	5,882,772 (19,300,431)	93,925 (308,153)	2,908,961 (9,543,835)	6,563,374 (21,533,379)	-3454.27 (-11,332.91)	75.80 (248.69)	6983.64 (22,912.20)	7791.60 (25,562.99)	0.00179
	Observed Postflight Trajectory	5,882,950 (19,301,018)	93,881 (308,010)	2,908,740 (9,543,109)	6,563,435 (21,533,581)	-3454.92 (-11,335.04)	76.89 (252.26)	6983.19 (22,910.73)	7791.42 (25,562.40)	-0.0064
	Postflight Operational Trajectory	5,883,463 (19,302,701)	93,919 (308,132)	2,907,773 (9,539,936)	6,563,467 (21,533,686)	-3452.94 (-11,328.54)	75.83 (248.78)	6984.02 (22,913.46)	7791.35 (25,562.17)	-0.00020

10-5

Table 10-2. Guidance Comparisons (Continued)

EVENT	DATA SOURCE	POSITIONS METERS (FT)				VELOCITIES M/S (FT/S)				FLIGHT PATH ANGLE (DEG)
		X _s	Y _s	Z _s	R	\dot{X}_s	\dot{Y}_s	\dot{Z}_s	V _s	γ
Parking Orbit Insertion	Guidance	5,847,815 (19,185,745)	94,677 (310,619)	2,978,600 (9,772,308)	6,563,380 (21,533,400)	-3537.66 (-11,606.50)	74.60 (244.75)	6943.82 (22,781.56)	7793.41 (25,568.93)	0.00260
	Observed Postflight Trajectory	5,847,847 (19,185,849)	94,642 (310,506)	2,978,439 (9,771,781)	6,563,335 (21,533,252)	-3538.19 (-11,608.23)	75.72 (248.43)	6943.18 (22,779.46)	7793.09 (25,567.88)	-0.00494
	Postflight Operational Trajectory	5,848,514 (19,188,037)	94,671 (310,600)	2,977,423 (9,768,447)	6,563,469 (21,533,690)	-3536.30 (-11,602.03)	74.63 (244.85)	6944.23 (22,782.91)	7793.16 (25,568.11)	0.0010
Second S-IVB ECO	Guidance	191,624 (628,688)	-123,594 (-405,493)	-6,690,747 (-21,951,270)	6,694,620 (21,963,976)	10,799.27 (35,430.67)	230.74 (757.02)	-1003.50 (-3292.32)	10,848.24 (35,591.34)	6.92400
	Observed Postflight Trajectory	188,203 (617,462)	-124,409 (-408,167)	-6,692,918 (-21,958,391)	6,696,719 (21,970,863)	10,797.04 (35,423.76)	229.34 (752.43)	-1009.00 (-3310.37)	10,846.56 (35,585.83)	6.927
	Postflight Operational Trajectory	172,344 (565,432)	-123,812 (-406,208)	-6,690,556 (-21,950,643)	6,693,920 (21,961,681)	10,798.20 (35,427.16)	231.87 (760.72)	-1024.03 (-3359.68)	10,849.12 (35,594.23)	6.8673
Translunar Injection	Guidance	299,613 (982,982)	-121,275 (-397,885)	-6,700,340 (-21,982,743)	6,710,259 (22,015,286)	10,799.97 (35,432.97)	232.66 (763.32)	-915.13 (-3002.40)	10,841.17 (35,568.14)	7.37843
	Observed Postflight Trajectory	296,191 (971,755)	-122,100 (-400,589)	-6,702,548 (-21,989,987)	6,710,200 (22,015,093)	10,797.91 (35,426.21)	231.99 (761.12)	-920.85 (-3021.16)	10,839.59 (35,562.96)	7.379
	Postflight Operational Trajectory	280,349 (919,780)	-121,482 (-398,562)	-6,700,355 (-21,982,793)	6,707,318 (22,005,637)	10,799.01 (35,429.83)	233.85 (767.23)	-935.57 (-3069.45)	10,841.98 (35,570.80)	7.3219

10-6

Table 10-3. Guidance Component Comparisons

PARAMETERS	OBSERVED-GUIDANCE	POSTFLIGHT-GUIDANCE
PARKING ORBIT INSERTION DIFFERENCES		
$\Delta \dot{x}_S$ m/s (ft/s)	-0.53 (-1.73)	1.36 (4.47)
$\Delta \dot{y}_S$ m/s (ft/s)	1.12 (3.67)	0.03 (0.10)
$\Delta \dot{z}_S$ m/s (ft/s)	-0.64 (-2.10)	0.41 (1.35)
ΔV_S m/s (ft/s)	-0.31 (-1.02)	-0.25 (-0.82)
ΔR m (ft)	45.0 (148.0)	89.0 (290.0)
$\Delta \theta$ deg	-0.00754	-0.0016
TRANSLUNAR INJECTION DIFFERENCES		
$\Delta \dot{x}_S$ m/s (ft/s)	-2.06 (-6.76)	-0.96 (-3.14)
$\Delta \dot{y}_S$ m/s (ft/s)	-0.67 (-2.20)	1.19 (3.91)
$\Delta \dot{z}_S$ m/s (ft/s)	-5.72 (-18.76)	-20.44 (-67.05)
ΔV_S m/s (ft/s)	-1.58 (-5.18)	0.81 (2.67)
ΔR m (ft)	-59.0 (-193.0)	-2941.0 (-9649.0)
$\Delta \theta$ deg	0.00277	-0.0546

The ST-124M-3 platform measurements and the LVDC flight programs were highly successful in guiding the AS-505 vehicle to near nominal end conditions. A minimum of corrections were required for the spacecraft to accomplish its mission.

10.3 NAVIGATION AND GUIDANCE SCHEME EVALUATION

All analyzed guidance performance measurements indicated satisfactory guidance during S-IVB first and second burns. The active guidance phases start and stop times are given in Table 10-4. Included in this table are the start and stop times for the artificial tau phases and chi freezes. The minor loop chi attitude commands and orbital guidance commands are given in Figures 10-2 and 10-3, respectively. The lower than predicted geocentric radius and the higher crossrange velocity component at Iterative Guidance Mode (IGM) initiation were compensated for by commanding pitch approximately 2 degrees more positive than predicted and yaw approximately 0.5 degree more negative than predicted, as shown in Figure 10-2. The deletion of the attitude freeze resulted in a smoother transition from S-II to S-IVB guidance phases than the same transition during AS-503 and AS-504 missions. Pre-IGM guidance functioned satisfactorily as programmed. Orbital guidance events for which telemetry was available were accomplished satisfactorily. The guidance during S-IVB second burn resulted in satisfactory TLI parameters as shown in Table 10-5.

Table 10-4. Start and Stop Times for IGM Guidance Commands

EVENT*	IGM PHASE (SEC)		ARTIFICIAL TAU (SEC)		STEERING MISALIGNMENT CORRECTION (SEC)		TERMINAL GUIDANCE (SEC)		CHI FREEZE (SEC)	
	START	STOP	START	STOP	START	STOP	START	STOP	START	STOP
First Phase IGM	202.9	484.8			222.6	491.9				
Second Phase IGM	484.8	552.7	484.8	490.2	493.8	552.7				
Third Phase IGM	552.7	695.7	560.1	568.9	567.1	695.7	669.4	697.3	697.3	704.9**
Fourth Phase IGM	9218.2	9333.2			9223.9					
Fifth Phase IGM	9333.2	9547.7	9333.2	9339.6		9549.2	9521.1	9549.3	9549.3	9568.7**

* All times are for the start of the computation cycle in which the event occurred.

** Start orbital time line.

Control parameters indicate slight attitude perturbations at IGM initiation and S-IVB Programmed Mixture Ratio (PMR) shift. The perturbations were expected and were not significant. The minor loop satisfactorily converted the guidance commands into steering signals throughout the mission.

10.4 GUIDANCE SYSTEM COMPONENT EVALUATION

10.4.1 LVDC Performance

The LVDC performed as predicted for the AS-505 mission. No valid error monitor words and no self-test error data have been observed that indicate any deviation from correct operation.

10.4.2 LVDA Performance

The LVDA performance was nominal. No valid error monitor words and no self-test error data indicating deviations from correct performance were observed.

10.4.3 Ladder Outputs

The ladder networks and converter amplifiers performed satisfactorily. No data have been observed that indicate an out-of-tolerance condition between channel A and the reference channel converter-amplifiers.

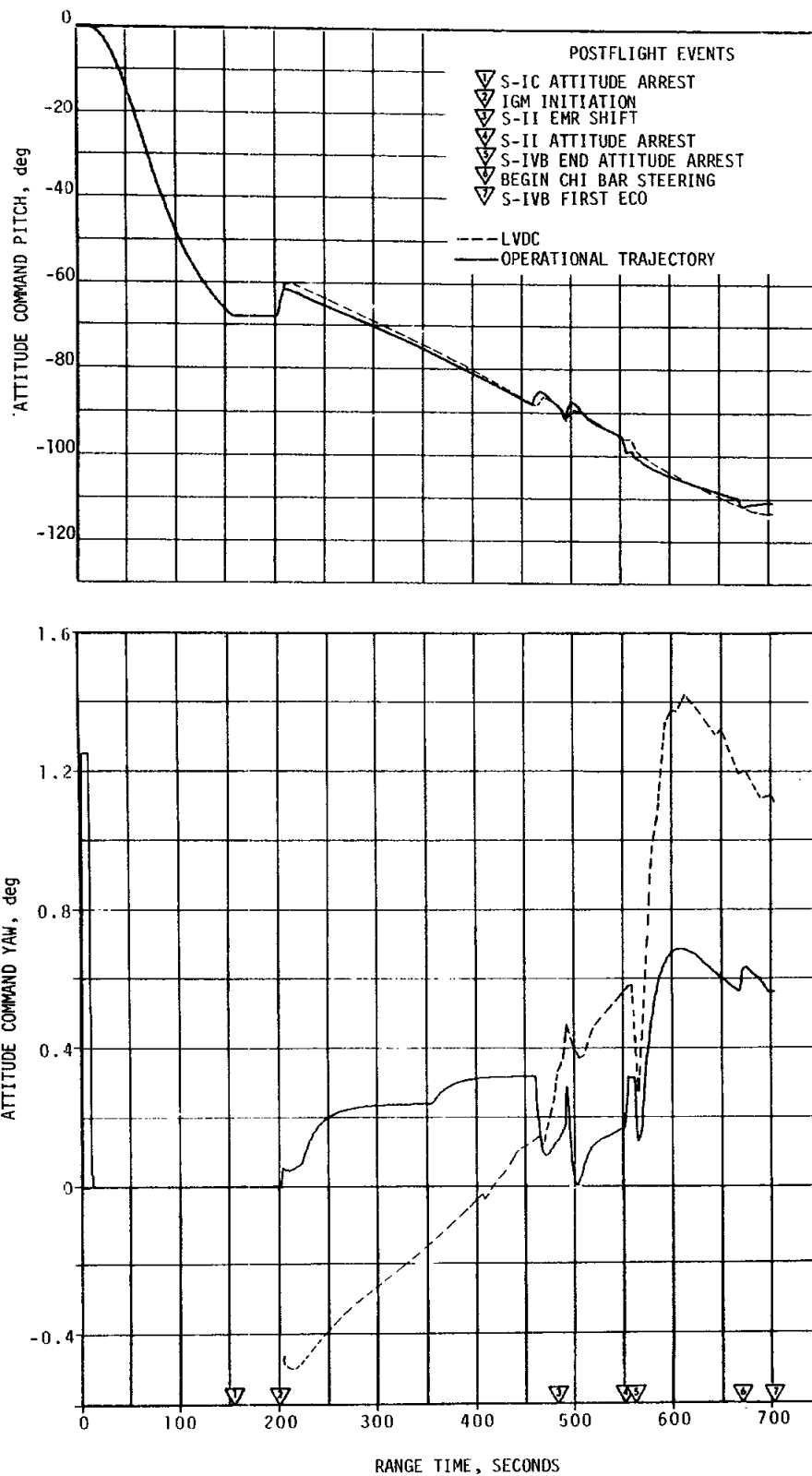


Figure 10-2. Attitude Commands During Active Guidance Period

10-10

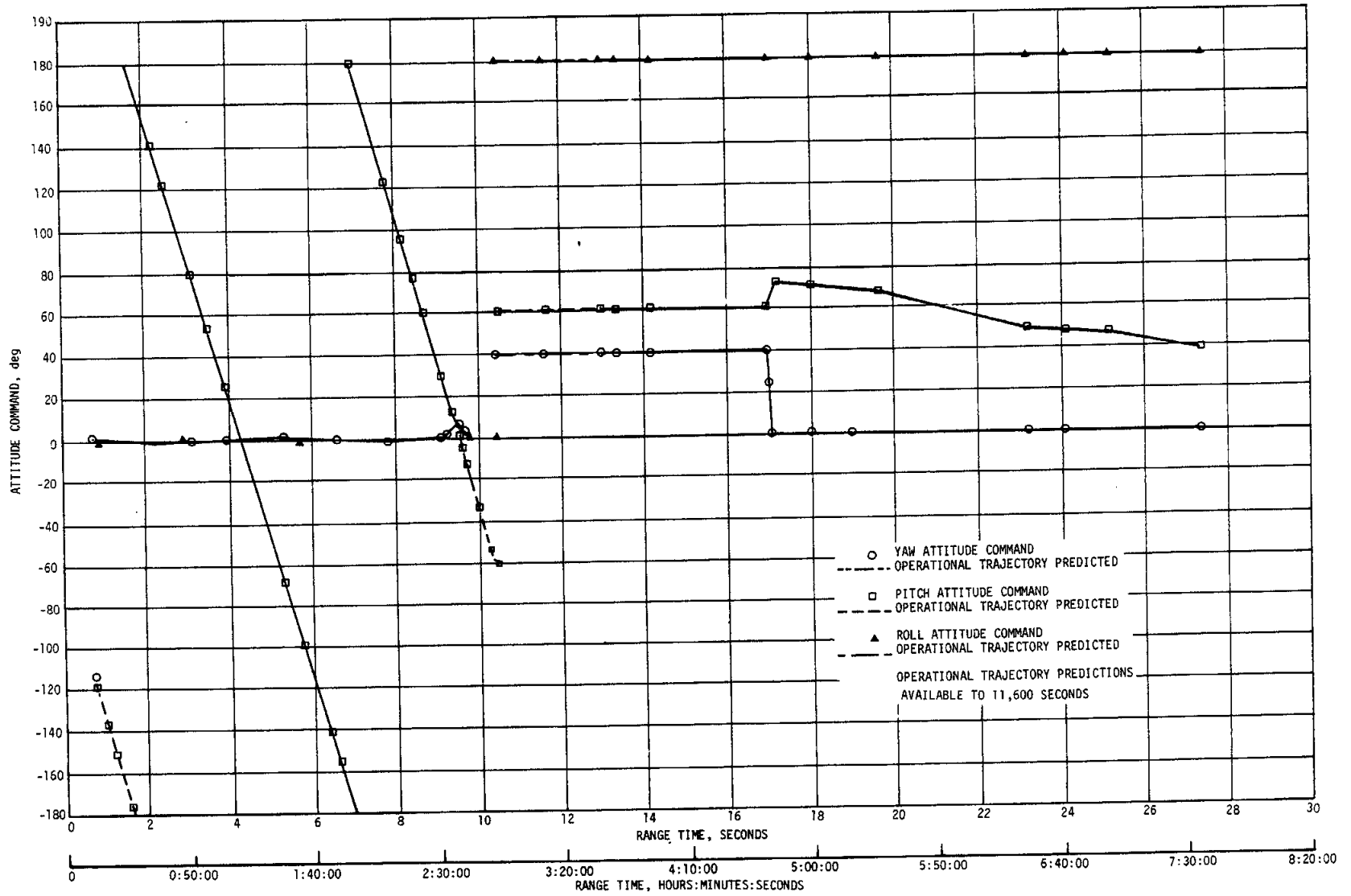


Figure 10-3. Orbital Attitude Commands

Table 10-5. Translunar Injection Parameters

PARAMETER	PREDICTED	POSTFLIGHT TRAJECTORY	TRAJECTORY MINUS PREDICTED	LVDC	LVDC MINUS PREDICTED
Inertial Velocity m/s (ft/s)	10,841.98 (35,570.80)	10,839.59 (35,562.96)	-2.39 (-7.84)	10,841.17 (35,568.14)	-0.81 (-2.66)
Flight Path Angle deg	7.322	7.379	0.057	7.378	0.056
Descending Mode deg	123.537	123.515	-0.022	123.527	-0.010
Inclination deg	31.691	31.698	0.007	31.698	0.007
Eccentricity	0.97836	0.97834	-0.00002	0.97830	-0.00006
c_3 m ² /s ² (ft ² /s ²)	-1,307,603 (-14,074,922)	-1,308,471 (-14,084,267)	-868 (-9345)	-1,310,867 (-14,110,055)	-3,264 (-35,133)

10.4.4 Telemetry Outputs

Analysis of the available LVDA telemetry buffer and flight control computer attitude error plots indicated symmetry between the buffer outputs and the ladder outputs. The available LVDC power supply plots indicated satisfactory power supply performance. The H60-603 guidance computer telemetry was completely satisfactory.

10.4.5 Discrete Outputs

No valid discrete output register words (tags 043 and 052) were observed to indicate guidance or simultaneous memory failure.

10.4.6 Switch Selector Functions

Switch selector data indicate that the LVDA switch selector functions were performed satisfactorily. No error monitor words were observed that indicate disagreement in the Triple Modular Redundant (TMR) switch selector register positions or in the switch selector feedback circuits. No mode code 24 words or switch selector feedback words were observed that indicated a switch selector feedback was in error. In addition, no indications were observed to suggest that the B channel input gates to the switch selector register positions were selected.

10.4.7 ST-124M-3 Inertial Platform Performance

The inertial platform system performed as designed. The inertial gimbal temperature fell below specifications; however, there are no indications

of degraded inertial platform performance. The temperature went below the minimum specification of 313.15°K (104.0°F) at 10,000 seconds, reaching 310.15°K (98.6°F) at approximately 25,000 seconds.

The accelerometer servo loops functioned as designed and maintained the accelerometer float within the measuring head stops (± 6 degrees) throughout the flight. The accelerometer encoder outputs indicated that the accelerometers accurately measured the vehicle acceleration.

The X, Y, and Z gyro servo loops for the stable element functioned as designed. The operational limits of the servo loops were not reached at any time during the mission.

SECTION 11

CONTROL SYSTEM

11.1 SUMMARY

The AS-505 Flight Control Computer (FCC), Thrust Vector Control (TVC), and Auxiliary Propulsion System (APS) satisfied all requirements for vehicle attitude control during the flight. Bending and slosh dynamics were adequately stabilized. The preprogrammed S-IC boost phase yaw, roll, and pitch maneuvers were properly executed. The S-IC outboard cant was accomplished as planned.

The peak winds observed during the flight were slightly less than the 95-percentile May wind and were well within the capabilities of the control system. The maximum pitch and yaw engine deflections were caused by wind shears.

S-IC/S-II first and second plane separations were accomplished with no significant attitude deviations. At Iterative Guidance Mode (IGM) initiation a pitch up transient occurred similar to that seen on previous flights. At S-II early Center Engine Cutoff (CECO), the guidance parameters were modified by the loss in thrust. There was a change in yaw attitude due to the slight thrust misalignment of the center engine. S-II/S-IVB separation occurred as expected and without producing any significant attitude deviations.

Satisfactory control of the vehicle was maintained during first and second S-IVB burns and during parking orbit. During the Command and Service Module (CSM) separation from the S-IVB/Instrument Unit (IU) and during the Transposition, Docking and Ejection (TD&E) maneuver, the control system maintained the vehicle in a fixed inertial attitude to provide a stable docking platform.

After Translunar Injection (TLI) attitude control was maintained for the propellant dumps and chilldown experiment. For AS-505 the APS propellants were not depleted by the last ullage burn, and control was maintained until the batteries were exhausted.

11.2 CONTROL SYSTEM DESCRIPTION

The control system was essentially the same as that on AS-503. The flight program was modified to provide for early S-II Center Engine Cutoff (CECO).

11.3 S-IC CONTROL SYSTEM EVALUATION

The AS-505 control system performed satisfactorily during S-IC powered flight. Less than 15 percent of available engine deflection was used although the actual flight wind magnitude was at times close to a 95-percentile May wind.

All dynamics were well within vehicle capability. In the region of high dynamic pressure, the maximum angles-of-attack were -3.3 degrees in pitch and 2.8 degrees in yaw. The maximum average pitch engine deflection was -0.6 degree and was caused by a wind shear. The maximum average yaw engine deflection was 0.6 degree and was due to a wind shear. Absence of any divergent bending or slosh frequencies in vehicle motion indicates that bending and slosh dynamics were adequately stabilized.

Vehicle attitude errors required to trim out the effects of thrust imbalance, thrust misalignment, and control system misalignments were well within predicted envelopes. Vehicle dynamics at S-IC/S-II first plane separation were well within staging requirements.

11.3.1 Liftoff Clearances

The vehicle cleared the mobile launcher structure well within the available clearance envelopes. Reduction of the camera data showing liftoff motion was not performed for the AS-505 flight, but simulations with flight data show that less than 20 percent of the available clearance was used. The ground wind was from the southeast with a magnitude of 8.2 m/s (16.0 knots) at the 18.3-meter (60-ft) level.

The predicted and measured misalignments, soft release forces, winds, and the thrust-to-weight ratio are shown in Table 11-1.

11.3.2 S-IC Flight Dynamics

The control parameter maximums for the period of S-IC burn are listed in Table 11-2. The pitch, yaw, and roll plane time histories during S-IC boost are shown in Figures 11-1, 11-2, and 11-3. Dynamics in the region between liftoff and 40 seconds resulted primarily from guidance commands. During the period from 40 to 115 seconds, maximum dynamics were caused by the pitch tilt program, wind magnitude, and wind shears. Significant dynamics due to wind shears occurred in pitch and yaw between 70 and 100 seconds. Dynamics between 115 seconds and S-IC/S-II separation were caused by high-altitude winds, separated airflow aerodynamics, CECO, and tilt arrest. The prominent pitch attitude error at 119 seconds may be caused by the loss of fin stabilizing action due to separated airflow. The transient at CECO indicates that the center engine cant was -0.1 degree in pitch and -0.15 degree in yaw.

Table 11-1. AS-505 Misalignment and Liftoff Conditions Summary

PARAMETER	PREFLIGHT PREDICTED			LAUNCH		
	PITCH	YAW	ROLL	PITCH	YAW	ROLL
Thrust Misalignment, deg*	±0.34	±0.34	±0.34	0.073	-0.038	-0.049
Center Engine Cant, deg	-	-	-	-0.1	-0.15	-
Servo Amp Offset, deg/eng	±0.1	±0.1	±0.1	-	-	-
Vehicle Stacking and Pad Misalignment, deg	±0.29	±0.29	0.0	0.022	-0.017	0.0
Attitude Error at Holddown Arm Release, deg				-0.034	-0.035	-0.003
Peak Soft Release Force Per Rod, N (lbf)	316,000 (71,000)			391,000 (88,200)		
Wind	95 Percentile Envelope			8.2 m/s (16.0 knots) at 18.3 meters (60 ft)		
Thrust-to-Weight Ratio	1.197			**		
<p>*Thrust misalignment of 0.34 degree encompasses the center engine cant. A positive polarity was used to determine minimum fin tip/umbilical tower clearance. A negative polarity was used to determine vehicle/GSE clearances.</p> <p>**Data not available for update.</p>						

At Outboard Engine Cutoff (OECO), the vehicle had attitude errors of -0.48, 0.05, and -0.2 degree in pitch, yaw, and roll, respectively. These errors are required to trim out the effects of thrust imbalance, offset Center of Gravity (CG), thrust vector misalignment, and control system misalignments. The maximum equivalent thrust misalignments were 0.07, -0.038, and -0.049 degree in pitch, yaw, and roll, respectively.

There was no significant sloshing observed. The engine response to the observed slosh frequencies showed that the slosh was well within the capabilities of the control system.

- ▽ BEGIN YAW MANEUVER
- ▽ END YAW MANEUVER
- ▽ BEGIN PITCH AND ROLL MANEUVER
- ▽ OUTBOARD ENGINE CANT
- ▽ END ROLL MANEUVER
- ▽ MACH 1
- ▽ MAX Q
- ▽ S-IC CECO
- ▽ TILT ARREST
- ▽ S-IC OEEO

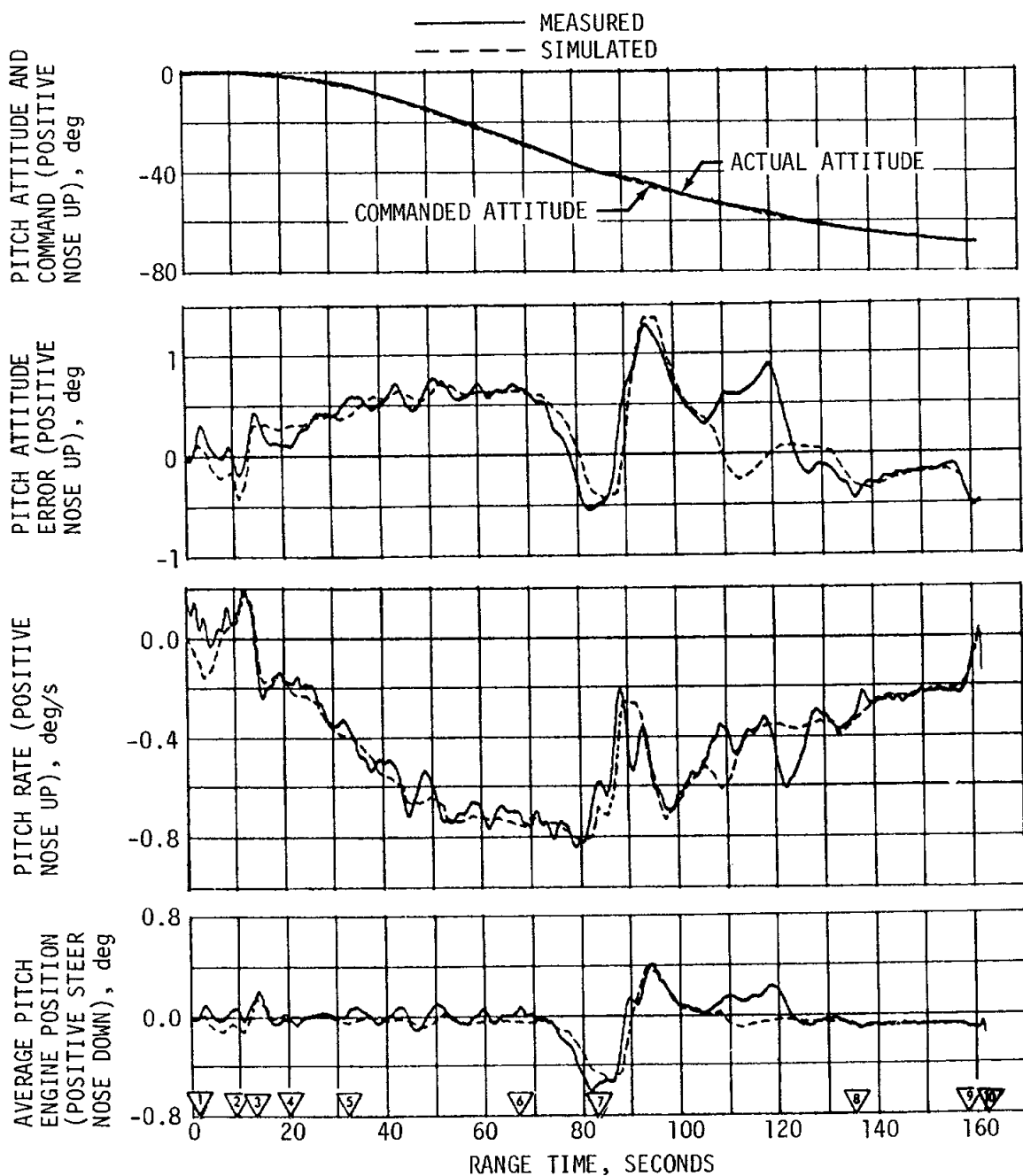


Figure 11-1. Pitch Plane Dynamics During S-IC Burn

- 1 BEGIN YAW MANEUVER
- 2 END YAW MANEUVER
- 3 BEGIN PITCH AND ROLL MANEUVER
- 4 OUTBOARD ENGINE CANT
- 5 END ROLL MANEUVER
- 6 MACH 1
- 7 MAX Q
- 8 S-IC CECO
- 9 TILT ARREST
- 10 S-IC OECO

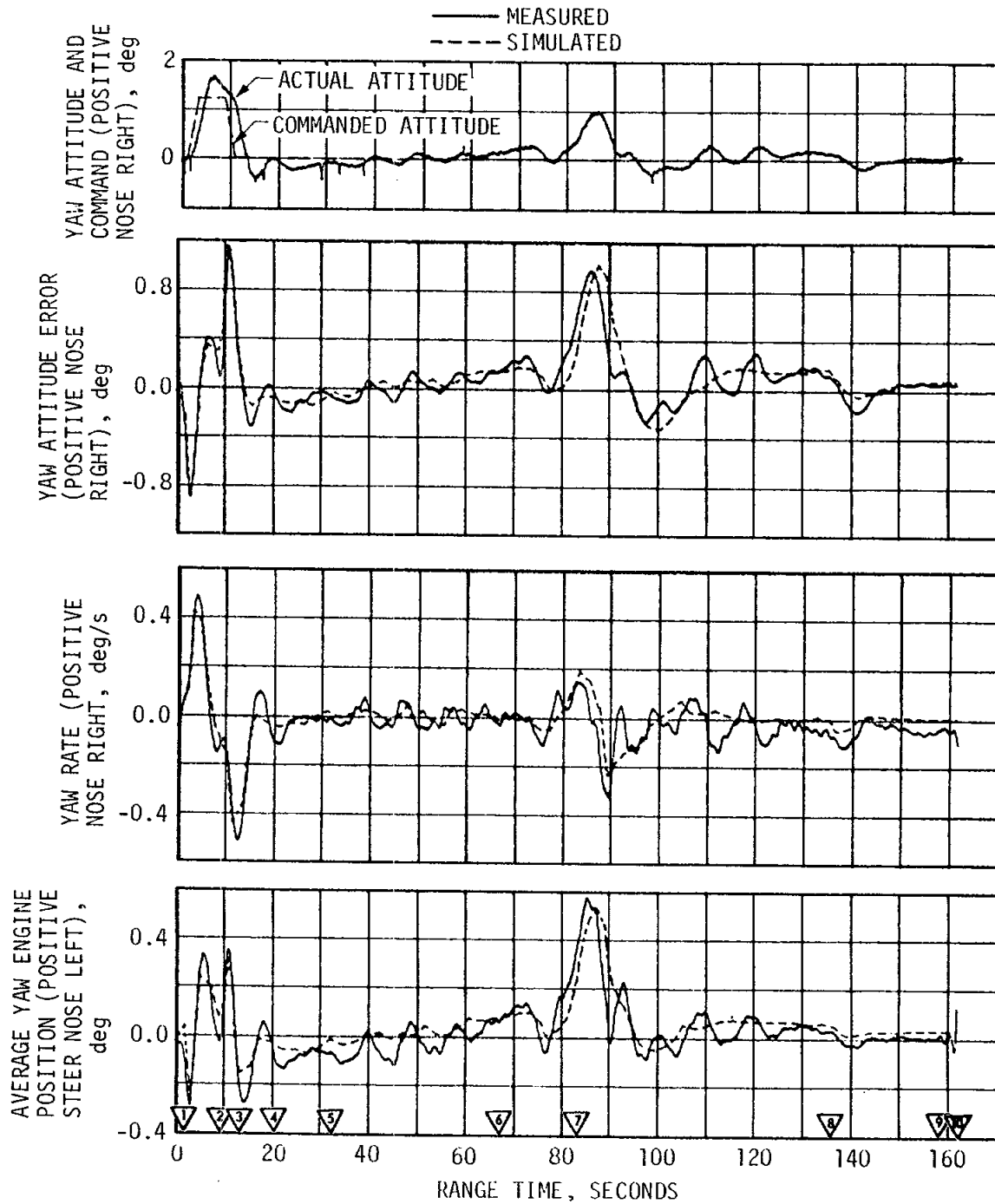


Figure 11-2. Yaw Plane Dynamics During S-IC Burn

- | | | | |
|---|-------------------------------|---|-------------|
| ▽ | BEGIN YAW MANEUVER | ▽ | MACH 1 |
| ▽ | END YAW MANEUVER | ▽ | MAX Q |
| ▽ | BEGIN PITCH AND ROLL MANEUVER | ▽ | S-IC CECO |
| ▽ | OUTBOARD ENGINE CANT | ▽ | TILT ARREST |
| ▽ | END ROLL MANEUVER | ▽ | S-IC OECC |

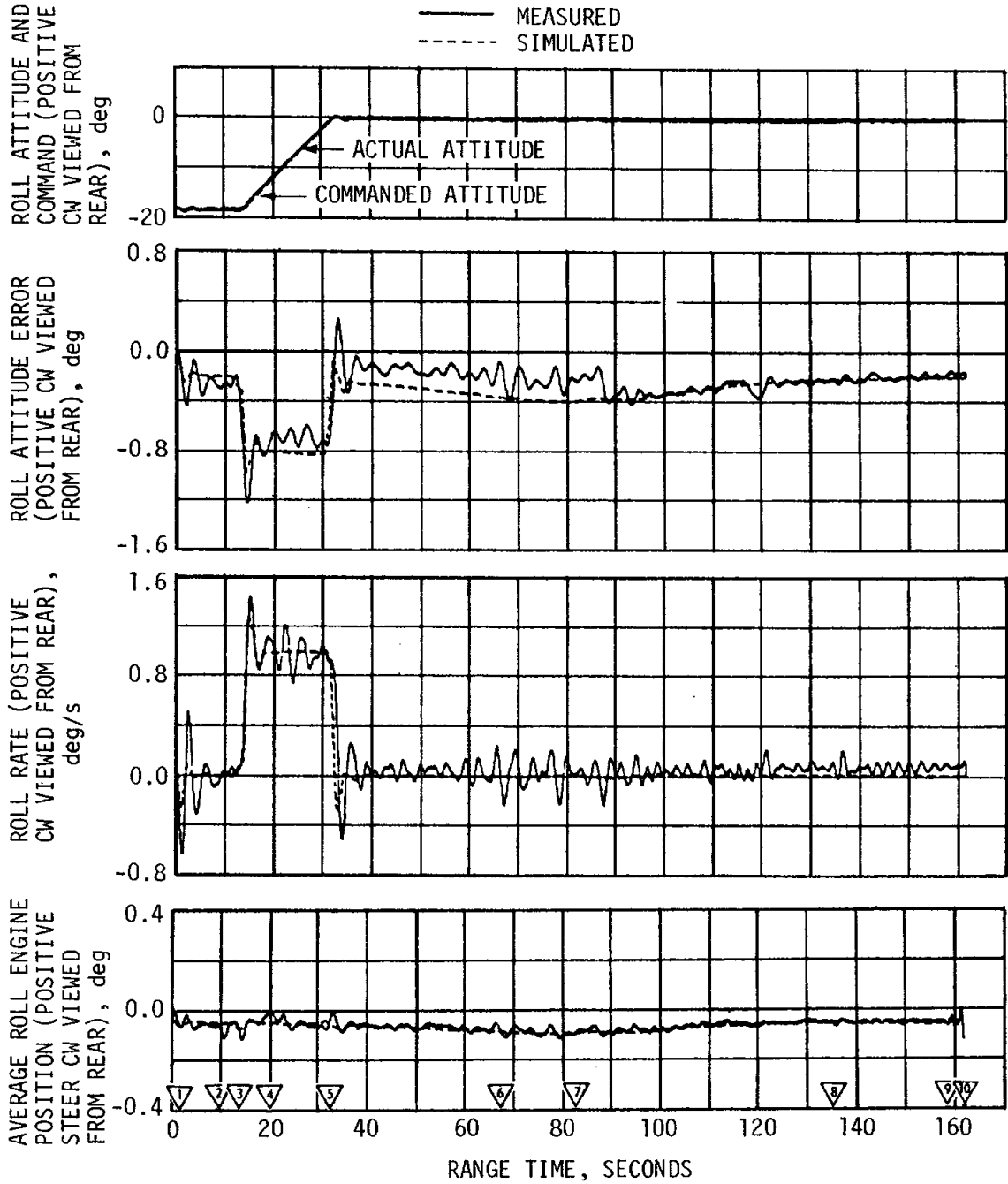


Figure 11-3. Roll Plane Dynamics During S-IC Burn

Table 11-2. Maximum Control Parameters During S-IC Boost Flight

PARAMETERS	UNITS	PITCH PLANE		YAW PLANE		ROLL PLANE	
		MAGNITUDE	RANGE TIME (SEC)	MAGNITUDE	RANGE TIME (SEC)	MAGNITUDE	RANGE TIME (SEC)
Attitude Error	deg	1.3	94.4	1.2	11.3	-1.2	14.5
Angular Rate	deg/s	-0.8	78.9	-0.5	12.7	1.4	15.3
Average Gimbal Angle	deg	-0.6	81.6	0.6	85.5	-0.1	79.2
Angle-of-Attack	deg	-3.3	84.1	2.8	86.9	-	-
Angle-of-Attack Dynamic Pressure Product	deg-N/cm ²	10.81	84.1	8.90	86.9	-	-
Normal Acceleration	m/s ²	0.443	84.2	0.345	85.6	-	-

The normal accelerations observed during the S-IC burn portion of flight are shown in Figure 11-4. The pitch and yaw plane wind velocities and angles-of-attack are shown in Figure 11-5. The winds are shown both as determined from balloon and rocket measurements and as derived from the vehicle Q-ball.

11.4 S-II CONTROL SYSTEM EVALUATION

The S-II stage attitude control system performance was satisfactory. Analysis of the magnitude of modal components in the engine deflection revealed that vehicle structural bending and propellant sloshing had negligible effect on control system performance. The maximum values of pitch control parameters occurred in response to IGM Phase 1 initiation. The maximum values of yaw control parameters occurred at S-II CECO. The maximum values of roll control parameters occurred in response to S-IC/S-II separation disturbances. The response at other times was within expectations, except for a pitch rate of -0.6 deg/s which occurred at the end of the artificial tau guidance mode.

- ▽ BEGIN YAW MANEUVER
- ▽ END YAW MANEUVER
- ▽ BEGIN PITCH AND ROLL MANEUVER
- ▽ END ROLL MANEUVER
- ▽ MACH 1
- ▽ MAX Q
- ▽ S-IC CECO
- ▽ TILT ARREST

—— MEASURED
 - - - - SIMULATED

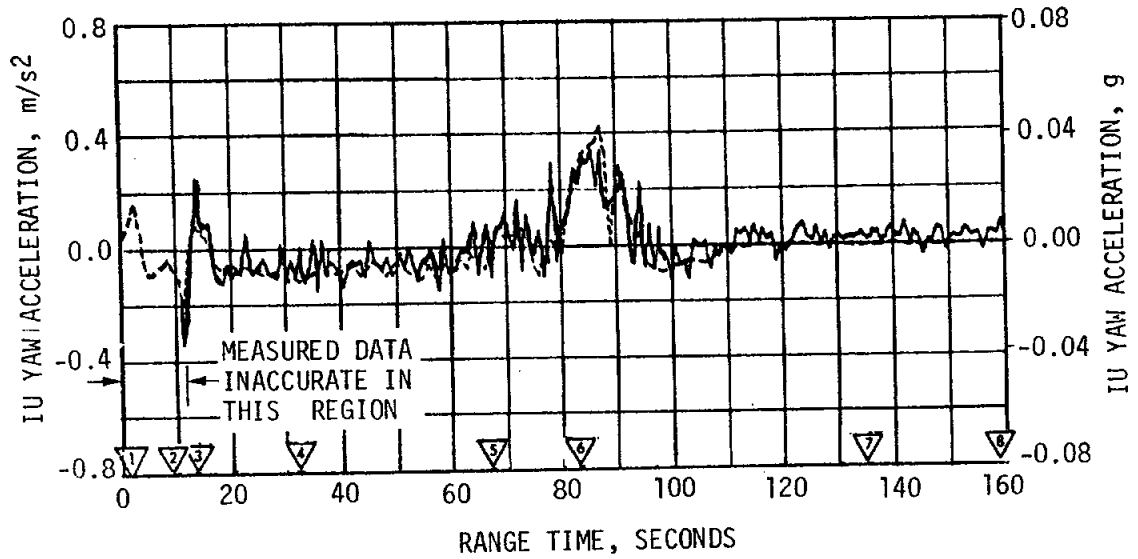
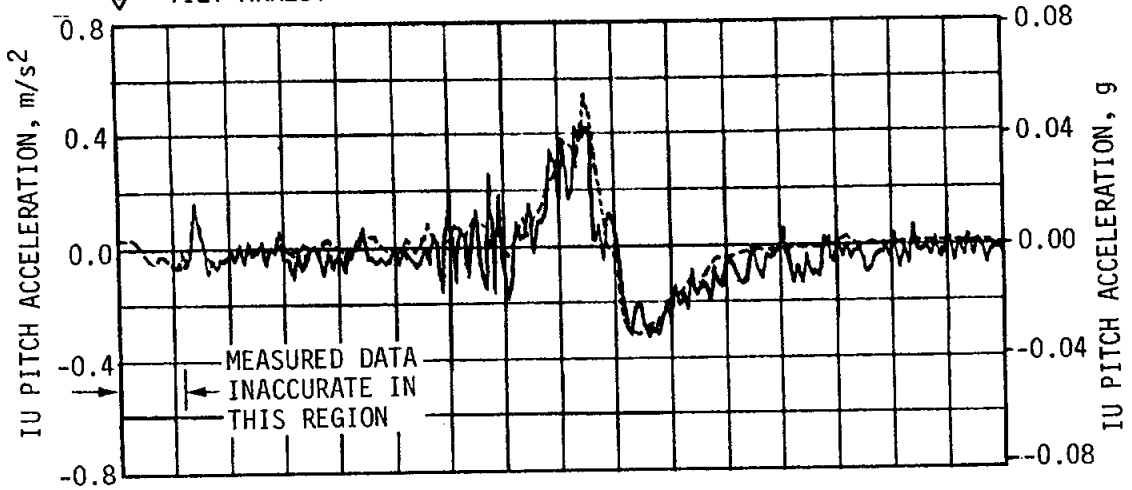


Figure 11-4. Normal Acceleration During S-IC Burn

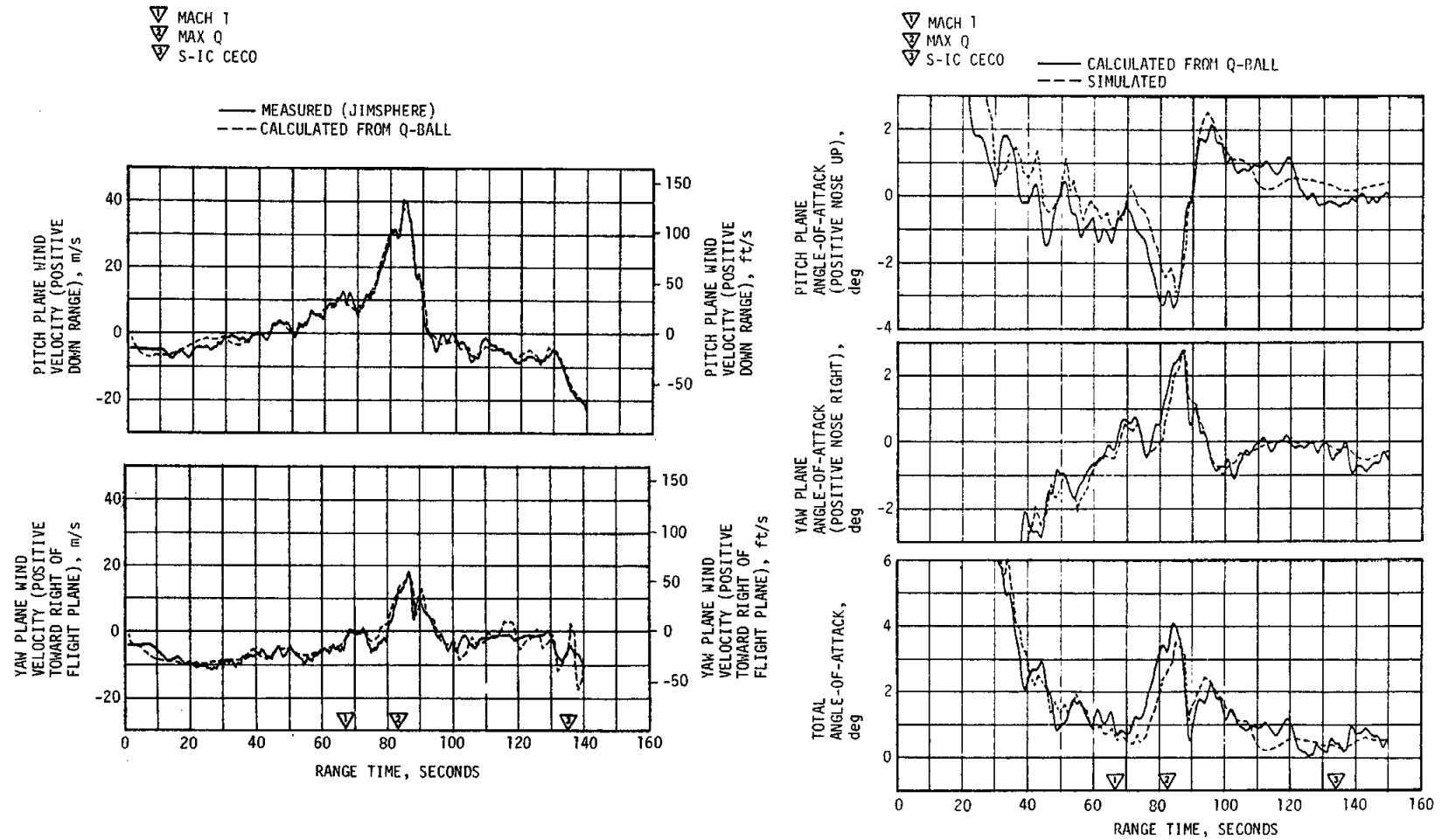


Figure 11-5. Pitch and Yaw Plane Wind Velocity and Free-Stream Angles-of-Attack During S-IC Burn

Table 11-3. Maximum Control Parameters During S-II Boost Flight

PARAMETERS	UNITS	PITCH PLANE		YAW PLANE		ROLL PLANE	
		MAGNITUDE	RANGE TIME (SEC)	MAGNITUDE	RANGE TIME (SEC)	MAGNITUDE	RANGE TIME (SEC)
Attitude Error	deg	-2.1	207.6	-0.5	464.5	-1.1	165.5
Angular Rate	deg/s	1.2	208.5	-0.25	207.5	1.1	166.5
Average Gimbal Angle	deg	-0.9	215.1	-0.3	464.4	0.2	167.1

The maximum control parameter values for the period of S-II burn are shown in Table 11-3. Between the events of S-IC OECO and initiation of IGM, these commands were held constant. Significant events occurring during that interval were S-IC/S-II separation, S-II stage J-2 engine start, second plane separation, and Launch Escape Tower (LET) jettison. The attitude control dynamics throughout this interval indicated stable operation, as shown in Figures 11-6, 11-7, and 11-8. Steady state attitudes were achieved within 20 seconds from S-IC/S-II separation. The maximum control excursions following S-IC/S-II separation occurred in the roll axis.

At IGM initiation the FCC received TVC commands to pitch the vehicle up. During IGM, the vehicle pitched down at a constant commanded rate of approximately -0.1 deg/s. The transient magnitudes experienced at IGM initiation were similar to those on AS-504.

A steady state yaw attitude error of approximately -0.04 degree occurred following S-II engine start. At S-II CECO an additional steady state yaw attitude error of -0.2 degree appeared. Peak transient after CECO was -0.5 degree and occurred at 465 seconds. This yaw error occurred in response to the loss of the compliance deflection of the center engine cutoff. The center engine was not precanted to allow for compliance deflection. This compliance effect occurred in the yaw plane because of the location of the fixed links. Consequently, the outboard engines were deflected in yaw after CECO to compensate for the yaw attitude error and to stabilize the vehicle. The deflections of the outboard engines in pitch after CECO occurred later and were a result of a pitch up guidance command. This command was generated to compensate for the effect on the trajectory due to loss of center engine thrust.

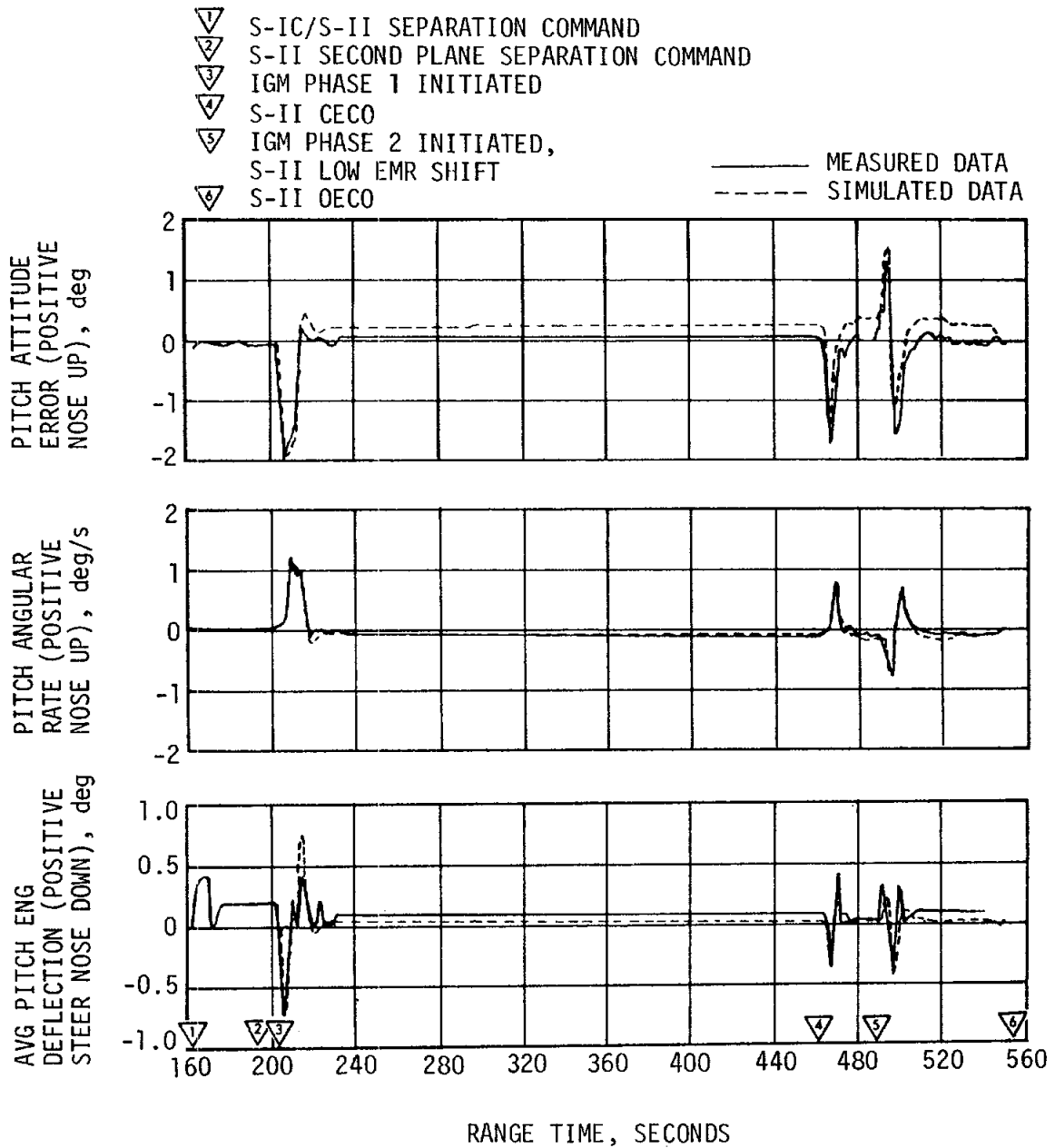


Figure 11-6. Pitch Plane Dynamics During S-II Burn

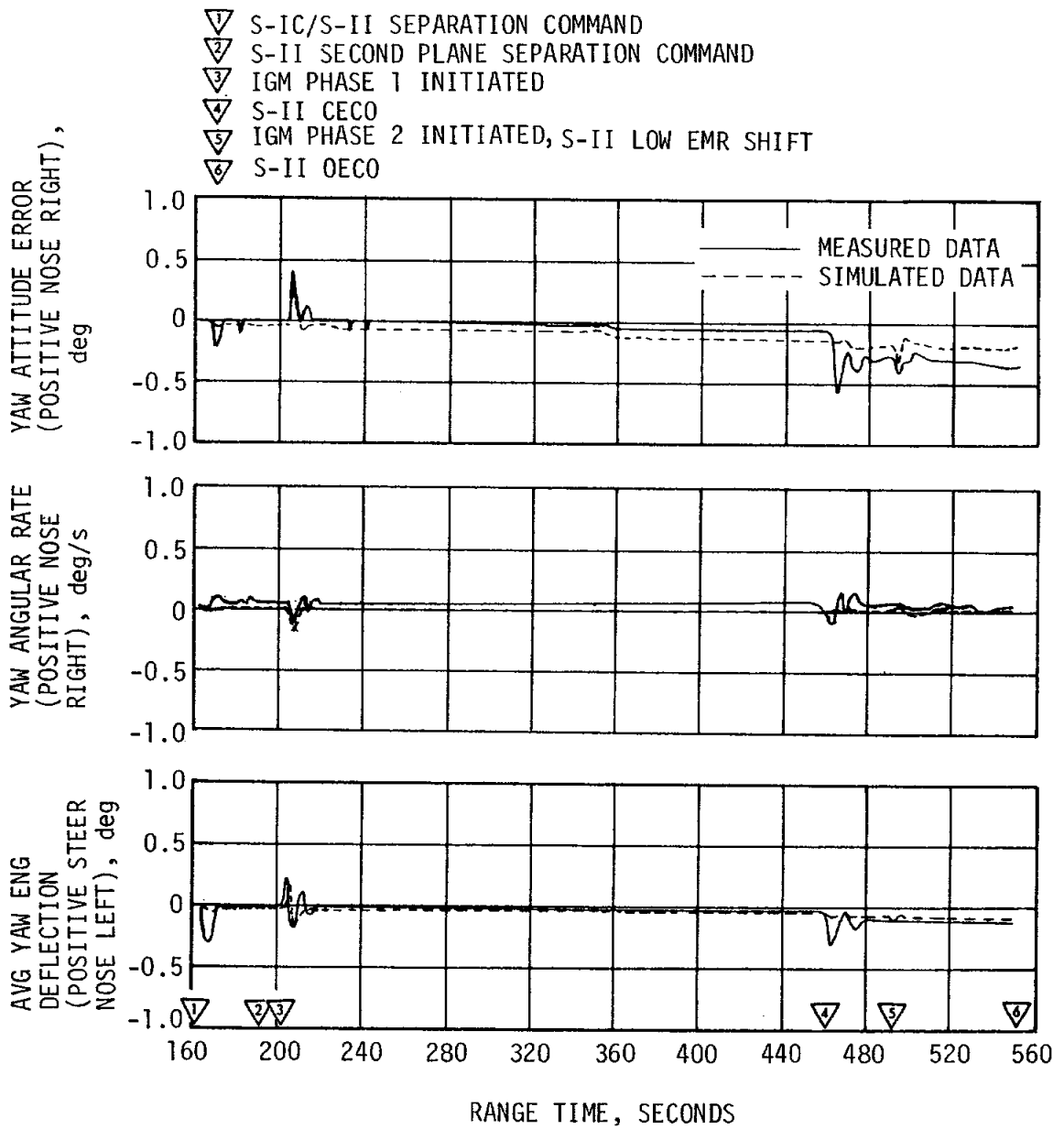


Figure 11-7. Yaw Plane Dynamics During S-II Burn

▽ S-IC/S-II SEPARATION COMMAND
 ▽ S-II SECOND PLANE SEPARATION COMMAND
 ▽ IGM PHASE 1 INITIATED
 ▽ S-II CECO

▽ IGM PHASE 2 INITIATED,
 S-II LOW EMR SHIFT
 ▽ S-II OECO

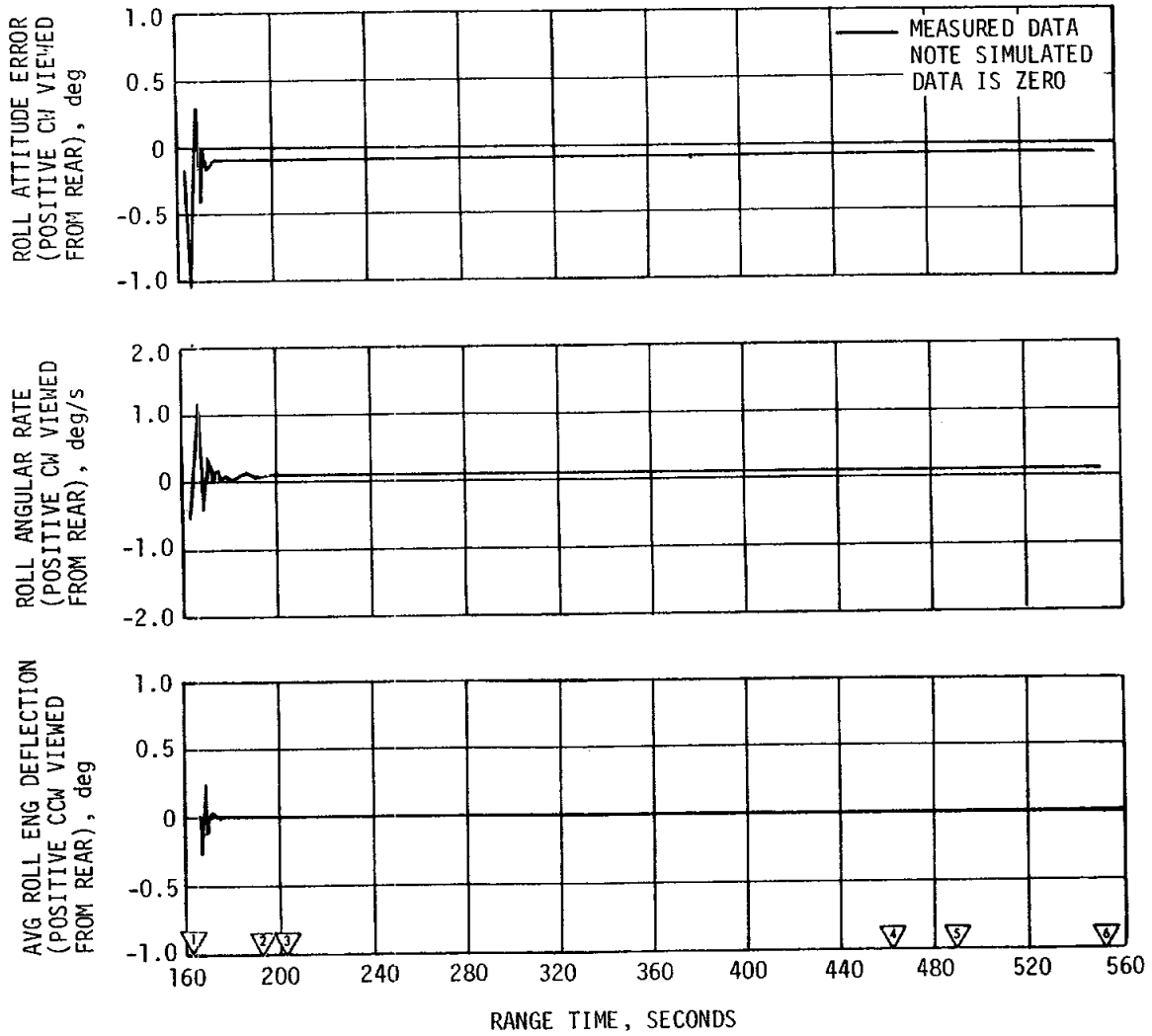


Figure 11-8. Roll Plane Dynamics During S-II Burn

Simulated and flight data are compared in Figures 11-6, 11-7, and 11-8. The major differences were as follows: steady state yaw attitude error caused by early CECO, which reflects a lower compliance than predicted for the center engine; initial transients in the roll axis, which could be attributed to uncertainties in thrust buildup of the J-2 engines; and steady state attitude errors, which were caused by engine location misalignments and thrust vector misalignments.

11.5 S-IVB CONTROL SYSTEM EVALUATION

The S-IVB TVC system provided satisfactory pitch and yaw control during powered flight. The APS provided satisfactory roll control during first and second burns.

During S-IVB first and second burns, control system transients were experienced at S-II/S-IVB separation, guidance initiation, Engine Mixture Ratio (EMR) shift, chi freeze, and J-2 engine cutoff. These transients were expected and were well within the capabilities of the control system.

11.5.1 Control System Evaluation During First Burn

The S-IVB first burn attitude control system response to guidance commands for pitch, yaw, and roll are presented in Figures 11-9, 11-10, and 11-11, respectively. The maximum attitude errors and rates occurred at IGM initiation. A summary of the maximum values of critical flight control parameters during first burn is presented in Table 11-4.

The pitch and yaw effective thrust vector misalignments during first burn were +0.33 and -0.38 degree, respectively. A steady state roll torque of 14.1 N-m (10.4 lbf-ft), clockwise looking forward, required roll APS firings during first burn. The steady state roll torque experienced on previous flights has ranged between 27 N-m (20 lbf-ft) counterclockwise and 54 N-m (40 lbf-ft) clockwise.

11.5.2 Control System Evaluation During Parking Orbit

The coast attitude control system provided satisfactory orientation and stabilization of the S-IVB/CSM in the parking orbit. APS engines I_p and III_{IV} responded on an average of one pulse every 40 seconds during steady-state operation of the LH₂ Continuous Vent System (CVS), which indicates that the CVS-induced moments were nose up, nose left, and clockwise (assuming fin position I down and posigrade orientation). APS engine I_p responded an average of one pulse every 4 seconds during O₂/H₂ burner operation, which indicates that the induced moment was nose up. Pitch attitude control during parking orbit is shown in Figure 11-12. The data of the figure show only the first 2600 seconds of parking orbit since there were no significant perturbations beyond that point.

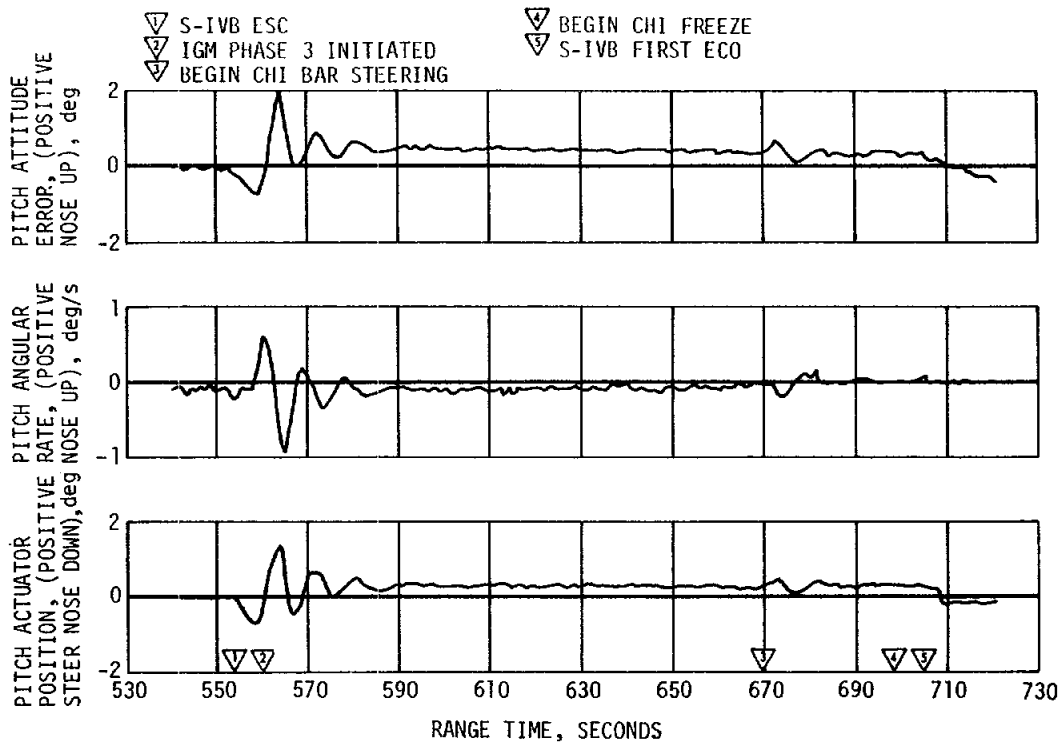


Figure 11-9. Pitch Attitude Control During S-IVB First Burn

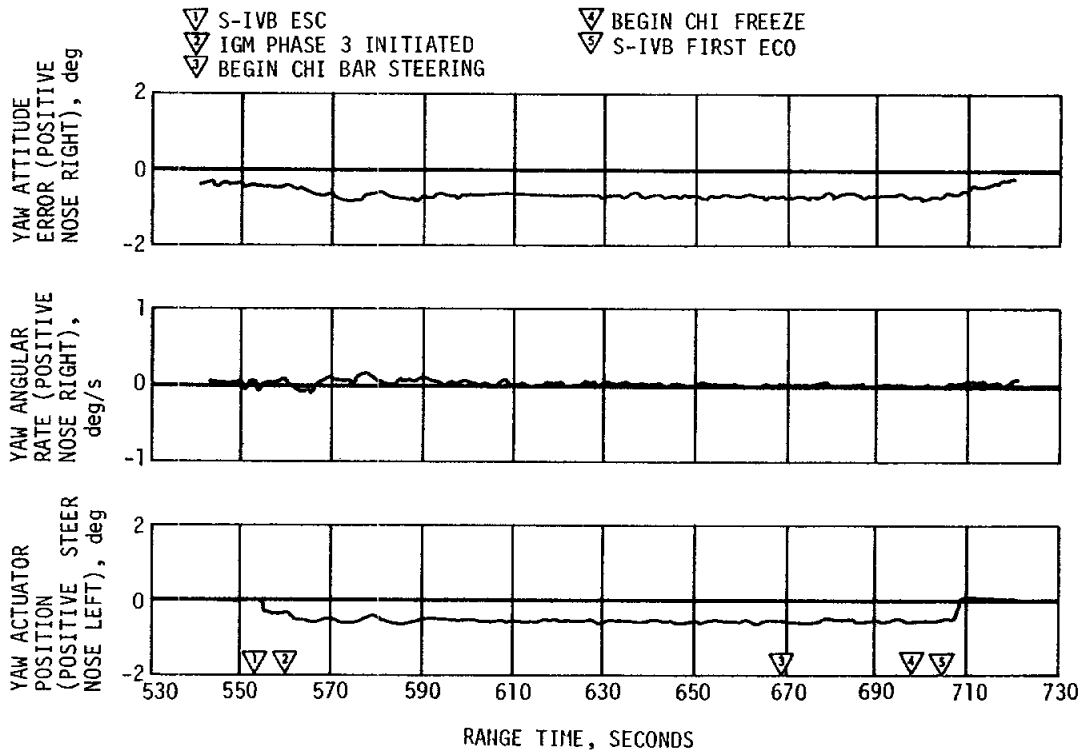


Figure 11-10. Yaw Attitude Control During S-IVB First Burn

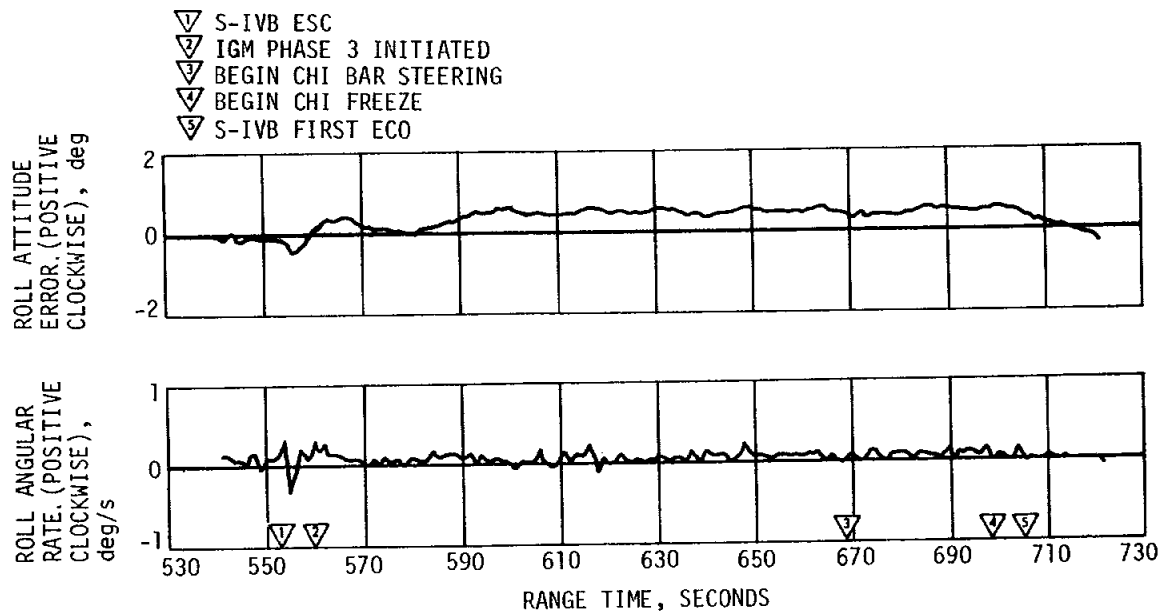


Figure 11-11. Roll Attitude Control During S-IVB First Burn

Table 11-4. Maximum Control Parameters During S-IVB First Burn

PARAMETERS	UNITS	PITCH PLANE		YAW PLANE		ROLL PLANE	
		MAGNITUDE	RANGE TIME (SEC)	MAGNITUDE	RANGE TIME (SEC)	MAGNITUDE	RANGE TIME (SEC)
Attitude Error	deg	+2.0	563.5	-0.8	573.0	0.6	600.0
Angular Rate	deg/s	-0.9	565.1	-0.2	562.4	-0.6	554.5
Average Gimbal Angle	deg	1.4	563.2	-0.6	573.7	---	---

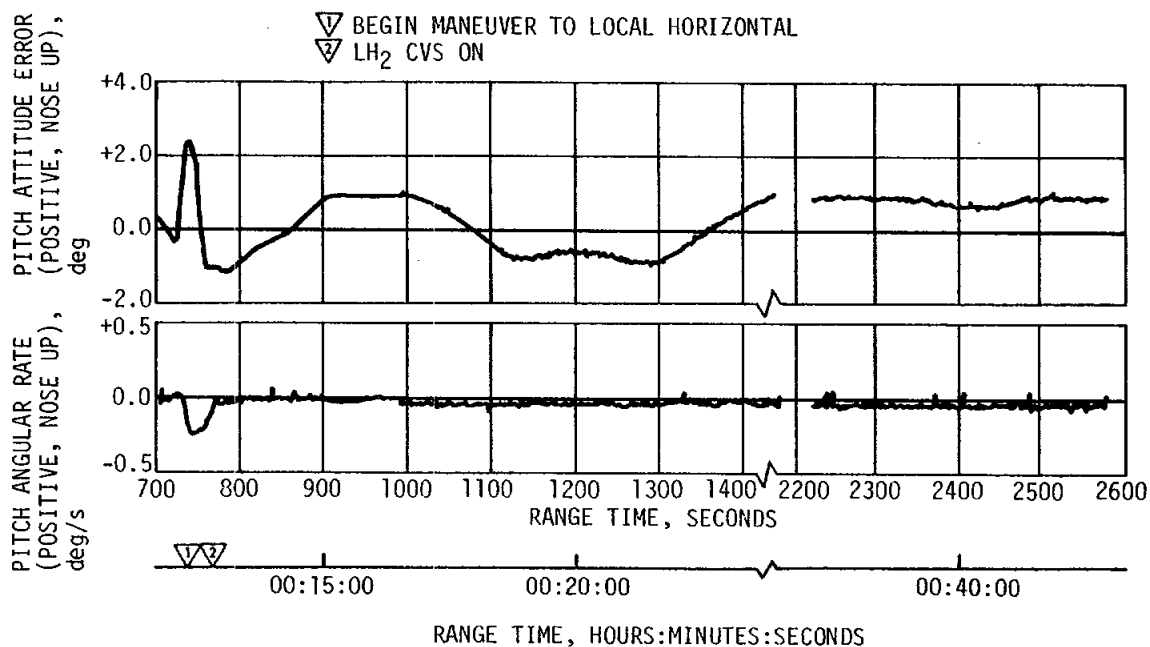


Figure 11-12. Pitch Attitude Control During Parking Orbit

11.5.3 Control System Evaluation During Second Burn

The S-IVB second burn attitude control system response to guidance commands for pitch, yaw, and roll are presented in Figures 11-13, 11-14, and 11-15, respectively. The significant events are indicated in each figure. The maximum attitude errors and rates occurred at IGM initiation and EMR shift. A summary of the maximum values of critical flight control parameters during second burn is presented in Table 11-5.

The maximum pitch and yaw effective thrust vector misalignments during second burn were +0.57 and -0.45 degree, respectively. The steady state roll torque during second burn was 16.8 N-m (12.4 lbf-ft) clockwise.

The pitch actuator trim position changed distinctly at EMR shift and at chi bar guidance mode initiation. The trim position change was approximately 0.1 degree in the retract direction following EMR shift and 0.1 degree in the extend direction at chi bar. No change in yaw actuator trim position was evident at either of these times.

The pitch trim position change at EMR shift has been observed on previous flights and is attributed to compression in the area of the gimbal due to the increased thrust. This compression requires the actuator to shorten to return the thrust vector to its original position. The trim position change at chi bar is attributed to a sudden change in thrust vector misalignment since there was no thrust change at this point.

Table 11-5. Maximum Control Parameters During S-IVB Second Burn

PARAMETERS	UNITS	PITCH PLANE		YAW PLANE		ROLL PLANE	
		MAGNITUDE	RANGE TIME (SEC)	MAGNITUDE	RANGE TIME (SEC)	MAGNITUDE	RANGE TIME (SEC)
Attitude Error	deg	2.2	9219.5	-1.7	9343.0	-0.9	9244.0
Angular Rate	deg/s	-1.3	9220.2	0.6	9344.5	0.2	9347.0
Average Gimbal Angle	deg	1.3	9219.0	-1.0	9343.5	----	----

11.5.4 Control System Evaluation after S-IVB Second Burn

The coast attitude control system provided satisfactory orientation and stabilization of the S-IVB/CSM after S-IVB second burn. APS engines IIIp and IIIv fired in response to induced moments from the LH₂ CVS. The difference in the polarity of the induced moment in the pitch plane can be attributed to a normal change in the location of the engine CG. The LH₂ CVS operation was terminated at approximately 10,451 seconds; therefore, there was minimal operation of APS subsequent to the TD&E maneuver. The S-IVB was controlled during S-IVB/CSM separation, docking, and ejection. Pitch attitude control after S-IVB second burn is shown in Figure 11-16.

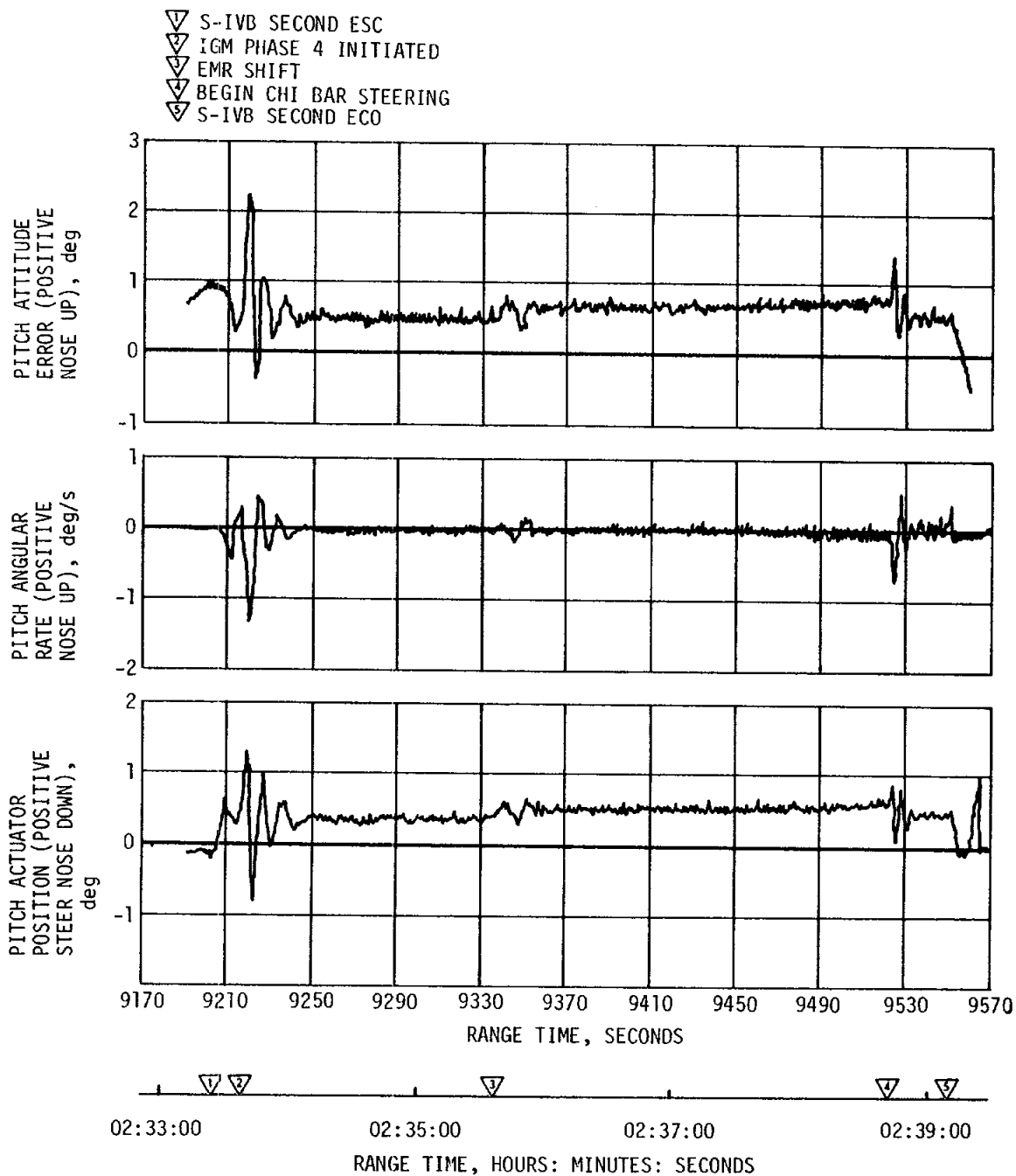


Figure 11-13. Pitch Attitude Control During S-IVB Second Burn

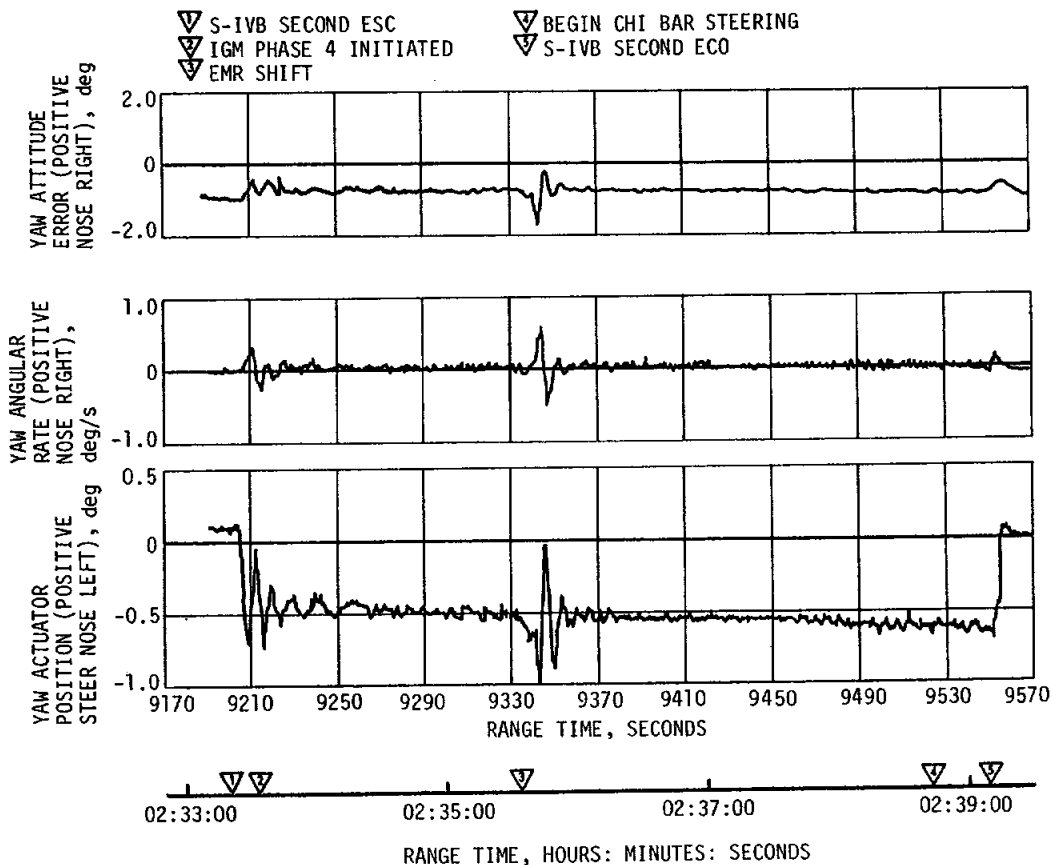


Figure 11-14. Yaw Attitude Control During S-IVB Second Burn

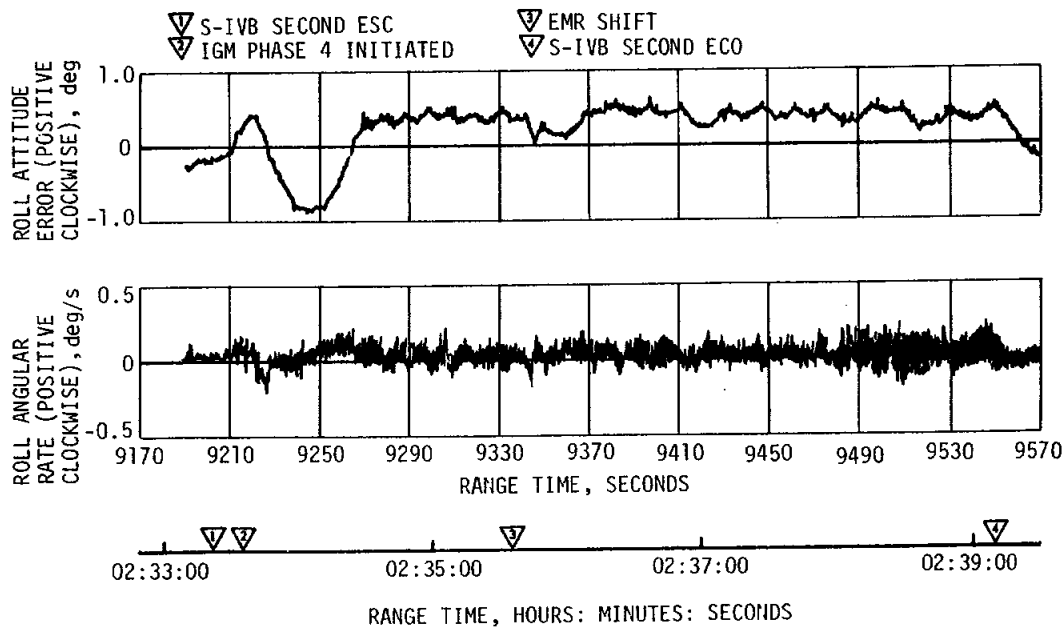


Figure 11-15. Roll Attitude Control During S-IVB Second Burn

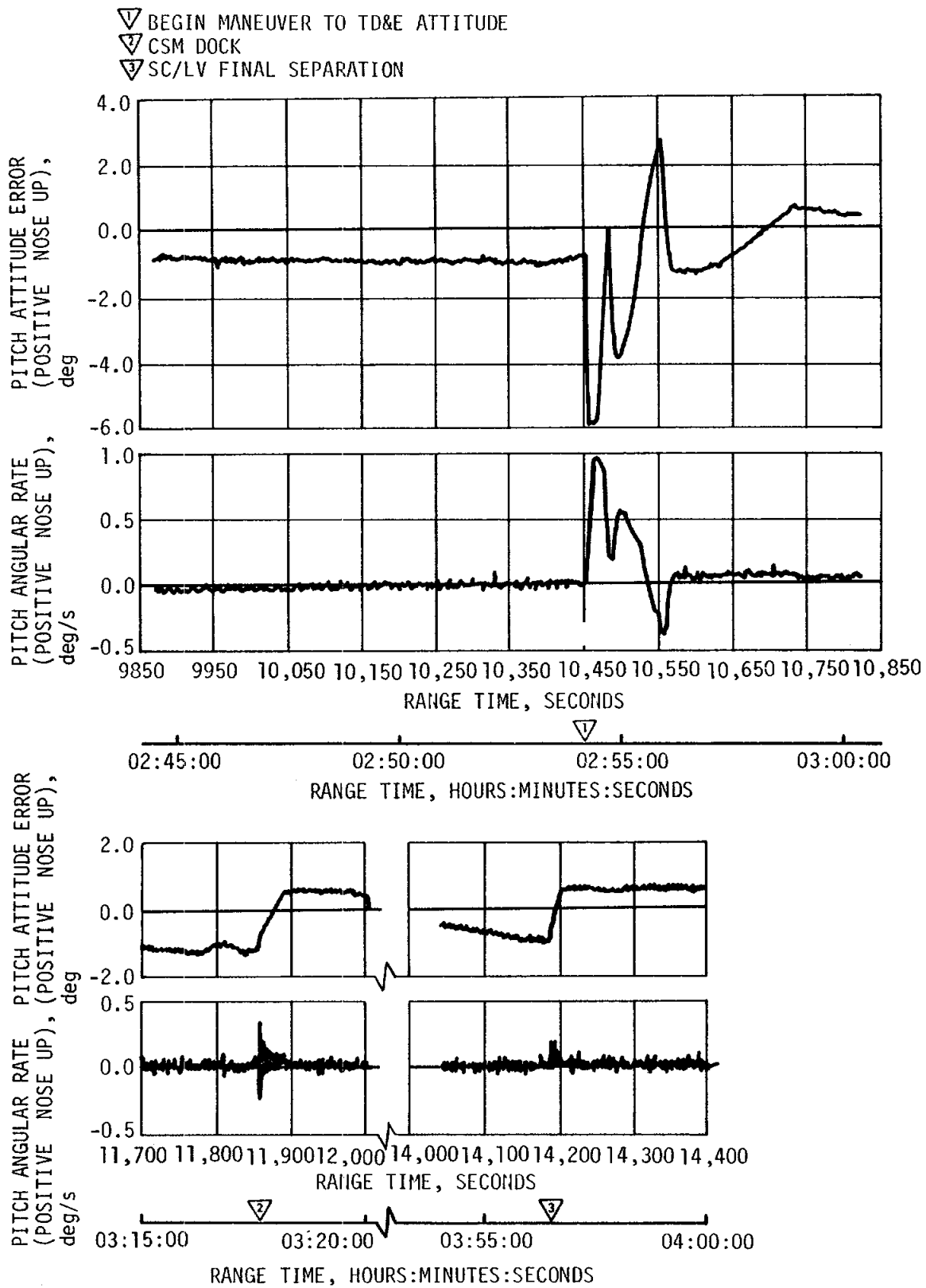


Figure 11-16. Pitch Attitude Control After S-IVB Second Burn

SECTION 12

SEPARATION

12.1 SUMMARY

S-IC/S-II first plane separation was satisfactory. The S-IC retro motors performed as expected. S-II second plane separation was satisfactory. S-II/S-IVB separation was nominal. The S-II retro motors and S-IVB ullage motors performed as expected.

Command and Service Module (CSM) separation from the Launch Vehicle (LV) occurred as predicted during translunar coast. The Transposition, Docking, and Ejection (TD&E) maneuver occurred as expected. Attitude control of the LV was maintained during each separation sequence.

12.2 S-IC/S-II SEPARATION EVALUATION

12.2.1 S-IC Retro Motor Performance

The S-IC retro motors performed as expected and provided for a successful separation of the S-IC and S-II stages. The telemetered chamber pressure data were high as on previous flights. The data, when biased according to previous analyses, showed a slightly lower than nominal chamber pressure.

12.2.2 S-II Ullage Motor Performance

The S-II ullage motors performed as predicted providing satisfactory propellant seating for S-II engine start.

12.2.3 S-IC/S-II Stage Separation

S-IC/S-II separation and associated sequencing were accomplished as planned. Dynamic conditions at separation were well within staging limits. Longitudinal oscillations were observed after separation, as they were on AS-504. No problems were caused by the oscillations.

12.3 S-II SECOND PLANE SEPARATION EVALUATION

S-II second plane separation occurred as predicted. There were no observable vehicle dynamics caused by second plane separation.

12.4 S-II/S-IVB SEPARATION EVALUATION

12.4.1 S-II Retro Motor Performance

The S-II retro motors performed satisfactorily and provided a nominal S-II/S-IVB separation.

12.4.2 S-IVB Ullage Motor Performance

The S-IVB ullage motor performance was as expected during staging, maintaining propellant seating for engine start.

12.4.3 S-II/S-IVB Separation Dynamics

S-II/S-IVB separation and associated sequencing were accomplished as planned. Dynamic conditions at separation were well within staging limits. The separation conditions were very similar to those observed on previous flights.

12.5 S-IVB/IU/LM/CSM SEPARATION EVALUATION

The separation of the CSM from the launch vehicle was accomplished as planned. There were no large control disturbances noted during the separation.

12.6 LUNAR MODULE DOCKING AND EJECTION EVALUATION

The attitude of the LV was adequately maintained during the docking of the CSM with the Lunar Module (LM). The LM was then successfully ejected from the LV by the CSM. There were no significant control disturbances during the ejection.

SECTION 13
ELECTRICAL NETWORKS

13.1 SUMMARY

The AS-505 launch vehicle electrical systems performed satisfactorily throughout all phases of flight. Operation of the batteries, power supplies, inverters, Exploding Bridge Wire (EBW) firing units, switch selectors and interconnecting cabling was normal.

13.2 S-IC STAGE ELECTRICAL SYSTEM

Both Battery No. 1 (Operational) and Battery No. 2 (Instrumentation) voltages remained within performance limits of 26.5 to 32 vdc during powered flight. Battery currents were near predicted and below the maximum limits of 64 amperes for Battery No. 1 and 125 amperes for Battery No. 2. Battery power consumption was well within the rated capacities of 640 and 1250 ampere-minutes for Batteries No. 1 and No. 2, respectively, as shown in Table 13-1. Electrical shorts were experienced on bus 1D20 (Battery No. 2) from 170 to 173 seconds and 183 to 199 seconds. Current drain from the battery was not excessive and had no effect on tape recorder playback. Similar shorts have been experienced after separation on AS-501 and AS-502.

Table 13-1. S-IC Stage Battery Power Consumption

BATTERY	BUS DESIGNATION	RATED CAPACITY (AMP-MIN)	POWER CONSUMPTION*	
			AMP-MIN	PERCENT OF CAPACITY
Operational No. 1	1D10	640	27.3	4.3
Instrumentation No. 2	1D20	1250	303.3	24.3

*Operational battery power consumption was calculated from power transfer until S-IC/S-II separation.

Instrumentation battery power consumption was calculated from power transfer through 7 seconds of tape recorder playback.

The seven measuring power supplies remained within the 5 ± 0.05 vdc limit during powered flight.

All switch selector channels functioned correctly and all outputs were issued within their required time limits in response to commands from the IU.

The separation and retromotor EBW firing units were armed and triggered as programmed. Charging times and voltages were within the requirements of 1.5 seconds for maximum allowable charging time and 4.2 ± 0.4 volts for the allowable voltage level.

The command destruct EBW firing units were in the required state of readiness if needed.

13.3 S-II STAGE ELECTRICAL SYSTEM

All battery bus voltages remained within specified limits throughout the prelaunch and flight periods and bus currents remained within required and predicted limits. Main bus current averaged 38 amperes during S-IC boost and varied from 50 to 55 amperes during S-II boost. Instrumentation bus current varied from 52 to 55 amperes during S-IC and S-II boost. Recirculation bus current averaged 95 amperes during S-IC boost and ignition bus current averaged 30 amperes during the S-II ignition sequence. Battery power consumption was well within the rated capacities of the batteries as shown in Table 13-2.

Table 13-2. S-II Stage Battery Power Consumption

BATTERY	BUS DESIGNATION	RATED CAPACITY (AMP-HR)	POWER CONSUMPTION*		TEMPERATURE	
			AMP-HR	PERCENT OF CAPACITY	MAX	MIN
Main	2D11	35	7.86	22.5	311.5°K (101°F)	305.9°K (91°F)
Instrumentation	2D21	35	12.1	34.6	312.0°K (102°F)	304.8°K (89°F)
Recirculation No. 1	2D51	30	5.59	18.6	304.0°K (87.5°F)	300.9°K (82.0°F)
Recirculation No. 2	2D51 and 2D61	30	5.63	18.8	303.1°K (86°F)	299.5°K (79.5°F)

*Power consumption calculated from -50 seconds.

The fifteen temperature bridge power supplies and five 5-vdc instrumentation power supplies all performed within acceptable limits. The five LH₂ recirculation inverters which furnish power to the recirculation pumps operated properly throughout the J-2 engine chilldown period.

All switch selector channels functioned correctly and all outputs were issued within their required time limits in response to commands from the IU. Performance of the EBW circuitry for the separation system was satisfactory. Firing units charge and discharge responses were within predicted time and voltage limits. The command destruct EBW firing units were in the required state of readiness if needed.

13.4 S-IVB STAGE ELECTRICAL SYSTEM

The three 28-vdc and one 56-vdc battery voltages, currents and temperatures stayed well within acceptable limits as shown in Figures 13-1 through 13-4. Electrical performance was not affected by the anomaly reported in paragraph 8.7 since Aft Battery No. 2 responded properly to the load demand placed on it. Battery temperatures remained below the 322°K (120°F) limits during the powered portions of flight (this limit does not apply after insertion into orbit). The highest temperature of 316.5°K (110°F) was reached on Aft Battery No. 2, Unit 1, after S-IVB first burn cutoff. Battery power consumption is shown in Table 13-3.

All switch selector channels functioned correctly and all outputs were issued within their required time limits in response to commands from the IU.

The three 5-vdc and nine 20-vdc excitation modules all performed within acceptable limits. The LOX and LH₂ chilldown inverters which furnish power to the LOX and LH₂ recirculation pumps performed in a satisfactory manner and met their load requirements.

Table 13-3. S-IVB Stage Battery Power Consumption

BATTERY	RATED CAPACITY (AMP-HRS)*	POWER CONSUMPTION**	
		AMP-HRS	PERCENT OF CAPACITY
Forward No. 1	300.0	150.24	50.1
Forward No. 2	24.75	28.47	115.0
Aft. No. 1	300.0	84.37	28.1
Aft. No. 2	75.0	39.72	53.0

*Rated capacities are minimum guaranteed by vendor.
 **Actual usage for 29,000 seconds (08:03:20) based on flight data.
 Stage design lifetime is nominally 6 hours 30 minutes.

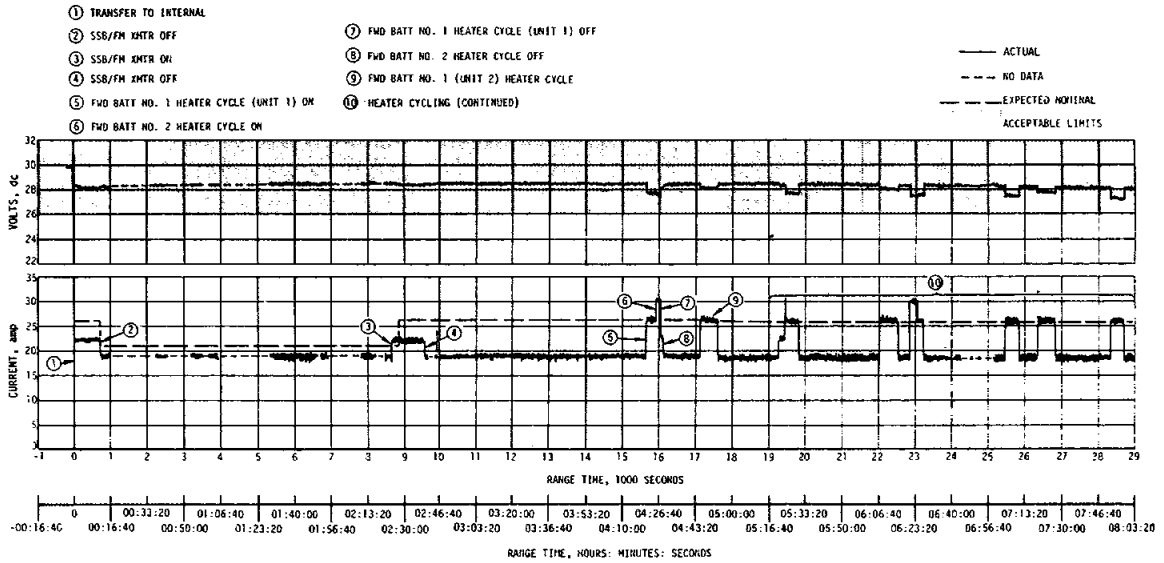


Figure 13-1. S-IVB Stage Forward Battery No. 1 Voltage and Current

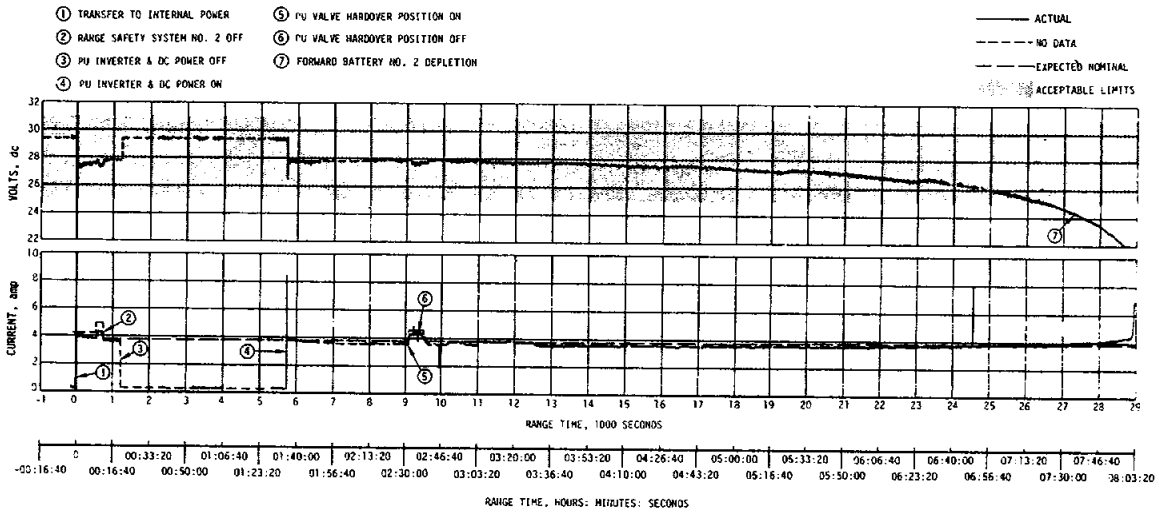


Figure 13-2. S-IVB Stage Forward Battery No. 2 Voltage and Current

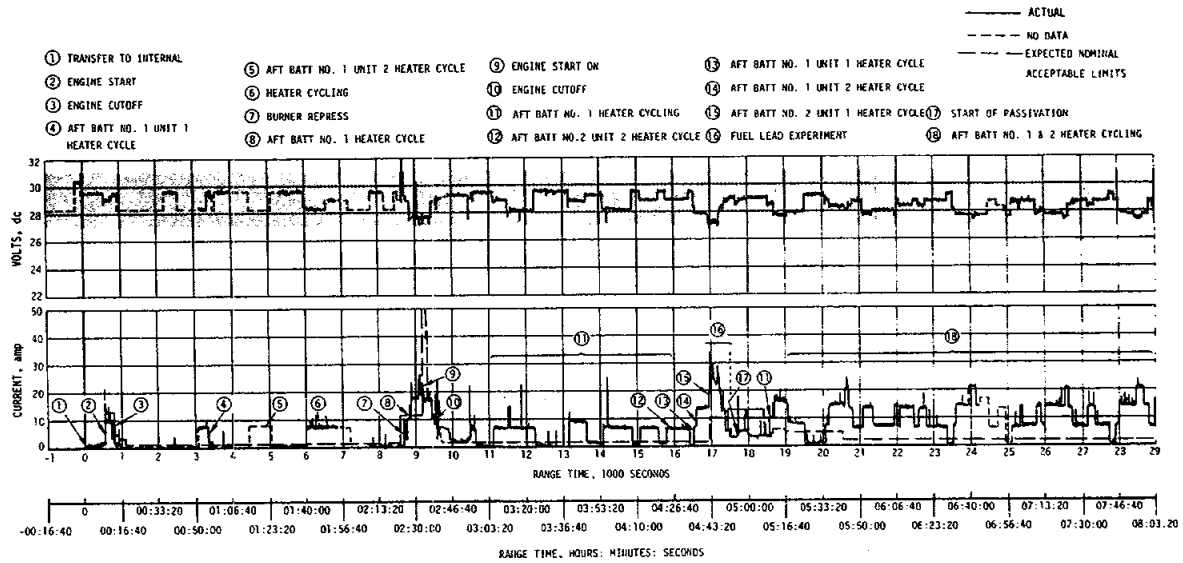


Figure 13-3. S-IVB Stage Aft Battery No. 1 Voltage and Current

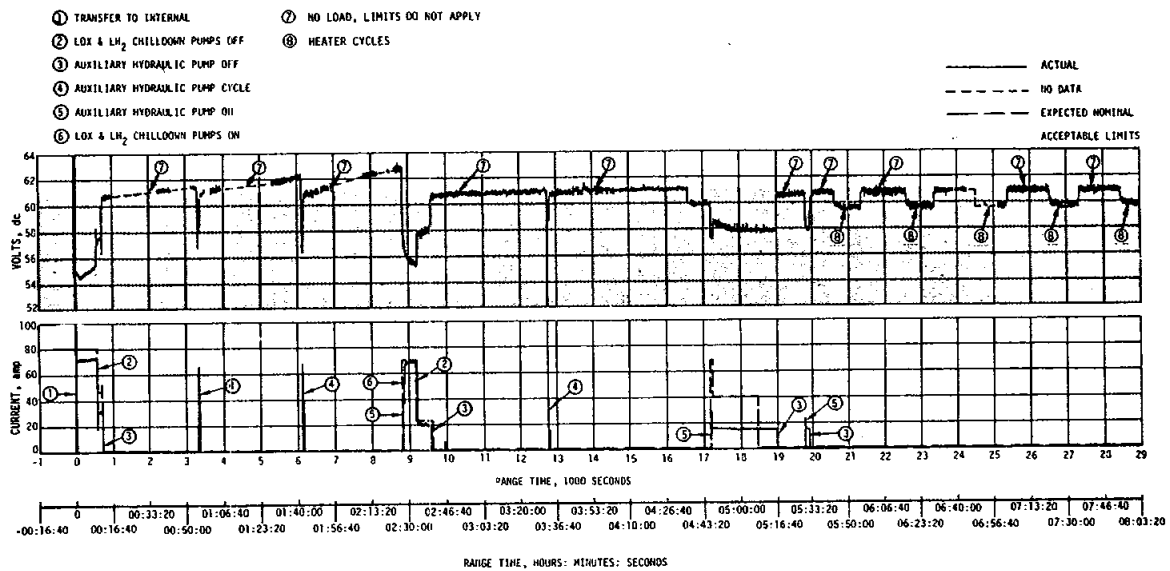


Figure 13-4. S-IVB Stage Aft Battery No. 2 Voltage and Current

Performance of the EBW circuitry for the separation system was satisfactory. Firing units charge and discharge responses were within predicted time and voltage limits. The command destruct EBW firing units were in the required state of readiness if needed.

13.5 INSTRUMENT UNIT ELECTRICAL SYSTEM

Voltages on all three batteries showed a gradual rise as the flight progressed. This voltage increase is expected as battery temperatures increase. All battery voltages remained within normal limits. Battery currents remained normal during launch and coast periods of flight. The expected peaks in battery currents were observed during launch with average currents near predicted levels. The 6D40 battery, which had the highest average current drain, experienced the greatest temperature increase to 340.0°K (152.3°F). Battery temperature, however, remained within normal limits. Battery power consumption and estimated depletion times are shown in Table 13-4. Battery voltages, currents and temperatures are shown in Figures 13-5 through 13-7.

The 56 volt power supply maintained an output voltage 55.6 to 56.6 vdc, well within the required tolerance of 56 \pm 2.5 vdc.

The 5-volt measuring power supply performed nominally, maintaining a constant voltage within specified tolerances.

Voting circuits in the Emergency Detection System (EDS) Distributor all performed nominally. There is no evidence to indicate deviations in the other distributors or network cabling.

No forced reset commands were issued to the switch selector indicating that all commands to the switch selector were received properly and no complement commands were necessary.

Table 13-4. IU Battery Power Consumption

BATTERY	RATED CAPACITY (AMP-HRS)	POWER CONSUMPTION*		ESTIMATED* LIFE TIME (HOURS)
		AMP-HRS	PERCENT OF CAPACITY	
6D10	350	225.8	64.5	16.4
6D30	350	219.4	62.7	16.9
6D40	350	350.9	100.3	>10.6**
*Based on 10.6 hours of available flight data. **CCS loss reported at 11.2 hours.				

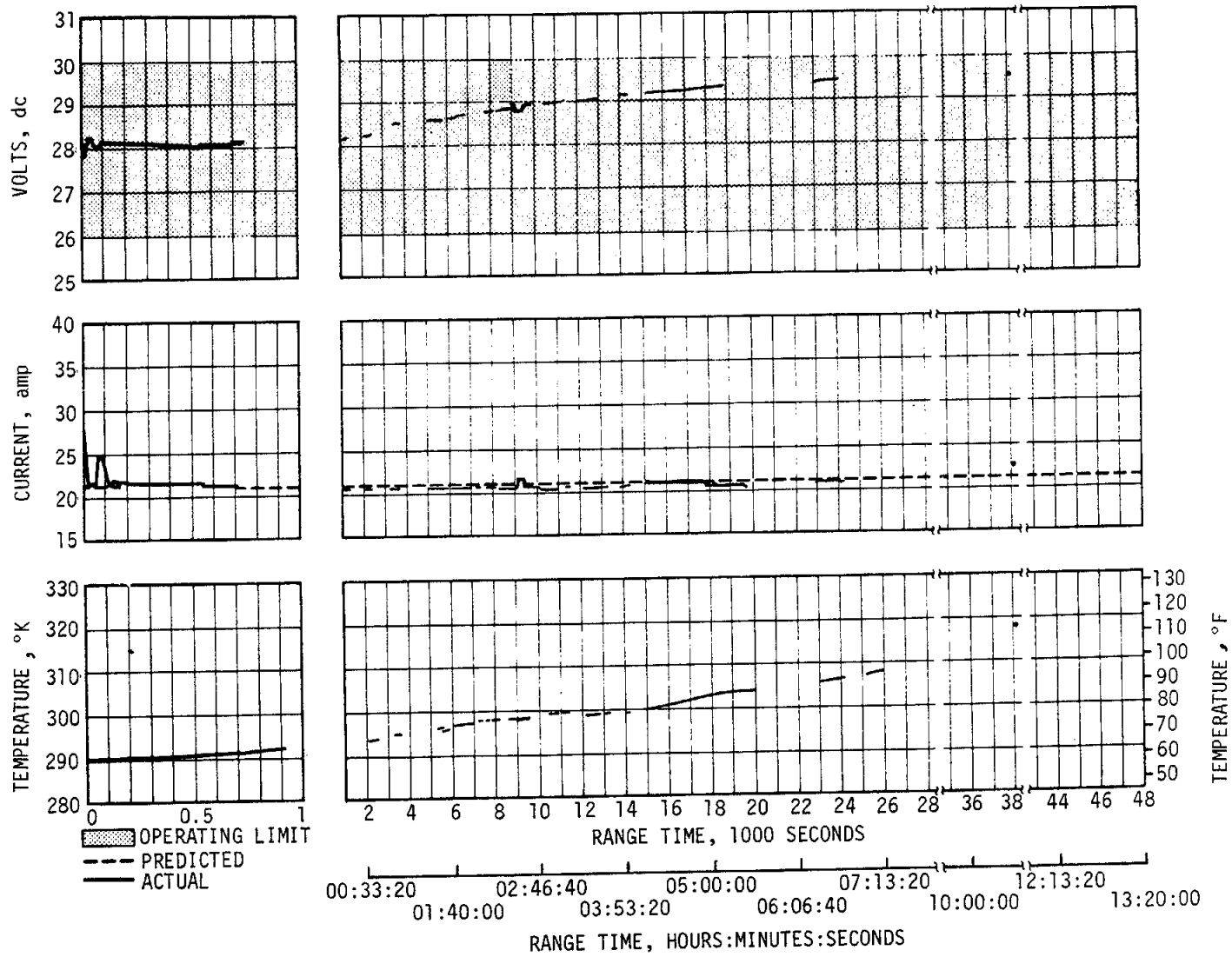


Figure 13-5. Battery 6D10 Voltage, Current and Temperature

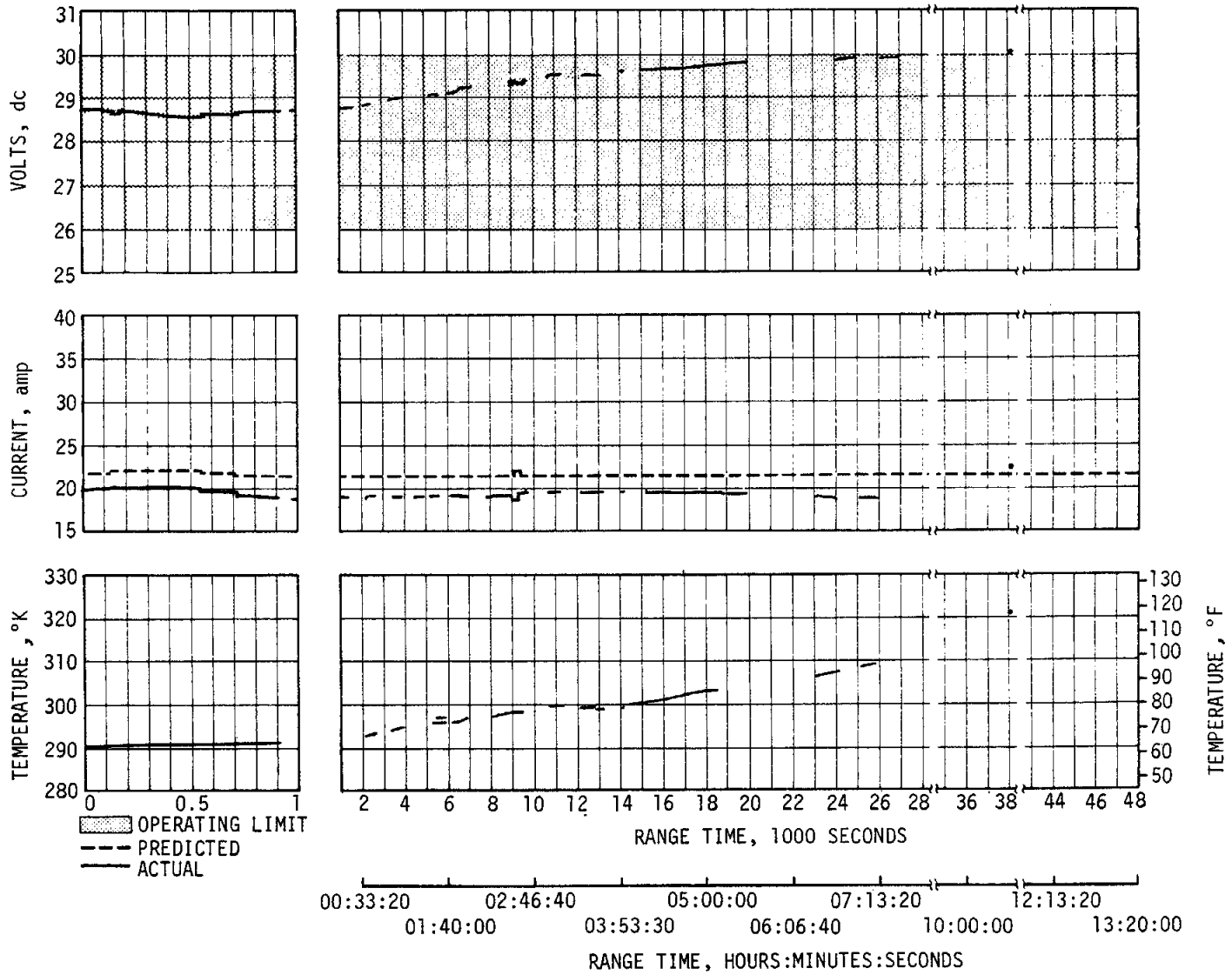


Figure 13-6. Battery 6D30 Voltage, Current and Temperature

13-9/13-10

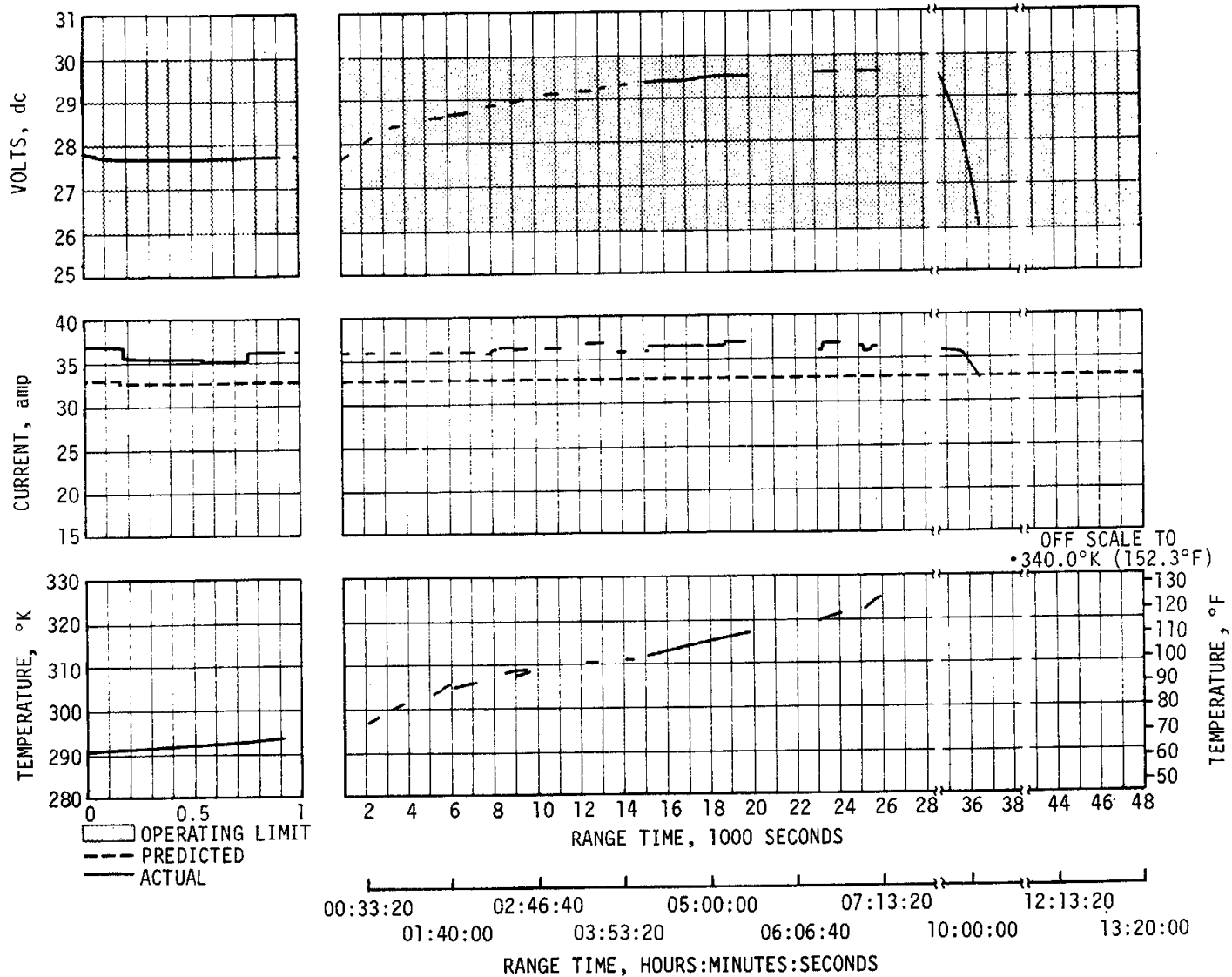


Figure 13-7. Battery 6D40 Voltage, Current and Temperature

SECTION 14

RANGE SAFETY AND COMMAND SYSTEMS

14.1 SUMMARY

Data indicated that the redundant Secure Range Safety Command Systems (SRSCS) on the S-IC, S-II and S-IVB stages were ready to perform their functions properly on command if flight conditions during the launch phase had required vehicle destruct. The system properly safed the S-IVB SRSCS on command transmitted from Bermuda (BDA). The performance of the Command and Communications System (CCS) in the Instrument Unit (IU) was satisfactory, except during the time period from 23,601 seconds (06:33:21) when CCS downlink signal strength dropped sharply until 25,097 seconds (06:58:17), when the antenna was switched to the omni mode. The drop in signal strength is suspected to be a malfunction in the directional antenna system.

14.2 SECURE RANGE SAFETY COMMAND SYSTEMS

Telemetered data indicated that the command antennas, receiver/decoders, exploding bridge wire networks, and destruct controllers on each powered stage functioned properly during flight and were in the required state of readiness if flight conditions during the launch phase had required vehicle destruct. Since no arm/cutoff or destruct commands were required, all data except receiver signal strength remained unchanged during the flight. Power to the system was cut off at 715.3 seconds, by ground command from BDA, thereby deactivating (safing) the system. Both S-IVB stage systems, the only systems in operation at this time, responded properly to the safing command.

Radio Frequency (RF) performance aspects of the system are discussed in paragraph 19.5.3.1.

14.3 COMMAND AND COMMUNICATIONS SYSTEM

The performance of the command section of the CCS was satisfactory. A total of 51 known commands, consisting of 234 command words, were attempted from the ground stations as shown in Table 14-1 with 210 words being accepted by the CCS. Transmission of the 24 words not accepted was attempted either when the command subcarrier was off at the station, or out of lock onboard the vehicle.

Table 14-1. Command and Communications System Commands History, AS-505

RANGE TIME		TRANSMITTING STATION	COMMAND	NUMBER OF WORDS	REMARKS
SECONDS	HRS:MIN:SEC				
9555.0	02:39:15.0	Redstone	Ambient Repress. System Off and Cryo On	4	Not Transmitted
9565.5	02:39:25.5	Redstone	Ambient Repress. System Off and Cryo On	3	Accepted
15,232.7	04:13:52.7	Goldstone	Switch Antenna Low Gain	1	Accepted
16,935.0	04:42:15.0	Goldstone	Enable Time Base 8	1	Accepted
16,952.2	04:42:32.2	Goldstone	LH ₂ Tank Continuous Vent Valve Close On	6	Accepted
16,955.0	04:42:35.0	Goldstone	LH ₂ Tank Continuous Vent Valve Close Off	3	Accepted
17,095.5	04:44:55.5	Goldstone	LH ₂ Tank Repress. Control Valve Open Off	3	Accepted
17,096.8	04:44:56.8	Goldstone	Terminate	1	Accepted
17,097.3	04:44:57.3	Goldstone	LH ₂ Tank Repress. Control Valve Open Off	3	Accepted
17,098.7	04:44:58.7	Goldstone	Ambient Repress. On and Cryo Off	3	Accepted
17,135.3	04:45:35.3	Goldstone	S-IVB Ullage Engine No. 1 On	3	Accepted
17,136.7	04:45:36.7	Goldstone	S-IVB Ullage Engine No. 2 On	3	Accepted
17,152.0	04:45:52.0	Goldstone	LOX Repress. Control Valve Open On	3	Accepted
17,185.3	04:46:25.3	Goldstone	Aux. Hydraulic Pump On	3	Accepted
17,299.0	04:48:19.0	Goldstone	Passivation Enable	3	Accepted
17,299.8	04:48:19.8	Goldstone	Engine He Control Valve Open On	3	Accepted
17,300.6	04:48:20.6	Goldstone	Engine Mainstage Valve Open On	3	Accepted
17,301.4	04:48:21.4	Goldstone	8 Second Lead Dummy Words	31	Accepted, No CRP's
17,309.3	04:48:29.3	Goldstone	Terminate	1	Accepted
17,309.6	04:48:29.6	Goldstone	Engine Mainstage Valve Open Off	3	Accepted
17,310.4	04:48:30.4	Goldstone	Terminate	1	Accepted
17,310.7	04:48:30.7	Goldstone	Prevalves Close On	3	Accepted
17,311.5	04:48:31.5	Goldstone	Engine He Control Valve Open Off	3	Accepted
17,324.0	04:48:44.0	Goldstone	Engine He Control Valve Open On	3	Accepted
17,324.7	04:48:44.7	Goldstone	Dummy Words	42	Accepted, No CRP's
17,335.5	04:48:55.5	Goldstone	Engine He Control Valve Open Off	3	Accepted
17,336.3	04:48:56.3	Goldstone	Passivation Disable	3	Accepted
17,354.3	04:49:14.3	Goldstone	LOX Tank Repress. Control Valve Open Off	3	Accepted
17,355.7	04:49:15.7	Goldstone	LH ₂ Tank Repress. Control Valve Open On	3	Accepted
17,357.2	04:49:17.2	Goldstone	Prevalves Close Off	3	Accepted
17,385.1	04:49:45.1	Goldstone	Ambient Repress. System Mode Selector Off and Cryo On	3	Accepted
17,407.3	04:50:07.3	Goldstone	Passivation Enable	3	Accepted
17,408.7	04:50:08.7	Goldstone	Engine Ignition Phase Control Valve Open On	3	Accepted
17,410.1	04:50:10.1	Goldstone	Engine He Control Valve Open On	9	Accepted
17,414.4	04:50:14.4	Goldstone	S-IVB Ullage Engine No. 1 Off	3	Accepted
17,415.8	04:50:15.8	Goldstone	S-IVB Ullage Engine No. 2 Off	3	Accepted
17,457.7	04:50:57.7	Goldstone	Engine Ignition Phase Control Valve Open Off	3	Accepted
17,459.1	04:50:59.1	Goldstone	Engine He Control Valve Open Off	3	Accepted
17,494.9	04:51:34.9	Goldstone	LH ₂ Continuous Vent Open On	3	Accepted
17,496.3	04:51:36.3	Goldstone	LH ₂ Continuous Vent Relief Override Open On	6	Accepted
17,499.1	04:51:39.1	Goldstone	LH ₂ Continuous Vent Open Off	3	Accepted
17,500.6	04:51:40.6	Goldstone	LH ₂ Continuous Vent Relief Override Open Off	3	Accepted
19,741.7	05:29:01.7	Goldstone	S-IVB Ullage Engine No. 1 Off	3	Accepted
19,743.5	05:29:03.5	Goldstone	S-IVB Ullage Engine No. 2 Off	3	Accepted
19,790.6	05:29:50.6	Goldstone	Aux. Hydraulic Pump On	3	Accepted
19,926.6	05:32:06.6	Goldstone	Aux. Hydraulic Pump Off	3	Accepted
24,051.8	06:40:51.8	Goldstone	Set Antenna High Gain	3*	Accepted
25,096.7	06:58:16.7	Goldstone	Set Antenna Omni	3*	Accepted
35,994.2	09:59:54.2	Goldstone	Set Antenna Low Gain	4	Not Accepted
36,033.2	10:00:33.2	Goldstone	Set Antenna Low Gain	4	Not Accepted
36,426.0	10:07:06.0	Goldstone	Set Antenna Low Gain	4	Not Transmitted
36,502.0	10:08:22.0	Goldstone	Set Antenna Low Gain	4	Not Transmitted
36,671.0	10:11:11.0	Goldstone	Set Antenna Low Gain	4	Not Accepted

*One word is normally required to switch antennas. These commands were repeated due to missed verification pulses at the ground station because of noisy telemetry.

A command attempted at 9555 seconds (02:39:15) from the ship Redstone was not transmitted because two-way lock with the vehicle had not been established and the subcarrier was off. The command was successfully transmitted at 9566 seconds (02:39:26).

Commands to switch the CCS transmitter to the high-gain directional antenna at 24,052 seconds (06:40:52) and to omni antenna at 25,097 seconds (06:58:17) had to be repeated because the station failed to capture the address verification pulses and the computer reset pulses. These pulses were missed because of noisy telemetry data, which was due to the low downlink signal problem discussed in paragraph 19.5.3.2. Signal strength data indicate these commands were accepted on the first transmission.

Commands to switch the CCS transmitter to the low-gain directional antenna after 35,994 seconds (09:59:54) were not received on board because of low signal strength. The low signal strength was caused by the extended range and low vehicle antenna gain at this time. The CCS transponder tracking threshold is approximately 20 decibels better than the command subcarrier threshold. Consequently, although two-way lock was being maintained during part of this time period, 70-kilohertz subcarrier lock was never established.

SECTION 15
EMERGENCY DETECTION SYSTEM

15.1 SUMMARY

The performance of the AS-505 Emergency Detection System (EDS) was normal and no abort limits were exceeded.

15.2 SYSTEM EVALUATION

15.2.1 General Performance

The AS-505 EDS was the same configuration as on AS-504. All launch vehicle EDS parameters remained well within acceptable limits during the AS-505 mission. Sequential events and discrete indications occurred as expected.

15.2.2 Propulsion System Sensors

The operation of all thrust OK sensors, which monitor engine status, was nominal insofar as EDS operation was concerned as was the associated voting logic. S-IVB tank ullage pressure remained within the abort limits, and displays to the crew were nominal.

15.2.3 Flight Dynamics and Control Sensors

None of the triple redundant rate gyros gave any indication of angular overrate in the pitch, yaw, or roll axes. The maximum angular rates experienced are shown in Table 15-1. The switch selector command, which deactivates the overrate automatic abort and changes the rate limit settings, was given at 134.7 seconds.

Table 15-1. Maximum Angular Rates

PHASE	PITCH	YAW	ROLL
Liftoff to 134.7 seconds	0.8 (4) deg/s	0.5 (4) deg/s	1.4 (20) deg/s
134.7 seconds to Spacecraft Separation	1.3 (9.2) deg/s	0.6 (9.2) deg/s	1.1 (20) deg/s
Note: Abort limits are shown in parentheses.			

The maximum angle-of-attack dynamic pressure sensed by a redundant Q-ball mounted atop the launch escape tower was 0.76 N/cm² (1.1 psid) from about 84 to 87 seconds. This was only 34 percent of the EDS abort limit of 2.2 N/cm² (3.2 psid).

15.2.4 EDS Event Times

All EDS related switch selector events and discrete indications occurred as expected and are shown in Tables 15-2 and 15-3 respectively.

Table 15-2. EDS Related Event Times

FUNCTION	STAGE	RANGE TIME, SECONDS	TIME FROM BASE, SECONDS
Start of T ₁	--	0.6	--
Multiple Engine Cutoff Enable	S-IC	14.5	T ₁ +14.0
Launch Vehicle Engines EDS Cutoff Enable	IU	30.5	T ₁ +30.0
S-IC Two Engines Out Auto-Abort Inhibit Enable	IU	134.2	T ₁ +133.6
S-IC Two Engines Out Auto-Abort Inhibit	IU	134.3	T ₁ +133.8
Excess Rate (P,Y,R) Auto-Abort Inhibit Enable	IU	134.6	T ₁ +134.0
Excess Rate (P,Y,R) Auto-Abort Inhibit and Switch Rate Gyros SC Indication "A"	IU	134.7	T ₁ +134.2
T ₂ (Center Engine Cutoff)	--	135.3	--
Q-Ball Power Off	IU	152.3	T ₂ +17.0
T ₃ (Outboard Engines Cutoff)	--	161.7	--
S/C Control of Saturn Enable	IU	708.9	T ₃ +5.0
S/C Control of Saturn Disable	IU	8629.5*	T ₆ +0.3*
S/C Control of Saturn Enable	IU	9555.8	T ₇ +5.0
S-IVB Engine EDS Cutoff No. 2 Disable	S-IVB	16,936.0	T ₈ +0.2
*Calculated Value			

Table 15-3. EDS Associated Discretes

DISCRETE MEASUREMENT	DISCRETE EVENT	RANGE TIME SECONDS
K73-602 On	EDS or Manual Cutoff of LV Engines Armed (Switch Selector)	30.0
K74-602 On	EDS or Manual Cutoff of LV Engines Armed (Timer)	31.3
K81-602 On	EDS S-IC One Engine Out	135.3
K82-602 On	EDS S-IC One Engine Out	135.3
K57-603 Off	Q-Ball Off Indication (+6D21)	152.3
K58-603 Off	Q-Ball Off Indication (+6D41)	152.3
K79-602 On	EDS S-IC Two Engines Out	161.9
K80-602 On	EDS S-IC Two Engines Out	161.9
K88-602 Off	S-IC Stage Separation	162.5

SECTION 16

VEHICLE PRESSURE AND ACOUSTIC ENVIRONMENT

16.1 SUMMARY

The internal, external, and base region pressure environments for the S-IC, S-II and S-IVB stages were monitored by a series of differential and absolute pressure gages. These measurements were used in confirming the vehicle external, internal, and base region design pressure environments. The flight data were generally in good agreement with the predictions and compared well with previous flight data. The pressure environment was well below design levels.

The vehicle internal and external acoustic environment was monitored by a series of microphones positioned to measure both the rocket engine and aerodynamically induced fluctuating pressure levels. The measured acoustic levels were generally in good agreement with the liftoff and inflight predictions, and with data from previous flights. The spectral analysis of the ten (one of which failed) additional S-IC intertank acoustic measurements has not been completed. Preliminary estimates indicate acoustic levels exceeded 160 decibels.

16.2 SURFACE PRESSURE AND COMPARTMENT VENTING

16.2.1 S-IC Stage

External and internal pressure environments on the S-IC stage were recorded by 12 measurements located on and inside the engine fairings, aft skirt, intertank, and forward skirt. Representative data from a portion of these instruments are compared, in Figures 16-1 through 16-3, with the AS-504 flight data and a band consisting of data from the first three Saturn V flights.

Differential pressure is the difference between measured pressure and free stream static pressure ($P_{int} - P_{amb}$). Pressure loading is the difference between structural internal and external pressures ($P_{int} - P_{ext}$) defined such that a positive loading is in the burst direction.

The AS-505 S-IC engine fairing compartment pressure differentials, shown in Figure 16-1, agree very well with previous flight data.

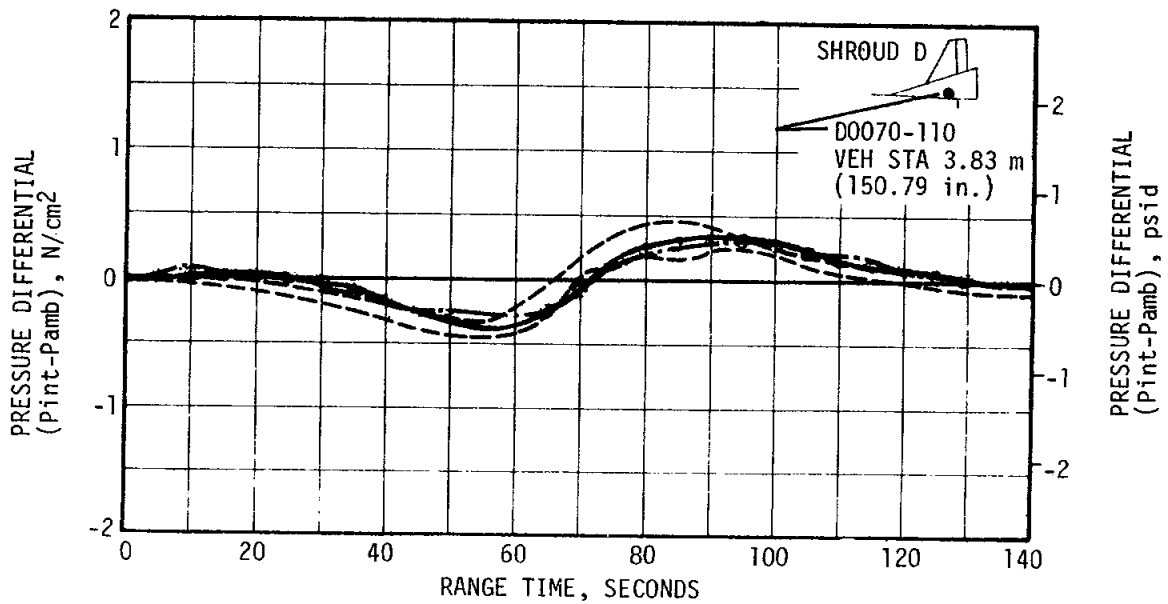
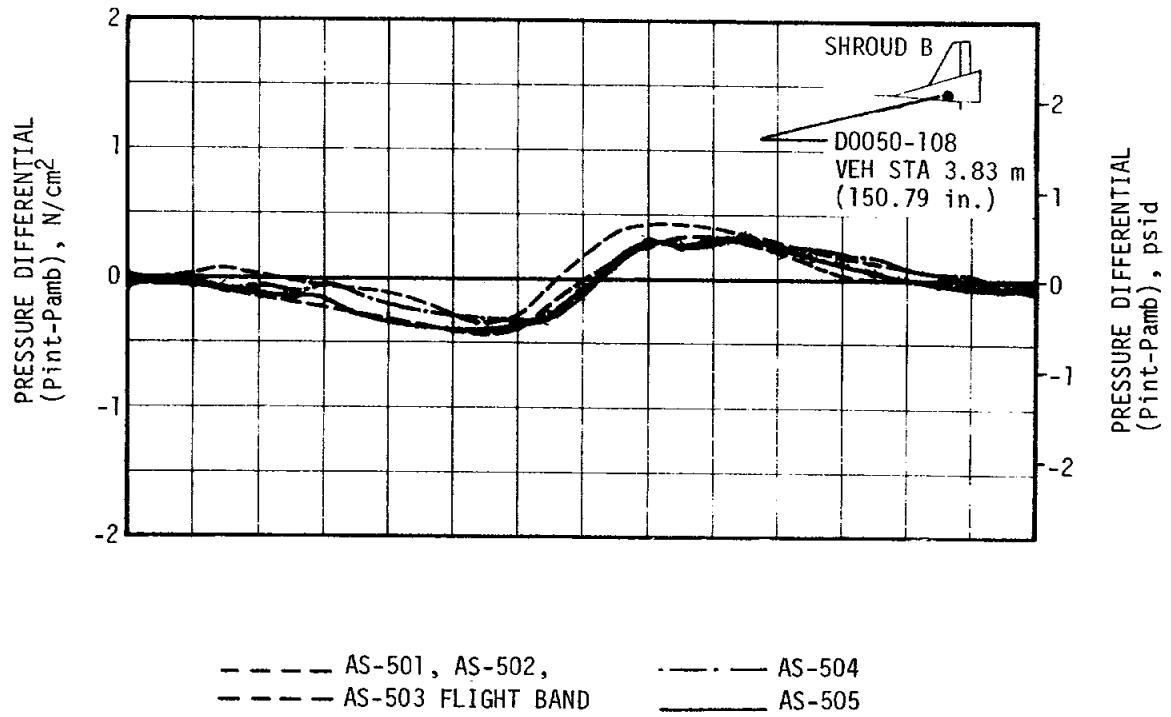


Figure 16-1. S-IC Engine Fairing Compartment Pressure Differential

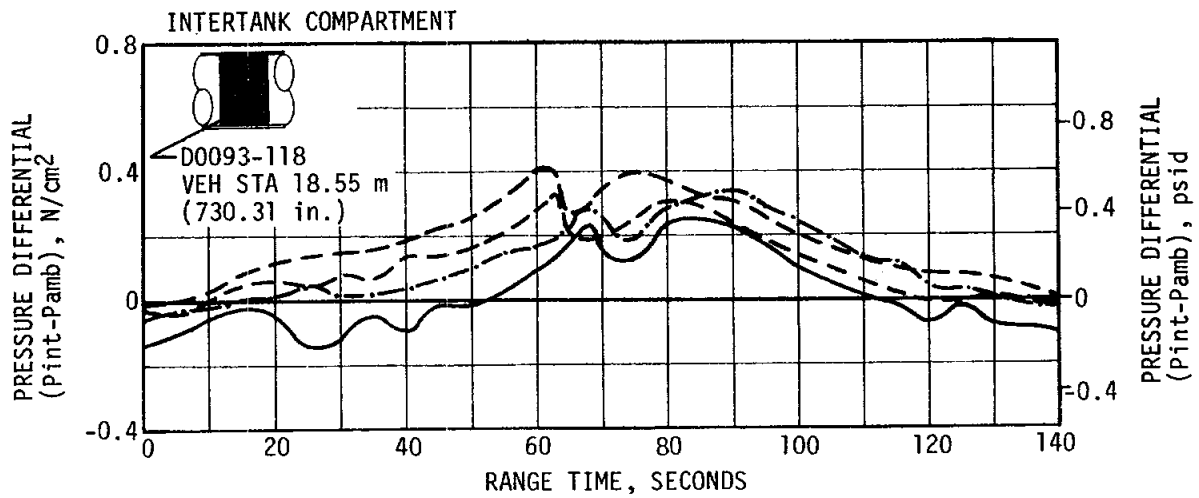
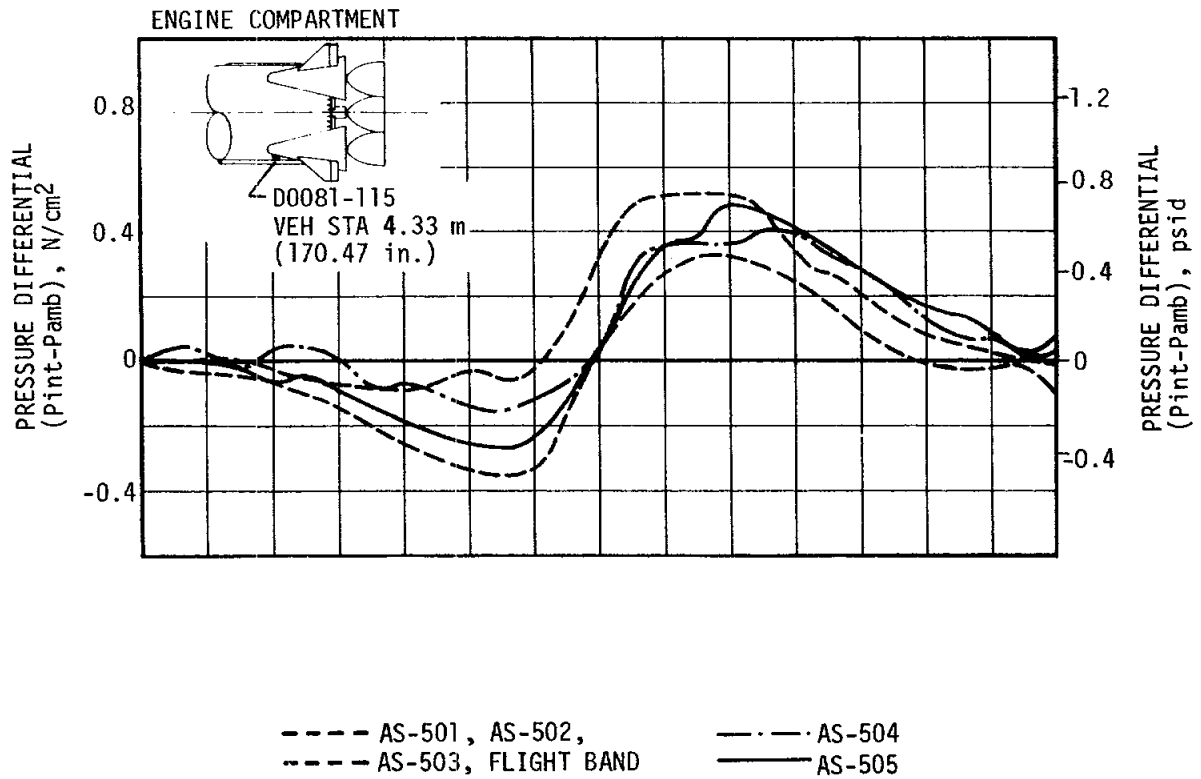


Figure 16-2. S-IC Compartment Pressure Differentials

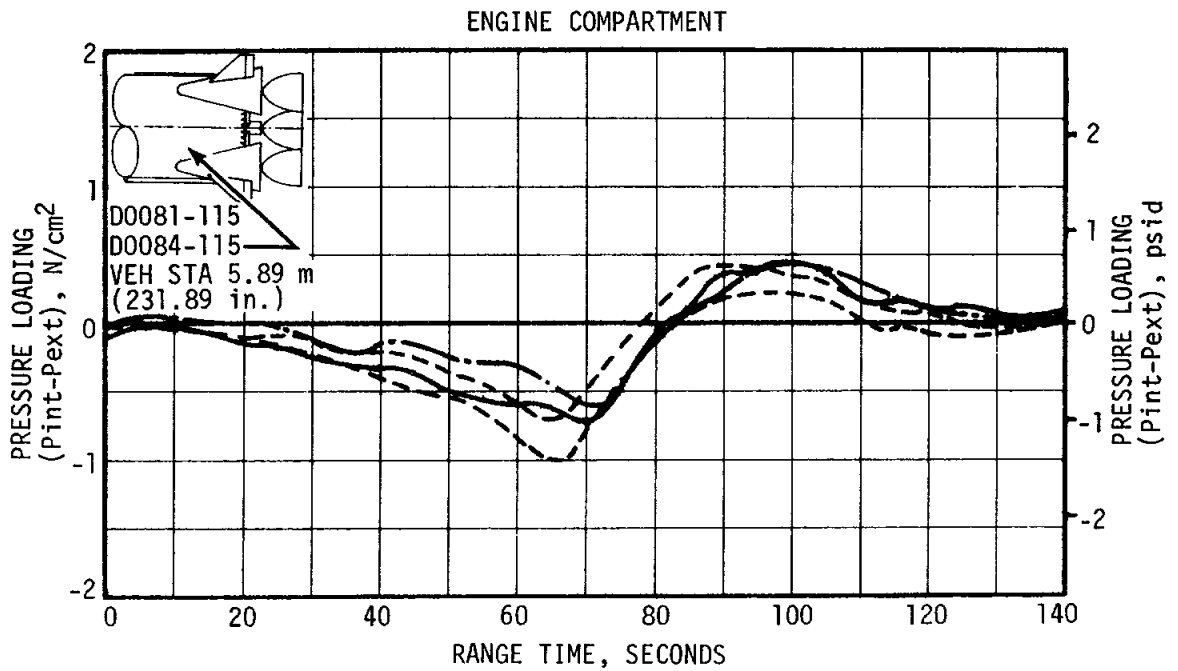
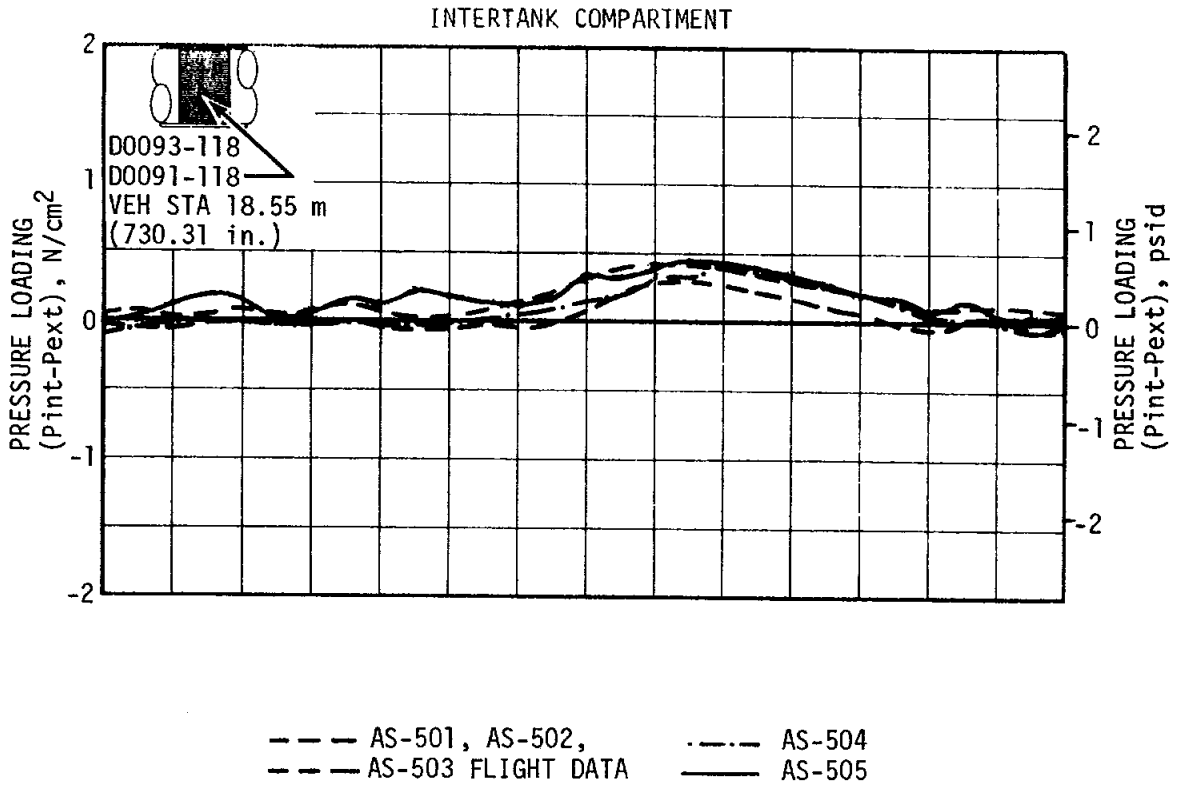


Figure 16-3. S-IC Compartment Pressure Loading

The S-IC engine and intertank compartment pressure differentials are shown in Figure 16-2. The AS-505 engine compartment pressure differential agrees well with previous data. The delay in the peak of the AS-505 and AS-504 intertank pressure differential was caused by the slower trajectories of these flights. However, the trends and magnitudes of the AS-505 data show good agreement with previous data.

The intertank pressure differential showed the characteristic drop as the vehicle passed through Mach 1. On the first three Saturn V flights, Mach 1 occurred between 60 and 62 seconds, while on AS-504 Mach 1 occurred at 68 seconds and on AS-505 Mach 1 occurred at 67 seconds.

The engine and intertank compartment pressure loadings are shown in Figure 16-3. The intertank compartment pressure loading agrees well with previous data. The AS-505 engine compartment pressure loading agrees in magnitude and trend with previous flight data. However, the slower trajectories flown on AS-505 and AS-504 delayed the data peak by approximately 10 seconds.

16.2.2 S-II Stage

The pressure environment on the S-II stage forward skirt was measured by 14 external absolute pressure measurements and one internal absolute pressure measurement.

A plot of the pressure loading acting across the forward skirt wall is presented in Figure 16-4. The AS-505 flight data and postflight predicted values are presented in the form of maximum-minimum data bands (positive values denote burst pressure). The AS-501 through AS-504 flight data bands are also shown for comparison. Both flight and predicted pressure loadings were obtained by taking the difference between the respective external pressure values and the assumed uniform internal pressure, which was measured at vehicle station 62.2 meters (2448.8 in.) and peripheral angle of 191 degrees. The AS-505 forward skirt pressure loadings were well within the design limits and agreed with predicted values and previous flight data.

16.3 BASE PRESSURES

16.3.1 S-IC Base Pressures

Static pressures on the S-IC base heat shield were recorded by four measurements, two of which are heat shield differential pressures. Representative AS-505 data are compared with AS-504 data and a band of data from the first three Saturn V flights.

S-IC base pressure differential is shown in Figure 16-5 as a function of altitude. In general, the agreement is good between AS-505 base pressure data and previous flight data.

* COMPLETE DATA FAILURE		
** QUESTIONABLE DATA		
--- POSTFLIGHT PREDICTION		
— AS-505 FLIGHT DATA		
I DATA FROM PREVIOUS FLIGHTS		
▽ MACH 1		
▽ MAX Q		
▽ S-IC/S-II FIRST PLANE SEPARATION		

	MEASUREMENT	VEHICLE STATION m (ft.)
EXTERNAL	D108-219	63.88 (2515)
	D109-219	63.75 (2510)
	D110-219	63.50 (2500)
	D111-219	62.99 (2480)
	D112-219	62.74 (2470)
	D113-219 *	61.54 (2423)
	D114-219	63.25 (2490)
	D115-219	63.25 (2490)
	D116-219 **	63.25 (2490)
	D117-219 **	63.25 (2490)
	D118-219	61.98 (2440)
	D119-219	63.75 (2510)
D120-219 **	63.25 (2490)	
D121-219 **	63.25 (2490)	
INTERNAL	D163-219	62.20 (2449)

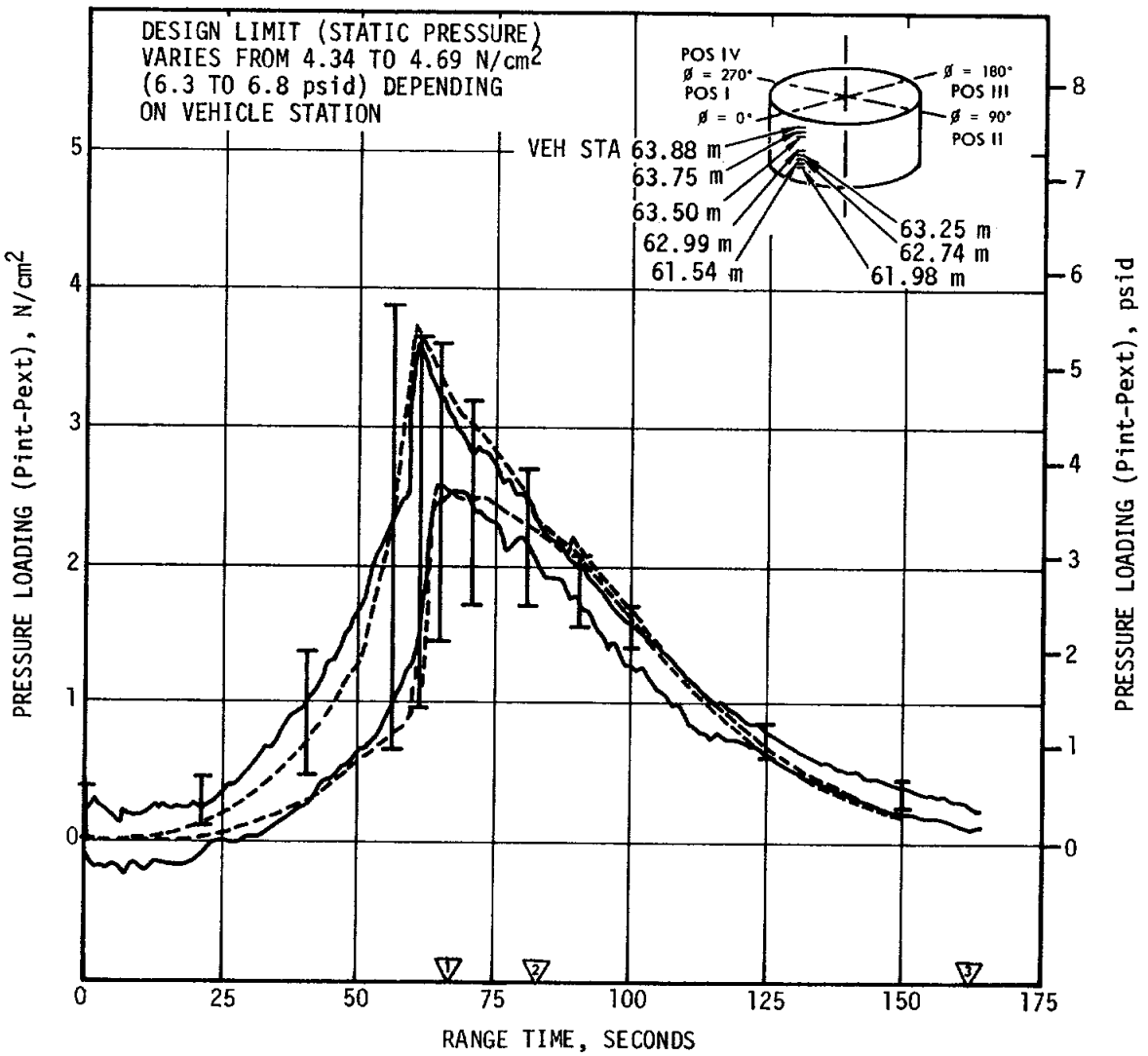


Figure 16-4. S-II Forward Skirt Pressure Loading

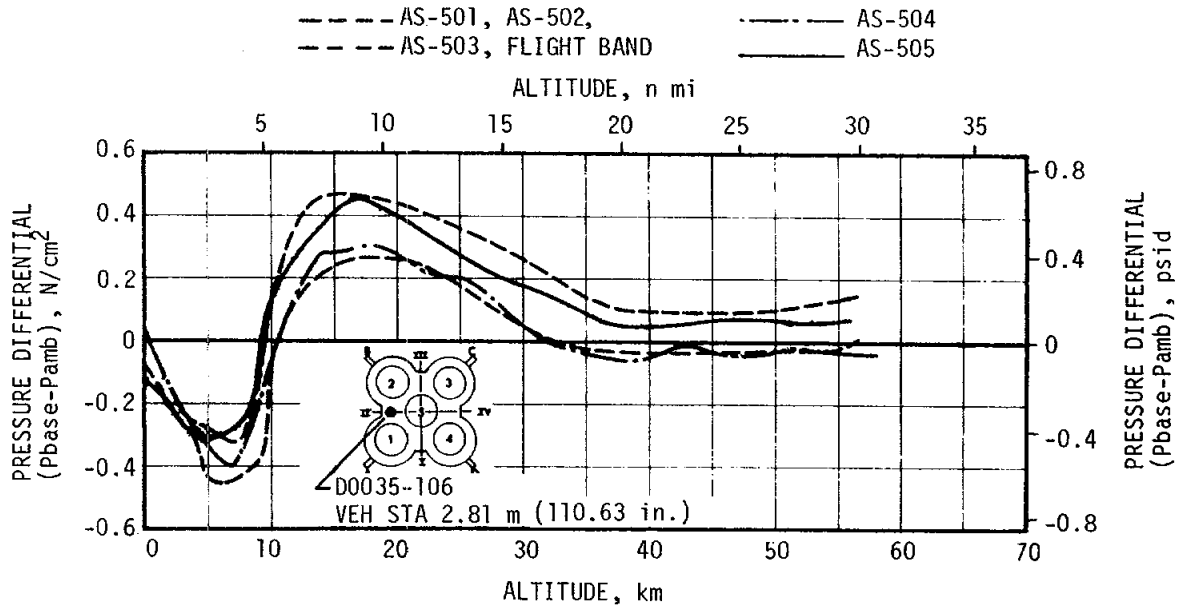


Figure 16-5. S-IC Base Pressure Differential

S-IC base heat shield pressure loading is shown in Figure 16-6 as a function of altitude. AS-505 data shows good agreement with previous flight data. The heat shield loadings were well within the 1.38 N/cm^2 (2.0 psid) design differential.

16.3.2 S-II Base Pressures

The S-II stage heat shield and thrust cone pressure environment was determined by six absolute pressure measurements on the aft face of the heat shield, by four absolute pressure measurements on the forward face, and a single absolute pressure measurement on the thrust cone.

Figure 16-7 shows the static pressure variation with range time on the forward face of the heat shield and in the thrust cone region. The predictions are based on the AS-501 through AS-504 flight data and predicted AS-505 heat shield aft face pressures. The AS-505 flight static pressure in this region was approximately the same as that measured during previous flights. The pressure peaks observed on previous flights during inter-stage separation are also present in the AS-505 flight data. The forward face pressures were not significantly affected by S-II stage Center Engine Cutoff (CECO).

Figure 16-8 compares the AS-505 flight heat shield aft face static pressure data with predicted values and prior flight data. It is noted that the AS-505 flight data band enveloping all heat shield aft face pressure measurements is wider than that corresponding to previous flights. Also, there is a larger than normal discrepancy between the predicted and the

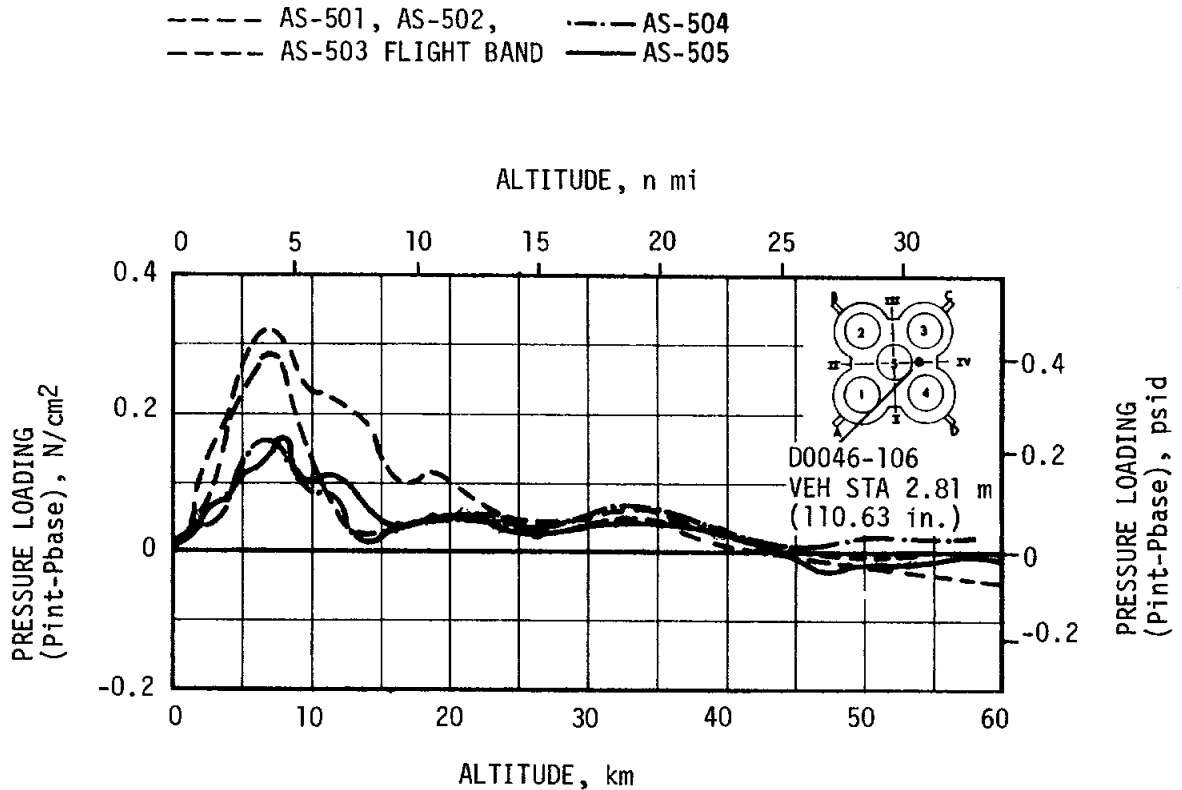


Figure 16-6. S-IC Base Heat Shield Pressure Loading

AS-505 flight data band. These effects can be attributed to widening of the data band caused by an unpredicted local increase of static pressure after second plane separation. The gradual decay in heat shield aft face pressure from second plane separation to S-II Outboard Engine Cutoff (OECO), noted on flights AS-503 and AS-504, was not as pronounced during the AS-505 flight.

The predicted pressures after S-II CECO were based on four- and five-engine 1/25 S-II stage scale model test results. It is shown that the predicted minimum pressure during this time interval does not follow the flight data trend. The flight data show a pressure drop after CECO at all measured locations, while the pressure measured during model testing increased or decreased depending on location. These model data are not strictly applicable, because the effect on the pressure distribution as a result of the center engine shutdown was not simulated.

16.4 ACOUSTIC ENVIRONMENT

16.4.1 External Acoustics

The AS-505 external fluctuating pressures were measured at six vehicle stations located on the S-IC aft skirt, Fin D base, S-IC intertank, S-II forward and aft skirts, and S-IVB forward and aft skirts. Figure 16-9

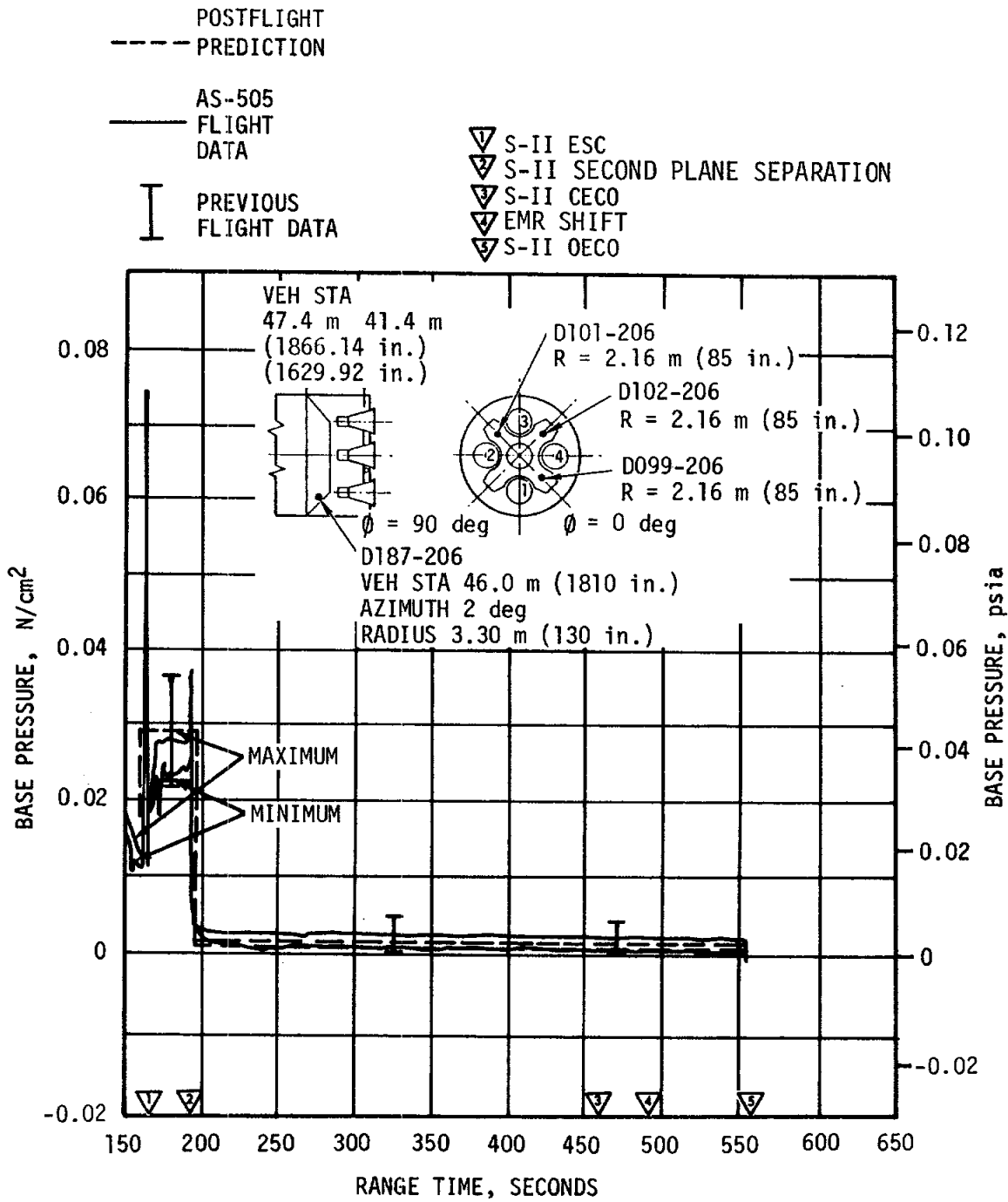


Figure 16-7. Thrust Cone and Base Heat Shield Forward Face Pressures

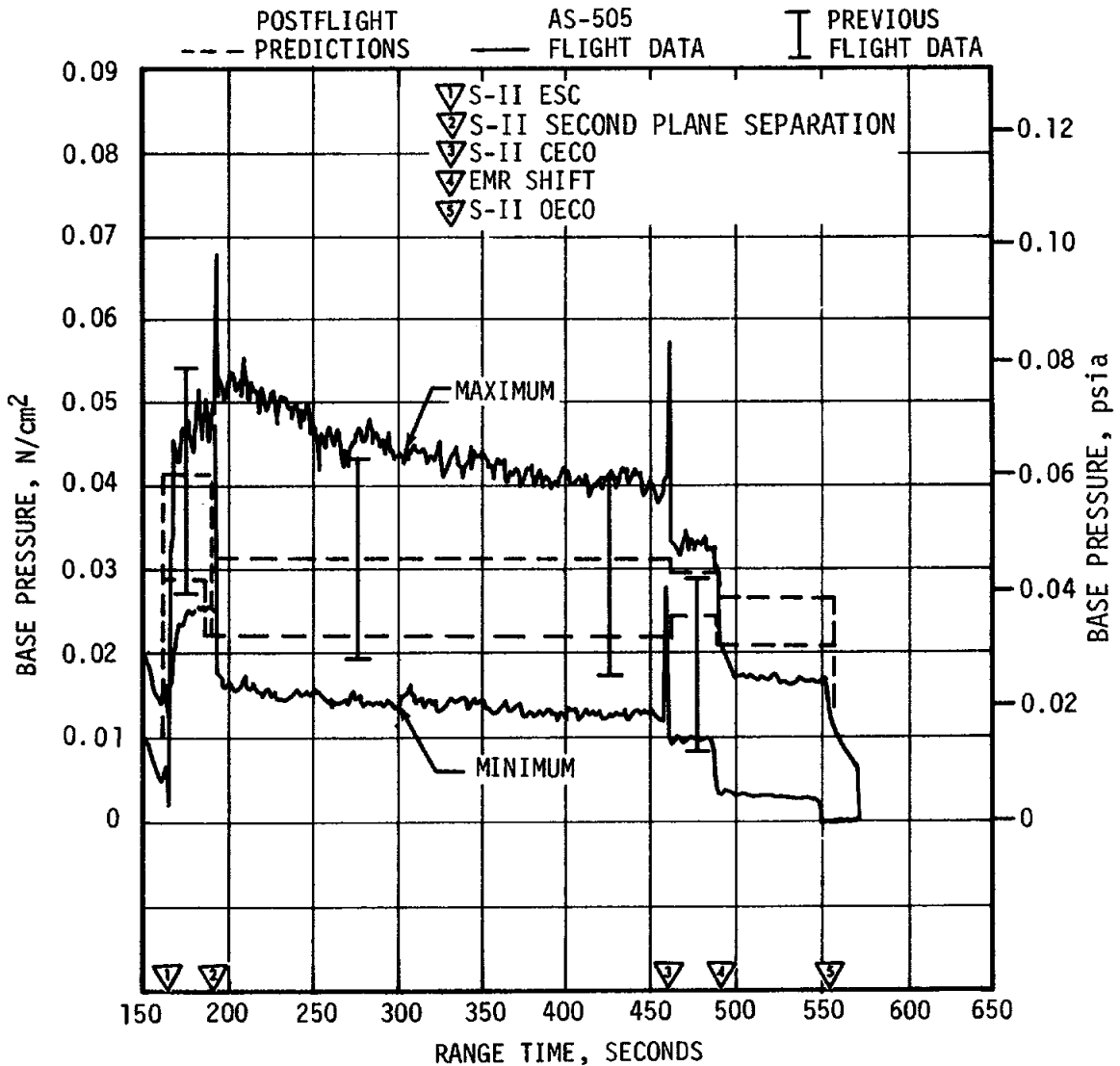
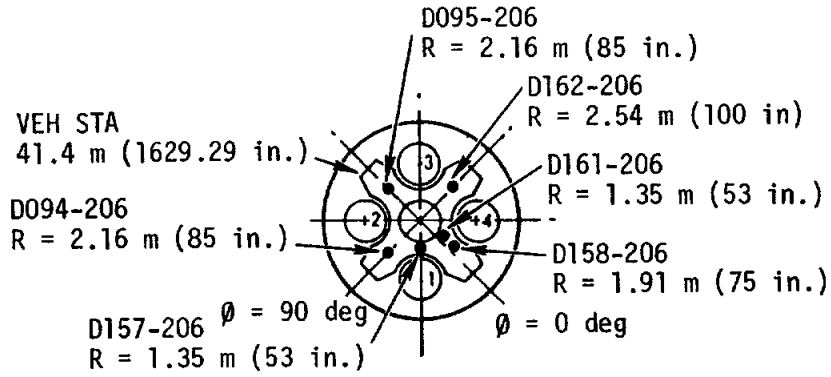


Figure 16-8. S-II Heat Shield Aft Face Pressures

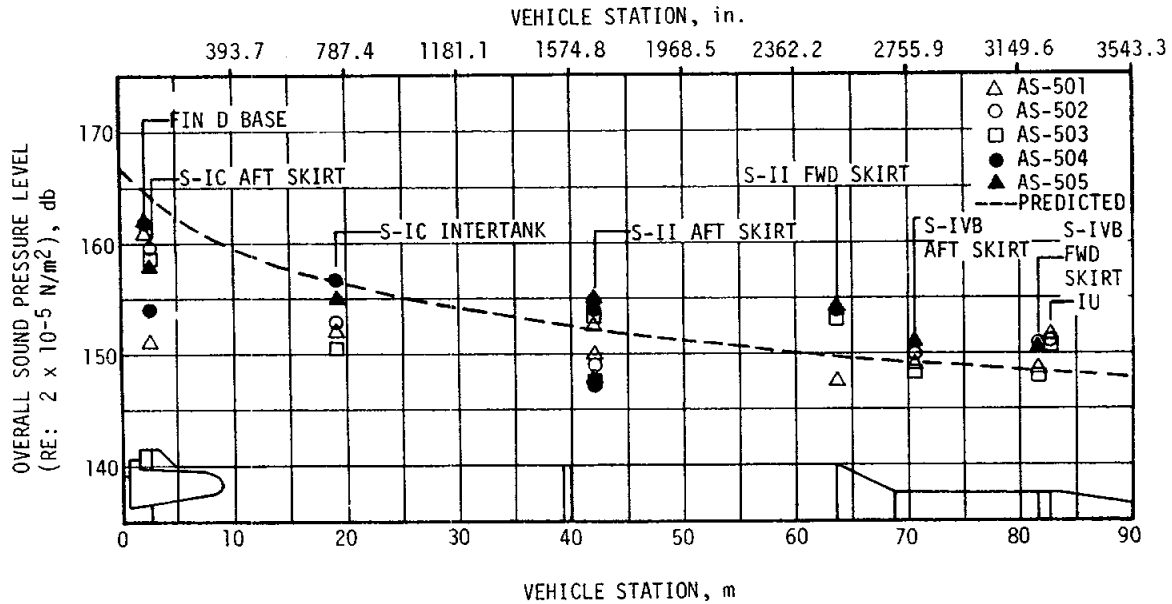


Figure 16-9. Vehicle External Overall Sound Pressure Level At Liftoff

presents overall sound pressure levels versus vehicle body station at liftoff and shows good agreement with data from AS-501 through AS-504. Pressure spectral densities at liftoff are presented in Figure 16-10 and are shown to be reasonably consistent with previous flight data.

Overall fluctuating pressure level time histories for S-IC boost are presented in Figure 16-11. No significant variations from previous flight data are noted. Pressure spectral densities at maximum aerodynamic noise are presented in Figure 16-12. S-IC intertank measurement B0003-118 shows the only significant spectral variation between flights. This variation is characterized by the appearance of isolated peaks in the various flight spectrums.

Ten additional acoustic measurements were installed on the S-IC intertank to study the unstable dynamic pressures induced in that area by the recirculating gases from the exhaust plume. One measurement was a total failure and data from the other nine were clipped during some time periods due to higher than expected pressure levels. However, the data is considered usable since only the more positive voltage signals were clipped.

Spectral analysis of this data has not been completed at this time, but preliminary estimates indicate acoustic levels exceeded 160 decibels (about 0.3 psi or approximately 20 times the pressures anticipated). The frequency range, in general, varied from 1 hertz to as high as 110 hertz. The greatest acoustic energy appears to be in the 1 to 5 hertz range during the plume passage. The vehicle response to these pressures depends

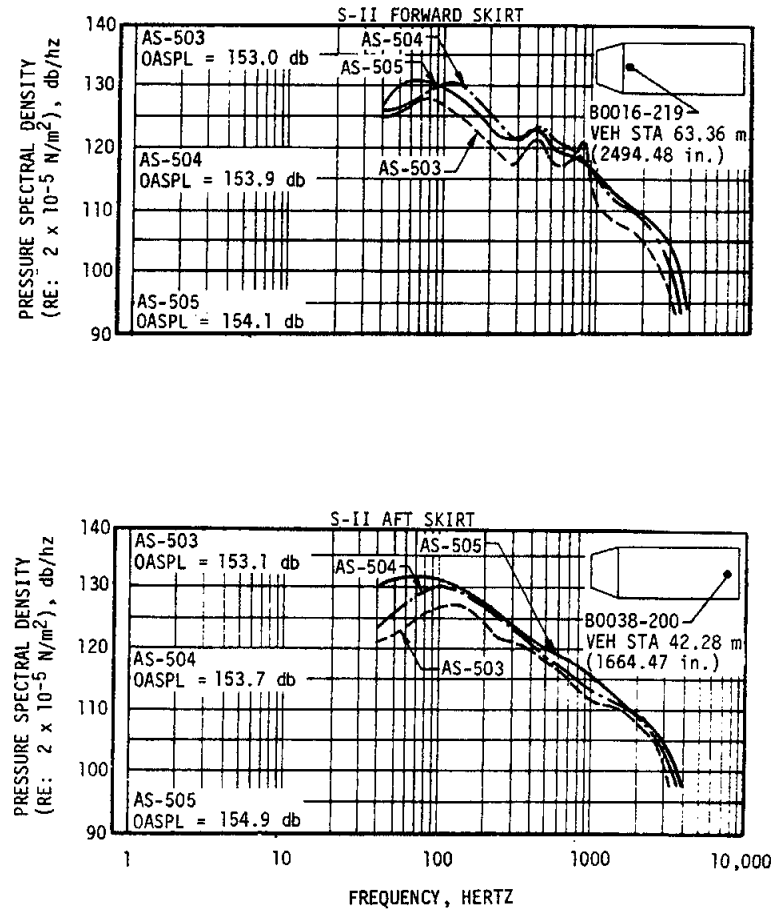
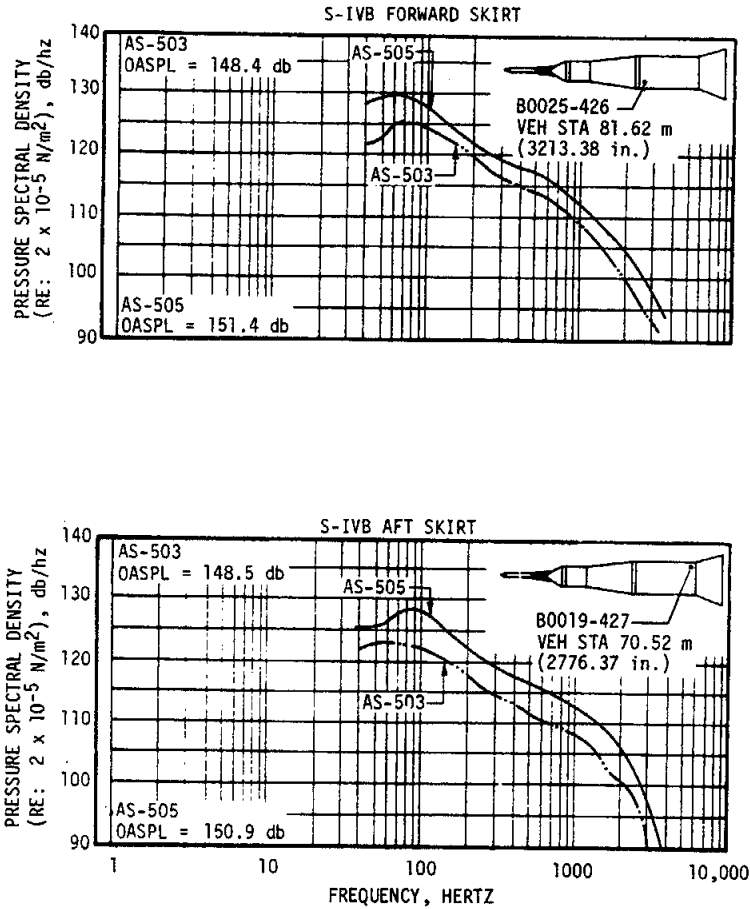


Figure 16-10. Vehicle External Sound Pressure Spectral Densities at Liftoff (Sheet 1 of 2)

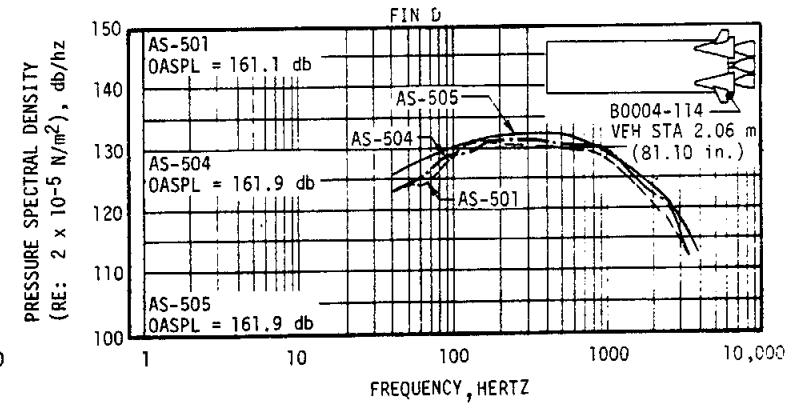
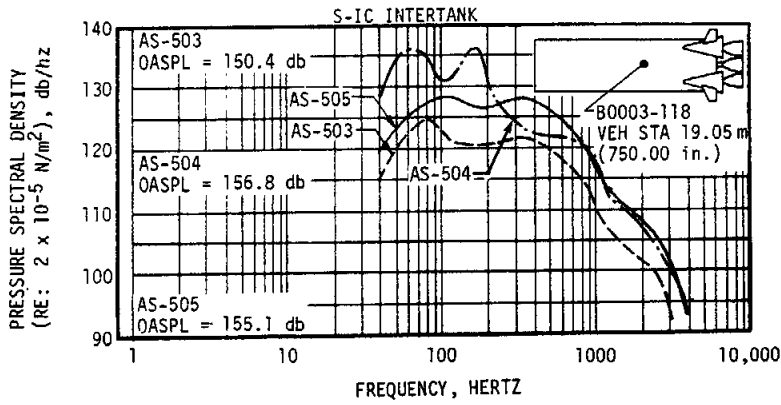
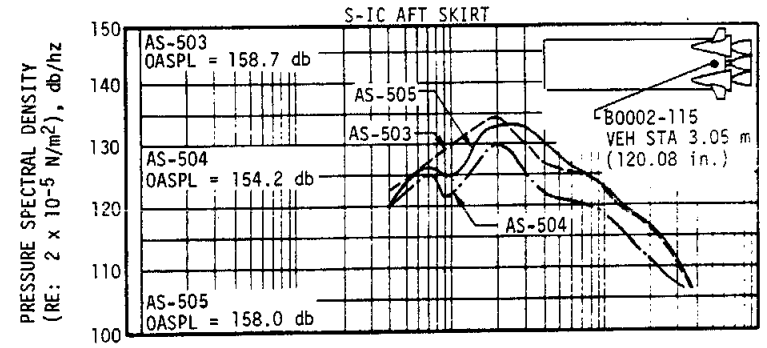
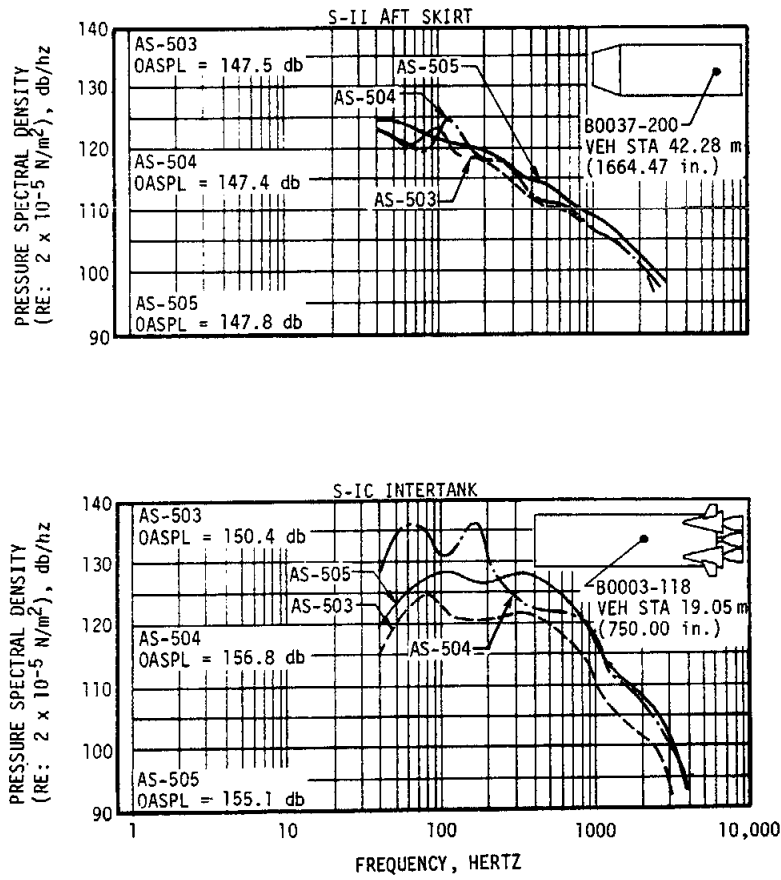


Figure 16-10. Vehicle External Sound Pressure Spectral Densities at Liftoff (Sheet 2 of 2)

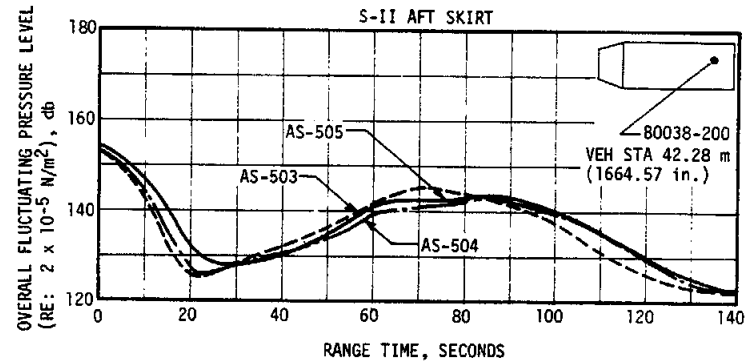
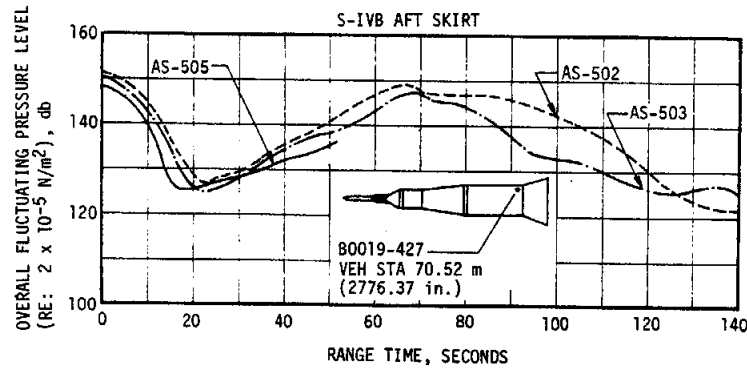
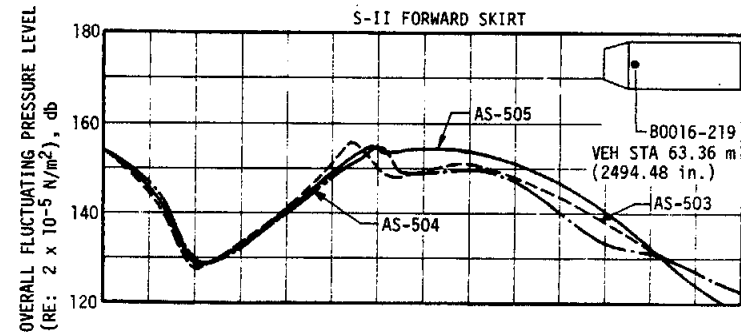
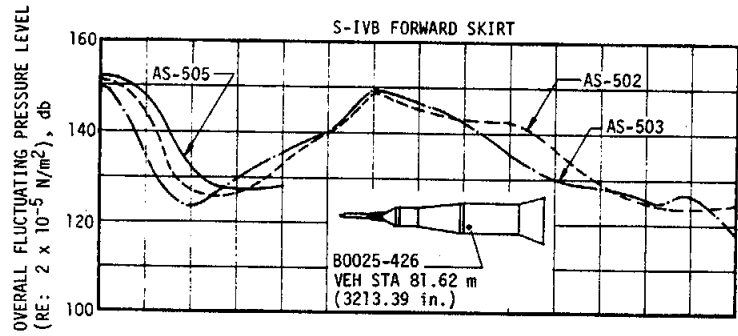


Figure 16-11. Vehicle External Overall Fluctuating Pressure Level (Sheet 1 of 2)

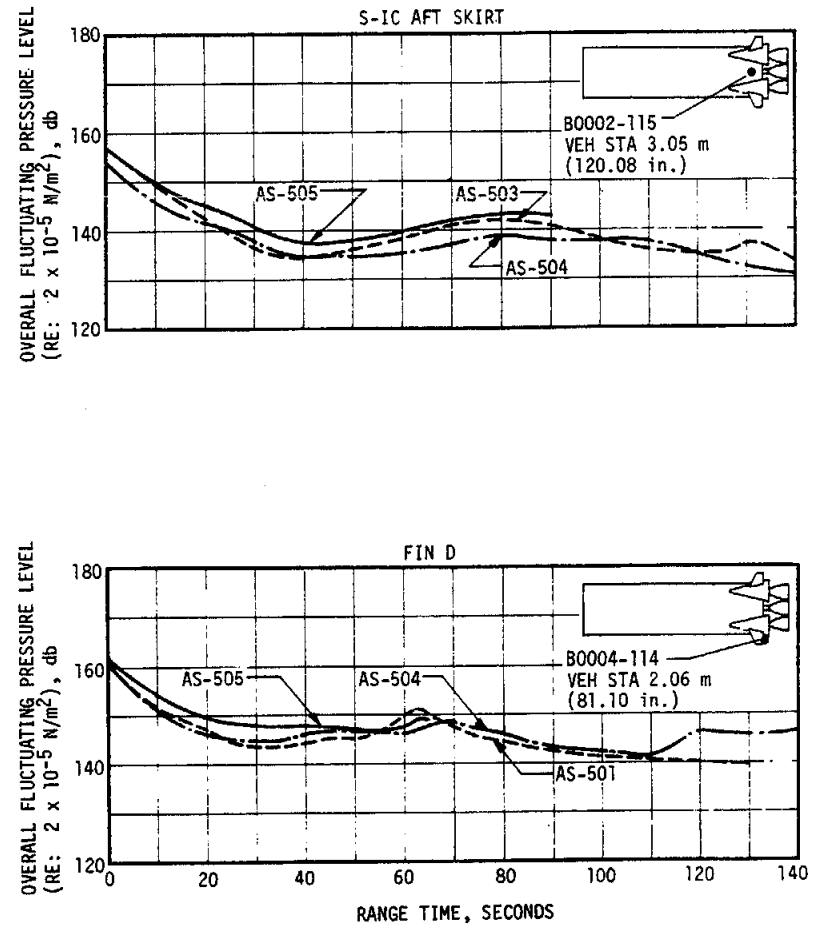
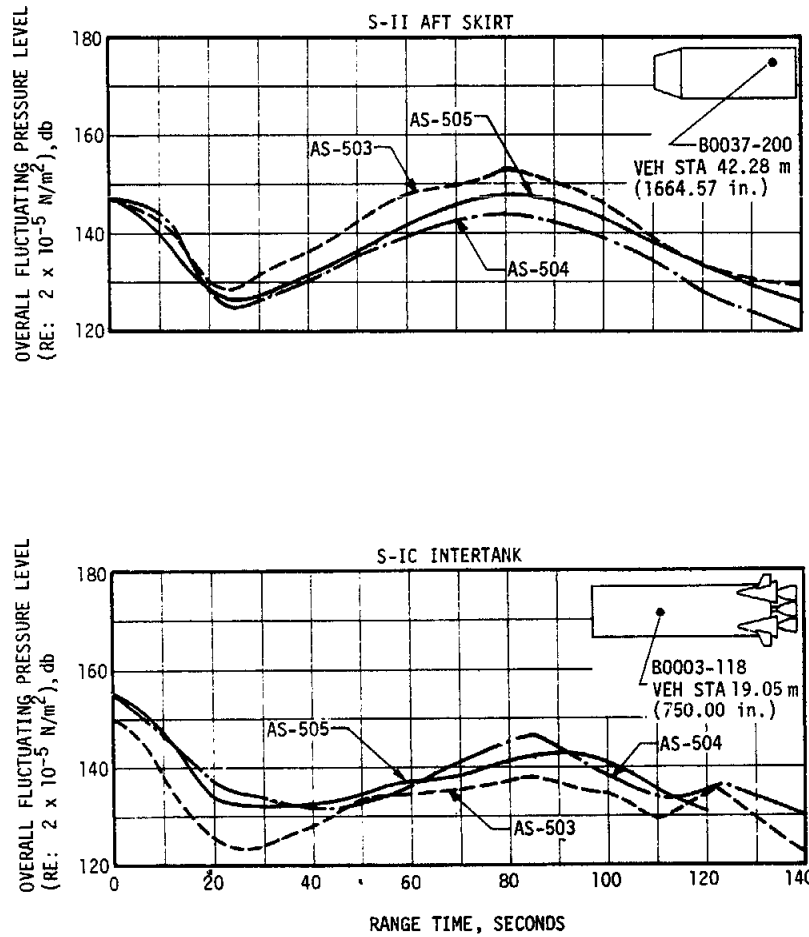


Figure 16-11. Vehicle External Overall Fluctuating Pressure Level (Sheet 2 of 2)

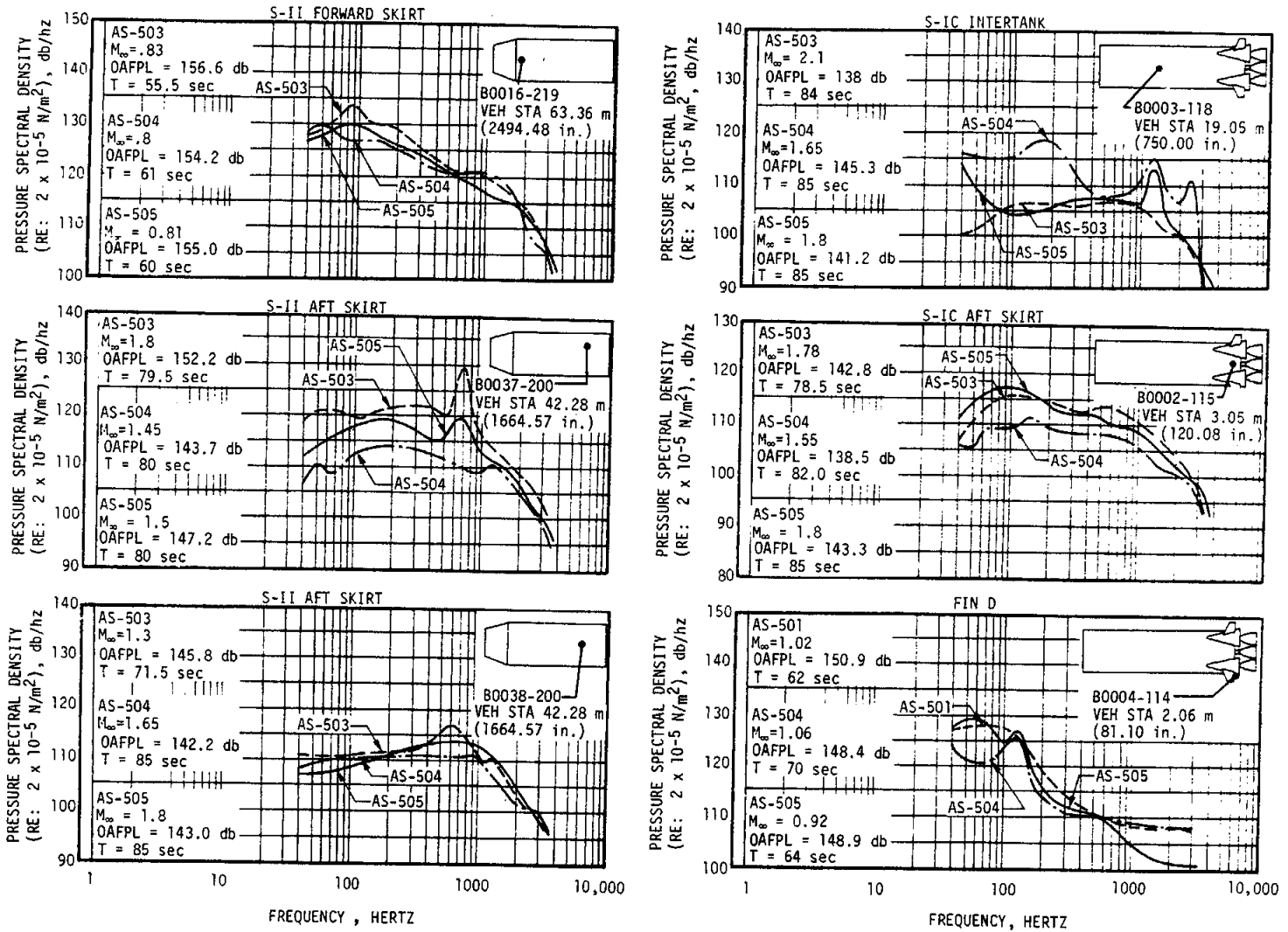


Figure 16-12. Vehicle External Fluctuating Pressure Spectral Densities at Maximum Inflight Aerodynamic Noise




on the phasing of the loads (pressures). An estimate of the phasing and pressure amplitudes can be established when the spectral analysis of all the data is completed.


16.4.2 Internal Acoustics

16.4.2.1 S-IC Stage. Internal acoustics were measured at two locations on the S-IC stage. One measurement was located in the intertank section, and the other in the thrust structure above the heat shield. The acoustic data at these locations are shown in Figures 16-13 and 16-14. Data from both measurements agree with previous flight data, except AS-505 data were somewhat lower between 20 and 60 seconds.

16.4.2.2 S-II Stage. The two internal microphones, used on the S-II stage, are located on the forward skirt and thrust cone. Figure 16-15 presents the internal overall acoustic levels versus range time for AS-505. The forward compartment internal acoustics show agreement with previous flight data during liftoff. The lower level for the aft compartment internal acoustics is due to the measurement commutation occurring after the liftoff acoustic maximum.

AS-505 internal and external acoustics are shown in Table 16-1 and compared with data from previous flights. The microphone located away from

MEASUREMENT	MAXIMUM SPL 		OVERALL SPL LIMIT	LEGEND
	PREVIOUS FLIGHT DATA	AS-505		
B005-106	144.8 at 0 seconds	143.7 at 0 seconds	169.0	 PREVIOUS FLIGHT DATA ENVELOPE  AS-505 FLIGHT DATA

 SPL in db referenced to $2 \times 10^{-5} \text{ N/m}^2$

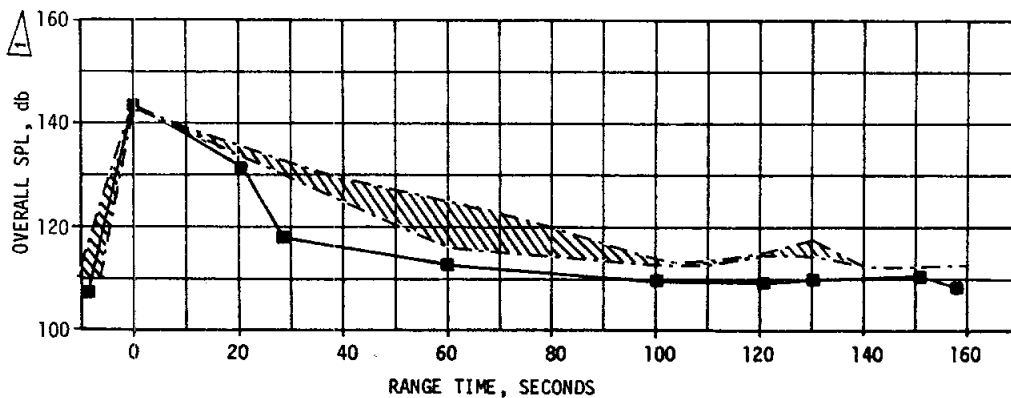





Figure 16-13. S-IC Heat Shield Panels Internal Acoustic Environment

MEASUREMENT	MAXIMUM SPL 		OVERALL SPL LIMIT	LEGEND
	PREVIOUS FLIGHT DATA	AS-505		
B001-118	144.7 at 0 seconds	139.5 at 0 seconds	157	 PREVIOUS FLIGHT DATA ENVELOPE  AS-505 FLIGHT DATA

 SPL in db referenced to $2 \times 10^{-5} \text{ N/m}^2$

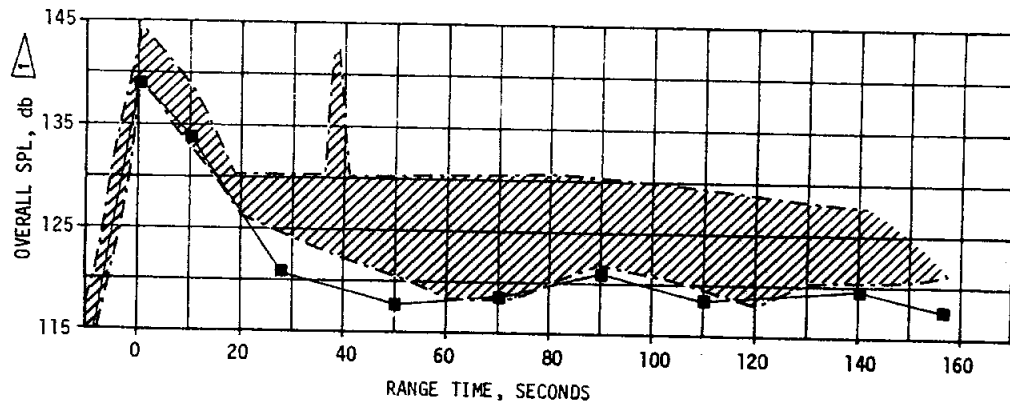


Figure 16-14. S-IC Intertank Internal Acoustic Environment

the tower (270 degrees azimuth) shows the higher level, as expected. The differential between the forward external and internal acoustic levels is approximately 8 decibels at liftoff. The differentials for Mach 1 and Max Q conditions are 18 decibels or higher because the greater high frequency contents are more attenuated across the vehicle skin. The differential between the aft external and internal acoustic levels is not realistic because the internal measurement was commutated after the lift-off acoustic maximum.

16.4.2.3 S-IVB Stage. The S-IVB acoustic environment was measured at four positions, internal and external on the forward skirt, and internal and external on the aft skirt. Both external measurements provided valid data only during portions of the flight due to an instrumentation malfunction.

Time histories of the composite levels, 50 to 3000 hertz, for these locations are presented in Figure 16-16. The AS-505 structural transmissibility for the sound pressure at liftoff is indicated by the difference (shaded band) between the external and the internal measurements. The maximum external levels and minimum internal levels measured during the AS-503 flight are also shown, indicating that the AS-505 levels were nominal.

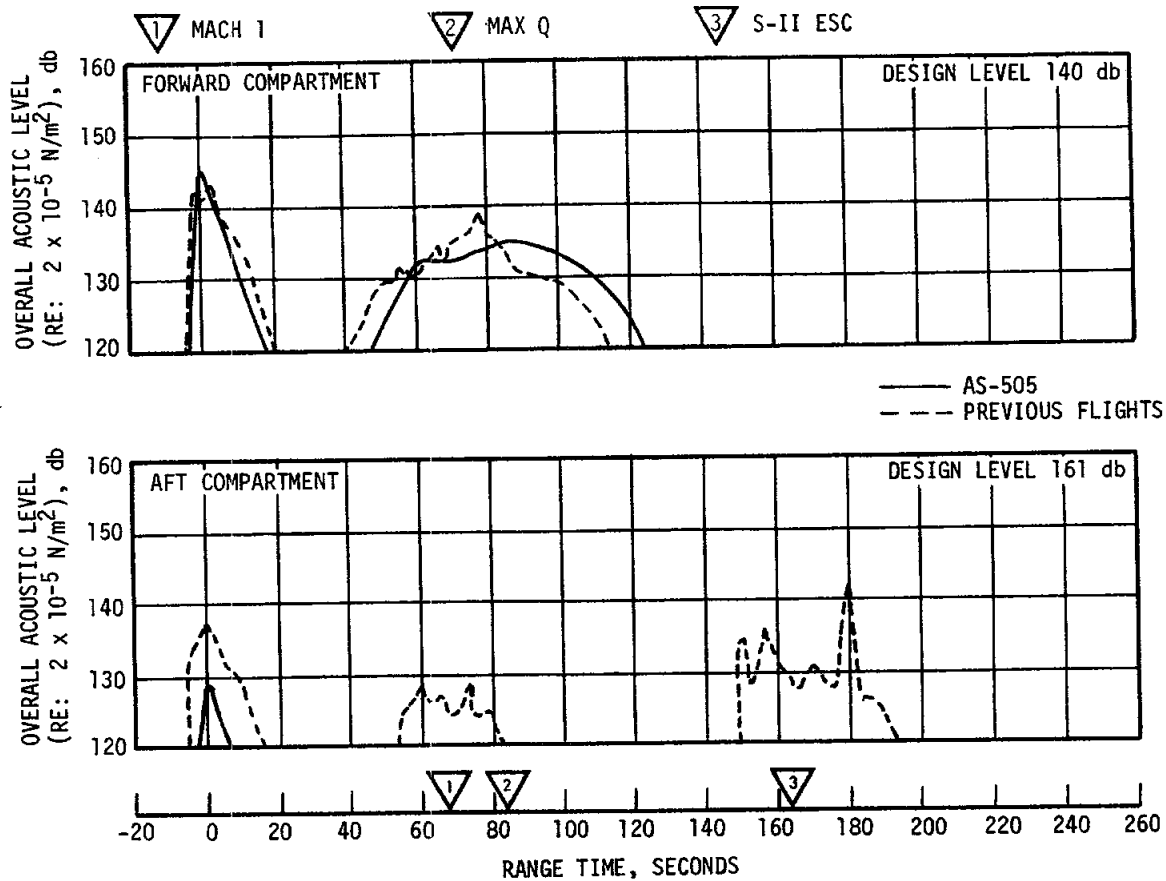


Figure 16-15. S-II Internal Acoustic History

Table 16-1. Sound Pressure Level Comparison of AS-505 With Previous Saturn V Flight Data

EVENT	MAXIMUM OVERALL DB							
	FORWARD COMPARTMENT				AFT COMPARTMENT			
	EXTERNAL (B016-219)		INTERNAL (B017-219)		EXTERNAL (B037-200 & B038-200)		INTERNAL (B039-206)	
	AS-505	AS-501/503/504	AS-505	AS-501/502/503/504	AS-505	AS-501/503/504	AS-505	AS-501/502/503/504
Liftoff	154.1	154.0	145.7	142.0	154.9	153.7	128.7	137.5
Transonic	153.5	156.5	133.9	133.0	143.5	147.8		129.0
Max Q	154.0	151.2	137.0	138.0	147.2	152.2		129.0
Max Static Firing	139.5		134.0		150.3		161.8	

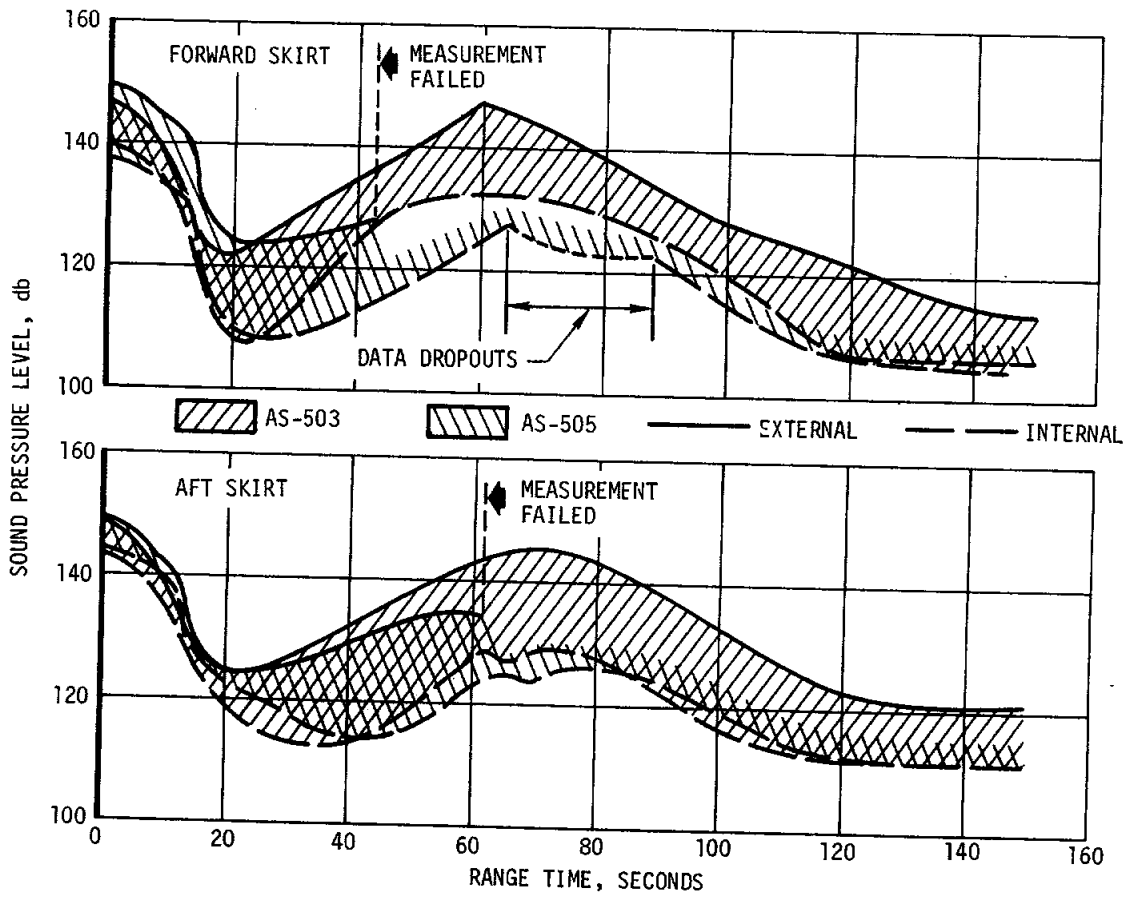


Figure 16-16. S-IVB Acoustic Levels During S-IC Burn

SECTION 17
VEHICLE THERMAL ENVIRONMENT

17.1 SUMMARY

The AS-505 S-IC base region thermal environment was similar to that experienced on earlier flights with the maximum temperatures generally higher as a result of higher ambient temperatures at liftoff. Heat shield temperatures and structural temperatures forward of the heat shield were generally within the bands of previous data and well below design allowances. The forward surface and bondline measurements did not indicate loss of M-31 insulation on AS-505.

S-IC fuel tank and intertank skin temperatures exceeded the predicted maximum during the early portion of flight. This condition was a result of the higher ambient temperatures and wind velocity at liftoff.

Base thermal environments on the AS-505 S-II stage were similar to those measured on previous flights and were well below design limits. Heat shield aft surface temperatures increased between S-II Center Engine Cutoff (CECO) and Engine Mixture Ratio (EMR) stepdown, but were well below the design predictions.

The aeroheating rates on the AS-505 S-II stage interstage, body structure and fairings were similar to those on previous flights.

The AS-505 S-IVB stage aeroheating environment was comparable to that of AS-501, AS-503, and AS-504 and cooler than that of AS-502.

17.2 S-IC BASE HEATING AND STAGE SEPARATION ENVIRONMENT

17.2.1 S-IC Base Heating

Thermal environments in the base region of the S-IC stage were recorded by 29 measurements, which were located on the heat shield and F-1 engines. This instrumentation included 6 radiation calorimeters, 16 total calorimeters, and 7 gas temperature probes. Representative data from these instruments are compared with the AS-502 through AS-504 flight data band. See Figures 17-1 and 17-2. Data are shown versus altitude to minimize trajectory differences. AS-501 flight data, which showed less severity than subsequent flight data because of flow deflector effects, are not shown.

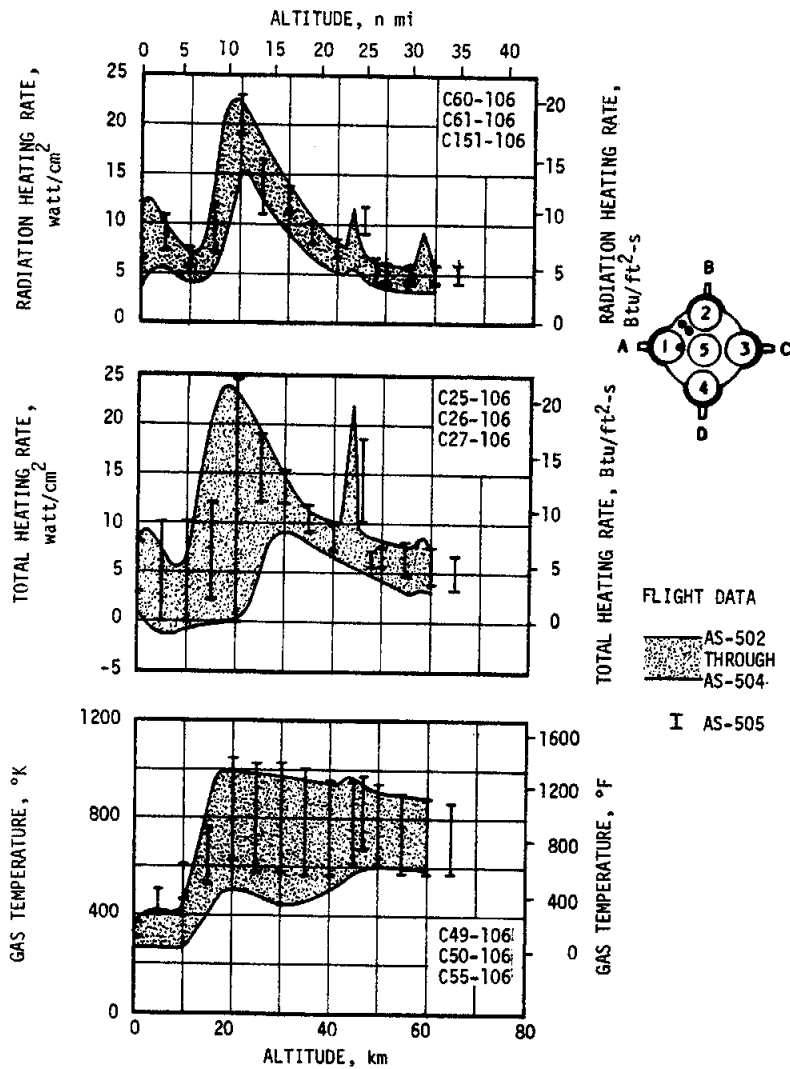


Figure 17-1. S-IC Base Heat Shield Thermal Environment

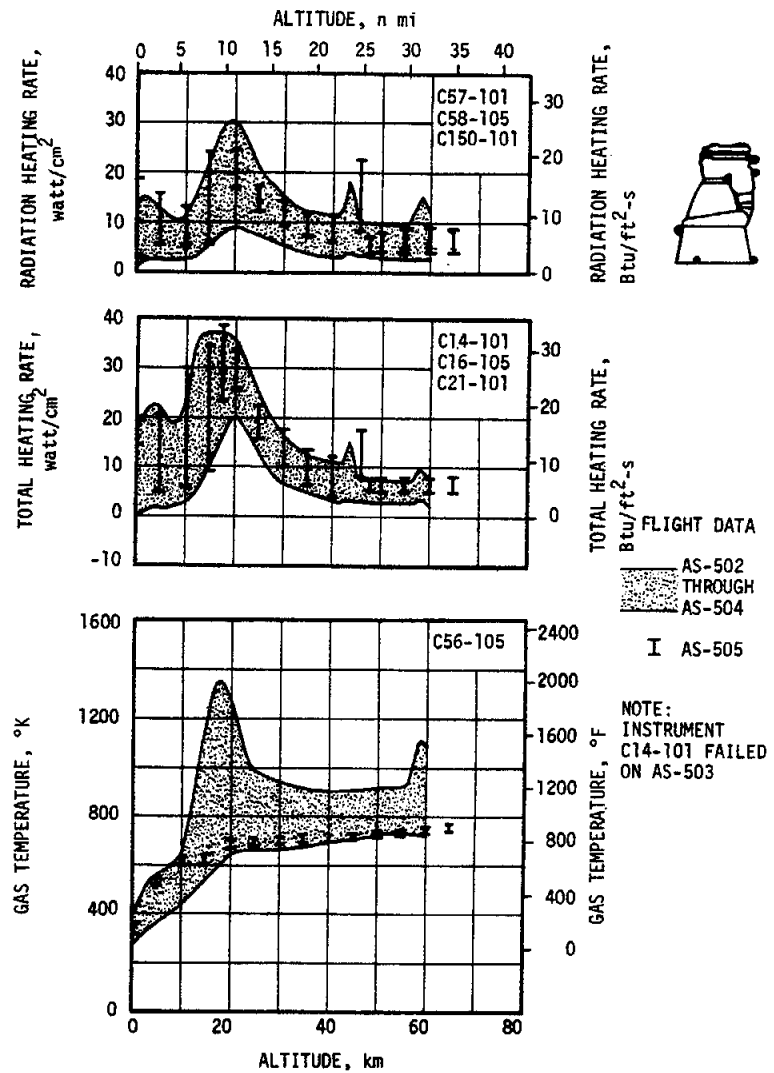


Figure 17-2. F-1 Engine Thermal Environment

AS-505 S-IC base thermal environments have similar trends and magnitudes as those measured during the previous flights, as shown in Figures 17-1 and 17-2. In general, AS-505 radiation heating rates were slightly higher than AS-504. Maximum values of radiation and total heating rate occurred at altitudes between 15 and 22 kilometers (8.1 and 11.9 n mi). The maximum total heating rate measured in the AS-505 base region was 39.5 watt/cm² (34.8 Btu/ft²-s), recorded on the inboard surface of engine No. 3 (C123-103). CECO on AS-505 produced a spike in the environments with a magnitude and duration similar to previous flight data at CECO. AS-505 base gas temperatures show good comparison with AS-502 through AS-504 flight data. However, AS-505 gas temperature data do not show the decrease between 4 and 9 kilometers (2 and 5 n mi) that previous flight data indicated.

The heat shield temperature data are compared to previous flight data in Figures 17-3 and 17-4. Measurement locations for the S-IC base heat shield are shown in Figure 17-5. The temperatures were generally higher than on previous flights largely because of a higher ambient temperature at liftoff. The forward surface and bondline measurements did not indicate M-31 insulation loss, and temperatures were well below design levels. Measured temperatures showed reasonable agreement with a flight reconstruction (not shown in the figures) based on flight radiation data, gas temperature data, and design heat transfer coefficients.

Engine temperature data were normal. The thermal response of the turbine exhaust manifold under the insulation on the inboard side of engine No. 1 at vehicle station -1.1 meters (-44 in.) is shown in Figure 17-6. The measurement trace is similar to previous flight data. Temperatures under the insulation on the gimbal actuator and on the fuel discharge line were well below design limits while gas temperatures inside the engine cocoons remained within the band of previous flight data.

17.2.2 S-IC/S-II Separation Environment

Forward skirt compartment gas temperatures, shown in Figure 17-7, were similar to those encountered during separation on previous flights. Two spikes in the gas temperature were noted. The first spike was due to the S-II ullage motor flow field and the second spike was due to the five J-2 engine plumes. Peak temperatures, due to the J-2 engine plumes, may have reached slightly higher peaks than those shown, at approximately 4.0 seconds after separation since data at this point exceeded the upper limit of the transducers, requiring extrapolation between 3.7 and 4.4 seconds after separation.

17.3 S-II BASE REGION ENVIRONMENT

The S-II base heat shield and thrust cone flight environment was, in general, in good agreement with previous flight data and postflight predictions. Base heat shield measured heating rates, gas temperatures,

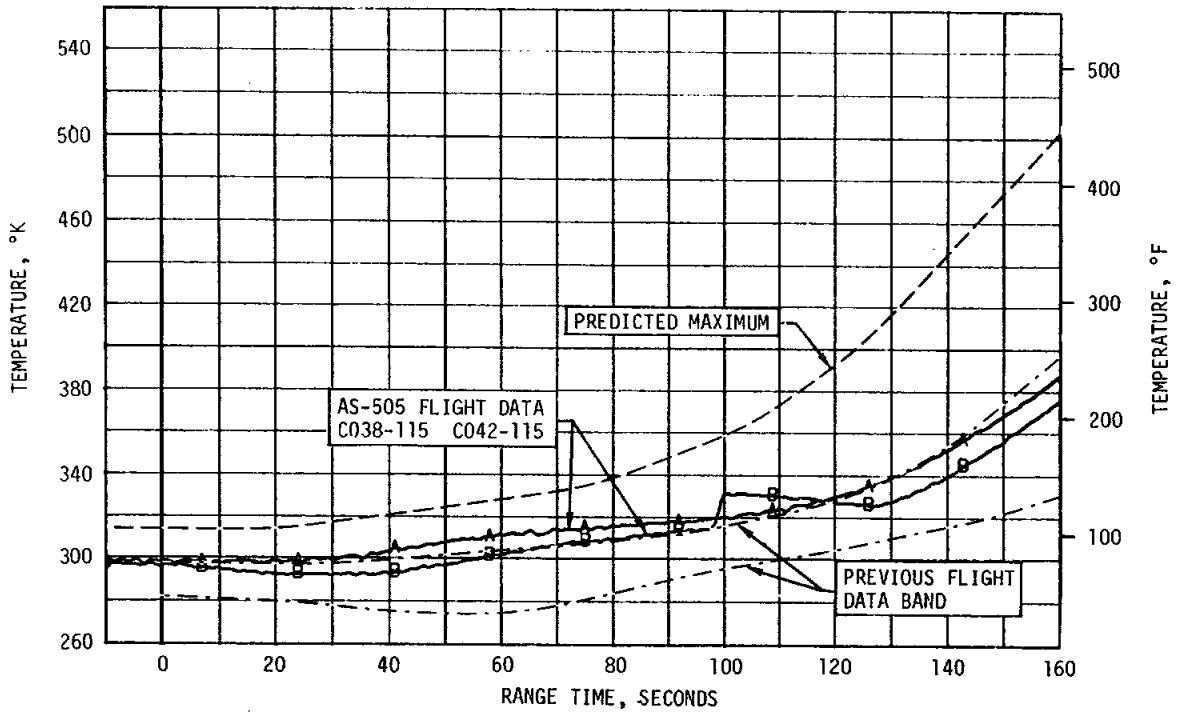


Figure 17-3. S-IC Heat Shield Forward Surface Temperature

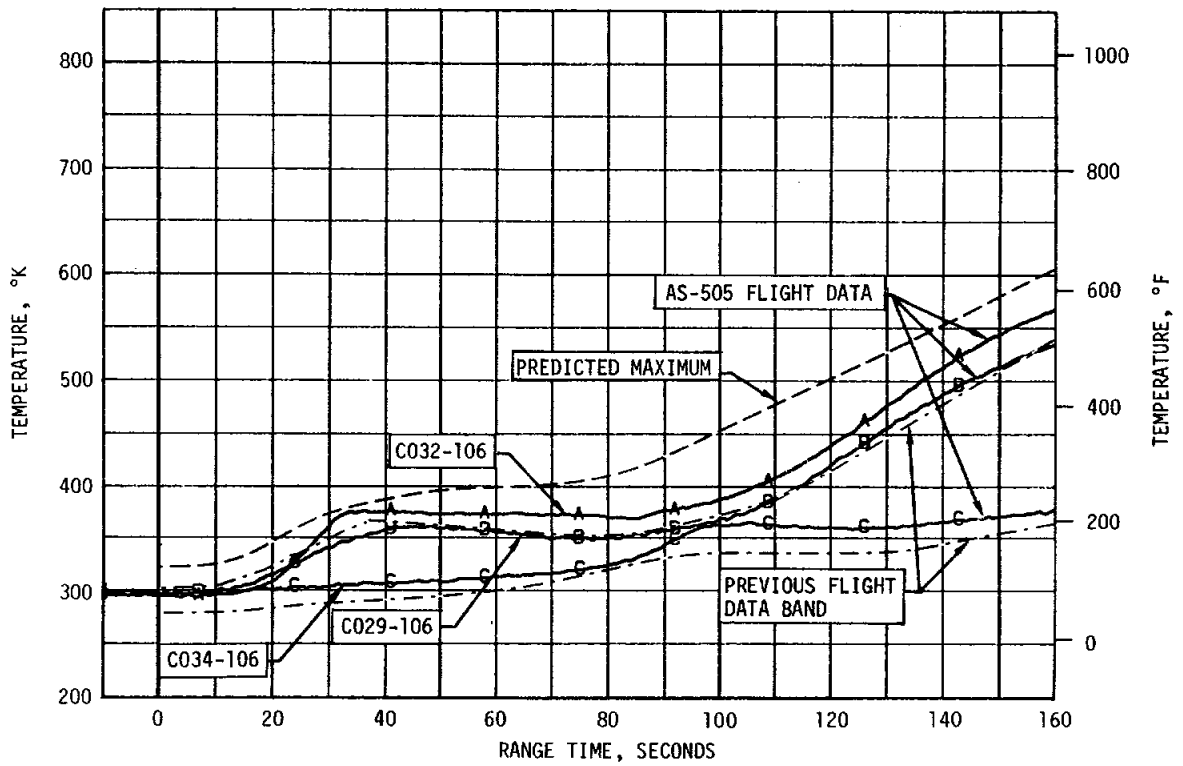
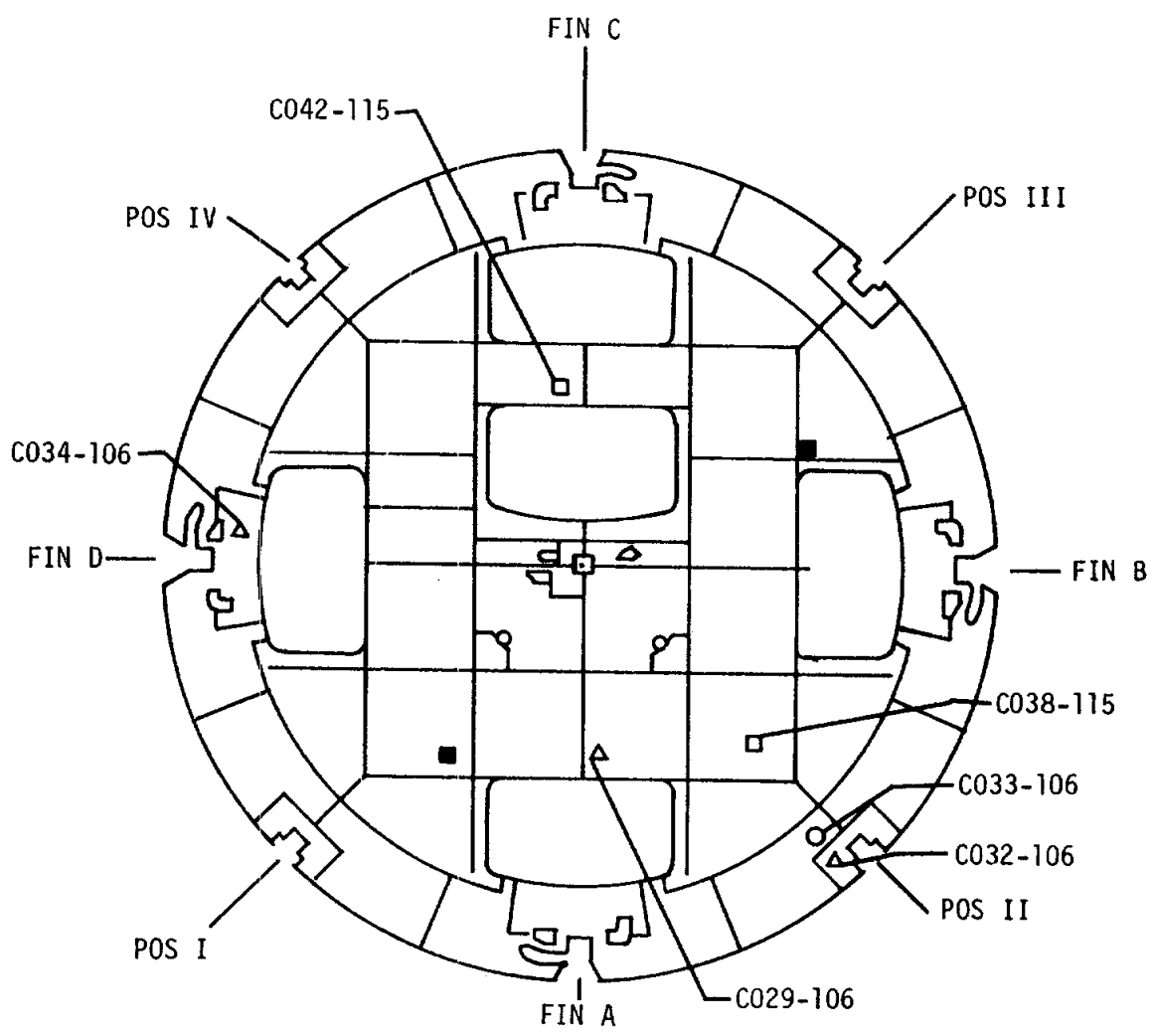


Figure 17-4. S-IC Heat Shield Bondline Temperature



LOCATION

CODE

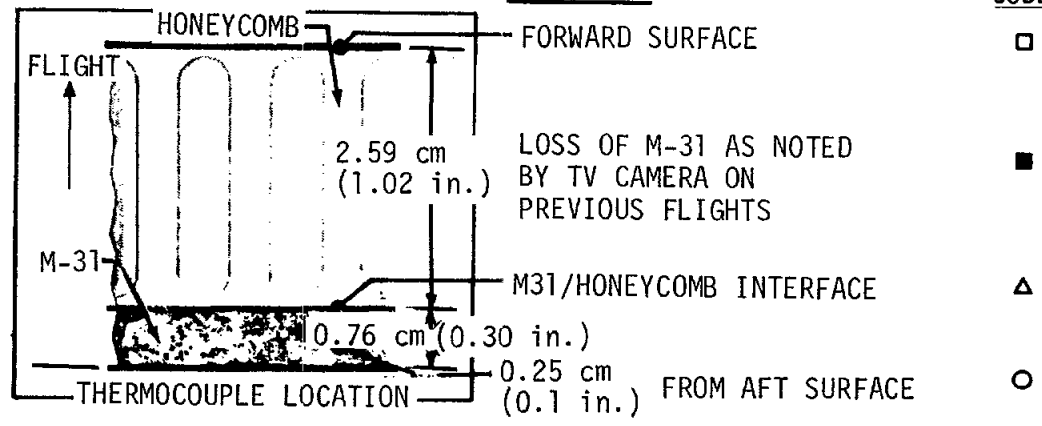


Figure 17-5. S-IC Base Heat Shield Measurement Locations

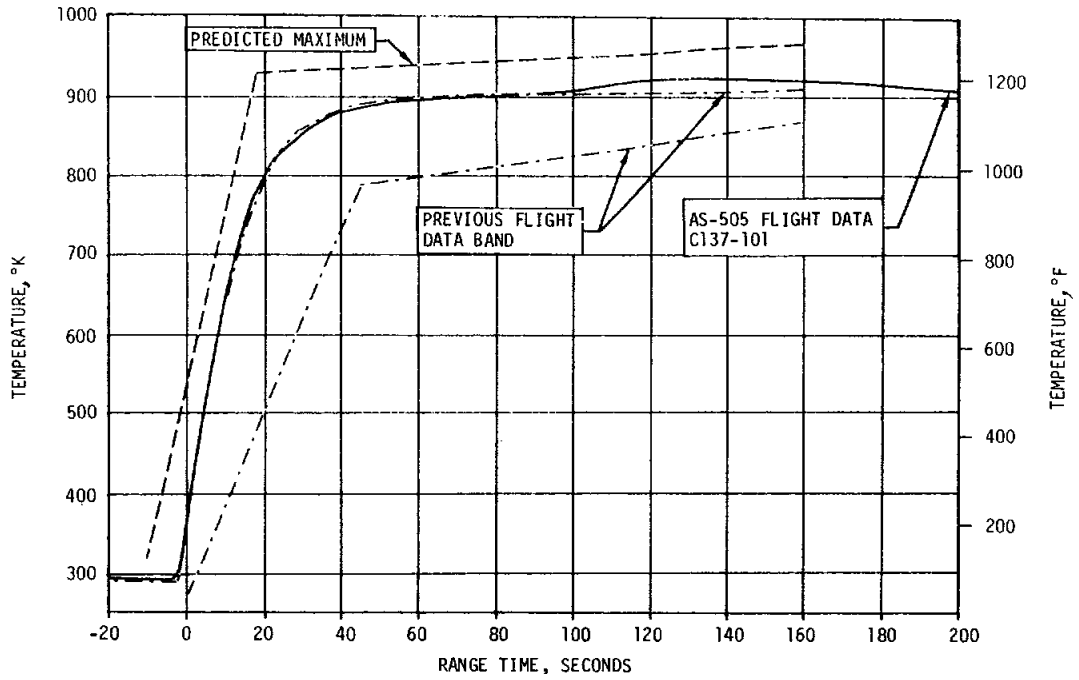


Figure 17-6. S-IC Temperature Under Insulation, Inboard Side Engine No. 1

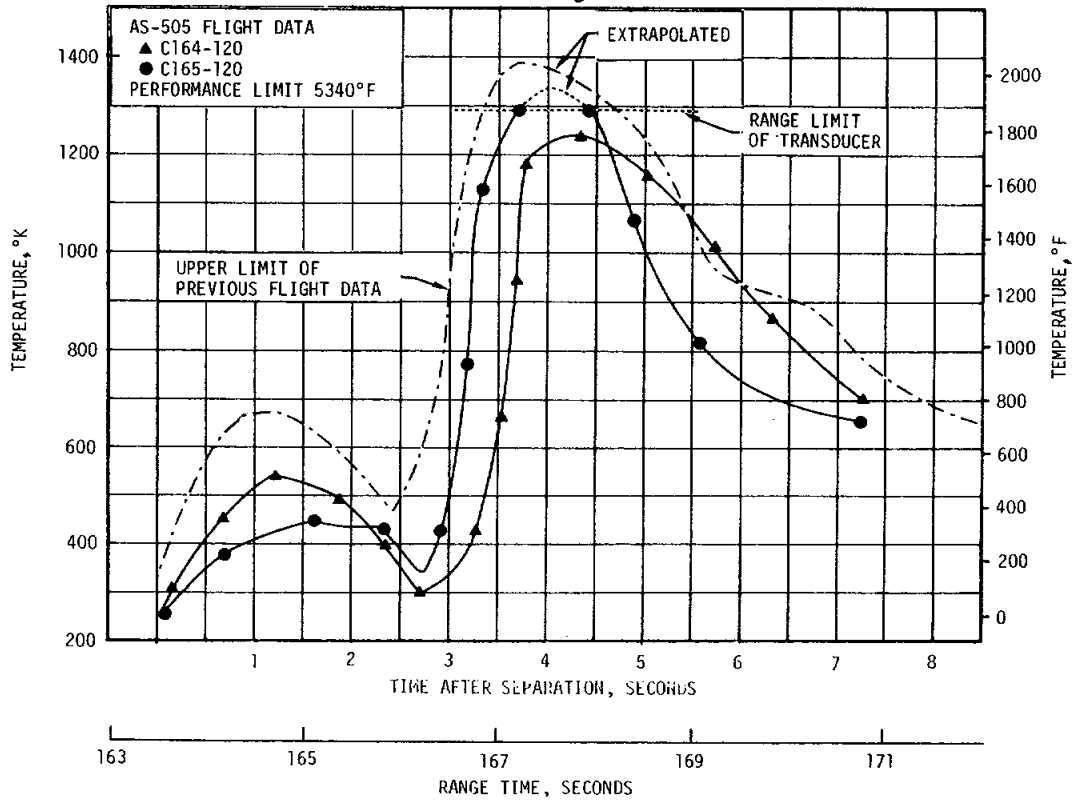


Figure 17-7. S-IC Forward Skirt Compartment Ambient Air Temperature During S-IC/S-II Stage Separation

thrust cone heating rates and aft face temperatures are presented in Figures 17-8 through 17-11, along with previous flight data and post-flight predictions. The predicted effects of CECO on the heat shield heating rates were determined from four- and five-engine 1/25 scale S-II stage model test results; other predictions were accomplished by the same analytical methods described in previous flight evaluation reports.

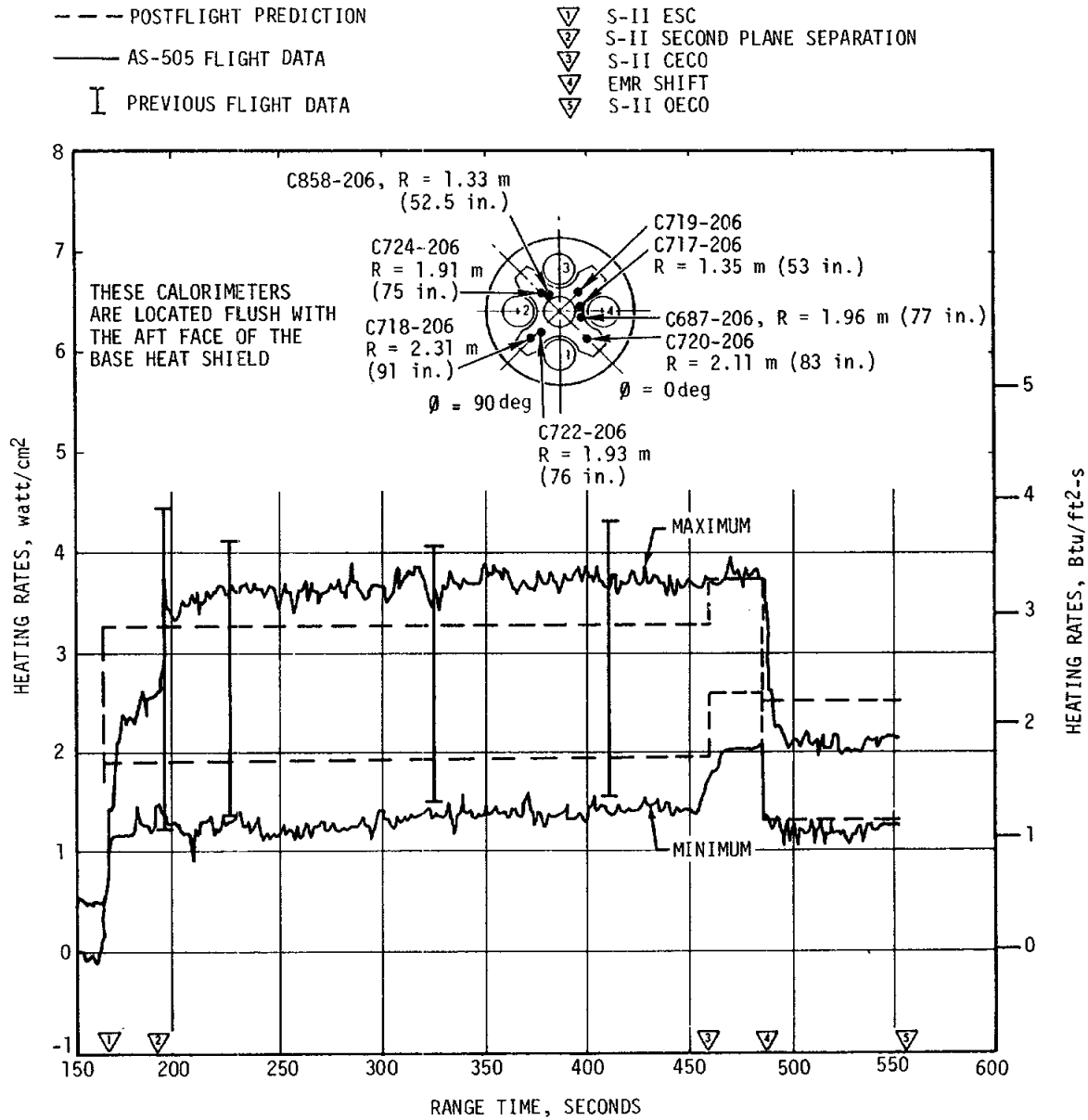


Figure 17-8. S-II Heat Shield Base Region Heating Rates

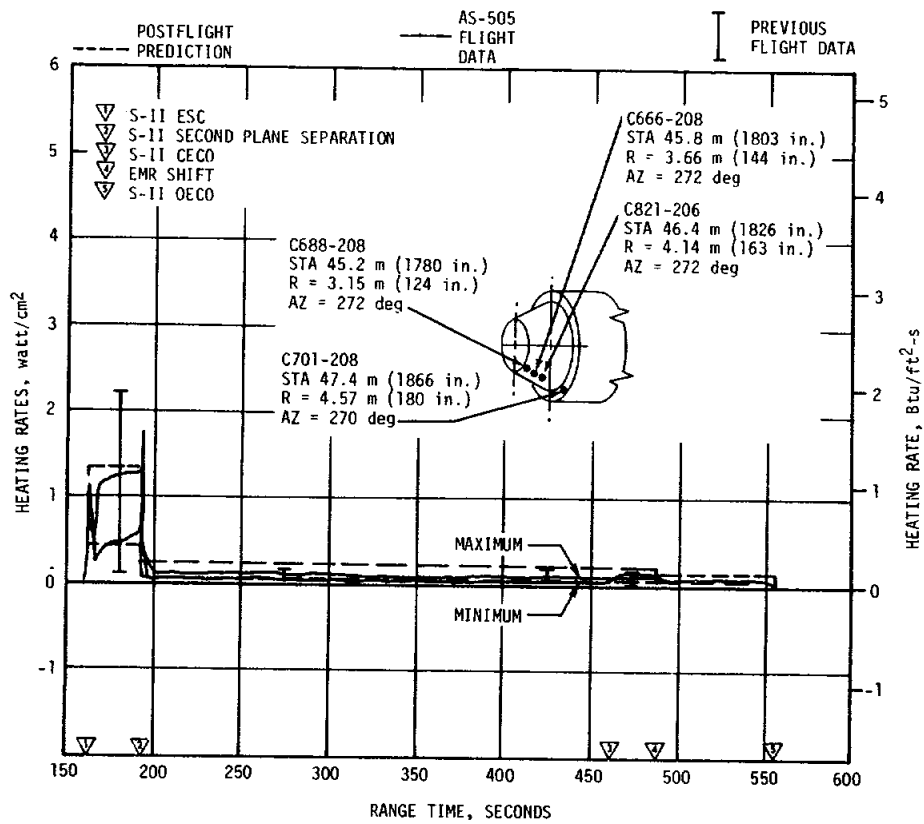


Figure 17-9. S-II Thrust Cone Heating Rates

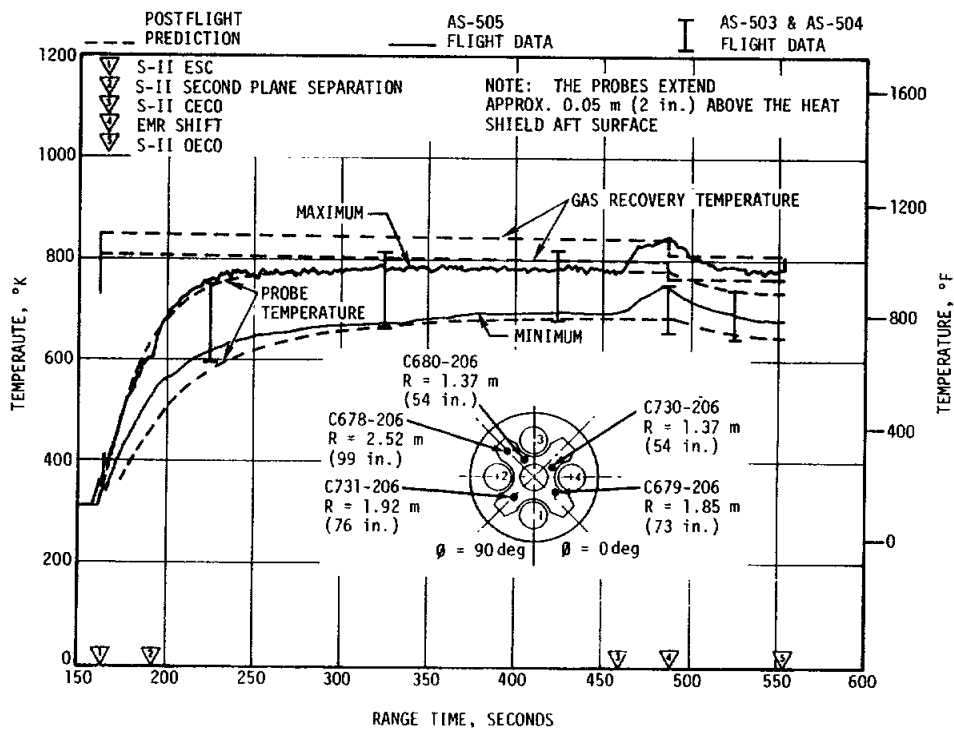





Figure 17-10. S-II Base Gas Temperatures

THESE SURFACE TEMPERATURE MEASUREMENTS ARE LOCATED FLUSH WITH THE AFT FACE OF THE HEAT SHIELD

-  DESIGN PREDICTION
-  PAST FLIGHT DATA
-  AS-505 FLIGHT DATA

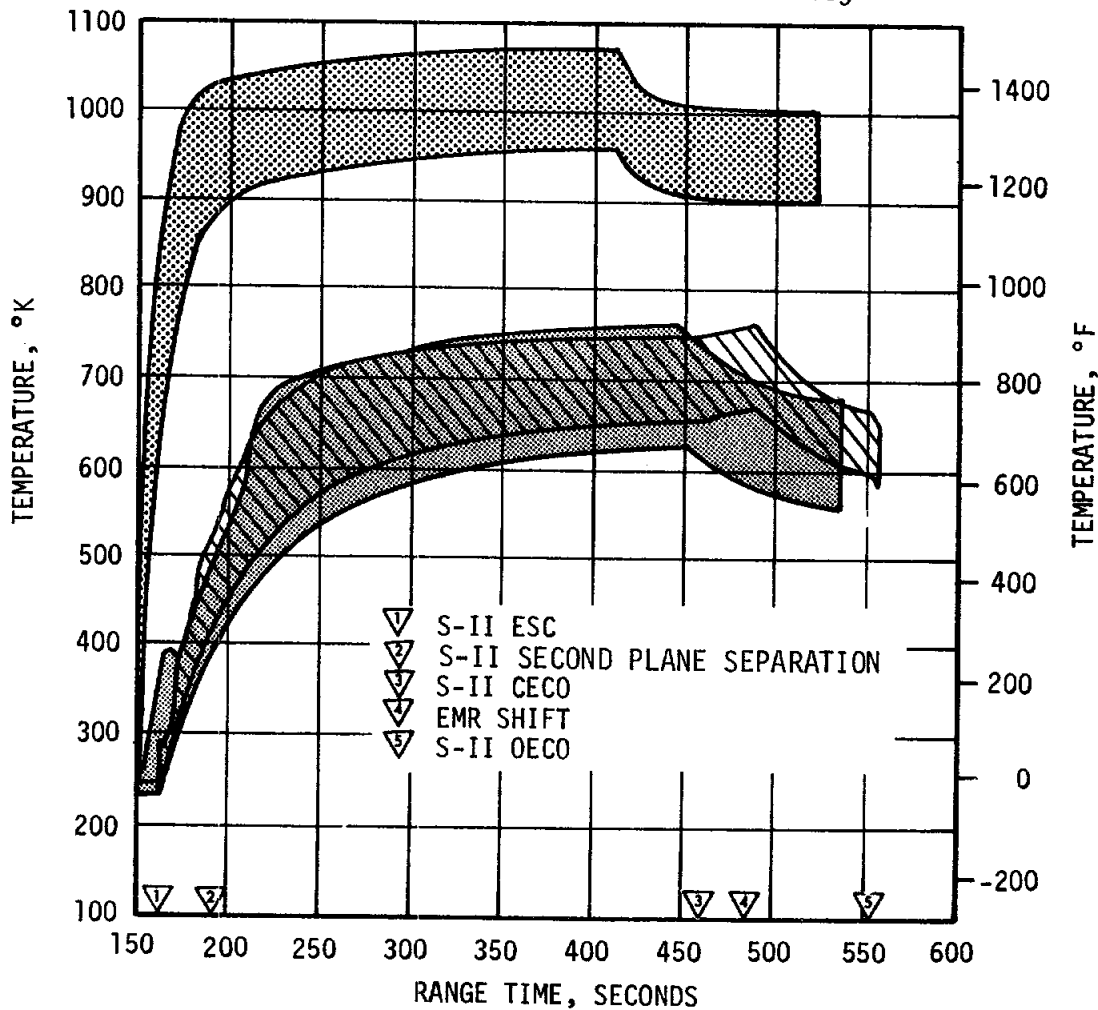
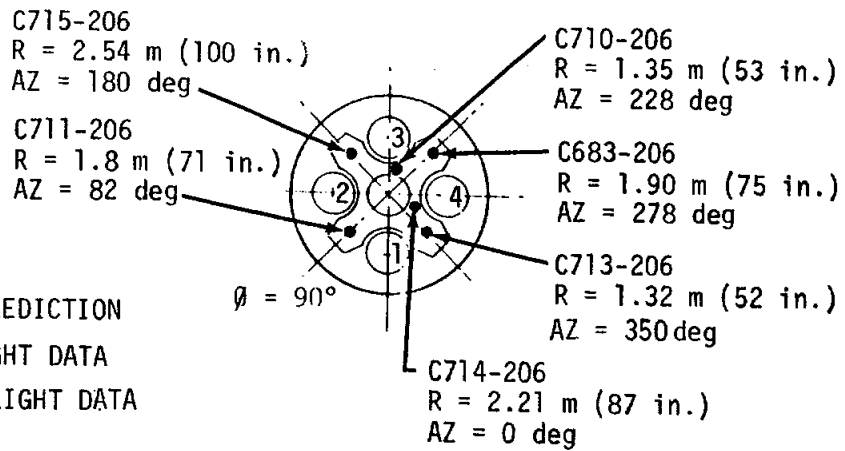


Figure 17-11. S-II Heat Shield Aft Face Temperatures

As expected, an increase in the base region environment after CECO was noted, except for the heat shield maximum heating rates. After CECO these heating rates continued at approximately the same level of magnitude until engine mixture ratio shift and did not experience the predicted increase as shown in Figure 17-8. At the lower heating levels, an increase in total heating rate of approximately 0.6 watt/cm^2 ($0.5 \text{ Btu/ft}^2\text{-s}$) was observed, consistent with the predicted values. Thrust cone heating rates, shown in Figure 17-9; base gas temperatures, shown in Figure 17-10, and heat shield aft face temperatures shown in Figure 17-11, exhibited slight increases after CECO.

17.4 VEHICLE AEROHEATING THERMAL ENVIRONMENT

17.4.1 S-IC Stage Aeroheating Environment

Aerodynamic heating environments were measured with thermocouples attached internally to the structural skin on the S-IC forward skirt and intertank. Generally, the aerodynamic heating environments were higher than for the AS-504 flight but were below design limits.

Measured skin temperatures and derived heating rates for the S-IC intertank are shown in Figure 17-12. Postflight simulations of skin temperatures and heating rates are also presented. These simulations are based on analytically determined heat transfer coefficients and recovery temperatures until flow separation reaches the intertank. During the period of flow separation, a radiation heating environment, determined from previous flight data (AS-502 and AS-503), is used in the simulation. Good correlation was obtained between the flight data and the simulations.

The S-IC forward skirt skin temperatures and derived heating rates are presented in Figure 17-13. The AS-505 S-IC forward skirt skin temperatures and derived heating rates were higher than recorded on AS-504. The S-IC forward skirt was uninsulated on both AS-504 and AS-505.

Flow separation on the AS-505 flight, according to ALOTS data, occurred at approximately 116 seconds. The forward point of flow separation versus flight time is plotted in Figure 17-14. The effects of CECO on the separated flow region during AS-505 flight were the same as observed on AS-503 and AS-504. It should be noted that at higher altitudes, the measured location of the forward point of flow separation is questionable because of loss of resolution in the flight optical data.

LOX tank skin temperatures were well below the predicted maximum throughout flight, as shown in Figure 17-15. There was a noticeable measurement response when the LOX level passed corresponding thermocouples.

Fuel tank skin temperatures exceeded the predicted maximum during the early portion of flight, as shown in Figure 17-16. The higher initial temperatures are attributed to higher ambient temperature and wind velocity at liftoff. These temperatures were within design limits.

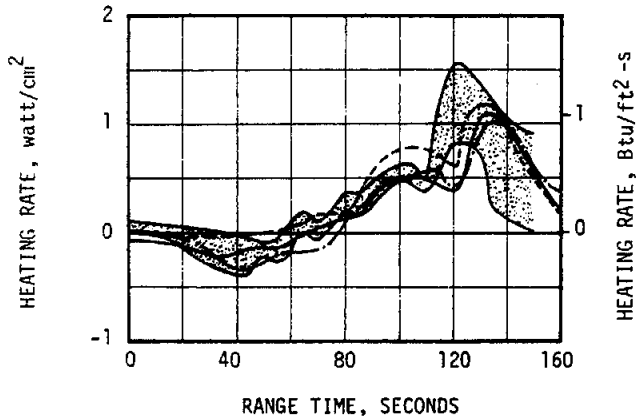
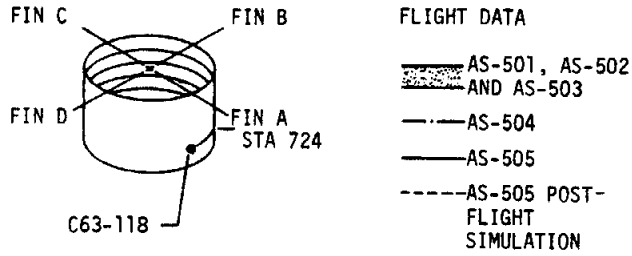
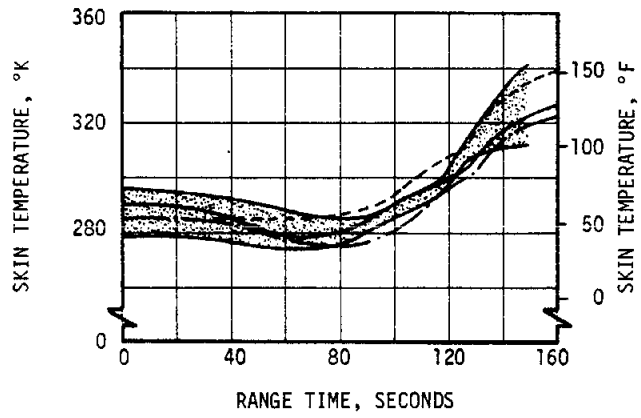


Figure 17-12. S-IC Intertank Aerodynamic Heating

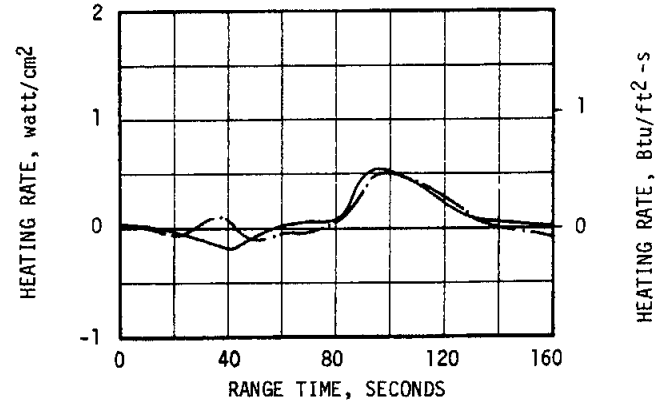
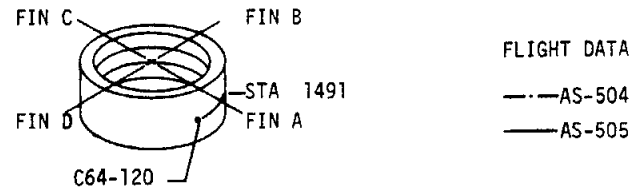
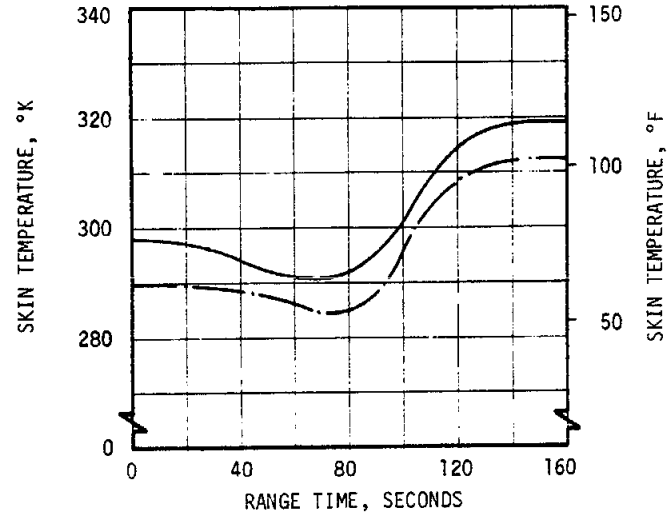


Figure 17-13. S-IC Forward Skirt Aerodynamic Heating

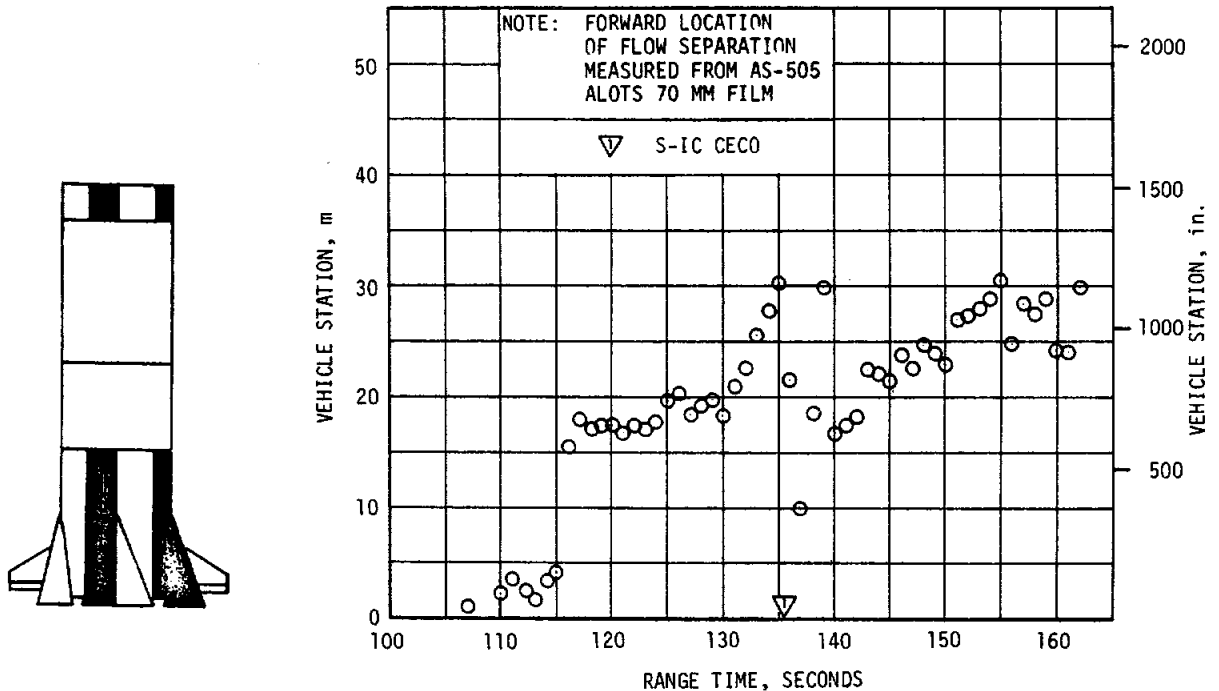


Figure 17-14. Forward Location of Separated Flow

Intertank skin temperatures exceeded the predicted maximum during the early portion of flight, as shown in Figure 17-17. This condition was due to the higher ambient temperature and wind velocity at liftoff.

The forward skirt skin temperatures were slightly higher than on AS-504 and were considerably higher than the first three flights, which had insulation on the forward skirt of the S-IC stage, as shown in Figure 17-18. However, temperatures reached a maximum of 319°K (115°F) at the end of the flight which was well below the predicted maximum.

17.4.2 S-II Stage Aeroheating Environment

S-II stage aeroheating data were in good agreement with previous flight data and postflight predictions and were within design limits. Measured heating rates for the aft interstage, ullage motor fairing, LH₂ aft and forward feedline fairings, forward skirt and systems tunnel forward fairing are shown in Figures 17-19 through 17-24.

Flight data from measurement C863-200, located on the forward fairing of ullage motor No. 6, are lower than data from C861-200 at a similar location on the forward fairing of ullage motor No. 4 and the predicted heat rates, as shown in Figure 17-20. Ullage motor No. 6 is located in the vicinity of the LOX vent valve. Cold gases from the LOX vent valve in the form of either a cooled boundary layer or allowable leakage from the vent valves, or a combination of both, could be flowing over the calorimeter

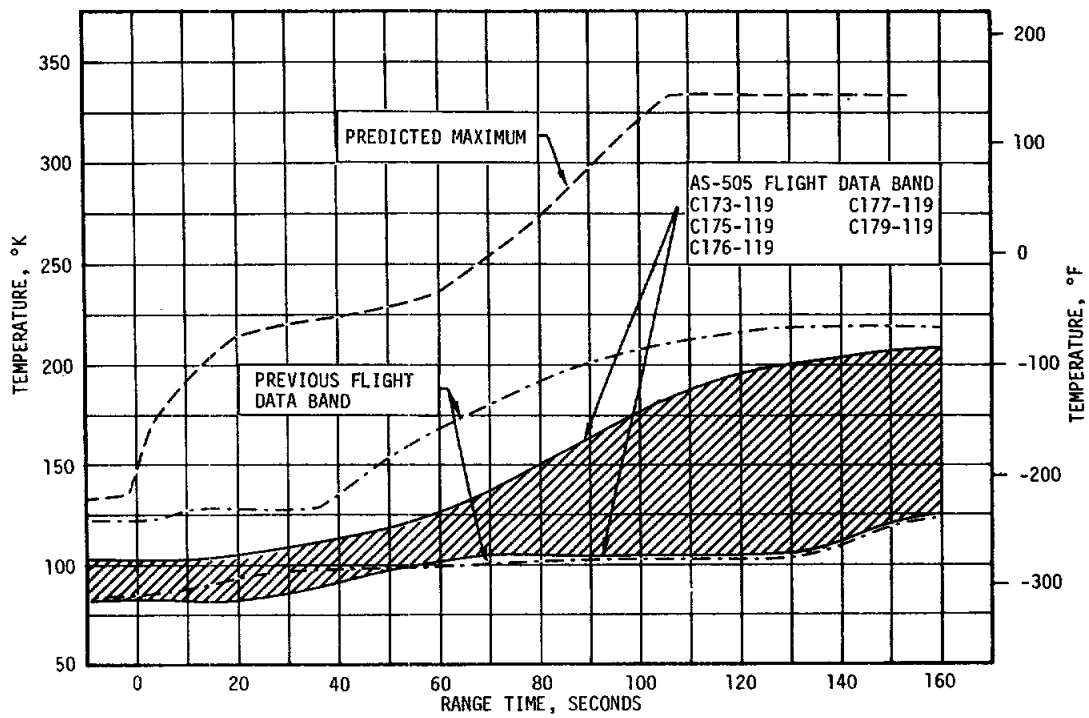


Figure 17-15. S-IC LOX Tank Skin Temperature

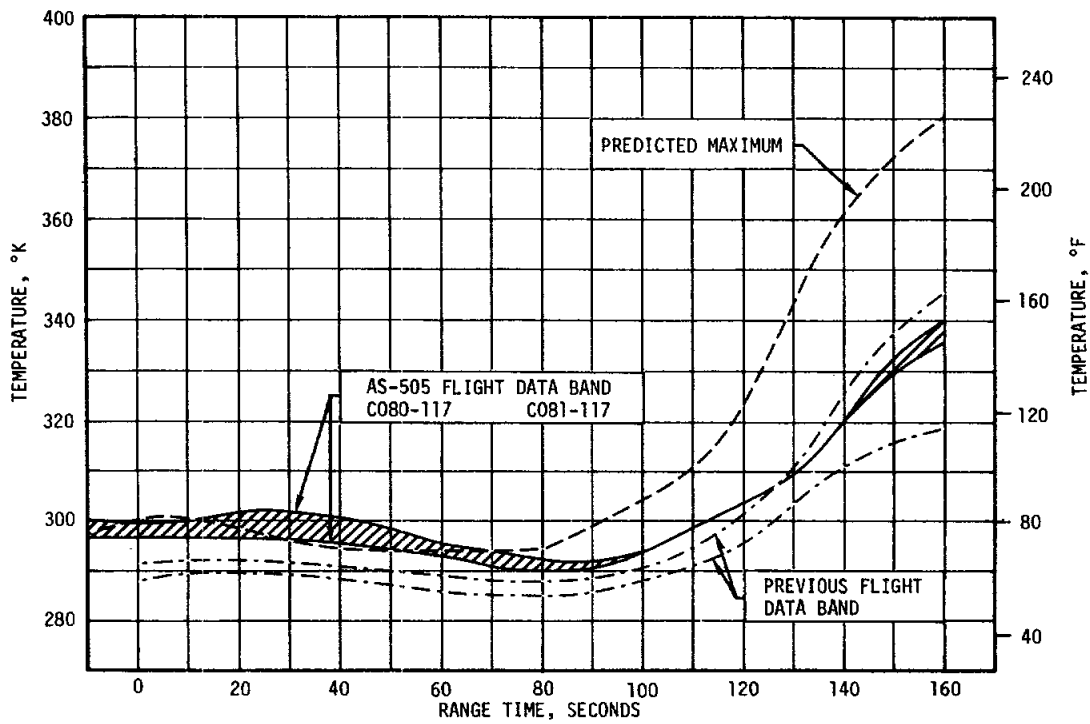


Figure 17-16. S-IC Fuel Tank Skin Temperature

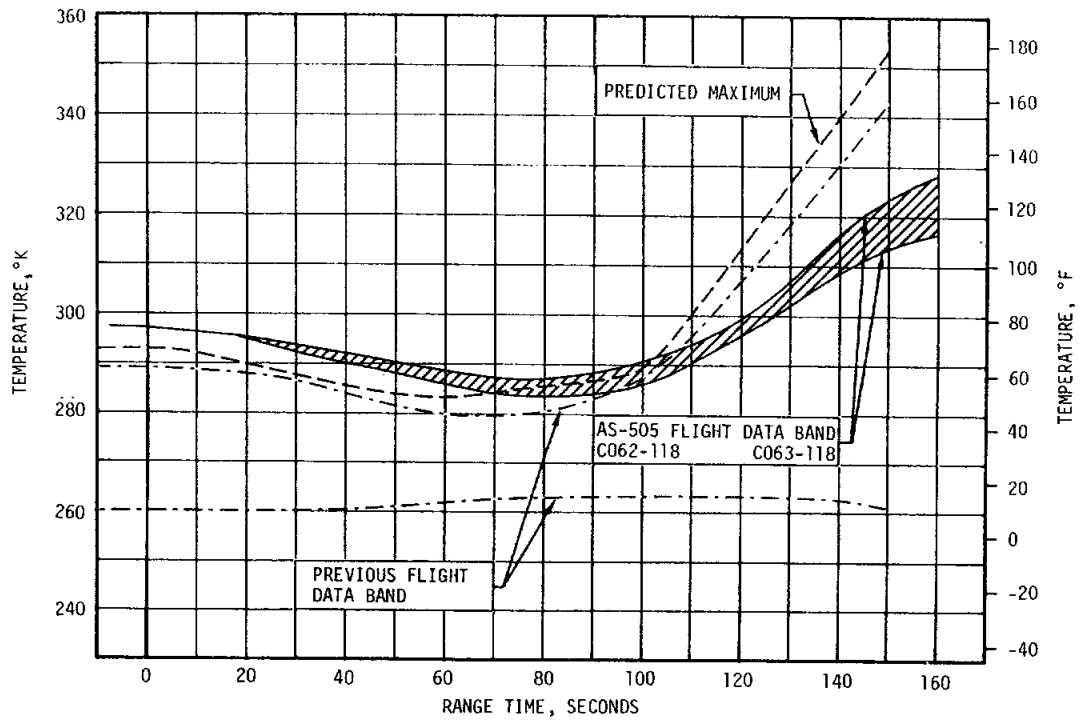


Figure 17-17. S-IC Intertank Skin Temperatures

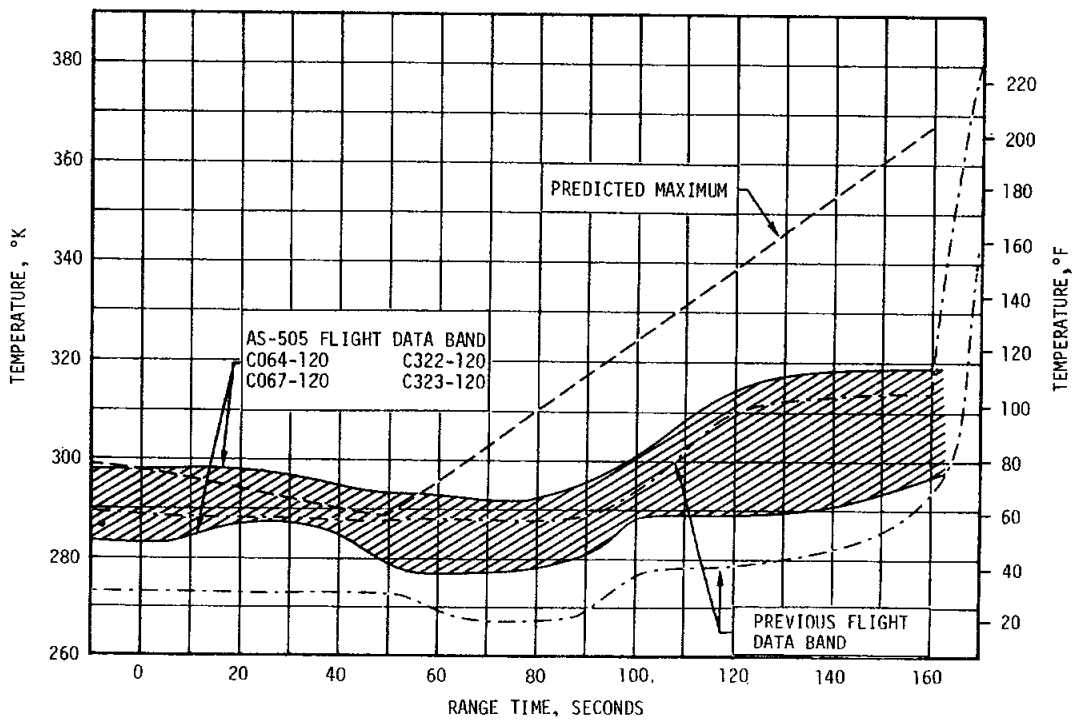


Figure 17-18. S-IC Forward Skirt Skin Temperature

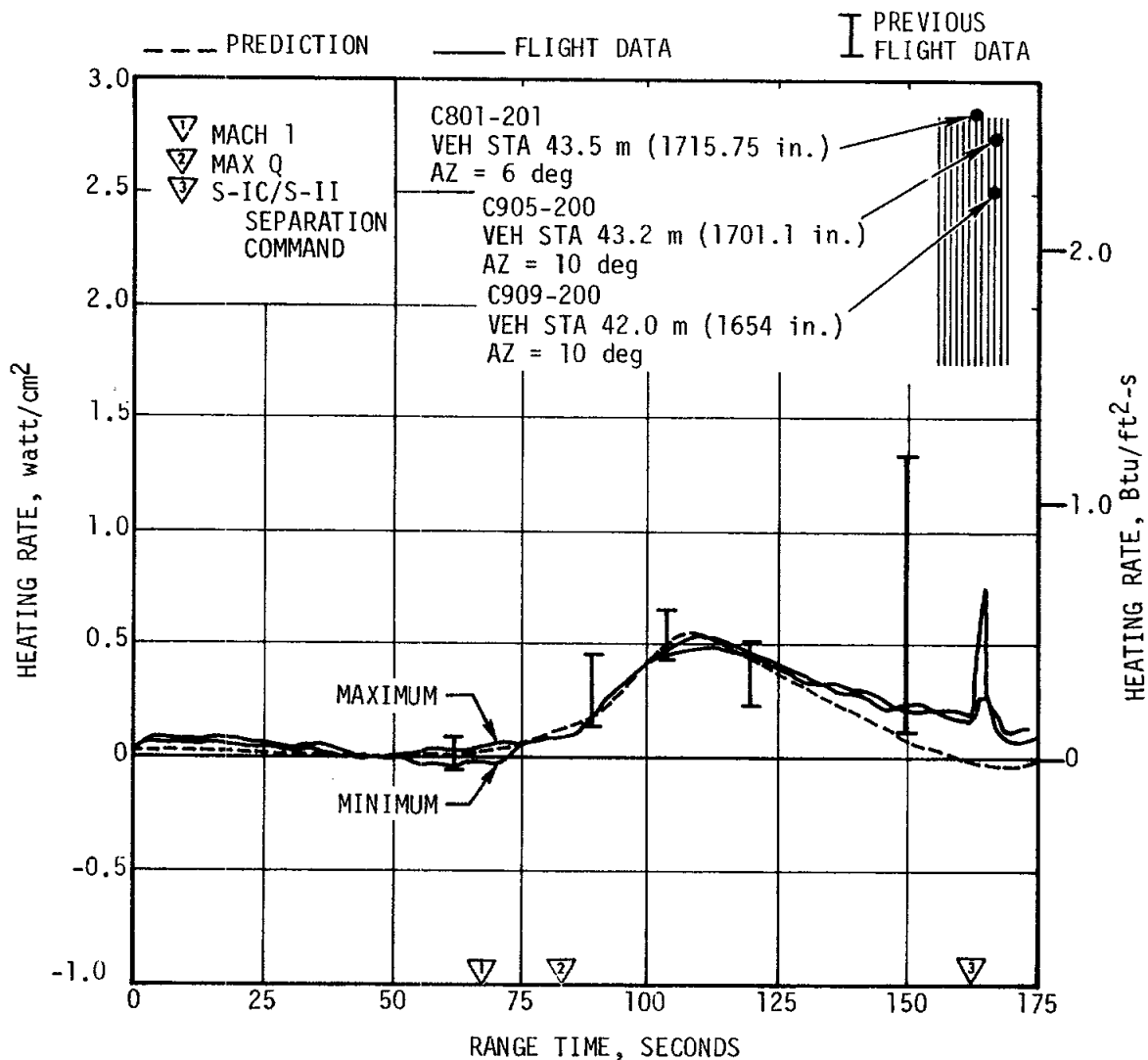


Figure 17-19. S-II Aft Interstage Aeroheating Environment

disk and thus indicating a reduced heating rate. The data from C861-200 are higher than the predictions during the period of 105 to 125 seconds; this difference is presently under investigation.

Lower than expected heating rates were recorded by calorimeter C846-218 on the LH₂ aft feedline fairing. This condition is possibly a result of cool gases from within the fairing being driven out of the aft joggle due to rapidly decreasing pressure outside the fairing.

At range times greater than 135 seconds, flight data from measurements C801-201, C905-200, and C909-200, shown in Figure 17-19; C846-218 and C847-218, shown in Figure 17-21; and measurement C811-216, shown in Figure

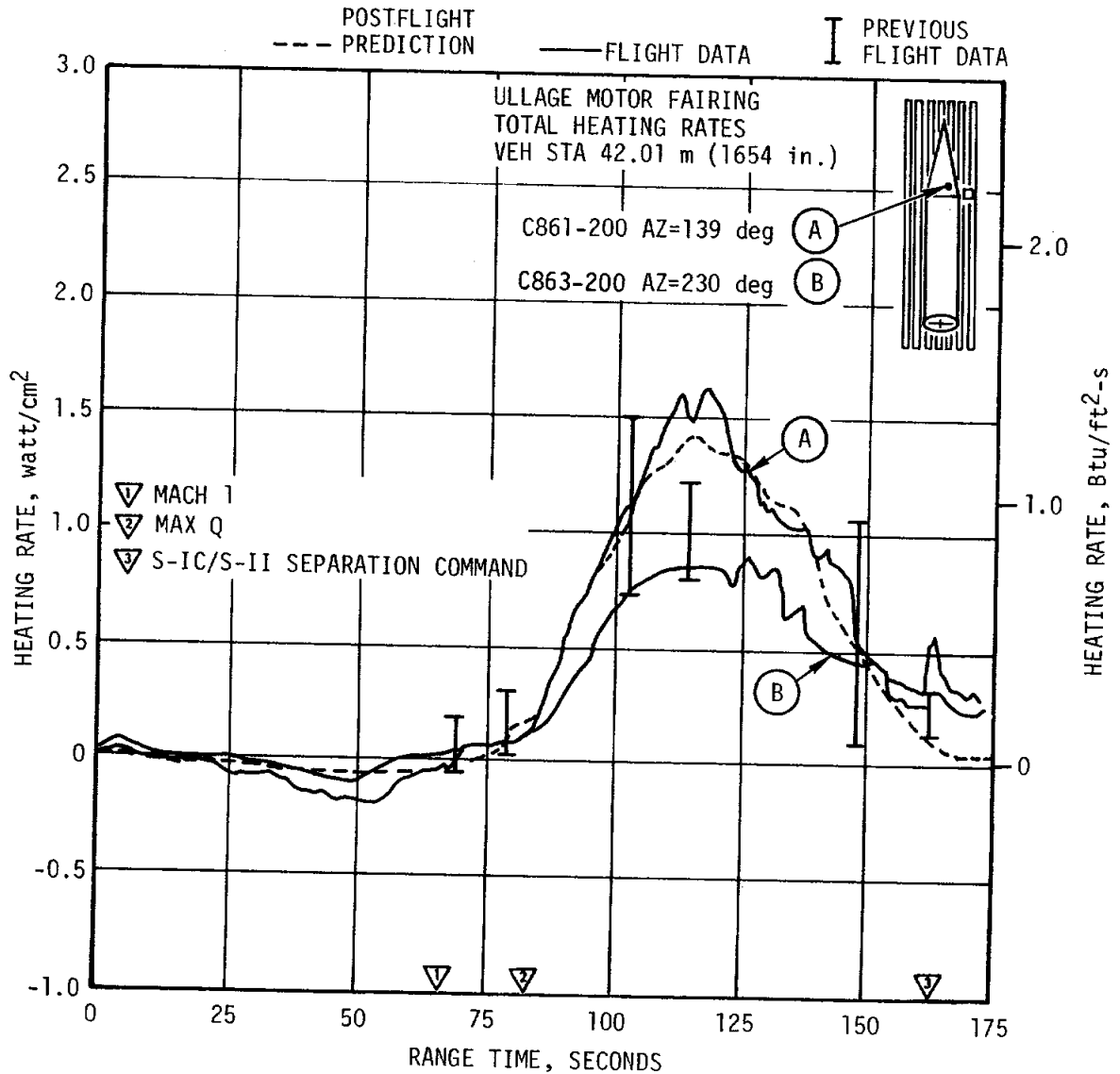


Figure 17-20. S-II Aft Interstage Aeroheating Environment, Ullage Motor Fairing

17-24 are higher than predicted. At the higher altitude, F-1 engine exhaust gases are drawn forward along the vehicle surface into the low pressure region created by the separation of the boundary layer. Radiation from this exhaust gas could cause the higher heating rates indicated by the calorimeters.

Additional measurements in the form of S-II stage structural, fairing, and insulation surface temperatures were made during the AS-505 flight. Data from these measurements (not shown in the figures) agree well with previous flight data and postflight predictions and were within design limits.

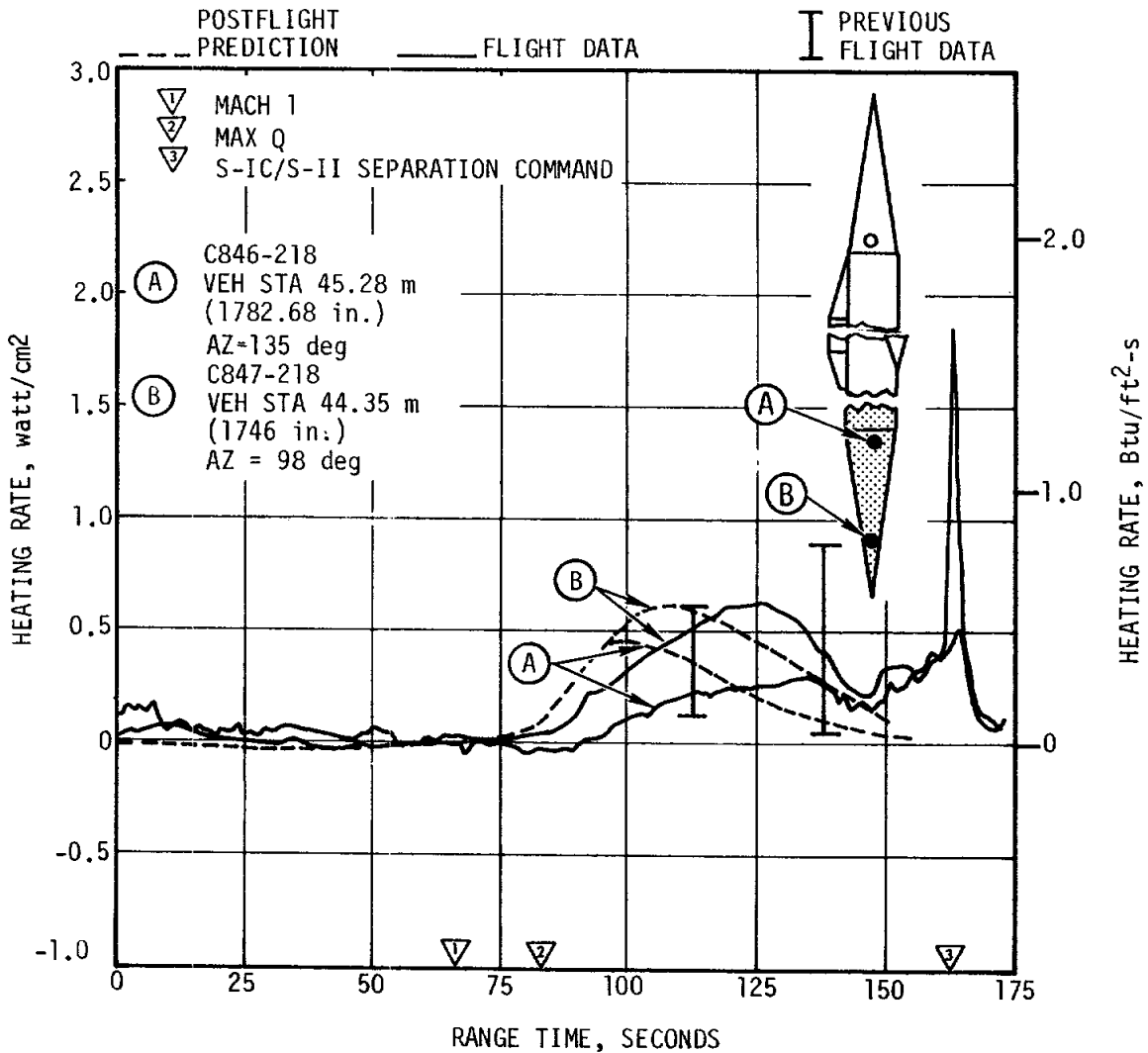


Figure 17-21. S-II Aft Interstage Aeroheating Environment, LH₂ Feedline Aft Fairing

17.4.3 S-IVB Stage Aeroheating Environment

The mission profile of the AS-505 flight produced nominal thermal environments for the S-IVB stage components and structure. The thermal severity of the AS-505 boost trajectory was comparable to that of AS-504, AS-503, and AS-501, and cooler than that of AS-502 and the thermal design trajectory. There was no instrumentation from which structural temperatures could be obtained; however, since the thermal severity of AS-505 was less than that for the design trajectory, the S-IVB stage structural temperatures should be within the design limits for the boost phase.

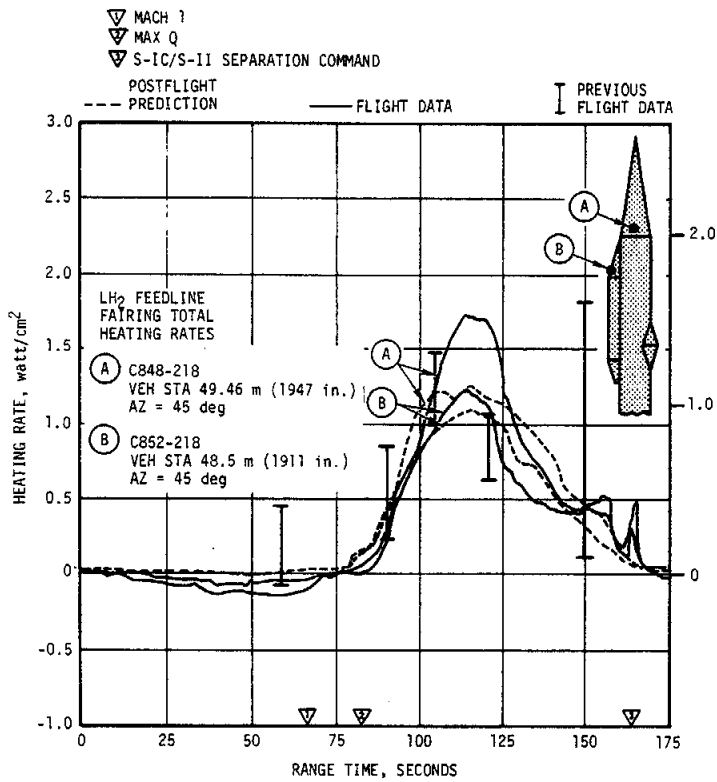


Figure 17-22. S-II Body Aeroheating Environment, LH₂ Feedline Forward Fairing

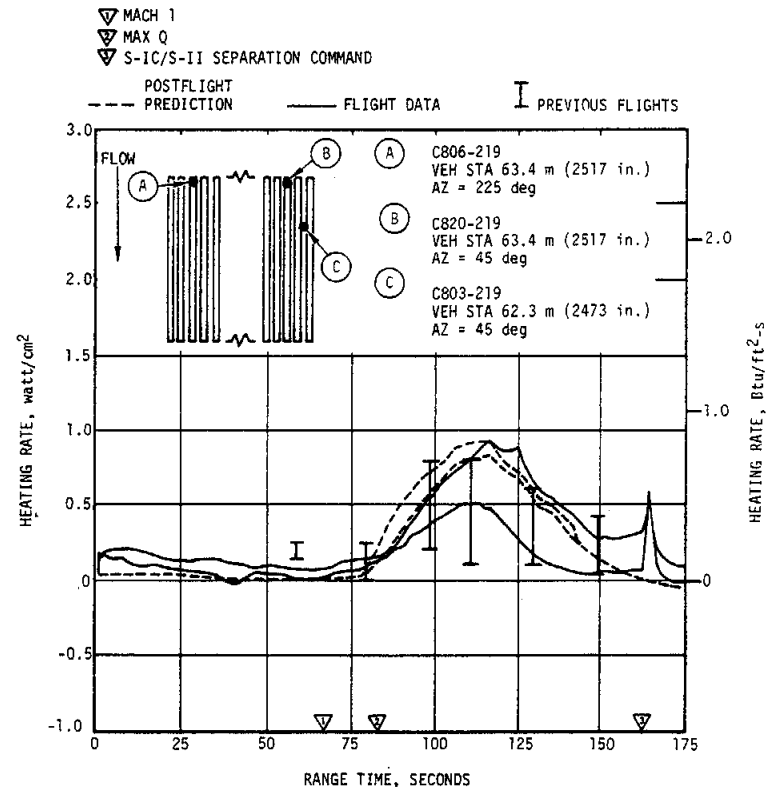


Figure 17-23. S-II Body Aeroheating Environment, Forward Skirt

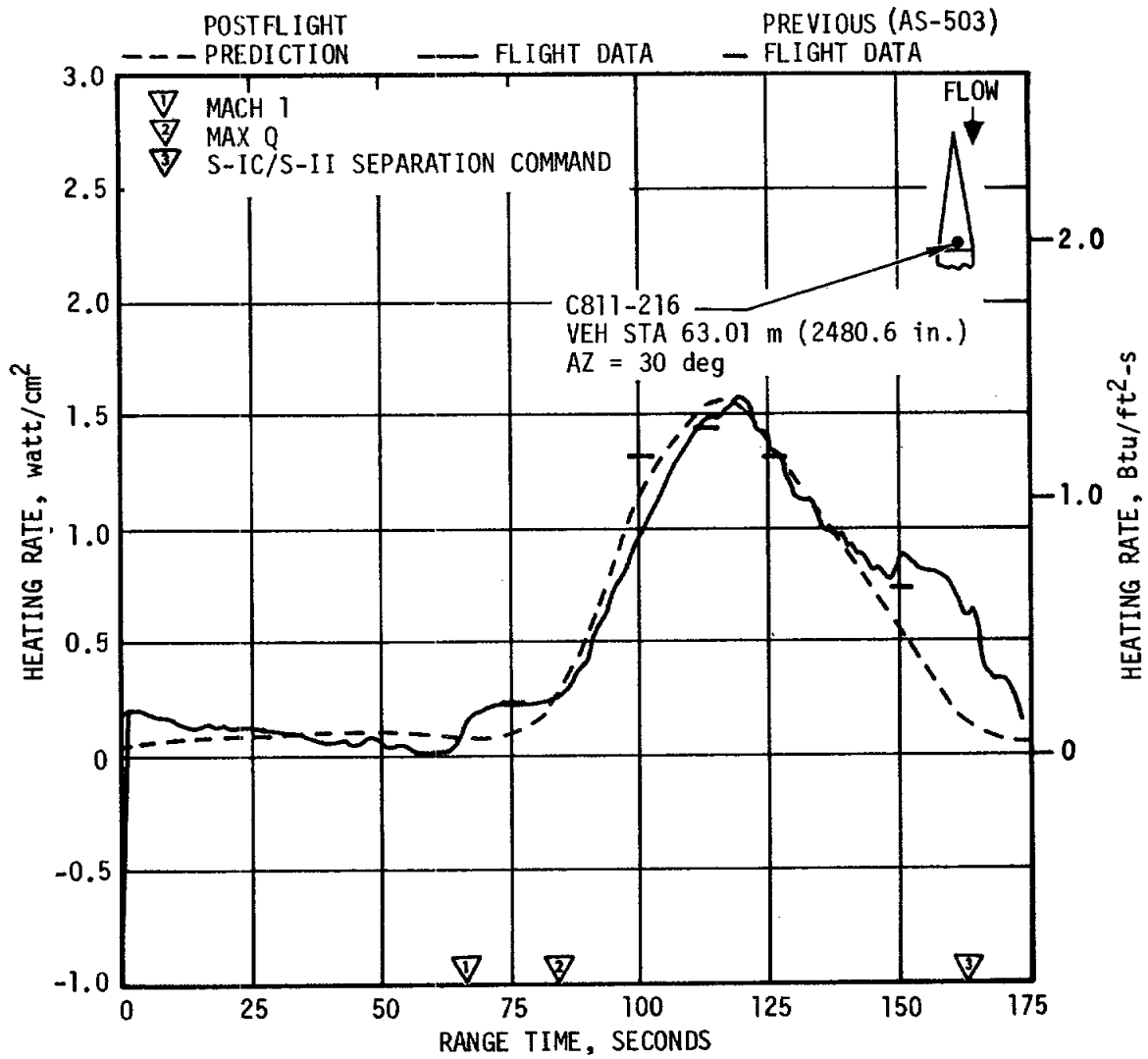


Figure 17-24. S-II Body Aeroheating Environment, Systems Tunnel Forward Fairing

SECTION 18

ENVIRONMENTAL CONTROL SYSTEM

18.1 SUMMARY

The S-IC canister conditioning system and the aft environmental conditioning system performed satisfactorily during the AS-505 countdown.

The S-II thermal control and compartment conditioning system maintained temperatures within the design limits throughout the prelaunch operations.

Available data show that the Instrument Unit (IU) Environmental Control System (ECS) performed satisfactorily. The IU environmental conditioning purge duct exhibited a pressure loss and flow increase during prelaunch operations but IU performance was unaffected.

18.2 S-IC ENVIRONMENTAL CONTROL

The ambient temperatures of the 10 canisters in the S-IC forward skirt compartment must be maintained at $299.8 \pm 11.1^\circ\text{K}$ ($80 \pm 20^\circ\text{F}$); however, the canisters can operate at 324.8 to 277.6°K (125 to 40°F) for no more than a 10 minute period. No canister conditioning is required after S-IC forward umbilical disconnect.

The ambient temperatures within the canisters remained within the required limits during the countdown. Canister No. 1 recorded the lowest temperature, 289°K (60.5°F), during prelaunch. The lowest canister temperature measured in flight (Figure 18-1) was 259°K (6.5°F) in canister No. 2.

During J-2 engine chilldown prior to launch, the thermal environment is at the most critical point. Within this period the ambient temperature in the forward skirt compartment dropped, as shown in Figure 18-2. The lowest temperature, 185°K (-126.7°F) was recorded at instrument C207-120 which is located under a J-2 engine nozzle and received the maximum effect of the cold helium. All other ambient temperatures were above the 205.4°K (-90°F) design minimum. The band of ambient temperatures during flight (Figure 18-2) exceeded the predicted maximum but this did not cause a problem.

The design requirement for the aft compartment is that the prelaunch temperature be maintained at $299.7 \pm 8.3^\circ\text{K}$ ($80 \pm 15^\circ\text{F}$). Aft compartment temperatures are shown in Figure 18-3. Prior to LOX loading the aft compartment temperature was a maximum of 311°K (100.4°F). This is 3°K (5.4°F) above the maximum performance limit but did not cause a problem.

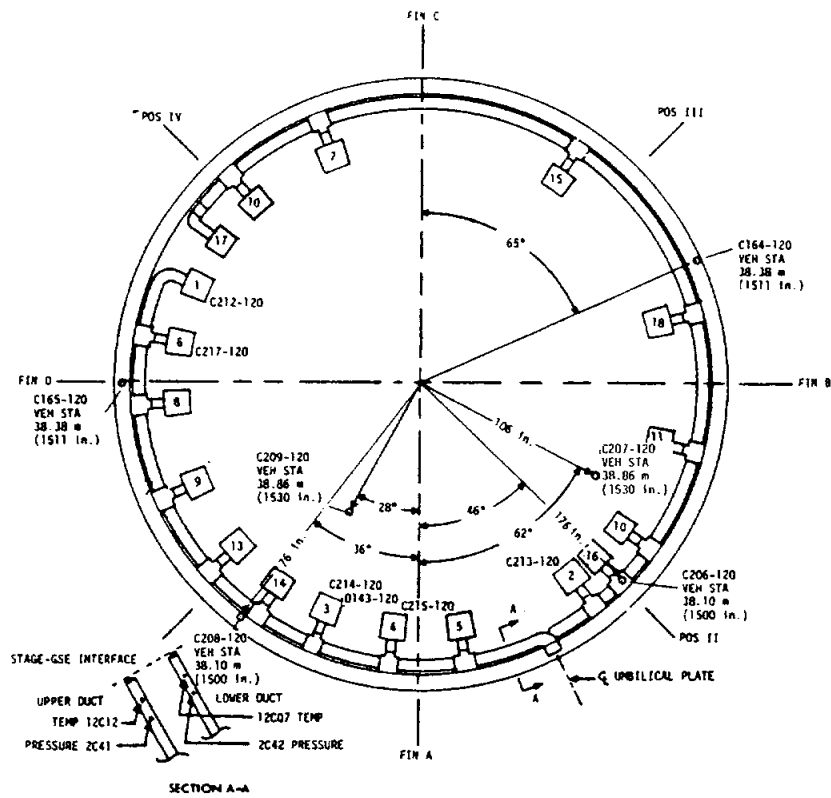
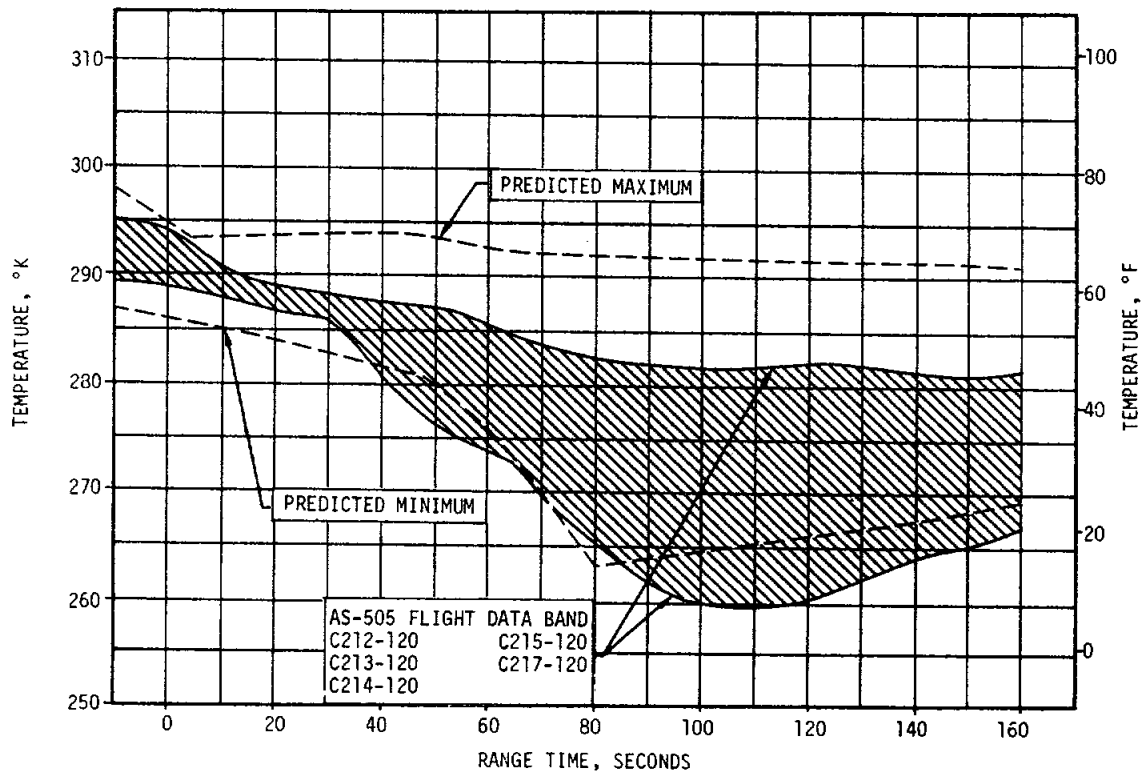


Figure 18-1. S-IC Forward Compartment Canister Temperature

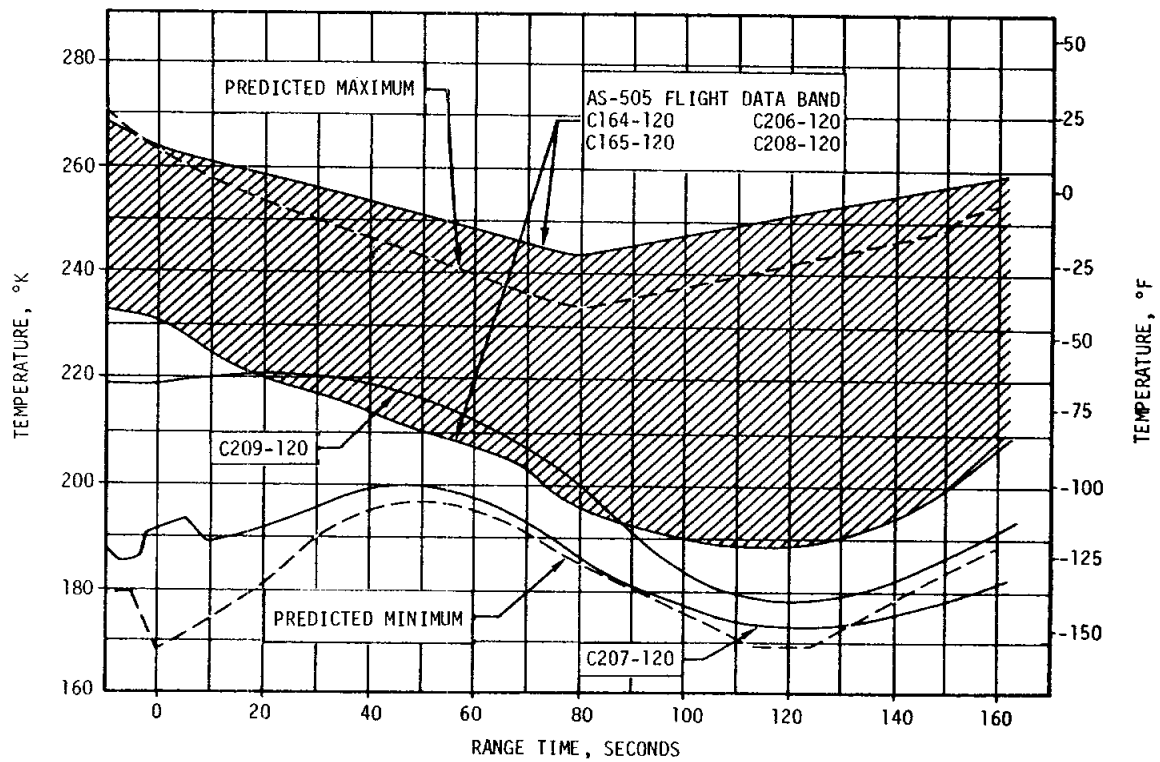
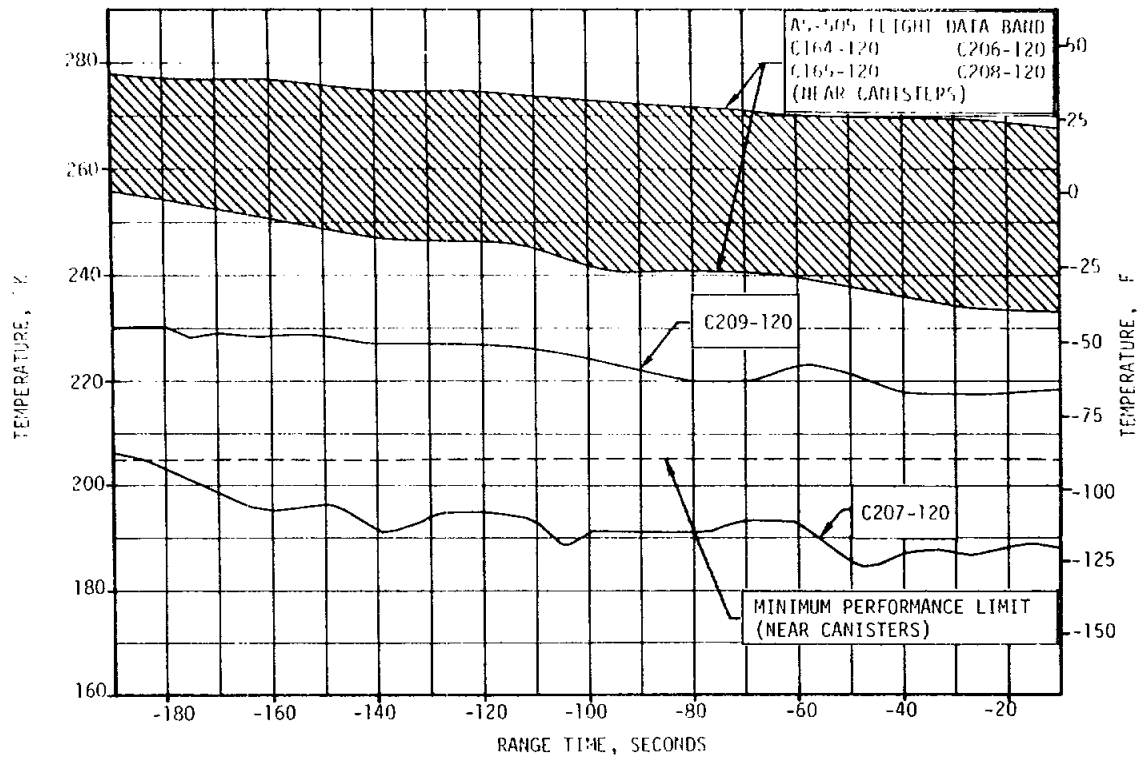


Figure 18-2. S-IC Forward Compartment Ambient Temperature

18-4

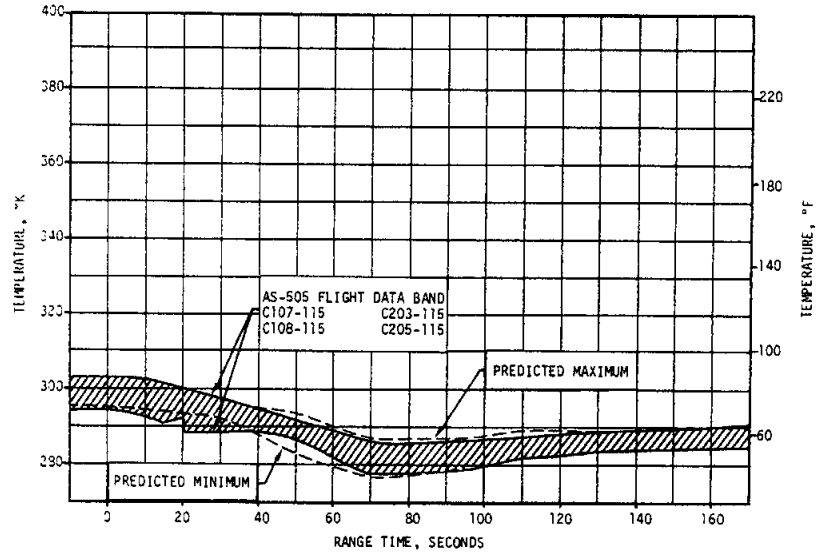
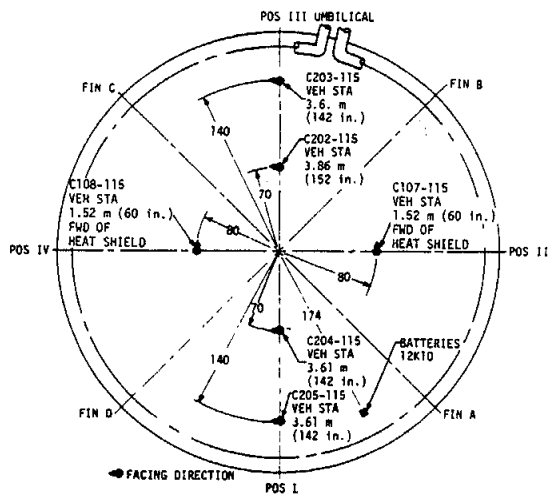
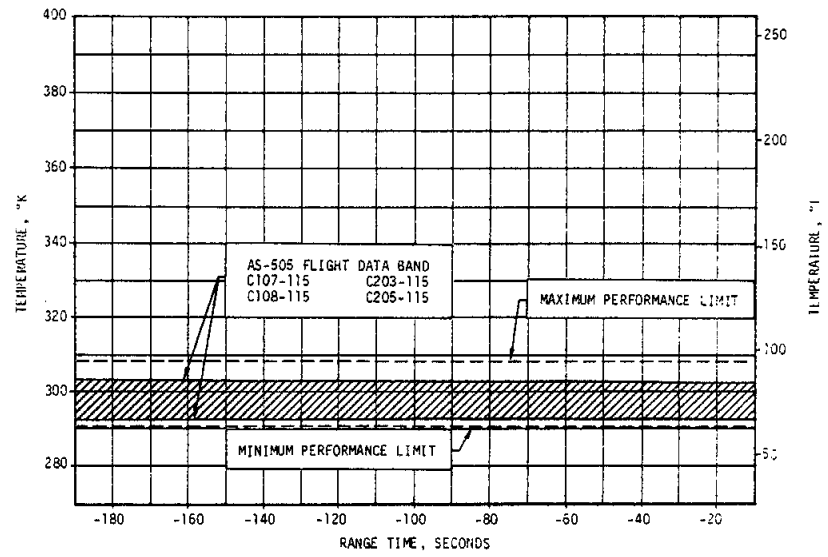
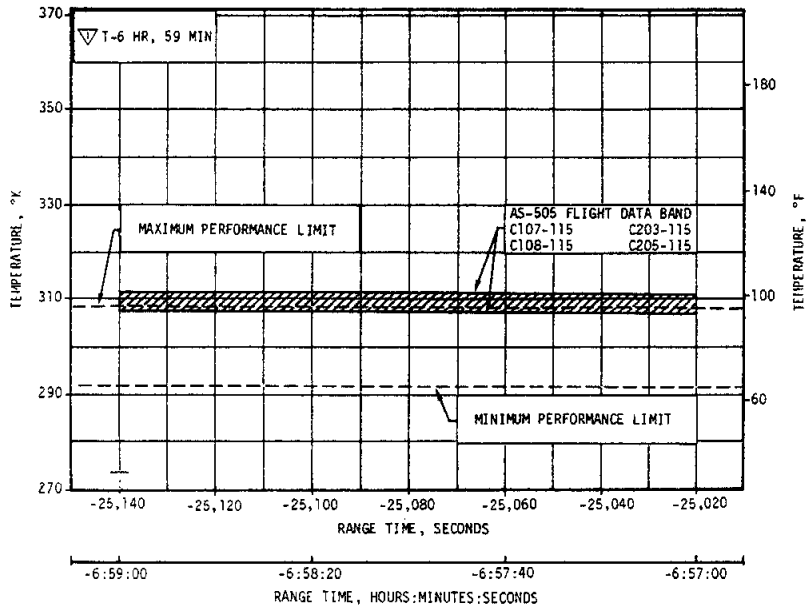


Figure 18-3. S-IC Aft Compartment Temperature Range

18.3 S-II ENVIRONMENTAL CONTROL

The S-II environmental control system performed satisfactorily throughout the launch countdown. All container temperatures in the forward thermal control system and the temperature of the one instrumented container in the aft system were essentially identical with previous vehicles. Ambient temperatures in the S-II/S-IC interstage were also similar to those of prior vehicles. No design temperatures were exceeded. There were no detectable indications (less than 0.04 percent) of oxygen or hydrogen in the interstage indicating that the purge maintained an inert atmosphere.

18.4 IU ENVIRONMENTAL CONTROL

The ECS is composed of a Thermal Conditioning System (TCS) and a Gas Bearing Supply System (GBS). The ECS maintained acceptable operating conditions for components mounted within the Instrument Unit (IU) and the S-IVB stage forward skirt during preflight and flight operations. The IU compartment temperature of 290.2 to 295.8°K (63 to 73°F) was maintained. However, a deviation associated with the preflight purge subsystem did occur during the terminal countdown operation.

The purge subsystem on IU-505 was modified to incorporate the Radio Isotope Thermo-Electrical Generator (RTG) purge ducting as seen in Figure 18-4. At approximately -9.8 hours, pressure measurement D68-603 decreased to zero while the purge inlet pressure at the swing arm decreased and the purge flow increased. This deviation occurred approximately 25 minutes after successful switchover of the purge medium from air to GN₂. Investigation through analysis and tests showed that the deviation occurred as a result of the separation of the IU purge duct at a connection in the vicinity of the umbilical door (see Figure 18-4). Evaluation of the suspect connections revealed that design deficiencies did exist.

Corrective action with effectivity IU 506 and subsequent, was taken by adding a second clamp at the umbilical door-purge duct "boot" connection and increasing the torque requirements on the three purge duct "boot" connection clamps from 0.678 to 0.904 N-m (6 to 8 lbf-in.) to 2.260 ±0.2260 N-m (20 ±2 lbf-in.). In addition, a torque reverification will be performed prior to both Countdown Demonstration Test (CDDT) and terminal countdown on these three clamps. Laboratory tests have shown that the corrective action will preclude any future occurrences of this deviation in the IU.

Recommendations for future action are as follows:

- a. Pursue elimination of torque verification requirement during CDDT and terminal count.
- b. Perform "long term" torque relaxation tests.
- c. Investigate redesign of "boot" connections.
- d. Institute stripping of duct wire at bead connections.

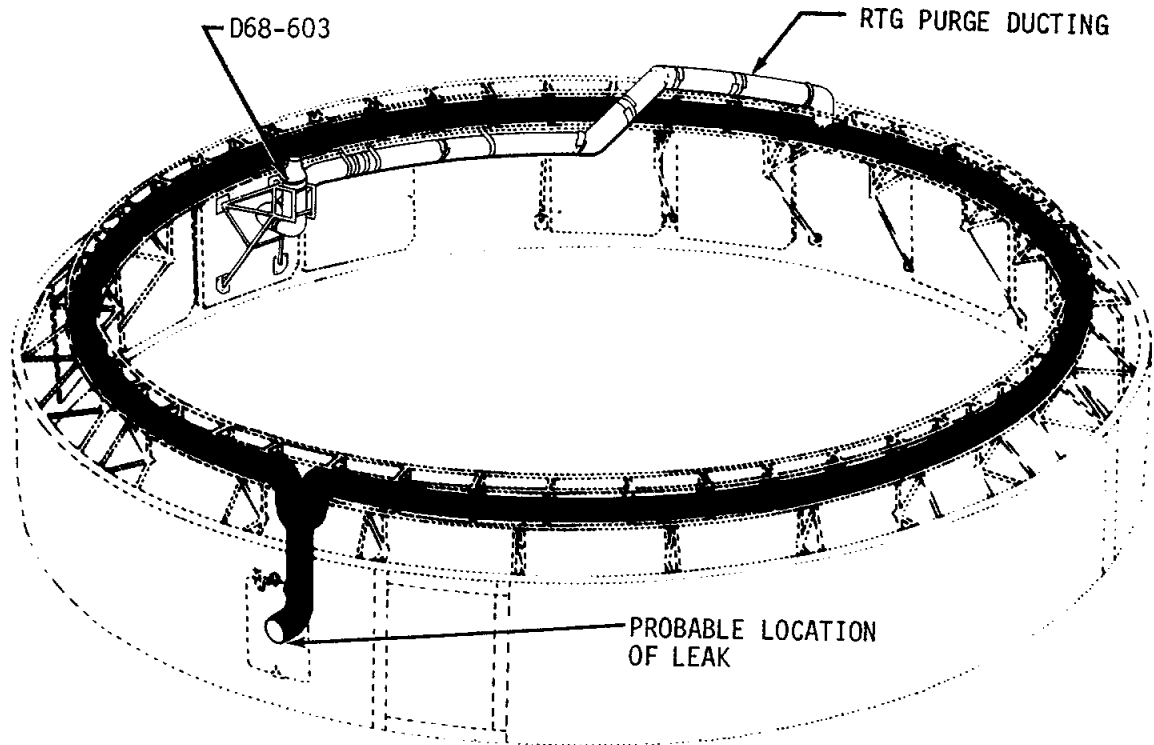


Figure 18-4. RTG Purge Ducting Modification

18.4.1 Thermal Conditioning System

Sublimator performance and coolant temperature during ascent are presented in Figure 18-5. Immediately after liftoff, the Modulating Flow Control Valve (MFCV) began driving toward the full heatsink position which was achieved at approximately 20 seconds. The water valve opened at 181 seconds allowing water to flow to the sublimator. Full cooling from the sublimator was not evidenced until approximately 530 seconds. At this time, the coolant temperature at the control point began to decrease rapidly. The low cooling rate during the first 300 seconds after the water valve opened is typical of a slow-starting sublimator. At the first thermal switch sampling, the coolant temperature was still above the actuation point and the water valve remained open. The second thermal switch sampling occurred at 783 seconds and the water valve closed.

The IU coolant flowrate was slightly below the minimum specification limits as shown in Table 18-1. The out-of-specification flowrate will be evaluated in regard to applied pump voltage. No degradation of system performance occurred.

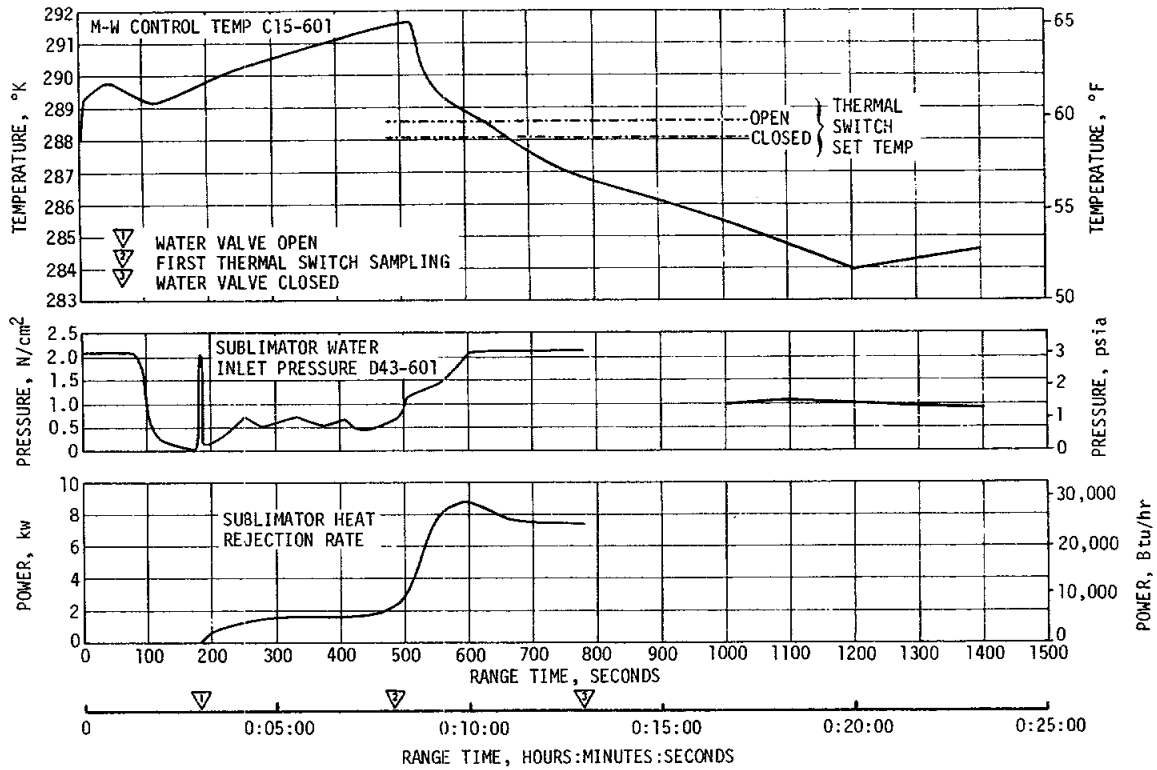


Figure 18-5. IU Sublimator Performance During Ascent

Table 18-1. TCS Coolant Flowrates and Pressures

PARAMETER	REQUIREMENT	MINIMUM OBSERVED	MAXIMUM OBSERVED
IU Coolant Flowrate F9-602 m ³ /s (gpm)	6.06 x 10 ⁻⁴ (9.6 Minimum)	5.87 x 10 ⁻⁴ (9.3)	5.99 x 10 ⁻⁴ (9.5)
S-IVB Coolant Flowrate F10-602 m ³ /s (gpm)	49.2 ± 2.52 x 10 ⁻⁵ (7.8 ± 0.4)	4.80 x 10 ⁻⁴ (7.6)	4.92 x 10 ⁻⁴ (7.8)
Pump Inlet Pressure D24-601 N/cm ² (psia)	10.82 to 11.72 (15.7 to 17.0)	11.17 (16.2)	11.24 (16.3)
Pump Outlet Pressure D17-601 N/cm ² (psia)	28.89 to 33.23 (41.9 to 48.2)	29.32 (42.5)	30.70 (44.5)

The TCS GN₂ sphere pressure decay, which is indicative of the GN₂ usage rate, was approximately as expected for the nominal case as shown in Figure 18-6. The rapid pressure drop during the first 780 seconds, though not predicted, is not considered an abnormal condition. The same type of drop was present during the AS-504 boost phase, and is regarded as a cooling effect of compartment outgassing during boost.

The Flight Control Computer (FCC) contains an internal coolant flow passage which is normally connected in parallel with the TCS flow loop. Due to a potential failure of coolant tube connecting flares inside the FCC cover, the IU-505 FCC was disconnected from the TCS flow loop. Thermal vacuum test performed prior to launch showed that with no internal cooling the upper allowable temperature limit of the FCC would not be exceeded under worst case hot conditions. The predicted worst case temperature and available flight data are presented in Figure 18-7. The internal temperature remained well below the allowable and predicted worst case temperature limits.

Component temperatures appear to be within the expected ranges, but insufficient data preclude any conclusive comments at this time (Figure 18-8). Limited real-time information and second-burn data indicate all component environmental parameters were satisfactory.

18.4.2 Gas Bearing Supply System

The gas bearing subsystem performed nominally through the time period for which data are available. The GBS GN₂ sphere pressure decay is nominal as can be seen in Figure 18-9. Figure 18-10 shows the platform pressure differential and internal ambient pressure. The platform internal pressure (D12-603) decreased as expected to 8.63 N/cm² (12.5 psia) at 4000 seconds then increased to 9.80 N/cm² (14.2 psia) at 24,000 seconds, however the gas bearing differential pressure (D11-603) exhibited the expected tendency to increase during the initial portion of the flight, which has been seen in most previous flights. Data after mission completion show the differential pressure steady and below the maximum allowable value.

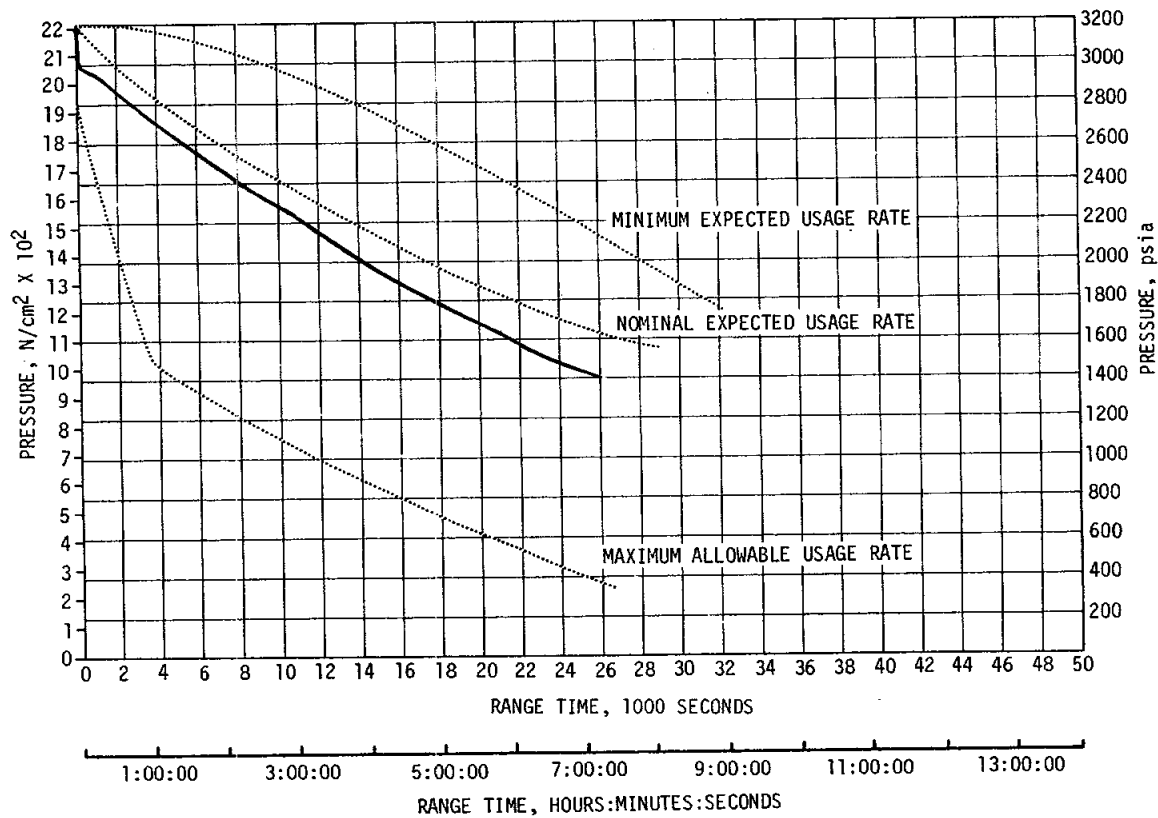


Figure 18-6. Thermal Conditioning System GN₂ Sphere Pressure (D25-601)

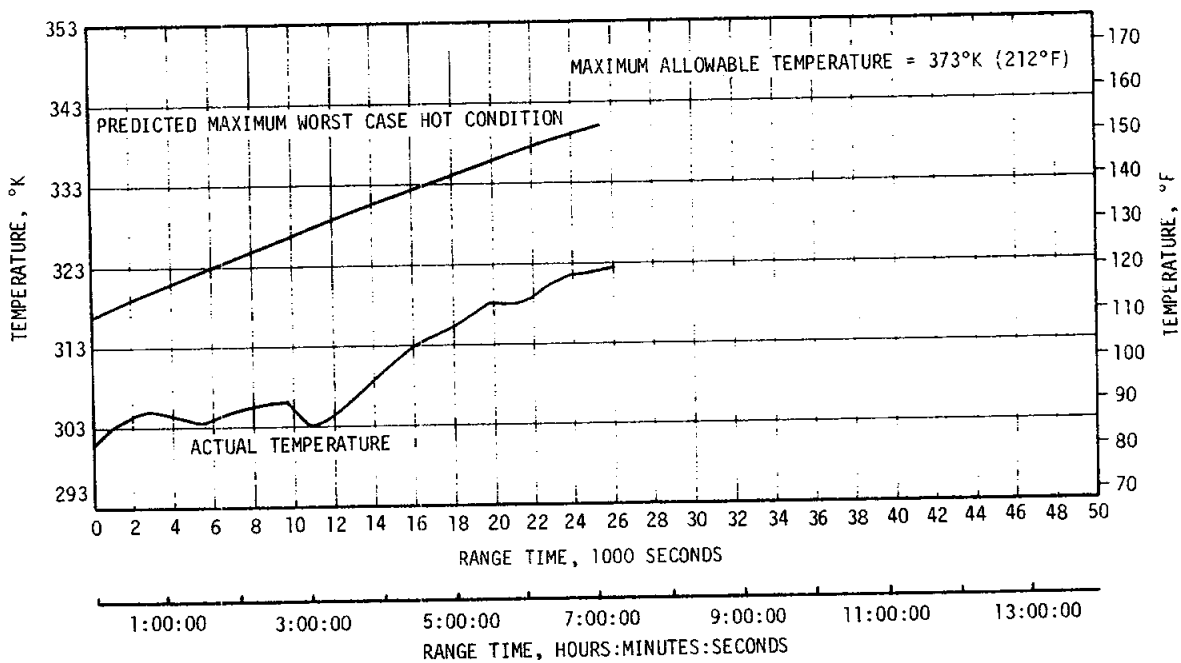


Figure 18-7. Flight Control Computer Temperatures (C69-602)

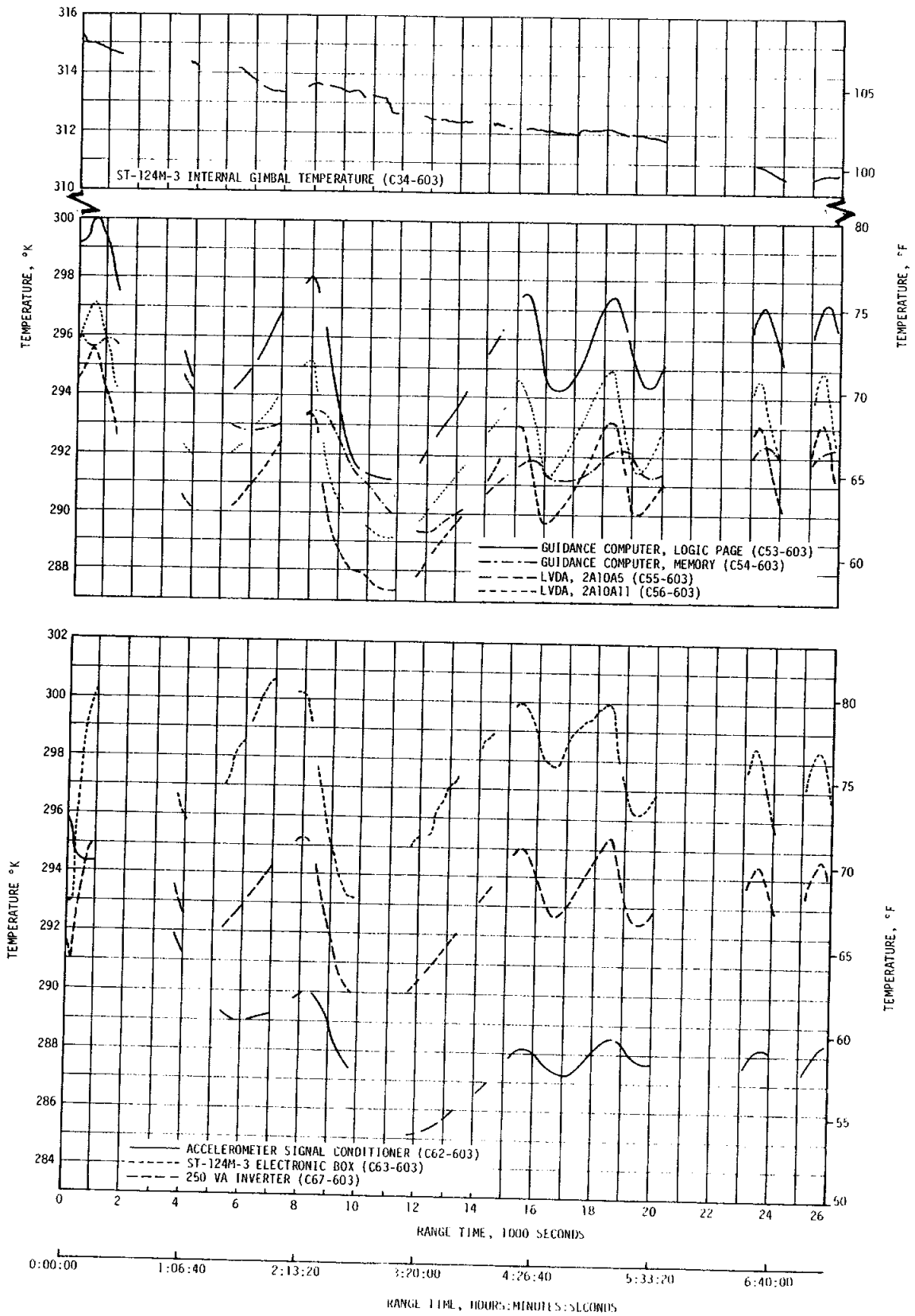


Figure 18-8. Selected Component Temperatures

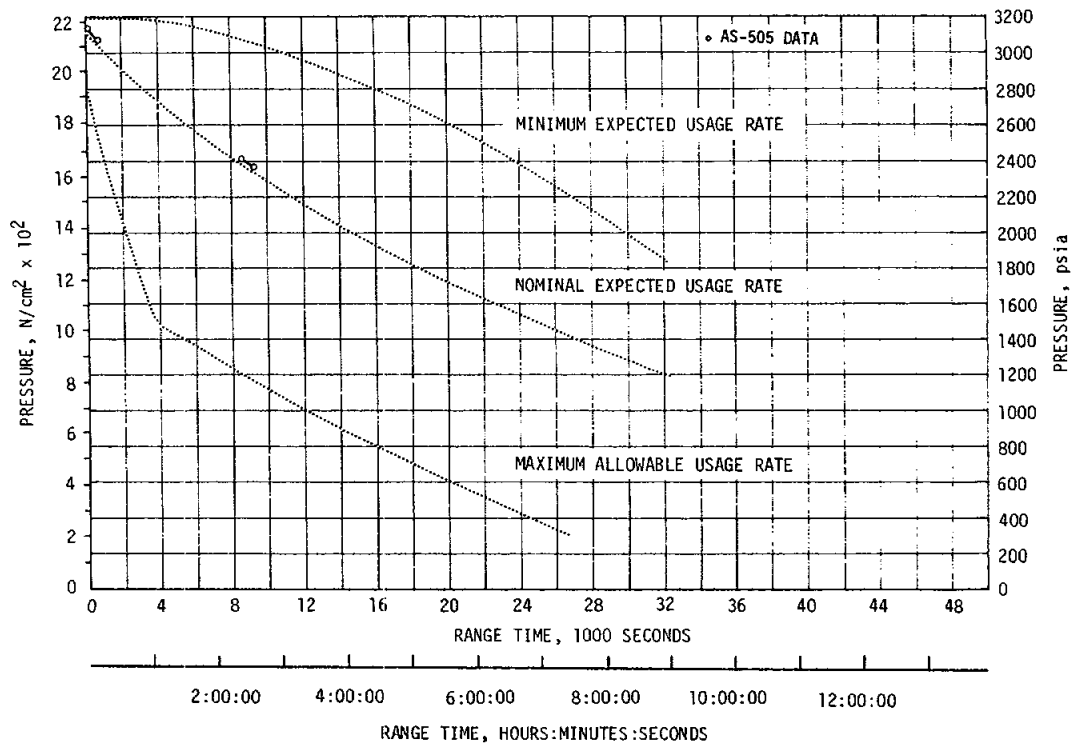


Figure 18-9. Gas Bearing GN₂ Sphere Pressure

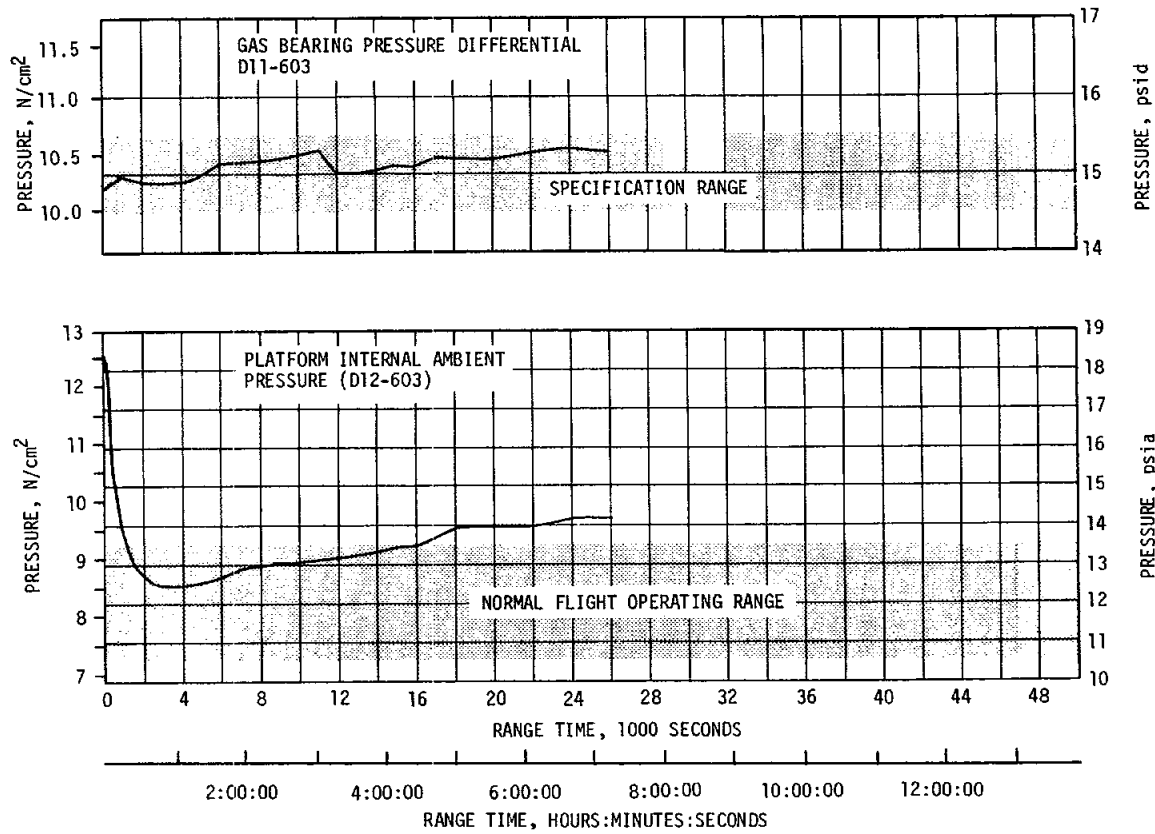


Figure 18-10. Inertial Platform GN₂ Pressures

SECTION 19
DATA SYSTEMS

19.1 SUMMARY

All elements of the data system performed satisfactorily except for a problem with the Command and Communications System (CCS) downlink during translunar coast.

Measurement performance was excellent, as evidenced by 99.2 percent reliability. This is the highest reliability attained on any Saturn V flight.

Telemetry performance was nominal, with the exception of a minor calibration deviation. The onboard tape recorder performance was satisfactory. Very High Frequency (VHF) telemetry Radio Frequency (RF) propagation was generally good, though the usual problems due to flame effects and staging were experienced. VHF data were received to 15,780 seconds (04:23:00). Command systems RF performance for both the Secure Range Safety Command Systems (SRSCS) and CCS was nominal except for the CCS downlink problem noted. Goldstone (GDS) and Guaymas (GYM) reported receiving CCS signal to 40,191 seconds (11:09:51). Good tracking data were received from the C-Band radar, with Bermuda (BDA) indicating final Loss of Signal (LOS) at 35,346 seconds (09:49:06).

The 73 ground engineering cameras provided good data during the launch.

19.2 VEHICLE MEASUREMENT EVALUATION

The AS-505 launch vehicle had 2286 measurements scheduled for flight. Fifteen measurements were waived prior to the start of automatic countdown sequence leaving 2271 measurements active for flight. Of the waived measurements, 2 provided valid data during flight.

Table 19-1 presents a summary of measurement performance for the total vehicle and for each stage. Measurement performance was exceptionally good, as evidenced by 99.2 percent reliability, which is the highest attained on any Saturn V flight.

Tables 19-2, 19-3, and 19-4 tabulate by stage the waived measurements, totally and partially failed measurements, and questionable measurements. None of the listed failures had any significant impact on postflight evaluation.

Table 19-1. AS-505 Flight Measurement Summary

MEASUREMENTS CATEGORY	S-IC STAGE	S-II STAGE	S-IVB STAGE		INSTRUMENT UNIT	TOTAL VEHICLE
			PHASE I*	PHASE II*		
Scheduled	669	1018	378	378	221	2286
Waived	3	9	2	2	1	15
Failures	5	6	4	8	0	19
Partial Failures	22	13	5	5	0	40
Questionable	0	4	0	0	0	4
Reliability, Percent	99.2	99.4	98.9	97.9	100.0	99.2

*Notes: 1. S-IVB Phase I period of performance is from liftoff to parking orbit insertion.
 2. S-IVB Phase II period of performance is from liftoff until end of S-IVB stage required flight period of performance as specified in the Detailed Flight Test Plan.

Table 19-2. AS-505 Flight Measurements Waived Prior to Launch

MEASUREMENT NUMBER	MEASUREMENT TITLE	NATURE OF FAILURE	REMARKS
S-IC STAGE			
C343-115 D119-104 D128-115	LOX Prevalve, Engine 5 Gimbal System Filter Manifold LOX Suction Line, Engine 2	Data negative Transducer failure Noisy data prior to launch.	KSC waiver I-8-505-4 MICH-505-4 MICH-505-3. Data satisfactory during flight.
S-II STAGE			
C758-217 C850-218 D030-201 D030-202 D030-203 D030-204 D030-205 D152-202 S013-218	LOX Tank Liquid Temperature E4 LH ₂ Feedline Heat Rate LH ₂ Recirc Pump Disch Pressure LH ₂ Recirc Pump Disch Pressure LH ₂ Recirc Pump Disch Pressure LH ₂ Recirc Pump Disch Pressure LH ₂ Recirc Pump Disch Pressure LH ₂ Recirc Pump Inlet Pressure Stringer 20 Side Long Strain	Transducer open Transducer open Transducer failure Transducer failure Transducer failure Transducer failure Transducer failure Transducer failure Transducer open	Installation Installation Installation Installation Installation Installation
S-IVB STAGE			
D0254-403 L0019-408	Press-LOX Tank Repress Sphere Level-Liquid Hydrogen Pos C	Drifted low Dropped out when wet	Return to "ON" state after several minutes.
INSTRUMENT UNIT			
D17-601	Methanol/Water Coolant Pump Exit Pressure	Noisy	Waived during CDDT. Provided useful data during flight.

Table 19-3. AS-505 Measurement Malfunctions

MEASUREMENT NUMBER	MEASUREMENT TITLE	NATURE OF FAILURE	TIME OF FAILURE (RANGE TIME)	DURATION SATISFACTORY OPERATION	REMARKS
TOTAL MEASUREMENT FAILURES, S-IC STAGE					
B015-118 C033-106 D047-106	Acoustic, External Heat Shield, Internal Differential, Heat Shield	Data low Transducer failure Protective cover for sensing port not removed before flight	0 sec 0 sec 0 sec	None None None	No usable data. Positive port sealed.
E038-101 E054-115	Vibration, Fuel Pump Flange, Rad Vibration, Retromotor	Data level too high Transducer failure.	Ignition See Remarks.	None None	
TOTAL MEASUREMENT FAILURES, S-II STAGE					
D113-219 E001-203	Forward Skirt Static P E3 Long Vib Conbstn Dome	Transducer failure. Cable and/or connector open.	0 sec 0 sec	None None	
E003-204	E4 Radial Vib Fuel Pump	Cable and/or connector open.	0 sec	None	
E326-219	Long Vib Fwd Skirt Stringer	Cable and/or connector open.	0 sec	None	
E339-206	Norm Vib Thrust Cone	Cable and/or connector open.	0 sec	None	
E352-206	Tan Vib Interstage Frame	Cable and/or connector open.	0 sec	None	
TOTAL MEASUREMENT FAILURES, S-IVB STAGE, PHASE I (ALSO INCLUDED IN PHASE II)					
B0019-427 B0025-426	Acous Aft Skirt Sta 2880 Ext Acous Sta 3220, Pos 1 Ext	Envelope decrease. Envelope decrease.	65 sec 45 sec	65 sec 45 sec	Decrease in amplifier gain suspected. Decrease in amplifier gain suspected.
C0200-401 D0230-403	Temp-Fuel Injection Press-GOX/GH ₂ Burner GH ₂ Inj	6 to 8 percent low 10 percent upward shift	-10 minutes Prior to liftoff	None None	
ADDITIONAL MEASUREMENT FAILURES, S-IVB STAGE, PHASE II					
A0010-403* D0104-403	Accel-Gimbal Block-Pitch-LF Press-LH ₂ Press Module Inlet	Data drifted to upper band edge. Steady state varied during second burn	1200 sec 9270 sec	1200 sec 9270 sec	Low temperature failure. Degradation of amplifier suspected.
D0236-403 E0239-401	Press-Ambient Helium Pneu Sphere Vib-LOX Turbine Bypass Vlv Tan	Off scale high at 9750 seconds. Data erratic during second engine burn	9750 sec 9210 sec	9750 sec 9210 sec	
PARTIAL MEASUREMENT FAILURES, S-IC STAGE					
A001-118 B004-114 B006-118 B007-118 B008-118 B009-118 B010-118 B011-118 B012-118 B013-118	Accel, Long Acoustic, Fin D Acoustic, External Acoustic, External Acoustic, External Acoustic, External Acoustic, External Acoustic, External Acoustic, External Acoustic, External	Data went to negative at liftoff High amplitude low frequency noise Bias level too high Bias level too high Bias level too high Data clipping Data clipping Data clipping Data clipping Data clipping	0 sec 0 sec 115 sec 37 sec 51 to 61 sec 37 sec 118 sec 0 sec 0 sec 0 sec	10 sec to end of flight Intermittent 0 to 115 sec 0 to 37 sec 0 to 51 sec and 61 sec to end of flight Intermittent Intermittent Intermittent Intermittent Intermittent	Positive clipping and negative Positive clipping Positive clipping Positive clipping Positive clipping Some usable data. Some usable data. Some usable data.
*Contractor position is that this measurement failed outside the period of interest.					

Table 19-3. AS-505 Measurement Malfunctions (Continued)

MEASUREMENT NUMBER	MEASUREMENT TITLE	NATURE OF FAILURE	TIME OF FAILURE (RANGE TIME)	DURATION SATISFACTORY OPERATION	REMARKS
PARTIAL MEASUREMENT FAILURES, S-IC STAGE (Continued)					
B014-118 C003-102 C131-105	Acoustic, External Temp. Turbine Manifold Temperature Solenoid Valve	Data clipping Data drops unexpectedly Data noisy	0 sec 115 sec 35 sec	Intermittent 115 sec 35 sec	Some usable data. Minor loss of data.
D011-101 D020-101	Press, Eng Control Heat Exchanger Outlet	Data level too high Transducer failure	70 sec 52 sec	70 sec 52 sec	Data usable prior to 52 sec.
D145-115 D150-115	Helium Inlet LOX Pump Inlet	Data trend low Transducer failure	7 sec 100 sec	7 sec 100 sec	Data usable. Data usable prior to 100 sec.
E042-102 E042-103 E042-104	Fuel Pump Flange Radial Fuel Pump Flange Radial Vibration, Fuel Pump Flange Radial	High amplitude low frequency noise High amplitude low frequency noise Data dropouts	0 sec 0 sec 0 sec	Intermittent Intermittent Intermittent	Some usable data. Some usable data.
D007-102 D007-104	Pressure, Fuel Pump Discharge, Engine 2 Pressure, Fuel Pump Discharge, Engine 4	Unexpected decrease from 85 to 95 sec Unexpected decrease from 50 to 60 sec	85 sec 50 sec	All but 10 seconds All but 10 seconds	
PARTIAL MEASUREMENT FAILURES, S-II STAGE					
C003-201 C680-206	E1 Fuel Turbine Inlet T Heat Shield Aft Gas T	Transducer failure Intermittent and noisy throughout	177.5 sec	177.5 sec	
C72T-206 C815-206 D012-202 D060-200	Heat Shield Aft Heat Rate LOX Vent Valve Heat Rate E2 Engine Reg Outlet P Ullage Rocket 8 Chamber P	Transducer failure Transducer failure Transducer failure 10 percent DC bias shift in transducer	195 sec 102 sec 210 sec	195 sec 102 sec 210 sec	
D100-206 E001-204	Heat Shield Fwd Face P E4 Long Vib Combstn Dome	Transducer failure Periods of amplifier saturation	200 sec	200 sec	
E002-203 E002-204	E3 Radial Vib LOX Pump E4 Radial Vib LOX Pump	Periods of amplifier saturation Periods of amplifier saturation			
E003-203	E3 Radial Vib Fuel Pump	Periods of amplifier saturation			
E215-202	E5 Rad Main Fuel Valve	Amplifier saturation	261 to 276 sec	537 sec	
E342-203	Tan Vib LH ₂ Prevlv/Fdln	Periods of amplifier saturation			
PARTIAL MEASUREMENT FAILURES, S-IVB STAGE					
B0016-411 C0001-401 C0199-401 D0233-403 E0092-404	Acoustic Fwd Skirt Station 3216-INT Temp-Fuel Turbine Inlet Temp-Thrust Chamber Jacket Press-O ₂ H ₂ Inj Spool Chamber Dff Vibration-Station 2748 Position II-Thrust	Approximately 19 data dropouts were observed between 65 and 85 sec Data lower than expected Slow response during first engine burn Approximately 8 percent noise from liftoff to liftoff plus 20 seconds. Data level lower than expected	65 sec 0 sec first burn 0 to 20 sec 0 sec	All but 20 sec All but 20 seconds	A loose cable is suspected. Data believed to be usable. Slight sensor debonding during first engine burn is suspected. Susceptible to vibration. Data believed to be usable.

Table 19-4. AS-505 Questionable Flight Measurements

MEASUREMENT NUMBER	MEASUREMENT TITLE	REASON QUESTIONED	REMARKS
QUESTIONABLE MEASUREMENTS, S-II STAGE			
D116-219	Forward Skirt Static P	Decay not proper; questionable after 50 seconds.	Full scale range of instrument is extremely low.
D117-219	Forward Skirt Static P	Decay not proper; questionable after 50 seconds.	Full scale range of instrument is extremely low.
D120-219	Forward Skirt Static P	Decay not as predicted.	Full scale range of instrument is extremely low.
D121-219	Forward Skirt Static P	Decay not proper; questionable after 75 seconds.	Full scale range of instrument is extremely low.

19.3 AIRBORNE TELEMETRY SYSTEMS

Performance of the 17 VHF telemetry links was generally satisfactory with the minor exceptions noted. A brief performance summary of these links is shown in Table 19-5.

There was a variation of approximately 10 counts in the 100 percent level of the inflight calibrations for the DP-1 telemetry link. This is equivalent to 50 millivolts as compared to 41 millivolts in the specifications. This type of high variation has been previously experienced on AS-205 and during checkout. Examination of 5-vdc measuring voltage supply data as seen on word 28-frame 10 of the DP1-A0 links also indicates variations of this magnitude. This problem is under further investigation.

Data degradation and dropouts were experienced at various times during boost as on previous flights due to attenuation of RF transmission at these times as discussed in paragraph 19.5.1.

Usable VHF telemetry data were received to 15,780 seconds (04:23:00) at both GYM and Hawaii (HAW).

Performance of the CCS telemetry was generally satisfactory except for the period during translunar coast from 23,601 seconds (06:33:21) to 25,111 seconds (06:58:17). This problem is discussed in detail in paragraph 19.5.3.2. Usable CCS data were received at GDS to 39,305 seconds (10:55:05).

19.4 AIRBORNE TAPE RECORDERS

The performance of the three onboard tape recorders installed to record real time data during predicted RF blackout periods was satisfactory. Noise levels, timer operations and recorder response times remained within

Table 19-5. AS-505 Launch Vehicle Telemetry Links

LINK	FREQUENCY (MHz)	MODULATION	STAGE	FLIGHT PERIOD (RANGE TIME, SEC)	PERFORMANCE SUMMARY	
					Range Time (sec)	Duration (sec)
AF-1 AF-2 AF-3 AP-1 AS-1 AS-2	240.2 252.4 231.9 244.3 235.0 256.2	PAM/FM/FM PAM/FM/FM PAM/FM/FM PCM/FM SS/FM SS/FM	S-IC S-IC S-IC S-IC S-IC S-IC	0-405 0-405 0-405 0-405 0-405 0-405	Satisfactory except for AF-3 calibration. Data Dropouts	
					162.5	1.0
					165.6	1.4
BF-1 BF-2 BF-3 BP-1 BS-1 BS-2	241.5 234.0 229.9 248.6 227.2 236.2	PAM/FM/FM PAM/FM/FM PAM/FM/FM PCM/FM SS/FM SS/FM	S-II S-II S-II S-II S-II S-II	0-762 0-762 0-762 0-762 0-762 0-762	Satisfactory Data Dropouts	
					162.4	0.7
					192.3	1.0
					552 (FM/FM only)	0.5
CF-1 CP-1 CS-1	253.8 258.5 246.3	FM/FM PCM/FM SS/FM	S-IVB S-IVB S-IVB	Flight Duration Flight Duration 0-726; 8640-9576	Satisfactory Data Dropouts	
					162.5	1.0
DF-1 DP-1 DP-1B	250.7 255.1 2282.5	FM/FM/FM PCM/FM PCM/FM	S-IU S-IU S-IU	Flight Duration Flight Duration Flight Duration	Satisfactory except for DP-1 calibration. Data Dropouts	
					162.5 (VHF)	0.8
					162.8	5.6
					193.4	5.6
					5880.5	9.5
					6120.3	5.2
					23,601	See 19.5.3.2

Table 19-6. Tape Recorder Summary

RECORDER	LINK RECORDED	RECORD TIME (RANGE TIME, SECONDS)		PLAYBACK TIME (RANGE TIME, SECONDS)	
		START	STOP	START	STOP
LAUNCH PHASE					
S-IC Recorder	AF-1, AF-2	135.15	186.25	186.25	237.85
S-II Recorder No. 1	BF-1, BF-2	75.54 494.11	173.52 575.85	575.85	757.13
S-II Recorder No. 2	BF-3, BT-1	75.54 494.11	173.52 575.85	575.85	757.13

required operating limits. Recorded data agreed favorably with data obtained in real-time. Approximately 51.1 seconds of S-IC data and 179.7 seconds of S-II data were recorded. All of the recorded data were successfully played back.

Recorder assignments and their periods of performance are listed in Table 19-6.

19.5 RF SYSTEMS EVALUATION

The performance of the RF systems, based on data received to date, was good. Measured flight data, with few exceptions agreed favorably with expected trends. RF performance of the telemetry, SRSCS and tracking systems was good. CCS performance was generally satisfactory with the exception of the problem discussed in paragraph 19.5.3.

VHF final LOS was reported by BDA at 18,900 seconds (05:15:00) and CCS LOS at 40,191 seconds (11:09:51) by GYM and GDS. BDA indicated C-Band tracking LOS at 35,346 second (09:49:06).

19.5.1 Telemetry System RF Propagation Evaluation

The performance of the 17 VHF telemetry links was excellent and generally agreed with predictions. Ultra High Frequency (UHF) telemetry link DP-1A was deleted on AS-505.

Moderate to severe signal attenuation was experienced at various times during the boost due to main engine flame effects, S-IC/S-II and S-II/S-IVB staging, S-II engine ignition and S-II second plane separation. Magnitude of these effects was comparable to that experienced on previous flights. At S-IC/S-II staging, signal strength on all VHF telemetry links and on the CCS downlink dropped to threshold for approximately 1 and 5.6 seconds respectively. Signal degradation due to S-II engine ignition and S-II flame effects was sufficient to cause loss of VHF telemetry data on the S-IC and S-II stages. CCS and S-II VHF data were lost during S-II second plane separation. In addition there were intervals during the launch phase where some data were so degraded as to be unusable. Loss of these data, however, posed no problem since much of the data was recovered from onboard tape recorder playback, other stations providing overlapping coverage, or losses were of such short duration as to have little or no impact on flight analysis.

The performance of the S-IVB and IU telemetry systems was nominal during orbit, although the Mercury (MER) ship experienced a drop in RF signal strength to -127 dbm, shortly after start of S-IVB Restart Preparations (Time Base 6). This dropout was at least 90 seconds in duration. Valid data were received during this period from Carnarvon (CRO), indicating that vehicle instrumentation systems were operating satisfactorily. Performance was nominal during second burn and final coast, except for the CCS downlink problem discussed in paragraph 19.5.3.2.

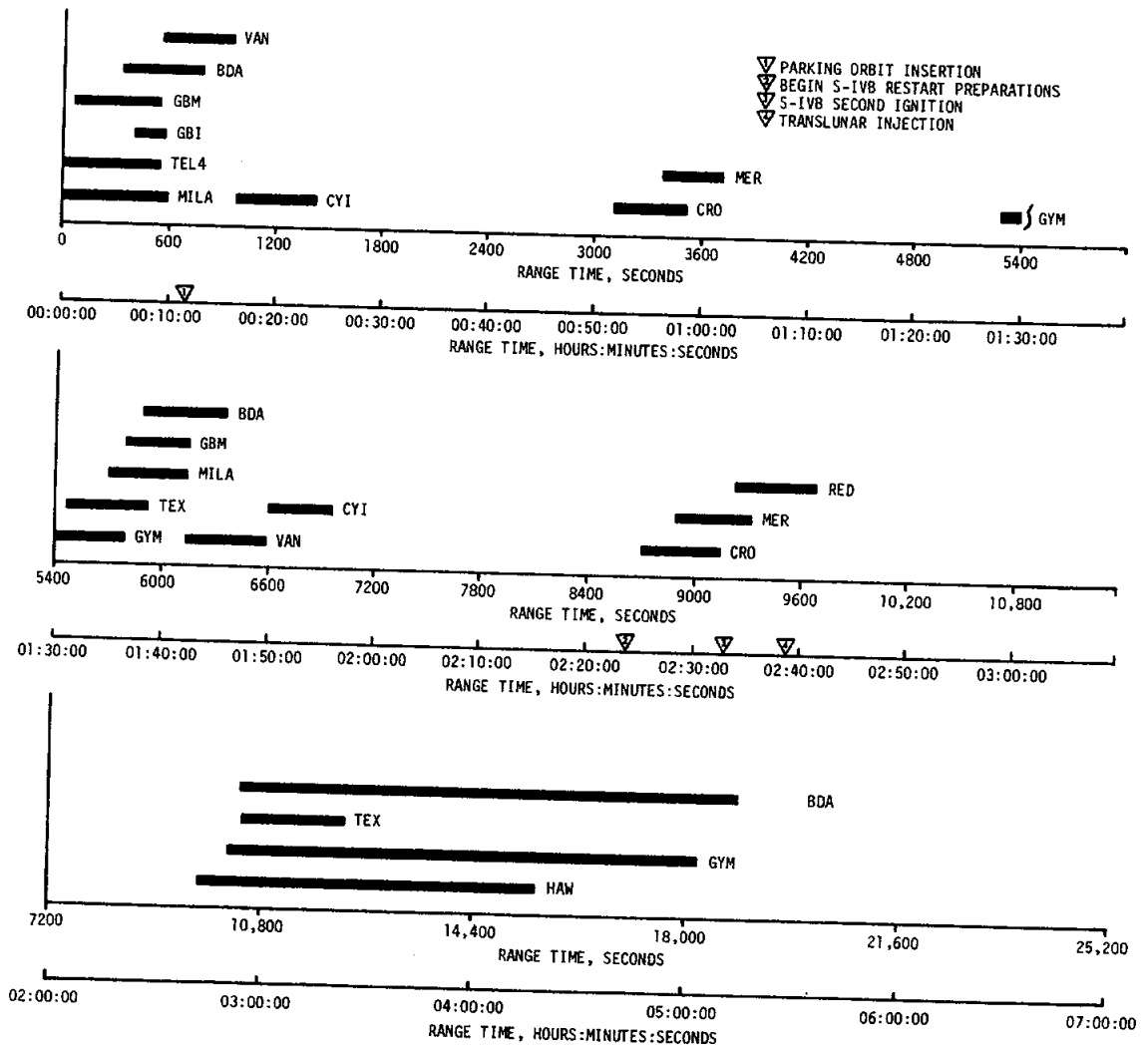


Figure 19-1. VHF Telemetry Coverage Summary

BDA reported VHF LOS at 18,900 seconds (05:15:00) and GYM and GDS reported CCS LOS at 40,191 seconds (11:09:51).

A summary of available VHF telemetry coverage showing Acquisition of Signal (AOS) and LOS for each station is shown in Figure 19-1.

19.5.2 Tracking Systems RF Propagation Evaluation

Analysis of data received to date indicates that the C-Band radar functioned satisfactorily during this flight, although several stations experienced tracking problems due to phase front distortions and equipment malfunctions. The ODOP system, previously flown on the S-IC stage, was deleted on this flight.

The Cape Kennedy Air Force Site (CKAFS), Merritt Island Launch Area (MILA), and Grand Bahama Island (GBI) sites reported tracking problems during launch, caused by balance point shifts. The most serious problem was a 5 second loss of track by MILA at 22 seconds when the operator tried to verify main lobe track. Grand Turk Island (GTI) lost track twice due to bad aspect angles.

No problems were experienced during the first orbital revolution. During the second revolution, however, both BDA radars had short dropouts caused by high elevation angles. The vehicle was almost directly overhead during this time requiring azimuth tracking rates in excess of station capabilities. The Vanguard (VAN) ship lost track during this revolution because of apparent interference from another radar. CRO was unable to track during the second revolution because of ground station transmitter problems.

Performance during the second burn and final coast was generally satisfactory. Rapid fluctuations on the Automatic Gain Control (AGC) were experienced at HAW for a two minute period beginning at 10,160 seconds (02:49:20). GTI acquired track late at 12,210 seconds (03:23:30) due to an erroneous "Parametric Amplifiers On" indication caused by a burned out lamp. BDA indicated final LOS at 35,346 seconds (09:49:06).

A summary of available C-Band radar coverage showing AOS and LOS for each station is shown in Figure 19-2.

There is no mandatory tracking requirement of the CCS; however, the CCS transponder has turnaround ranging capabilities and provided a backup to the Command and Service Module (CSM) transponder used for tracking in case of failure or desire for a cross check. Since the same transponder is used for all CCS functions, discussion of the tracking performance of this system is included in the general discussion of the CCS RF evaluation.

19.5.3 Command Systems RF Evaluation

The AS-505 command systems consisted of the SRSCS and the CCS. All indications were that these systems performed satisfactorily except for the CCS downlink problem discussed below.

19.5.3.1 Secure Range Safety Command System. VHF telemetry measurements received by the ground stations from the S-IC, S-II and S-IVB stages indicated that the SRSCS RF subsystems functioned properly. Canaveral (CNV) and BDA were the command stations used for this flight. The carrier signal was turned off at CNV at 404 seconds. At BDA the carrier was turned on at 371 seconds and turned off at 745 seconds. A momentary dropout occurred at approximately 121 seconds when the command station switched transmitting antennas.

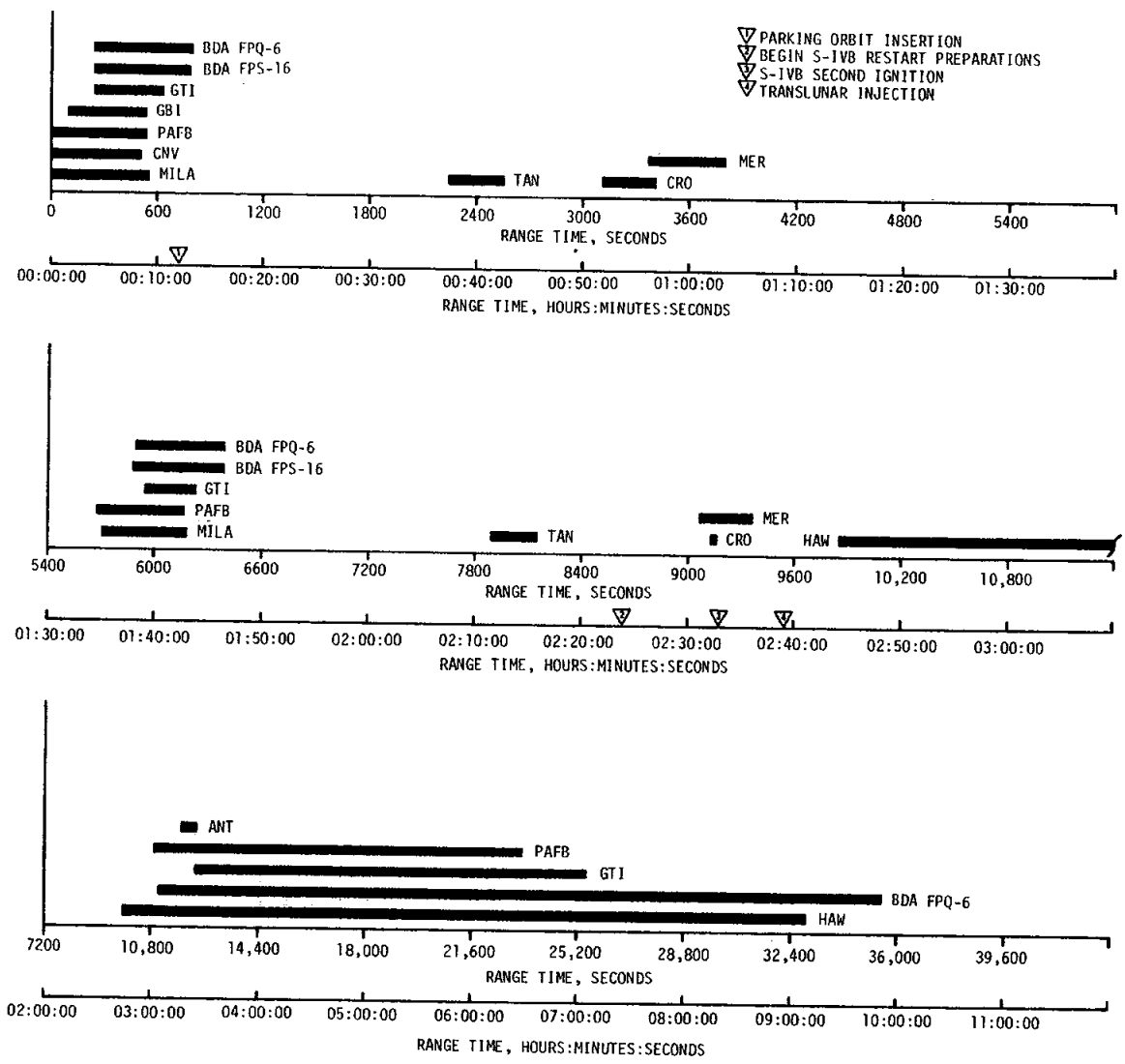


Figure 19-2. C-Band Radar Coverage Summary

19.5.3.2 Command and Communications System. Available data indicated satisfactory CCS performance during boost and parking orbit with minor exceptions. Downlink dropouts occurred during S-IC/S-II staging and at S-II second plane separation. Dropouts at these times are expected. Station handover was accomplished with minimum data loss (less than 5 seconds) from MILA to BDA at 362 seconds and from BDA to VAN at 690 seconds. Downlink dropouts were also experienced during the second revolution during handover from MILA to Grand Bahama (GBM) at 5880.5 seconds (01:42:00.5) and during handover from GBM to BDA at 6120.3 seconds (01:42:00.3). Duration of these dropouts were 9.5 and 5.2 seconds respectively.

Performance during second burn and translunar injection was nominal.

During the final coast, a sharp drop in downlink CCS signal strength was noted at GYM and GDS at 23,601 seconds (06:33:21). The onboard antenna system, which had been on low gain since 15,233 seconds (04:13:53), was switched to the high gain mode at 24,052 seconds (06:40:52) to improve signal quality. Signal strength picked up and was maintained at a high level until 24,160 seconds (06:42:40) at which time the signal level again dropped, then was completely lost approximately 1 minute later. The signal fluctuated intermittently at low levels until 25,097 seconds (06:58:17) at GDS and 25,111 seconds (06:58:31) at GYM. The system, which had been commanded to the omni-directional mode at 25,097 seconds (06:58:17), remained in this mode until final loss of signal at 40,191 seconds (11:09:51). Figure 19-3 shows the fluctuation in signal level experienced during this time at the GYM site. The GDS station experienced similar fluctuations at corresponding times as shown in Figure 19-4. Signal levels were slightly higher at GDS due to the 85 foot antenna used versus the 30 foot antenna at GYM.

Normally, the directional high and low gain antennas would be expected to provide higher signal levels than the omni-directional antennas. During this time period the vehicle was at a sufficiently high elevation angle and vehicle attitude was such that good signal could be expected.

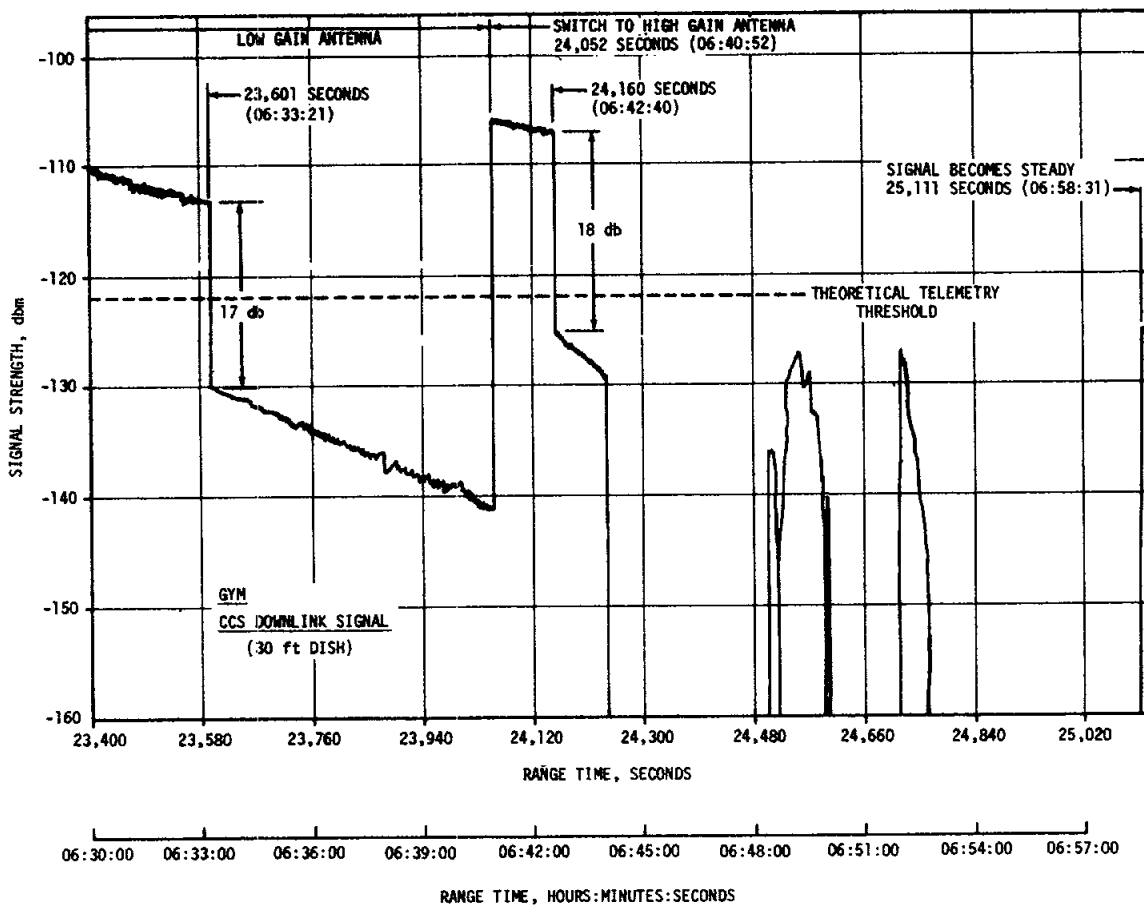


Figure 19-3. CCS Signal Strength Fluctuations at Guaymas

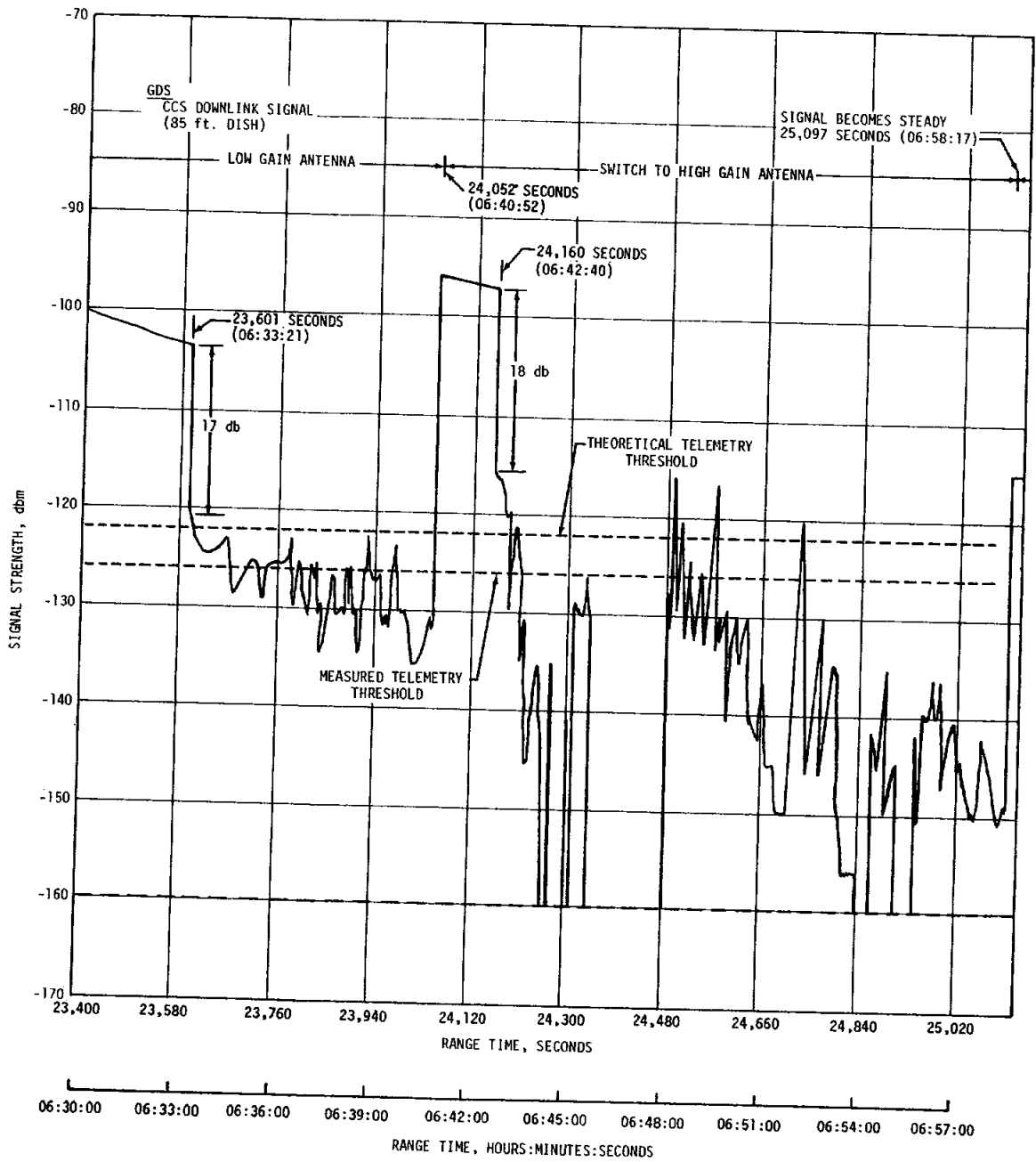


Figure 19-4. CCS Signal Strength Fluctuations at Goldstone

Figure 19-5 shows that the output from the CCS power amplifier is routed through a coaxial switch to the low gain, high gain, or omni antenna. GDS had intervals during the period of fluctuating signal strength when valid CCS telemetered data were received. These data indicate that the CCS power amplifier helix current was constant throughout the period when the problems were experienced. Constant helix current and satisfactory CCS operation using the omni-directional antenna implies that the source of the problem is in the directional antenna system, with the most likely source the coaxial switch.

Figure 19-6 shows an electrical schematic of the coaxial switch. When relay A is energized, the switch is positioned in the low gain mode. When relay B is energized, the switch is positioned in the omni-mode. When neither relay is energized the switch is held in the high gain (fail safe) position by a mechanical spring. Energizing either of the two relays breaks the high gain contacts through a mechanical linkage and switches to low gain or omni, dependent on the relay. A leak in the hermetic seal of a flight configuration switch was simulated by drilling a small hole in the housing. The switch was then operated in a vacuum chamber with a normal 15 watt RF load applied. At a pressure equivalent to approximately 80,000 feet altitude, signal was attenuated about 15 db, both during switching operations and when under load for a sustained period of time. Low signal levels would continue until another switching operation was accomplished. The above test indicates that breakdown occurs when a leaking switch, exposed to vacuum conditions, reaches a critical pressure region. After further leakage, the internal pressure would decrease below the critical pressure region, thereby accounting for occurrence of the problem during only a portion of flight. Effective on AS-507 a new configuration of coaxial switch will be flown, replacing the present configuration. This configuration change was implemented prior to experiencing the problem and is not the result of the present problem. To replace the switch on AS-506 with the new configuration would require some network changes, since the parts, though electrically interchangeable are not physically interchangeable because of configuration differences.

Other possible causes in the antenna system and associated cabling are being investigated.

A summary of CCS coverage showing AOS and LOS for each station is shown in Figure 19-7.

19.6 OPTICAL INSTRUMENTATION

In general, ground camera coverage was very good. Seventy-three items were received from Kennedy Space Center (KSC) and evaluated. Two cameras provided unusable data due to bad time. Four cameras malfunctioned, one camera jammed before acquiring requested data and one camera had no image on the film. As a result of the eight failures listed above, system efficiency was 95 percent.

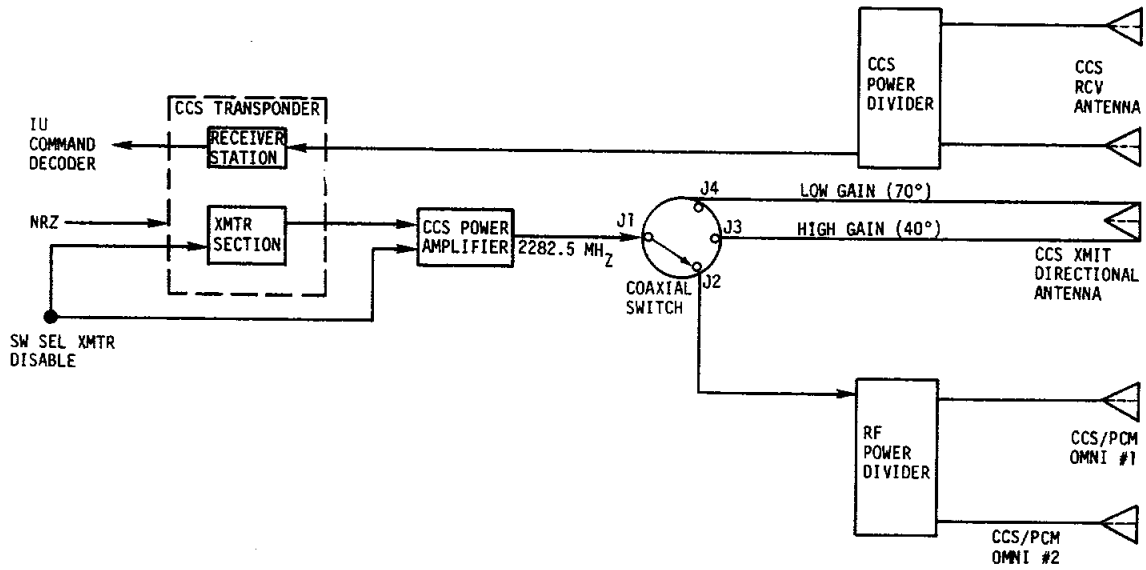


Figure 19-5. CCS System Block Diagram

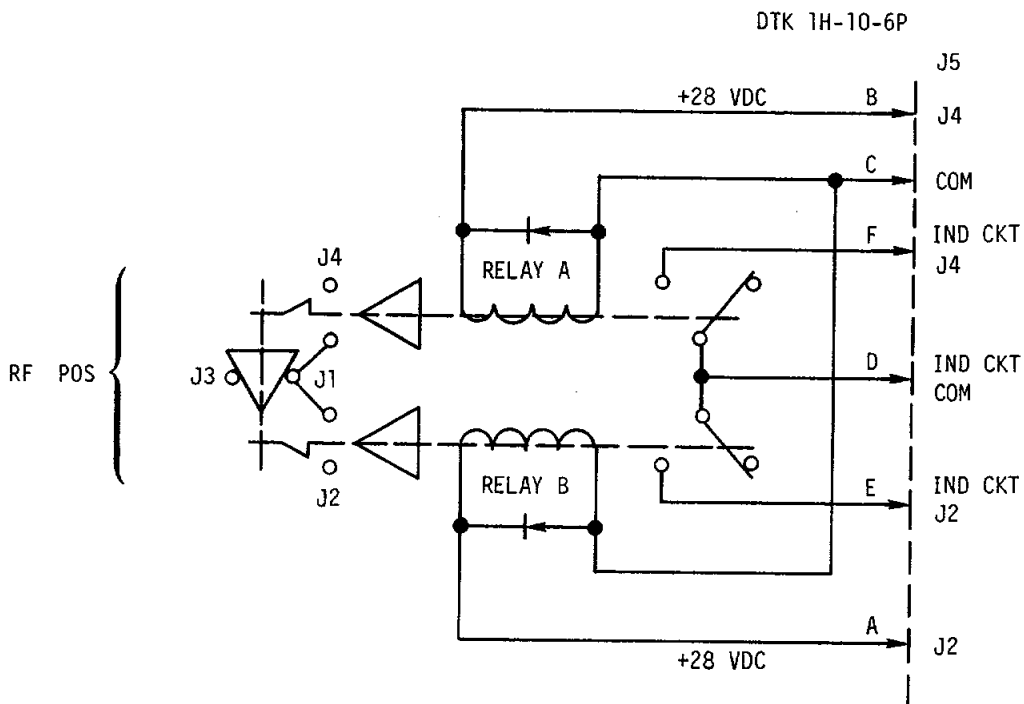


Figure 19-6. Electrical Schematic of CCS Coaxial Switch

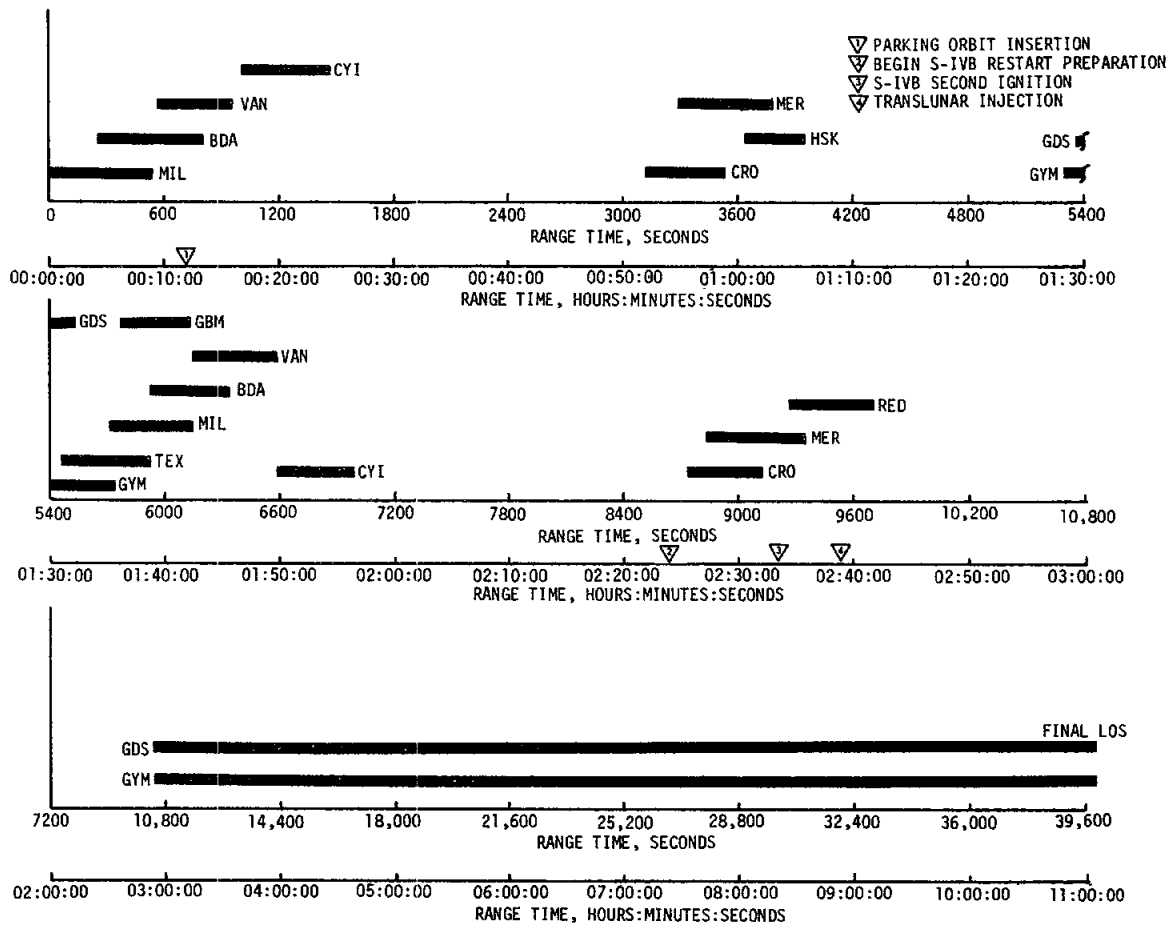


Figure 19-7. CCS Coverage Summary

SECTION 20

MASS CHARACTERISTICS

20.1 SUMMARY

Postflight analysis indicates that total vehicle mass was within 0.50 percent of the prediction from ground ignition through S-IVB stage final shutdown. This very small deviation signifies that the initial propellant loads and propellant utilization throughout vehicle operation were close to predicted.

20.2 MASS EVALUATION

Postflight mass characteristics are compared with the final predicted mass characteristics (MSFC Memorandum S&E-ASTN-SAE-69-M-53) which were used in the determination of the final operational trajectory (MSFC Memorandum S&E-AERO-FMT-106-69).

The postflight mass characteristics were determined from an analysis of all available actual and reconstructed data from S-IC stage ignition through S-IVB stage second burn cutoff. Dry weights of the launch vehicle were based on actual stage weighings and evaluation of the weight and balance log books (MSFC Form 998). Propellant loading and utilization was evaluated from propulsion system performance reconstructions. Spacecraft data were obtained from the Manned Spacecraft Center (MSC).

Deviations from predicted in dry weights of the inert stages and the loaded spacecraft were all less than 0.5 percent which is well within the 3-sigma deviation limits.

During S-IC powered flight, mass of the total vehicle was determined to be 2673 kilograms (5892 lbm) or 0.09 percent lower than predicted at ignition, and 2125 kilograms (4684 lbm) or 0.25 percent lower at S-IC/S-II separation. These very small deviations are attributed to a less than predicted S-IC propellant load and a slightly less than predicted upper stage mass. S-IC burn phase total vehicle mass is shown in Tables 20-1 and 20-2.

During S-II burn phase, the total vehicle mass varied from 142 kilograms (313 lbm) or 0.02 percent lower than predicted at start command to 559 kilograms (1233 lbm) or 0.27 percent higher than predicted at S-II/S-IVB separation. The initial deviation may be attributed to a slightly less

than predicted total propellant loading, and the deviation at separation was due mainly to a higher than predicted S-II LOX residual. Total vehicle mass for the S-II burn phase is shown in Tables 20-3 and 20-4.

During S-IVB stage operation, the total vehicle mass varied from 309 kilograms (681 lbm) or 0.19 percent higher than predicted at first start command to 260 kilograms (572 lbm) or 0.42 percent higher than predicted at end of second burn thrust decay. These deviations are due mainly to a slight excess of S-IVB propellants. Total vehicle mass at spacecraft separation was 367 kilograms (808 lbm) or 2.04 percent higher than predicted. Tables 20-5 through 20-8 show the vehicle mass history during both S-IVB burn phases.

A summary of mass utilization and loss, actual and predicted, from S-IC stage ignition through completion of S-IVB second burn is presented in Table 20-9. A comparison of actual and predicted mass, center of gravity and moment of inertia is shown in Table 20-10.

Table 20-1. Total Vehicle Mass - S-IC Burn Phase - Kilograms

EVENTS	GROUND IGNITION		HOLDDOWN ARM RELEASE		CENTER ENGINE CUTOFF		OUTBOARD ENGINE CUTOFF		S-IC/S-II SEPARATION	
	PRED	ACT	PRED	ACT	PRED	ACT	PRED	ACT	PRED	ACT
RANGE TIME--SEC	-6.39	-6.37	.25	.25	135.26	135.16	160.20	161.63	160.91	152.31
S-IC STAGE DRY	133447.	133344.	133447.	133344.	133447.	133344.	133447.	133344.	133447.	133344.
LOX IN TANK	1477931.	1477050.	1446718.	1443231.	189409.	194713.	668.	1559.	599.	1043.
LOX BELOW TANK	21000.	21087.	21737.	21847.	21720.	21778.	16761.	16853.	14629.	14994.
LOX ULLAGE GAS	190.	191.	210.	222.	2590.	2878.	3062.	3377.	3068.	3382.
RP1 IN TANK	642892.	641271.	632749.	630605.	92682.	91987.	9997.	6993.	8897.	5854.
RP1 BELOW TANK	4313.	4306.	5996.	5989.	5996.	5989.	5958.	5951.	5958.	5951.
RP1 ULLAGE GAS	35.	73.	35.	76.	211.	230.	240.	254.	241.	255.
N2 PURGE GAS	36.	36.	36.	36.	20.	20.	20.	20.	20.	20.
HELIUM IN BOTTLE	289.	288.	289.	285.	113.	132.	83.	108.	83.	107.
FROST	635.	635.	635.	635.	340.	340.	340.	340.	340.	340.
RETROMOTOR PROP	1027.	1027.	1027.	1027.	1027.	1027.	1027.	1027.	1027.	1027.
OTHER	239.	239.	239.	239.	239.	239.	239.	239.	239.	239.
TOTAL S-IC STAGE	2282034.	2279549.	2243118.	2237537.	447793.	452677.	171842.	170065.	168548.	166566.
TOTAL S-IC/S-II IS	5262.	5255.	5262.	5255.	5262.	5255.	5262.	5255.	5229.	5222.
TOTAL S-II STAGE	484590.	484159.	484590.	484159.	484331.	483901.	484331.	483901.	484331.	483901.
TOT S-II/S-IVB IS	3665.	3649.	3665.	3649.	3665.	3649.	3665.	3649.	3665.	3649.
TOTAL S-IVB STAGE	118858.	119223.	118858.	119223.	118722.	119132.	118722.	119132.	118722.	119132.
TOTAL INSTRU UNIT	1930.	1935.	1930.	1935.	1930.	1935.	1930.	1935.	1930.	1935.
TOTAL SPACECRAFT	48731.	48625.	48731.	48625.	48731.	48625.	48731.	48625.	48731.	48625.
TOTAL UPPER STAGE	663035.	662847.	663035.	662847.	662641.	662497.	662641.	662497.	662607.	662464.
TOTAL VEHICLE	2945069.	2942396.	2906153.	2900383.	1110434.	1115175.	834483.	832562.	831155.	829031.

Table 20-2. Total Vehicle Mass - S-IC Burn Phase - Pounds Mass

EVENTS	GROUND IGNITION		HOLDDOWN ARM RELEASE		CENTER ENGINE CUTOFF		OUTBOARD ENGINE CUTOFF		S-IC/S-II SEPARATION	
	PRED	ACT	PRED	ACT	PRED	ACT	PRED	ACT	PRED	ACT
RANGE TIME--SEC	-6.39	-6.37	.25	.25	135.26	135.16	160.20	161.63	160.91	162.31
S-IC STAGE DRY	294200.	293974.	294200.	293974.	294200.	293974.	294200.	293974.	294200.	293974.
LOX IN TANK	3258280.	3256338.	3199469.	3181780.	417575.	429259.	1472.	3437.	1321.	2300.
LOX BELOW TANK	46296.	46489.	47921.	48164.	47884.	48013.	36953.	37155.	32251.	33056.
LOX ULLAGE GAS	418.	422.	463.	489.	5710.	6346.	6750.	7444.	6763.	7457.
RP1 IN TANK	1417335.	1413761.	1394972.	1390245.	204328.	202797.	22039.	15417.	19615.	12927.
RP1 BELOW TANK	9509.	9493.	13219.	13203.	13219.	13203.	13136.	13120.	13136.	13120.
RP1 ULLAGE GAS	77.	161.	77.	168.	464.	507.	529.	560.	531.	562.
N2 PURGE GAS	80.	80.	80.	80.	43.	43.	43.	43.	43.	43.
HELIUM IN BOTTLE	636.	636.	636.	629.	249.	290.	183.	237.	182.	235.
FROST	1400.	1400.	1400.	1400.	750.	750.	750.	750.	750.	750.
RETROMOTOR PROP	2264.	2264.	2264.	2264.	2264.	2264.	2264.	2264.	2264.	2264.
OTHER	528.	528.	528.	528.	528.	528.	528.	528.	528.	528.
TOTAL S-IC STAGE	5031024.	5025546.	4945228.	4932924.	987215.	997983.	378848.	374929.	371584.	367215.
TOTAL S-IC/S-II IS	11600.	11585.	11600.	11585.	11600.	11585.	11600.	11585.	11527.	11512.
TOTAL S-II STAGE	1068337.	1067389.	1068337.	1067389.	1067767.	1066819.	1067767.	1066819.	1067767.	1066819.
TOT S-II/S-IVB IS	8081.	8045.	8081.	8045.	8081.	8045.	8081.	8045.	8081.	8045.
TOTAL S-IVB STAGE	262037.	262841.	262037.	262841.	261737.	262641.	261737.	262641.	261737.	262641.
TOTAL INSTRU UNIT	4254.	4267.	4254.	4267.	4254.	4267.	4254.	4267.	4254.	4267.
TOTAL SPACECRAFT	107433.	107200.	107433.	107200.	107433.	107200.	107433.	107200.	107433.	107200.
TOTAL UPPER STAGE	1461742.	1461327.	1461742.	1461327.	1460872.	1460557.	1460872.	1460557.	1460799.	1460484.
TOTAL VEHICLE	6492766.	6486873.	6406970.	6394251.	2448087.	2458540.	1839720.	1835486.	1832384.	1827700.

20-4

Table 20-3. Total Vehicle Mass - S-II Burn Phase - Kilograms

EVENTS	S-IC IGNITION		S-II IGNITION		S-II MAINSTAGE		S-II ENGINE CUTOFF		S-II/S-IVB SEPARATION	
	PRED	ACT	PRED	ACT	PRED	ACT	PRED	ACT	PRED	ACT
RANGE TIME--SEC	-6.89	-6.37	162.61	164.05	164.61	166.30	554.13	552.64	555.04	553.50
S-IC/S-II IS SMALL	612.	611.								
S-IC/S-II IS LARGE	4032.	4033.	4032.	4033.	4032.	4033.				
S-IC/S-II IS PROP	617.	610.	313.	309.	0.	0.				
TOTAL S-IC/S-II IS	5262.	5255.	4345.	4343.	4032.	4033.				
S-II STAGE DRY	38268.	38226.	38268.	38226.	38268.	38226.	38268.	38226.	38268.	38225.
LOX IN TANK	373249.	372717.	373249.	372717.	372788.	372270.	656.	816.	543.	689.
LOX BELOW TANK	737.	737.	737.	737.	800.	800.	787.	787.	797.	737.
LOX ULLAGE GAS	179.	184.	179.	184.	181.	186.	2320.	2444.	2322.	2444.
LH2 IN TANK	71668.	71808.	71661.	71801.	71448.	71592.	1966.	1973.	1916.	1930.
LH2 BELOW TANK	105.	105.	111.	112.	128.	128.	123.	123.	123.	123.
LH2 ULLAGE GAS	77.	77.	77.	77.	77.	78.	708.	737.	709.	737.
INSULATION PURGE	54.	54.								
FROST	204.	204.								
START TANK GAS	14.	14.	14.	14.	2.	2.	2.	2.	2.	2.
OTHER	34.	34.	34.	34.	34.	34.	34.	34.	34.	34.
TOTAL S-II STAGE	484590.	484159.	484331.	483901.	483727.	483315.	44866.	45143.	44705.	44972.
TOT S-II/S-IVB IS	3665.	3649.	3665.	3649.	3665.	3649.	3665.	3649.	3565.	3543.
TOTAL S-IVB STAGE	118958.	119223.	118722.	119132.	118722.	119132.	118722.	119132.	118720.	119130.
TOTAL INSTRU UNIT	1930.	1935.	1930.	1935.	1930.	1935.	1930.	1935.	1930.	1935.
TOTAL SPACECRAFT	48731.	48625.	48731.	48625.	48731.	48625.	44679.	44572.	44679.	44572.
TOTAL UPPER STAGE	173184.	173432.	173048.	173342.	173048.	173342.	168996.	169288.	168993.	169286.
TOTAL VEHICLE	663035.	662847.	661724.	661585.	660807.	660690.	213862.	214432.	213699.	214258.

Table 20-4. Total Vehicle Mass - S-II Burn Phase - Pounds Mass

EVENTS	S-IC IGNITION		S-II IGNITION		S-II MAINSTAGE		S-II ENGINE CUTOFF		S-II/S-IVB SEPARATION	
	PRED	ACT	PRED	ACT	PRED	ACT	PRED	ACT	PRED	ACT
RANGE TIME--SEC	-6.39	-6.37	162.61	164.05	164.61	166.30	554.13	552.64	555.04	553.50
S-IC/S-II IS SMALL	1350.	1348.								
S-IC/S-II IS LARGE	8890.	8892.	8890.	8892.	8890.	8892.				
S-IC/S-II IS PROP	1360.	1345.	689.	682.	0.	0.				
TOTAL S-IC/S-II IS	11600.	11585.	9579.	9574.	8890.	8892.				
S-II STAGE DRY	84367.	84273.	84367.	84273.	84367.	84273.	84367.	84273.	84367.	84273.
LOX IN TANK	822874.	821700.	822874.	821700.	821856.	820714.	1447.	1800.	1197.	1513.
LOX BELOW TANK	1625.	1625.	1625.	1625.	1764.	1764.	1736.	1736.	1736.	1736.
LOX ULLAGE GAS	395.	405.	395.	405.	399.	409.	5114.	5387.	5119.	5337.
LH2 IN TANK	158000.	158310.	157986.	158295.	157516.	157834.	4335.	4350.	4224.	4254.
LH2 BELOW TANK	231.	231.	245.	246.	282.	282.	272.	272.	272.	272.
LH2 ULLAGE GAS	169.	169.	169.	169.	171.	171.	1561.	1625.	1562.	1625.
INSULATION PURGE	120.	120.								
FROST	450.	450.								
START TANK GAS	30.	30.	30.	30.	5.	5.	5.	5.	5.	5.
OTHER	76.	76.	76.	76.	76.	76.	76.	76.	76.	76.
TOTAL S-II STAGE	1068337.	1067389.	1067767.	1066819.	1066436.	1065528.	98913.	99524.	98558.	99146.
TOT S-II/S-IVB IS	8081.	8045.	8081.	8045.	8081.	8045.	8081.	8045.	8081.	8045.
TOTAL S-IVB STAGE	262037.	262841.	261737.	262641.	261737.	262641.	261737.	262641.	261732.	262536.
TOTAL INSTRU UNIT	4254.	4267.	4254.	4267.	4254.	4267.	4254.	4267.	4254.	4267.
TOTAL SPACECRAFT	107433.	107200.	107433.	107200.	107433.	107200.	99500.	99264.	98500.	98264.
TOTAL UPPER STAGE	381805.	382353.	381505.	382153.	381505.	382153.	372572.	373217.	372567.	373212.
TOTAL VEHICLE	1461742.	1461327.	1458851.	1458546.	1456831.	1456573.	471485.	472741.	471125.	472359.

20-6

Table 20-5. Total Vehicle Mass - S-IVB First Burn Phase - Kilograms

EVENTS	S-IC IGNITION		S-IV3 IGNITION		S-IVB MAINSTAGE		S-IVB ENGINE CUTOFF		S-IVB END DECAY	
	PRED	ACT	PRED	ACT	PRED	ACT	PRED	ACT	PRED	ACT
RANGE TIME--SEC	-6.39	-6.37	558.14	556.81	560.64	559.31	703.54	703.76	703.74	703.96
S-IVB STAGE DRY	11680.	11648.	11657.	11525.	11657.	11625.	11596.	11563.	11596.	11563.
LOX IN TANK	86539.	86964.	86539.	86964.	86376.	86801.	80306.	80548.	80275.	80516.
LOX BELOW TANK	166.	166.	166.	166.	180.	180.	180.	180.	180.	180.
LOX ULLAGE GAS	18.	22.	18.	22.	25.	23.	102.	100.	102.	101.
LH2 IN TANK	19709.	19659.	19705.	19654.	19649.	19598.	14429.	14291.	14415.	14277.
LH2 BELOW TANK	22.	22.	26.	26.	26.	26.	26.	26.	26.	26.
LH2 ULLAGE GAS	20.	21.	20.	21.	21.	21.	66.	65.	67.	66.
ULLAGE MOTOR PROP	54.	54.	10.	10.	1.	1.	1.	1.	1.	1.
APS PROPELLANT	286.	303.	286.	303.	286.	303.	295.	298.	285.	298.
HELIUM IN BOTTLES	200.	200.	200.	200.	200.	200.	178.	176.	178.	176.
START TANK GAS	2.	2.	2.	2.	0.	0.	3.	3.	3.	3.
FROST	136.	136.	0.	45.	0.	45.	0.	45.	0.	45.
OTHER	25.	25.	25.	25.	25.	25.	25.	25.	25.	25.
TOTAL S-IVB STAGE	118858.	119223.	118655.	119065.	118445.	118848.	87197.	87322.	87152.	87278.
TOTAL INSTFU UNIT	1930.	1935.	1930.	1935.	1930.	1935.	1930.	1935.	1930.	1935.
TOTAL SPACECRAFT	44679.	44572.	44579.	44572.	44679.	44572.	44679.	44572.	44679.	44572.
TOTAL UPPER STAGE	46608.	46507.	46608.	46507.	46608.	46507.	46608.	46507.	46608.	46507.
TOTAL VEHICLE	165466.	165730.	165263.	165573.	165054.	165355.	133806.	133830.	133760.	133786.

20-7

Table 20-6. Total Vehicle Mass - S-IVB First Burn Phase - Pounds Mass

EVENTS	S-IC IGNITION		S-IVB IGNITION		S-IVB MAINSTAGE		S-IVS ENGINE CUTOFF		S-IVB END DECAY	
	PRED	ACT	PRED	ACT	PRED	ACT	PRED	ACT	PRED	ACT
RANGE TIME--SEC	-6.39	-6.37	558.14	556.81	560.64	559.31	703.54	703.76	733.74	733.98
S-IVB STAGE DRY	25750.	25680.	25699.	25629.	25699.	25629.	25564.	25492.	25564.	25432.
LOX IN TANK	190785.	191722.	190785.	191722.	190426.	191363.	132953.	133486.	132883.	133416.
LOX BELOW TANK	367.	367.	367.	367.	397.	397.	397.	397.	397.	397.
LOX ULLAGE GAS	40.	49.	40.	49.	56.	50.	224.	221.	225.	223.
LH2 IN TANK	43452.	43340.	43442.	43330.	43318.	43206.	31810.	31506.	31779.	31476.
LH2 BELOW TANK	48.	48.	58.	58.	58.	58.	58.	58.	58.	58.
LH2 ULLAGE GAS	45.	46.	45.	45.	46.	46.	147.	144.	147.	145.
ULLAGE MOTOR PROP	118.	118.	22.	22.	0.	0.	0.	0.	0.	0.
APS PROPELLANT	630.	668.	630.	668.	630.	668.	628.	658.	628.	658.
HELIUM IN BOTTLES	441.	442.	441.	442.	440.	441.	393.	388.	392.	388.
START TANK GAS	5.	5.	5.	5.	1.	1.	7.	7.	7.	7.
FROST	300.	300.	0.	100.	0.	100.	0.	100.	0.	100.
OTHER	56.	56.	56.	56.	56.	56.	56.	56.	56.	56.
TOTAL S-IVB STAGE	262037.	262841.	261589.	262494.	261127.	262015.	192237.	192513.	192137.	192415.
TOTAL INSTRU UNIT	4254.	4267.	4254.	4267.	4254.	4267.	4254.	4267.	4254.	4257.
TOTAL SPACECRAFT	98500.	98264.	98500.	98264.	98500.	98264.	98500.	98264.	98500.	98264.
TOTAL UPPER STAGE	102754.	102531.	102754.	102531.	102754.	102531.	102754.	102531.	102754.	102531.
TOTAL VEHICLE	364791.	365372.	364343.	365025.	363881.	364546.	294991.	295044.	294891.	294947.

20-8

Table 20-7. Total Vehicle Mass - S-IVB Second Burn Phase - Kilograms

EVENTS	S-IVB IGNITION		S-IVB MAINSTAGE		S-IVB ENGINE CUTOFF		S-IVB END DECAY		SPACECRAFT SEPARATION	
	PRED	ACT	PRED	ACT	PRED	ACT	PRED	ACT	PRED	ACT
RANGE TIME--SEC	9204.92	9207.52	9207.42	9210.02	9548.64	9550.58	9548.79	9550.83	14904.87	14195.72
S-IVB STAGE DRY	11596.	11563.	11596.	11563.	11596.	11563.	11596.	11563.	11596.	11563.
LOX IN TANK	60194.	60375.	60030.	60211.	2068.	2244.	2037.	2212.	2037.	2212.
LOX BELOW TANK	166.	166.	180.	180.	180.	180.	180.	180.	166.	166.
LOX ULLAGE GAS	159.	156.	162.	158.	252.	269.	252.	269.	252.	269.
LH2 IN TANK	13151.	13187.	13086.	13116.	892.	973.	879.	961.	879.	951.
LH2 BELOW TANK	26.	26.	26.	26.	26.	26.	26.	26.	22.	22.
LH2 ULLAGE GAS	156.	143.	156.	144.	272.	274.	272.	274.	272.	274.
ULLAGE MOTOR PROP	0.	0.	0.	0.	0.	0.	0.	0.	0.	0.
APS PROPELLANT	183.	246.	183.	246.	179.	241.	179.	241.	144.	206.
HELIUM IN BOTTLES	149.	163.	149.	163.	90.	99.	90.	99.	90.	99.
START TANK GAS	2.	2.	0.	0.	3.	3.	3.	3.	3.	3.
FROST	0.	45.	0.	45.	0.	45.	0.	45.	0.	45.
OTHER	25.	25.	25.	25.	25.	25.	25.	25.	25.	25.
TOTAL S-IVB STAGE	85809.	86092.	85594.	85878.	15584.	15943.	15539.	15899.	15486.	15845.
TOTAL INSTRU UNIT	1930.	1935.	1930.	1935.	1930.	1935.	1930.	1935.	1930.	1935.
TOTAL SPACECRAFT	44679.	44572.	44679.	44572.	44679.	44572.	44679.	44572.	525.	525.
TOTAL UPPER STAGE	46608.	46507.	46608.	46507.	46608.	46507.	46608.	46507.	2556.	2561.
TOTAL VEHICLE	132417.	132600.	132203.	132385.	62192.	62450.	62147.	62407.	18041.	18408.

20-9

Table 20-8. Total Vehicle Mass - S-IVB Second Burn Phase - Pounds Mass

EVENTS	S-IVB IGNITION		S-IVB MAINSTAGE		S-IVB ENGINE CUTOFF		S-IVB END DECAY		SPACECRAFT SEPARATION	
	PRED	ACT	PRED	ACT	PRED	ACT	PRED	ACT	PRED	ACT
RANGE TIME--SEC	9204.92	9207.52	9207.42	9210.02	9548.64	9550.58	9548.79	9550.83	14904.87	14185.72
S-IVB STAGE DRY	25564.	25492.	25564.	25492.	25564.	25492.	25564.	25492.	25564.	25492.
LOX IN TANK	132705.	133104.	132343.	132742.	4560.	4947.	4491.	4877.	4491.	4877.
LOX BELOW TANK	367.	367.	397.	397.	397.	397.	397.	397.	367.	367.
LOX ULLAGE GAS	351.	343.	358.	349.	555.	593.	555.	593.	555.	593.
LH2 IN TANK	28993.	29058.	28850.	28915.	1967.	2146.	1937.	2119.	1937.	2119.
LH2 BELOW TANK	58.	58.	58.	58.	58.	58.	58.	58.	48.	48.
LH2 ULLAGE GAS	344.	316.	345.	317.	599.	603.	599.	604.	599.	604.
ULLAGE MOTOR PROP	0.	0.	0.	0.	0.	0.	0.	0.	0.	0.
APS PROPELLANT	403.	542.	403.	542.	395.	531.	395.	531.	318.	454.
HELIUM IN BOTTLES	329.	350.	329.	359.	198.	218.	198.	218.	198.	218.
START TANK GAS	5.	5.	1.	1.	7.	7.	7.	7.	7.	7.
FPOST	0.	100.	0.	100.	0.	100.	0.	100.	0.	100.
OTHER	56.	56.	56.	56.	56.	56.	56.	56.	56.	56.
TOTAL S-IVB STAGE	189176.	189801.	188703.	189328.	34356.	35148.	34257.	35052.	34140.	34935.
TOTAL INSTRU UNIT	4254.	4267.	4254.	4267.	4254.	4267.	4254.	4267.	4254.	4267.
TOTAL SPACECRAFT	98500.	98264.	98500.	98264.	98500.	98264.	98500.	98264.	1380.	1380.
TOTAL UPPER STAGE	102754.	102531.	102754.	102531.	102754.	102531.	102754.	102531.	5634.	5647.
TOTAL VEHICLE	291930.	292332.	291457.	291859.	137110.	137679.	137011.	137583.	39774.	40582.

20-10

Table 20-9. Flight Sequence Mass Summary

MASS HISTORY	PREDICTED		ACTUAL	
	KG	LBM	KG	LBM
S-IC STAGE, TOTAL	2282034.	5031024.	2279549.	5025546.
S-IC/S-II INTERSTAGE, TOTAL	5262.	11600.	5255.	11585.
S-II STAGE, TOTAL	484590.	1068337.	484159.	1067389.
S-II/SIIVB INTERSTAGE	3665.	8081.	3649.	8045.
S-IVB STAGE, TOTAL	118858.	262037.	119223.	262841.
INSTRUMENT UNIT	1930.	4254.	1935.	4267.
SPACECRAFT INCLUDING LES	48731.	107433.	48625.	107200.
1ST FLT STG AT IGN	2945069.	6492766.	2942396.	6486873.
S-IC THRUST BUILDUP	-38916.	-85795.	-42013.	-92622.
1ST FLT STG HOLDDOWN ARM REL	2906153.	6406970.	2900383.	6394251.
S-IC FROST	-295.	-650.	-295.	-650.
S-IC MAINSTAGE PROPELLANT	-2069955.	-4563470.	-2066096.	-4554962.
S-IC N2 PURGE	-17.	-37.	-17.	-37.
S-IC INBD ENGINE T.O. PROP	-824.	-1816.	-875.	-1928.
S-IC INBD ENG EXPENDED PROP	-185.	-408.	-190.	-418.
S-II INSULATION PURGE GAS	-54.	-120.	-54.	-120.
S-II FROST	-204.	-450.	-204.	-450.
S-IVB FROST	-136.	-300.	-91.	-200.
1ST FLT STAGE AT S-IC OECOS	834483.	1839720.	832562.	1835486.
S-IC OTBD ENGINE T.O. PROP	-3295.	-7263.	-3499.	-7713.
S-IC/S-II ULLAGE RKT PROP	-33.	-73.	-33.	-73.
1ST FLT STAGE AT SIC/SII SEP	831155.	1832384.	829031.	1827700.
S-IC STAGE AT SEPARATION	-168548.	-371584.	-166566.	-367216.
S-IC/S-II INTERSTAGE SMALL	-612.	-1350.	-611.	-1348.
S-IC/S-II ULLAGE RKT PROP	-83.	-184.	-83.	-184.
2ND FLT STAGE AT S-II SSC	661912.	1459265.	661769.	1458952.
S-II FUEL LEAD	0.	0.	0.	0.
S-IC/S-II ULLAGE RKT PROP	-188.	-414.	-184.	-406.
2ND FLT STAGE AT S-II IGN	661724.	1458851.	661585.	1458546.
S-II T.B. PROPELLANT	-593.	-1306.	-574.	-1266.
S-II START TANK	-11.	-25.	-11.	-25.
S-IC/S-II ULLAGE RKT PROP	-313.	-689.	-309.	-682.
2ND FLT STAGE AT MAINSTAGE	660807.	1456831.	660690.	1456573.
S-II MAINSTAGE + VENTING	-438804.	-967396.	-438112.	-965871.
LAUNCH ESCAPE SYSTEM	-4052.	-8933.	-4053.	-8936.
S-IC/S-II INTERSTAGE LARGE	-4032.	-8890.	-4033.	-8892.
S-II T.O. PROPELLANT	-57.	-127.	-60.	-132.
2ND FLT STAGE AT S-II C.O.S.	213862.	471485.	214432.	472741.
S-II T.O. PROPELLANT	-161.	-355.	-171.	-378.
S-IVB ULLAGE PROPELLANT	-2.	-5.	-2.	-5.
2ND FLT STG AT SII/SIVB SEP	213699.	471125.	214258.	472358.
S-II STAGE AT SEPARATION	-44705.	-98558.	-44972.	-99146.
S-II/S-IVB INTERSTAGE-DRY	-3185.	-7021.	-3167.	-6982.
S-II/S-IVB IS PROP	-481.	-1060.	-482.	-1063.
S-IVB AFT FRAME	-22.	-48.	-22.	-48.
S-IVB ULLAGE PROPELLANT	-1.	-3.	-1.	-3.
S-IVB DET PACKAGE	-1.	-3.	-1.	-3.
3RD FLT STG AT 1ST SSC	165304.	364432.	165612.	365113.
S-IVB ULLAGE PROPELLANT	-40.	-88.	-40.	-88.
S-IVB FUEL LEAD LOSS	-0.	-0.	0.	0.

Table 20-9. Flight Sequence Mass Summary (Continued)

MASS HISTORY	PREDICTED		ACTUAL	
	KG	LBM	KG	LBM
3RD FLT STG AT 1ST SIVB IGN	165263.	364343.	165573.	365025.
S-IVB ULLAGE PROPELLANT	-10.	-22.	-10.	-22.
S-IVB START TANK	-2.	-4.	-2.	-4.
S-IVB T.B. PROPELLANT	-198.	-437.	-205.	-453.
3RD FLT STG AT MAINSTAGE	165054.	363881.	165355.	364546.
S-IVB ULLAGE ROCKET CASES	-61.	-135.	-62.	-137.
S-IVB MAINSTAGE PROP	-31186.	-68753.	-31459.	-69355.
S-IVB APS PROPELLANT	-1.	-2.	-5.	-10.
3RD FLT STG AT 1ST SIVB COS	133806.	294991.	133830.	295044.
S-IVB T.D. PROPELLANT	-45.	-99.	-44.	-97.
3RD FLT STG AT END 1ST TD	133760.	294891.	133786.	294947.
S-IVB ENG PROP EXPENDED	-18.	-40.	-18.	-40.
S-IVB FUEL TANK LOSS	-1188.	-2619.	-1014.	-2236.
S-IVB LOX TANK LOSS	-20.	-43.	-83.	-184.
S-IVB APS PROPELLANT	-102.	-225.	-53.	-116.
S-IVB START TANK	-1.	-2.	-1.	-2.
S-IVB O2/H2 BURNER	-7.	-16.	-7.	-16.
3RD FLT STG AT 2ND SSC	132424.	291946.	132609.	292353.
S-IVB FUEL LEAD LOSS	-7.	-16.	-10.	-21.
3RD FLT STG AT 2ND SIVB IGN	132417.	291930.	132600.	292332.
S-IVB START TANK	-2.	-4.	-2.	-4.
S-IVB T.B. PROPELLANT	-213.	-468.	-213.	-469.
3RD FLT STG AT MAINSTAGE	132203.	291457.	132385.	291859.
S-IVB MAINSTAGE PROP	-70007.	-154339.	-69930.	-154169.
S-IVB APS PROPELLANT	-4.	-8.	-5.	-11.
3RD FLT STG AT 2ND SIVB COS	62192.	137110.	62450.	137679.
S-IVB T.D. PROPELLANT	-45.	-99.	-44.	-96.
3RD FLT STG AT END 2ND TD	62147.	137011.	62407.	137583.
S-IVB ENG PROP EXPENDED	-18.	-40.	-18.	-40.
S-IVB APS PROPELLANT	-35.	-77.	-35.	-77.
SPACECRAFT SEPARATED	-44053.	-97120.	-43946.	-96884.
SPACECRAFT NOT SEPARATED	-626.	-1380.	-626.	-1380.
INSTRUMENT UNIT	-1930.	-4254.	-1935.	-4267.
S-IVB STAGE AT SEPARATION	-15486.	-34140.	-15846.	-34935.

Table 20-10. Mass Characteristics Comparison

EVENT	MASS		LONGITUDINAL C.G. (X STR.)		RADIAL C.G.		ROLL MOMENT OF INERTIA		PITCH MOMENT OF INERTIA		YAW MOMENT OF INERTIA	
	KILO POUNDS	O/O DEV.	METERS INCHES	DELTA	METERS INCHES	DELTA	KG-M2 X 10-6	O/O DEV.	KG-M2 X 10-6	O/O DEV.	KG-M2 X 10-6	O/O DEV.
S-TC STAGE DRY	PRED	133447. 294200.	9.401 370.1		.0703 2.7659		2.642		17.185		17.100	
	ACTUAL	133345. 293974.	9.401 370.1	.000 .00	.0703 2.7659	.0000 .0007	2.640	-.07	17.172	-.07	17.087	-.07
S-TC/S-II INTER-STAGE TOTAL	PRED	5262. 11600.	41.623 1638.7		.1546 6.0877		.134		.081		.081	
	ACTUAL	5255. 11585.	41.626 1638.8	.003 .10	.1563 6.1555	.0017 .0678	.134	-.12	.080	-.12	.081	-.12
S-II STAGE DRY	PRED	38269. 84367.	44.113 1894.2		.1116 4.3932		.633		2.176		2.188	
	ACTUAL	38226. 84273.	44.090 1893.3	-.023 -.90	.1116 4.3932	.0000 .0000	.632	-.11	2.174	-.11	2.185	-.11
S-II/S-IVR INTER-STAGE TOTAL	PRED	3666. 8081.	65.860 2592.9		.0573 2.2561		.065		.043		.044	
	ACTUAL	3650. 8045.	65.936 2595.9	.076 3.00	.0598 2.3537	.0025 .0976	.065	-.44	.043	-.44	.044	-.44
S-IVR STAGE DRY	PRED	11681. 25750.	72.601 2858.3		.1978 7.7878		.082		.309		.308	
	ACTUAL	11649. 25680.	72.601 2858.3	.000 .00	.1978 7.7878	.0000 .0000	.082	-.27	.308	-.27	.308	-.27
VEHICLE INSTRUMENT UNIT	PRED	1930. 4254.	82.415 3244.7		.3511 13.8232		.019		.010		.009	
	ACTUAL	1936. 4267.	82.415 3244.7	.000 .31	.3511 13.8232	.0000 .0000	.019	.31	.010	.31	.009	.31
SPACECRAFT TOTAL	PRED	48731. 107433.	91.653 3608.4		.1085 4.2720		.090		1.552		1.555	
	ACTUAL	48626. 107200.	91.658 3608.6	.005 .20	.1099 4.3267	.0014 .0547	.088	-1.70	1.549	-.21	1.550	-.30
1ST FLIGHT STAGE AT IGNITION	PRED	2945070. 6492766.	30.311 1193.4		.0042 .1640		3.786		915.749		915.659	
	ACTUAL	2942397. 6486874.	30.317 1193.6	.006 -.24	.0042 .1640	.0000 .0000	3.779	-.18	915.682	-.00	915.592	-.00
1ST FLIGHT STAGE AT HOLD/DOWN ARM RELEASE	PRED	2906153. 6406970.	30.257 1191.2		.0042 .1640		3.789		914.514		914.424	
	ACTUAL	2900384. 6394252.	30.259 1191.3	.002 -.19	.0042 .1640	.0000 .0000	3.782	-.18	914.236	-.03	914.146	-.03
1ST FLIGHT STAGE AT OUTBOARD ENGINE CUTOFF SIGNAL	PRED	834484. 1839720.	46.216 1819.5		.0141 .5547		3.773		445.816		445.729	
	ACTUAL	832563. 1835486.	46.332 1824.1	.117 4.59	.0142 .5604	.0001 .0056	3.767	-.15	441.940	-.86	441.853	-.86
1ST FLIGHT STAGE AT SEPARATION	PRED	831156. 1832384.	46.359 1825.2		.0141 .5547		3.771		441.412		441.345	
	ACTUAL	829031. 1827700.	46.481 1830.0	.122 4.79	.0142 .5604	.0001 .0056	3.765	-.15	437.485	-.89	437.348	-.89
2ND FLIGHT STAGE AT START SEQUENCE COMMAND	PRED	661912. 1459265.	55.750 2194.9		.0142 .5601		1.020		134.833		134.819	
	ACTUAL	661770. 1458952.	55.762 2195.4	.012 .48	.0142 .5600	-.0000 -.0001	1.018	-.25	134.848	.02	134.861	.02
2ND FLIGHT STAGE AT MAINSTAGE	PRED	660808. 1456831.	55.762 2195.4		.0142 .5601		1.009		134.714		134.720	
	ACTUAL	660691. 1456573.	55.773 2195.8	.011 .44	.0142 .5600	-.0000 -.0001	1.006	-.24	134.731	.02	134.744	.02
2ND FLIGHT STAGE AT CUTOFF SIGNAL	PRED	713862. 471485.	70.792 2787.1		.0415 1.6325		.905		45.508		45.513	
	ACTUAL	714432. 472741.	70.754 2785.6	-.038 -1.50	.0415 1.6325	.0000 .0000	.902	-.27	45.694	.41	45.706	.43

Table 20-10. Mass Characteristics Comparison (Continued)

EVENT	MASS		LONGITUDINAL C.G. (X STA.)		RADIAL C.G.		ROLL MOMENT OF INERTIA		PITCH MOMENT OF INERTIA		YAW MOMENT OF INERTIA	
	KILO POUNDS	O/O DEV.	METERS INCHES	DELTA	METERS INCHES	DELTA	KG-M ² X10 ⁻⁶	O/O DEV.	KG-M ² X10 ⁻⁶	O/O DEV.	KG-M ² X10 ⁻⁶	O/O DEV.
2ND FLIGHT STAGE AT SEPARATION	PRED	213699. 471125.	70.811 2787.8		.0417 1.6425		.905		45.407		45.407	
	ACTUAL	214258. 472358.	70.775 2786.4	-.036 -1.43	.0415 1.6325	-.0001 -.0100	.902	-.27	45.580	-.40	45.593	-.41
3RD FLIGHT STAGE AT 1ST START SEQUENCE COMMAND	PRED	165304. 364472.	77.084 3034.8		.0377 1.4841		.195		13.342		13.339	
	ACTUAL	165613. 365113.	77.063 3034.0	-.020 .19	.0378 1.4872	.0001 .0031	.194	-.46	13.331	-.08	13.328	-.08
3RD FLIGHT STAGE AT 1ST IGNITION	PRED	165264. 364343.	77.081 3034.7		.0377 1.4841		.195		13.343		13.340	
	ACTUAL	165573. 365025.	77.060 3033.9	-.020 .19	.0378 1.4872	.0001 .0031	.194	-.46	13.331	-.08	13.328	-.08
3RD FLIGHT STAGE AT 1ST MAINSTAGE	PRED	165054. 363881.	77.084 3034.8		.0377 1.4841		.195		13.341		13.337	
	ACTUAL	165356. 364546.	77.062 3034.0	-.021 .19	.0380 1.4957	.0003 .0116	.194	-.46	13.329	-.08	13.326	-.08
3RD FLIGHT STAGE AT 1ST CUTOFF SIGNAL	PRED	133806. 294991.	78.015 3071.5		.0463 1.8224		.194		12.518		12.515	
	ACTUAL	133830. 295044.	77.994 3070.6	-.021 .02	.0466 1.8338	.0003 .0115	.193	-.50	12.512	-.04	12.509	-.04
3RD FLIGHT STAGE AT 1ST END THRUST DECAY, START COAST	PRED	133761. 294891.	78.017 3071.6		.0463 1.8224		.194		12.517		12.514	
	ACTUAL	133796. 294947.	77.996 3070.7	-.021 .02	.0466 1.8338	.0003 .0115	.193	-.50	12.511	-.04	12.508	-.04
3RD FLIGHT STAGE AT 2ND START SEQUENCE COMMAND	PRED	132425. 291946.	78.027 3071.9		.0464 1.8250		.193		12.512		12.510	
	ACTUAL	132610. 292353.	78.006 3071.1	-.021 .14	.0467 1.8392	.0004 .0142	.192	-.11	12.506	-.04	12.504	-.05
3RD FLIGHT STAGE AT 2ND IGNITION	PRED	132418. 291930.	78.026 3071.9		.0464 1.8250		.193		12.514		12.512	
	ACTUAL	132600. 292332.	78.006 3071.1	-.020 .14	.0467 1.8392	.0004 .0142	.192	-.11	12.509	-.04	12.506	-.05
3RD FLIGHT STAGE AT 2ND MAINSTAGE	PRED	132203. 291457.	78.033 3072.2		.0464 1.8250		.193		12.509		12.507	
	ACTUAL	132386. 291859.	78.012 3071.3	-.021 .14	.0467 1.8392	.0004 .0142	.192	-.11	12.503	-.04	12.501	-.05
3RD FLIGHT STAGE AT 2ND CUTOFF SIGNAL	PRED	62192. 137109.	85.722 3374.9		.0974 3.8365		.192		5.315		5.312	
	ACTUAL	62450. 137678.	85.631 3371.3	-.091 .42	.0976 3.8413	.0001 .0048	.192	-.14	5.391	1.43	5.388	1.43
3RD FLIGHT STAGE AT 2ND END THRUST DECAY	PRED	62147. 137010.	85.734 3375.3		.0974 3.8365		.192		5.304		5.301	
	ACTUAL	62407. 137582.	85.642 3371.7	-.092 .42	.0976 3.8413	.0001 .0048	.192	-.14	5.380	1.45	5.377	1.44
CSM SEPARATED	PRED	32034. 70622.	78.477 3089.6		.0766 3.0153		.136		1.633		1.628	
	ACTUAL	32353. 71326.	78.387 3086.1	-.090 1.00	.0774 3.0458	.0004 .0305	.136	-.52	1.655	1.34	1.649	1.31
CSM DOCKED	PRED	60906. 134273.	85.162 3352.8		.1262 4.9695		.183		4.758		4.752	
	ACTUAL	61179. 134875.	85.073 3349.3	-.088 .45	.1261 4.9640	-.0001 -.0056	.182	-.22	4.831	1.53	4.824	1.52
SPACECRAFT SEPARATED	PRED	18041. 39773.	73.603 2897.7		.1377 5.4205		.108		.620		.617	
	ACTUAL	18408. 40581.	73.556 2895.9	-.047 2.04	.1347 5.3040	-.0030 -.1165	.108	-.47	.627	1.13	.624	1.06

SECTION 21

MISSION OBJECTIVES ACCOMPLISHMENT

Table 21-1 presents the MSFC AS-505 major flight objectives and detailed test objectives as defined in the Saturn V Mission Implementation Plan, Mission F. An assessment of the degree of accomplishment of each objective is shown. Discussion supporting the assessment can be found in the indicated sections of the Saturn V Launch Vehicle Flight Evaluation Report - AS-505, Apollo 10 Mission.

Table 21-1. Mission Objectives Accomplishment Summary

NO.	MSFC MAJOR FLIGHT OBJECTIVES (MFO) AND MSFC SECONDARY DETAILED TEST OBJECTIVES (DTO)*	DEGREE OF ACCOMPLISHMENT	DISCREPANCIES	PARAGRAPH IN WHICH DISCUSSED
1	Demonstrate launch vehicle capability to inject the Spacecraft (SC) onto the specified translunar trajectory. (MFO)	Complete	None	4.3
2	Demonstrate launch vehicle capability to maintain a specified attitude for Transposition, Docking and SC Ejection (TD&E) maneuver. (MFO)	Complete	None	11.5.4 12.6
3	Demonstrate S-IVB propellant dump and safing. (MFO)	Complete	None	7.13
4	Verify J-2 engine modifications. (DTO)	Complete	None	7.3 9.3.3.3
5	Confirm J-2 engine environment in S-II and S-IVB stages. (DTO)	Complete	None	9.3,16.3.2, 17.3
6	Confirm launch vehicle longitudinal oscillation environment during S-IC burn period.(DTO)	Complete	None	9.2.3
7	Verify that modifications incorporated in the S-IC stage suppress low frequency longitudinal oscillations. (DTO)	Complete	None	9.2.3
8	Confirm launch vehicle longitudinal oscillation environment during S-II stage burn period.(DTO)	Complete	None	9.2.3
9	Demonstrate that early S-II center engine cutoff suppresses S-II stage low frequency longitudinal oscillations. (DTO)	Complete	None	6.3 9.2.3

*There were no MSFC principal test objectives; all test objectives were classified as secondary.

SECTION 22
FAILURES, ANOMALIES AND DEVIATIONS

22.1 SUMMARY

Evaluation of the launch vehicle performance during the AS-505 flight test revealed one area of concern with a mission criticality category of three. Action is planned to prevent reoccurrence of this problem on future flights.

22.2 SYSTEM FAILURES AND ANOMALIES

Table 22-1 defines the criticality categories assigned to the failures and anomalies listed in Table 22-2, which complies with Apollo Program Directive No. 19. Reference paragraph numbers are given for sections in which the specific problem area is discussed in more detail.

Table 22-1. Hardware Criticality Categories For Flight Hardware

CATEGORY	DESCRIPTION
1	Hardware failure which results in loss of life of any crew member. This includes normally passive systems such as the Emergency Detection System (EDS), Launch Escape System (LES), etc.
2	Hardware failure which results in abort of mission but does not cause loss of life.
3	Hardware failure which will not result in abort of mission nor cause loss of life.

22.3 SYSTEM DEVIATIONS

Nine system deviations occurred without any significant effects on the flight or operation of that particular system. Table 22-3 presents these deviations with the recommended corrective actions and a reference to the paragraphs containing further discussion of the deviation. These deviations are of no major concern, but are presented in order to complete the summary of deviations experienced on AS-505.

Table 22-2. Summary of Failures and Anomalies

FAILURE/ANOMALY IDENTIFICATION						RECOMMENDED CORRECTIVE ACTION			
VEHICLE SYSTEM	DESCRIPTION (CAUSE)	EFFECT ON MISSION	MISSION CRITICALITY	EFFECT ON NEXT MISSION	TIME OCCURRENCE (AVERAGE TIME)	DESCRIPTION	ACTION STATUS	VEHICLE EFFECTIVITY	PARAGRAPH REFERENCE
S-IVB Hydraulics	Auxiliary hydraulic pump stopped producing full pressure during Second burn. (Suspect failure of auxiliary hydraulic pump compensator spring guide.)	None	3	None	9425 seconds	Inspection of spring guides for proper fillet radius and proper Rockwell Hardness. Inspect compensator springs to insure all tolerances are met.	Closed for AS-506	AS-506 and Subs	8.7

Table 22-3. Summary of Deviations

VEHICLE SYSTEM	DEVIATION	PROBABLE CAUSE	CORRECTIVE ACTION BEING CONSIDERED	PARAGRAPH REFERENCE
S-IC Propulsion	Low performance of engine No. 1 thrust reduced to standard conditions was 97,000 Newtons (22,000 lbf) below predicted.	Unknown	None. Average thrust over full burn was more nominal.	5.3
S-IC Propulsion	Unexplained LOX suction duct pressure decay of engine No. 5 after CECD.	Unknown	None. Similar occurrences during AS-503 and AS-504 with no effect on mission.	5.6.2
S-II Propulsion	Slightly sharper pressure decay of engine No. 5 helium tank pressure than expected, after ESC.	Leak through J-2 engine helium regulator	None. Decay rate returned to normal at 60 seconds after ESC.	6.2
S-IVB Propulsion/Mechanical	Astronauts reported mild low frequency oscillations (12 to 19 hertz) during first and second burns.	Data indicate S-IVB had typical buildup and decay periods of very mild 12 to 19 hertz oscillations without indications of propulsion/structural coupling.	None anticipated, but MDAC ECP 3218 adds 5 measurements for stability model analyses and flight evaluation of low frequency oscillations.	9.2.3
S-IVB Propulsion/Mechanical	Astronauts reported noisy low level vibrations during latter part of second burn which were superimposed on the 12 to 19 hertz vibrations.	Cycling of the LH ₂ tank NPV valves	Test program at AEDC underway to confirm interacting of LH ₂ tank NPV valves.	9.2.3
S-IVB Propulsion/Hydraulics	Unexpected increase in S-IVB engine driven hydraulic pump outlet pressure (3 percent) shortly after second burn start.	Unknown	None. Has been experienced on other systems (F-100 Aircraft) and is not considered a problem.	8.6
S-IVB Auxiliary/Propulsion System	APS Module No. 1 helium supply pressure decay at approximately 23,400 seconds.	Unknown. Similar problem on AS-504 resulted in change of seal material and additional leak check at KSC.	Being investigated. Leakage rate insufficient to impact mission.	7.12
IU/RF System	Erratic signal strength at receiving station beginning at 23,601 seconds.	Malfunction of coaxial switch.	None. (Coaxial switch to be replaced on AS-507 per previously planned ECP). Omni directional antenna system provided sufficient signal strength to maintain satisfactory communications.	19.5.3.2
IU/GN ₂ Purge System	Sharp drop in IU inlet pressure and increased flowrate at -9.8 hours accompanied by a complete loss of pressure to the Radio-Isotope Thermo-Electrical Generator on the LM.	Opening in the purge duct.	Installation of dual clamps on umbilical connection boat with increased clamp torque.	18.4

SECTION 23
SPACECRAFT SUMMARY

The purpose of the Apollo 10 Mission was to verify lunar module systems operation in the lunar environment, to confirm validity of crew activity schedules designed for the lunar landing mission, to obtain additional data on lunar gravitational harmonics, and to evaluate mission support performance for the combined spacecraft at lunar distance. The Apollo 10 crew was Thomas P. Stafford, Commander; John W. Young, Command Module (CM) Pilot; and Eugene A. Cernan, Lunar Module (LM) Pilot.

The space vehicle was launched from Kennedy Space Center, Florida, at 12:49:00, Eastern Daylight Time (EDT) on May 18, 1969. Following a nominal launch phase, the spacecraft and S-IVB/IU combination was inserted into an earth parking orbit of 185.79 by 184.66 kilometers (100.32 by 99.71 n mi). After checkout of onboard systems, the S-IVB was reignited at 2:33:27.5 elapsed time to place the spacecraft on a translunar trajectory.

The command and service modules were separated from the S-IVB, and then transposed and docked with the LM at about 3 hours. Approximately an hour later, the spacecraft was ejected and excellent color television pictures of earth were transmitted. A separation maneuver of 5.7 m/s (18.7 ft/s) was then performed, and the S-IVB was placed in a solar orbit by an auxiliary propulsion system ullage engine firing, propulsive venting, and dumping the residual propellants. The option for the first spacecraft midcourse correction at 12 hours was not exercised, and the passive thermal control technique was initiated at about 13 hours. The first midcourse correction, approximately 15.2 m/s (50 ft/s), was made at about 26.5 hours, and no further translunar corrections were required.

The spacecraft was inserted into a lunar orbit of 111 by 317 kilometers (60 by 171 n mi) at about 76 hours. Following two revolutions of tracking and ground updates, a maneuver was performed to circularize the orbit at approximately 111 kilometers (60 n mi). The LM pilot entered the LM, made a preliminary check of all systems, and then returned to the CM for the scheduled rest period.

Transfer to the LM was accomplished at approximately 95 hours. All systems were activated in preparation for undocking, which occurred at 98:47:17. After station-keeping, a small separation maneuver was performed by the command and service modules, and the LM was normally inserted into the descent orbit at about 99.8 hours. The first pass over Apollo Landing

Site 2 was made approximately 1 hour later, highlighted by a test of the landing radar, visual observation of lunar lighting conditions, stereo photography, and execution of the phasing maneuver using the descent engine at about 101 hours. Following one revolution in the phasing orbit, about 14.8 by 359 kilometers (8 by 195 n mi), the LM was staged, and the ascent engine was used to perform the insertion maneuver at about 103 hours. The cutoff conditions following this maneuver were identical to those expected after a normal ascent from the lunar surface, and the rendezvous which followed was therefore valid.

The rendezvous operation commenced with the coelliptic sequence initiation maneuver about one-half revolution from insertion, followed by a small constant differential height maneuver at approximately 104.7 hours. With the altitude difference between the two orbits established at the proper 28 kilometers (15 n mi), the terminal phase was initiated normally at 105:22:56, with the planned line-of-sight elevation angle in the midpoint of darkness. Final braking was performed on schedule to bring the two vehicles to within 30.5 meters (100 ft), at which time station-keeping was conducted. Final docking was completed at 106:22:02, and the crew transferred into the CM in preparation for ascent stage jettison. The ascent stage was jettisoned, and the ascent engine was fired to propellant depletion at about 108.5 hours.

After a rest period, the crew conducted landmark tracking and photography exercises prior to preparation for transearth injection, which was performed at about 137.5 hours.

Passive thermal control and navigation procedures used on the translunar portion of flight were also performed during earth return. One midcourse correction of 0.49 m/s (1.6 ft/s) was required about 3 hours prior to command and service modules separation. Entry occurred at 191:48:54, and the CM landed near the primary recovery vessel, USS Princeton, at 192:03:23. The crew was retrieved by helicopter at daybreak.

All system and vehicle temperatures varied within acceptable limits and essentially exhibited predicted behavior. Consumables usage was always maintained at a safe level.

For further details on the spacecraft performance, refer to the Apollo 10 Mission Report published by the NASA Manned Spacecraft Center at Houston, Texas.

APPENDIX A

ATMOSPHERE

A.1 SUMMARY

This appendix presents a summary of the atmospheric environment at launch time of the AS-505. The format of these data is similar to that presented on previous launches of Saturn vehicles to permit comparisons. Surface and upper winds, and thermodynamic data near the launch time are given.

A.2 GENERAL ATMOSPHERIC CONDITIONS AT LAUNCH TIME

A high pressure cell, in the Atlantic Ocean off the New England coast, caused southeasterly surface winds and brought moisture into the Cape Kennedy, Florida area, which contributed to the overcast conditions during launch.

A.3 SURFACE OBSERVATIONS AT LAUNCH TIME

At launch time, skies were overcast with 4/10 cumulus at 0.7 kilometer (2200 ft), 2/10 altostratus at 3.4 kilometers (11,000 ft) and 10/10 cirrus at an unknown altitude. Surface observations at launch time are summarized in Table A-1. Solar radiation data are given in Table A-2.

Table A-1. Surface Observations at AS-505 Launch Time

LOCATION	TIME AFTER T-0 (MIN)	PRES-SURE N/CM ² (PSIA)	TEM-PERATURE °K (°F)	POINT DEW °K (°F)	VISI-BILITY KM (STAT MI)	SKY COVER			WIND	
						AMOUNT (TENTHS)	TYPE	HEIGHT OF BASE M (FT)	SPEED M/S (KNOTS)	DIR (DEG)
Kennedy Space Center, Station Merritt Island, Florida	0	10.190 (14.78)	299.82 (80.0)	295.37 (72.0)	18 (11)	4	Cumulus	671 (2200)	5.7 (11.0)	130
						2	Alto-cumulus	E3350 (E11000)		
						10	Cirrus	high		
Cape Kennedy Rawinsonde Measurements	10	10.184 (14.77)	300.25 (80.8)	295.25 (71.8)	--	--	--	6.0 (11.7)	120	
Pad 39 B Lightpole SE (20.1 m)*	0	--	--	--	--	--	--	8.2 (16.0)	125	

*Above Natural Grade

Table A-2. Solar Radiation at AS-505 Launch Time, Launch Pad 39B

DATE	HOUR ENDING EST	TOTAL HORIZONTAL G-CAL/CM ² (MIN)	NORMAL INCIDENT G-CAL/CM ² (MIN)	DIFFUSE SKY G-CAL/CM ² (MIN)
May 17, 1969	0600	0.01	0.01	0.01
	0700	0.16	0.33	0.06
	0800	0.41	0.53	0.14
	0900	0.73	0.70	0.25
	1000	1.04	0.81	0.36
	1100	1.13	0.46	0.70
	1200	1.19	0.33	0.87
	1300	1.42	0.57	0.87
	1400	1.34	0.50	0.89
	1500	1.20	0.41	0.88
	1600	0.96	0.28	0.78
	1700	0.64	0.19	0.56
	1800	0.33	0.11	0.31
1900	0.07	0.03	0.07	
May 18, 1969	0600	0.01	0.00	0.01
	0700	0.14	0.16	0.09
	0800	0.41	0.46	0.17
	0900	0.74	0.61	0.32
	1000	1.04	0.68	0.47
	1100	1.19	0.58	0.65
	1200	1.15	0.26	0.89
	1300	1.36	0.37	1.00
	1400	0.94	0.09	0.86
	1500	0.54	0.02	0.52

A.4 UPPER AIR MEASUREMENTS

Data were used from four of the upper air wind systems to compile the final meteorological tape. Table A-3 summarizes the data systems used. It was necessary to use interpolated wind and thermodynamic data from 57 to 70 kilometers (187,000 to 229,660 ft).

A.4.1 Wind Speed

Wind speed increased with altitude, reaching a speed of 42.5 m/s (82.6 knots) at 14.18 kilometers (46,520 ft). Wind speeds at higher altitudes

Table A-3. Systems Used to Measure Upper Air Wind Data for AS-505

TYPE OF DATA	RELEASE TIME		PORTION OF DATA USED			
	TIME (UT)	TIME AFTER T-0 (MIN)	START		END	
			ALTITUDE M (FT)	TIME AFTER T-0 (MIN)	ALTITUDE M (FT)	TIME AFTER T-0 (MIN)
FPS-16 Jimsphere	1704	15	0	15	15,750 (51,670)	69
Rawinsonde	1659	10	16,000 (52,490)	62	24,750 (81,200)	91
Loki Dart	1928	159	56,750 (186,190)	159	25,000 (82,020)	187
Viper Dart	2030	221	89,750 (294,450)	221	70,250 (230,480)	222

were less than this peak, except near 90 kilometers (295,270 ft) altitude. See Figure A-1 for more information of the wind speeds.

A.4.2 Wind Direction

The surface wind was from the southeast, but shifted through the south to westerly at 14.0 kilometers (45,930 ft) altitude. Above this altitude winds shifted through the north and stayed generally from the east above 18.0 kilometers (59,050 ft), as shown in Figure A-2.

A.4.3 Pitch Wind Component

The surface pitch wind speed component was a head wind of 4.0 m/s (7.8 knots) and shifted to a tail wind by 3.0 kilometers (9840 ft) altitude. A maximum tail wind of 40.8 m/s (79.3 knots) was observed at 13.8 kilometers (45,280 ft) altitude. Head winds were observed from 16.9 kilometers (55,450 ft) to 83.5 kilometers (273,950 ft) altitude, with a peak head wind of 39.5 m/s (76.8 knots) at 71.0 kilometers (232,940 ft) altitude. See Figure A-3.

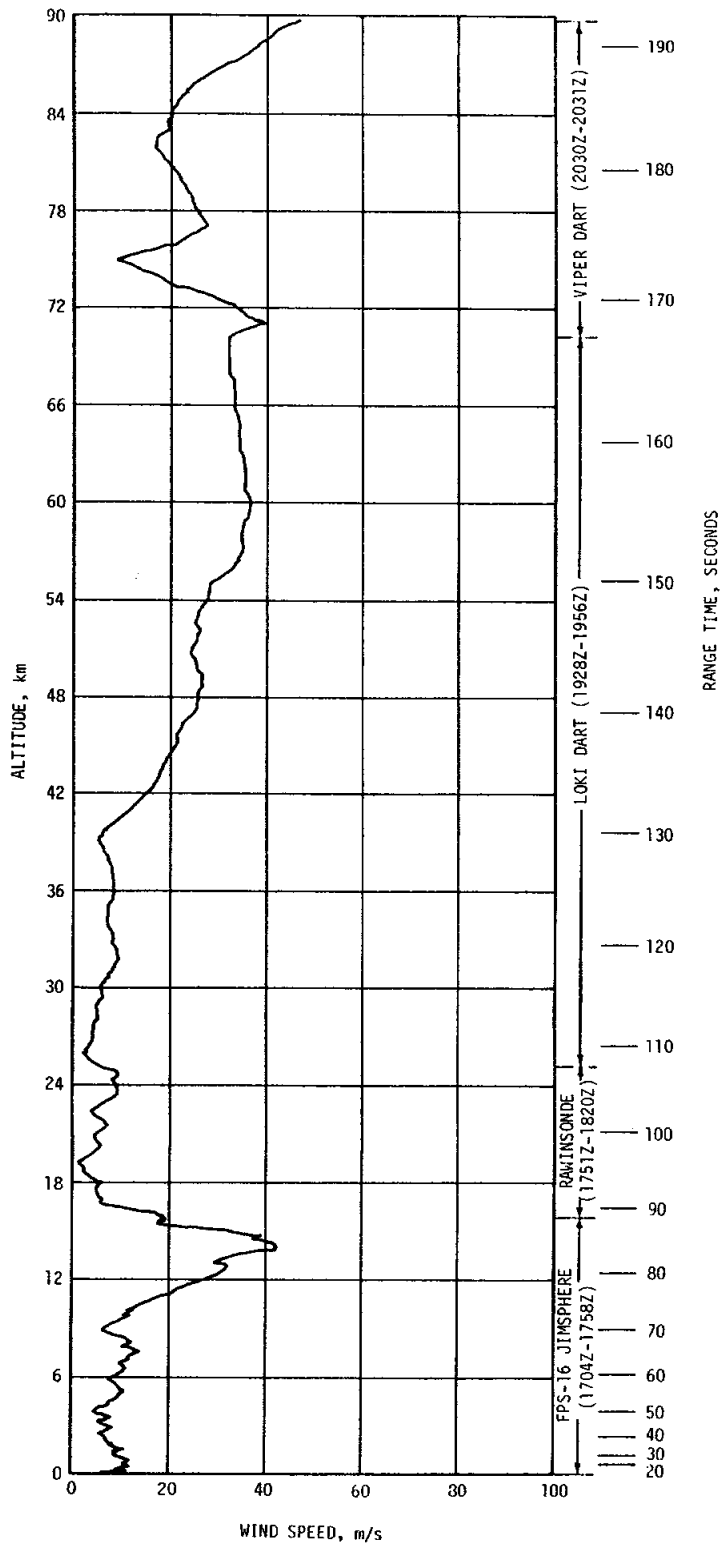


Figure A-1. Scalar Wind Speed at Launch Time of AS-505

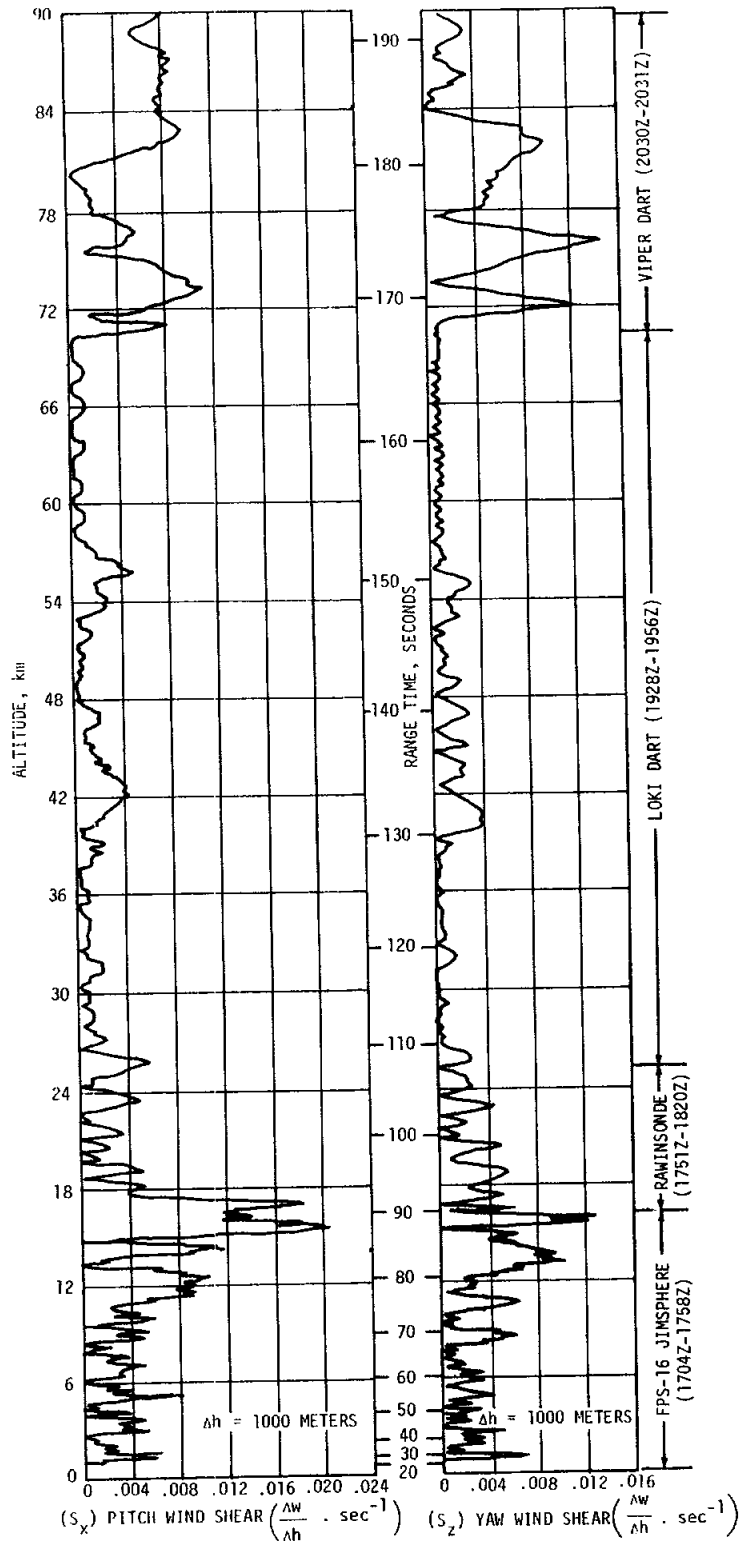


Figure A-5. Pitch (S_x) and Yaw (S_z) Component Wind Shears At Launch Time of AS-505

Table A-4. Maximum Wind Speed in High Dynamic Pressure Region for Apollo/Saturn 501 through Apollo/Saturn 505 Vehicles

VEHICLE NUMBER	MAXIMUM WIND			MAXIMUM WIND COMPONENTS			
	SPEED M/S (KNOTS)	DIR (DEG)	ALT KM (FT)	PITCH (w_x) M/S (KNOTS)	ALT KM (FT)	YAW (w_z) M/S (KNOTS)	ALT KM (FT)
AS-501	26.0 (50.5)	273	11.50 (37,700)	24.3 (47.2)	11.50 (37,700)	12.9 (25.1)	9.00 (29,500)
AS-502	27.1 (52.7)	255	12.00 (42,600)	27.1 (52.7)	12.00 (42,600)	12.9 (25.1)	15.75 (51,700)
AS-503	34.8 (67.6)	284	15.22 (49,900)	31.2 (60.6)	15.10 (49,500)	22.6 (43.9)	15.80 (51,800)
AS-504	76.2 (148.1)	264	11.73 (38,480)	74.5 (144.8)	11.70 (38,390)	21.7 (42.2)	11.43 (37,500)
AS-505	42.5 (82.6)	270	14.18 (46,520)	40.8 (79.3)	13.80 (45,280)	18.7 (36.3)	14.85 (48,720)

Table A-5. Extreme Wind Shear Values in the High Dynamic Pressure Region for Apollo/Saturn 501 through Apollo/Saturn 505 Vehicles

$(\Delta h = 1000 \text{ m})$				
VEHICLE NUMBER	PITCH PLANE		YAW PLANE	
	SHEAR (SEC ⁻¹)	ALTITUDE KM (FT)	SHEAR (SEC ⁻¹)	ALTITUDE KM (FT)
AS-501	0.0066	10.00 (32,800)	0.0067	10.00 (32,800)
AS-502	0.0125	14.90 (48,900)	0.0084	13.28 (43,500)
AS-503	0.0103	16.00 (52,500)	0.0157	15.78 (51,800)
AS-504	0.0248	15.15 (49,700)	0.0254	14.68 (48,160)
AS-505	0.0203	15.30 (50,200)	0.0125	15.53 (50,950)

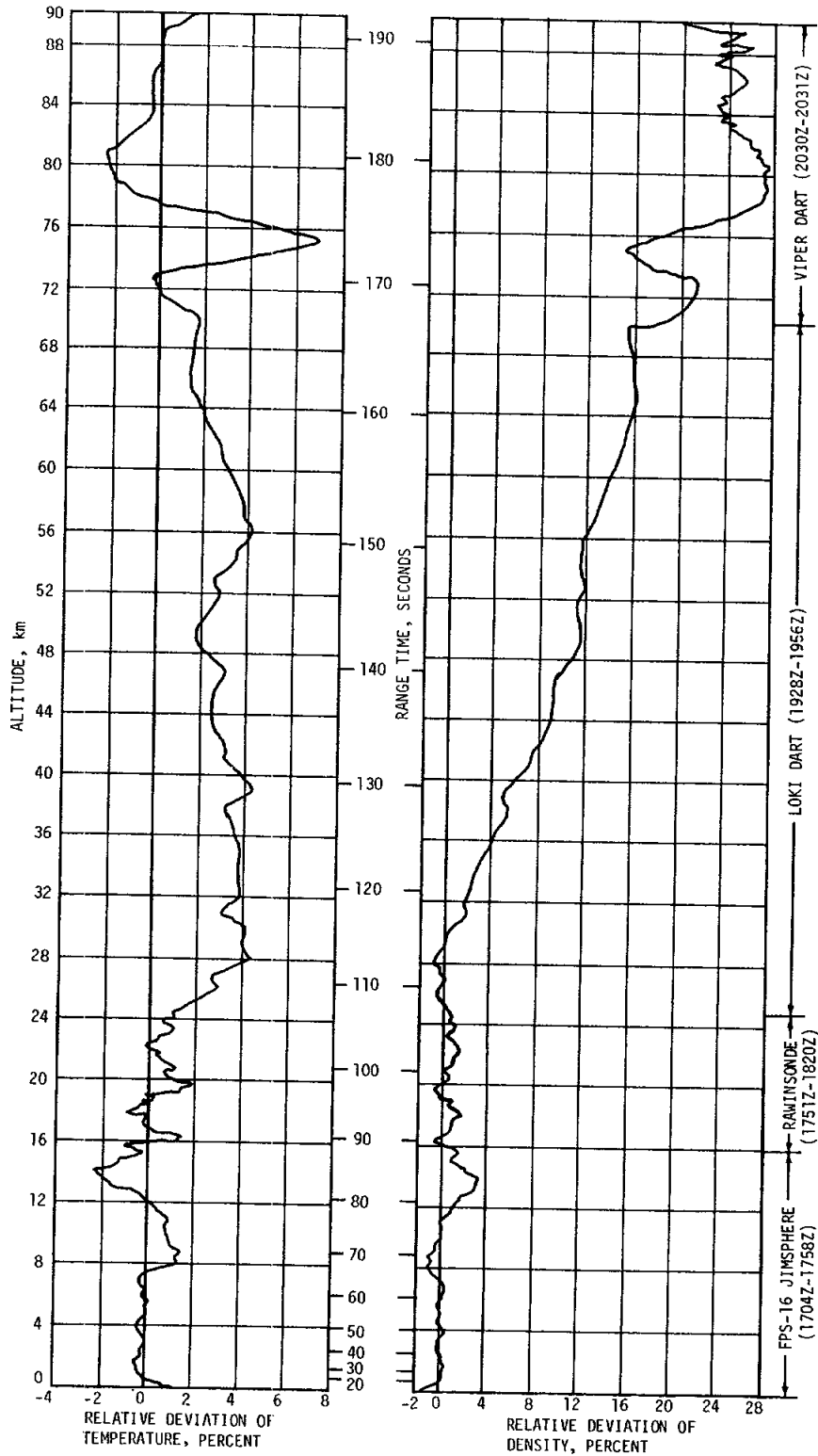


Figure A-6. Relative Deviation of Temperature and Density From the PRA-63 Reference Atmosphere, AS-505

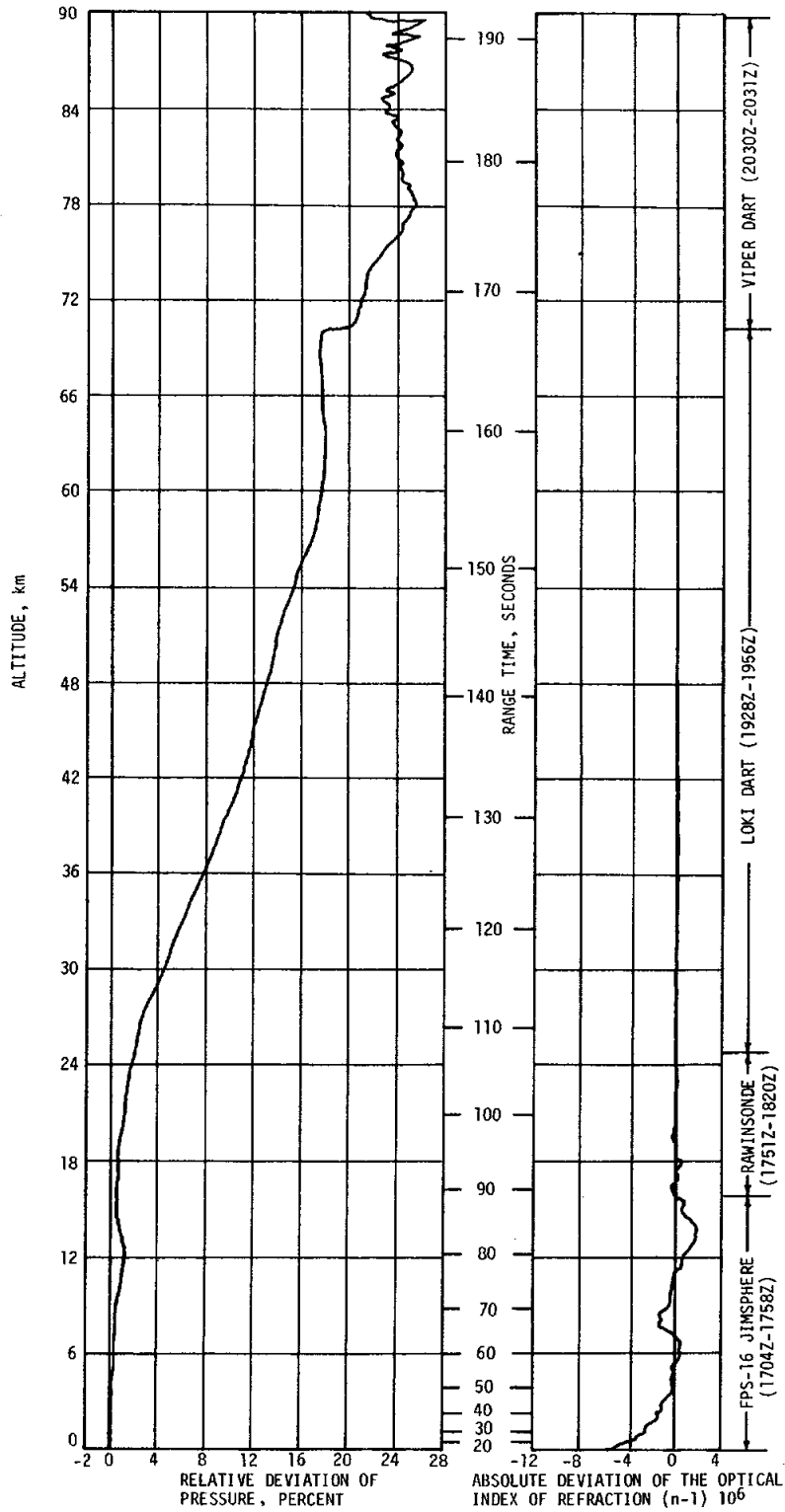


Figure A-7. Relative Deviation of Pressure and Absolute Deviation of the Index of Refraction From the PRA-63 Reference Atmosphere, AS-505

A.5.3 Atmospheric Density

Atmospheric density deviations were small, being less than 4 percent deviation from the PRA-63 to 36 kilometers (118,110 ft) altitude. Since density generally follows pressure patterns, there was an increase in density differences above 36 kilometers (118,110 ft) altitude, with a peak percentage difference at 27.6 percent from the PRA-63 at 80.5 kilometers (264,100 ft) altitude.

A.5.4 Optical Index of Refraction

At the surface, the Optical Index of Refraction was $9.81 (n-1) \times 10^{-6}$ units lower than the corresponding value of the PRA-63. The deviation decreased with altitude, becoming a maximum of $1.92 (n-1) \times 10^{-6}$ greater than the corresponding value of the PRA-63 at 13.3 kilometers (43,630 ft). Above this altitude the Optical Index of Refraction approximates the PRA-63 values.

A.6 COMPARISON OF SELECTED ATMOSPHERIC DATA FOR SATURN V LAUNCHES

A summary of the atmospheric data for each Saturn V launch is shown in Table A-6.

Table A-6. Selected Atmospheric Observations for Apollo/Saturn 501 through Apollo/Saturn 505 Vehicle Launches at Kennedy Space Center, Florida

VEHICLE NUMBER	VEHICLE DATA			SURFACE DATA						INFLIGHT CONDITIONS		
	DATE	TIME NEAREST MINUTE	LAUNCH COMPLEX	PRESSURE N/CM ²	TEMPERATURE °C	RELATIVE HUMIDITY PERCENT	SPEED M/S	WIND* DIRECTION DEG	CLOUDS	MAXIMUM WIND IN 8-16 KM LAYER ALTITUDE M	SPEED M/S	DIRECTION DEG
AS-501	9 Nov 67	0700 EST	39A	10.261	17.6	55	8.0	70	1/10 cumulus	11.50	26.0	273
AS-502	4 Apr 68	0600 EST	39A	10.200	20.9	83	5.4	132	5/10 stratocumulus	13.00	27.1	255
AS-503	21 Dec 68	0751 EST	39A	10.207	15.0	88	1.0	360	4/10 cirrus	15.22	34.8	284
AS-504	3 Mar 69	1100 EST	39A	10.095	19.6	61	6.9	160	10/10 strato-cumulus	11.73	26.2	264
AS-505	18 May 69	1149 EDT	39C	10.190	26.7	75	8.2	125	4/10 cumulus, 2/10 altocumulus, 10/10 cirrus	14.18	42.5	270

*Instantaneous readings from charts at T-0 from anemometers on launch pad at 18.3 m (60.0 ft) on launch complex 39 (A&B). Heights of anemometers are above natural grade.

APPENDIX B

AS-505 SIGNIFICANT CONFIGURATION CHANGES

B.1 INTRODUCTION

AS-505, fifth flight of the Saturn V series, was the third manned Apollo Saturn V vehicle. The AS-505 launch vehicle was configured the same as AS-504 with significant exceptions as shown in Tables B-1 through B-4. The AS-505 Apollo 10 spacecraft structure and components were essentially unchanged from the AS-504 Apollo 9 configurations. The basic AS-504 vehicle description is presented in Appendix B of the Saturn V Launch Vehicle Flight Evaluation Report AS-504, Apollo 9 Mission, MPR-SAT-FE-69-4.

Table B-1. S-IC Significant Configuration Changes

SYSTEM	CHANGE	REASON
Structures	Integral machine fittings replace welded fittings on LOX and fuel tank bulkheads.	Increase reliability of bulkheads.
Data	Deleted ODOP transponder and instrumentation. Ten acoustic measurements added to intertank. Deleted fuel tank slosh probes.	ODOP system no longer required for tracking. To determine effect of exhaust plume on vehicle. R&D instrumentation which is no longer required.

Table B-2. S-II Significant Configuration Changes

SYSTEM	CHANGE	REASON
Structures	Incorporate redesign of LH ₂ feedline elbows.	Improve weldability and reliability.
Propellant Management	Use PU system open loop mode (was closed loop mode on S-II-4).	Improve reliability.
Propulsion	Command early cutoff of center engine (No. 5) by switch selector.	Avoid low frequency oscillations experienced during flights of S-II-3 and S-II-4.
Launch Vehicle Ground Support Equipment	Add redundant vent system to S7-41 for vent valve actuation system.	Assure venting of vent valve actuation pressure prior to -15 seconds to avoid inadvertent opening of stage vent valves and consequent loss of ullage pressures.

Table B-3. S-IVB Significant Configuration Changes

SYSTEM	CHANGE	REASON
Instrumentation	AS-502 anomalies instrumentation package is installed and incorporates the FM/FM and single side-band telemetry systems and additional measurements.	Program requires AS-502 anomalies instrumentation on AS-503 and AS-505 stages only.
Propulsion	<p>Two S-IVB J-2 engine burns. First restart propellant tank repressurization performed by O₂/H₂ burner with ambient spheres as backup.</p> <p>Remove and inspect the bulkhead fittings and tube assembly flares in the APS high pressure system, and the temperature transducer fittings. Reinstall the fittings using MS-28778, Nitrile Rubber, 90 durometer hardness "O" rings.</p> <p>Delete one LH₂ tank ambient repressurization bottle.</p> <p>Connect the 2 LOX tank ambient repressurization bottles to the stage pneumatics bottle.</p>	<p>Normal TLI mission.</p> <p>To eliminate leakage of APS helium which was observed during the AS-504 flight.</p> <p>Payload savings.</p> <p>Increase the reserves capability for propulsion dumping and stage safing.</p>
Thermo-conditioning System	The number of cold plates located in the S-IVB forward skirt increased from 5 to 8.	To accommodate the additional electrical components.

Table B-4. IU Significant Configuration Changes

SYSTEM	CHANGE	REASON
Electrical	The S-IVB Engine Cutoff Enable Circuitry was not installed on S-IU-505.	The S-IVB restart requirement after Spacecraft separation is not required for S-IU-505.
	Permanent fix to isolate Flight Control Computer (FCC) from CCS generated noise during ground checkout.	CCS generated noise on 6D41 bus was fed back through ESE power buses to the FCC (6D31). Procedural change had been used to operate ESE + 6D211 (CCS) to prevent noise from CCS feeding back to the FCC.
Environmental Control	Cable Modifications	Minimum cable and network modifications were made to facilitate disabling UHF control circuitry and reroute IU and S-IVB PCM signals.
	Preflight GN ₂ /Air Purge Duct modifications at Locations 19 and 23.	Additional ducts were routed to the RTG Fuel Cask located in the LM Descent Stage to provide preflight cooling.
Guidance	The FCC M/W supply was disconnected.	The possibility of M/W leakage was eliminated; FCC cooling not required.
	LVDA P-23 Circuit changes.	LVDA circuit changes were made to inhibit recurrent generation of Error Time Words for a single error condition. These changes ensure only one error time word will be generated for a solid failure condition.
Instrumentation and Communications	Delete UHF RF telemetry link. Remove the following equipment: UHF RF Assembly, UHF RF Filter, PCM Coaxial Switch, CCS Hybrid Ring, CCS TM antenna. Add CCS Power Divider to replace the Hybrid Ring. S-IVB and IU PCM signals rerouted.	The CCS is considered operational and the backup UHF link is unnecessary.
	Add D68-603	The S-IVB PCM was removed from the CCS and replaced with IU PCM that had been routed to the UHF Transmitter.
Structures	Delete K133-603 and K134-603.	LM RTG Cask Diffuser Inlet Pressure. UHF Coaxial Switch measurement deleted.
	Add cork insulating material to outer IU surface and a sheet of vibration damping material in place of steel channels for the ST124M vibration damping.	Without cork and with steel channels, the safety factor at S-IC CECO was 1.14. The cork and vibration damping compound increase this factor to 1.55 (1.40 is required for manned flight).
	The Double Volume M/W Accumulator mounting brackets were changed from aluminum to steel.	The steel brackets provide adequate support for the increased load of the new Accumulator. Dynamic tests had revealed hairline cracks in the aluminum brackets.
	Add heavy core material in the region of the Water Accumulator attach points. (Location 3).	This gives a higher margin of safety against core crushing under the attach pads.
Flight Program	Redesigned umbilical plated added to S-IU-505 and Subs.	Internal stiffening was added to increase the strength of the plates. Swing Arm tests revealed excessive deflection of the old plate when the disconnect mechanism failed to release cleanly.
	A list of significant logic changes added to the S-IU-503 C Prime LVDC Flight Program to define the S-IU-505F Mission Program is given below:	
	Digital Command System (DCS) target and navigation update.	
	S-II Guidance to cutoff.	
	S-II CECO.	
	Open loop P/U S-II and S-IVB; different S-IVB EMR Shift time for first and second opportunities.	
Propellant Dump and Slingshot maneuver as separate Time Base (8) rather than included in TB7.		
DCS Command - Enable TB8.		
DCS Command - TD&E Enable.		
DCS Command - Enable Maneuver A.		
Guidance Switchover.		
Continuous real-time telemetry.		

APPROVAL

SATURN V LAUNCH VEHICLE FLIGHT EVALUATION REPORT

AS-505, APOLLO 10 MISSION

By Saturn Flight Evaluation Working Group

The information in this report has been reviewed for security classification. Review of any information concerning Department of Defense or Atomic Energy Commission programs has been made by the MSFC Security Classification Officer. The highest classification has been determined to be unclassified.



Stanley L. Fragge
Security Classification Officer

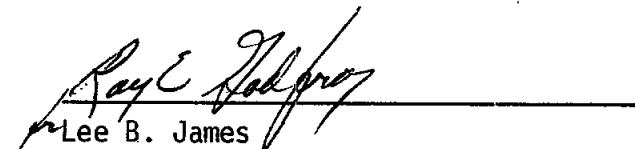
This report has been reviewed and approved for technical accuracy.



George H. McKay, Jr.
Chairman, Saturn Flight Evaluation Working Group



Herman K. Weidner
Director, Science and Engineering



Lee B. James
Saturn Program Manager

DISTRIBUTION:

MSFC:

Dr. von Braun, DIR
 Mr. Shepherd, DIR
 Dr. Rees, DEP-T
 Mr. Gorman, DEP-M
 Dr. Stuhlinger, ADIR-S

E

Mr. Maus, E-DIR
 Mr. Smith, E-S

PA

Mr. Slattery, PA-DIR

PD

Dr. Lucas, PD-DIR
 Mr. Williams, PD-DIR
 Mr. Driscoll, PD-DIR
 Mr. Thomason, PD-DO-DIR
 Mr. Goerner, PD-DO
 Mr. Nicaise, PD-DO
 Mr. Jean, PD-RV
 Mr. Digesu, PD-DO-E
 Mr. Palaoro, PD-SS
 Mr. Blumrich, PD-DO-SL

PM

Gen. O'Connor, PM-DIR
 Mr. Andressen, PM-PR-CM
 Col. Teir, PM-SAT-IB-MGR
 Mr. Huff, PM-SAT-E
 Dr. Speer, PM-MO-MGR
 Mr. Belew, PM-AA-MGR
 Mr. Brown, PM-EP-MGR
 Mr. Smith, PM-EP-J
 V. J. Norman, PM-MO
 Mr. Stewart, PM-EP-F
 Mr. L. James, PM-SAT-MGR
 Mr. Bramlet, PM-SAT-MGR
 Mr. Godfrey, PM-SAT-MGR
 Mr. Burns, PM-SAT-T
 Mr. Bell, PM-SAT-E
 Mr. Rowan, PM-SAT-E
 Mr. Moody, PM-SAT-Q
 Mr. Webb, PM-SAT-P
 Mr. Urlaub, PM-SAT-S-IB/S-IC
 Mr. Lahatte, PM-SAT-S-II
 Mr. McCullough, PM-SAT-S-IVB
 Mr. Duerr, PM-SAT-IU
 Mr. Smith, PM-SAT-G
 Col. Montgomery, PM-KM
 Mr. Peters, PM-SAT-S-IVB
 Mr. Weir, PM-SAT-IU
 Mr. Ferrell, PM-EP-EJ
 Dr. Constan, PM-MA-MGR
 Mr. Riemer, PM-MA-QP
 Mr. Balch, PM-MT-MGR
 Mr. Auter, PM-MT-T
 Mr. Sparks, PM-SAT-G
 Mr. Ginn, PM-SAT-E
 Mr. Haley, PM-SAT-S-IB/S-IC
 Mr. Higgins, PM-SAT-S-IVB
 Mr. Odom, PM-SAT-S-II
 Mr. Stover, PM-SAT-S-II
 Mr. Reaves, PM-SAT-Q
 Mr. Wheeler, PM-EP-F
 Mr. Johnson, PM-SAT-T
 Mr. Cushman, PM-SAT-T

S&E

Mr. Weidner, S&E-DIR
 Mr. Richard, S&E-DIR
 Dr. Johnson, S&E-R
 Mr. Hamilton, MSC-RL

S&E-AERO

Dr. Geissler, S&E-AERO-DIR
 Mr. Horn, S&E-AERO-DIR
 Mr. Dahm, S&E-AERO-A (2)
 Mr. Holderer, S&E-AERO-A
 Mr. Dunn, S&E-AERO-ADV
 Mr. Elkin, S&E-AERO-AT
 Mr. Wilson, S&E-AERO-AT
 Mr. Jones, S&E-AERO-AT
 Mr. Reed, S&E-AERO-AU
 Mr. Guest, S&E-AERO-AU
 Mr. Ryan, S&E-AERO-DD
 Mr. Cremin, S&E-AERO-M (10)
 Mr. Lindberg, S&E-AERO-M
 Mr. Baker, S&E-AERO-G
 Mr. Jackson, S&E-AERO-P
 Mr. Cummings, S&E-AERO-T
 Mr. O. E. Smith, S&E-AERO-Y
 Mr. J. Sims, S&E-AERO-P
 Dr. Lovingood, S&E-AERO-D
 Mr. Vaughan, S&E-AERO-Y

S&E-CSE

Dr. Haeussermann, S&E-CSE-DIR
 Mr. Hoberg, S&E-CSE-DIR
 Mr. Mack, S&E-CSE-DIR
 Dr. McDonough, S&E-CSE-A
 Mr. Aberg, S&E-CSE-S
 Mr. Fichtner, S&E-CSE-G
 Mr. Vann, S&E-CSE-GA
 Mr. Hammers, S&E-CSE-I
 Mr. Wolfe, S&E-CSE-I
 Mr. R. Smith, S&E-CSE-L
 Mr. McKay, S&E-CSE-LF (4)
 Mr. R. L. Smith, S&E-CSE-V
 Mr. Brooks, S&E-CSE-V
 Mr. Hagood, S&E-CSE-M (3)

S&E-ASTR

Mr. Moore, S&E-ASTR-DIR
 Mr. Stroud, S&E-ASTR-SC
 Mr. Robinson, S&E-P-ATM (4487)
 Mr. Erickson, S&E-ASTR-SE
 Mr. Darden, S&E-ASTR-SD
 Mr. Justice, S&E-ASTR-SD
 Mr. Vallely, S&E-ASTR-FO
 Mr. Mink, S&E-ASTR-FR
 Mr. Mandel, S&E-ASTR-G
 Mr. Ferrell, S&E-ASTR-GS
 Mr. Powell, S&E-ASTR-I
 Mr. Avery, S&E-ASTR-SC
 Mr. Kerr, S&E-ASTR-IRD
 Mr. Threlkeld, S&E-ASTR-ITA
 Mr. Boehm, S&E-ASTR-M
 Mr. Lominick, S&E-ASTR-GMF
 Mr. Taylor, S&E-ASTR-R

S&E COMP

Dr. Hoelzer, S&E-COMP-DIR
 Mr. Prince, S&E-COMP-DIR
 Mr. Fortenberry, S&E-COMP-A
 Mr. Cochran, S&E-COMP-R
 Mr. Houston, S&E-COMP-RR
 Mr. Craft, S&E-COMP-RR

S&E-ME

Mr. Siebel, S&E-ME-DIR
 Mr. Wuencher, S&E-ME-DIR
 Mr. Orr, S&E-ME-A
 Mr. Franklin, S&E-ME-T (10)

S&E-ASTN

Mr. Heimburg, S&E-ASTN-DIR
 Mr. Kingsbury, S&E-ASTN-DIR

Mr. Hellebrand, S&E-ASTN-DIR
 Mr. Edwards, S&E-ASTN-DIR
 Mr. Sterett, S&E-ASTN-A
 Mr. Schwinghamer, S&E-ASTN-M
 Mr. Earle, S&E-ASTN-P
 Mr. Reilmann, S&E-ASTN-P
 Mr. Thompson, S&E-ASTN-E
 Mr. Fuhrmann, S&E-ASTN-EM (2)
 Mr. Cobb, S&E-ASTN-PP
 Mr. Black, S&E-ASTN-PPE
 Mr. Wood, S&E-ASTN-P
 Mr. Hunt, S&E-ASTN-A
 Mr. Beam, S&E-ASTN-AD
 Mr. Riquelmy, S&E-ASTN-SDF
 Mr. Katz, S&E-ASTN-SER
 Mr. Showers, S&E-ASTN-SL
 Mr. Frederick, S&E-ASTN-SS
 Mr. Furman, S&E-ASTN-AA
 Mr. Green, S&E-ASTN-SVM
 Mr. Grafton, S&E-ASTN-T
 Mr. Mammann, S&E-ASTN-VAM
 Mr. Lutonsky, S&E-ASTN-VAW (2)
 Mr. Devenish, S&E-ASTN-VNP
 Mr. Sells, S&E-ASTN-VOO
 Mr. Schulze, S&E-ASTN-V (2)
 Mr. Rothe, S&E-ASTN-XA
 Mr. Griner, S&E-ASTN-XSJ
 Mr. Boone, S&E-ASTN-XEK

S&E-QUAL

Mr. Grau, S&E-QUAL-DIR
 Mr. Chandler, S&E-QUAL-DIR
 Mr. Henritze, S&E-QUAL-A
 Mr. Rushing, S&E-QUAL-PI
 Mr. Klaus, S&E-QUAL-J
 Mr. Hughes, S&E-QUAL-P
 Mr. Landers, S&E-QUAL-PC (3)
 Mr. Peck, S&E-QUAL-F
 Mr. Brien, S&E-QUAL-Q
 Mr. Wittmann, S&E-QUAL-T
 Mr. Davis, S&E-QUAL-F

S&E-SSL

Mr. Heller, S&E-SSL-DIR
 Mr. Sieber, S&E-SSL-S

MS

MS-H
 MS-I
 MS-IP
 MS-IL (8)
 MS-D

CC-P

Mr. Wofford, CC-P

KSC

Dr. Debus, CD
 Adm. Middleton, AP (5)
 Mr. Petrone, LO
 Dr. Gruene, LV
 Mr. Rigell, LV-ENG
 Mr. Sandler, IN
 Mr. Mathews, AP
 Dr. Knothe, EX-SCI
 Mr. Edwards, LV-INS
 Mr. Fannin, LV-MEC
 Mr. Pickett, LV-TMO
 Mr. Rainwater, LV-TMO
 Mr. Bell, LV-TMO-3
 Mr. Lealman, LV-GDC
 Mr. Preston, DE
 Mr. Mizell, LV-PLN-12
 Mr. O'Hara, LV-TMO
 Mr. Brown, AP-SVO-3
 Mr. Smith, AP-SVO

EXTERNAL

Headquarters, National Aeronautics & Space Administration
Washington, D. C. 20546

Dr. Mueller, M
Gen. Phillips, MA
Gen. Stevenson, MO (3 copies)
Mr. Hage, MO
Mr. Schneider, MO-2
Capt. Freitag, MC
Capt. Holcomb, MAO
Mr. White, MAR (2 copies)
Mr. Day, MAT (10 copies)
Mr. Wilkinson, MAB
Mr. Kubat, MAP
Mr. Wagner, MAS (2 copies)
Mr. Armstrong, MB
Mr. Mathews, ML (3 copies)
Mr. Lord, MT
Mr. Lederer, MY

Director, Ames Research Center: Dr. H. Julian Allen
National Aeronautics & Space Administration
Moffett Field, California 94035

Director, Flight Research Center: Paul F. Bikle
National Aeronautics & Space Administration
P. O. Box 273
Edwards, California 93523

Goddard Space Flight Center
National Aeronautics & Space Administration
Greenbelt, Maryland 20771
Attn: Herman LaGow, Code 300

John F. Kennedy Space Center
National Aeronautics & Space Administration
Kennedy Space Center, Florida 32899
Attn: Technical Library, Code RC-42
Mrs. L. B. Russell

Director, Langley Research Center: Dr. Floyd L. Thompson
National Aeronautics & Space Administration
Langley Station
Hampton, Virginia 23365

Lewis Research Center
National Aeronautics & Space Administration
21000 Brookpark Road
Cleveland, Ohio 44135
Attn: Dr. Abe Silverstein, Director
Robert Washko, Mail Stop 86-1
E. R. Jonash, Centaur Project Mgr.

Manned Spacecraft Center
National Aeronautics & Space Administration
Houston, Texas 77058
Attn: Director: Dr. Robert R. Gilruth, AA
Mr. Low, PA
Mr. Arabian, ASPQ-PT (15 copies)
Mr. Paules, FC-5
J. Hamilton, PF (MSFC Resident Office)
G. F. Prude, CF-33 (3 copies)

Director, Wallops Station: R. L. Krieger
National Aeronautics & Space Administration
Wallops Island, Virginia 23337

Director, Western Operations Office: Robert W. Kamm
National Aeronautics & Space Administration
150 Pico Blvd.
Santa Monica, California 90406

Scientific and Technical Information Facility
P. O. Box 5700
Bethesda, Maryland 20014
Attn: NASA Representative (S-AK/ARIT) (25 copies)

Jet Propulsion Laboratory
4800 Oak Grove Drive
Pasadena, California 91103
Attn: Irl Newlan, Reports Group (Mail 111-172)
H. Levy, CCMA (Mail 179-203) (4 copies)

Office of the Asst. Sec. of Defense for Research
and Engineering
Room 3E1065
The Pentagon
Washington, D. C. 20301
Attn: Tech Library

Director of Guided Missiles
Office of the Secretary of Defense
Room 3E131
The Pentagon
Washington, D. C. 20301

Central Intelligence Agency
Washington, D. C. 20505
Attn: OCR/DD/Publications (5 copies)

Director, National Security Agency
Ft. George Mead, Maryland 20755
Attn: C3/TDL

U. S. Atomic Energy Commission, Sandia Corp.
University of California Radiation Lab.
Technical Information Division
P. O. Box 808
Livermore, California 94551
Attn: Clovis Craig

U. S. Atomic Energy Commission, Sandia Corp.
Livermore Br, P. O. Box 969
Livermore, California 94551
Attn: Tech Library

Commander, Armed Services Technical Inf. Agency
Arlington Hall Station
Arlington, Virginia 22212
Attn: TIPCR (Transmittal per Cognizant Act
Security Instruction) (5 copies)

Commanding General
White Sands Missile Range,
New Mexico 88002
Attn: RE-L (3 copies)

Chief of Staff, U. S. Air Force
The Pentagon
Washington, D. C. 20330
1 Cpy marked for DCS/D AFDRD
1 Cpy marked for DCS/D AFORD-EX

Headquarters SAC (DPLBS)
Offutt AFB, Nebraska 68113

Commander
Arnold Engineering Development Center
Arnold Air Force Station, Tennessee 37389
Attn: Tech Library (2 copies)

Commander
Air Force Flight Test Center
Edwards AFB, California 93523
Attn: FTOTL

Commander
Air Force Missile Development Center
Holloman Air Force Base
New Mexico 88330
Attn: Tech Library (SRLT)

Headquarters
6570th Aerospace Medical Division (AFSC)
U. S. Air Force
Wright-Patterson Air Force Base, Ohio 45433
Attn: H. E. Vongierke

Systems Engineering Group (RTD)
Attn: SEPIR
Wright-Patterson, AFB, Ohio 45433

AFETR (ETLLG-1)
Patrick AFB, Florida 32925

EXTERNAL (CONT.)

Director
U. S. Naval Research Laboratory
Washington, D. C. 20390
Attn: Code 2027

Chief of Naval Research
Department of Navy
Washington, D. C. 20390
Attn: Code 463

Chief, Bureau of Weapons
Department of Navy
Washington, D. C. 20390
1 Cpy to RESI, 1 Cpy to SP,
1 Cpy to AD3, 1 Cpy to REW3

Commander
U. S. Naval Air Missile Test Center
Point Mugu, California 93041

AMSML-RBLD; RSIC (3 copies)
Bldg. 4484
Redstone Arsenal, Alabama 35809

Aerospace Corporation
2400 East El Segundo
El Segundo, California 90245
Attn: D. C. Bakeman

Aerospace Corporation
Reliability Dept.
P. O. Box 95085
Los Angeles, California 90045
Attn: Don Herzstein

Bellcomm, Inc.
1100 Seventeenth St. N. W.
Washington, D. C. 20036
Attn: Miss Scott, Librarian

The Boeing Company
P.O. Box 1680
Huntsville, Alabama 35807
Attn: S. C. Krausse, Mail Stop AD-60
(30 copies)
J. B. Winch, Mail Stop JA-52
(1 copy)

The Boeing Company
P.O. Box 58747
Houston, Texas 77058
Attn: H. J. McClellan, Mail Stop HH-05
(2 copies)

The Boeing Company
P.O. Box 29100
New Orleans, Louisiana 70129
Attn: S. P. Johnson, Mail Stop LT-84
(10 copies)

Mr. Norman Sissenwine, CREW
Chief, Design Climatology Branch
Aerospace Instrumentation Laboratory
Air Force Cambridge Research Laboratories
L. G. Hanscom Field
Bedford, Massachusetts 01731

Lt/Col. H. R. Montague
Det. 11, 4th Weather Group
Eastern Test Range
Patrick Air Force Base, Florida 33564

Mr. W. Davidson
NASA Resident Management Office
Mail Stop 8890
Martin Marietta Corporation
Denver Division
Denver, Colorado 80201

Chrysler Corporation Space Division
Huntsville Operation
1312 N. Meridian Street
Huntsville, Alabama 35807
Attn: J. Fletcher, Dept. 4830
M. L. Bell, Dept. 4830

McDonnell Douglas Astronautics Company
Missile & Space Systems Division/SSC
5301 Bolsa Avenue
Huntington Beach, California 92646
Attn: R. J. Mohr (40 copies)

Grumman Aircraft Engineering Corp.
Bethpage, Long Island, N. Y. 11714
Attn: NASA Resident Office
John Johansen

International Business Machine
Mission Engineering Dept. F103
150 Sparkman Dr. NW
Huntsville, Alabama 35805
Attn: C. N. Hansen (15 copies)

Martin Company
Space Systems Division
Baltimore, Maryland 21203
Attn: W. P. Sommers

North American Rockwell/Space Division
12214 S. Lakewood Blvd.
Downey, California 90241
Attn: R. T. Burks (35 copies)

Radio Corporation of America
Defense Electronic Products
Data Systems Division
8500 Balboa Blvd.
Van Nuys, California 91406

Rocketdyne
6633 Canoga Avenue
Canoga Park, California 91303
Attn: T. L. Johnson (10 copies)

Foreign Technology Division
FTD (TDPSL)
Wright-Patterson Air Force Base, Ohio 45433

Mr. George Mueller
Structures Division
Air Force Flight Dynamics Laboratory
Research and Technology Division
Wright-Patterson Air Force Base, Ohio 45433

Mr. David Hargis
Aerospace Corporation
Post Office Box 95085
Los Angeles, California 90045

Mr. H. B. Tolefson
DLA-Atmospheric Physics Branch
Mail Stop 240
NASA-Langley Research Center
Hampton, Virginia 23365

Mr. Chasteen
Sperry Rand
Dept. 223
Blue Spring Road
Huntsville, Ala.